DESIGN AND DEVELOPMENT OF NEW PYRAZINE-BASED MOLECULES AS POTENT ANTITUBERCULAR AGENTS

Thesis

Submitted in partial fulfillment of the requirements for the degree of

DOCTOR OF PHILOSOPHY

by

SHIVAKUMAR

DEPARTMENT OF CHEMISTRY

NATIONAL INSTITUTE OF TECHNOLOGY KARNATAKA

SURATHKAL, MANGALORE - 575025

August, 2024

DECLARATION

BY THE PH.D. RESEARCH SCHOLAR

I HEREBY *DECLARE* THAT THE RESEARCH THESIS ENTITLED **"DESIGN AND DEVELOPMENT OF NEW PYRAZINE-BASED MOLECULES AS POTENT ANTITUBERCULAR AGENTS."** WHICH IS BEING SUBMITTED TO THE **NATIONAL INSTITUTE OF TECHNOLOGY KARNATAKA, SURATHKAL** IN PARTIAL FULFILLMENT OF THE REQUIREMENTS FOR THE AWARD OF THE DEGREE OF ***DOCTOR OF PHILOSOPHY*** INCHEMISTRY IS A *BONAFIDE REPORT OF THE RESEARCH WORK CARRIED OUT BY ME*. THE MATERIAL CONTAINED IN THIS THESIS HAS NOT BEEN SUBMITTED TO ANY UNIVERSITY OR INSTITUTION FOR THE AWARD OF ANY DEGREE.

Shivakumar 20/08/24

Shivakumar

Reg. No.: 207114CY010

Department of Chemistry

Place: NITK, Surathkal

Date: 20-08-2024

CERTIFICATE

THIS IS TO *CERTIFY* THAT THE THESIS ENTITLED **"DESIGN AND DEVELOPMENT OF NEW PYRAZINE-BASED MOLECULES AS POTENT ANTITUBERCULAR AGENTS."** SUBMITTED BY **MR. SHIVAKUMAR (REGISTER NUMBER: 207114CY010)** AS THE RECORD OF THE RESEARCH WORK CARRIED OUT BY HIM IS ACCEPTED AS THE *RESEARCH THESIS* SUBMISSION IN PARTIAL FULFILLMENTOF THE REQUIREMENTS FOR THE AWARD OF THE DEGREE OF **DOCTOR OF PHILOSOPHY.**

Dr. Udayakumar Dalimba
Research Guide
Date: 20-08-2024

Dr. UDAYA KUMAR D.
Professor
Department of Chemistry
National Institute of Technology Karnataka
Surathkal, MANGALORE- 575 025

20/08/2024
Chairman-DRPC

Head / H.O.D.
रसायन शास्त्र विभाग/ Chemistry Dept.
राष्ट्रीय प्रौद्योगिकी संस्थान कर्नाटक, सुरत्कल
NITK SURATHKAL
मंगलूरु-५७५ ०२५, कर्नाटक
MANGALURU-575 025, KARNATAKA

ACKNOWLEDGEMENTS

I extend my heartfelt gratitude to everyone who has contributed directly and indirectly to my research endeavours.

Firstly, I am deeply thankful to my research supervisor, Dr. Udayakumar D., Professor in the Department of Chemistry at NITK, Surathkal, for offering me the invaluable opportunity to pursue my research under his expert guidance.

I am also grateful to NITK Surathkal for providing the research fellowship and necessary laboratory facilities, enabling me to conduct my research.

Special appreciation goes to the RPAC members, Dr. N. K. Udayashankar and Dr. A. Chitharanjan Hegde, for their time, evaluation, and insightful suggestions, which greatly enhanced the quality of my work.

I acknowledge the support received from the Head of the Department, Dr. Darshak R. Trivedi, and other faculty members including Dr. A. Nithyananda Shetty, Dr. B. Ramchandra Bhat, Dr. D. Krishna Bhat, Dr. Arun M. Isloor, Dr. Sib Sankar Mal, Dr. Beneesh P. B., Dr. Saikat Dutta, Dr. Debasree Chakraborty, Dr. Vijayendra S. Shetti, and Dr. Lakshmi Vellanki, for their encouragement and guidance.

I am grateful to my research colleagues and fellow scholars, namely Dr. Rajkumar R., Mr. Vigenshwar Ganesh Bhat, Miss. Archana S, Mr. Dinesha P., Mr. Subramanya K. S., Mr. Sampat P. Vibhutimath, Mr. Shreeganesh Subraya Hegde, Mr. Poornachandra S. P., and others, for their support throughout my Ph.D. journey.

Special thanks to Dr. M. Murali Krishna Kumar from the College of Pharmaceutical Sciences, Andhra University, Visakhapatnam, and collaborators from Nitte University, Mangalore, including Dr. Revanasiddappa B. C., Dr. Deekshit V. K.,

and Miss. Varsha, for their assistance in biological studies, which were integral to the success of my research.

I express my gratitude to the Central Research Facility at NITK Surathkal for providing analytical support, and to the non-teaching staff members of the Chemistry Department, namely Mr. Prashant, Mr. Pradeep, Mr. Santhosh, Mrs. Rashmi, Mrs. Sharmila, Mrs. Divya, and Mrs. Deepa for their timely assistance.

Lastly, my deepest appreciation goes to my family members, especially my mother Mrs. Lakshmibai, my late father Mr. Linga Naik, my sisters Mrs. Susheela Bai, Mrs. Vasanta Bai, Mrs. Roja Bai, Mrs. Lalitha Bai, and my brothers in law Mr. Ramanji Naik, Mr. Shivanna Naik, Mr. Ramesh Naik, and Mr. Harish Naik, along with my nephews and niece, for their unwavering support and inspiration throughout my research journey.

Thank you.

Mr. Shivakumar

ABSTRACT

Tuberculosis (TB) remains a significant global health concern, with millions of new cases and deaths reported each year. The emergence of drug-resistant strains, such as multidrug-resistant tuberculosis (MDR-TB) and extensively drug-resistant tuberculosis (XDR-TB), has underscored the need for more effective antitubercular treatments. Pyrazine, a versatile compound capable of forming hydrogen bonds and dipole-dipole interactions, has garnered attention for its potential in developing new drugs due to its wide range of pharmacological applications. To capitalize on this, we aimed to create novel molecules by incorporating various potent heterocyclic motifs into the pyrazine structure. We successfully designed five new series of pyrazine-based compounds through molecular hybridization, structural modification, and bioisosterism. These series include derivatives incorporating 1,3,4-oxadiazole/[1,2,4] triazolo[3,4-b][1,3,4]thiadiazine (**T1-T18**), 1,2,4-triazole (**T19-T36**), pyrazine hydrazinylidene derivatives with a benzenesulfonate scaffold (**T37-T52**), 4-quinazolinone (**T53-T68**), and 2-aminophenyl and 2-oxoacetyl incorporated pyrazine-2-carbohydrazide derivatives (**T69-T88**). These compounds were synthesized using multistep synthetic protocols and characterized using ^{1}H-NMR, ^{13}C-NMR, and HRMS techniques. Furthermore, we evaluated the synthesized compounds for their *in vitro* antitubercular activity against the *mycobacterium tuberculosis* H37Rv strain, as well as their antibacterial activity against *S. aureus*, *S. mutans*, *E. coli*, and *S.* Typhi, and antifungal activity against *A. niger*. Additionally, we assessed the cytotoxicity of active molecules on non-cancerous cells using an MTT assay. To gain insights into their mechanism of action, we conducted *in silico* ADMET, DFT calculations, and molecular docking studies.

Keywords: Pyrazine, *Mycobacterium tuberculosis* H37Rv, antitubercular activity, antibacterial activity, antifungal activity, cytotoxicity studies, ADMET, DFT, *in silico* molecular docking.

CONTENTS

CHAPTER 1

INTRODUCTION, LITERATURE REVIEW, AND OBJECTIVES OF THE WORK

1.1 Medicinal Chemistry 1

1.2 Heterocyclic Chemistry 2

1.3 Chemistry of Pyrazine and its Derivatives 5

1.3.1 Synthesis of Pyrazine 6

1.4 Pharmacological Significance of Pyrazine and its Derivatives 10

1.5 Tuberculosis 13

1.6 Literature Survey 17

1.7 Scope and Objectives of the Present Work 27

1.8 Organization of the Thesis 29

CHAPTER 2

SYNTHESIS AND CHARACTERIZATION OF PYRAZINE-BASED COMPOUNDS

2.1 Introduction 31

2.2 Experimental 33

2.2.1 Materials And Methods 33

2.2.2 Synthesis and Characterization 34

2.3 Results and Discussions 63

2.3.1 Synthesis and Characterization of 1,3,4-oxadiazole/[1,2,4] triazolo[3,4-b] [1,3,4]thiadiazine incorporated pyrazine Derivatives 64

2.3.2 Synthesis and Characterization of 1,2,4-triazole incorporated Pyrazine Derivatives 69

2.3.3 Synthesis and Characterization of Pyrazine hydrazinylidene Derivatives containing Benzenesulfonate Scaffold 75

2.3.4 Synthesis and Characterization of 4-quinazolinone incorporated pyrazine Derivatives 80

2.3.5 Synthesis and Characterization of 2-aminophenyl and 2-oxoacetyl incorporated pyrazine-2-carbohydrazide Derivatives 85

2.4 Conclusions 90

CHAPTER 3

BIOLOGICAL SCREENING: *IN VITRO* STUDIES ON ANTITUBERCULAR, ANTIBACTERIAL, ANTIFUNGAL ACTIVITY, AND CYTOTOXICITY

3.1 Introduction 213

3.1.1 Mode of Action of Antimicrobials 215

3.1.2 Antimicrobial Screening 217

3.1.2.1 Diffusion Method 218

3.1.2.2 Dilution Method 218

3.1.2.3 Diffusion and Dilution Method 219

3.2 Materials and Methods 220

3.2.1 Antitubercular Activity 220

3.2.2 Antibacterial Activity 221

3.2.3 Antifungal Activity 222

3.2.4 Cytotoxicity Studies 223

3.3 Results and Discussions 223

3.3.1 Antitubercular, Antibacterial, and Antifungal Activity of 1,3,4-oxadiazole/[1,2,4] triazolo[3,4-b][1,3,4]thiadiazine incorporated pyrazine Derivatives 223

3.3.2 Antitubercular, Antibacterial, and Antifungal Activity of 1,2,4-triazole incorporated pyrazine Derivatives 227

3.3.3 Antitubercular, Antibacterial, and Antifungal Activity of pyrazine hydrazinylidene Derivatives containing Benzenesulfonate Scaffold 230

3.3.4 Antitubercular, Antibacterial, and Antifungal Activity of 4-quinazolinone incorporated pyrazine Derivatives 233

3.3.5 Antitubercular, Antibacterial, and Antifungal Activity of 2-aminophenyl and 2-oxoacetyl incorporated pyrazine-2-carbohydrazide Derivatives 236

3.3.6 *In vitro* Cytotoxicity of the active Compounds 239

3.4 Structure-Activity Relationship 242

3.5 Conclusions 247

CHAPTER 4

***IN SILICO* STUDIES: A COMPREHENSIVE EXPLORATION OF ADMET, DFT, AND MOLECULAR DOCKING OF PYRAZINE-BASED DERIVATIVES**

4.1 Introduction 249

4.2 Materials and Methods 251

4.2.1 Pharmacokinetics and Physicochemical Studies 251

4.2.2 DFT Studies 252

4.2.3 *In silico* Molecular Docking Studies 252

4.3 Results and Discussions 253

4.3.1 Pharmacokinetics and Physicochemical Studies 253

4.3.2 DFT Studies 261

4.3.3 *In silico* Molecular Docking Studies 276

4.4 Conclusions 287

CHAPTER 5

SUMMARY AND CONCLUSIONS

5.1 Summary 289

5.2 Conclusions 292

5.3 Scope for the Future Work 293

References 295

List of Publications 305

Biodata 309

NOMENCLATUREJ

ABBREVIATIONS

AIDS	Acquired immunodeficiency syndrome
AmB	Amphotericin B
A. niger	*Aspergillus niger*
AntiTB	Antitubercular
AST	Antimicrobial Susceptibility Testing
B. subtilis	*Bacillus subtilis*
C. albicans	*Candida albicans*
CHL	Chloramphenicol
DNA	Deoxyribonucleic acid
E. coli	*Escherichia coli*
EMB	Ethambutol
FDA	Food and Drug Administration
GLP	Good laboratory practices
HEK	Human Embryonic Kidney
HIV	Human immunodeficiency virus
IND	Investigational new drug process
INH	Isoniazid
INN	Ciprofloxacin
KOH	Potassium Hydroxide
m.p.	Melting point
MABA	Microplate Alamar blue assay

M. avium	*Mycobacterium avium*
MBC	Minimum Bactericidal Concentrations
MDR-TB	Multidrug resistant tuberculosis
MIC	Minimum inhibitory concentration
M. kansasii	*Mycobacterium kansasii*
Mtb	*Mycobacterium tuberculosis*
NCCLS	National Committee for Clinical Laboratory Standards
NMR	Nuclear magnetic resonance
OLEDs	organic light-emitting diodes
PZA	pyrazinamide
P. aeruginosa	*Pseudomonas aeruginosa*
RIF	Rifampicin
RNA	Ribonucleic acid
RT	Room temperature
SAR	Structure-activity relationship
S. aureus	*Staphylococcus aureus*
S. Typhi	*Salmonella typhi*
SCXRD	Single-crystal X-Ray diffraction
TB	Tuberculosis
TLC	Thin layer chromatography
WHO	World health organization
XDR-TB	Extensively drug-resistant tuberculosis

SYMBOLS AND UNIT

α	Alpha
β	Beta
γ	Gamma
δ	Delta
g	Gram
µg	Microgram
µL	Microlitre
mL	Millilitre
µM	Micromolar
mmol	Millimole
ppm	Parts per million
min	Minutes
sec	seconds
h	hours
%	Percent
°C	Degree Celsius
K	Kelvin
Hz	Hertz
<	Less than
≤	Less than or equal to
>	Greater than
≥	Greater than or equal to
±	Plus or minus
kcal/mol	kilocalorie per mole
Å	Angstrom
ev	electron volt
Da	Dalton

CHAPTER 1

INTRODUCTION, LITERATURE REVIEW AND OBJECTIVES OF THE WORK

Abstract:

This chapter provides a comprehensive introduction to medicinal and heterocyclic chemistry. It starts by introducing pyrazine and its derivatives, highlighting their pharmacological significance. Additionally, it provides a brief overview of tuberculosis. The chapter further explores a detailed literature review on pyrazine-based molecules, demonstrating their promising pharmaceutical properties. It also outlines the scope and objectives of the current work.

1.1 Medicinal Chemistry

Medicinal chemistry is a dynamic field at the interface of chemistry, biology, and pharmacology, focused on the design, synthesis, and optimization of chemical compounds for therapeutic purposes. It plays a crucial role in drug discovery and development by identifying molecules that can interact with biological targets to treat diseases effectively and safely. Medicinal chemists employ their knowledge of organic and synthetic chemistry to synthesize new compounds and analyze their structure-activity relationships. They also investigate how these compounds are absorbed, distributed, metabolized, and excreted in the body, ensuring their efficacy and safety.

In the realm of medicinal chemistry research, effective drug design is paramount. Key strategies in this endeavor include:

i) Computer-aided drug design, which relies on the analysis of receptor-lead interactions (Åqvist et al. 1994).

ii) Incorporating two active pharmacophoric units into a single molecular framework through hybridization (Lazar et al. 2004).

iii) Structural modification of the known drug molecule (Lima and Barreiro 2005).

iv) Random screening of different structural units within a defined activity window (Cappoen et al. 2014).

Developing a new drug is a highly intricate process that necessitates the expertise of various professionals from fields such as organic chemistry, analytical chemistry, biochemistry, molecular biology, and pharmacology. From the initial discovery to its public availability, the process typically spans 12 to 20 years and requires an investment ranging from $270 million to $2.8 billion (Rennane et al. 2021). This process typically involves five key steps (Deore et al. 2019).

i) **Discovery and Development Research**: This phase commences in the laboratory, where extensive research is conducted to identify potential drug candidates.

ii) **Preclinical Research**: Before testing a drug on humans, it undergoes rigorous laboratory and animal testing to assess its safety profile. This phase involves both *in vitro* (laboratory-based) and *in vivo* (animal-based) studies. These studies adhere to good laboratory practices (GLP) as per the Food and Drug Administration (FDA) regulations and provide essential data on dosing and toxicity levels.

iii) **Clinical Research**: This step involves conducting studies or trials on humans to evaluate the safety and effectiveness of the drug. Clinical trials are designed according to different phases, and before initiating them, developers must complete the Investigational New Drug (IND) process.

iv) **FDA Review and Approval**: If the evidence from preclinical and clinical research suggests that the drug is safe and effective for its intended use, the drug developer can apply for FDA approval to market the drug. The FDA thoroughly evaluates all submitted data before making a decision.

v) **FDA Post-Market Safety Monitoring**: Even after approval, the FDA continues to monitor the safety of drugs and devices once they are available to the public. This monitoring allows for identifying any previously unseen safety

issues, and the FDA can take appropriate actions, such as updating dosage or usage information or issuing warnings.

Despite the rigorous steps involved in drug development, limitations exist, and the complete safety profile of a drug may only become clear over time as the public uses it. The FDA remains vigilant in monitoring drug safety and takes necessary actions to ensure public health.

1.2 Heterocyclic Chemistry

Heterocyclic chemistry is a distinct branch of organic chemistry that has been studied for many years and holds significant promise for future research. Heterocyclic chemistry deals with the synthesis, characterization, and application of heterocycles. Heterocyclic compounds are cyclic organic compounds that contain at least one atom other than a carbon atom. Nitrogen, oxygen, and sulfur are the most common heteroatoms present in these systems. However, a heterocyclic ring containing other heteroatoms such as phosphorus and silicon is also widely known. Some of the commonly encountered heterocycles are given below (Figure 1.1).

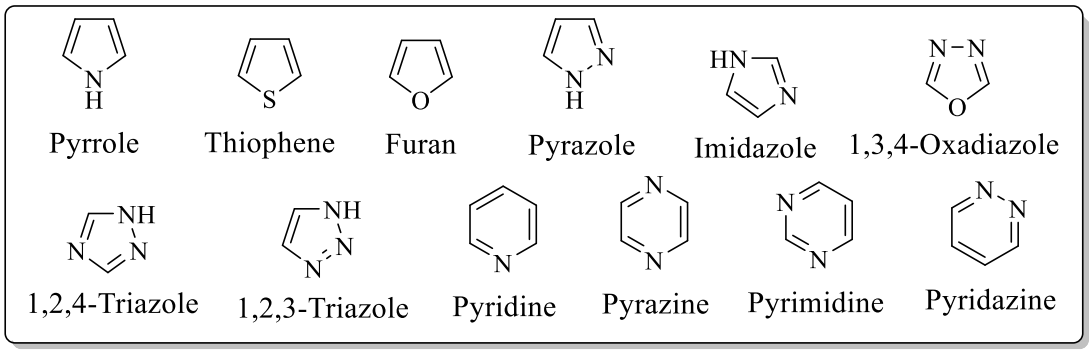

Figure 1.1 *Structures of a few important heterocycles*

Heterocyclic compounds play pivotal roles in biological molecules like DNA and RNA, essential for life. Nucleotides, the building blocks of these molecules, stem from pyrimidine and purine ring structures. Several crucial dietary components, including Thiamin (Vitamin B1), Riboflavin (Vitamin B2), Niacin (Vitamin B3), pyridoxal (Vitamin B6), Ascorbic acid (Vitamin C), as well as two essential amino acids,

tryptophan, and histidine, are classified as heterocyclic compounds. Moreover, vital biological entities such as hemoglobin (oxygen carriers in the blood), chlorophyll, and various enzymes are comprised of heterocyclic core structures, emphasizing their significance in biological systems.

Heterocycles play a crucial role in various fields including pharmaceuticals, natural products, biomolecules, and biologically active compounds. They are found in a wide range of drugs, vitamins, and other bioactive substances, serving as key components in treatments for conditions like tumors, infections, inflammation, depression, malaria, and HIV. Additionally, heterocycles are utilized in materials science for applications such as dyes, fluorescent sensors, corrosion inhibitors, and analytical reagents. They also hold significance in supramolecular and polymer chemistry, particularly in the development of conjugated molecules and polymers derived from aromatic heterocyclic systems. These materials exhibit promising properties for optoelectronic devices like organic photovoltaic cells, organic light-emitting diodes (OLEDs), and organic field-effect transistors, as well as electrochromic devices.

Heterocyclic compounds possess a fascinating feature wherein they can accommodate multiple functional groups, either as integral parts or within the ring system itself. Even slight alterations in their molecular structure can lead to significant changes in their physical, chemical, and biological properties. These modifications are influenced by both steric and electronic factors. Various factors such as solubility, partition coefficient, hydrogen bonding, bioisosterism, and the presence of hydrophilic and hydrophobic groups play pivotal roles in selecting lead molecules. Some of the interesting properties of heterocyclic compounds make it more passionate for the medicinal chemist to develop a variety of new molecules having pharmacological importance. These properties include:

i) Availability of low-cost raw materials
ii) Synthetic feasibility
iii) Chemical stability
iv) Ability to incorporate functional groups, either as constituents or as part of

the ring system.

The Pyrazine ring system possesses all the above-mentioned properties and hence it is considered as one of the key members in the field of medicinal chemistry, protein chemistry, natural product chemistry, and so on.

1.3 Chemistry of pyrazine and its derivatives

Diazine is described as a compound with a monocyclic aromatic ring that contains two nitrogen atoms with a molecular formula of $C_4H_4N_2$. The three isomers of diazine are pyridazine, pyrimidine, and pyrazine (Figure 1.2).

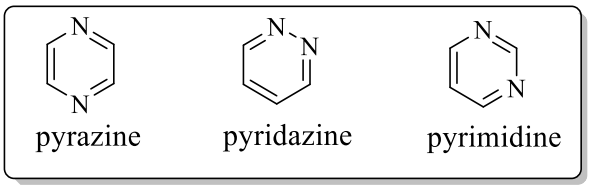

Figure 1.2 *Isomers of diazine*

Pyrazine, also known as 1,4- diazine, is a 6-membered heterocyclic compound with two nitrogen atoms in the *para* position. This heteroaromatic compound is 6π-electron-deficient and resembles a planar configuration. Pyrazine can be represented as a resonance hybrid of several canonical structures as shown in Figure 1.3 having a resonance energy of 24.3 kcal/mole and a dipole moment of zero because of the symmetric nature of the pyrazine molecule. Pyrazine demonstrates the weakest basicity (pKa = 0.65) among diazine compounds (Dolezal and Zitko 2015). This is due to the electron-withdrawing effect of nitrogen atoms positioned at the *para* position. It is a stable, colorless compound with a boiling point of 118 ℃ and a melting point of 54℃. It is soluble in water. Most of the lower homologs are liquid at room temperature. From an X-ray study, it was shown that the carbon-carbon bond distance is longer than benzene which is 1.40Å (Miniyar et al. 2015).

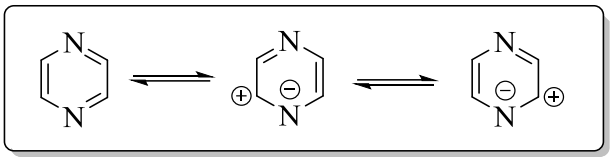

Figure 1.3 *Canonical structures of pyrazine*

Pyrazine is a naturally occurring compound, typically present in small amounts in various natural sources (Müller and Rappert 2010). It plays a significant role in enhancing the flavor of both raw and processed food (Maga 1992). Moreover, synthetic derivatives of pyrazine find extensive applications not only in the fragrance and flavor sectors but also in pharmaceuticals (Maga 1992). Living organisms such as plants, animals, insects, marine organisms, and microorganisms naturally produce pyrazine (Dolezal and Zitko 2015).

1.3.1 Synthesis of pyrazine

Several synthetic protocols have been reported in the literature to prepare pyrazine derivatives. Some of the important methods which give a variety of pyrazine derivatives are as follows.

Jones et al. reported a new method for the synthesis of pyrazine derivatives based on the condensation of α-amino acid amides and 1,2-dicarbonyl. The reaction was carried out in methanol in the presence of sodium hydroxide (NaOH). Typically, when unsymmetrical dicarbonyl compounds and α-amino acid amides undergo condensation, multiple isomers are anticipated. Surprisingly, Jones managed to isolate only one compound from the reaction of α-amino acid with either methylglyoxal or phenylglyoxal, resulting in the formation of pyrazine (Jones 1949).

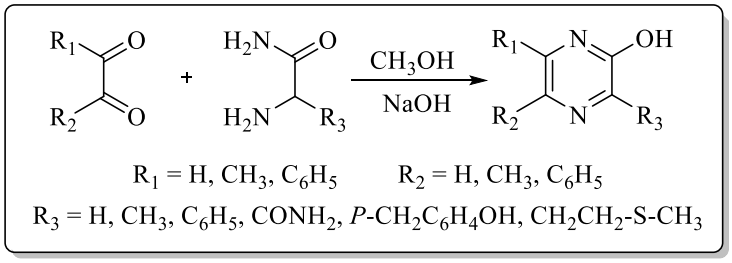

R_1 = H, CH_3, C_6H_5 R_2 = H, CH_3, C_6H_5

R_3 = H, CH_3, C_6H_5, $CONH_2$, *P*-$CH_2C_6H_4OH$, CH_2CH_2-S-CH_3

Scheme 1.1

Vogl et al. reported a condensation reaction involving aminomalonamidamidine dihydrochloride and dry glyoxal bisulfate in presence of dilute ammonium hydroxide at temperatures ranging from 0 to 20 °C. This reaction yielded 76% of 2-aminopyrazine-3-carboxamide (Vogl and Taylor 1959).

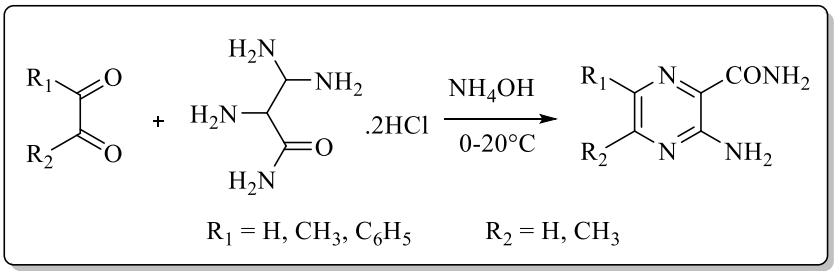

Scheme 1.2

Begland et al. documented a reaction involving diiminosuccinonitrile and diaminomaleonitrile under the influence of a strong acid catalyst. The strong acid was used to protonate the diiminosuccinonitrile and facilitate the elimination of ammonia. Depending on the amount of acid used, three distinct pyrazine products were obtained. Specifically, the addition of one equivalent of acid resulted in aminotricyanopyrazine, while an excess of acid led to the formation of tetracyanopyrazine. Interestingly, when a catalytic amount of acid was employed, 2,3-diamino-5,6-dicyanopyrazine was produced (Begland et al. 1974).

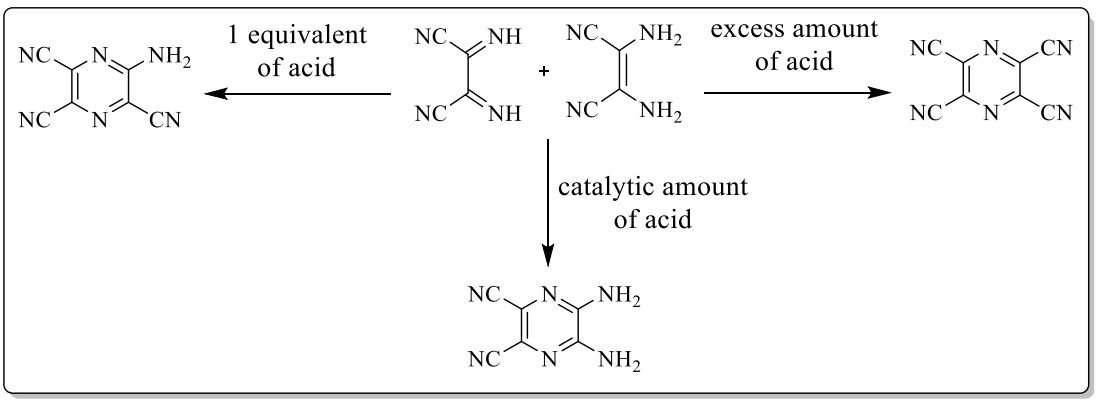

Scheme 1.3

Jing et al. reported a method for synthesizing pyrazine using a gas-phase reaction

at temperatures ranging from 300 to 600 °C, with zinc serving as the catalyst. The reaction involves the interaction of diamine and diol, facilitated by silica, alumina, or silica-alumina as the catalyst carrier. The catalyst for the reaction can either be zinc oxide (ZnO) alone or a blend comprising 10% zinc combined with metals like cobalt, nickel, iron, aluminum, and chromium (Jing et al. 2010).

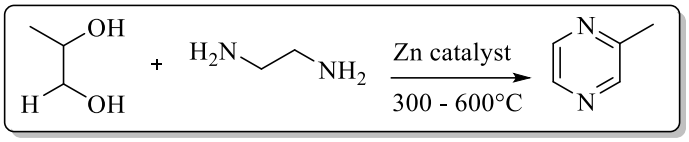

Scheme 1.4

Ohta et al. described a process involving the condensation of phenylglyoxal with 1,2-Diaminopropane, followed by dehydrogenation in the presence of a base NaOH. This resulted in the formation of a mixture containing both 2-methyl-1,5-phenylpyrazine and 2-methyl-6-phenylpyrazine. The mixture was subsequently separated using column chromatography (Ohta et al. 1979).

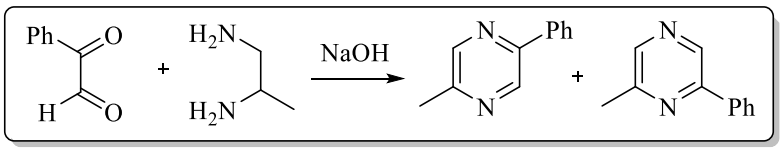

Scheme 1.5

Lee et al. patented a method for synthesizing pyrazine using a copper-chromite ($Cu_2Cr_2O_5$) catalyst (Patent No.: US4966970). They claimed that this process could yield over 90% of the desired product with up to 97% conversion. The catalytic reaction involved adding the $Cu_2Cr_2O_5$ catalyst to a diamine compound and heating it to temperatures between 300 °C and 450 °C for a duration of one to three hours. The researchers emphasized the importance of maintaining the reaction temperature within this range for optimal results. The reaction below 300 °C resulted in incomplete dehydrogenation, leading to the formation of piperazine instead of pyrazine. Conversely, temperatures exceeding 450 °C led to the production of several by-products due to the breakdown of pyrazine (Young K. Lee et al. 1990).

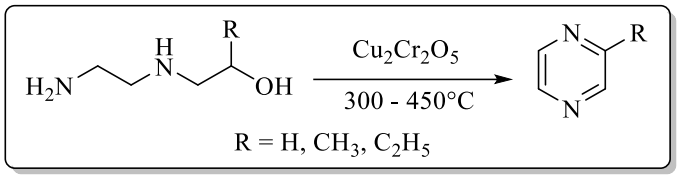

Scheme 1.6

Itoh et al. investigated the catalytic activity of Ferric chloride ($FeCl_3$) in the synthesis of pyrazine. They conducted a reaction between isonitroso-acetophenone and aminoacetonitrile in the presence of one equivalent of $FeCl_3$. This process resulted in the formation of N-oxide pyrazine, which was subsequently subjected to hydrogenation using a 10% Pd-C catalyst, yielding 55-80% pyrazine (Itoh et al. 2002).

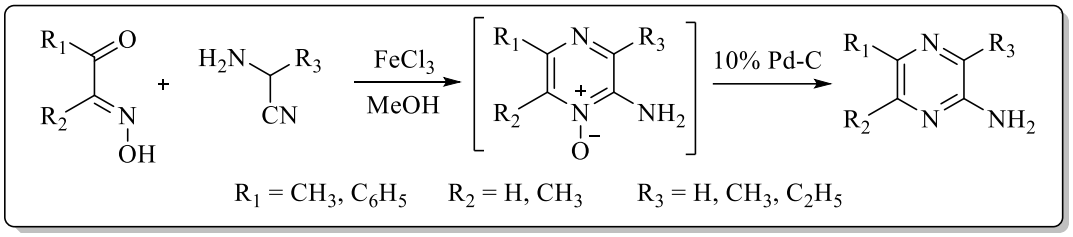

Scheme 1.7

Raw et al. documented a catalytic method for generating pyrazine by employing excess manganese dioxide (MnO_2). The process involved reacting α-hydroxyl ketones with 1,2-diamino in the presence of MnO_2. The addition of KOH in methanol proved crucial to the reaction, resulting in yields ranging from 10% to 66% of pyrazine (Raw et al. 2003).

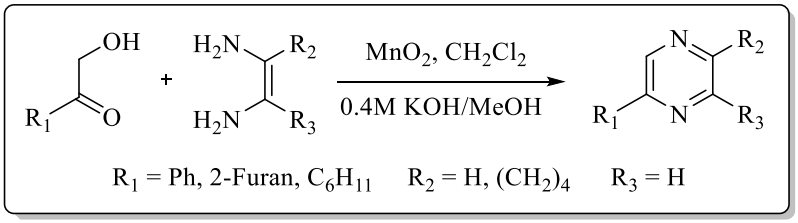

Scheme 1.8

Ghosh et al. reported an environmentally friendly method for synthesizing pyrazine. The process entailed a straightforward condensation reaction between 1,2-

diamine and 1,2-dicarbonyl in the presence of potassium tert-butoxide (t-BuOK) at room temperature. This approach yielded pyrazine in quantities ranging from 72% to 88%. They concluded that the reaction initially formed dihydropyrazine, which then underwent aromatization to produce pyrazine (Ghosh and Mandal 2012).

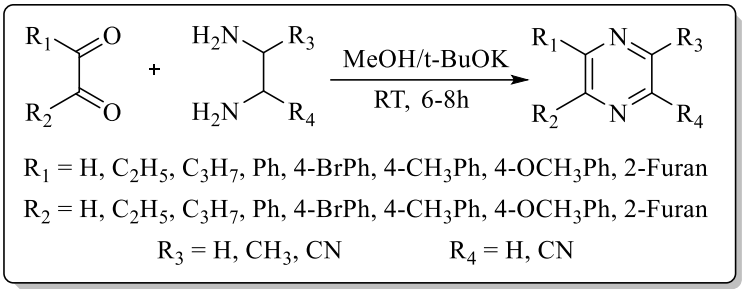

Scheme 1.9

1.4 Pharmacological significance of pyrazine and its derivatives

Pyrazine derivatives are highly valued in drug discovery due to their wide range of pharmaceutical and therapeutic applications. They are utilized in various treatments such as antibacterial, antitubercular, antifungal, anti-HIV, antiviral, anti-inflammatory, antidiabetic, and anticonvulsant therapies (Miniyar et al. 2015). The pyrazine core serves as a fundamental component in many biologically active compounds, including numerous approved drugs and compounds undergoing advanced clinical trials. Specifically, excluding certain condensed structures like quinoxalines, imidazopyrazines, pteridines, phenazines, and other bi- or polycycles, the non-condensed pyrazine ring is currently found in over 12 approved drugs. Additionally, 22 investigational drugs containing this core have been identified in the Drug Bank database. Below is a list detailing some of the pyrazine-containing drugs, along with their structures and biological applications (Table 1.1).

Table 1.1 *Pyrazine-containing drugs, their structure, and their biological application.*

S. No.	Name	Structure	Importance

1	Pyrazinamide	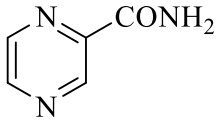	antitubercular
2	Amiloride	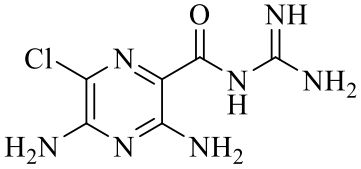	diuretic
3	Thionazine	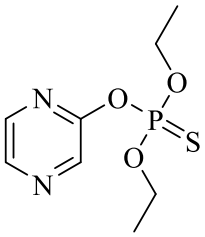	Insecticide and nematicide
4	Glipizide	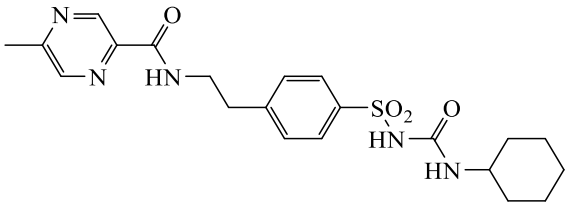	Anti-diabetic
5	Bortezomib	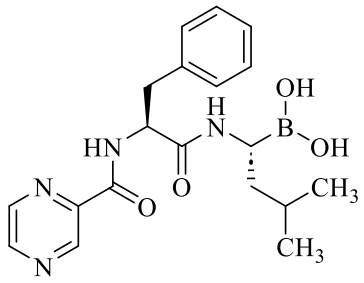	anticancer
6	Favipiravir	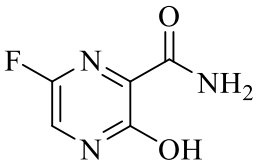	antiviral
7	Pyrazine diazohydroxide	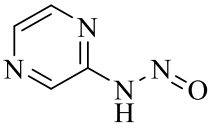	antineoplastic

8	Flutamide	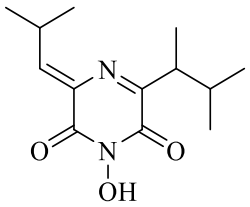	antiviral
9	Acipimox	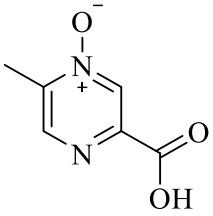	Used to treat high cholesterol
10	Oltipraz	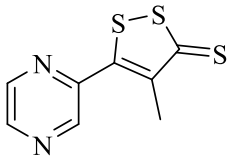	anticancer
11	Varenicline	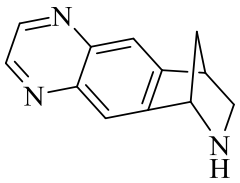	Used to quit smoking
12	Elpetrigine	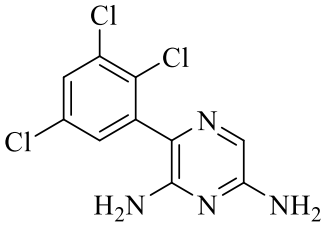	anticonvulsant
13	Brimonidine	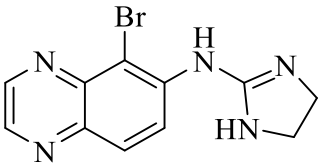	Used in the treatment of ocular hypertension and glaucoma

14	Mirfentanil	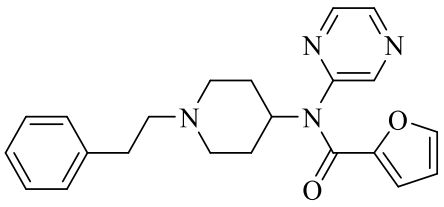	High selectivity for the mu-opioid receptor
15	Sulfalene	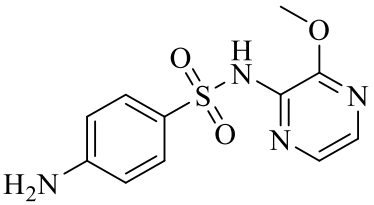	antibacterial
16	Eszopiclone	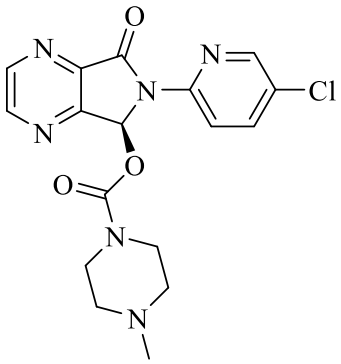	Used to treat insomnia
17	Telaprevir	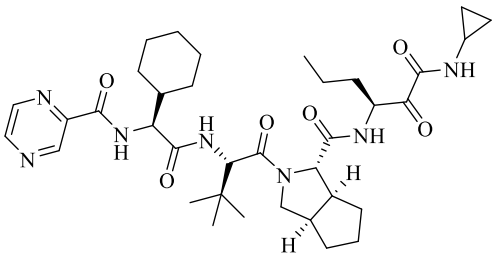	Protease inhibitor for the treatment of hepatitis C

1.5 Tuberculosis

Among all microbial diseases, Tuberculosis (TB) is one of the most dangerous and deadly diseases. TB is one of the most ancient diseases. It has been referred to in the Vedas and Ayurvedic Samhitas. It is the second greatest killer worldwide due to a single infectious agent after COVID-19. According to the Global Tuberculosis Report 2023 released by the World Health Organization (WHO), 10.6 million people fell ill with TB worldwide (Figure 1.4), and 1.3 million died in 2022 (Figure 1.5). Over 95% of TB cases and deaths occur in low and middle-income countries of Asia and Africa.

Out of 10.6 million cases of TB incidences, in India alone, 2.8 million cases were reported (Figure 1.6) which is a very large number compared to other global countries (*Global tuberculosis report 2023* 2023).

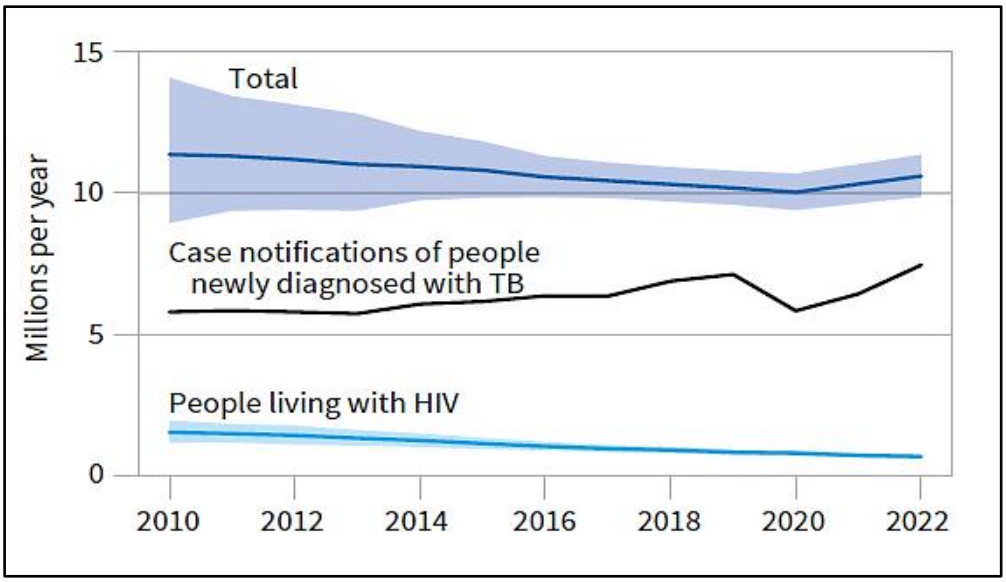

Figure 1.4 *Global trends in the estimated number of TB incidence*

(Source: WHO Global Tuberculosis Report 2023)

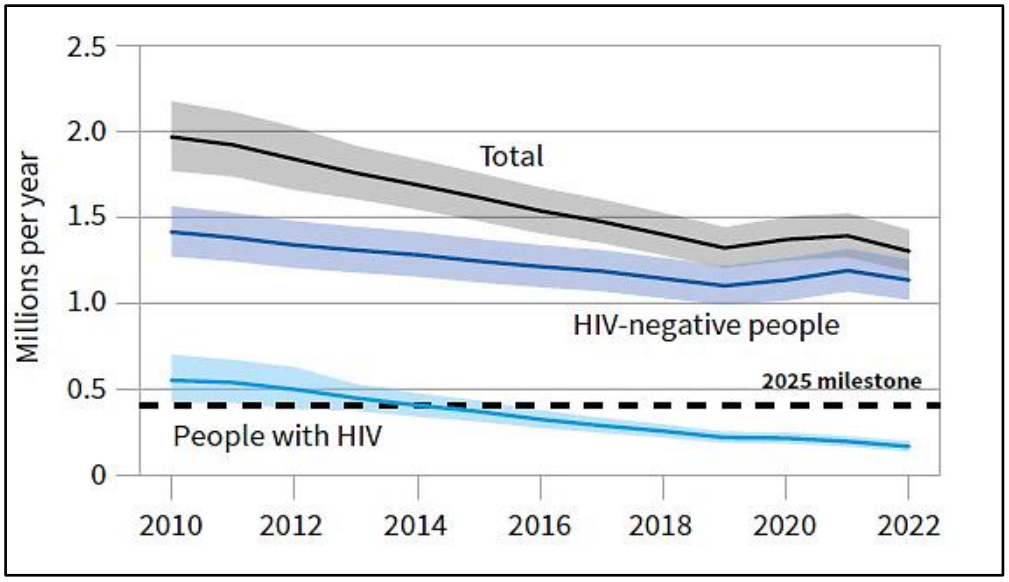

Figure 1.5 *Global trends in the estimated number of TB deaths*

(Source: WHO Global Tuberculosis Report 2023)

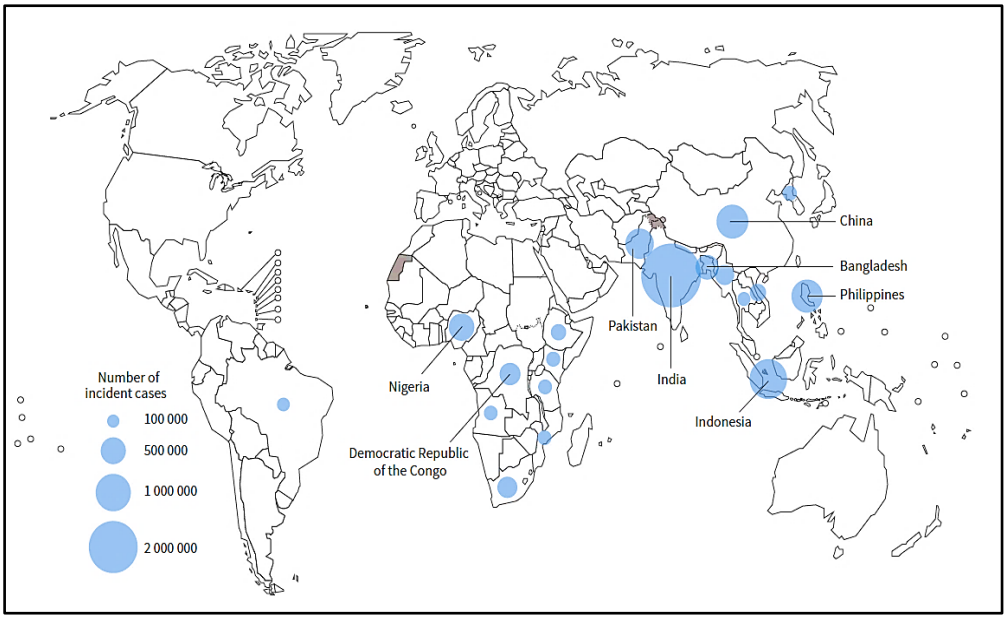

Figure 1.6 *Estimated TB incidences in top ten countries, 2022*

(Source: WHO Global Tuberculosis Report 2023)

Tuberculosis is an infectious disease caused by a bacterium known as *Mycobacterium tuberculosis (Mtb)*. While it primarily affects the lungs, it can also target other organs such as those in the central nervous, lymphatic, and circulatory systems. When TB infects someone, the bacteria multiply in the lungs, leading to symptoms like pneumonia, chest pain, coughing up blood, and persistent coughing. Additionally, it causes enlargement of the lungs and nearby lymph nodes. If TB spreads to other body parts, it can weaken the immune system, progressing to an active state that includes pneumonia and damage to bones, kidneys, and the protective layers surrounding the spinal cord and brain. The typical signs of TB include a persistent cough with blood-tinged mucus, fever, weight loss, and night sweats (*Global tuberculosis report 2023*).

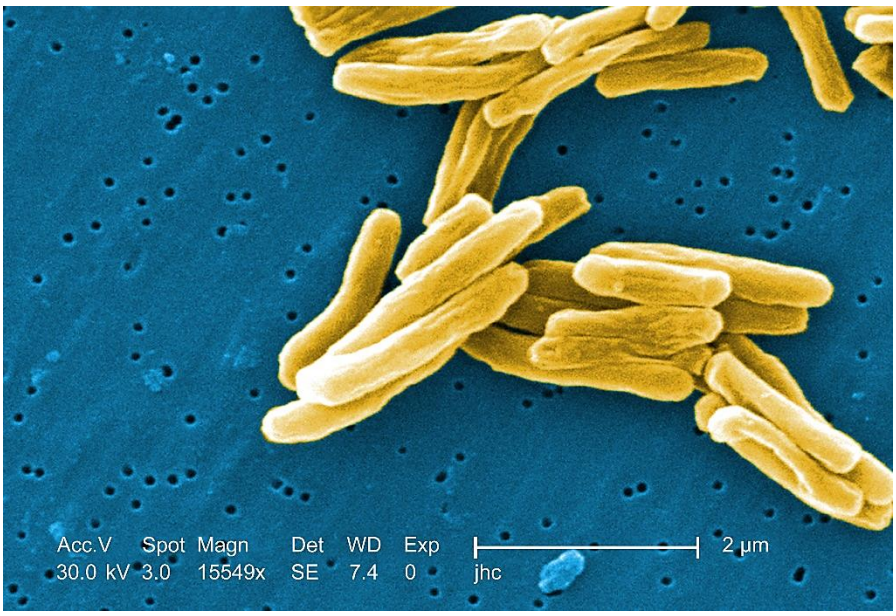

Figure 1.7 *Scanning electron microscopic image of Mycobacterium tuberculosis*

(Source: Public Health Image Library)

The standard treatment for tuberculosis involves a combination of four drugs: isoniazid (INH), rifampicin (RMP), pyrazinamide (PZA), and ethambutol (EMB) for the initial two months, followed by isoniazid and rifampicin alone for an additional four months (Zumla et al. 2013). These drugs are referred to as first-line TB medications. However, there are instances where TB shows resistance to these first-line drugs, leading to conditions like extensively drug-resistant tuberculosis (XDR-TB) or multidrug-resistant tuberculosis (MDR-TB). In such cases, second-line drugs are used for treatment (Zheng and Av-Gay 2016). Second-line drugs are generally less favored for several reasons: they may be less effective compared to first-line drugs (such as p-aminosalicylic acid), they might cause harmful side effects (like cycloserine), or they could be costly and not readily available in many developing nations (such as fluoroquinolones).

First-line drugs for tuberculosis treatment also come with potential side effects. Isoniazid may lead to adverse reactions such as rashes, abnormal liver function, and hepatitis. Pyrazinamide commonly causes joint pain (arthralgia). Long-term use of rifampicin can result in hepatotoxicity, a serious liver problem, prompting patients to

undergo regular liver function tests. Ethambutol may cause optic neuritis, red-green color blindness, joint pain, hyperuricemia, and skin reactions (Yee et al. 2003). Due to the serious nature of these adverse effects, many second and third-line TB drugs are not recommended by the WHO.

Despite the existence of many potent anti-tubercular drugs, tuberculosis remains a significant global threat. The emergence of drug-resistant forms like MDR-TB and XDR-TB poses a serious challenge to TB control efforts. Additionally, a more concerning and fatal form known as totally drug-resistant tuberculosis (TDR-TB) has been identified in countries like India, Iran, and Italy. The mortality rate and transmission of TB are notably higher in individuals infected with Human Immunodeficiency Virus (HIV) compared to those without HIV (*Global Tuberculosis Report 2023*). It's noteworthy that no new first-line TB drug has been discovered in the past fifty years following rifampicin. However, there are ongoing clinical trials for several new drugs, and recently, Bedaquiline (Worley and Estrada 2014), Delamanid (Xavier and Lakshmanan 2014), and Pretomanid (Occhineri et al. 2022) have been approved by the FDA for use in drug-resistant TB. Presently, there is a clear demand for tuberculosis medications that act quickly, have minimal side effects, and can eradicate the infection within a short timeframe.

1.6 Literature survey

From the literature reports it is evident that pyrazine derivatives possess promising antitubercular activity. Some of the important literatures are listed below.

Miniyar et al. synthesized a series of pyrazine-2-carbohydrazides (**P1**-**P14**) and evaluated all target compounds for their *in vitro* antimicrobial activity against Gram-positive (*S. aureus, B. subtilis*) and Gram-negative (*E. coli, S.* Typhi) strains of bacteria using Ofloxacin as a standard drug. Compound **P4** showed better antimicrobial activity against *S. aureus*, compound **P8** showed better antimicrobial activity against *B. subtilis*, compound **P7** showed better antimicrobial activity against *E. coli* and compound **P14** showed better antimicrobial activity against *S.* Typhi compared to other derivatives (Miniyar and Makhija 2009).

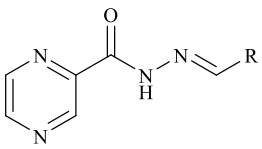

P1-P14

P1, R = C_6H_5
P2, R = CH=CH-C_6H_5
P3, R = 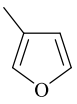
P4, R = C_6H_4-p-OCH_3
P5, R = C_6H_4-o-Cl
P6, R = C_6H_4-m-Cl
P7, R = C_6H_4-p-Cl
P8, R = C_6H_4-o-NO_2
P9, R = C_6H_4-m-NO_2
P10, R = C_6H_4-p-NO_2
P11, R = C_6H_4-o-OH
P12, R = C_6H_4-m-OH
P13, R = C_6H_4-p-OH
P14, R = C_6H_4-N$(CH_3)_2$

Abdel-Aziz et al. synthesized a series of pyrazine-2-carboxylic acid hydrazide derivatives (**P15-P23**) and scanned for their activity against *Mycobacterium tuberculosis* H37Rv strain by Microplate Alamar Blue Assay (MABA) method using pyrazinamide as standard drug. The result shows that pyrazine-2-carboxylic acid hydrazide-hydrazone derivatives were less active than pyrazinamide. In contrast, the N_4-ethyl-N_1-pyrazinoyl-thiosemicarbazide (**P24**) showed the highest activity against *M. tuberculosis* H37Rv (MIC_{90} = 16.87 µg/mL) (Abdel-Aziz and Abdel-Rahman 2010).

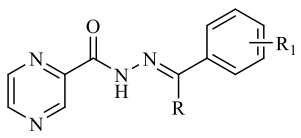

P15-P23

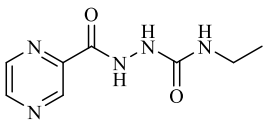

P24

P15, R = H, R_1 = 4-Cl
P16, R = H, R_1 = 2-OH
P17, R = H, R_1 = 3-OH
P18, R = H, R_1 = 4-OH
P19, R = H, R_1 = 3-NH_2
P20, R = H, R_1 = 4-OCH_3
P21, R = CH_3, R_1 = H
P22, R = CH_3, R_1 = 4-OCH_3
P23, R = CH_3, R_1 = 4-Br

Lima et al. synthesized a series of nine N-(E)-heteroatomic-pyrazine-2-carbohydrazide derivatives (**P25-P33**) and screened for their antitubercular activity against *M. tuberculosis* ATCC 27294 by the MABA method using pyrazinamide as a standard drug. Compounds **P25** and **P30** exhibited potent activities (MIC = 3.12 and 50 µg/mL, respectively) compared to first-line drug pyrazinamide (MIC > 100 µg/mL). Afterward, these compounds were evaluated for their cell viabilities in non-infected and infected macrophages with *Mycobacterium Bovis Bacillus Calmette-Guerin* (BCG) and

compound **P30** was not toxic to host cells in the effective concentration to inhibit the growth of *M. tuberculosis* (H. S. Lima et al. 2011).

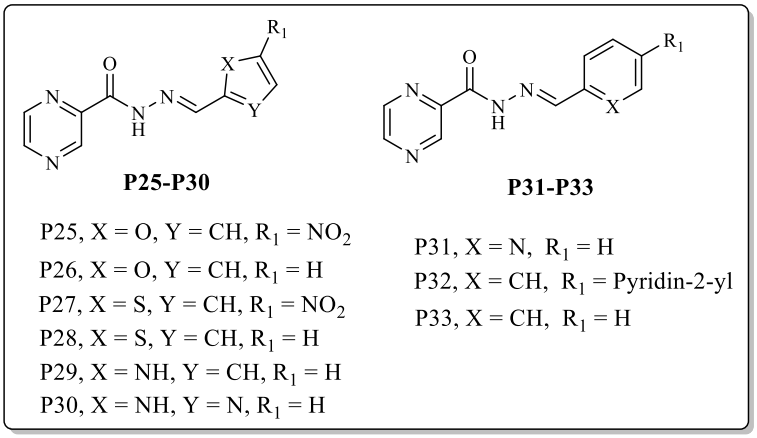

Miniyar et al. synthesized a series of 5-methylpyrazine-2-carbohydrazide derivatives (**P34-P47**) and evaluated their *in vitro* antitubercular activity against *Mycobacterium tuberculosis* strain H37Rv using the Middle brook 7H-9 broth dilution method using pyrazinamide as a standard drug. Among the tested compounds, seven compounds (**P38**, **P39**, **P40**, **P44**, **P45**, **P46** & **P47**) showed remarkable antitubercular activity (Miniyar et al. 2017).

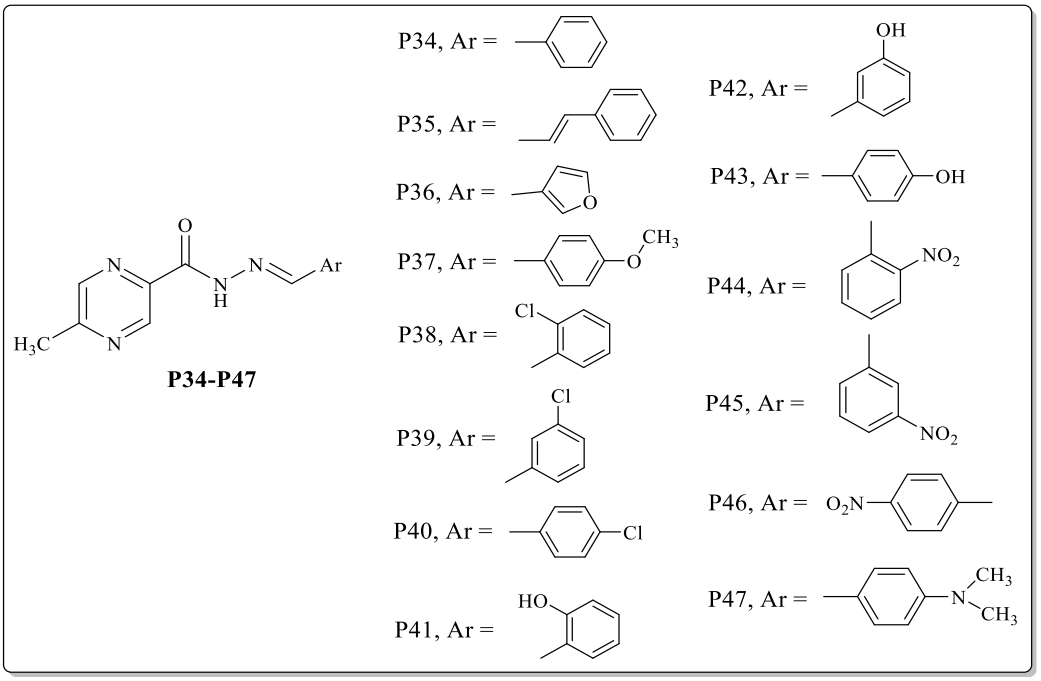

R. Das et al. synthesized 1,3,4-Oxadiazole molecules bearing pyrazine moiety (**P48-P51**) and screened for their *in vitro* antimycobacterial activity against *Mycobacterium tuberculosis* H37Rv strain by Lowenstein-Jensen Agar method using isoniazid and rifampicin as standard drugs. Compound **P49** with a MIC value of 6.25 µg/mL displayed significant antitubercular activity (still less active compared to standard drugs). Also, the synthesized compounds were screened for their *in vitro* antibacterial activity against gram-positive (*S. aureus, B. subtilis*) and gram-negative (*P. aeruginosa, E. coli*) bacteria taking Amoxicillin as a standard drug and *in vitro* antifungal activity against two fungal strains *C. Albicans* and *A. niger* taking Miconazole as a standard drug. Compounds **P48** and **P49** show remarkable antibacterial and antifungal activity (Das et al. 2015).

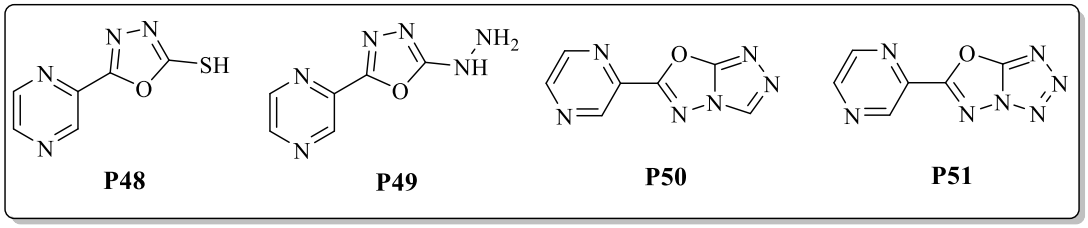

Zitko et al. synthesized a series of N-phenylpyrazine-2-carboxamides (**P52-P76**) and scanned for their *in vitro* antimycobacterial activity against *M. tuberculosis* H37Rv strain and nontuberculous mycobacterial strains of M. kansasii and *M. avium* by microdilution method using isoniazid and pyrazinamide as a standard drug. Compounds **P64**, **P65** & **P70** displayed significant antimycobacterial activity against H37Rv with MIC around 10 µM. Compound **P63** and **P73** exhibited significant activity against M. kansasii with MIC = 3.13 (12.6 µM and 8.7 µM, respectively). No activity was detected against *M. avium* (Zitko et al. 2015).

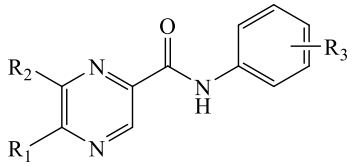

P52-P76

P52, R_1 = H, R_2 = H, R_3 = 2-Cl
P53, R_1 = CH_3, R_2 = H, R_3 = 2-Cl
P54, R_1 = H, R_2 = Cl, R_3 = 2-Cl
P55, R_1 = $C(CH_3)_3$, R_2 = H, R_3 = 2-Cl
P56, R_1 = $C(CH_3)_3$, R_2 = Cl, R_3 = 2-Cl
P57, R_1 = H, R_2 = H, R_3 = 2-CH_3-5-F
P58, R_1 = CH_3, R_2 = H, R_3 = 2-CH_3-5-F
P59, R_1 = H, R_2 = Cl, R_3 = 2-CH_3-5-F
P60, R_1 = $C(CH_3)_3$, R_2 = H, R_3 = 2-CH_3-5-F
P61, R_1 = $C(CH_3)_3$, R_2 = Cl, R_3 = 2-CH_3-5-F
P62, R_1 = H, R_2 = H, R_3 = 3-Cl-4-CH_3
P63, R_1 = CH_3, R_2 = H, R_3 = 3-Cl-4-CH_3
P64, R_1 = H, R_2 = Cl, R_3 = 3-Cl-4-CH_3
P65, R_1 = $C(CH_3)_3$, R_2 = H, R_3 = 3-Cl-4-CH_3
P66, R_1 = $C(CH_3)_3$, R_2 = Cl, R_3 = 3-Cl-4-CH_3
P67, R_1 = H, R_2 = H, R_3 = 2-CH_3-5-I
P68, R_1 = CH_3, R_2 = H, R_3 = 2-CH_3-5-I
P69, R_1 = H, R_2 = Cl, R_3 = 2-CH_3-5-I
P70, R_1 = $C(CH_3)_3$, R_2 = H, R_3 = 2-CH_3-5-I
P71, R_1 = $C(CH_3)_3$, R_2 = Cl, R_3 = 2-CH_3-5-I
P72, R_1 = H, R_2 = H, R_3 = 2-CH_3-5-I
P73, R_1 = CH_3, R_2 = H, R_3 = 2-CH_3-5-I
P74, R_1 = H, R_2 = Cl, R_3 = 2-CH_3-5-I
P75, R_1 = $C(CH_3)_3$, R_2 = H, R_3 = 2-CH_3-5-I
P76, R_1 = $C(CH_3)_3$, R_2 = Cl, R_3 = 2-CH_3-5-I

Ahmad et al. synthesized a series of pyrazine carbohydrazide-based hydrazones (**P77-P84**) and evaluated their Urease inhibition, antioxidant, and antimicrobial activities by agar well diffusion method using Thiourea, Gallic acid, and Tazocin as a standard drug respectively. All the compounds showed non-significant activities (Ahmad et al. 2016).

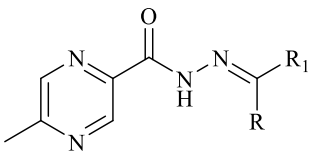

P77-P84

P77, R = CH_3, R_1 = Phenyl
P78, R = H, R_1 = Hydroxyphenyl
P79, R = CH_3, R_1 = 2-Hydroxyphenyl
P80, R = H, R_1 = 4-Chlorophenyl
P81, R = H, R_1 = 3-Bromophenyl
P82, R = H, R_1 = 4-Bromophenyl
P83, R = H, R_1 = 2,6-Dichloroyphenyl
P84, R = H, R_1 = 2-Hydroxy-1-naphthyl

El-Azab et al. synthesized a series of 1,3,4-Oxadiazole molecules containing pyrazine moiety (**P85-P87**) and all the compounds were tested for *in vitro* antitubercular activity against *M. tuberculosis* strain H37Rv by MABA method using

pyrazinamide and streptomycin as a standard drug. Compounds **P85**, **P86** & **P87** displayed significant antimycobacterial activity against H37Rv with MIC values 1.6, 3.1, and 1.6 µg/mL respectively (El-Azab et al. 2018).

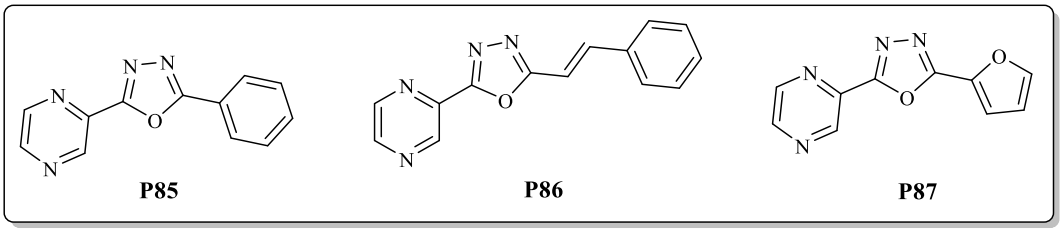

Al-Tamimi et al. synthesized a series of 2-substituted-1,3,4-oxadiazole-5-pyrazine derivatives (**P88-P90**) and scanned for their *in vitro* antimycobacterial activity against *M. tuberculosis* H37Rv strain using pyrazinamide and streptomycin as a standard drug. Compound **P88** (MIC = 0.8 µg/mL), **P89** (MIC=0.8 µg/mL), and **P90** (MIC=1.6 µg/mL) were more active than pyrazinamide (MIC = 3.125 µg/mL) and streptomycin (MIC=6.25 µg/mL). The synthesized compounds were also tested for their *in vitro* antibacterial activity against gram-positive (*S. aureus, B. subtilis*) and gram-negative (*E. coli, S.* Typhi) bacteria. However, all the tested compounds show no activity against *B. subtilis* and *E. coli*. All compounds were found to be active against *S. aureus* and compound **P88** was found to be active against *S.* Typhi (Al-Tamimi et al. 2018).

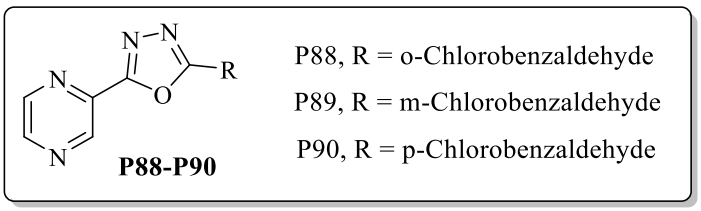

Bouz et al. synthesized a series of N-substituted-3-aminopyrazine-2-carboxamides with free amino groups in position-3 on the pyrazine ring (**P91-P110**). Based on various substituents on the carboxamide moiety, the series is subdivided into benzyl, alkyl, and phenyl derivatives. The compounds were evaluated for their *in vitro* antimycobacterial, antibacterial, and antifungal activities. Compound **P107** was most active against *M. tuberculosis* H37Rv with a MIC value of 12.5 µg/mL. Antimycobacterial activity

against *Mtb* and *M. kansasii* along with antibacterial activity increased among the alkyl derivatives with increasing the length of the carbon side chain. Antibacterial activity was observed for phenyl and alkyl derivatives but not for benzyl derivatives. Antifungal activity was observed in all structural subtypes mainly against *Trichophyton interdigitale* and *Candida albicans*. The four most active compounds (**P100**, **P106**, **P107**, and **P110**) were evaluated for their *in vitro* cytotoxicity in the HepG2 cancer cell line, only compound **P110** was found to exert some level of cytotoxicity (Bouz et al. 2019).

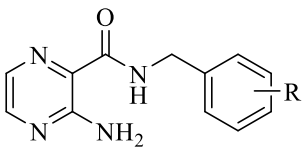

P91-P98

P91, R = H
P92, R = 2-CH_3
P93, R = 4-CH_3
P94, R = 4-OCH_3
P95, R = 2,4-diOCH_3
P96, R = 3,4-diCl
P97, R = 3-CF_3
P98, R = 4-CF_3

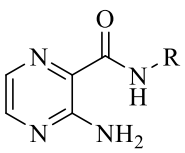

P99-P102

P99, R = C_5H_{11}
P100, R = C_6H_{13}
P101, R = C_7H_{15}
P102, R = C_8H_{17}

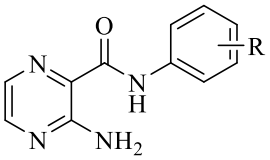

P103-P110

P103, R = H
P104, R = 2-OH
P105, R = 2,5-diCH_3
P106, R = C_2H_5
P107, R = 2,4-diOCH_3
P108, R = 2,4-diF
P109, R = 3,4-diCl
P110, R = 4-CF_3

Bouz et al. synthesized a series of *N*-(pyrazin-2-yl) benzenesulfonamides (**P111-P135**). All compounds were evaluated for their *in vitro* antimycobacterial activity against *M. tuberculosis* H37Rv, M. kansasii, and *M. avium* by the MABA method using isoniazid as a standard drug. Compounds **P117** (MIC = 6.25 µg/mL, 25 µM) and **P118** (MIC = 6.25 µg/mL, 22 µM) showed good antimycobacterial activity against *Mtb* (Bouz et al. 2019).

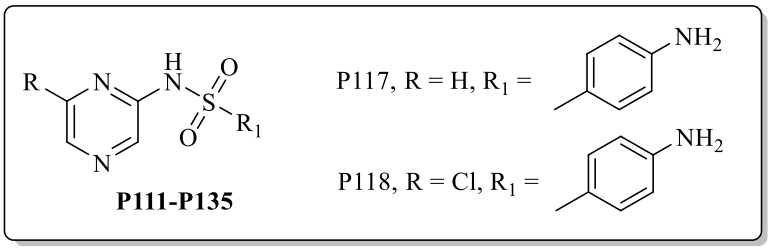

Hassan et al. synthesized some pyrazine-2-carbohydrazides (**P136-P139**) and all compounds were screened for their *in vitro* antimycobacterial activity against *M. tuberculosis* H37Rv strain by MABA method using Pyrazinamide, isoniazid, and ethambutol as a standard drug. All compounds exhibited promising inhibition with MIC values ≤ 6.25 μg/mL, a value postulated by the global program for the discovery of new antitubercular drugs as an upper threshold for the evolution of new *Mtb* therapies (Hassan et al. 2020).

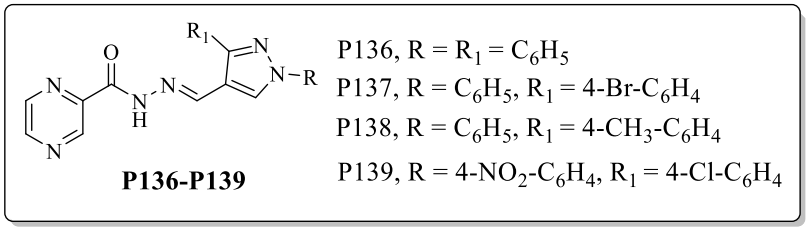

Juhas et al. synthesized a series of *N*-pyrazinoyl substituted amino acids (**P140**) and evaluated for their *in vitro* antimycobacterial activity against *M. tuberculosis* H37Rv and H37Ra strains by MABA method using pyrazinamide, isoniazid, rifampicin, and ciprofloxacin as a standard drug. The notable activity was detected only against *Mtb* H37Ra at pH=6 (Juhás et al. 2020).

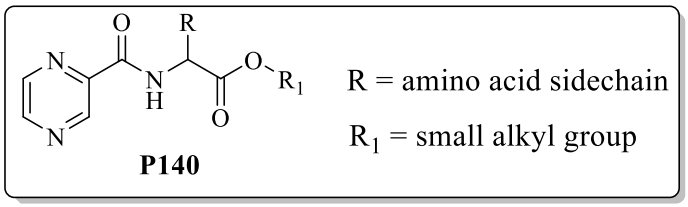

Srinivasarao et al. synthesized a series of novel substituted-N-(6-(4-(pyrazine-2-carbonyl)piperazine/homopiperazine-1-yl)pyridine-3-yl)benzamide derivatives (**P141-P167**) and evaluated for their *in vitro* antitubercular activity against *M.*

tuberculosis H37Ra using isoniazid as a standard drug. Among the tested compounds, six compounds (**P141**, **P145**, **P148**, **P151**, and **P159**) exhibited significant activity with 50% inhibitory concentrations (IC_{50}) ranging from 1.35 to 2.18 µM. All active compounds were evaluated for their cytotoxicity on HEK-293 (human embryonic kidney) cells. The result indicates that all compounds are non-toxic to human cells (Srinivasarao et al. 2020).

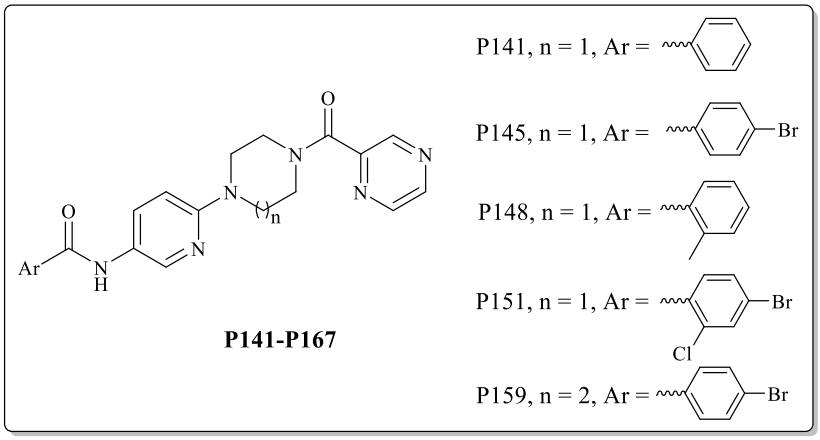

Reddyrajula et al. synthesized a series of pyrazine-1,2,3-triazoles (**P168-P209**) and screened for their *in vitro* antitubercular activity against *M. tuberculosis* H37Rv strain by MABA method using pyrazinamide as a standard drug. Among the tested compounds, seven compounds (**P183**, **P184**, **P185**, **P186**, **P188**, **P189**, and **P191**) demonstrated significant antitubercular activity with the MIC value 1.56 µg/mL, which is two-fold more potent than the parent compound pyrazinamide. Further, the synthesized pyrazinamide analogs demonstrated moderate inhibition activity against several bacterial strains and possessed an acceptable *in vitro* cytotoxicity profile as well (Reddyrajula and Dalimba 2020).

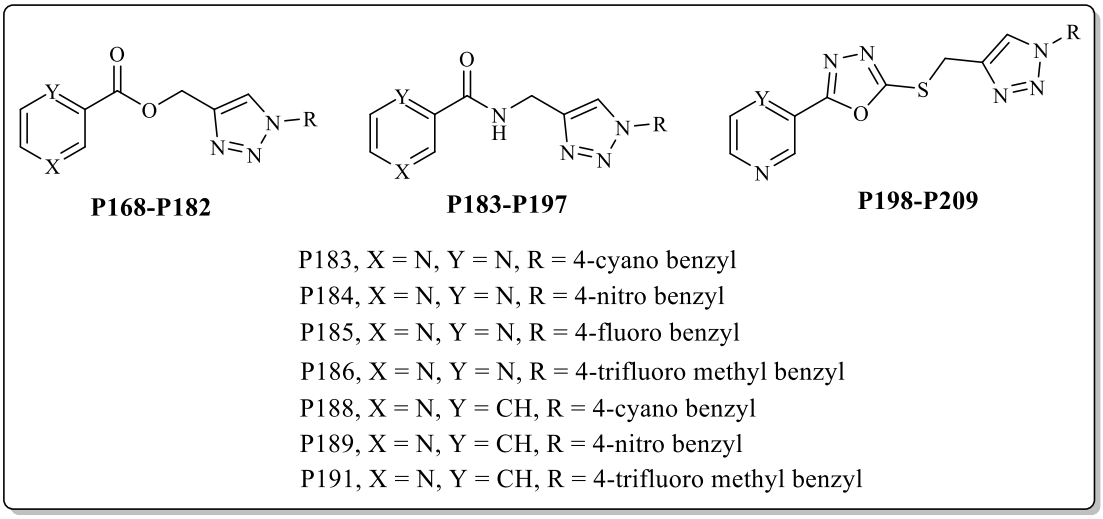

P183, X = N, Y = N, R = 4-cyano benzyl
P184, X = N, Y = N, R = 4-nitro benzyl
P185, X = N, Y = N, R = 4-fluoro benzyl
P186, X = N, Y = N, R = 4-trifluoro methyl benzyl
P188, X = N, Y = CH, R = 4-cyano benzyl
P189, X = N, Y = CH, R = 4-nitro benzyl
P191, X = N, Y = CH, R = 4-trifluoro methyl benzyl

Shamsel-Din et al. synthesized ethyl 2- (2-(5-((pyrazin-2-ylamino) methyl)-1,3,4-oxadiazol-2-ylthio)acetamido)acetamido)-3-(4-hydroxyphenyl) propanoate (EPOGTP) (**P210**) and iodinated EPOGTP (**P211**) and screened for their *in vitro* antitubercular activity against *M. tuberculosis* H37Ra 7131 strain by MIC method using pyrazinamide as a standard drug. Both compounds indicated a good IC_{50} value of 210 µg/mL for EPOGTP and 86 µg/mL for iodinated EPOGTP (Shamsel-Din and Gizawy 2021).

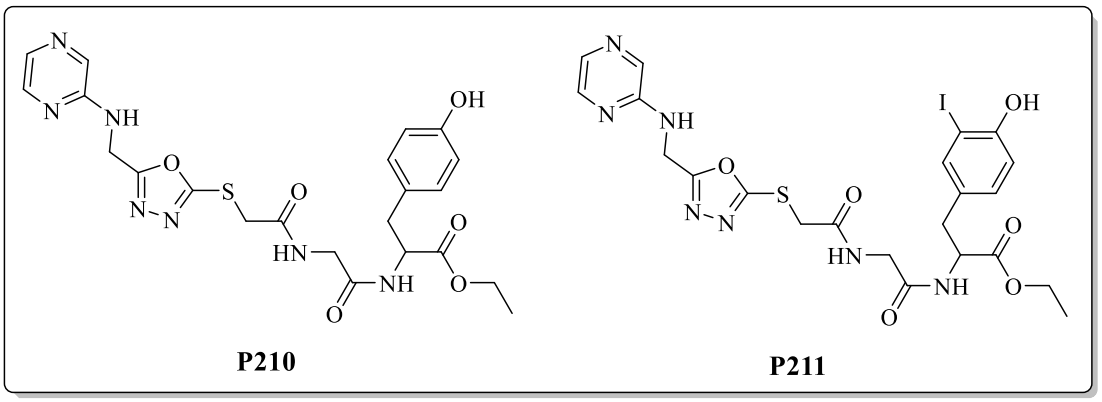

Bouz et al. synthesized a series of hybrid compounds containing pyrazinamide and 4-aminosalicylic acid moiety (**P212-P219**). All compounds were evaluated for their *in vitro* antimycobacterial activity against *M. tuberculosis* H37Rv strain by the MABA method using pyrazinamide, isoniazid, and rifampicin as standard drugs. Compound **P219** was most active against *M. tuberculosis* H37Rv with a MIC value of 10.7 µM.

The findings suggest that the active compound exhibits non-toxic properties, as its IC_{50} greater than 1000 µM (Bouz et al. 2023).

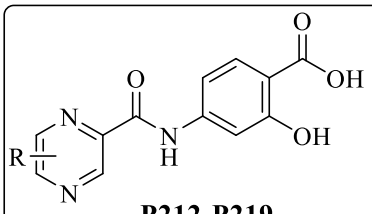

P212-P219

P212, R = H	P216, R = 3-CH_3
P213, R = 3-$CONH_2$	P217, R = 5-CH_3
P214, R = 3,5-diCl	P218, R = 6-CH_3
P215, R = 3-OH	P219, R = 6-Cl

Zulqurnain et al. synthesized a series of pyrazinamide analogs (**P220-P227**) and screened for their *in vitro* antitubercular activity against *M. tuberculosis* H37Rv strain by resazurin microtiter method using pyrazinamide and rifampicin as a standard drug. Among the tested compounds, **P223** and **P226** demonstrated the highest activity with MIC values ≤ 6.25 µg/mL (Zulqurnain et al. 2023).

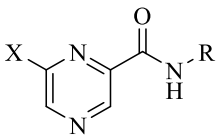

P220-P227

P220, X = H, R = 4-ethylphenyl	P224, X = H, R = adamantan-1-yl
P221, X = H, R = cycloheptyl	P225, X = Cl, R = 4-ethylphenyl
P222, X = H, R = n-octyl	P226, X = Cl, R = cycloheptyl
P223, X = H, R = 4-chlorobenzyl	P227, X = Cl, R = n-octyl

1.7 Scope and objectives of the present work

Tuberculosis is one of the most fatal infectious diseases caused by the bacillus *Mycobacterium tuberculosis (Mtb)*. It causes a huge number of human deaths despite the availability of more than 20 antitubercular drugs and the Bacillus Calmette-Guerin (BCG) antitubercular vaccine. According to the WHO Global Tuberculosis Report 2023, every day more than 3600 people die from tuberculosis and nearly 30000 people fall ill with TB disease, despite it being preventable and curable. The emergence of extensively drug-resistant tuberculosis and multidrug-resistant tuberculosis, against which the traditional antitubercular drugs showed limited efficacy, further caused a serious problem in controlling TB. According to the WHO Global Tuberculosis Report 2023, globally 3.5% of new and 20.5% of previously treated TB cases were estimated to be multidrug-resistant. In view of this, a great deal of research work is being devoted

to identifying newer molecular entities that are active against the bacterial strains. Moreover, some of the currently available drugs have been shown to exhibit some side effects and toxicity. The cost of the drug happens to be another factor that makes it difficult for the public to afford the present drugs available on the market.

Hence, there is a continuous requirement for better drugs synthesized by facile routes and with higher efficacy. The synthesis of new drugs and investigation of their pharmacological importance is a continuous process. However, it is not a simple process, and it involves plenty of effort from scientists working in different fields of research. It is a well-known fact that around 2-3 lakhs of organic compounds have to be synthesized and analyzed to obtain one potential drug. Besides, it is a challenging task to prepare new molecules that combine high activity and selectivity, drug-likeness, and good pharmacokinetic properties. Currently, extensive research is in progress all over the world to synthesize and develop effective drugs that can selectively control the infection/disease without side effects.

Against this background, the present research study has been planned to design new pyrazine-based compounds carrying biologically important pharmacophores in their active positions and synthesize them using standard procedures. Also, it has been thought to investigate their preliminary antitubercular properties to understand the structure-activity relationship. It has been hoped that the study would lead to the development of new active antitubercular agents, which may enter as potential candidates for the next phase of clinical studies.

In this perception and based on the literature studies, the following objectives have been proposed for the present research work.

1. To design a new series of molecules based on Pyrazine and assess their drug-likeness through *in silico* studies.
2. To synthesize the designed molecules and characterize the intermediate and final products using analytical techniques such as ^{1}H-NMR, ^{13}C-NMR, and HR-MS/ESI-MS.

3. To investigate the *in vitro* antitubercular activity of the synthesized molecules against the *Mycobacterium tuberculosis* H37Rv strain.
4. To examine the *in vitro* antibacterial and antifungal activity of the synthesized molecules against a range of bacterial and fungal strains.
5. To carry out *in vitro* cytotoxic studies of the active molecules among all synthesized molecules on a mammalian Vero cell line.

1.8 Organization of the Thesis

The thesis consists of five chapters, each chapter addressing specific aspects of the present research work. **Chapter 1** provides an introduction to medicinal chemistry, and heterocyclic chemistry, specifically focusing on pyrazine and its derivatives. It discusses the pharmacological importance of pyrazine derivatives, especially concerning antimicrobial properties. Additionally, it conducts a comprehensive literature review on pyrazine-based molecules with antitubercular properties and outlines the scope and objectives of the present research work. **Chapter 2** covers the design and synthesis of five new series of pyrazine-based molecules. It includes the characterization of these compounds using various spectral techniques such as ^{1}H-NMR, ^{13}C-NMR, and HRMS/ESI-MS. Detailed experimental procedures, mechanisms, and analytical characterization data for intermediates and final compounds are presented. **Chapter 3** focuses on the biological studies of the synthesized compounds. It provides a thorough investigation of *in vitro* antitubercular, antibacterial, and antifungal activities, along with *in vitro* cytotoxicity studies of the compounds. **Chapter 4** delves into the computational studies of the synthesized compounds. It includes *in silico* ADMET studies, *in silico* molecular docking, and DFT calculations. In **Chapter 5**, the research work is summarized, and the outcomes of the present investigation are highlighted, providing a cohesive conclusion to the thesis.

****

CHAPTER 2

SYNTHESIS AND CHARACTERIZATION OF PYRAZINE-BASED COMPOUNDS

Abstract:

This chapter outlines the design and synthesis of five new series of pyrazine-based compounds. It explains the experimental procedures followed for the synthesis of target compounds and their characterization using various spectral techniques.

2.1 Introduction:

Pyrazine is a six-membered heterocyclic ring containing nitrogen at the para position. It is found in numerous bioactive molecules and essential components of various clinically utilized drugs. Its presence in these compounds is crucial for their biological activity, often in combination with other structural moieties like oxadiazole, triazole, quinazoline, thiadiazole, benzothiazoles, imidazole, benzamides, oxazole, and piperazine (Ong et al. 2017). One such drug containing a pyrazine ring is pyrazinamide, which plays a vital role in tuberculosis treatment when used alongside other antitubercular medications. It acts as a prodrug, converting to pyrazinoic acid through enzymatic processes facilitated by pyrazinamides enzyme under acidic conditions (pH: 5-6) (**Figure 2.1**). This conversion process is crucial for its antitubercular efficacy, contributing significantly to the shortened duration of TB therapy (Zhang et al. 2003). Despite its recognition as an essential drug by the WHO, pyrazinamide is associated with notable side effects such as joint pain, gout, and hepatotoxicity.

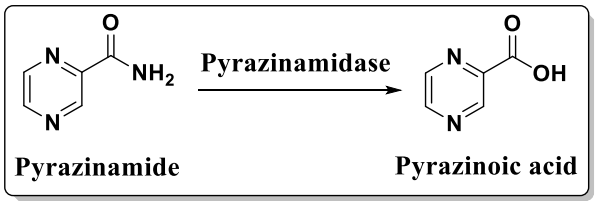

Figure 2.1 *Mechanism of action of pyrazinamide*

Recent studies have highlighted the potential of various modified pyrazinamide derivatives in combating tuberculosis. For example, Reddyrajula explored bioisosteric modifications to pyrazinamide derivatives, resulting in the development of potent antitubercular compounds (Reddyrajula and Dalimba 2020). Srinivasarao and team focused on N-(6-(4-(pyrazine-2-carbonyl)piperazine/homopiperazine-1-yl)pyridin-3-yl)benzamide derivatives as effective agents against tuberculosis. Panda reported pyrazolopyridones as a new class of noncovalent DprE1 inhibitors with strong anti-mycobacterial activity (Srinivasarao et al. 2020). Zhou's team reported pyrazine-2-carboxamide derivatives with notable antitubercular properties (Zhou et al. 2017). Vanaskova reported N-benzylpyrazine-2-carboxamide alkylamino derivatives, which showed superior inhibition against *M. tuberculosis* compared to pyrazinamide. Stringer reported a series of pyrazinyl ferrocenyl-derived complexes as moderate antitubercular agents (Servusova-Vanaskova et al. 2015). Servusova reported N-substituted 5-chloropyrazine-2-carboxamides with excellent inhibitory activity against various strains of mycobacteria including *M. tuberculosis* H37Rv, *M. kansasii*, and two strains of *M. avium* (Servusová et al. 2013).

The potent antitubercular activity of pyrazinamide and its derivatives has inspired us to enhance their efficacy by incorporating various bioactive moieties. We aimed to modify pyrazinamide by introducing diverse chemical groups such as 1,3,4-oxadiazole, 1,2,4-triazole, and quinazoline rings, to boost their antimycobacterial activity. To achieve this, we designed and synthesized five new series of pyrazine-based molecules (**Figure 2.2**). In the first series, we focused on synthesizing 18 new pyrazine-1,3,4-oxadiazole derivatives (**T1-T18**) using a molecular hybridization approach, leveraging the pharmacological significance of both pyrazine and 1,3,4-oxadiazole moieties. For the second series, we replaced the 1,3,4-oxadiazole moiety with 1,2,4-triazole through rational modification, resulting in the synthesis of 18 new pyrazine-1,2,4-triazole derivatives (**T19-T36**). In the third series, we synthesized 16 new pyrazine hydrazinylidene derivatives containing a benzenesulfonate scaffold (**T37-T52**). The fourth series involved the synthesis of 16 new 4-quinazolinone-incorporated pyrazine derivatives (**T53-T68**). Finally, in the fifth series, we synthesized 20 new pyrazine-2-

carbohydrazide derivatives (**T69-T88**), incorporating 2-aminophenyl and 2-oxoacetyl groups. Subsequently, we evaluated the effects of these structural modifications on the inhibitory activity against the *M. tuberculosis* H37Rv strain.

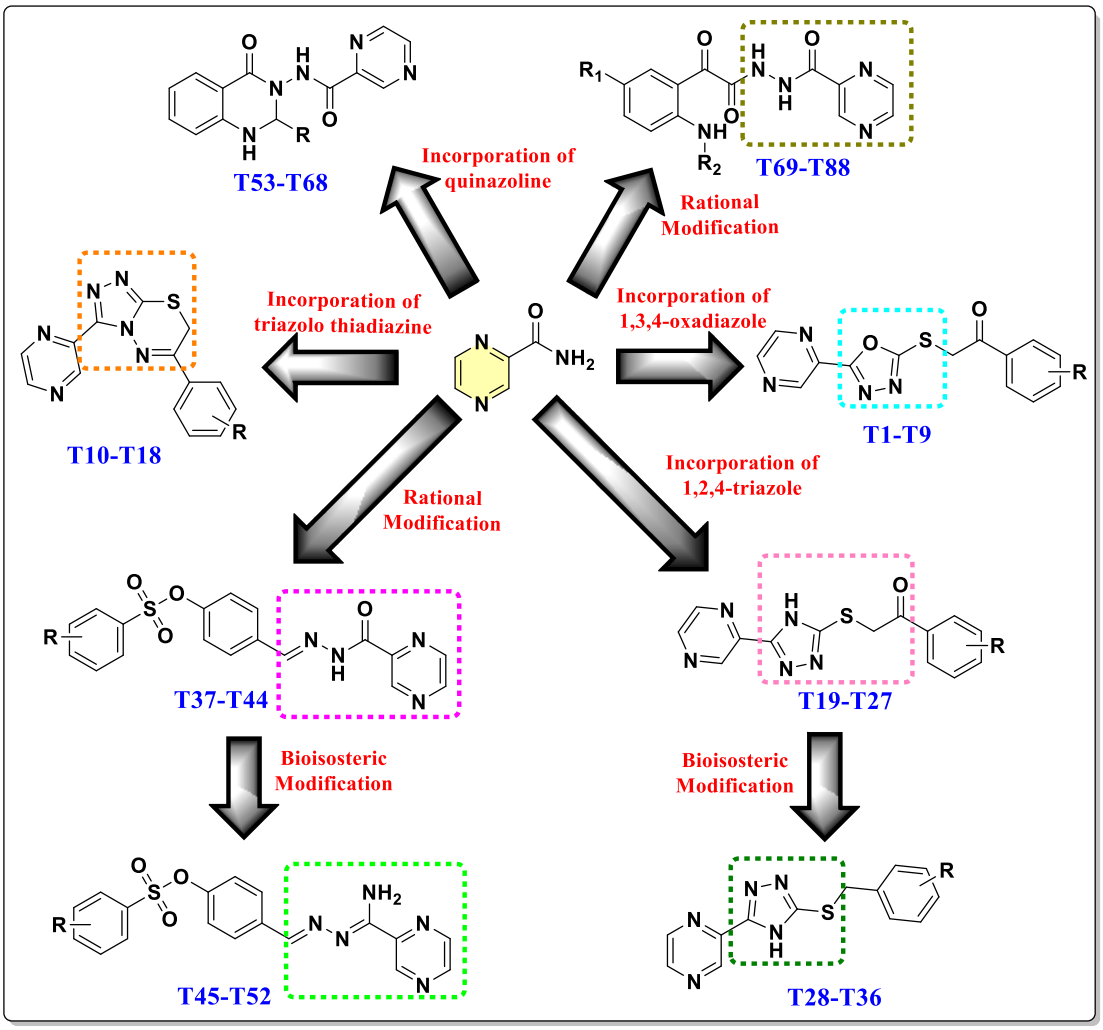

Figure 2.2 *Design strategy for new pyrazine-based compounds (**T1-T88**)*

2.2 Experimental

2.2.1 Materials and Methods

The reagents employed in this study were purchased from commercial suppliers such as Sigma Aldrich, TCI, and Alfa-aesar, and all are of analytical grade. To monitor the progress of the reaction, we utilized thin-layer chromatography with alumina plates coated with silica gel (Merck 60 F254) as the stationary phase and ethyl acetate -

petroleum ether (3:7) solvent mixture as the mobile phase. The resulting spots were examined under a UV chamber. The melting points of the newly synthesized compounds were measured using a digital melting point apparatus without correction. We obtained Proton NMR (^{1}H-NMR) and carbon NMR (^{13}C-NMR) spectra of the synthesized compounds using an FT-NMR Bruker Advance spectrometer operating at 400 MHz and 100 MHz. We used $CDCl_3$ or DMSO-D_6 as solvents and tetramethyl silane (TMS) as an internal standard. Chemical shifts are reported in parts per million (δ-scale), and coupling constants were reported in Hertz (Hz). NMR splitting patterns are indicated as follows: s for singlet, d for doublet, t for triplet, q for quadruplet, m for multiplet, and dd for doublet of doublet. We conducted NMR spectral analysis using Bruker NMR Software (TopSpin 4.1.4). Additionally, we recorded the Mass (HR-MS) spectra of the synthesized compounds using a Waters Xevo QTOF MS system.

2.2.2 Synthesis and characterization

2.2.2.1 Procedure for the synthesis of Methyl pyrazine-2-carboxylate (2):

Pyrazine-2-carboxylic acid (1) (10 g, 80.58 mmol) was taken in anhydrous methanol (250 mL) in a clean, dry 500 mL round bottom flask. A few drops of concentrated sulfuric acid (0.1 mL) were added and the reaction mixture was refluxed for 10 hours at 65 ℃. The progress of the reaction was monitored using thin-layer chromatography. The reaction mixture was then cooled to room temperature and the excess solvent was removed using a rotorvap. Then the reaction mixture was poured into crushed ice and made alkaline using 10% KOH followed by extraction with dichloromethane. The dichloromethane layer was evaporated and kept aside to obtain the crystals of the desired product. Recrystallization was done using methanol (Zhang et al. 2012). White crystals, Yield: 9.47 g, 85%; m.p.: 58-59 ℃; ^{1}H-NMR ($CDCl_3$, 400 MHz, δ in ppm): 9.27 (s,1H), 8.90 (d, J = 2.4 Hz, 1H), 8.76 (d, J = 2.2 Hz, 1H), 3.97 (s, 3H); ^{13}C-NMR ($CDCl_3$, 100 MHz, δ in ppm): 164.7, 147.8, 146.5, 144.4, 143.6, 53.2; HR-MS (m/z) = 139.0429 $[M+H]^+$.

2.2.2.2 Procedure for the synthesis of Pyrazine-2-carbohydrazide (3):

Methyl pyrazine-2-carboxylate (2) (9 g, 65.15 mmol) was taken in anhydrous methanol (50mL) in a clean, dry 250 mL round bottom flask. Hydrazine hydrate (3.26 mL, 65.15 mmol) was added to the reaction mixture and refluxed for 4 hours at 65 ℃. The progress of the reaction was monitored using thin-layer chromatography. The reaction mixture was then cooled to room temperature and the excess solvent was removed using a rotorvap. The obtained solid was filtered, washed with cold methanol, and dried. Recrystallization was done using methanol (Zhang et al. 2012). White crystals, Yield: 8.74 g, 97%; m.p.: 168-169 ℃; ^{1}H-NMR (DMSO-D_6, 400 MHz, δ in ppm): 10.16 (s, 1H), 9.12 (d, *J* = 1.48 Hz, 1H), 8.83 (d, *J* = 2.48 Hz, 1H), 8.68 (m, 1H), 4.67 (s, 2H); ^{13}C-NMR (DMSO-D_6, 100 MHz, δ in ppm): 161.52, 147.28, 144.88, 143.48, 143.25; HR-MS (m/z) = 139.0542 $[M+H]^+$.

2.2.2.3 Procedure for the synthesis of 5-(pyrazin-2-yl)-1,3,4-oxadiazole-2-thiol (4):

Pyrazine-2-carbohydrazide (3) (8.5 g, 61.53 mmol) and potassium hydroxide (3.45 g, 61.53 mmol) were taken in anhydrous methanol (50 mL) in a clean, dry 250 mL round bottom flask. Carbon disulfide was added dropwise at 0 ℃ and the resulting reaction mixture was refluxed for 16 hours at 65 ℃. The progress of the reaction was monitored using thin-layer chromatography. The reaction mixture was then cooled to room temperature and the excess solvent was removed using a rotorvap. The reaction pH was adjusted to 7.0 by adding 1N hydrochloric acid. The precipitated solid was filtered, washed with water, and dried. Recrystallization was done using methanol (Zhang et al. 2012). White solid, Yield: 10.3 g, 93%; m.p.: 206-207 ℃; ^{1}H-NMR (DMSO-D_6, 400 MHz, δ in ppm): 15.04 (s, 1H), 9.20 (s, 1H), 8.86 – 8.84 (m, 2H); ^{13}C-NMR (DMSO-D_6, 100 MHz, δ in ppm): 177.91, 158.10, 147.00, 144.96, 143.14, 138.19; HR-MS (m/z) = 181.0106 $[M+H]^+$.

2.2.2.4 General procedure for the synthesis of 1-phenyl-2-((5-pyrazin-2-yl)-1,3,4-oxadiazol-2-yl)thio)ethane-1-one derivatives (T1 - T9):

A mixture of 5-(pyrazin-2-yl)-1,3,4-oxadiazole-2-thiol (4) (1.0 mmol) and sodium hydroxide (1.1 mmol) was taken in aqueous methanol (80%) (10 mL) in a clean,

dry 50 mL round bottom flask and the reaction mixture was stirred for 10 minutes at room temperature. Then substituted phenacyl bromide (1.0 mmol) was added and the reaction mixture was allowed to stir at room temperature for 4 hours. The progress of the reaction was monitored using thin-layer chromatography. The reaction mixture was then poured into ice-cold water. The precipitated solid was filtered, washed with ice-cold water, and dried. Recrystallization was done using methanol (Zhang et al. 2012).

1-Phenyl-2-((5-(pyrazin-2-yl)-1,3,4-oxadiazol-2-yl)thio)ethan-1-one (T1): White solid, Yield: 95%; m.p.: 162-163 ℃; ^{1}H-NMR ($CDCl_3$, 400 MHz, δ in ppm): 9.37 (s, 1H), 8.70 (s, 2H), 8.02 (t, *J* = 4.2 Hz, 2H), 7.61 (t, *J* = 7.4 Hz, 1H), 7.49 (t, *J* = 7.7 Hz, 2H), 5.01 (s, 2H); ^{13}C-NMR ($CDCl_3$, 100 MHz, δ in ppm): 191.91, 166.40, 163.37, 146.63, 144.76, 144.07, 139.41, 134.92, 134.49, 129.15, 128.69, 41.97; HR-MS (m/z) = 299.0525 $[M+H]^+$.

1-(4-Hydroxyphenyl)-2-((5-(pyrazin-2-yl)-1,3,4-oxadiazol-2-yl)thio)ethan-1-one (T2): White solid, Yield: 97%; m.p.: 235-236 ℃; ^{1}H-NMR (DMSO-D_6, 400 MHz, δ in ppm): 10.58 (s, 1H), 9.31 (s, 1H), 8.85 (t, *J* = 3.4 Hz, 2H), 7.95 (d, *J* = 8.5 Hz, 2H), 6.90 (d, *J* = 8.5 Hz, 2H), 5.14 (s, 2H); ^{13}C-NMR (DMSO-D_6, 100 MHz, δ in ppm): 190.28, 165.39, 162.90, 162.87, 146.95, 145.02, 143.43, 138.69, 131.21, 126.43, 115.48, 40.62; HR-MS (m/z) = 315.0474 $[M+H]^+$.

2-((5-(Pyrazin-2-yl)-1,3,4-oxadiazol-2-yl)thio)-1-(p-tolyl)ethan-1-one (T3): White solid, Yield: 94%; m.p.: 166-167 ℃; ^{1}H-NMR (DMSO-D_6, 400 MHz, δ in ppm): 9.38 (s, 1H), 8.70 (s, 2H), 7.92 (d, *J* = 8.0 Hz, 2H), 7.29 (d, *J* = 7.9 Hz, 2H), 4.99 (s, 2H), 2.41 (s, 3H); ^{13}C-NMR (DMSO-D_6, 100 MHz, δ in ppm): 191.53, 166.57, 163.36, 146.63, 145.66, 144.77, 144.09, 139.45, 132.45, 129.84, 128.83, 42.07, 21.99; HR-MS (m/z) = 313.0681 $[M+H]^+$.

1-(4-Methoxyphenyl)-2-((5-(pyrazin-2-yl)-1,3,4-oxadiazol-2-yl)thio)ethan-1-one (T4): White solid, Yield: 93%; m.p.: 162-163 ℃; ^{1}H-NMR ($CDCl_3$, 400 MHz, δ in ppm): 9.38 (s, 1H), 8.71 (s, 2H), 8.00 (d, *J* = 8.8 Hz, 2H), 6.96 (d, *J* = 8.8 Hz, 2H), 4.98 (s, 2H), 3.87 (s, 3H); ^{13}C-NMR ($CDCl_3$, 100 MHz, δ in ppm): 190.39, 166.70, 164.64,

163.35, 146.64, 144.79, 144.10, 139.47, 131.15, 127.95, 114.35, 55.81, 41.94; HR-MS (m/z) = 329.0630 $[M+H]^+$.

1-(4-Fluorophenyl)-2-((5-(pyrazin-2-yl)-1,3,4-oxadiazol-2-yl)thio)ethan-1-one (T5): White solid, Yield: 94%; m.p.: 164-165 °C; ^{1}H-NMR ($CDCl_3$, 400 MHz, δ in ppm): 9.38 (d, *J* = 0.6 Hz, 1H), 8.72 - 8.70 (m, 2H), 8.09 - 8.05 (m, 2H), 7.17 (t, *J* = 8.5 Hz, 2H), 4.97 (s, 2H); ^{13}C-NMR ($CDCl_3$, 100 MHz, δ in ppm): 190.42, 167.87, 166.30, 165.32, 163.46, 146.70, 144.79, 144.11, 139.40, 131.57, 131.47, 116.56, 116.34, 41.69; HR-MS (m/z) = 317.0431 $[M+H]^+$.

1-(4-Chlorophenyl)-2-((5-(pyrazin-2-yl)-1,3,4-oxadiazol-2-yl)thio)ethan-1-one (T6): White solid, Yield: 95%; m.p.: 168-169 °C; ^{1}H-NMR ($CDCl_3$, 400 MHz, δ in ppm): 9.37 (s, 1H), 8.72 - 8.70 (m, 2H), 7.97 (d, *J* = 8.5 Hz, 2H), 7.47 (d, *J* = 8.5 Hz, 2H), 4.96 (s, 2H); ^{13}C-NMR ($CDCl_3$, 100 MHz, δ in ppm): 190.84, 190.84, 166.21, 163.48, 146.70, 144.79, 144.11, 141.14, 139.38, 130.11, 129.55, 41.64; HR-MS (m/z) = 333.0135 $[M+H]^+$.

1-(4-Bromophenyl)-2-((5-(pyrazin-2-yl)-1,3,4-oxadiazol-2-yl)thio)ethan-1-one (T7): White solid, Yield: 97%; m.p.: 180-181 °C; ^{1}H-NMR ($CDCl_3$, 400 MHz, δ in ppm): 9.38 (s, 1H), 8.72 - 8.70 (m, 2H), 7.89 (d, *J* = 8.5 Hz, 2H), 7.65 (d, *J* = 8.5 Hz, 2H), 4.95 (s, 2H); ^{13}C-NMR ($CDCl_3$, 100 MHz, δ in ppm): 191.07, 166.21, 163.50, 146.72, 144.80, 144.13, 139.40, 133.73, 132.57, 130.18, 129.97, 41.61; HR-MS (m/z) = 376.9630 $[M+H]^+$.

1-(4-Nitrophenyl)-2-((5-(pyrazin-2-yl)-1,3,4-oxadiazol-2-yl)thio)ethan-1-one (T8): Yellow solid, Yield: 96%; m.p.: 202-203 °C; ^{1}H-NMR (DMSO-D_6, 400 MHz, δ in ppm): 9.32 (d, *J* = 1.3 Hz, 1H), 8.89 - 8.85 (m, 2H), 8.41 (d, *J* = 8.8 Hz, 2H), 8.31 (d, *J* = 8.8 Hz, 2H), 5.31 (s, 2H); ^{13}C-NMR (DMSO-D_6, 100 MHz, δ in ppm): 191.83, 164.80, 162.96, 150.21, 146.90, 144.92, 143.35, 139.54, 138.53, 129.85, 129.85, 123.88, 40.82; HR-MS (m/z) = 344.0375 $[M+H]^+$.

4-(2-((5-(Pyrazin-2-yl)-1,3,4-oxadiazol-2-yl)thio)acetyl)benzonitrile (T9): Pale brown solid, Yield: 94%; m.p.: 213-214 °C; ^{1}H-NMR (DMSO-D_6, 400 MHz, δ in ppm):

9.31 (s, 1H), 8.85 (t, *J* = 4.1 Hz, 2H), 8.22 (d, *J* = 8.2 Hz, 2H), 8.08 (d, *J* = 8.1 Hz, 2H), 5.25 (s, 2H); ^{13}C-NMR (DMSO-D_6, 100 MHz, δ in ppm): 190.28, 165.39, 162.90, 162.87, 146.95, 145.02, 143.43, 138.69, 131.21, 126.43, 121.44, 115.48, 40.62; HR-MS (m/z) = 324.0477 $[M+H]^+$.

2.2.2.5 General procedure for the synthesis of 6-phenyl-3-(pyrazin-2-yl)-7*H*-[1,2,4]triazolo[3,4-*b*][1,3,4]thiadiazin derivatives (T10 – T18):

A mixture of 1-phenyl-2-((5-pyrazin-2-yl)-1,3,4-oxadiazol-2-yl)thio)ethane-1-one derivatives (**T1-T9**) (1.0 mmol) and hydrazine hydrate (2.0 mmol) was taken in glacial acetic acid (5 mL) in a clean, dry 25 mL round bottom flask. The reaction mixture was refluxed for 3 hours at 100 ℃. The progress of the reaction was monitored using thin-layer chromatography. The reaction mixture was then poured into ice-cold water. The precipitated solid was filtered, washed with ice-cold water, and dried. Recrystallization was done using methanol (Sasaki et al. 1982).

6-Phenyl-3-(pyrazin-2-yl)-7*H*-[1,2,4]triazolo[3,4-*b*][1,3,4]thiadiazine (T10): White solid, Yield: 98%; m.p.: 201-202 ℃; ^{1}H-NMR ($CDCl_3$, 400 MHz, δ in ppm): 9.36 (s, 1H), 8.73 (s, 1H), 8.66 (d, *J* = 1.8 Hz, 1H), 7.87 (d, *J* = 7.5 Hz, 2H), 7.57 - 7.45 (m, 3H), 4.04 (s, 2H); ^{13}C-NMR ($CDCl_3$, 100 MHz, δ in ppm): 154.79, 150.53, 145.32, 145.00, 144.60, 144.09, 142.09, 133.37, 132.49, 129.40, 127.70, 23.56; HR-MS (m/z) = 295.0688 $[M+H]^+$.

4-(3-(Pyrazin-2-yl)-7*H*-[1,2,4]triazolo[3,4-*b*][1,3,4]thiadiazin-6-yl)phenol (T11): White solid, Yield: 97%; m.p.: 203-204 ℃; ^{1}H-NMR (DMSO-D_6, 400 MHz, δ in ppm): 10.36 (s, 1H), 9.23 (d, *J* = 1.2 Hz, 1H), 8.88 (t, *J* = 1.8 Hz, 1H), 8.82 (d, *J* = 2.4 Hz, 1H), 7.87 (d, *J* = 8.8 Hz, 2H), 6.93 (d, *J* = 8.7 Hz, 2H), 4.41 (s, 2H); ^{13}C-NMR (DMSO-D_6, 100 MHz, δ in ppm): 161.25, 155.94, 149.47, 145.49, 144.85, 144.52, 144.10, 141.49, 129.74, 123.60, 115.92, 22.61; HR-MS (m/z) = 311.0636 $[M+H]^+$.

3-(Pyrazin-2-yl)-6-(p-tolyl)-7*H*-[1,2,4]triazolo[3,4-*b*][1,3,4]thiadiazine (T12): White solid, Yield: 98%; m.p.: 281-282 ℃; ^{1}H-NMR (DMSO-D_6, 400 MHz, δ in ppm): 9.36 (s, 1H), 8.69 (d, *J* = 27.9 Hz, 2H), 7.76 (s, 2H), 7.26 (s, 2H), 4.01 (s, 2H), 2.41 (s,

3H); ^{13}C-NMR (DMSO-D_6, 100 MHz, δ in ppm): 154.72, 150.46, 145.27, 145.00, 144.61, 144.10, 143.35, 142.17, 130.52, 130.11, 127.67, 23.47, 21.77; HR-MS (m/z) = 309.0844 $[M+H]^+$.

6-(4-Methoxyphenyl)-3-(pyrazin-2-yl)-7*H*-[1,2,4]triazolo[3,4-*b*][1,3,4]thiadiazine (T13): White solid, Yield: 99%; m.p.: 207-208 °C; ^{1}H-NMR ($CDCl_3$, 400 MHz, δ in ppm): 9.36 (s, 1H), 8.72 (s, 1H), 8.65 (s, 1H), 7.84 (d, *J* = 8.6 Hz, 2H), 6.97 (d, *J* = 8.6 Hz, 2H), 3.99 (s, 2H), 3.85 (s, 3H); ^{13}C-NMR ($CDCl_3$, 100 MHz, δ in ppm): 163.15, 154.24, 150.36, 145.22, 144.99, 144.60, 144.03, 142.23, 129.55, 125.51, 114.78, 55.76, 23.32; HR-MS (m/z) = 325.0793 $[M+H]^+$.

6-(4-Fluorophenyl)-3-(pyrazin-2-yl)-7*H*-[1,2,4]triazolo[3,4-*b*][1,3,4]thiadiazine (T14): White solid, Yield: 96%; m.p.: 244-245 °C; ^{1}H-NMR (DMSO-D_6, 400 MHz, δ in ppm): 9.23 (d, *J* = 1.1 Hz, 1H), 8.88 (t, *J* = 1.8 Hz, 1H), 8.83 (d, *J* = 2.4 Hz, 1H), 8.01 (d, *J* = 8.6 Hz, 2H), 7.66 (d, *J* = 8.6 Hz, 2H), 4.48 (s, 2H); ^{13}C-NMR (DMSO-D_6, 100 MHz, δ in ppm): 155.27, 149.70, 145.65, 144.86, 144.56, 144.12, 141.31, 136.98, 132.09, 129.47, 129.26, 22.80; HR-MS (m/z) = 313.0593 $[M+H]^+$.

6-(4-Chlorophenyl)-3-(pyrazin-2-yl)-7*H*-[1,2,4]triazolo[3,4-*b*][1,3,4]thiadiazine (T15): White solid, Yield: 96%; m.p.: 252-253 °C; ^{1}H-NMR (DMSO-D_6, 400 MHz, δ in ppm): 9.24 (d, *J* = 1.3 Hz, 1H), 8.89 (t, *J* = 1.9 Hz, 1H), 8.83 (d, *J* = 2.5 Hz, 1H), 8.09 - 8.04 (m, 2H), 7.44 (t, *J* = 8.8 Hz, 2H), 4.49 (s, 2H); ^{13}C-NMR (DMSO-D_6, 100 MHz, δ in ppm): 165.60, 155.31, 149.67, 145.62, 144.86, 144.56, 144.08, 141.35, 130.40, 130.31, 129.79, 116.40, 116.17, 22.89; HR-MS (m/z) = 329.0299 $[M+H]^+$.

6-(4-Bromophenyl)-3-(pyrazin-2-yl)-7*H*-[1,2,4]triazolo[3,4-*b*][1,3,4]thiadiazine (T16): White solid, Yield: 98%; m.p.: 248-259 °C; ^{1}H-NMR (DMSO-D_6, 400 MHz, δ in ppm): 9.23 (s, 1H), 8.86 (t, *J* = 10.0 Hz, 2H), 7.93 (d, *J* = 8.5 Hz, 2H), 7.80 (d, *J* = 8.5 Hz, 2H), 4.48 (s, 2H); ^{13}C-NMR (DMSO-D_6, 100 MHz, δ in ppm): 155.39, 149.69, 145.64, 144.85, 144.55, 144.12, 141.30, 132.44, 132.18, 129.60, 125.98, 22.75; HR-MS (m/z) = 372.9793 $[M+H]^+$.

6-(4-Nitrophenyl)-3-(pyrazin-2-yl)-7*H*-[1,2,4]triazolo[3,4-*b*][1,3,4]thiadiazine (T17): Yellow solid, Yield: 99%; m.p.: 258-259 °C; ^{1}H-NMR (DMSO-D_6, 400 MHz, δ in ppm): 9.25 (s, 1H), 8.89 (s, 1H), 8.85 (d, *J* = 2.3 Hz, 1H), 8.41 (d, *J* = 8.8 Hz, 2H), 8.23 (d, *J* = 8.8 Hz, 2H), 4.56 (s, 2H); ^{13}C-NMR (DMSO-D_6, 100 MHz, δ in ppm): 166.93, 164.80, 162.96, 150.21, 146.90, 144.92, 143.35, 139.54, 138.53, 129.85, 123.88, 22.61; HR-MS (m/z) = 340.0538 $[M+H]^+$.

4-(3-(Pyrazin-2-yl)-7*H*-[1,2,4]triazolo[3,4-*b*][1,3,4]thiadiazin-6-yl)benzonitrile (T18): Yellow solid, Yield: 96%; m.p.: 266-267 °C; ^{1}H-NMR (DMSO-D_6, 400 MHz, δ in ppm): 9.23 (s, 1H), 8.88 (s, 1H), 8.83 (d, *J* = 2.4 Hz, 1H), 8.15 (d, *J* = 8.4 Hz, 2H), 8.06 (d, *J* = 8.3 Hz, 2H), 4.52 (s, 2H); ^{13}C-NMR (DMSO-D_6, 100 MHz, δ in ppm): 161.25, 155.94, 149.47, 145.49, 144.85, 144.52, 144.10, 141.49, 129.74, 123.60, 120.49, 115.92, 22.61; HR-MS (m/z) = 320.0640 $[M+H]^+$.

2.2.2.6 Procedure for the synthesis of (Z)-pyrazine-2-carbohydrazonamide (6):

In a clean and dry 100 mL round bottom flask, pyrazine-2-carbonitrile (5) (10 g, 95.14 mmol) was combined with anhydrous methanol (50 mL). To this mixture, hydrazine hydrate (8.33 mL, 166.50 mmol) was introduced. The reaction mixture was then stirred at room temperature for 24 hours. The progression of the reaction was scrutinized using thin-layer chromatography. Following the reaction, the obtained solid product was isolated by filtration, washed with cold methanol, and subsequently dried. The purification process involved recrystallization in methanol, resulting in the formation of yellow crystals (Bradford et al. 2004). Yield: 12.83 g, 98%; m.p.: 127-128 °C; ^{1}H-NMR ($CDCl_3$, 400 MHz, δ in ppm): 9.24 (s, 1H), 8.48 (d, *J* = 2.36 Hz, 1H), 8.40 (d, *J* = 1.28 Hz, 1H), 5.10 (s, 2H), 4.70 (s, 2H); ^{13}C-NMR ($CDCl_3$, 100 MHz, δ in ppm): 146.60, 146.44, 144.11, 142.81, 142. 40; ESI-MS (m/z) = 106.03 $[M+H]^+$.

2.2.2.7 Procedure for the synthesis of 5-(pyrazin-2-yl)-4*H*-1,2,4-triazole-3-thiol (7):

pyrazine-2-carbohydrazonamide (6) (10 g, 72 mmol) and KOH (4.5g, 80 mmol) were taken in anhydrous methanol (100 mL) in a clean 250 mL round bottom flask. Carbon disulfide (4.40 g, 72 mmol) was introduced to the reaction mixture and refluxed

for 24 hours at 65 ℃. The progress of the reaction was scrutinized using TLC. The reaction mixture was then cooled to room temperature and the excess solvent was removed using a rotorvap. The obtained residue was poured into crushed ice and made acidic (pH = 6) using 20% HCl, and the obtained solid was filtered and dried. Recrystallization was done using methanol (Patil et al. 2017). Pale Yellow solid**,** Yield: 92%, m.p.: 176-177ºC, ^{1}H-NMR (DMSO-D_6, 400 MHz, δ in ppm): 14.1692 (s, 1H), 13.9546 (s, 1H), 9.1809 (s, 1H), 8.7571 (s, 2H); ^{13}C-NMR (DMSO-D_6, 100 MHz, δ in ppm):167.9086, 148.3865, 145.8394, 144.3842, 142.3343, 140.5931, 40.1253, 39.9179, 39.7089, 39.5005, 39.2919, 39.0836, 38.8748; ESI-MS (m/z) = 180.03 $[M+H]^+$.

2.2.2.8 General procedure for the synthesis of 1-phenyl-2-((5-(pyrazin-2-yl)-4*H*-1,2,4-triazol-3-yl)thio)ethan-1-one derivatives (T19 – T27):

A mixture of 5-(pyrazin-2-yl)-4H-1,2,4-triazole-3-thiol (7) (1.0 mmol) and sodium hydroxide (1.1 mmol) was taken in aqueous methanol (80%) (10 mL) in a clean 50 mL round bottom flask and the reaction mixture was stirred for 10 minutes at room temperature. Then substituted phenacyl bromide (1.0 mmol) was added and the reaction mixture was stirred at room temperature for 4 hours. The progression of the reaction was scrutinized using thin-layer chromatography. The reaction mixture was then poured into ice-cold water. The precipitated solid was filtered, washed with ice-cold water, and dried. Recrystallization was done using methanol (Zhang et al. 2012).

1-phenyl-2-((5-(pyrazin-2-yl)-4*H*-1,2,4-triazol-3-yl)thio)ethan-1-one (T19): White solid, Yield: 86%; m.p.: 193-194 ℃; ^{1}H-NMR ($CDCl_3$, 400 MHz, δ in ppm): 12.7680 (s, 1H), 9.4716 (s, 1H), 8.6173 (s, 1H), 8.5612 (s, 1H), 8.0357 (s, 2H), 7.5983 (s, 1H), 7.4901 (d, *J* = 5.68 Hz, 2H), 5.0396 (s, 2H); ^{13}C-NMR ($CDCl_3$, 100 MHz, δ in ppm): 191.91, 166.40, 163.37, 146.63, 144.76, 144.07, 139.41, 134.92, 134.49, 129.15, 128.69, 41.97; ESI-MS (m/z) = 298.11 $[M+H]^+$.

2-((5-(pyrazin-2-yl)-4*H*-1,2,4-triazol-3-yl)thio)-1-(p-tolyl)ethan-1-one (T20): White solid, Yield: 88%; m.p.: 190-191 ℃; ^{1}H-NMR ($CDCl_3$, 400 MHz, δ in ppm):

12.9680 (s, 1H), 9.4716 (s, 1H), 8.6260 (d, *J* = 2.16 Hz, 1H), 8.5711 (s, 1H), 7.9356 (d, *J* = 8.16 Hz, 2H), 7.2870 (d, *J* = 8.08 Hz, 2H), 5.0317 (s, 2H), 2.4134 (s, 3H); ^{13}C-NMR ($CDCl_3$, 100 MHz, δ in ppm): 191.53, 166.57, 163.36, 146.63, 145.66, 144.77, 144.09, 139.45, 132.45, 129.84, 128.83, 42.07, 21.99; ESI-MS (m/z) = 312.09 $[M+H]^+$.

1-(4-methoxyphenyl)-2-((5-(pyrazin-2-yl)-4*H*-1,2,4-triazol-3-yl)thio)ethan-1-one (T21): White solid, Yield: 93%; m.p.: 198-199 °C; ^{1}H-NMR ($CDCl_3$, 400 MHz, δ in ppm): 12.7783 (s, 1H), 9.4574 (s, 1H), 8.6143 (d, *J* = 2.44 Hz, 1H), 8.5622 (d, *J* = 1.44 Hz, 1H), 8.0076 (d, *J* = 8.8 Hz, 2H), 6.9419 (d, *J* = 8.84, 2H), 5.0007 (s, 2H), 3.8567 (s, 3H); ^{13}C-NMR ($CDCl_3$, 100 MHz, δ in ppm): 190.39, 166.70, 164.64, 163.35, 146.64, 144.79, 144.10, 139.47, 131.15, 127.95, 114.35, 55.81, 41.94; ESI-MS (m/z) = 328.13 $[M+H]^+$.

1-(4-hydroxyphenyl)-2-((5-(pyrazin-2-yl)-4*H*-1,2,4-triazol-3-yl)thio)ethan-1-one (T22): White solid, Yield: 87%; m.p.: 250-251 °C; ^{1}H-NMR (DMSO-D_6, 400 MHz, δ in ppm): 12.9889 (s, 1H), 10.5739 (s, 1H), 9.3073 (s, 1H), 8.8451 (t, *J* = 5.80 Hz, 2H), 7.9481 (d, *J* = 8.52 Hz, 2H), 6.9016 (d, *J* = 8.52 Hz, 2H), 5.1359 (s, 2H); ^{13}C-NMR (DMSO-D_6, 100 MHz, δ in ppm):190.28, 165.39, 162.90, 162.87, 146.95, 145.02, 143.43, 138.69, 131.21, 126.43, 115.48; ESI-MS (m/z) = 314.06 $[M+H]^+$.

1-(4-nitrophenyl)-2-((5-(pyrazin-2-yl)-4*H*-1,2,4-triazol-3-yl)thio)ethan-1-one (T23): White solid, Yield: 81%; m.p.: 229-230 °C; ^{1}H-NMR (DMSO-D_6, 400 MHz, δ in ppm): 12.6630 (s, 1H), 9.3847 (d, *J* = 1.20 Hz, 1H), 8.8110 (d, *J* = 2.48 Hz, 1H), 8.7697 (d, *J* = 1.52 Hz, 1H), 8.2163 (d, *J* = 8.68 Hz, 2H), 7.7926 (d, *J* = 8.64 Hz, 2H), 4.8030 (s, 2H); ^{13}C-NMR (DMSO-D_6, 100 MHz, δ in ppm): 191.83, 164.80, 162.96, 150.21, 146.90, 144.92, 143.35, 139.54, 138.53, 129.85, 123.88; ESI-MS (m/z) = 343.08 $[M+H]^+$.

4-(2-((5-(pyrazin-2-yl)-4*H*-1,2,4-triazol-3-yl)thio)acetyl)benzonitrile (T24): White solid, Yield: 85%; m.p.: 215-216 °C; ^{1}H-NMR (DMSO-D_6, 400 MHz, δ in ppm): 12.7140 (s, 1H), 9.3132 (d, *J* = 1.32 Hz, 1H), 8.8724 (d, *J* = 2.48 Hz, 1H), 8.8494 (t, *J* = 1.48 Hz, 1H), 8.4048 (d, *J* = 8.84 Hz, 2H), 8.3055 (d, *J* = 8.84 Hz, 2H), 5.2958 (s,

2H); ^{13}C-NMR (DMSO-D_6, 100 MHz, δ in ppm): 190.28, 165.39, 162.90, 162.87, 146.95, 145.02, 143.43, 138.69, 131.21, 126.43, 121.44, 115.48; ESI-MS (m/z) = 323.10 $[M+H]^+$.

1-(4-fluorophenyl)-2-((5-(pyrazin-2-yl)-4*H*-1,2,4-triazol-3-yl)thio)ethan-1-one (T25): White solid, Yield: 92%; m.p.: 202-203 °C; ^{1}H-NMR ($CDCl_3$, 400 MHz, δ in ppm): 12.9680 (s, 1H), 9.4573 (s, 1H), 8.6234 (t, *J* = 1.56 Hz, 2H), 8.0875 (d, *J* = 5.56 Hz, 1H), 8.0679 (d, *J* = 5.56 Hz, 1H), 7.2400 (s, 1H), 7.1642 (t, *J* = 8.28 Hz, 1H), 5.0019 (s, 2H); ^{13}C-NMR ($CDCl_3$, 100 MHz, δ in ppm): 190.42, 167.87, 166.30, 165.32, 163.46, 146.70, 144.79, 144.11, 139.40, 131.57, 131.47, 116.56, 116.34, 41.69; ESI-MS (m/z) = 316.09 $[M+H]^+$.

1-(4-chlorophenyl)-2-((5-(pyrazin-2-yl)-4*H*-1,2,4-triazol-3-yl)thio)ethan-1-one (T26): White solid, Yield: 96%; m.p.: 197-198 °C; ^{1}H-NMR ($CDCl_3$, 400 MHz, δ in ppm): 12.9686 (s, 1H), 9.4573 (s, 1H), 8.6234 (t, *J* = 1.56 Hz, 2H), 8.0875 (d, *J* = 5.56 Hz, 1H), 8.0679 (d, *J* = 5.56 Hz, 1H), 7.2400 (s, 1H), 7.1642 (t, *J* = 8.28 Hz, 1H), 5.0019 (s, 2H); ^{13}C-NMR ($CDCl_3$, 100 MHz, δ in ppm): 190.84, 166.21, 163.48, 146.70, 144.79, 144.11, 141.14, 139.38, 130.11, 129.55, 41.64; ESI-MS (m/z) = 332.04 $[M+H]^+$.

1-(4-bromophenyl)-2-((5-(pyrazin-2-yl)-4*H*-1,2,4-triazol-3-yl)thio)ethan-1-one (T27): White solid, Yield: 94%; m.p.: 203-204 °C; ^{1}H-NMR ($CDCl_3$, 400 MHz, δ in ppm): 12.8630 (s, 1H), 9.4631 (s, 1H), 8.6313 (s, 1H), 8.5737 (s,1H), 7.9071 (d, *J* = 7.00 Hz, 2H), 7.6406 (d, *J* = 7.08 Hz, 2H), 4.9843 (s, 2H); ^{13}C-NMR ($CDCl_3$, 100 MHz, δ in ppm): 191.07, 166.21, 163.50, 146.72, 144.80, 144.13, 139.40, 133.73, 132.57, 130.18, 129.97,41.61; ESI-MS (m/z) = 375.99 $[M+H]^+$.

2.2.2.9 General procedure for the synthesis of 2-(5-(benzylthio)-4*H*-1,2,4-triazol-3-yl)pyrazine derivatives (T28 - T36):

A mixture of 5-(pyrazin-2-yl)-4H-1,2,4-triazole-3-thiol (7) (1.0 mmol) and potassium carbonate (1.0 mmol) was taken in acetone (10 mL) in a clean 50 mL round bottom flask and the reaction mixture was stirred for 10 minutes at room temperature.

Then, substituted benzyl bromide (1.0 mmol) was introduced and the reaction mixture was stirred at room temperature for 2 hours. The progression of the reaction was scrutinized using thin-layer chromatography. The reaction mixture was then poured into ice-cold water. The precipitated solid was filtered, washed with ice-cold water, and dried. Recrystallization was done using methanol (Zhang et al. 2012).

2-(5-(benzylthio)-4*H*-1,2,4-triazol-3-yl)pyrazine (T28): Brown solid, Yield: 96%; m.p.: 198-199 ℃; ^{1}H-NMR ($CDCl_3$, 400 MHz, δ in ppm): 12.7482 (s, 1H), 9.5144 (d, *J* = 1.00 Hz, 1H), 8.6320 (d, *J* = 2.44 Hz, 1H), 8.5723 (d, *J* = 1.44 Hz, 1H), 7.4541 (d, *J* = 7.16 Hz, 2H), 7.3169 (m, *J* = 6.88 Hz, 3H), 4.6244 (s, 2H); ^{13}C-NMR ($CDCl_3$, 100 MHz, δ in ppm): 168.19, 162.49, 160.02, 145.89, 144.90, 144.38, 142.46, 131.67, 131.63, 130.20, 130.11, 124.49, 31.46; ESI-MS (m/z) = 270.08 $[M+H]^+$.

2-(5-((4-(trifluoromethyl)benzyl)thio)-4*H*-1,2,4-triazol-3-yl)pyrazine (T29): White solid, Yield: 92%; m.p.: 154-155 ℃; ^{1}H-NMR (DMSO-D_6, 400 MHz, δ in ppm): 12.9783 (s, 1H), 9.3917 (d, *J* = 1.36 Hz, 1H), 8.8125 (d, *J* = 2.56 Hz, 1H), 8.7720 (t, *J* = 1.52 Hz, 1H), 7.7360 (s, 2H), 7.6738 (s, 2H), 4.7617 (s, 2H); ^{13}C-NMR (DMSO-D_6, 100 MHz, δ in ppm): 168.19, 162.49, 160.02, 145.89, 144.90, 144.36, 142.46, 131.66, 131.63, 130.20, 130.11, 115.63; ESI-MS (m/z) = 338.11 $[M+H]^+$.

2-(5-((4-fluorobenzyl)thio)-4*H*-1,2,4-triazol-3-yl)pyrazine (T30): White solid, Yield: 86%; m.p.: 150-151 ℃; ^{1}H-NMR ($CDCl_3$, 400 MHz, δ in ppm): 12.8980 (s, 1H), 9.4857 (d, *J* = 1.12 Hz, 1H), 8.6161 (d, *J* = 2.44 Hz, 1H), 8.5516 (t, *J* = 1.52 Hz, 1H), 7.4241 (d, *J* = 5.40 Hz, 1H), 7.4030 (d, *J* = 5.36 Hz, 1H), 7.0115 (s, 1H), 6.9791 (d, *J* = 8.60 Hz, 1H), 4.5731 (s, 2H); ^{13}C-NMR ($CDCl_3$, 100 MHz, δ in ppm): 167.88, 163.78,161.34, 145.90, 144.85, 144.37, 142.45, 131.74, 131.71, 131.17, 131.09, 115.78, 37.44; ESI-MS (m/z) = 288.08 $[M+H]^+$.

2-(5-((2-fluorobenzyl)thio)-4*H*-1,2,4-triazol-3-yl)pyrazinepyrazine (T31): Yellow solid, Yield: 98%; m.p.: 130-131 ℃; ^{1}H-NMR ($CDCl_3$, 400 MHz, δ in ppm): 12.9637 (s, 1H), 9.5007 (d, 1H), 8.6205 (d, *J* = 2.52 Hz, 1H), 8.5582 (t, *J* = 1.56 Hz, 1H), 7.5256 (m, *J* = 1.56 Hz, 1H), 7.2660 (m, *J* = 2.04 Hz, 1H), 7.0876 (m, *J* = 7.60 Hz, 2H), 4.6542

(s, 2H); ^{13}C-NMR ($CDCl_3$, 100 MHz, δ in ppm):168.19, 162.49, 160.02, 145.89, 144.90, 144.38, 142.46, 131.67, 131.63, 130.20, 130.11, 115.73, 31.46 ; ESI-MS (m/z) = 288.10 $[M+H]^+$.

4-(((5-(pyrazin-2-yl)-4*H*-1,2,4-triazol-3-yl)thio)methyl)benzonitrile (T32): White solid, Yield: 89%; m.p.: 209-210 °C; ^{1}H-NMR (DMSO-D_6, 400 MHz, δ in ppm): 12.9220 (s, 1H), 9.3871 (d, 1H), 8.8122 (d, *J* = 2.52 Hz, 1H), 8.7701 (t, *J* = 1.56 Hz, 1H), 7.8314 (d, *J* = 8.28 Hz, 2H), 7.7139 (d, *J* = 8.24 Hz, 2H), 4.7464 (s, 2H); ^{13}C-NMR (DMSO-D_6, 100 MHz, δ in ppm): 167.39, 163.89, 159.34, 146.58, 144.95, 142.62, 141.39, 132.49, 130.13, 123.49, 120.13, 110.37; ESI-MS (m/z) = 295.07 $[M+H]^+$.

2-(5-((4-bromobenzyl)thio)-4*H*-1,2,4-triazol-3-yl)pyrazine (T33): Brown solid, Yield: 92%; m.p.: 155-156 °C; ^{1}H-NMR (DMSO-D_6, 400 MHz, δ in ppm): 12.9880 (s, 1H), 8.8150 (d, *J* = 2.52 Hz, 1H), 8.7779 (d, *J* = 1.52 Hz, 1H), 7.5579 (d, *J* = 8.40 Hz, 2H), 7.4731 (d, *J* = 8.44 Hz, 2H), 4.6444 (s, 2H); ^{13}C-NMR (DMSO-D_6, 100 MHz, δ in ppm): 168.09, 163.79, 161.34, 146.54, 144.93, 143.72, 141.37, 135.99, 131.50, 131.35, 120.89; ESI-MS (m/z) = 347.98 $[M+H]^+$.

2-(5-((2-bromobenzyl)thio)-4*H*-1,2,4-triazol-3-yl)pyrazine (T34): Brown solid, Yield: 92%; m.p.: 156-157 °C; ^{1}H-NMR ($CDCl_3$, 400 MHz, δ in ppm): 12.9889 (s, 1H), 9.5008 (d, *J* = 1.28 Hz, 1H), 8.6200 (d, *J* = 2.48 Hz, 1H), 8.5581 (t, *J* = 1.56 Hz, 1H), 7.6238 (m, *J* = 6.08 Hz, 1H), 7.5658 (m, *J* = 7.04 Hz, 1H), 7.2533 (m, *J* = 6.44 Hz, 1H), 7.1454 (m, *J* = 6.12 Hz, 1H), 4.7505 (s, 2H); ^{13}C-NMR ($CDCl_3$, 100 MHz, δ in ppm): 168.19, 162.49, 160.02, 145.89, 144.90, 144.38, 142.46, 131.67, 131.63, 130.20, 130.11, 115.94, 31.46; ESI-MS (m/z) = 347.97 $[M+H]^+$.

2-(5-((4-chlorobenzyl)thio)-4*H*-1,2,4-triazol-3-yl)pyrazine (T35): White solid, Yield: 94%; m.p.: 162-163 °C; ^{1}H-NMR ($CDCl_3$, 400 MHz, δ in ppm): 12.9881 (s, 1H), 9.4932 (d, J = 1.20 Hz, 1H), 8.6239 (d, *J* = 2.48 Hz, 1H), 8.5600 (t, *J* = 1.60 Hz, 1H), 7.3880 (d, *J* = 8.40 Hz, 2H), 7.2692 (t, *J* = 8.40 Hz, 2H), 4.5689 (s, 2H); ^{13}C-NMR

($CDCl_3$, 100 MHz, δ in ppm): 168.09, 163.79, 161.34, 145.90, 144.85, 144.37, 142.45, 131.74, 131.71, 131.17, 131.09, 116.00, 37.44; ESI-MS (m/z) = 304.05 $[M+H]^+$.

2-(5-((4-nitrobenzyl)thio)-4*H*-1,2,4-triazol-3-yl)pyrazine (T36): White solid, Yield: 97%; m.p.: 194-195 °C; ^{1}H-NMR (DMSO-D_6, 400 MHz, δ in ppm): 12.9680 (s, 1H), 9.3846 (d, *J* = 1.16 Hz, 1H), 8.8109 (d, *J* = 2.52 Hz, 1H), 8.7696 (d, *J* = 1.48 Hz, 1H), 8.2163 (d, *J* = 8.68 Hz, 2H), 7.7925 (d, *J* = 8.68 Hz, 2H), 4.8030 (s, 2H); ^{13}C-NMR (DMSO-D_6, 100 MHz, δ in ppm): 167.83, 167.34, 146.85, 146.57, 144.93, 144.78, 143.67, 141.37, 130.40, 123.67; ESI-MS (m/z) = 315.08 $[M+H]^+$.

2.2.2.10 General procedure for the synthesis of 4-formylphenyl benzenesulfonate derivatives (I1-I8):

4-hydroxybenzaldehyde (1.0 mmol) was placed in a clean and dry 50 mL round-bottom flask, and anhydrous THF (10 mL) was added. The mixture was then cooled to 0 °C, and a substituted benzenesulfonyl chloride (1.0 mmol) was introduced. To this mixture, TEA (1.1 mmol) in THF (10 mL) was added drop by drop while maintaining the temperature at 0 °C. Afterward, the reaction mixture was stirred at room temperature for 30 minutes and then refluxed for an additional 3 hours at 60 °C. The progression of the reaction was tracked using thin-layer chromatography. Any excess solvent was removed using a rotorvap, and the resulting solid product was obtained through filtration. It was subsequently washed with cold water and dried. Finally, the product was purified through recrystallization in methanol (Tian et al. 2006).

2.2.2.11 General procedure for the synthesis of (*E*)-4-((2-(pyrazine-2-carbonyl)hydrazineylidene)methyl)phenyl benzenesulfonate derivatives (T37 – T44):

A solution containing pyrazine-2-carbohydrazide (**3**) (1.0 mmol) and appropriate 4-formylphenyl benzenesulfonate derivatives (**I1-I8**) (1.0 mmol) was prepared in methanol (10 mL) in a clean and dry 25 mL round-bottom flask. A small amount of glacial acetic acid (2 drops), acting as a catalyst, was added to the mixture. The reaction mixture was then heated and refluxed at 65 °C for 3 hours. The progress

of the reaction was monitored using thin-layer chromatography. After completion of the reaction, the reaction mixture was poured into ice-cold water. As a result, a solid precipitated out. This solid was separated by filtration, washed with ice-cold water, and dried. To purify the product, recrystallization was carried out using methanol (Koçak Aslan et al. 2022).

(*E*)-4-((2-(pyrazine-2-carbonyl)hydrazineylidene)methyl)phenyl benzenesulfonate (T37): White solid, Yield: 94%; m.p.: 216-217 ℃; ^{1}H-NMR (DMSO-D_6, 400 MHz, δ in ppm): 12.3667 (s, 1H), 9.2610 (d, *J* = 1.24Hz, 1H), 8.9264 (d, *J* = 2.44 Hz, 1H), 8.7859 (t, *J* = 2.12 Hz, 1H), 8.6126 (s, 1H), 7.8727 (m, *J* = 1.08 Hz, 3H), 7.7046 (m, *J* = 8.00 Hz, 4H), 7.1301 (d, *J* = 8.64 Hz, 2H); ^{13}C-NMR (DMSO-D_6, 100 MHz, δ in ppm): 159.60, 150.02, 148.29, 147.91, 144.52, 144.17, 143.32, 135.19, 134.09, 133.38, 129.88, 128.84, 128.25, 122.66; HR-MS (m/z): 383.0734 $[M+H]^+$.

(*E*)-4-((2-(pyrazine-2-carbonyl)hydrazineylidene)methyl)phenyl 4-methylbenzene sulfonate (T38): White solid, Yield: 91%; m.p.: 261-262 ℃; ^{1}H-NMR (DMSO-D_6, 400 MHz, δ in ppm): 12.3742 (s, 1H), 9.2696 (d, *J* = 0.72 Hz, 1H), 8.9414 (d, *J* = 2.40 Hz, 1H), 8.8013 (d, *J* = 1.56 Hz, 1H), 8.6197 (s, 1H), 7.7486 (m, *J* = 2.00 Hz, 4H), 7.4915 (d, *J* = 8.28 Hz, 2H), 7.1338 (d, *J* = 8.60 Hz, 2H), 2.4341 (s, 3H); ^{13}C-NMR (DMSO-D_6, 100 MHz, δ in ppm): 150.10, 148.33, 146.01, 144.16, 143.33, 133.30, 131.17, 130.30, 128.83, 128.28, 122.67, 21.19; HR-MS (m/z): 397.0891 $[M+H]^+$.

(*E*)-4-((2-(pyrazine-2-carbonyl)hydrazineylidene)methyl)phenyl 4-methoxybenzene sulfonate (T39): White solid, Yield: 95%; m.p.: 235-236 ℃; ^{1}H-NMR (DMSO-D_6, 400 MHz, δ in ppm): 12.3688 (s, 1H), 9.2700 (d, *J* = 1.04 Hz, 1H), 8.9349 (d, *J* = 2.44 Hz, 1H), 8.7957 (t, *J* = 1.80 Hz, 1H), 8.6225 (s,1H), 7.7950 (d, *J* = 8.92 Hz, 2H), 7.7367 (d, *J* = 8.64 Hz, 2H), 7.1788 (d, *J* = 8.92 Hz, 2H),7.1251 (d, *J* = 8.6 Hz, 2H), 3.8751 (s, 3H); ^{13}C-NMR (DMSO-D_6, 100 MHz, δ in ppm): 164.13, 159.60, 150.16, 148.37, 147.91, 144.52, 144.16, 143.32, 133.24, 130.70, 128.81, 125.23, 122.73, 115.01, 55.95; HR-MS (m/z): 413.0842 $[M+H]^+$.

(*E*)-4-((2-(pyrazine-2-carbonyl)hydrazineylidene)methyl)phenyl 2-(trifluoromethyl) benzenesulfonate (T40): White solid, Yield: 93%; m.p.: 228-229 ℃; ^{1}H-NMR (DMSO-D_6, 400 MHz, δ in ppm): 12.3816 (s, 1H), 9.2695 (s, 1H), 8.9345 (d, *J* = 2.4 Hz, 1H), 8.7975 (d, *J* = 1.40 Hz, 1H), 8.6249 (s, 1H), 8.2117 (d, *J* = 7.76 Hz, 1H), 8.0782 (t, *J* = 7.68 Hz, 2H), 7.9432 (d, *J* = 7.68 Hz, 1H), 7.7549 (d, *J* = 8.68 Hz, 2H), 7.1689 (d, *J* = 8.60 Hz, 2H); ^{13}C-NMR (DMSO-D_6, 100 MHz, δ in ppm): 159.62, 149.69, 148.20, 147.92, 144.50, 144.17, 143.32, 135.94, 133.77, 133.66, 133.04, 132.14, 129.44, 129.38, 129.02, 127.26, 126.93, 123.73, 122.50; HR-MS (m/z): 451.0609 $[M+H]^+$.

(*E*)-4-((2-(pyrazine-2-carbonyl)hydrazineylidene)methyl)phenyl 4-fluorobenzene sulfonate (T41): White solid, Yield: 94%; m.p.: 234-235 ℃; ^{1}H-NMR (DMSO-D_6, 400 MHz, δ in ppm): 12.3777 (s, 1H), 9.2716 (s, 1H), 8.9351 (d, *J* = 2.40 Hz, 1H), 8.7980 (d, *J* = 1.28 Hz, 1H), 8.6282 (s, 1H), 7.9701 (m, *J* = 3.80 Hz, 2H), 7.7511 (d, *J* = 8.64 Hz, 2H), 7.5370 (t, *J* = 8.76 Hz, 2H), 7.1548 (d, *J* = 8.60 Hz, 2H); ^{13}C-NMR (DMSO-D_6, 100 MHz, δ in ppm): 166.93, 164.40, 159.61, 149.93, 148.27, 147.91, 144.51, 144.17, 143.32, 133.49, 131.74, 131.64, 130.35, 128.90, 122.73, 117.38, 117.15; HR-MS (m/z): 401.0642 $[M+H]^+$.

(*E*)-4-((2-(pyrazine-2-carbonyl)hydrazineylidene)methyl)phenyl 4-chlorobenzene sulfonate (T42): White solid, Yield: 90%; m.p.: 263-264 ℃; ^{1}H-NMR (DMSO-D_6, 400 MHz, δ in ppm): 12.3849 (s, 1H), 9.2729 (s, 1H), 8.9397 (d, *J* = 2.40 Hz, 1H), 8.8029 (d, *J* = 1.48 Hz, 1H), 8.6296 (s, 1H), 7.8982 (d, *J* = 8.60 Hz, 2H), 7.7661 (m, *J* = 3.04 Hz, 4H), 7.1717 (d, *J* = 8.64 Hz, 2H); ^{13}C-NMR (DMSO-D_6, 100 MHz, δ in ppm): 149.89, 148.26, 144.52, 144.17, 143.34, 140.26, 133.55, 132.86, 130.23, 130.11, 128.94, 122.73; HR-MS (m/z): 417.0344 $[M+H]^+$.

(*E*)-4-((2-(pyrazine-2-carbonyl)hydrazineylidene)methyl)phenyl 4-bromobenzene sulfonate (T43): White solid, Yield: 93%; m.p.: 272-273 ℃; ^{1}H-NMR (DMSO-D_6, 400 MHz, δ in ppm): 12.3766 (s, 1H), 9.2646 (s, 1H), 8.9314 (d, *J* = 2.40 Hz, 1H), 8.7946 (d, *J* = 1.48 Hz, 1H), 8.6213 (s, 1H), 7.8900 (d, *J* = 8.64 Hz, 2H), 7.7578 (m, *J* = 3.04 Hz, 4H), 7.1634 (d, *J* = 8.64 Hz, 2H); ^{13}C-NMR (DMSO-D_6, 100 MHz, δ in ppm):

166.92, 164.39, 159.60, 149.92, 148.26, 147.90, 144.50, 144.16, 143.31, 133.48, 131.73, 131.63, 130.34, 130.31, 128.89, 122.72, 117.37, 117.15; HR-MS (m/z): 460.9841 $[M+H]^+$.

(*E*)-4-((2-(pyrazine-2-carbonyl)hydrazineylidene)methyl)phenyl 4-(trifluoromethyl) benzenesulfonate (T44): White solid, Yield: 91%; m.p.: 226-227 ℃; ^{1}H-NMR (DMSO-D_6, 400 MHz, δ in ppm): 12.3733 (s, 1H), 9.2612 (s, 1H), 8.9262 (d, *J* = 2.40 Hz, 1H), 8.7893 (d, *J* = 1.36 Hz, 1H), 8.6166 (s, 1H), 8.2034 (d, *J* = 7.76 Hz, 2H), 8.0700 (t, *J* = 7.64 Hz, 2H), 7.9349 (d, *J* = 7.64 Hz, 1H), 7.7464 (d, *J* = 8.64 Hz, 2H), 7.1606 (d, *J* = 8.60 Hz, 2H); ^{13}C-NMR (DMSO-D_6, 100 MHz, δ in ppm): 159.61, 149.68, 148.19, 147.91, 144.49, 144.16, 143.31, 135.93, 133.76, 133.65, 133.03, 132.13, 129.43, 129.37, 129.01, 127.25, 126.92, 123.72, 122.49; HR-MS (m/z): 451.0611 $[M+H]^+$.

2.2.2.12 General procedure for the synthesis of 4-((*E*)-(((*Z*)-amino(pyrazin-2-yl)methylene)hydrazineylidene)methyl)phenyl benzenesulfonate derivatives (T45 – T52):

A solution containing (*Z*)-pyrazine-2-carbohydrazonamide (**6**) (1.0 mmol) and 4-formylphenyl benzenesulfonate derivatives (**I1-I8**) (1.0 mmol) in methanol (10 mL) was prepared in a clean and dry 25 mL round-bottom flask. Two drops of glacial acetic acid, acting as a catalyst, were added to the mixture. The reaction mixture was then heated and refluxed at 65 ℃ for 3 hours. The progress of the reaction was monitored using thin-layer chromatography. After completion of the reaction, the reaction mixture was poured into ice-cold water. As a result, a solid precipitated out. This solid was separated by filtration, washed with ice-cold water, and dried. To purify the product, recrystallization was carried out using methanol (Koçak Aslan et al. 2022).

4-((*E*)-(((*Z*)-amino(pyrazin-2-yl)methylene)hydrazineylidene)methyl)phenyl benzene sulfonate (T45): Yellow solid, Yield: 92%; m.p.: 176-177 ℃; ^{1}H-NMR (DMSO-D_6, 400 MHz, δ in ppm): 9.3653 (d, *J* = 1.24 Hz, 1H), 8.7325 (m, *J* = 1.56 Hz, 2H), 8.4826 (s, 1H), 7.9624 (d, *J* = 8.64 Hz, 2H), 7.8947 (d, *J* = 7.52 Hz, 2H), 7.8253

(d, *J* = 7.48 Hz, 1H), 7.6870 (t, *J* = 7.84 Hz, 2H), 7.0924 (s, 2H), 7.0708 (s, 2H); ^{13}C-NMR (DMSO-D_6, 100 MHz, δ in ppm): 155.77, 153.35, 149.90, 145.95, 145.82, 143.38, 143.05, 135.15, 134.52, 134.17, 129.86, 129.51, 128.28, 122.29; HR-MS (m/z): 382.0893 $[M+H]^+$.

4-((*E*)-(((*Z*)-amino(pyrazin-2-yl)methylene)hydrazineylidene)methyl)phenyl 4-methyl benzenesulfonate (T46): Yellow solid, Yield: 94%; m.p.: 185-186 ℃; ^{1}H-NMR (DMSO-D_6, 400 MHz, δ in ppm): 9.3747 (s, 1H), 8.7826 (d, *J* = 2.40, 1H), 8.7379 (d, *J* = 1.20 Hz, 2H), 8.4909 (s, 1H), 7.9697 (t, *J* = 8.48 Hz, 2H), 7.7718 (d, *J* = 8.08 Hz, 2H), 7.4894 (d, *J* = 8.20 Hz, 2H), 7.2922 (s, 2H), 7.0846 (d, *J* = 8.44 Hz, 2H), 2.4293 (s, 3H); ^{13}C-NMR (DMSO-D_6, 100 MHz, δ in ppm): 155.76, 153.38, 149.97, 145.92, 145.83, 143.37, 143.04, 134.43, 131.28, 130.27, 129.50, 128.30, 122.29; HR-MS (m/z): 396.1052 $[M+H]^+$.

4-((*E*)-(((*Z*)-amino(pyrazin-2-yl)methylene)hydrazineylidene)methyl)phenyl 4-methoxy benzenesulfonate (T47): Yellow solid, Yield: 91%; m.p.: 171-172 ℃; ^{1}H-NMR (DMSO-D_6, 400 MHz, δ in ppm): 9.3746 (s, 1H), 8.7838 (d, *J* = 2.40 Hz, 1H), 8.7391 (d, *J* = 1.16 Hz, 1H), 8.4932 (s, 1H), 7.9714 (d, *J* = 8.48 Hz, 2H), 7.8082 (d, *J* = 8.80 Hz 2H), 7.1932 (t, *J* = 8.80 Hz 4H), 7.0785 (d, *J* = 8.48 Hz, 2H), 3.8761 (s,3H); ^{13}C-NMR (DMSO-D_6, 100 MHz, δ in ppm): 164.08, 155.75, 153.42, 150.04, 145.94, 145.83, 143.38, 143.04, 134.37, 130.72, 129.48, 125.33, 122.35, 114.98; HR-MS (m/z): 412.1003 $[M+H]^+$.

4-((*E*)-(((*Z*)-amino(pyrazin-2-yl)methylene)hydrazineylidene)methyl)phenyl 2-(trifluoromethyl)benzenesulfonate (T48): Yellow solid, Yield: 92%; m.p.: 181-182 ℃; ^{1}H-NMR (DMSO-D_6, 400 MHz, δ in ppm): 9.3735 (s, 1H), 8.7838 (d, *J* = 2.44 Hz, 1H), 8.7376 (s, 1H), 8.4955 (s, 1H), 8.2128 (d, *J* = 7.76 Hz, 2H), 8.1000 (d, *J* = 7.96 Hz, 2H), 7.9800 (m, *J* = 9.44 Hz, 3H), 7.3072 (s, 2H), 7.1173 (d, *J* = 8.60 Hz, 2H); ^{13}C-NMR (DMSO-D_6, 100 MHz, δ in ppm): 155.81, 153.27, 149.61, 145.97, 145.81, 143.38, 143.05, 135.89, 134.79, 133.76, 133.04, 132.26, 129.68, 129.42, 129.36, 127.28, 126.95, 123.74, 122.09; HR-MS (m/z): 450.0769 $[M+H]^+$.

4-((*E*)-(((*Z*)-amino(pyrazin-2-yl)methylene)hydrazineylidene)methyl)phenyl 4-fluoro benzenesulfonate (T49): Yellow solid, Yield: 92%; m.p.: 178-179 ℃; ^{1}H-NMR (DMSO-D_6, 400 MHz, δ in ppm): 9.3764 (s, 1H), 8.7828 (d, *J* = 1.88 Hz, 1H), 8.7356 (t, *J* = 1.20 Hz, 1H), 8.4990 (s, 1H), 7.9807 (m, *J* = 3.28 Hz, 4H), 7.5388 (t, *J* = 8.56 Hz, 2H), 7.3063 (s, 2H), 7.1112 (d, *J* = 8.32 Hz, 2H); ^{13}C-NMR (DMSO-D_6, 100 MHz, δ in ppm): 166.90, 164.37, 155.79, 153.34, 149.81, 145.95, 145.82, 143.37, 143.05, 134.63, 131.76, 131.66, 130.43, 130.40, 129.57, 122.36, 117.35, 117.12; HR-MS (m/z): 400.0802 $[M+H]^+$.

4-((*E*)-(((*Z*)-amino(pyrazin-2-yl)methylene)hydrazineylidene)methyl)phenyl 4-chloro benzenesulfonate (T50): Yellow solid, Yield: 93%; m.p.: 183-184 ℃; ^{1}H-NMR (DMSO-D_6, 400 MHz, δ in ppm): 9.3775 (d, *J* = 1.16 Hz 1H), 8.7824 (d, *J* = 2.48 Hz 1H), 8.7357 (t, *J* = 2.16 Hz, 1H), 8.4998 (s, 1H), 7.9918 (d, *J* = 8.64 Hz, 2H), 7.9054 (d, *J* = 8.64 Hz, 2H), 7.7675 (d, *J* = 8.64 Hz, 2H), 7.3140 (s, 2H), 7.1207 (d, *J* = 8.60 Hz, 2H); ^{13}C-NMR (DMSO-D_6, 100 MHz, δ in ppm): 155.80, 153.32, 149.76, 145.95, 145.82, 143.37, 143.06, 140.20, 134.68, 132.93, 130.26, 130.06, 129.60, 122.35; HR-MS (m/z): 416.0506 $[M+H]^+$.

4-((*E*)-(((*Z*)-amino(pyrazin-2-yl)methylene)hydrazineylidene)methyl)phenyl 4-bromo benzenesulfonate (T51): Yellow solid, Yield: 94%; m.p.: 226-227 ℃; ^{1}H-NMR (DMSO-D_6, 400 MHz, δ in ppm): 9.3692 (d, *J* = 1.16 Hz, 1H), 8.7740 (d, *J* = 2.52 Hz, 1H), 8.7273 (t, *J* = 2.16 Hz, 1H), 8.4915 (s, 1H), 7.9834 (d, *J* = 8.68 Hz, 2H), 7.8971 (d, *J* = 8.64 Hz, 2H), 7.7591 (d, *J* = 8.64 Hz, 2H), 7.3056 (s, 2H), 7.1124 (d, *J* = 8.64 Hz, 2H); ^{13}C-NMR (DMSO-D_6, 100 MHz, δ in ppm): 155.79, 153.31, 149.75, 145.94, 145.81, 143.36, 143.05, 140.19, 134.67, 132.92, 130.25, 130.05, 129.59, 122.34; HR-MS (m/z): 460.0003 $[M+H]^+$.

4-((*E*)-(((*Z*)-amino(pyrazin-2-yl)methylene)hydrazineylidene)methyl)phenyl 4-(trifluoromethyl)benzenesulfonate (T52): Yellow solid, Yield: 91%; m.p.: 178-179 ℃; ^{1}H-NMR (DMSO-D_6, 400 MHz, δ in ppm): 9.3650 (s, 1H), 8.7754 (d, *J* = 2.48 Hz, 1H), 8.7292 (s, 1H), 8.4870 (s, 1H), 8.2043 (d, *J* = 7.80 Hz, 1H), 8.0916 (d, *J* = 8.00 Hz, 2H), 8.0537 (s, 2H), 7.9597 (m, *J* = 9.40 Hz, 1H), 7.2988 (s, 2H), 7.1089 (d, *J* =

8.60 Hz, 2H); ^{13}C-NMR (DMSO-D_6, 100 MHz, δ in ppm): 155.80, 153.26, 149.60, 145.96, 145.80, 143.37, 143.04, 135.88, 134.78, 133.75, 133.03, 132.35, 129.67, 129.41, 129.35, 127.27, 126.94, 123.73, 122.08; HR-MS (m/z): 450.0767 $[M+H]^+$.

2.2.2.13 Procedure for the synthesis of N-(2-aminobenzoyl)pyrazine-2-carbohydrazide (T53):

In a clean and dry 50 mL round-bottom flask, pyrazine-2-carbohydrazide (**3**) (1 g, 7.23 mmol) and isatoic anhydride (1.18 g, 7.23 mmol) were combined in methanol (15 mL). The resulting mixture was refluxed at 65 ℃ for 6 hours. The progress of the reaction was monitored using TLC. Subsequently, the mixture was allowed to cool to room temperature, leading to the formation of a solid precipitate, which was then filtered, washed with methanol, and dried. For purification, the product was subjected to recrystallization in methanol, resulting in the formation of a white solid (Takahashi et al., 2006). Yield: 0.52g, 97%; m.p.: 169-170 ℃; ^{1}H-NMR (DMSO-D_6, 400 MHz, δ in ppm): 12.6258 (s, 1H), 11.7764 (s, 1H), 9.2488 (s, 1H), 8.9996 (d, *J* = 1.32 Hz, 1H), 8.8780 (s, 1H), 8.0040 (d, *J* = 7.80 Hz, 1H), 7.8337 (t, *J* = 7.60 Hz, 1H), 7.4206 (m, *J* = 7.40 Hz, 2H), 6.2527 (s, 2H); ^{13}C-NMR (DMSO-D_6, 100 MHz, δ in ppm): 167.95, 162.50, 150.01, 148.00, 144.33, 143.72, 143.66, 132.41, 128.26, 116.46, 114.59, 112.24; ESI-MS (m/z) = 257.09 $[M+H]^+$.

2.2.2.14 Procedure for the synthesis of *N*-(4-oxo-2-thioxo-1,4-dihydroquinazolin-3(2*H*)-yl)pyrazine-2-carboxamide (T54):

A mixture of N-(2-aminobenzoyl)pyrazine-2-carbohydrazide (T53) (1 g, 3.88 mmol) and potassium hydroxide (0.22 g, 3.88 mmol) was taken in aqueous methanol (80%) (30 mL) in a clean, dry 100 mL round bottom flask and the reaction mixture was stirred for 5 minutes at room temperature. Carbon disulfide (0.35g, 4.66 mmol) was added dropwise at 0 ℃ and the resulting reaction mixture was refluxed for 18 hours at 65 ℃. The progress of the reaction was monitored using TLC. Afterwards, the reaction mixture was cooled to room temperature and the excess solvent was removed using a rotorvap. The precipitated solid was filtered, washed with methanol followed by water,

and dried. Recrystallization was done using methanol resulting in the formation of a white solid (Soltan et al. 2014). Yield: 0.82 g, 96%; m.p.: 259-260 ℃; ^{1}H-NMR (DMSO-D_6, 400 MHz, δ in ppm): 13.2681 (s, 1H), 11.7755 (s, 1H), 9.2480 (s, 1H), 9.0005 (d, *J* = 2.16 Hz, 1H), 8.8783 (s, 1H), 8.0058 (d, *J* = 7.80 Hz, 1H), 7.8360 (t, *J* = 7.56 Hz, 1H), 7.4238 (m, *J* = 7.60 Hz, 2H); ^{13}C-NMR (DMSO-D_6, 100 MHz, δ in ppm): 175.41, 161.37, 157.53, 148.73, 144.03, 143.99, 143.39, 139.21, 136.45, 127.78, 125.11, 116.13, 115.35; ESI-MS (m/z) = 299.05 $[M+H]^+$.

2.2.2.15 Procedure for the synthesis of 3-amino-2-(pyrazin-2-yl)-[1,2,4]triazolo[5,1-*b*]quinazolin-9(3*H*)-one (T55):

A mixture of *N*-(4-oxo-2-thioxo-1,4-dihydroquinazolin-3(2*H*)-yl)pyrazine-2-carboxamide (T54) (1g, 3.34 mmol) and hydrazine hydrate (0.17g, 3.34 mmol) was taken in methanol (15 mL) in a clean, dry 50 mL round bottom flask and the resulting reaction mixture was refluxed for 24 hours at 65 ℃. The progress of the reaction was monitored using TLC. Subsequently, the reaction mixture was cooled to room temperature, and the solid that precipitated was filtered, washed with methanol, and then dried. Recrystallization was done using methanol resulting in the formation of a white crystalline solid (Soltan et al. 2014). Yield: 1.02 g, 96%; m.p.: 268-269 ℃; ^{1}H-NMR (DMSO-D_6, 400 MHz, δ in ppm): 9.2488 (s, 1H), 8.996 (d, *J* = 1.32 Hz, 1H), 8.8780 (s, 1H), 8.0040 (d, *J* = 7.80 Hz, 1H), 7.8337 (t, *J* = 7.60 Hz, 1H), 7.4206 (m, *J* = 7.40 Hz, 2H), 6.2527 (s, 2H); ^{13}C-NMR (DMSO-D_6, 100 MHz, δ in ppm): 175.47, 161.47, 157.62, 148.79, 144.11, 144.04, 143.44, 139.26, 136.52, 127.85, 125.20, 116.19, 115.41; ESI-MS (m/z) = 279.09 $[M+H]^+$.

2.2.2.16 General procedure for the synthesis of 1,4-dihydroquinazolinylpyrazine-2-carboxamide derivatives (T56 – T68):

A mixture of N-(2-aminobenzoyl)pyrazine-2-carbohydrazide (**T53**) (1.0 equivalent) and substituted aromatic aldehyde (1.1 equivalent) was taken in anhydrous methanol (20 mL) in a clean, dry 50 mL round bottom flask. Three drops of glacial acetic acid were introduced, and the reaction mixture was subjected to reflux at 65 ℃

for 4 hours. The progress of the reaction was monitored using TLC. Following this, the reaction mixture was allowed to cool to room temperature (27 ℃), and excess solvent was removed through rotary evaporation. The remaining solution was poured into crushed ice, causing a solid precipitate to form. This solid was subsequently filtered, washed with water, and dried. To purify the product, recrystallization was performed using methanol.

***N*-(4-oxo-2-phenyl-1,4-dihydroquinazolin-3(2*H*)-yl)pyrazine-2-carboxamide (T56):** White solid, Yield: 93%; m.p.: 189-190 ℃; ^{1}H-NMR (DMSO-D_6, 400 MHz, δ in ppm): 10.7416 (s, 1H), 9.0478(d, *J* = 0.68 Hz, 1H), 8.8546 (d, *J* = 2.36 Hz, 1H), 8.6655 (d, *J* = 4.08 Hz, 1H), 7.7135 (d, *J* = 8.16 Hz, 1H), 7.5750 (m, *J* = 3.72 Hz, 2H), 7.3552 (d, *J* = 4.52 Hz, 5H), 6.8009 (m, *J* = 8.00 Hz, 2H), 6.1787 (s, 1H); ^{13}C-NMR (DMSO-D_6, 100 MHz, δ in ppm): 163.10, 162.06, 149.88, 148.10, 147.95, 143.74, 143.59, 137.70, 134.11, 129.28, 128.93, 128.31, 128.16, 128.05, 127.31, 117.87, 114.67, 113.56, 74.76; ESI-MS (m/z) = 345.12 $[M+H]^+$**.**

***N*-(2-(4-bromophenyl)-4-oxo-1,4-dihydroquinazolin-3(2*H*)-yl)pyrazine-2-carboxamide (T57):** White solid, Yield: 93%; m.p.: 237-238 ℃; ^{1}H-NMR (DMSO-D_6, 400 MHz, δ in ppm): 10.8204 (s, 1H), 9.0814 (s, 1H), 8.8737 (d, *J* = 1.60 Hz, 1H), 8.6902 (s, 1H), 7.6968 (t, *J* = 6.92 Hz, 2H), 7.5475 (m, *J* = 8.40 Hz, 4H), 7.3701 (s, 1H), 6.7959 (t, *J* = 7.84 Hz, 2H), 6.1735 (s, 1H); ^{13}C-NMR (DMSO-D_6, 100 MHz, δ in ppm): 162.97, 162.26, 148.75, 148.27, 147.76, 144.22, 143.71, 137.33, 134.32, 132.03, 131.21, 130.51, 129.25, 128.14, 122.52, 118.13, 114.75, 113.54, 74.18; ESI-MS (m/z) = 423.03 $[M+H]^+$.

***N*-(2-(4-fluorophenyl)-4-oxo-1,4-dihydroquinazolin-3(2*H*)-yl)pyrazine-2-carboxamide (T58):** White solid, Yield: 97%; m.p.: 203-204 ℃; ^{1}H-NMR (DMSO-D_6, 400 MHz, δ in ppm): 10.7723 (s, 1H), 9.0648 (s, 1H), 8.8669 (d, *J* = 2.20 Hz, 1H), 8.6834 (s, 1H), 7.7117 (d, *J* = 7.60 Hz, 1H), 7.6228 (m, *J* = 2.52 Hz, 2H), 7.3571 (t, *J* = 7.36 Hz, 2H), 7.7.1924 (t, *J* = 8.72 Hz, 2H), 6.8052 (m, *J* = 5.36 Hz, 2H), 6.1936 (s, 1H); ^{13}C-NMR (DMSO-D_6, 100 MHz, δ in ppm): 163.04, 162.08, 148.15, 147.87,

143.67, 143.60, 134.16, 134.01, 130.57, 130.49, 129.56, 129.47, 128.06, 117.98, 115.09, 114.87, 114.69, 113.56, 74.03; ESI-MS (m/z) = 363.11 $[M+H]^+$.

***N*-(2-(4-cyanophenyl)-4-oxo-1,4-dihydroquinazolin-3(2*H*)-yl)pyrazine-2-carboxamide (T59):** White solid, Yield: 96%; m.p.: 251-252 ℃; ^{1}H-NMR (DMSO-D_6, 400 MHz, δ in ppm): 10.9141 (s, 1H), 9.0860 (s, 1H), 8.8784 (d, *J* = 3.64 Hz, 1H), 8.7022 (d, *J* = 7.04 Hz, 1H), 7.8567 (d, *J* = 8.00 Hz, 2H), 7.7672 (d, *J* = 8.00 Hz, 2H), 7.7105 (d, *J* = 7.76 Hz, 1H), 7.4509 (s, 1H), 7.3613 (t, *J* = 7.36 Hz, 1H), 6.8037 (t, *J* = 4.72 Hz, 2H), 6.2544 (s, 1H); ^{13}C-NMR (DMSO-D_6, 100 MHz, δ in ppm): 162.57, 162.28, 148.27, 147.95, 147.47, 143.72, 143.66, 143.45, 143.35, 134.37, 132.89, 132.26, 129.19, 128.09, 127.90, 118.21, 114.75, 113.51, 111.89, 74.07; ESI-MS (m/z) = 370.12 $[M+H]^+$.

***N*-(2-(4-nitrophenyl)-4-oxo-1,4-dihydroquinazolin-3(2*H*)-yl)pyrazine-2-carboxamide (T60):** White solid, Yield: 91%; m.p.: 258-259 ℃; ^{1}H-NMR (DMSO-D_6, 400 MHz, δ in ppm): 10.9435 (s, 1H), 9.0906 (d, *J* = 1.12 Hz, 1H), 8.8722 (d, *J* = 2.44 Hz, 1H), 8.6877 (t, *J* = 2.04 Hz, 1H), 8.2270 (d, *J* = 8.72 Hz, 2H), 7.8565 (d, *J* = 8.68 Hz, 2H), 7.7284 (t, *J* = 6.96 Hz, 1H), 7.4976 (s, 1H), 7.3684 (m, *J* = 7.12 Hz, 1H), 6.8139 (m, *J* = 2.28 Hz, 2H), 6.3226 (s, 1H); ^{13}C-NMR (DMSO-D_6, 100 MHz, δ in ppm): 162.54, 162.35, 148.29, 148.04, 147.41, 145.28, 143.75, 143.66, 143.60, 134.43, 129.61, 128.31, 128.12, 124.21, 123.41, 118.27, 114.77, 113.48, 73.80; ESI-MS (m/z) = 390.11 $[M+H]^+$.

***N*-(4-oxo-2-(o-tolyl)-1,4-dihydroquinazolin-3(2*H*)-yl)pyrazine-2-carboxamide (T61):** White solid, Yield: 94%; m.p.: 205-206 ℃; ^{1}H-NMR (DMSO-D_6, 400 MHz, δ in ppm): 10.7143 (s, 1H), 9.0627 (s, 1H), 8.8590 (d, *J* = 1.60 Hz, 1H), 8.6771 (s, 1H), 7.7042 (d, *J* = 7.72 Hz, 1H), 7.4547 (d, *J* = 7.72 Hz, 2H), 7.3215 (t, *J* = 10.92 Hz, 2H), 7.1589 (d, *J* = 7.68 Hz, 2H), 6.8003 (t, *J* = 8.00 Hz, 2H), 6.1445 (s, 1H), 2.2596 (s, 3H); ^{13}C-NMR (DMSO-D_6, 100 MHz, δ in ppm): 163.18, 162.07, 148.11, 147.97, 143.76, 143.61, 140.32, 138.59, 134.84, 134.09, 129.54, 128.71, 128.20, 128.05, 127.32, 117.81, 114.66, 113.55, 74.55, 20.81; ESI-MS (m/z) = 359.14 $[M+H]^+$.

***N*-(4-oxo-2-(2-(trifluoromethyl)phenyl)-1,4-dihydroquinazolin-3(2*H*)-yl)pyrazine-2-carboxamide (T62):** White solid, Yield: 96%; m.p.: 128-129 ℃; ^{1}H-NMR (DMSO-D_6, 400 MHz, δ in ppm): 10.8271 (s, 1H), 9.0752 (s, 1H), 8.8621 (d, *J* = 2.12 Hz, 1H), 8.6718 (s, 1H), 8.2132 (d, *J* = 7.84 Hz, 1H), 7.7979 (d, *J* = 7.96 Hz, 1H), 7.7056 (m, *J* = 6.68 Hz, 2H), 7.6004 (d, *J* = 7.52 Hz, 1H), 7.3562 (t, *J* = 7.84 Hz, 2H), 6.80 (t, *J* = 6.92 Hz, 2H), 6.5630 (s, 1H); ^{13}C-NMR (DMSO-D_6, 100 MHz, δ in ppm): 162.97, 162.34, 148.27, 147.13, 144.31, 143.69, 143.65, 143.44, 137.30, 134.46, 132.91, 130.69, 129.69, 128.10, 127.10, 118.03, 114.44, 112.93; ESI-MS (m/z) = 413.11 $[M+H]^+$.

***N*-(2-(4-hydroxyphenyl)-4-oxo-1,4-dihydroquinazolin-3(2*H*)-yl)pyrazine-2-carboxamide (T63):** White solid, Yield: 91%; m.p.: 262-263 ℃; ^{1}H-NMR (DMSO-D_6, 400 MHz, δ in ppm): 10.6364 (s, 1H), 9.9845 (s, 1H), 9.5276 (s, 1H), 9.0477 (s, 1H), 8.8587 (d, *J* = 1.60 Hz, 1H), 7.6957 (d, *J* = 7.68 Hz, 1H), 7.5646 (d, *J* = 8.28 Hz, 2H), 7.3466 (m, *J* = 6.52 Hz, 3H), 7.2475 (s, 1H), 6.7055 (d, *J* = 8.24 Hz, 2H), 6.0766 (s, 1H); ^{13}C-NMR (DMSO-D_6, 100 MHz, δ in ppm): 163.30, 161.92, 150.10, 148.15, 144.02, 143.57, 143.27, 133.96, 129.66, 129.11, 128.03, 127.77, 125.10, 117.70, 115.77, 114.77, 114.77, 114.63, 113.57, 74.47; ESI-MS (m/z) = 361.12$[M+H]^+$.

***N*-(2-(5-bromo-2-hydroxyphenyl)-4-oxo-1,4-dihydroquinazolin-3(2*H*)-yl)pyrazine-2-carboxamide (T64):** White solid, Yield: 90%; m.p.: 231-232 ℃; ^{1}H-NMR (DMSO-D_6, 400 MHz, δ in ppm): 10.8862 (s, 1H), 10.0553 (s, 1H), 9.1195 (s, 1H), 8.8866 (d, *J* = 2.20 Hz, 1H), 8.7157 (s, 1H), 7.7059 (t, *J* = 2.32 Hz, 2H), 7.2931 (m, *J* = 8.64 Hz, 2H), 7.1874 (s, 1H), 6.7702 (m, *J* = 7.96 Hz, 3H), 6.4880 (s, 1H); ^{13}C-NMR (DMSO-D_6, 100 MHz, δ in ppm): 162.59, 162.03, 154.84, 148.06, 147.55, 143.98, 143.73, 143.60, 134.04, 132.32, 131.13, 127.93, 126.91, 117.63, 117.42, 114.57, 113.35, 109.93, 67.64; ESI-MS (m/z) = 439.03$[M+H]^+$.

***N*-(2-(3,4-dihydroxyphenyl)-4-oxo-1,4-dihydroquinazolin-3(2*H*)-yl)pyrazine-2-carboxamide (T65):** White solid, Yield: 92%; m.p.: 248-249 ℃; ^{1}H-NMR (DMSO-D_6, 400 MHz, δ in ppm): 10.6364 (s, 1H), 9.9845 (s, 1H), 9.5276 (s, 1H), 9.0477 (s, 1H), 8.8587 (d, *J* = 1.60 Hz, 1H), 8.6787 (s, 1H), 7.5646 (d, *J* = 8.28 Hz, 2H), 7.3466

(m, *J* = 6.52 Hz, 3H), 7.2475 (s, 1H), 6.7055 (d, *J* = 8.24 Hz, 2H), 6.0766 (s, 1H); ^{13}C-NMR (DMSO-D_6, 100 MHz, δ in ppm): 161.92, 159.68, 150.10, 148.15, 148.04, 147.69, 144.02, 143.57, 143.27, 133.96, 129.66, 129.11, 128.03, 127.77, 125.10, 117.70, 115.77, 114.77, 74.47; ESI-MS (m/z) = 377.11$[M+H]^+$.

***N*-(2-(isoquinolin-4-yl)-4-oxo-1,4-dihydroquinazolin-3(2*H*)-yl)pyrazine-2-carboxamide (T66):** White solid, Yield: 94%; m.p.: 267-268 ℃; ^{1}H-NMR (DMSO-D_6, 400 MHz, δ in ppm): 10.7971 (s, 1H), 9.3188 (s, 1H), 8.9702 (d, *J* = 5.76 Hz, 1H), 8.7859 (s, 1H), 8.6721 (s, 2H), 8.5533 (s, 1H), 8.1513 (d, *J* = 8.04 Hz, 1H), 7.7951 (d, *J* = 7.64 Hz, 2H), 7.6944 (t, *J* = 7.32 Hz, 1H), 7.5533 (s, 1H), 7.3830 (t, *J* = 7.56 Hz, 1H), 6.8445 (m, *J* = 7.72 Hz, 3H); ^{13}C-NMR (DMSO-D_6, 100 MHz, δ in ppm): 162.44, 162.15, 157.89, 148.22, 146.84, 146.29, 143.80, 143.69, 143.58, 134.39, 130.17, 128.95, 128.12, 128.07, 124.37, 124.01, 118.07, 114.64, 113.08; ESI-MS (m/z) = 396.13$[M+H]^+$.

***N*-(2-(2-chloro-6-methoxyquinolin-3-yl)-4-oxo-1,4-dihydroquinazolin-3(2*H*)-yl)pyrazine-2-carboxamide (T67):** White solid, Yield: 90%; m.p.: 254-255 ℃; ^{1}H-NMR (DMSO-D_6, 400 MHz, δ in ppm): 11.0568 (s, 1H), 9.1337 (s, 1H), 8.8764 (d, *J* = 2.00 Hz, 1H), 8.7877 (s, 1H), 8.6673 (s, 1H), 7.8571 (d, *J* = 9.08 Hz, 1H), 7.7608 (d, *J* = 7.72 Hz, 1H), 7.5556 (s, 1H), 7.4986 (d, *J* = 4.52 Hz, 2H), 7.3800 (t, *J* = 7.72 Hz, 1H), 6.8227 (t, *J* = 9.04 Hz, 2H), 6.7112 (s, 1H), 3.9026 (s, 3H); ^{13}C-NMR (DMSO-D_6, 100 MHz, δ in ppm): 162.44, 162.15, 157.89, 148.22, 146.84, 146.29, 143.80, 143.58, 143.00, 138.58, 134.60, 134.39, 130.17, 128.95, 128.12, 128.07, 124.01, 118.07, 114.64, 113.08, 106.30,71.17; ESI-MS (m/z) = 460.11$[M+H]^+$.

***N*-(4-oxo-2-(thiophen-2-yl)-1,4-dihydroquinazolin-3(2*H*)-yl)pyrazine-2-carboxamide (T68):** White solid, Yield: 92%; m.p.: 158-159 ℃; ^{1}H-NMR (DMSO-D_6, 400 MHz, δ in ppm): 10.8214 (s, 1H), 9.1044 (s, 1H), 8.8900 (d, *J* = 2.36 Hz, 1H), 8.7240 (d, *J* = 1.48 Hz, 1H), 7.7120 (d, *J* = 7.60 Hz, 1H), 7.6141 (s, 1H), 7.5377 (d, *J* = 4.96 Hz, 1H), 7.3722 (m, *J* = 7.20 Hz, 1H), 7.2090 (d, *J* = 3.28 Hz, 1H), 6.9417 (m, *J* = 1.16 Hz, 1H), 6.8436 (m, *J* = 7.56 Hz, 2H), 6.4453 (s, 1H); ^{13}C-NMR (DMSO-D_6, 100 MHz, δ in ppm): 162.40, 162.09, 148.11, 147.36, 143.84, 143.67, 141.28, 134.17,

128.18, 127.99, 127.25, 126.16, 118.27, 114.91, 113.76, 70.15; ESI-MS (m/z) = 351.08$[M+H]^+$.

2.2.2.17 General procedure for the synthesis of N-alkylindoline-2,3-dione (I9-I28):

In a clean, dry 50 mL round bottom flask, a mixture of indoline-2,3-dione (1.0 mmol), potassium iodide (1.1 mmol), potassium carbonate (1.1 mmol), the corresponding alkyl halide (1.1 mmol), and acetonitrile (10 mL) was taken. The mixture was then heated under reflux at 75 ℃ for 4 hours while observing the reaction's progress via thin-layer chromatography. Once the reaction was completed, the mixture was cooled to room temperature, and excess solvent was removed via a rotavapor. The resulting solution was poured into crushed ice. If the product precipitated, the solid was filtered, washed with cold water, dried, and further purified through recrystallization using methanol. In case no precipitation occurred, the suspension was treated by extraction with dichloromethane. The organic layer obtained was washed with water, dried, and subsequently purified by recrystallization using methanol (Shmidt et al. 2008).

2.2.2.18 General procedure for the synthesis of *N*'-(2-(2-aminophenyl)-2-oxoacetyl)pyrazine-2-carbohydrazide derivatives (T69-T88):

In a 50 mL round bottom flask, pyrazine-2-carbohydrazide (**3**) (1.0 mmol) and N-alkyl/acyl/aryl indoline-2,3-dione (**I1-I20**) (1.0 mmol) were mixed with a solvent system of acetonitrile and water (1.5:1 ratio, 15 mL). This mixture was stirred at room temperature for 15-16 hours while monitoring the reaction's progress using thin-layer chromatography. After completion, the mixture was poured into crushed ice. The resulting precipitate was filtered and washed five times with ice-cold water, and twice with ice-cold acetonitrile. The obtained compound underwent drying and purification through column chromatography using a mobile phase of ethyl acetate and petroleum ether (1:1 ratio) (Castelo-Branco et al. 2018).

***N*'-(2-(2-aminophenyl)-2-oxoacetyl)pyrazine-2-carbohydrazide (T69):** Yellow solid, Yield: 82%; m.p.: 211-212 ℃; ^{1}H-NMR (DMSO-D_6, 400 MHz, δ in ppm): 11.92

(s, 1H), 10.91 (s, 1H), 9.36 (s, 1H), 9.01 (s, 1H), 8.90 (s, 1H), 7.85 (s, 1H), 7.45 (s, 1H), 7.16 (s, 1H), 6.96 (d, *J* = 6.08 Hz, 1H), 6.19 (s, 2H); ^{13}C-NMR (DMSO-D_6, 100 MHz, δ in ppm): 193.89, 164.39, 148.76, 144.26, 144.14, 143.79, 133.42, 125.68, 122.72, 122.25, 121.26, 115.49, 111.27; HR-MS (m/z) = 286.0862 $[M+H]^+$.

***N*'-(2-(2-amino-5-fluorophenyl)-2-oxoacetyl)pyrazine-2-carbohydrazide (T70):** Orange solid, Yield: 85%; m.p.: 223-224 °C; ^{1}H-NMR (DMSO-D_6, 400 MHz, δ in ppm): 11.98 (s, 1H), 10.92 (s, 1H), 9.35 (s, 1H), 9.00 (s, 1H), 8.93 (s, 1H), 7.65 (d, *J* = 7.24 Hz, 1H), 7.34 (t, *J* = 8.36 Hz, 1H), 6.95 (dd, *J* = 3.96 Hz, 1H), 6.20 (s, 2H); ^{13}C-NMR (DMSO-D_6, 100 MHz, δ in ppm): 190.46, 164.39, 148.76, 144.26, 144.14, 143.79, 133.42, 125.68, 122.72, 122.25, 121.26, 115.49, 111.26; HR-MS (m/z) = 304.0767 $[M+H]^+$.

***N*'-(2-(2-amino-5-chlorophenyl)-2-oxoacetyl)pyrazine-2-carbohydrazide (T71):** Yellow solid, Yield: 83%; m.p.: 239-240 °C; ^{1}H-NMR (DMSO-D_6, 400 MHz, δ in ppm): 12.04 (s, 1H), 11.03 (s, 1H), 9.35 (s, 1H), 9.00 (s, 1H), 8.90 (s, 1H), 7.88 (s, 1H), 7.51 (d, *J* = 7.52 Hz, 1H), 6.97 (d, *J* = 7.76 Hz, 1H), 6.15 (s, 2H); ^{13}C-NMR (DMSO-D_6, 100 MHz, δ in ppm): 189.44, 162.15, 159.67, 148.77, 148.23, 144.33, 143.87, 134.40, 131.18, 130.01, 124.42, 123.36; HR-MS (m/z) = 320.0473 $[M+H]^+$.

***N*'-(2-(2-amino-5-bromophenyl)-2-oxoacetyl)pyrazine-2-carbohydrazide (T72):** Yellow solid, Yield: 85%; m.p.: 242-243 °C; ^{1}H-NMR (DMSO-D_6, 400 MHz, δ in ppm): 12.04 (s, 1H), 11.03 (s, 1H), 9.35 (s, 1H), 9.00 (s, 1H), 8.89 (s, 1H), 8.01 (s, 1H), 7.72 (s, 1H), 7.63 (d, *J* = 8.04 Hz, 1H), 6.40 (s, 2H); ^{13}C-NMR (DMSO-D_6, 100 MHz, δ in ppm): 189.35, 162.13, 159.65, 148.75, 148.21, 144.31, 143.85, 143.68, 137.26, 133.99, 124.74, 123.55, 115.02; HR-MS (m/z) = 363.9967 $[M+H]^+$.

***N*'-(2-(2-amino-5-methylphenyl)-2-oxoacetyl)pyrazine-2-carbohydrazide (T73):** Orange solid, Yield: 86%; m.p.: 267-268 °C; ^{1}H-NMR (DMSO-D_6, 400 MHz, δ in ppm): 11.90 (s, 1H), 11.21 (s, 1H), 9.34 (s, 1H), 8.98 (s, 1H), 8.84 (s, 1H), 7.45 (s, 1H), 7.20 (d, *J* = 7.08 Hz, 1H), 6.83 (d, *J* = 7.60 Hz, 1H), 6.47 (s, 2H), 2.30 (s, 3H); ^{13}C-NMR (DMSO-D_6, 100 MHz, δ in ppm): 189.35, 162.38, 159.65, 148.75, 148.21,

143.85, 143.68, 138.08, 136.26, 132.83, 124.74, 123.55, 115.02, 23.57; HR-MS (m/z) = 300.1019 $[M+H]^+$.

***N*'-(2-(2-(methylamino)phenyl)-2-oxoacetyl)pyrazine-2-carbohydrazide (T74):** Yellow solid, Yield: 89%; m.p.: 283-284 ℃; ^{1}H-NMR (DMSO-D_6, 400 MHz, δ in ppm): 11.97 (s, 1H), 11.25 (s, 1H), 9.36 (s, 1H), 9.00 (d, *J* = 2.04, 1H), 8.91 (s, 1H), 7.88 (d, *J* = 7.52, 1H), 7.55 (t, *J* = 7.72 Hz, 1H), 7.23 (t, *J* = 7.56 Hz, 1H), 7.16 (dd, *J* = 2.48 Hz, 1H), 6.77 (s, 1H), 3.20 (s, 3H); ^{13}C-NMR (DMSO-D_6, 100 MHz, δ in ppm): 187.00, 157.98, 150.39, 141.67, 139.99, 132.76, 132.29, 126.62, 119.25, 115.03, 114.29, 112.88, 111.02, 26.24; HR-MS (m/z) = 300.1018 $[M+H]^+$.

***N*'-(2-(5-fluoro-2-(methylamino)phenyl)-2-oxoacetyl)pyrazine-2-carbohydrazide (T75):** Orange solid, Yield: 81%; m.p.: 331-332 ℃; ^{1}H-NMR (DMSO-D_6, 400 MHz, δ in ppm): 12.05 (s, 1H), 10.92 (s, 1H), 9.36 (s, 1H), 9.00 (s, 1H), 8.93 (s, 1H), 7.73 (s, 1H), 7.44 (s, 1H), 7.19 (s, 1H), 6.95 (s, 1H), 3.21 (s, 3H); ^{13}C-NMR (DMSO-D_6, 100 MHz, δ in ppm): 189.99, 164.14, 158.91, 152.99, 147.39, 140.11, 134.12, 127.49, 123.87, 118.85, 112.39, 26.23; HR-MS (m/z) = 318.0925 $[M+H]^+$.

***N*'-(2-(5-chloro-2-(methylamino)phenyl)-2-oxoacetyl)pyrazine-2-carbohydrazide (T76):** Orange solid, Yield: 83%; m.p.: 257-258 ℃; ^{1}H-NMR (DMSO-D_6, 400 MHz, δ in ppm): 12.09 (s, 1H), 11.30 (s, 1H), 9.35 (s, 1H), 9.00 (s, 1H), 8.89 (s, 1H), 7.83 (dd, *J* = 1.84 Hz, 1H), 7.68 (d, *J* = 1.76 Hz, 1H), 7.12 (d, *J* = 8.28 Hz, 1H), 6.25 (s, 1H), 3.12 (s, 3H); ^{13}C-NMR (DMSO-D_6, 100 MHz, δ in ppm): 182.41, 157.98, 150.39, 141.67, 139.99, 132.76, 132.29, 126.62, 119.25, 115.03, 114.29, 112.88, 111.02, 26.24; HR-MS (m/z) = 334.0627 $[M+H]^+$.

***N*'-(2-(5-bromo-2-(methylamino)phenyl)-2-oxoacetyl)pyrazine-2-carbohydrazide (T77):** Orange solid, Yield: 84%; m.p.: 248-249 ℃; ^{1}H-NMR (DMSO-D_6, 400 MHz, δ in ppm): 12.09 (s, 1H), 11.25 (s, 1H), 9.36 (s, 1H), 9.00 (d, *J* = 1.80 Hz, 1H), 8.87 (s, 1H), 7.71 (t, *J* = 1.56 Hz, 1H), 7.59 (s, 1H), 7.17 (d, *J* = 8.32 Hz, 1H), 6.45 (s, 1H), 3.13 (s, 3H); ^{13}C-NMR (DMSO-D_6, 100 MHz, δ in ppm): 182.51, 162.99, 158.11, 149.99,

144.39, 137.12, 132.85, 127.49, 123.87, 118.85, 112.39, 26.23; HR-MS (m/z) = 378.0125 $[M+H]^+$.

***N*'-(2-(5-methyl-2-(methylamino)phenyl)-2-oxoacetyl)pyrazine-2-carbohydrazide (T78):** Orange solid, Yield: 82%; m.p.: 307-308 ℃; ^{1}H-NMR (DMSO-D_6, 400 MHz, δ in ppm): 11.97 (s, 1H), 11.21 (s, 1H), 9.36 (s, 1H), 9.00 (s, 1H), 8.93 (s, 1H), 7.73 (s, 1H), 7.51 (s, 1H), 7.33 (d, *J* = 9.00 Hz, 1H), 7.07 (s, 1H), 3.18 (s, 3H), 2.34 (s, 3H); ^{13}C-NMR (DMSO-D_6, 100 MHz, δ in ppm): 190.21, 168.99, 163.59, 162.24, 148.21, 143.87, 143.67, 137.56, 136.06, 133.06, 132.43, 121.33, 121.09, 24.46, 20.19; HR-MS (m/z) = 314.1175 $[M+H]^+$.

***N*'-(2-(2-(benzylamino)phenyl)-2-oxoacetyl)pyrazine-2-carbohydrazide (T79):** Yellow solid, Yield: 87%; m.p.: 225-226 ℃; ^{1}H-NMR (DMSO-D_6, 400 MHz, δ in ppm): 12.46 (s, 1H), 12.02 (s, 1H), 9.38 (s, 1H), 9.02 (s, 1H), 8.91 (s, 1H), 7.91 (d, *J* = 7.44 Hz, 1H), 7.46 (dd, *J* = 7.72 Hz, 1H), 7.41 (s, 1H), 7.30 (m, *J* = 6.4 Hz, 5H), 7.21 (d, *J* = 7.60 Hz, 1H), 7.09 (d, *J* = 7.68 Hz, 1H), 5.00 (s, 2H); ^{13}C-NMR (DMSO-D_6, 100 MHz, δ in ppm): 193.84, 163.34, 160.82, 148.82, 144.22, 144.19, 143.84, 136.03, 135.69, 133.23, 128.77, 127.30, 125.68, 123.43, 122.97, 121.15, 119.29, 115.15, 110.49, 42.77; HR-MS (m/z) = 376.1332 $[M+H]^+$.

***N*'-(2-(2-(benzylamino)-5-fluorophenyl)-2-oxoacetyl)pyrazine-2-carbohydrazide (T80):** Yellow solid, Yield: 83%; m.p.: 231-232 ℃; ^{1}H-NMR (DMSO-D_6, 400 MHz, δ in ppm): 12.08 (s, 1H), 11.29 (s, 1H), 9.37 (s, 1H), 9.01 (s, 1H), 8.93 (s, 1H), 7.73 (s, 1H), 7.53 (d, *J* = 7.08 Hz, 1H), 7.36 (m, *J* = 6.64 Hz, 6H), 7.09 (s, 1H), 5.01 (s, 2H); ^{13}C-NMR (DMSO-D_6, 100 MHz, δ in ppm): 192.02, 163.34, 160.82, 148.82, 144.31, 144.21, 144.19, 143.84, 143.10, 136.02, 133.23, 128.77, 127.60, 127.50, 127.30, 125.68, 122.97, 115.15, 110.49, 42.77; HR-MS (m/z) = 394.1237 $[M+H]^+$.

***N*'-(2-(2-(benzylamino)-5-chlorophenyl)-2-oxoacetyl)pyrazine-2-carbohydrazide (T81):** Yellow solid, Yield: 81%; m.p.: 217-218 ℃; ^{1}H-NMR (DMSO-D_6, 400 MHz, δ in ppm): 12.15 (s, 1H), 11.31 (s, 1H), 9.37 (d, *J* = 4.24 Hz, 1H), 9.01 (s, 1H), 8.90 (s, 1H), 7.95 (s, 1H), 7.68 (s, 1H), 7.36 (m, *J* = 7.52 Hz, 6H), 7.09 (d, *J* = 7.72 Hz, 1H),

5.01 (s, 2H); ^{13}C-NMR (DMSO-D_6, 100 MHz, δ in ppm): 190.50, 163.34, 160.82, 148.82, 144.21, 144.19, 143.84, 143.10, 136.02, 135.69, 133.23, 128.77, 127.60, 127.50, 127.30, 125.68, 122.97, 121.15, 115.15, 42.77; HR-MS (m/z) = 410.0940 $[M+H]^+$.

***N*'-(2-(2-(benzylamino)-5-bromophenyl)-2-oxoacetyl)pyrazine-2-carbohydrazide (T82):** Yellow solid, Yield: 80%; m.p.: 238-239 °C; ^{1}H-NMR (DMSO-D_6, 400 MHz, δ in ppm): 12.14 (s, 1H), 11.23 (s, 1H), 9.36 (s, 1H), 9.00 (s, 1H), 8.89 (s, 1H), 8.08 (s, 1H), 7.65 (d, *J* = 5.08 Hz, 1H), 7.34 (s, 6H), 7.04 (d, *J* = 6.96 Hz, 1H), 4.99 (s, 2H); ^{13}C-NMR (DMSO-D_6, 100 MHz, δ in ppm): 192.03, 163.34, 160.82, 148.82, 144.22, 144.19, 143.84, 136.03, 133.23, 132.04, 128.77, 127.60, 127.50, 127.30, 125.68, 123.43, 122.97, 119.29, 115.15, 42.77; HR-MS (m/z) = 454.0435 $[M+H]^+$.

***N*'-(2-(2-(benzylamino)-5-methylphenyl)-2-oxoacetyl)pyrazine-2-carbohydrazide (T83):** Yellow solid, Yield: 84%; m.p.: 272-273 °C; ^{1}H-NMR (DMSO-D_6, 400 MHz, δ in ppm): 12.01 (s, 1H), 11.23 (s, 1H), 9.37 (s, 1H), 9.01 (d, *J* = 4.64 Hz, 1H), 8.93 (s, 1H), 7.74 (s, 1H), 7.53 (s, 1H), 7.34 (m, *J* = 7.28 Hz, 6H), 6.97 (t, *J* = 8.04 Hz, 1H), 4.98 (s, 2H), 2.30 (s, 3H); ^{13}C-NMR (DMSO-D_6, 100 MHz, δ in ppm): 189.35, 162.38, 159.65, 148.75, 148.21, 143.85, 143.68, 143.28, 138.08, 137.26, 136.26, 133.99, 132.83, 132.03, 129.51, 125.14, 124.74, 123.55, 115.02, 23.57; HR-MS (m/z) = 390.1486 $[M+H]^+$.

***N*-(2-(2-oxo-2-(2-(pyrazine-2-carbonyl)hydrazineyl)acetyl)phenyl)acetamide (T84):** Yellow solid, Yield: 87%; m.p.: 263-264 °C; ^{1}H-NMR (DMSO-D_6, 400 MHz, δ in ppm): 11.05 (s, 1H), 10.98 (s, 1H), 10.72 (s, 1H), 9.24 (s, 1H), 8.94 (s, 1H), 8.80 (s, 1H), 8.19 (d, *J* = 7.40 Hz, 1H), 8.04 (d, *J* = 6.92 Hz, 1H), 7.70 (s, 1H), 7.31 (s, 1H), 2.17 (s, 3H); ^{13}C-NMR (DMSO-D_6, 100 MHz, δ in ppm): 192.07, 169.19, 163.50, 162.21, 148.23, 143.88, 143.70, 139.85, 135.50, 133.05, 125.62, 123.23, 121.38, 121.01, 24.53; HR-MS (m/z) = 328.0967 $[M+H]^+$.

***N*-(4-fluoro-2-(2-oxo-2-(2-(pyrazine-2-carbonyl)hydrazineyl)acetyl)phenyl) acetamide (T85):** Yellow solid, Yield: 85%; m.p.: 249-250 °C; ^{1}H-NMR (DMSO-D_6,

400 MHz, δ in ppm): 13.30 (s, 1H), 10.67 (s, 1H), 9.81 (s, 1H), 9.29 (s, 1H), 8.90 (s, 1H), 8.60 (s, 1H), 7.51 (dd, *J* = 3.08 Hz, 1H), 7.41 (t, *J* = 6.44 Hz, 1H), 7.33 (d, *J* = 6.44 Hz, 1H), 1.86 (s, 3H); ^{13}C-NMR (DMSO-D_6, 100 MHz, δ in ppm): 190.09, 168.16, 163.09, 159.64, 148.76, 144.32, 143.78, 143.29, 141.90, 133.19, 129.85, 125.61, 125.53, 116.69, 23.35; HR-MS (m/z) = 346.0871 $[M+H]^+$.

***N*-(4-chloro-2-(2-oxo-2-(2-(pyrazine-2-carbonyl)hydrazineyl)acetyl)phenyl) acetamide (T86):** Yellow solid, Yield: 82%; m.p.: 271-272 °C; ^{1}H-NMR (DMSO-D_6, 400 MHz, δ in ppm): 11.03 (s, 1H), 10.98 (s, 1H), 10.62 (s, 1H), 9.34 (s, 1H), 9.23 (s, 1H), 8.94 (d, *J* = 1.24 Hz, 1H), 8.80 (d, *J* = 1.16 Hz, 1H), 7.93 (d, *J* = 1.36 Hz, 1H), 7.50 (s, 1H), 2.16 (s, 3H); ^{13}C-NMR (DMSO-D_6, 100 MHz, δ in ppm): 189.44, 169.30, 162.42, 162.15, 148.77, 148.23, 143.87, 143.69, 137.72, 135.82, 134.40, 131.18, 130.01, 127.28, 24,17; HR-MS (m/z) = 362.0576 $[M+H]^+$.

***N*-(4-bromo-2-(2-oxo-2-(2-(pyrazine-2-carbonyl)hydrazineyl)acetyl)phenyl) acetamide (T87):** Yellow solid, Yield: 81%; m.p.: 252-253 °C; ^{1}H-NMR (DMSO-D_6, 400 MHz, δ in ppm): 11.03 (s, 1H), 10.98 (s, 1H), 10.62 (s, 1H), 9.23 (s, 1H), 8.94 (d, *J* = 1.24 Hz, 1H), 8.80 (d, *J* = 1.16 Hz, 1H), 8.03 (d, *J* = 1.92 Hz, 1H), 7.92 (d, *J* = 8.84 Hz, 1H), 7.87 (d, *J* = 1.92 Hz, 1H), 2.15 (s, 3H); ^{13}C-NMR (DMSO-D_6, 100 MHz, δ in ppm): 189.35, 169.27, 162.38, 162.13, 148.21, 143.88, 143.85, 143. 68, 137.26, 133.99, 132.83, 124.74, 123.55, 115.02, 24.18; HR-MS (m/z) = 406.0074 $[M+H]^+$.

***N*-(4-methyl-2-(2-oxo-2-(2-(pyrazine-2-carbonyl)hydrazineyl)acetyl)phenyl) acetamide (T88):** Yellow solid, Yield: 83%; m.p.: 296-297 °C; ^{1}H-NMR (DMSO-D_6, 400 MHz, δ in ppm): 11.03 (s, 1H), 10.96 (s, 1H), 10.62 (s, 1H), 9.25 (s, 1H), 8.94 (s, 1H), 8.80 (s, 1H), 8.08 (d, *J* = 8.20 Hz, 1H), 7.86 (s, 1H), 7.52 (d, *J* = 8.08 Hz, 1H), 2.35 (s, 3H), 2.15 (s, 3H); ^{13}C-NMR (DMSO-D_6, 100 MHz, δ in ppm): 192.22, 169.00, 163.60, 162.25, 148.21, 143.88, 143.68, 137.56, 136.07, 133. 07, 132.44, 121.34, 121.10, 24.46, 20.19; HR-MS (m/z) = 342.1124 $[M+H]^+$.

2.3 Results and Discussion

2.3.1 Synthesis and characterization of 1,3,4-oxadiazole/[1,2,4] triazolo[3,4-*b*][1,3,4]thiadiazine incorporated pyrazine derivatives (T1-T18)

The target compounds (**T1-T18**) were synthesized as outlined in **Scheme 2.1.** Initially, we treated commercially available pyrazine-2-carboxylic acid (**1**) with an excess of methanol in the presence of a catalytic amount of H_2SO_4. This reaction yielded the corresponding ester (**2**). Subsequently, the ester was subjected to further treatment with hydrazine hydrate, resulting in the formation of pyrazine-2-carbohydrazide (**3**). Compound 3 was then reacted with KOH and CS_2 to undergo cyclization, producing 5-(pyrazin-2-yl)-1,3,4-oxadiazole-2-thiol (**4**). Compounds **T1-T9** were synthesized by reacting compound 4 with commercially available phenacyl bromides. Compounds **T10-T18** were synthesized through the cyclization of compounds **T1-T9** in the presence of glacial acetic acid.

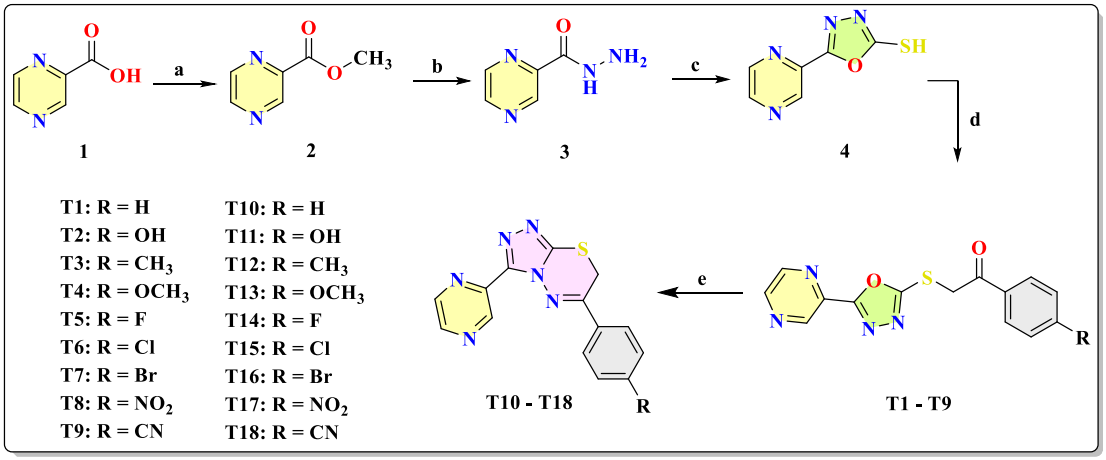

Scheme 2.1: Synthesis protocol for synthesizing title compounds (**T1-T18**). Reagents and conditions: **a)** CH_3OH, Conc. H_2SO_4, Reflux, 10 hours; **b)** CH_3OH, $N_2H_4.H_2O$, Reflux, 4 hours; **c)** CH_3OH, KOH, CS_2, 0 °C, Reflux, 16 hours; **d)** NaOH, aq. CH_3OH (80%), Phenacyl bromide derivatives, RT, 4 hours; **e)** $N_2H_4{\cdot}H_2O$, glacial CH_3COOH, Reflux, 3 hours.

The structure of the intermediates and target compounds (**T1-T18**) was confirmed by ^{1}H-NMR, ^{13}C-NMR, and mass spectral techniques. The ^{1}H-NMR spectrum of the compound **T7 (Figure 2.3)** showed one singlet and two doublet peaks at δ: 9.38, 8.71, and 8.70 ppm due to three aromatic protons of the pyrazine ring. The

presence of peaks in the region δ: 7.90-7.63 ppm is due to four aromatic protons of the phenyl ring, and the sharp singlet peaks at δ: 4.95 is due to the -CH_2 protons. The ^{13}C-NMR spectrum of compound **T7 (Figure 2.4)** displayed all characteristic peaks corresponding to its molecular structure. The peak at δ: 191.07 is due to carbonyl carbon, the peaks at δ: 166.21 and 163.50 ppm are due to the two carbons of the 1,3,4-oxadiazole ring, the peaks at δ: 146.72, 144.80, 144.13, and 139.40 ppm are due to the four carbons of pyrazine ring, the peaks at δ: 133.73, 132.57, 130.18, and 129.97 ppm are due to the six carbons of phenyl ring, the peaks at δ: 41.61 ppm is due to the -CH_2 carbon. The mass spectrum of the compound **T7 (Figure 2.5)** shows its molecular ion peak (M+H peak) at (m/z) 376.9630 thus confirming its molecular mass. Similarly, the ^{1}H-NMR spectrum of the compound **T17 (Figure 2.6)** displayed two singlet and one doublet peak at δ: 9.24, 8.88, and 8.84 ppm due to three aromatic protons of the pyrazine ring. The presence of two doublet peaks at δ: 8.40, and 8.22 ppm is due to four aromatic protons of the phenyl ring, and the sharp singlet peaks at δ: 4.55 are due to the -CH_2 protons. The ^{13}C-NMR spectrum of compound **T17 (Figure 2.7)** displayed all characteristic peaks corresponding to its molecular structure. The peak at δ: 166.93 is due to -C=N of 1,3,4-thiadiazine ring. The disappearance of the carbonyl carbon peak confirms the cyclization. The peaks at δ: 164.80 and 162.96 ppm are due to the two carbons of the 1,2,4-triazole ring, the peaks at δ: 150.21, 146.90, 144.92, and 143.35 ppm are due to the four carbons of pyrazine ring, the peaks at δ: 139.54, 138.53, 129.85, and 123.88 ppm are due to the six carbons of phenyl ring, the peak at δ: 22.61 ppm is due to the -CH_2 carbon. The mass spectrum of the compound **T17 (Figure 2.8)** shows its molecular ion peak (M+H peak) at (m/z) 340.0538 thus confirming its molecular mass.

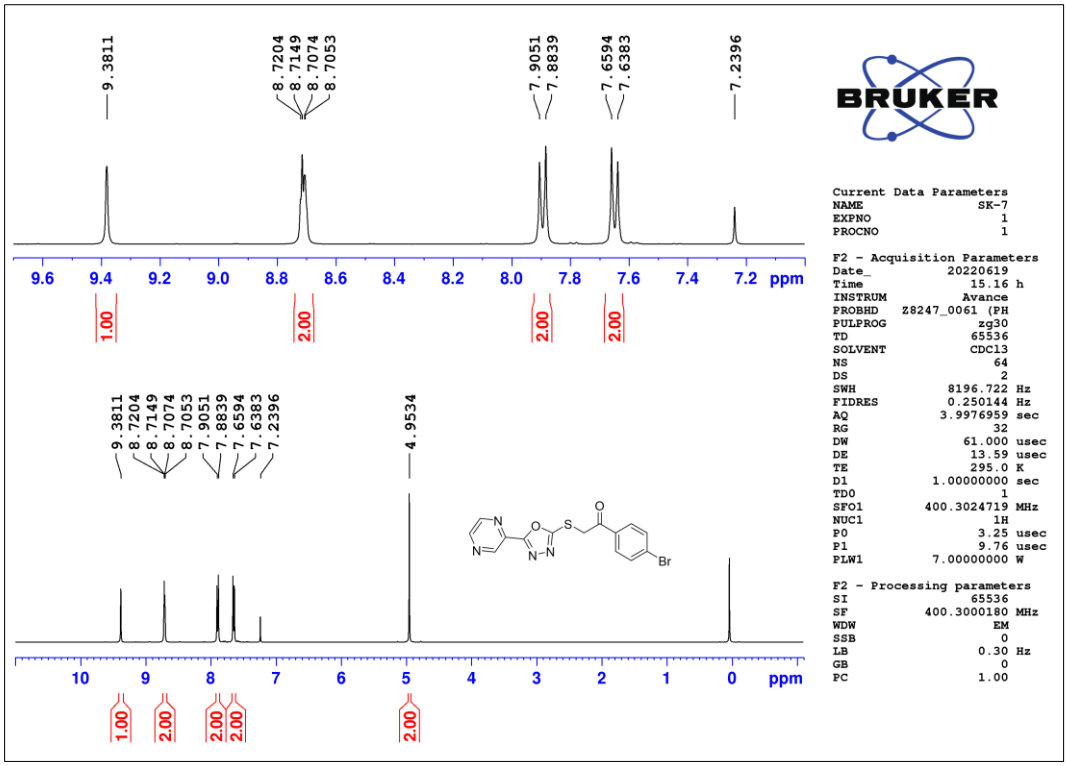

Figure 2.3 *^{1}H-NMR spectrum of compound* ***T7***

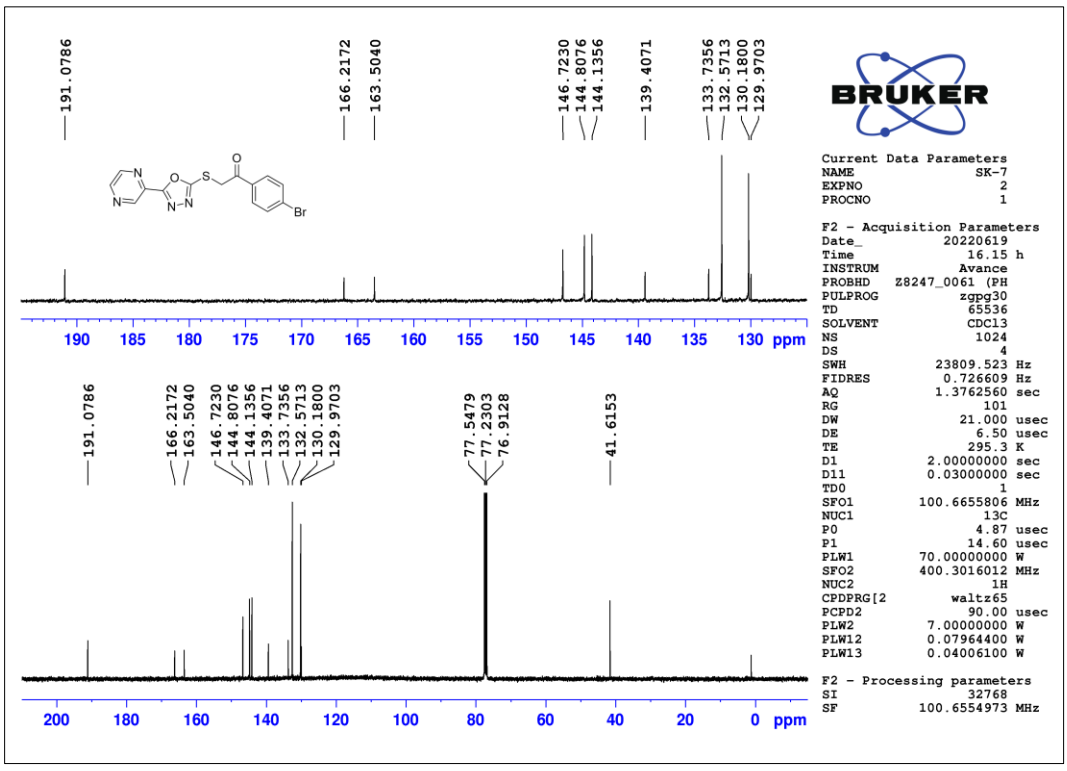

Figure 2.4 *^{13}C-NMR spectrum of compound* ***T7***

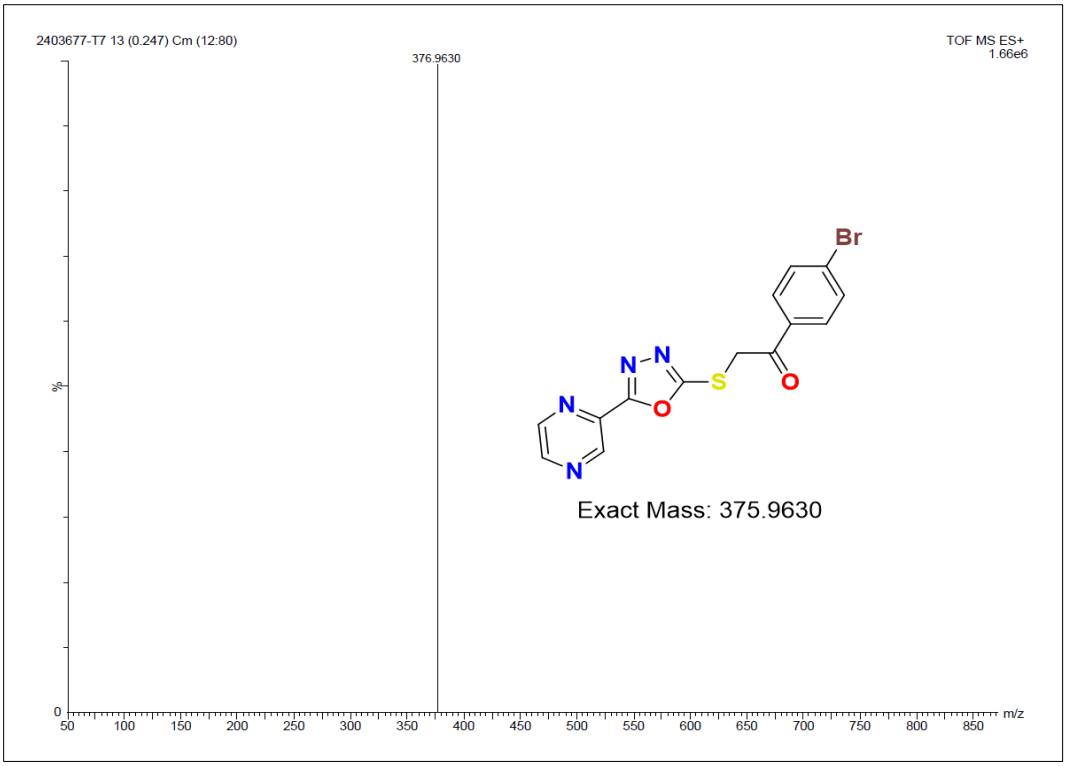

Figure 2.5 *HR-MS spectrum of compound* ***T7***

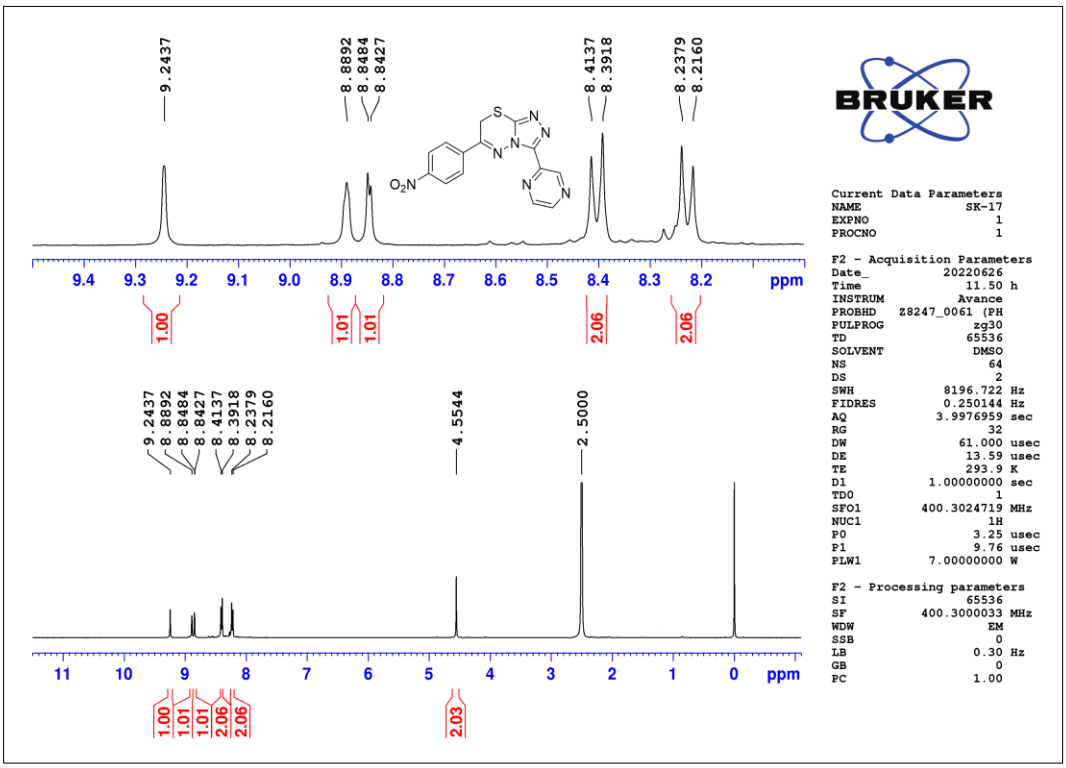

Figure 2.6 *^{1}H-NMR spectrum of compound* ***T17***

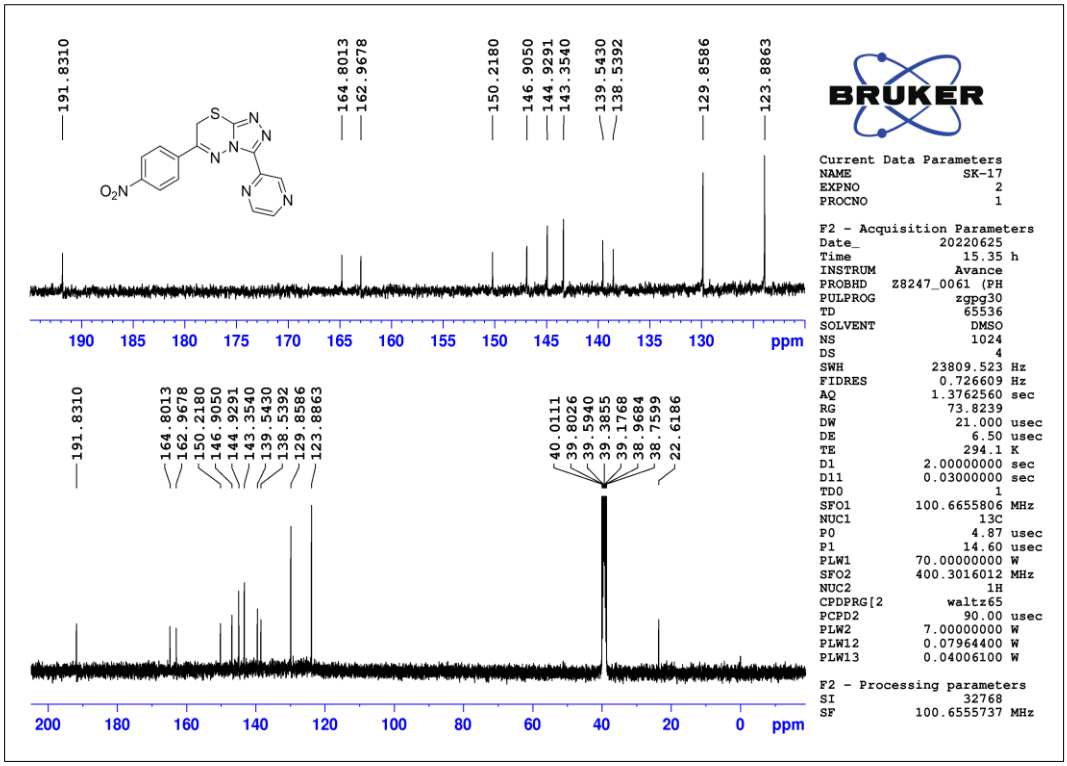

Figure 2.7 *^{13}C-NMR spectrum of compound* ***T17***

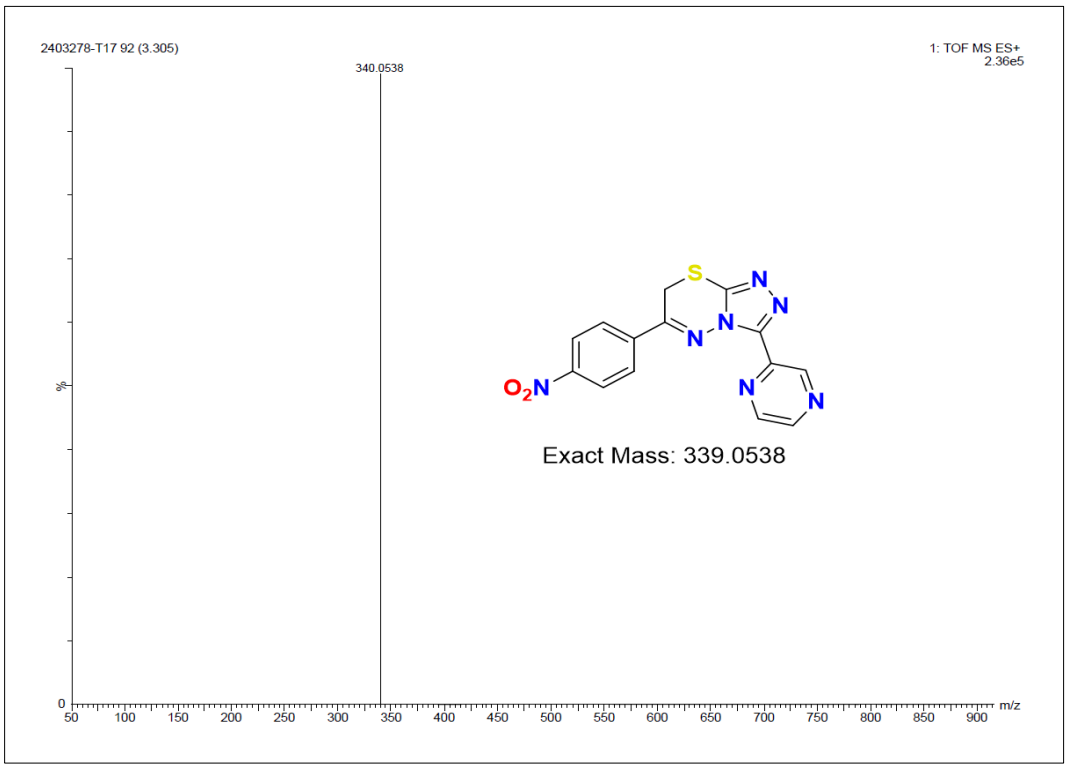

Figure 2.8 *HR-MS spectrum of compound* ***T17***

2.3.2 Synthesis and characterization of 1,2,4-triazole incorporated pyrazine derivatives (T19-T36)

The designed compounds (**T19-T36**) were synthesized as outlined in **Scheme 2.2.** The process started with the reaction of readily available pyrazine-2-carbonitrile (**5**) with hydrazine hydrate in the presence of methanol, yielding (Z)-pyrazine-2-carbohydrazonamide (**6**). Subsequently, compound 6 underwent cyclization when treated with KOH and CS_2, resulting in the formation of 5-(pyrazin-2-yl)-4*H*-1,2,4-triazole-3-thiol (**7**). Compounds **T19-T27** were synthesized by reacting compound 7 with commercially accessible phenacyl bromides, while compounds **T28-T36** were synthesized by reacting compound **7** with commercially available substituted benzyl bromides.

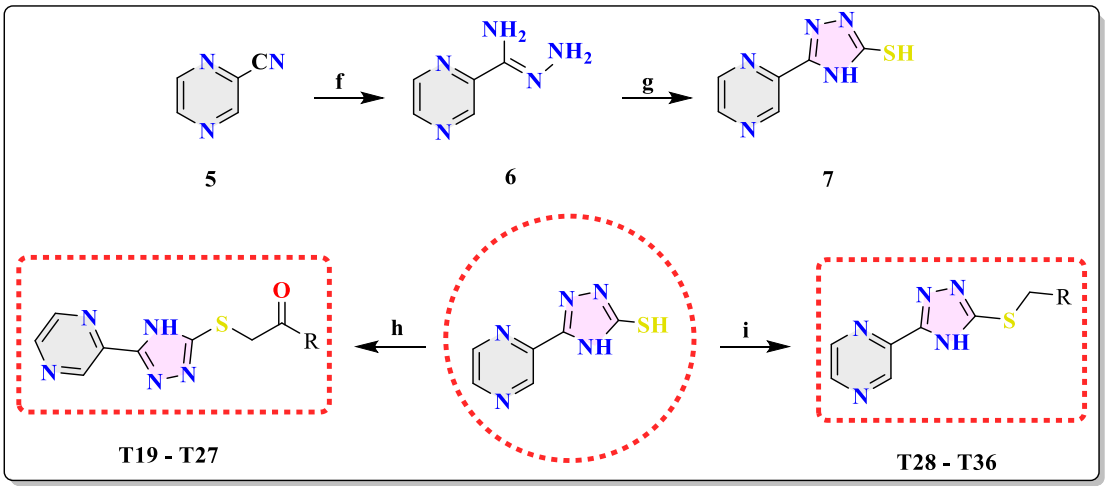

Scheme 2.2: Synthesis protocol for synthesizing target compounds (**T19-T36**). Reagents and conditions: **f)** $N_2H_4 \cdot H_2O$, CH_3OH, RT, 24 hours; **g)** CS_2, KOH, CH_3OH, reflux, 24 hours; **h)** Phenacyl bromide derivatives, 10% NaOH, CH_3OH, RT, 6 hours; **i)** Benzyl bromide derivatives, K_2CO_3, acetone, reflux, 2 hours.

Table 2.1 *Structural details of the target compounds (**T19-T36**)*

Compound Code	R	Compound Code	R

T19, T28	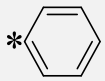	**T25, T30**	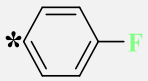
T20	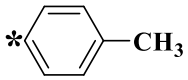	**T26, T35**	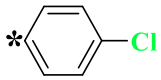
T21	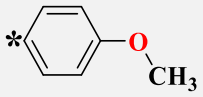	**T27, T33**	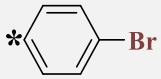
T22	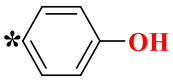	**T29**	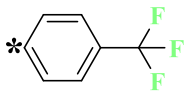
T23, T36	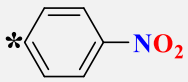	**T31**	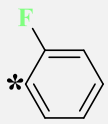
T24, T32	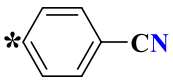	**T34**	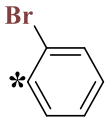

(The symbol '*' denotes the point of attachment)

The validation of the intermediates and target compounds (**T19-T36**) involved a combination of analytical techniques, including ^{1}H-NMR, ^{13}C-NMR, and mass spectrometry. The ^{1}H-NMR spectrum of compound **T22 (Figure 2.9)** showed two singlet peaks at δ: 12.98 and 10.57 ppm, corresponding to the -NH proton of the 1,2,4-triazole and the -OH proton, respectively. The pyrazine ring's three aromatic protons were observed with two singlet peaks at δ: 9.30 and 8.85 ppm and one doublet peak at δ: 8.84 ppm. Additionally, two doublet peaks at δ: 7.94 and 6.90 ppm indicated the presence of four aromatic protons from the phenyl ring. Finally, a sharp singlet peak at δ: 5.13 ppm was attributed to the -CH_2 protons. The ^{13}C-NMR spectrum of compound **T22 (Figure 2.10)** showed characteristic peaks corresponding to its molecular structure. The peaks at δ: 190.28 and 165.39 ppm were assigned to the carbonyl carbon and the carbon attached to the hydroxy group respectively. The two carbons of the

1,2,4-triazole were denoted by peaks at δ: 162.90 and 162.87 ppm. The four carbons of the pyrazine ring were represented by peaks at δ: 146.95, 145.02, 143.43, and 138.69 ppm. Five carbons from the phenyl ring were identified by three peaks at δ: 131.21, 126.43, and 115.48 ppm. Furthermore, a peak at δ: 38.88 ppm confirmed the presence of $-CH_2$ carbon. The molecular mass of compound **T22 (Figure 2.11)** was unambiguously confirmed through the mass spectrum, revealing a molecular ion peak (M+H peak) observed at (m/z) 314.06. Similarly, the ^{1}H-NMR spectrum of compound **T29 (Figure 2.12)** presented a singlet peak at δ: 12.97 ppm, signifying the -NH proton of the 1,2,4-triazole. The three aromatic protons within the pyrazine ring manifested as two doublet peaks at δ: 9.39 and 8.81 ppm, along with one triplet peak at δ: 8.77 ppm. In the region of δ: 7.73 - 7.67 ppm, four aromatic protons originating from the phenyl ring were detected. Additionally, a distinct sharp singlet peak at δ: 4.76 ppm represents the presence of $-CH_2$ protons. In the ^{13}C-NMR spectrum of compound **T29 (Figure 2.13)**, characteristic peaks aligned with its molecular structure. Peaks at δ: 168.19 and 162.49 ppm were assigned to two carbons of the 1,2,4-triazole. The four carbons of the pyrazine ring were represented by peaks at δ: 160.02, 145.89, 144.90, and 144.36 ppm. Furthermore, the phenyl ring contributed five peaks in the range of δ: 142.46 to 130.11 ppm, reflecting the presence of six carbon atoms. Peaks at δ: 115.63 and 36.59 ppm were attributed to the $-CF_3$ and $-CH_2$ carbons, respectively. The molecular mass of compound **T29 (Figure 2.14)** was conclusively confirmed through mass spectrometry, revealing the presence of the molecular ion peak (M+H peak) at (m/z) 338.18, thus validating its molecular weight.

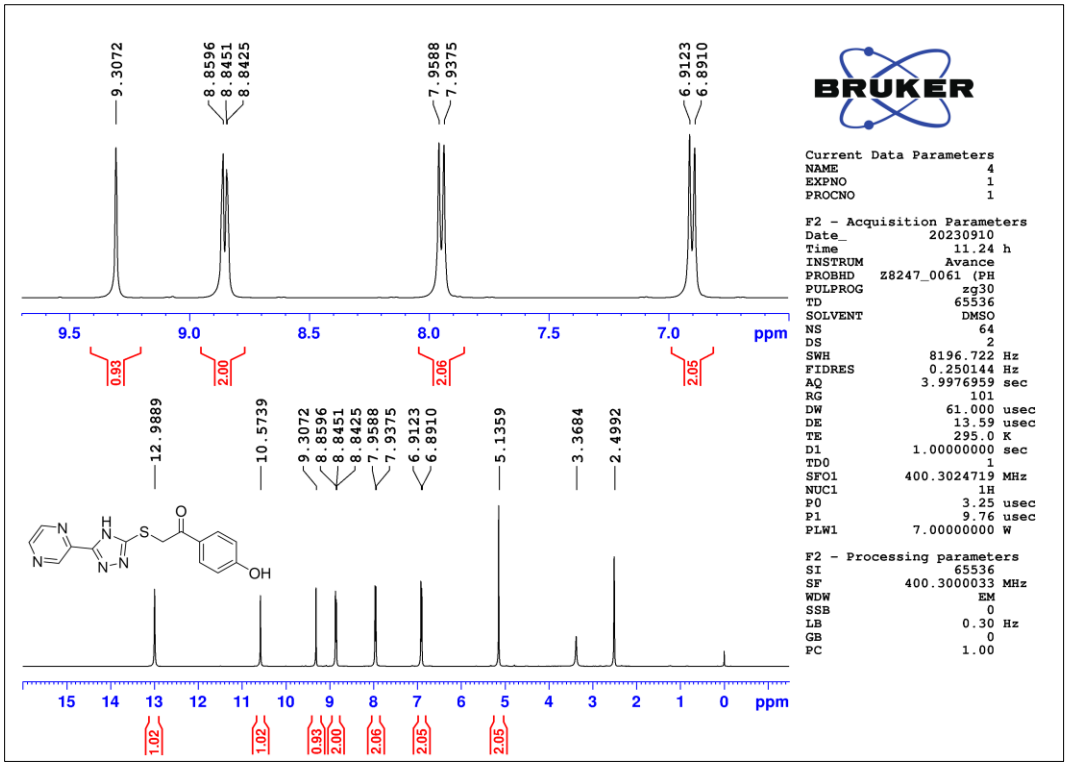

Figure 2.9 *[1]H-NMR spectrum of compound* ***T22***

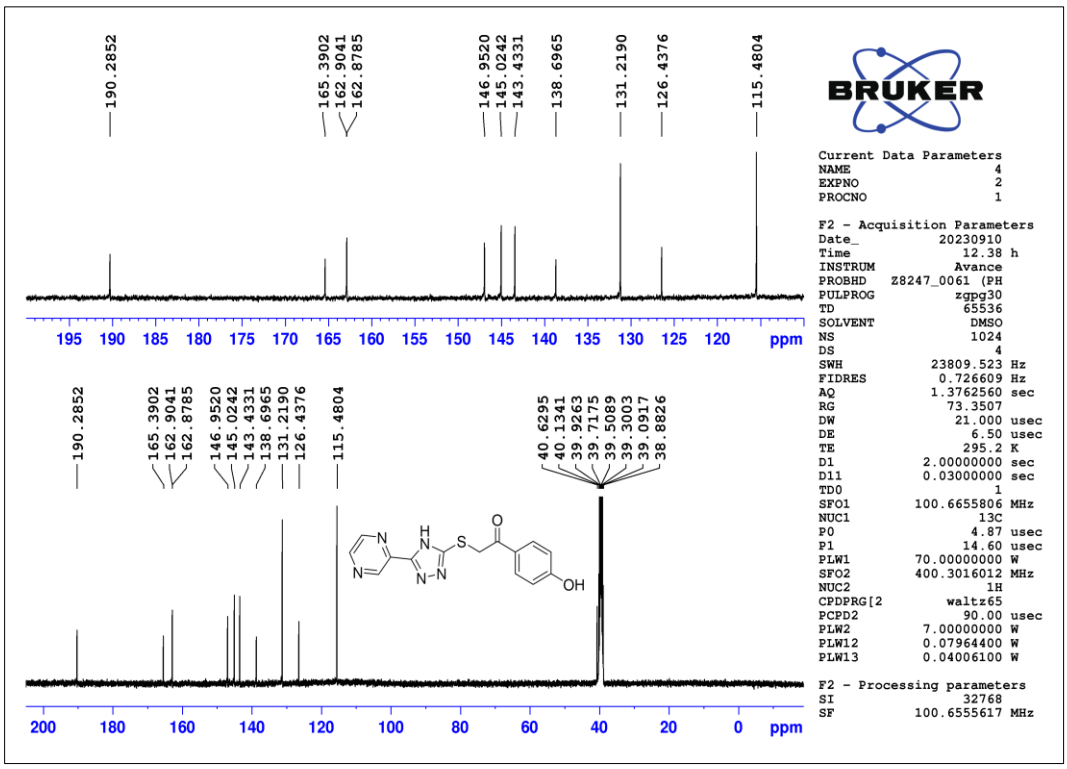

Figure 2.10 *[13]C-NMR spectrum of compound* ***T22***

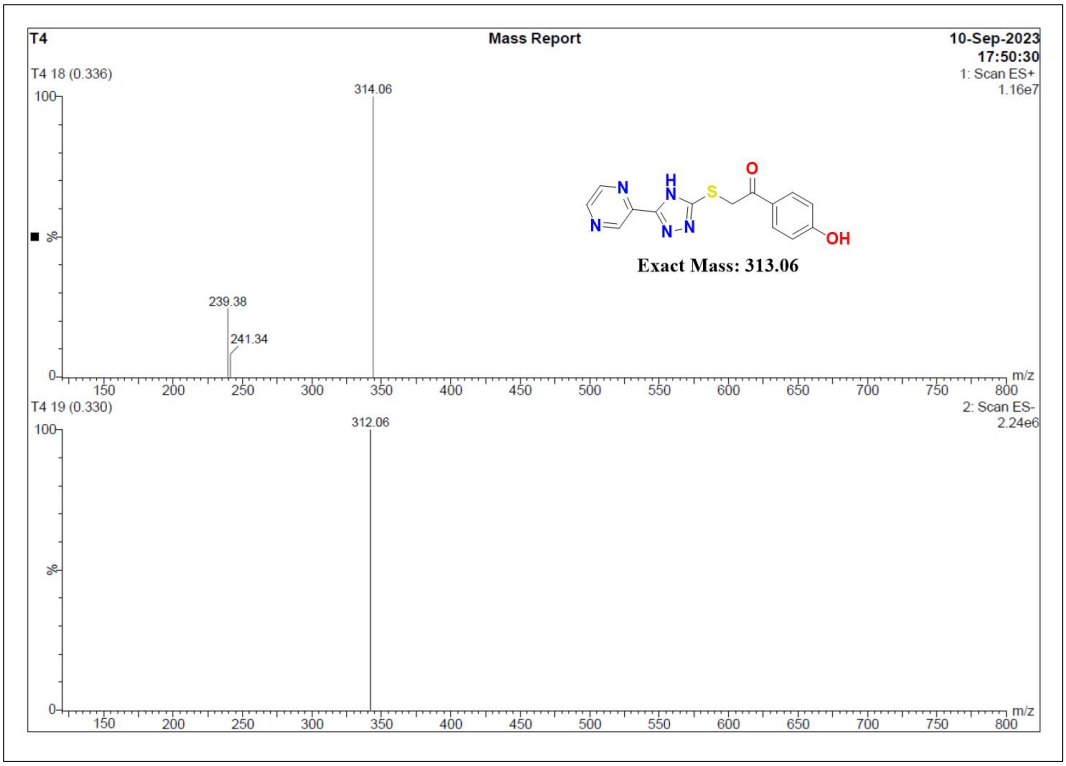

Figure 2.11 *ESI-MS spectrum of compound* ***T22***

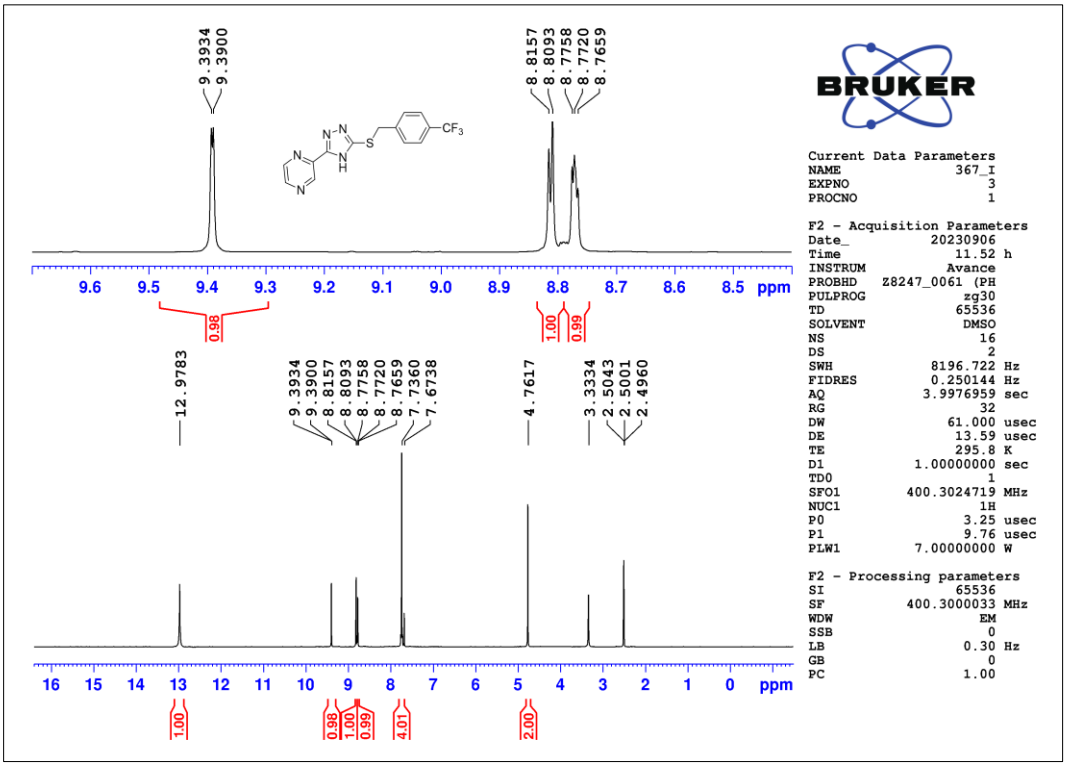

Figure 2.12 *[1]H-NMR spectrum of compound* ***T29***

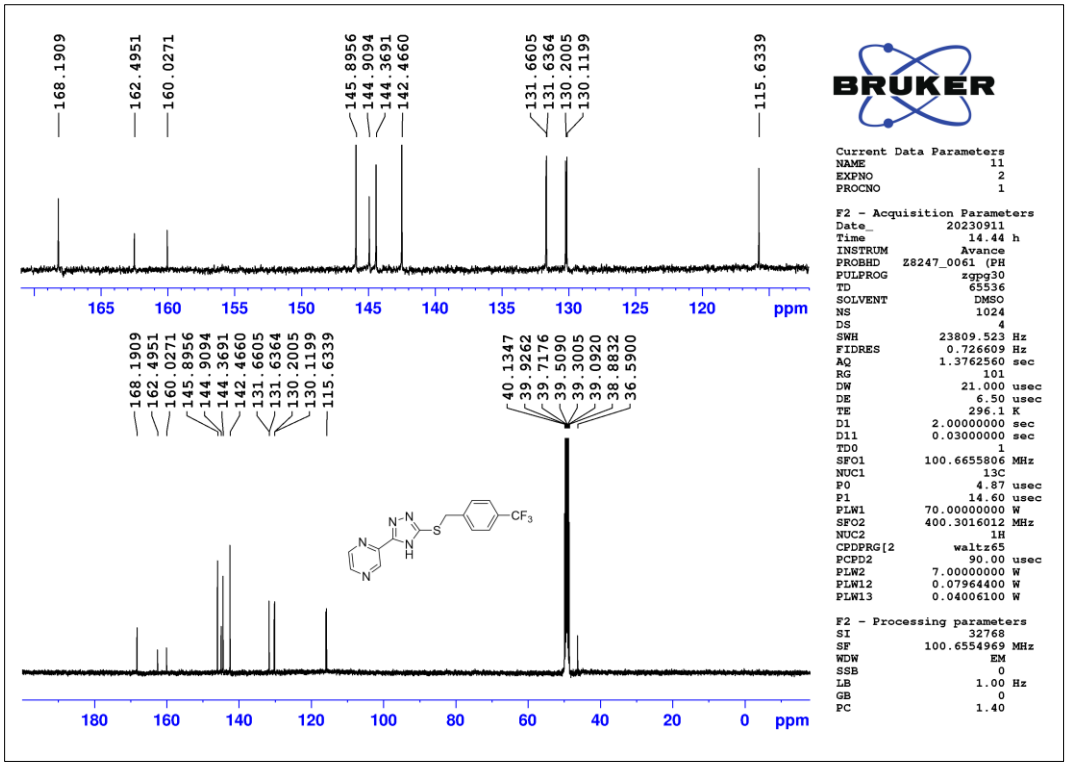

Figure 2.13 *^{13}C-NMR spectrum of compound* ***T29***

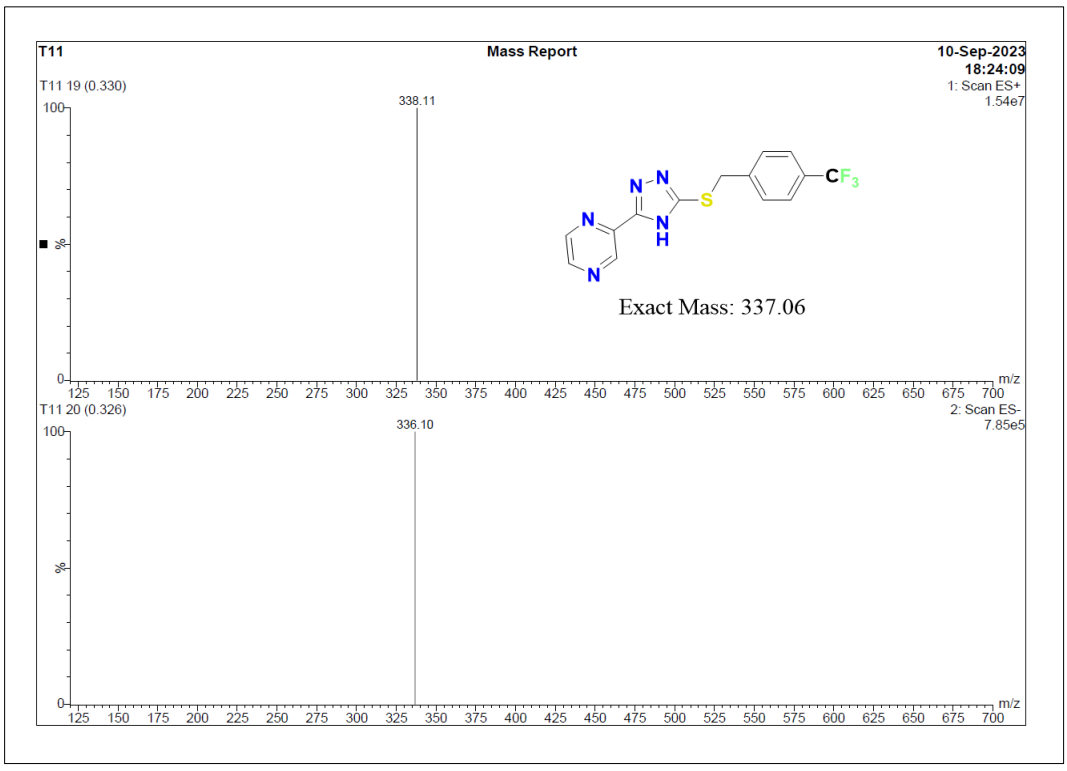

Figure 2.14 *ESI-MS spectrum of compound* ***T29***

2.3.3 Synthesis and characterization of pyrazine hydrazinylidene derivatives containing benzenesulfonate scaffold (T37-T52)

The target molecules (**T37-T52**) were synthesized following the synthetic routes outlined in **Scheme 2.3**. To begin, we utilized commercially available benzenesulfonyl chlorides and subjected them to a reaction with 4-hydroxybenzaldehyde, resulting in the formation of the corresponding sulfonate compounds (**I1-I8**). To synthesize compounds **T37-T44**, we reacted compound 3 with the previously obtained sulfonates (**I1-I8**). Similarly, compounds **T45-T52** were synthesized by treating compound 6 with the same set of sulfonates (**I1-I8**).

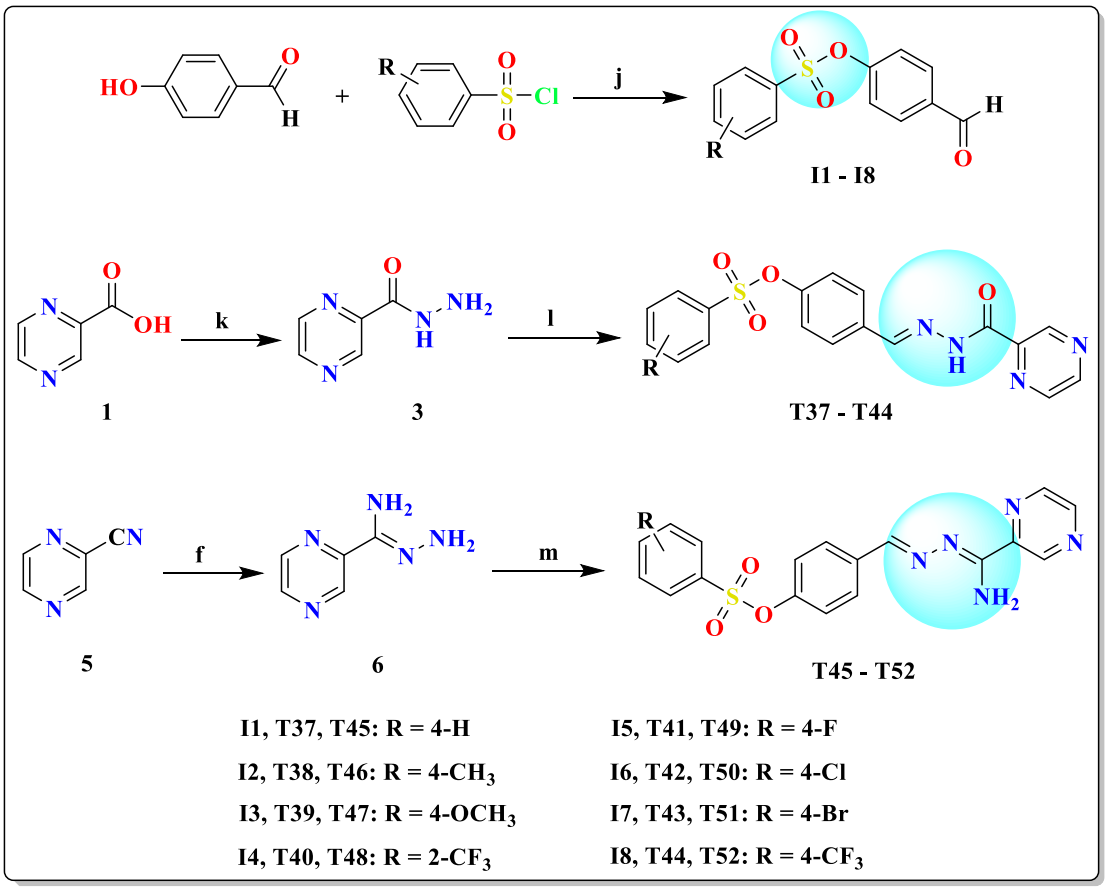

Scheme 2.3: Synthesis protocol for synthesizing title compounds (**T37-T52**). Reagents and conditions: **j)** THF, TEA, 0 °C - RT (30 min), Reflux, 3-4 hours; **k)** CH_3OH, Conc. H_2SO_4, $N_2H_4{\cdot}H_2O$, Reflux, 15 hours; **l)** I1-I8, CH_3OH, CH_3COOH, Reflux, 3 hours; **f)** CH_3OH, $N_2H_4{\cdot}H_2O$, RT, 24 hours; **m)** I1-I8, CH_3OH, CH_3COOH, Reflux, 3 hours.

The structure of the intermediates and target compounds (**T37-T52**) was confirmed by ^{1}H-NMR, ^{13}C-NMR, and mass spectral techniques. The ^{1}H-NMR spectrum of the compound **T40 (Figure 2.15)** displayed a singlet peak at δ: 12.38 ppm due to -NH proton, one singlet, and two doublet peaks at δ: 9.26, 8.93, and 8.79 ppm respectively due to three aromatic protons of the pyrazine ring and peaks in the region δ: 8.62 - 7.15 ppm are due to eight aromatic protons of the phenyl ring. The ^{13}C-NMR spectrum of compound **T40 (Figure 2.16)** displayed all characteristic peaks corresponding to its molecular structure. The peak at δ: 159.62 is due to carbonyl carbon, the peaks at δ: 149.69 and 148.20 ppm are due to the -C-O- and -C=N- carbons respectively, the peaks at δ: 147.92, 144.50, 144.17, and 143.32 ppm are due to the four carbons of pyrazine ring, the eight peaks in the region δ: 135.94 to 123.73 ppm are due to the eight carbons of the two phenyl rings, the peak at δ: 122.50 ppm is due to the -CF_3 carbon. The mass spectrum of the compound **T40 (Figure 2.17)** shows its molecular ion peak (M+H peak) at (m/z) 451.0609 thus confirming its molecular mass. Similarly, the ^{1}H-NMR spectrum of the compound **T48 (Figure 2.18)** displayed two singlet and one doublet peak at δ: 9.37, 8.78, and 8.73 ppm respectively due to three aromatic protons of the pyrazine ring. The presence of a sharp singlet peak at δ: 8.49 ppm is due to -HC=N- proton, the peaks in the region δ: 8.22 - 7.10 ppm are due to the eight aromatic protons two phenyl rings, the presence of a broad singlet peak at δ: 7.30 ppm is due to -NH_2 protons. The ^{13}C-NMR spectrum of compound **T48 (Figure 2.19)** displayed all characteristic peaks corresponding to its molecular structure. The peak at δ: 155.81 is due to H_2N-C=N carbon, the peaks at δ: 153.27 and 149.61 ppm are due to the -C-O- and -C=N- carbons respectively, the peaks at δ: 145.97, 145.81, 143.38, and 143.05 ppm are due to the four carbons of pyrazine ring, the eight peaks in the region δ: 135.89 to 123.74 ppm are due to the eight carbons of the two phenyl rings and the peak at δ: 122.09 ppm is due to the -CF_3 carbon. The mass spectrum of the compound **T48 (Figure 2.20)** shows its molecular ion peak (M+H peak) at (m/z) 450.0769 thus confirming its molecular mass.

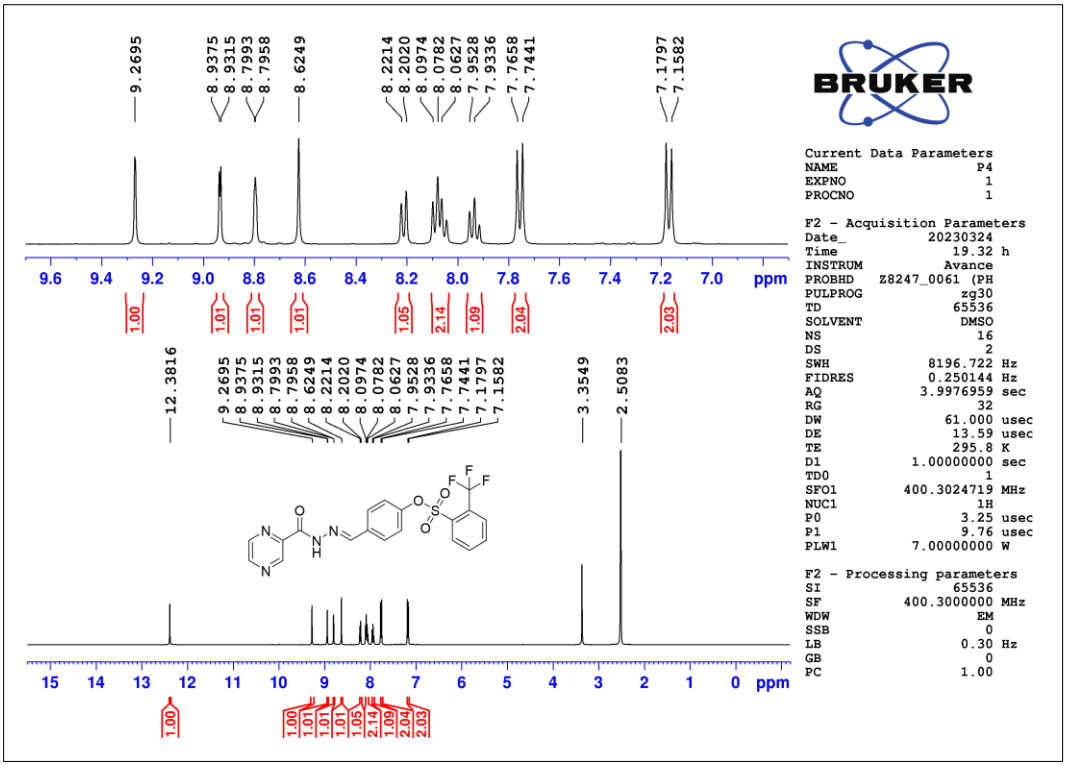

Figure 2.15 *^{1}H-NMR spectrum of compound* ***T40***

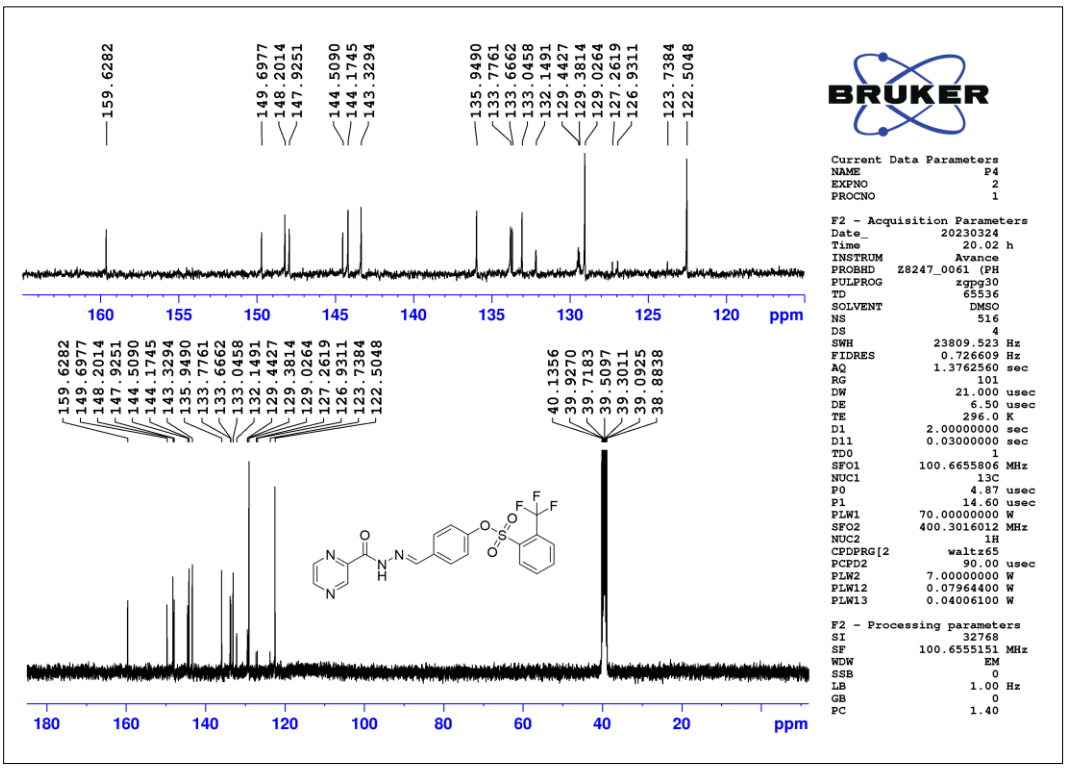

Figure 2.16 *^{13}C-NMR spectrum of compound* ***T40***

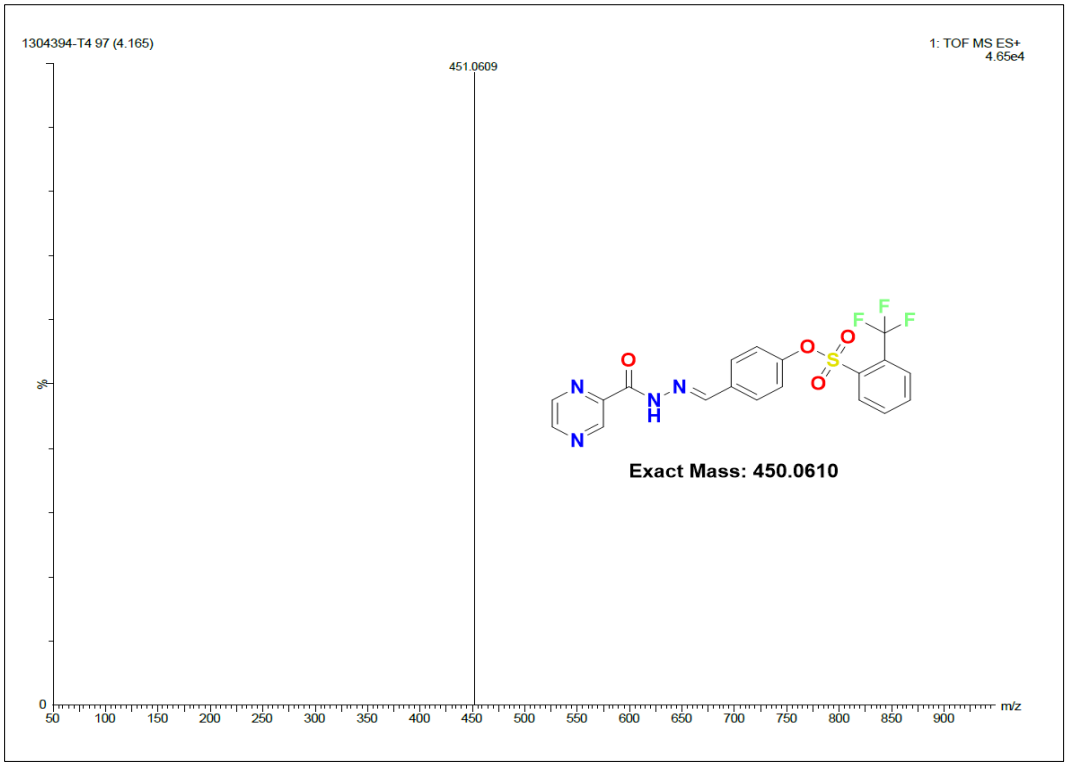

Figure 2.17 *HR-MS spectrum of compound* ***T40***

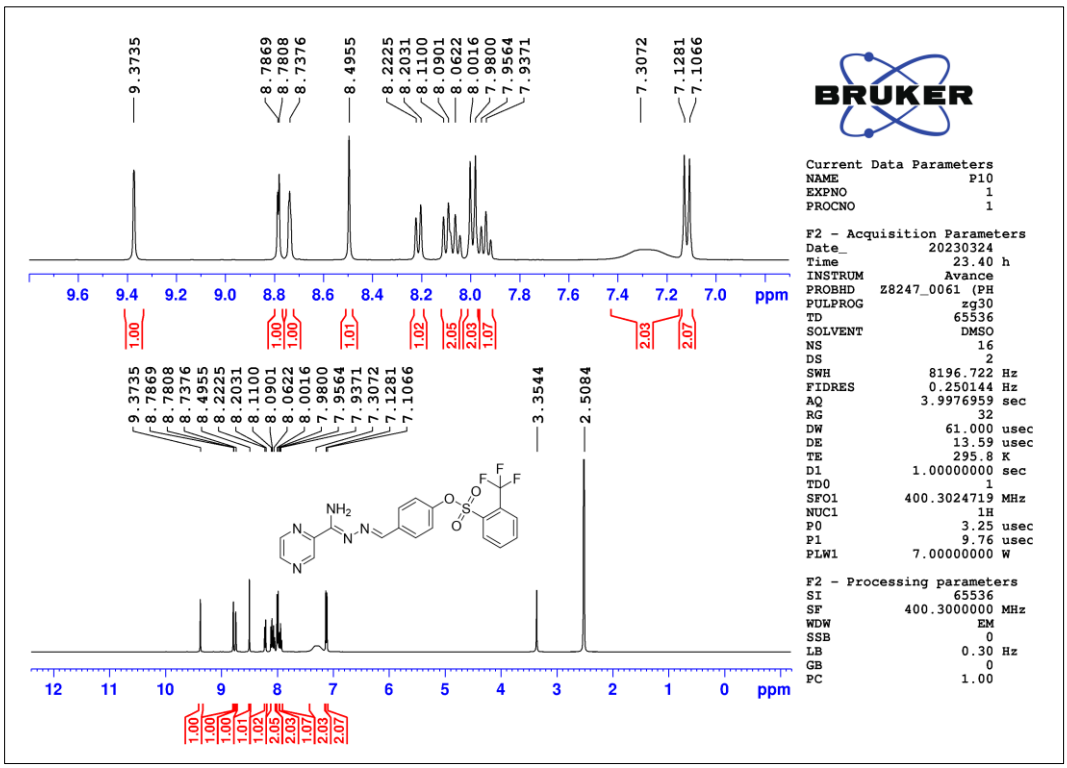

Figure 2.18 *^{1}H-NMR spectrum of compound* ***T48***

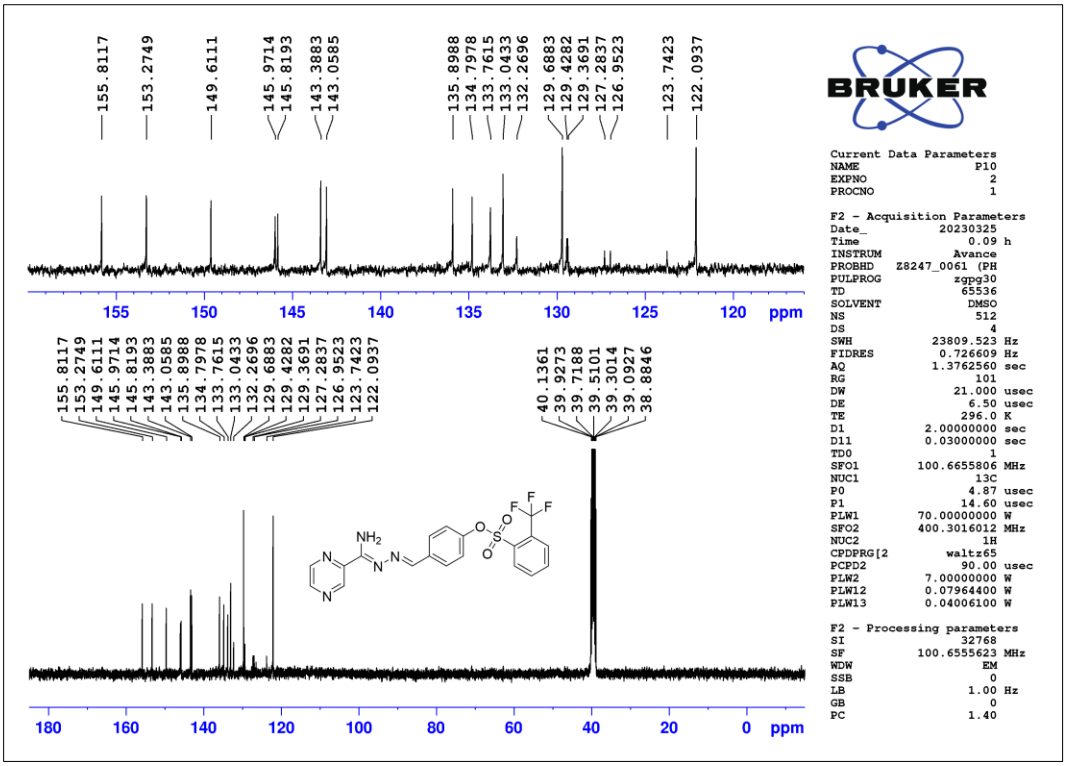

Figure 2.19 *^{13}C-NMR spectrum of compound* ***T48***

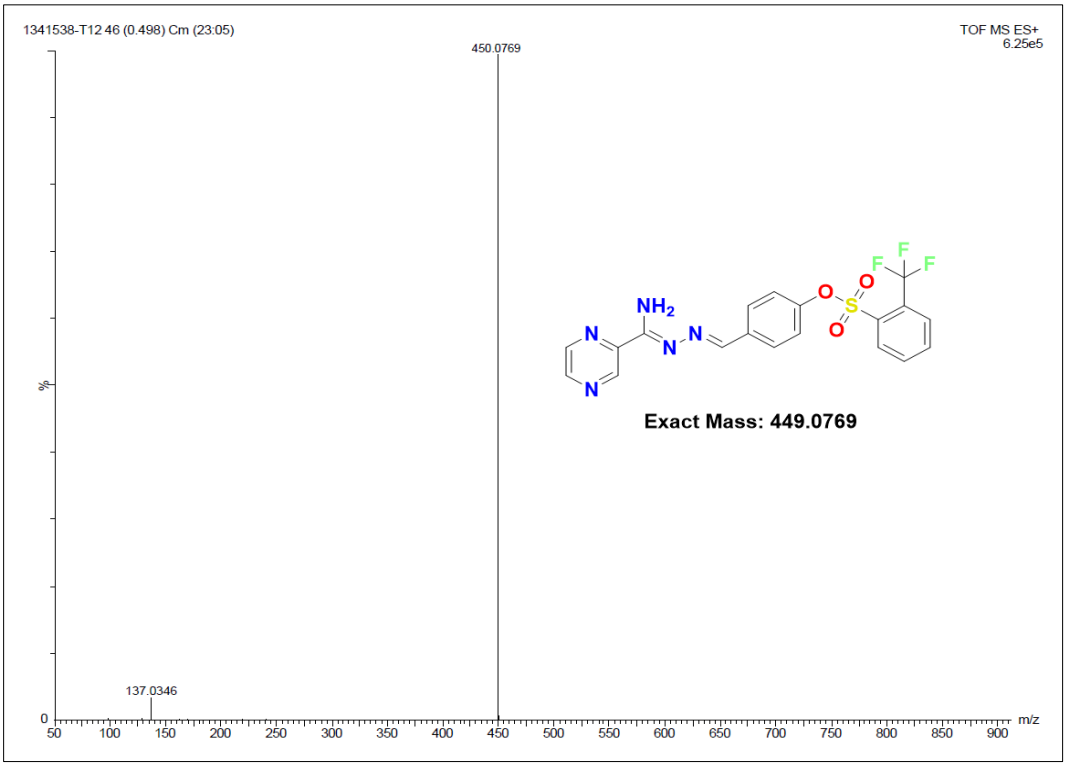

Figure 2.20 *HR-MS spectrum of compound* ***T48***

2.3.4 Synthesis and characterization of 4-quinazolinone incorporated pyrazine derivatives (T53-T68)

The target compounds (**T53-T68**) were synthesized following the synthetic pathways outlined in **Scheme 2.4.** We initiated the process by treating compound 3 with readily available isatoic anhydride, yielding *N*-(2-aminobenzoyl)pyrazine-2-carbohydrazide (**T53**). Compound **T53** was subjected to reaction with CS_2 and KOH yielding *N*-(4-oxo-2-thioxo-1,4-dihydroquinazolin-3(2*H*)-yl)pyrazine-2-carboxamide (**T54**). Compound **T54** was subsequently treated with hydrazine hydrate, leading to the formation of 3-amino-2-(pyrazin-2-yl)-[1,2,4]triazolo[5,1-*b*]quinazolin-9(3*H*)-one (**T55**). Compounds **T56-T68** were synthesized by reacting compound **T53** with commercially available substituted aromatic aldehydes in the presence of a catalytic quantity of glacial acetic acid.

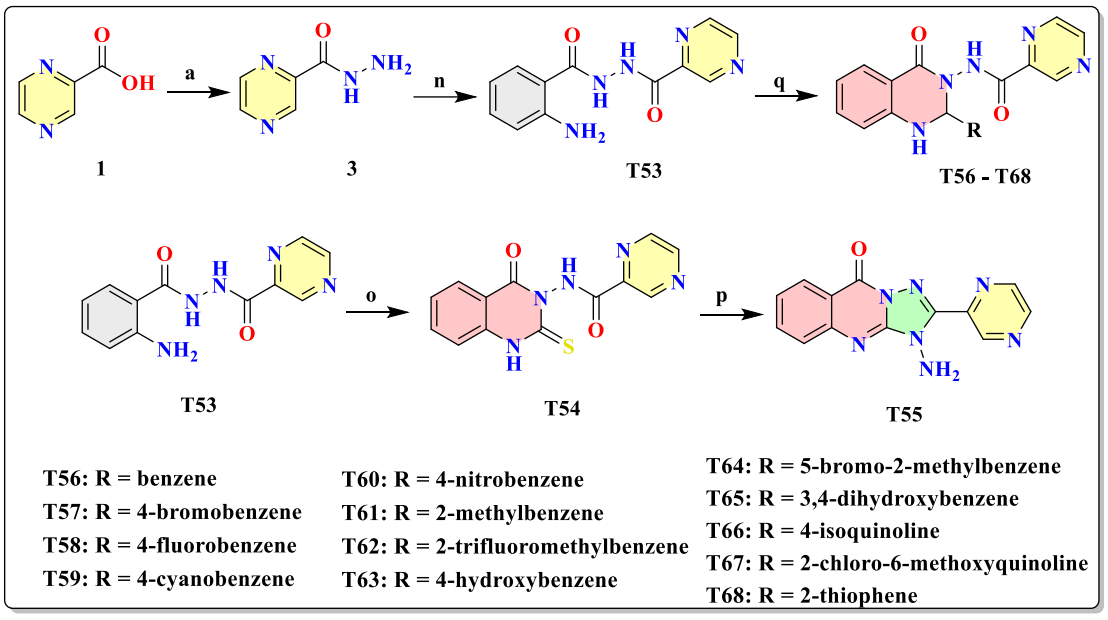

Scheme 2.4: Synthesis protocol for synthesizing title compounds (**T53-T68)**. Reagents and conditions: **a)** CH_3OH, Conc. H_2SO_4, $N_2H_4{\cdot}H_2O$, Reflux, 15 hours; **n)** CH_3OH, Isatoic anhydride, Reflux, 6 hours; **o)** CH_3OH/H_2O, CS_2, KOH, Reflux, 18 hours; **p)** CH_3OH, $N_2H_4{\cdot}H_2O$, Reflux, 24 hours; **q)** CH_3OH, glacial CH_3COOH, RCHO, Reflux, 4 hours.

The identification of the target compounds (**T53-T68**) was validated through a combination of spectral techniques, including ^{1}H-NMR, ^{13}C-NMR, and ESI-MS. In the ^{1}H-NMR spectrum of compound **T60 (Figure 2.21)**, a singlet at δ: 10.94 ppm is due to the -NH proton attached to the carbonyl carbon. The three aromatic protons in the pyrazine ring were observed as two doublets at δ: 9.09 and 8.87 ppm, and one triplet at δ: 8.68 ppm. Nine aromatic protons from the phenyl and quinazoline ring were detected in the region of δ: 8.23-6.79 ppm. Furthermore, a sharp singlet at δ: 6.32 ppm is due to -NH proton of the quinazoline moiety. The ^{13}C-NMR spectrum of compound **T60 (Figure 2.22)** exhibited all characteristic peaks. Peaks at δ 162.54 and 162.35 ppm were attributed to the presence of two carbonyl carbons. The pyrazine ring was represented by peaks at δ 148.29, 148.04, 147.41, and 145.28 ppm, corresponding to its four carbon atoms. Furthermore, the phenyl and quinazoline ring contributed thirteen peaks in the region of δ 143.75 to 73.80 ppm, reflecting the presence of the same number of carbon atoms. Confirmation of the molecular mass of compound **T60 (Figure 2.23)** was achieved through ESI-MS, which revealed the presence of the molecular ion peak (M+H peak) at (m/z) 391.18, thereby confirming its molecular weight. Similarly, the ^{1}H-NMR spectrum of the compound **T65 (Figure 2.24)** displayed a singlet at δ: 10.63 ppm which is attributed to the -NH proton attached to the carbonyl carbon. Two singlets at δ: 9.98 and 9.52 ppm indicate the presence of two -OH protons attached to the phenyl ring. Additionally, three aromatic protons of the pyrazine ring were detected with two singlets at δ: 9.04 and 8.67 ppm and one doublet at δ: 8.86 ppm. Further, peaks in the range of δ: 7.57-6.69 ppm correspond to seven aromatic protons originating from the phenyl and quinazoline ring. Lastly, sharp singlet peaks at δ: 7.24 and 6.07 ppm are attributed to the -CH and -NH protons of quinazoline respectively. In the ^{13}C-NMR spectrum of compound **T65 (Figure 2.25)**, characteristic peaks align with its molecular structure. Peaks at δ: 161.92 and 159.68 ppm are attributed to the two carbonyl carbons, while four carbons of the pyrazine ring are represented by peaks at δ: 150.10, 148.15, 148.04, and 147.69 ppm. Thirteen carbons from the phenyl and quinazoline ring are distinguished by thirteen peaks within the range of δ: 144.02 to 74.47 ppm. Furthermore, the ESI-MS of compound **T65 (Figure 2.26)** conclusively verifies its molecular mass by displaying a molecular ion peak (M+H peak) at (m/z) 378.13.

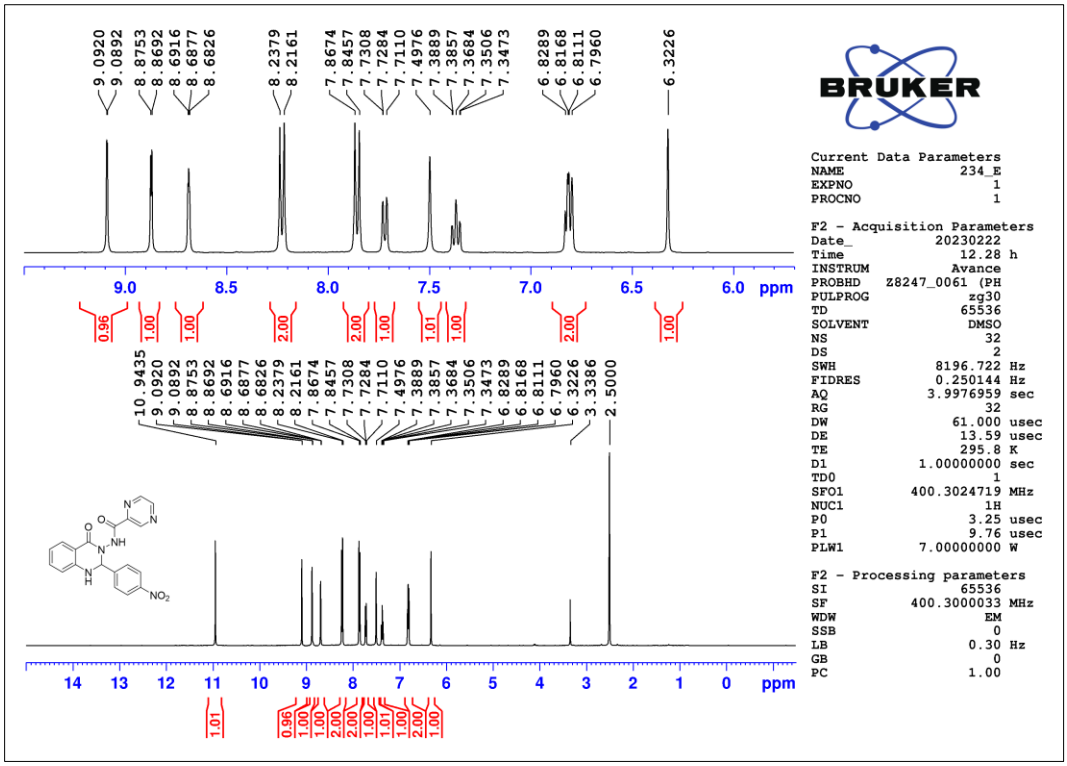

Figure 2.21 *^{1}H-NMR spectrum of compound* ***T60***

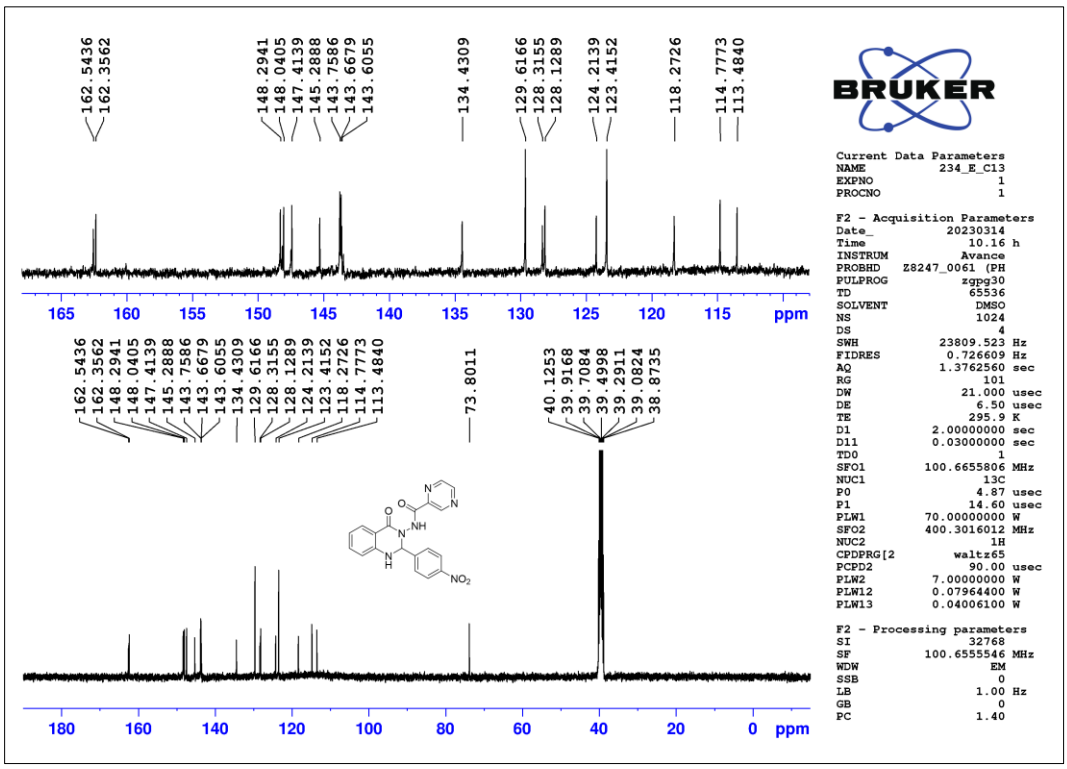

Figure 2.22 *^{13}C-NMR spectrum of compound* ***T60***

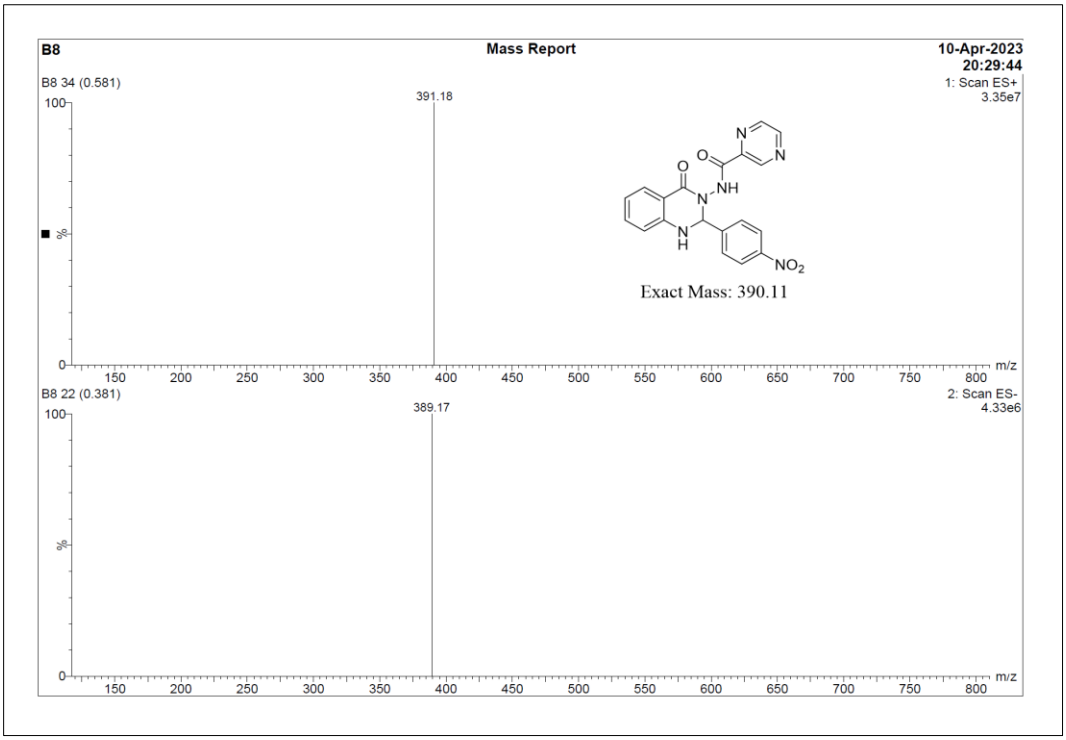

Figure 2.23 *ESI-MS spectrum of compound* ***T60***

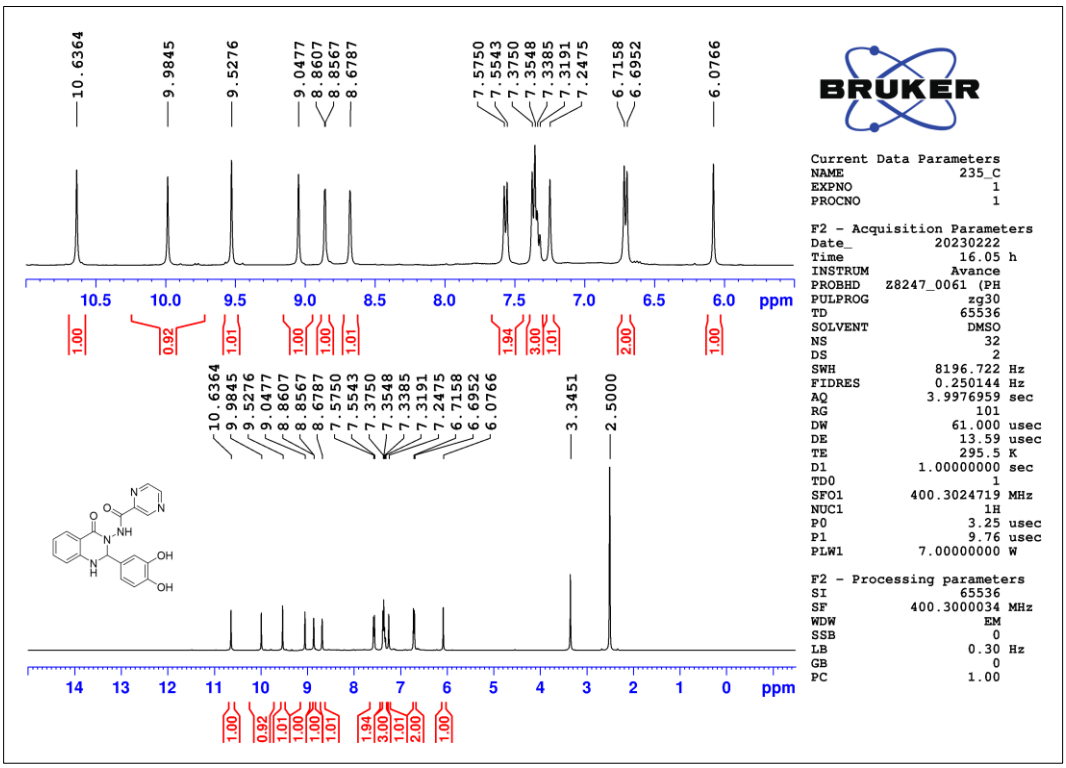

Figure 2.24 *^{1}H-NMR spectrum of compound* ***T65***

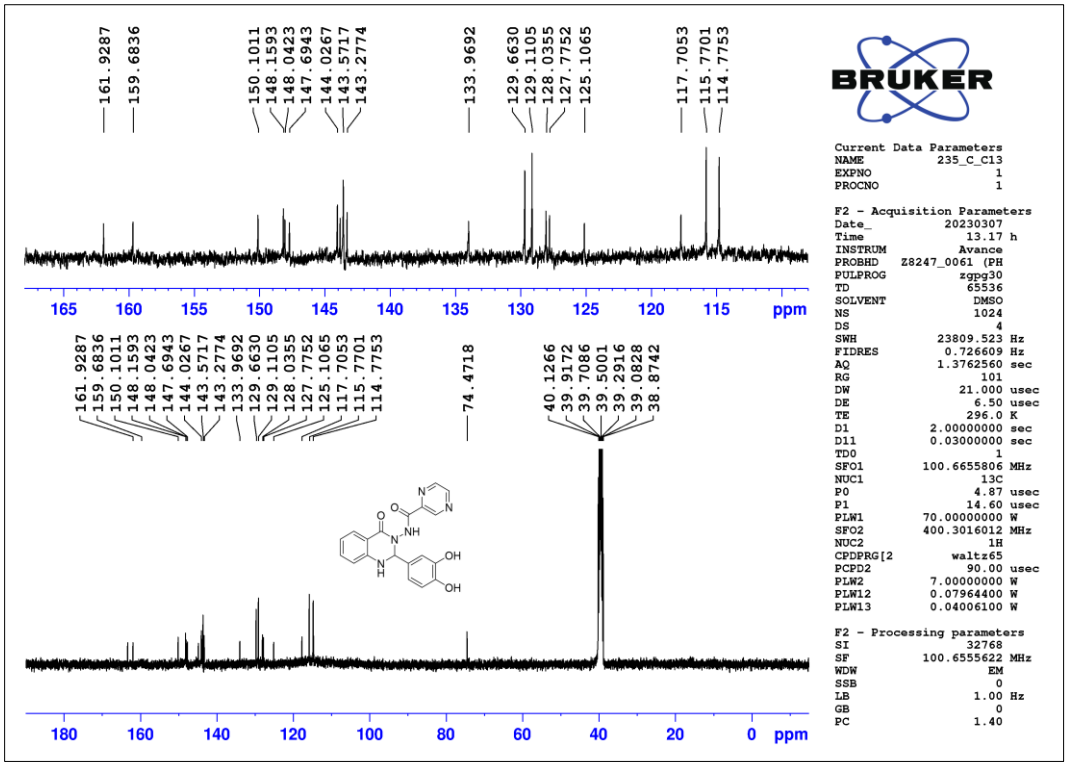

Figure 2.25 *^{13}C-NMR spectrum of compound* ***T65***

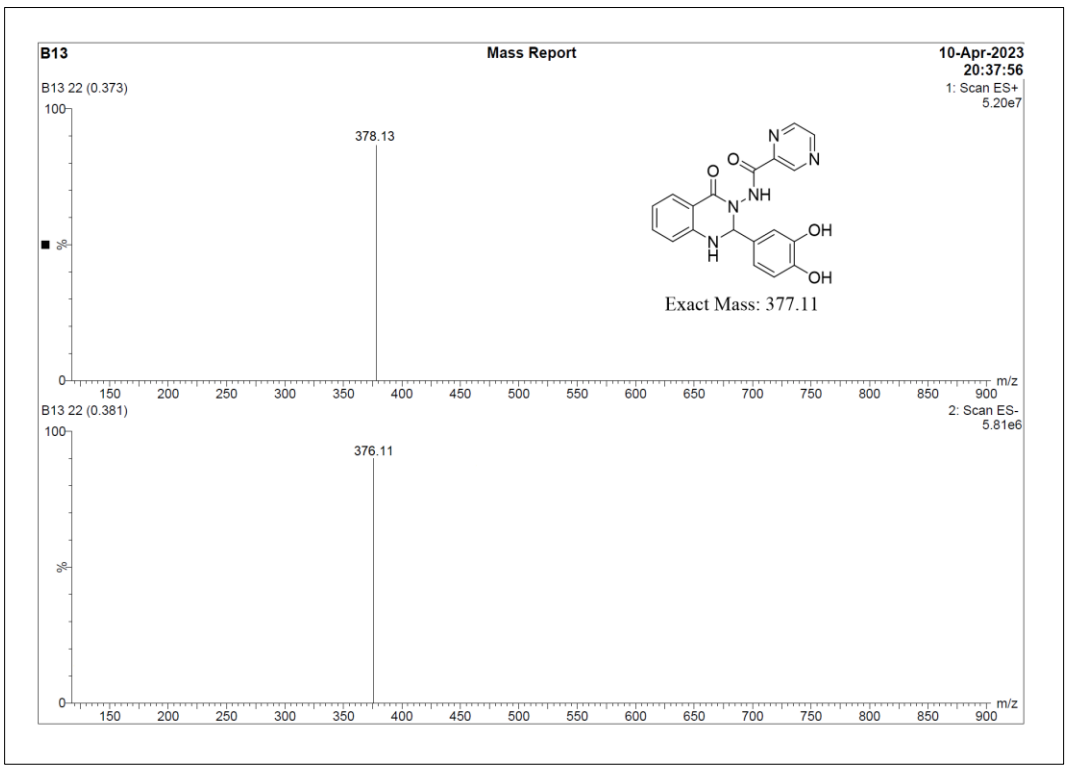

Figure 2.26 *ESI-MS spectrum of compound* ***T65***

2.3.5 Synthesis and characterization of 2-aminophenyl and 2-oxoacetyl incorporated pyrazine-2-carbohydrazide derivatives (T69-T88)

The target compounds (**T69-T88**) were synthesized as delineated in **Scheme 2.5.** Initially, we treated commercially procurable indoline-2,3-dione with alkyl/acyl/benzyl halides in the presence of K_2CO_3 and KI utilizing acetonitrile as the solvent. This reaction yielded the corresponding N-alkyl/acyl/benzylindoline-2,3-dione (**I9-I28**). Compounds **T69-T88** were synthesized by reacting compound **3** with the previously synthesized compounds **I9-I28** employing an acetonitrile and water system as the solvent.

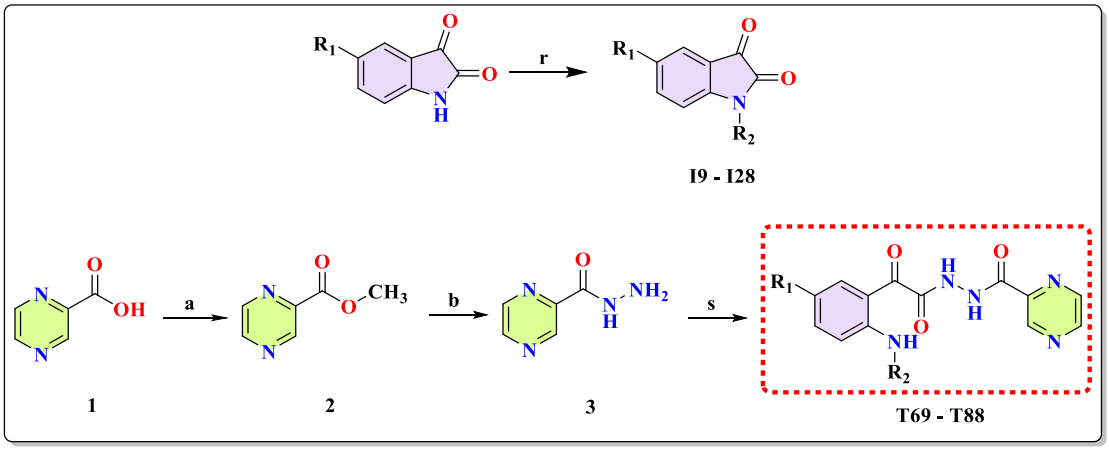

Scheme 2.5: Synthesis protocol for synthesizing title compounds (**T69-T88**). Reagents and conditions: **r)** CH_3CN, alkyl halides, K_2CO_3, KI, Reflux, 4 hours; **a)** CH_3OH, Conc. H_2SO_4, $N_2H_4{\cdot}H_2O$, Reflux, 15 hours; **b)** CH_3OH, $N_2H_4{\cdot}H_2O$, Reflux, 4 hours; **s)** CH_3CN/H_2O (1.5:1), N-alkylindoline-2,3-dione (I9-I28), RT, Stirr, 16 hours.

Table 2.2 *Structural details of the intermediate (**I9-I28**) and target compounds (**T69-T88**)*

Compound Code	R^1	R^2	Compound Code	R^1	R^2
I9, T69	H		**I19, T79**	H	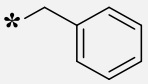
I10, T70	F		**I20, T80**	F	
I11, T71	Cl		**I21, T81**	Cl	

I12, T72	Br		**I22, T82**	Br	
I13, T73	CH_3		**I23, T83**	CH_3	
I14, T74	H	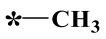	**I24, T84**	H	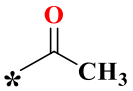
I15, T75	F		**I25, T85**	F	
I16, T76	Cl		**I26, T86**	Cl	
I17, T77	Br		**I27, T87**	Br	
I18, T78	CH_3		**I28, T88**	CH_3	

(The symbol '*' denotes the point of attachment)

The structure of the intermediates and target compounds (**T69-T88**) was confirmed by ^{1}H-NMR, ^{13}C-NMR, and HRMS. The ^{1}H-NMR spectrum of the compound **T69 (Figure 2.27)** displayed two singlets at δ: 11.92 and 10.91 ppm due to two -NH protons, the presence of three singlets at δ: 9.36, 9.01, and 8.90 ppm due to three aromatic protons of the pyrazine ring, the presence of peaks in the region δ: 7.85-6.95 ppm is due to four aromatic protons of the phenyl ring. A sharp singlet at δ: 6.19 is due to the -NH_2 protons. The ^{13}C-NMR spectrum of compound **T69 (Figure 2.28)** displayed all characteristic peaks corresponding to its molecular structure. The peaks at δ: 193.89, 164.39, and 148.76 are due to three carbonyl carbons, the peaks at δ: 144.26, 144.14, 143.79, and 133.42 ppm are due to the four carbons of pyrazine ring, the peaks at δ: 125.68, 122.72, 122.25, 121.26, 115.49 and 111.27 ppm are due to the six carbons of the phenyl ring. The mass spectrum of the compound **T69 (Figure 2.29)** shows its molecular ion peak (M+H peak) at (m/z) 286.0862 thus confirming its molecular mass. Similarly, the ^{1}H-NMR spectrum of the compound **T88 (Figure 2.30)** displayed three singlets at δ: 11.03, 10.96, and 10.62 ppm due to three -NH protons, the presence of three singlets at δ: 9.25, 8.94, and 8.80 ppm due to three aromatic protons of the pyrazine ring, the presence of peaks in the region δ: 8.09-7.51 ppm is due to three aromatic protons of the phenyl ring, and the presence of two sharp singlet peaks at δ: 2.35 and 2.15 ppm are due to the six -CH_3 protons. The ^{13}C-NMR spectrum of compound **T88 (Figure 2.31)** displayed all characteristic peaks corresponding to its molecular structure. The peak at δ: 192.22, 169.00, 163.60, and 162.25 is due to four carbonyl carbons, the peaks at δ: 148.21, 143.88, 143.68, and 137.56 ppm are due to

the four carbons of pyrazine ring, the peaks at δ: 136.07, 133.07, 132.44,121.34, and 121.10 ppm are due to the six carbons of the phenyl ring, the peaks at δ: 24.46 and 20.19 ppm are due to the -CH_3 carbon. The mass spectrum of the compound **T88 (Figure 2.32)** shows its molecular ion peak (M+H peak) at (m/z) 342.1124 thus confirming its molecular mass.

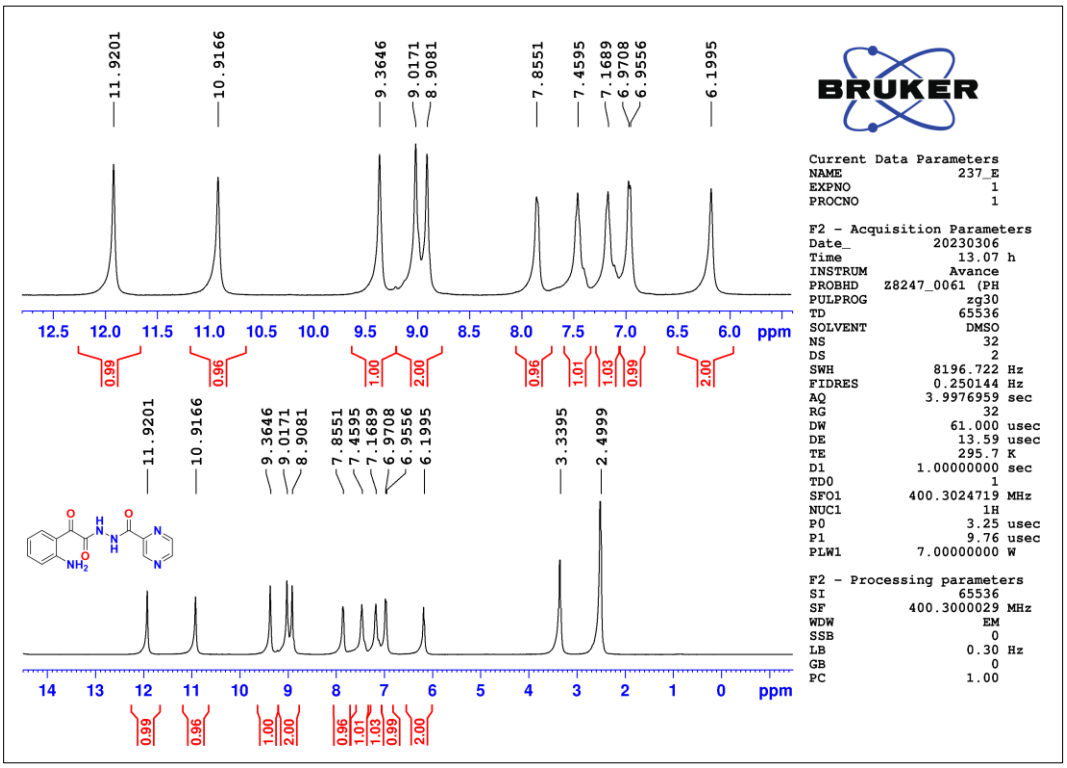

Figure 2.27 *^{1}H-NMR spectrum of compound* ***T69***

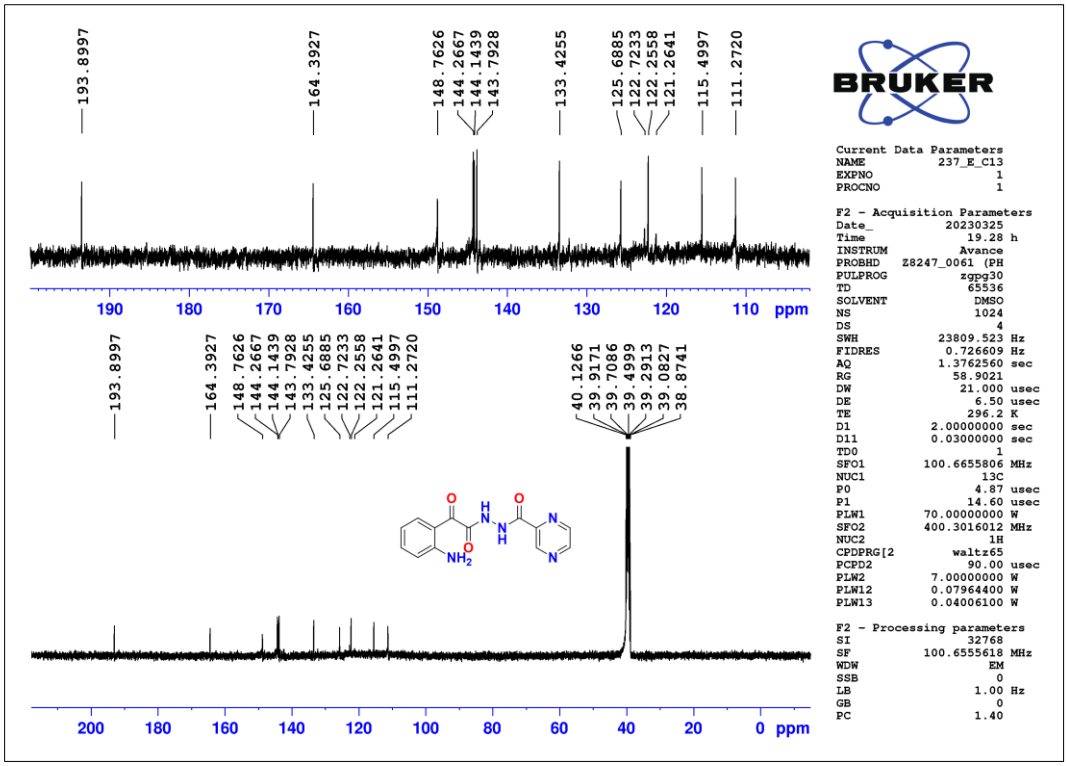

Figure 2.28 *^{13}C-NMR spectrum of compound* ***T69***

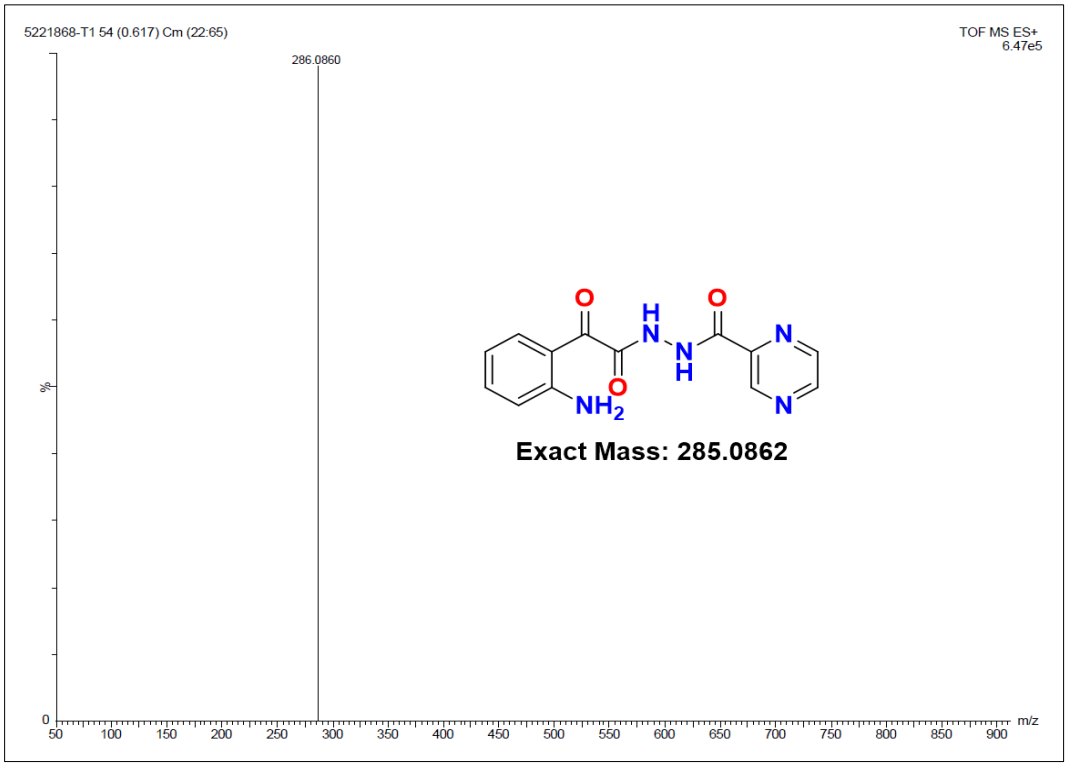

Figure 2.29 *HR-MS spectrum of compound* ***T69***

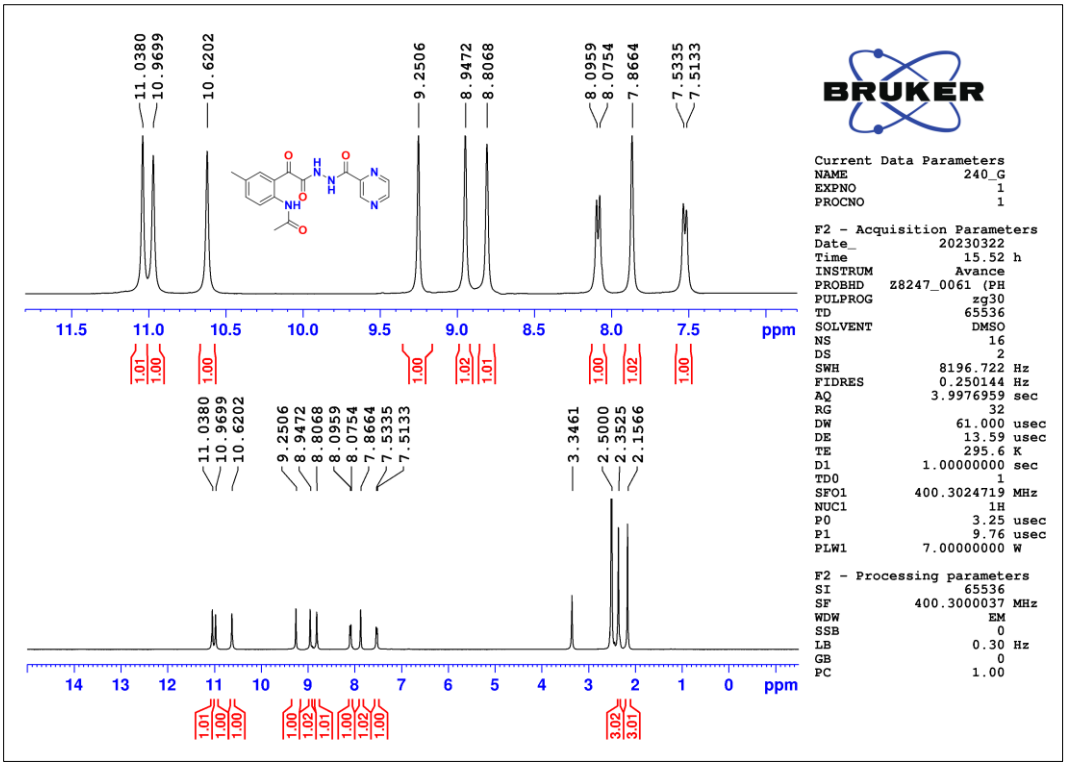

Figure 2.30 *^{1}H-NMR spectrum of compound* ***T88***

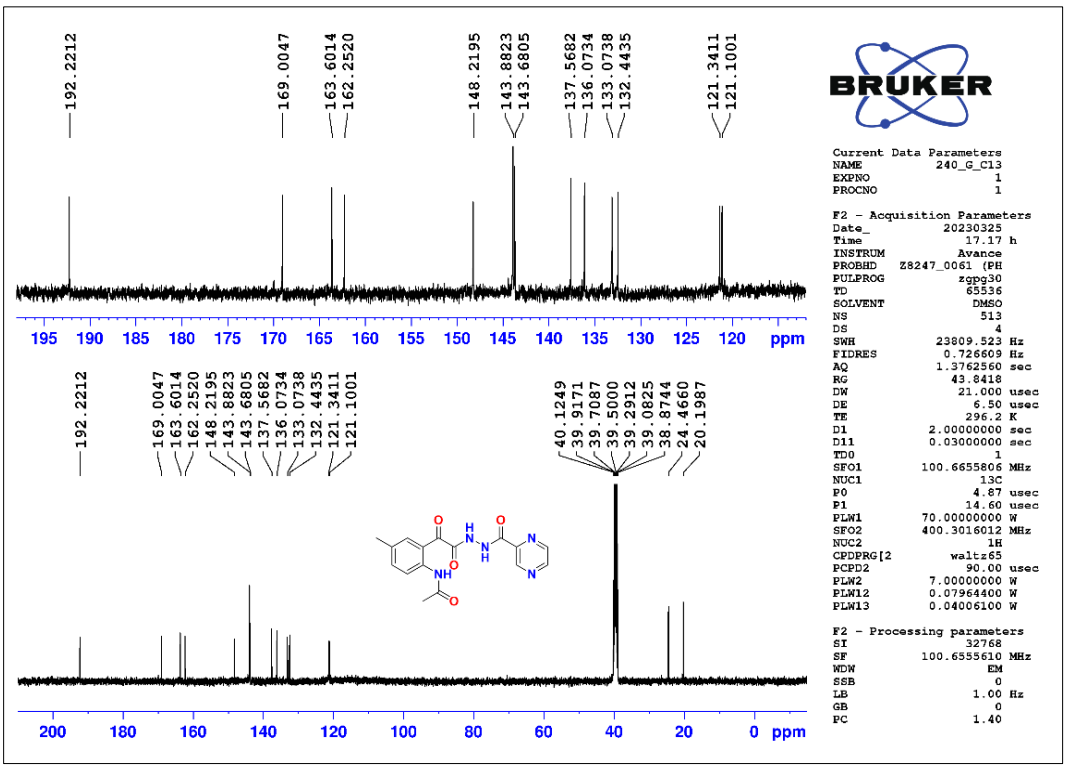

Figure 2.31 *^{13}C-NMR spectrum of compound* ***T88***

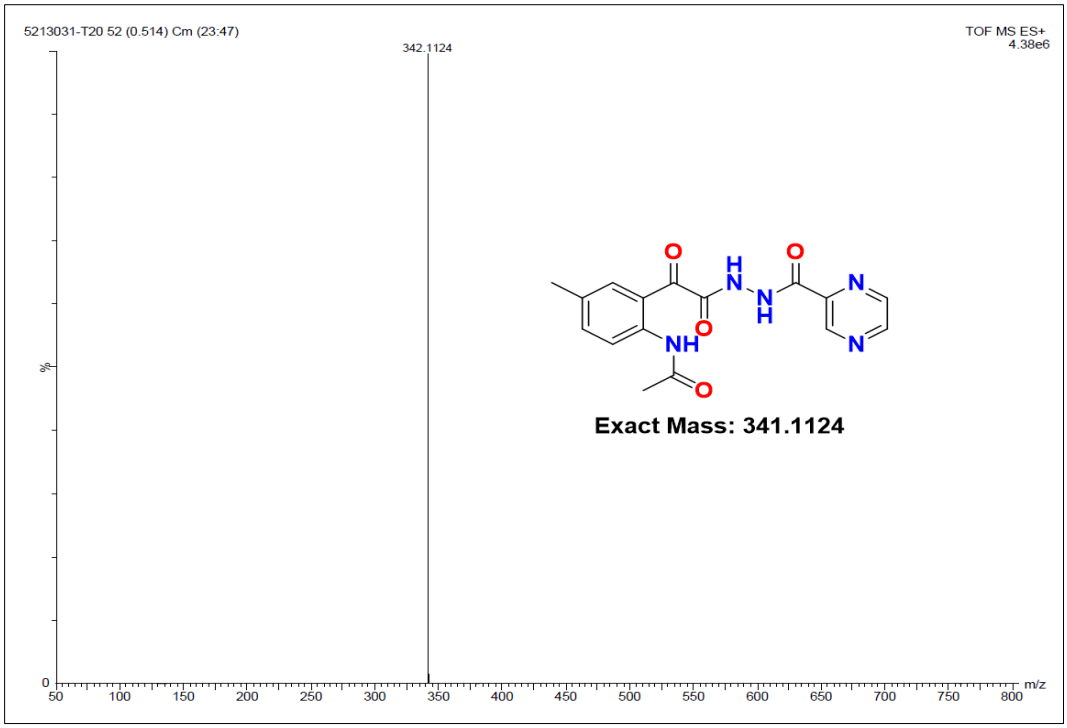

Figure 2.32 *HR-MS spectrum of compound* ***T88***

2.4 Conclusions

Five new series of pyrazine-based molecules such as 1,3,4-oxadiazole/[1,2,4] triazolo[3,4-b][1,3,4]thiadiazine incorporated pyrazine derivatives (**T1-T18**), 1,2,4-triazole incorporated pyrazine derivatives (**T19-T36**), pyrazine hydrazinylidene derivatives containing benzenesulfonate scaffold (**T37-T52**), 4-quinazolinone incorporated pyrazine derivatives (**T53-T68**), and 2-aminophenyl and 2-oxoacetyl incorporated pyrazine-2-carbohydrazide derivatives (**T69-T88**) were designed and synthesized using multistep synthetic protocol and were purified using recrystallization or column chromatography, resulting in yields ranging from 80% to 99%. The melting points of the final compounds were determined. All the intermediate and final compounds were characterized by ^{1}H-NMR, ^{13}C-NMR, and HRMS/ESI-MS. The target compounds (**T1-T88**) were screened for their *in vitro* antitubercular, antibacterial, and antifungal activities and *in vitro* cytotoxicity studies and the results were discussed in Chapter 3. The drug-likeness and possible action mechanism of the target compounds were determined using *in silico* studies and the results were discussed in Chapter 4.

Appendix 2.1

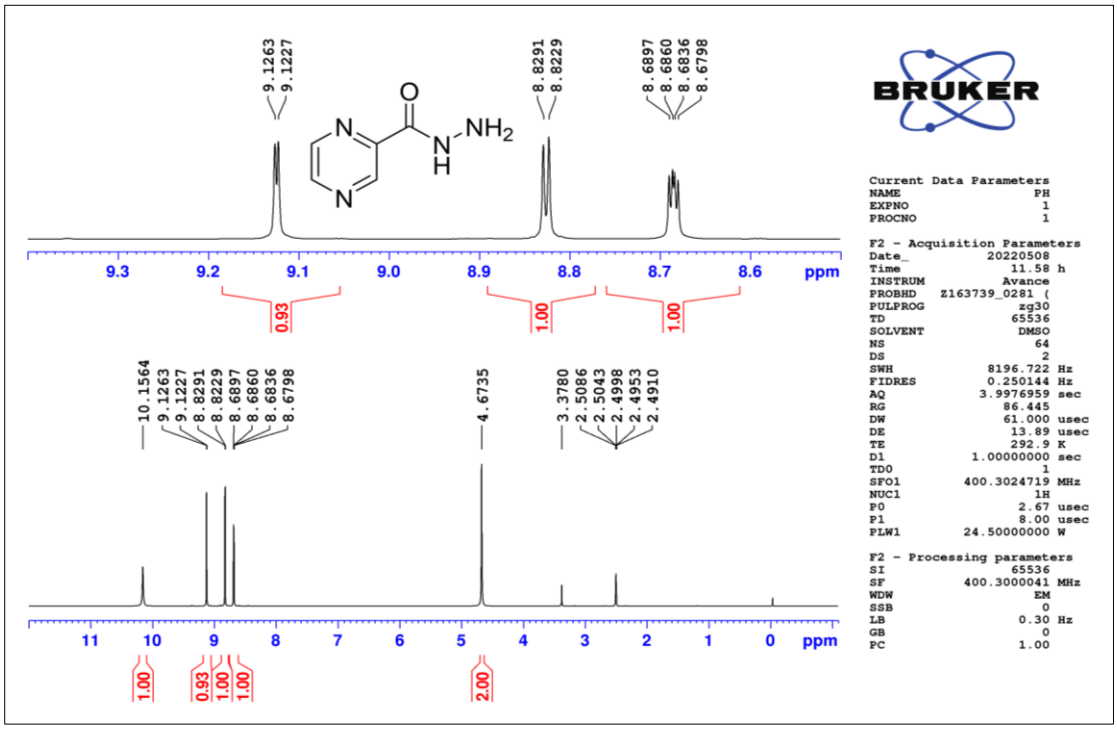

Figure 2.33 *^{1}H-NMR spectrum of compound* ***3***

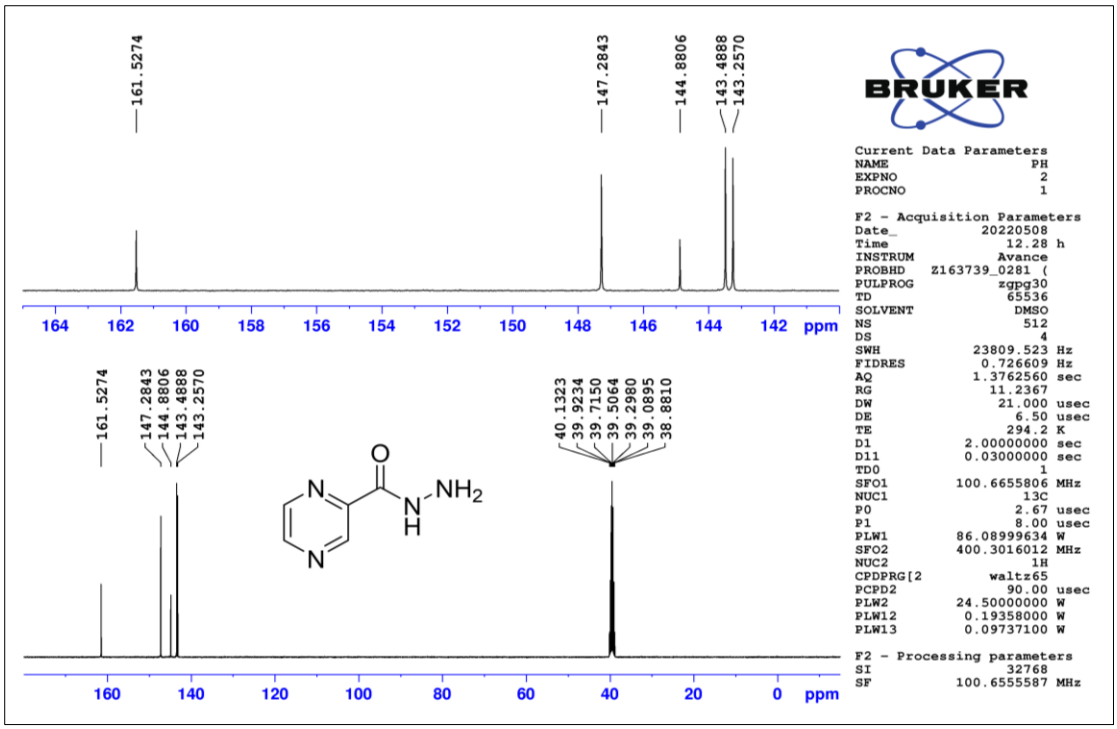

Figure 2.34 *^{13}C-NMR spectrum of compound* ***3***

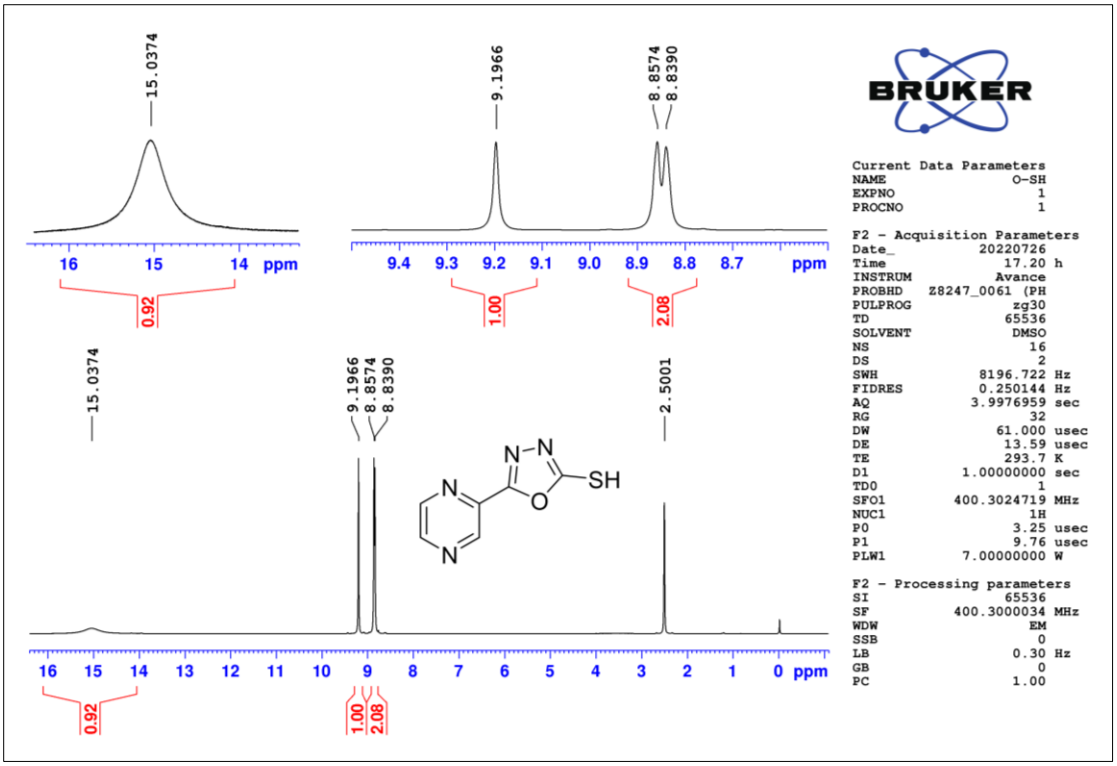

Figure 2.35 *^{1}H-NMR spectrum of compound* ***4***

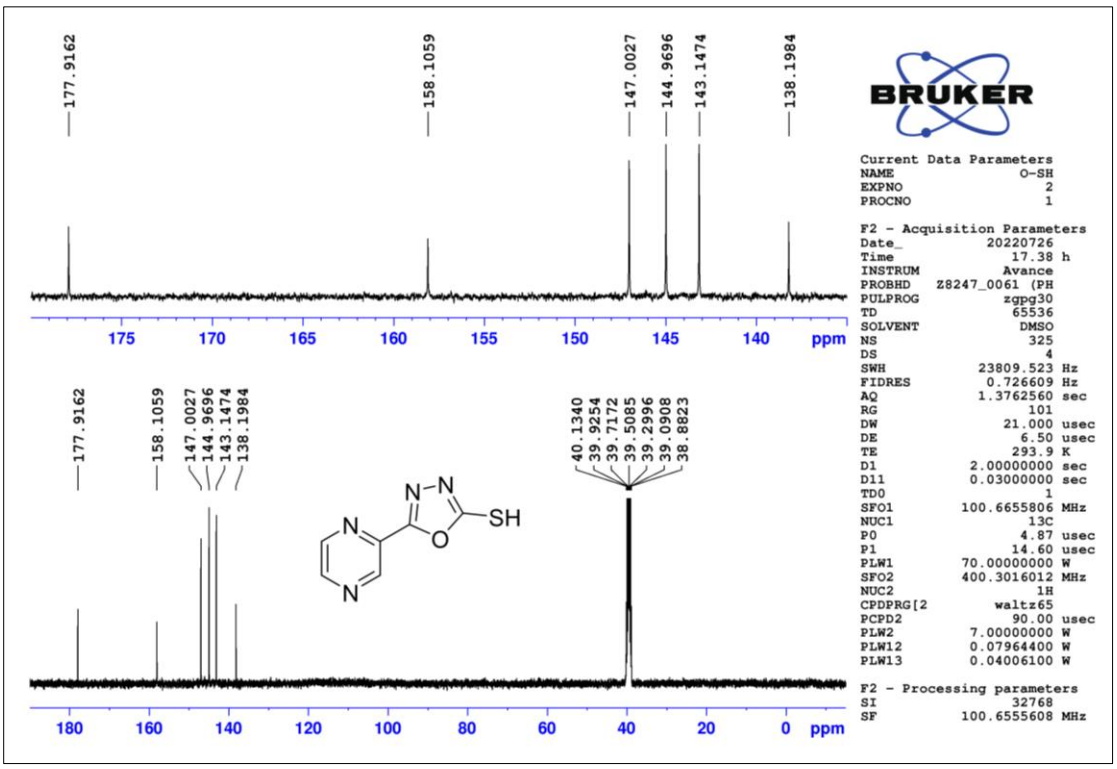

Figure 2.36 *^{13}C-NMR spectrum of compound* ***4***

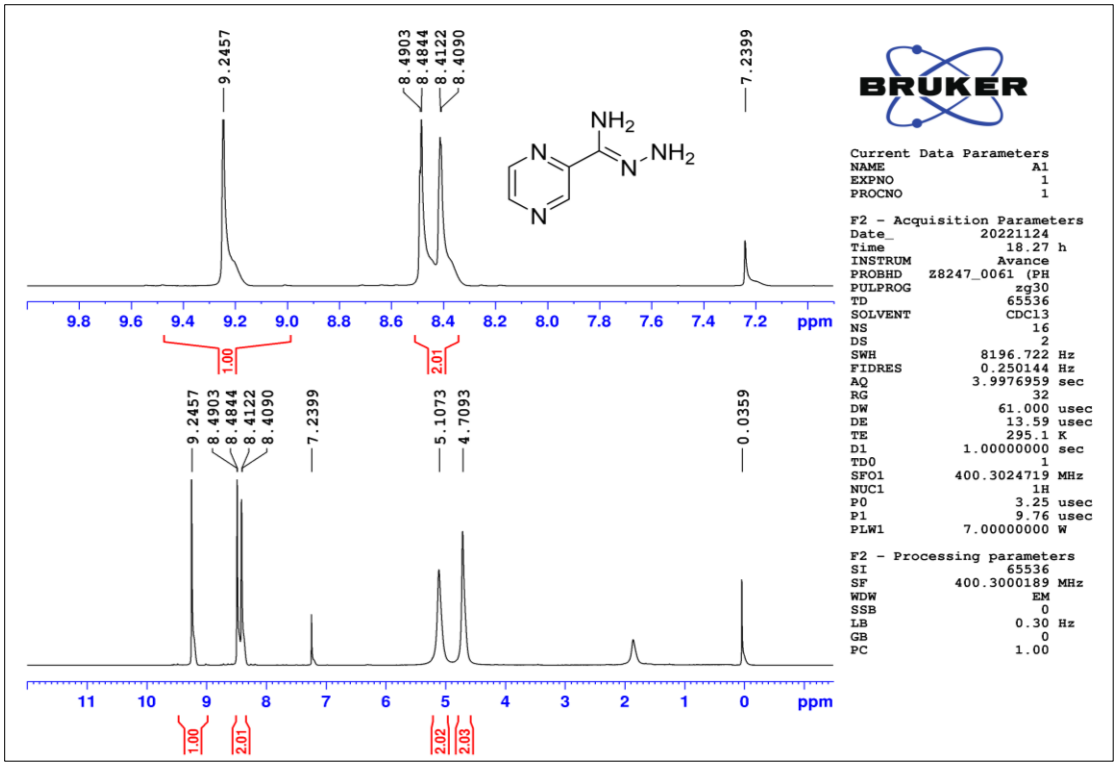

Figure 2.37 *^{1}H-NMR spectrum of compound* ***6***

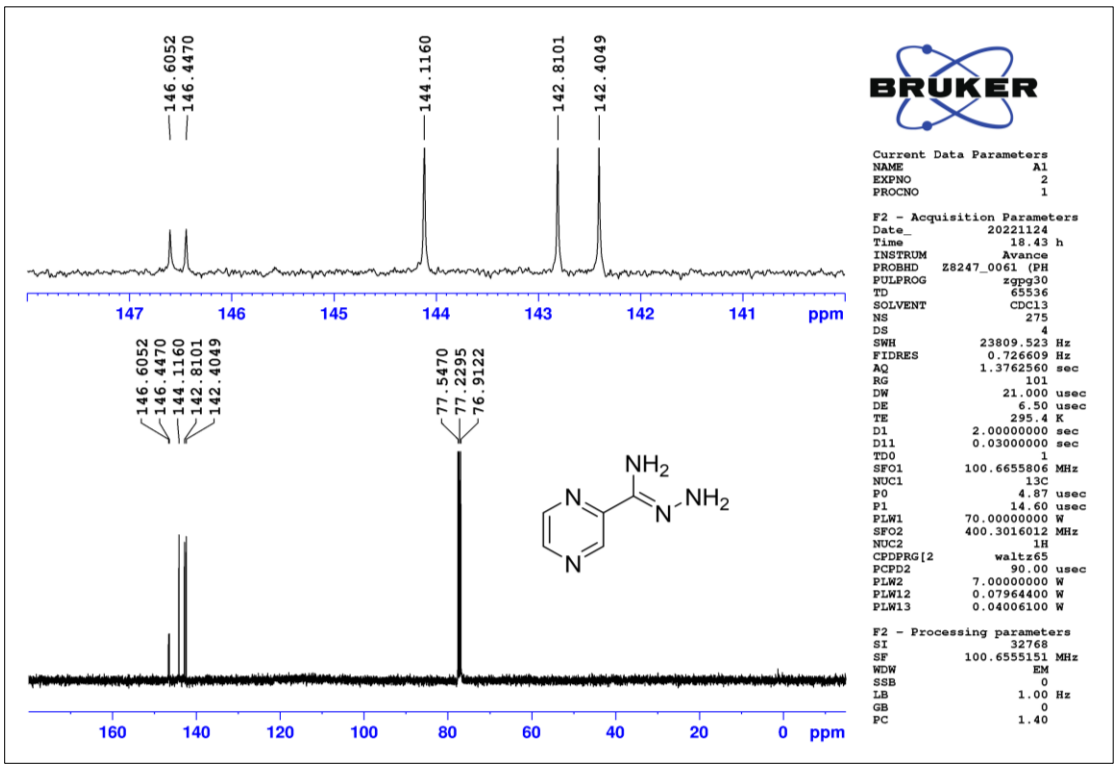

Figure 2.38 *^{13}C-NMR spectrum of compound* ***6***

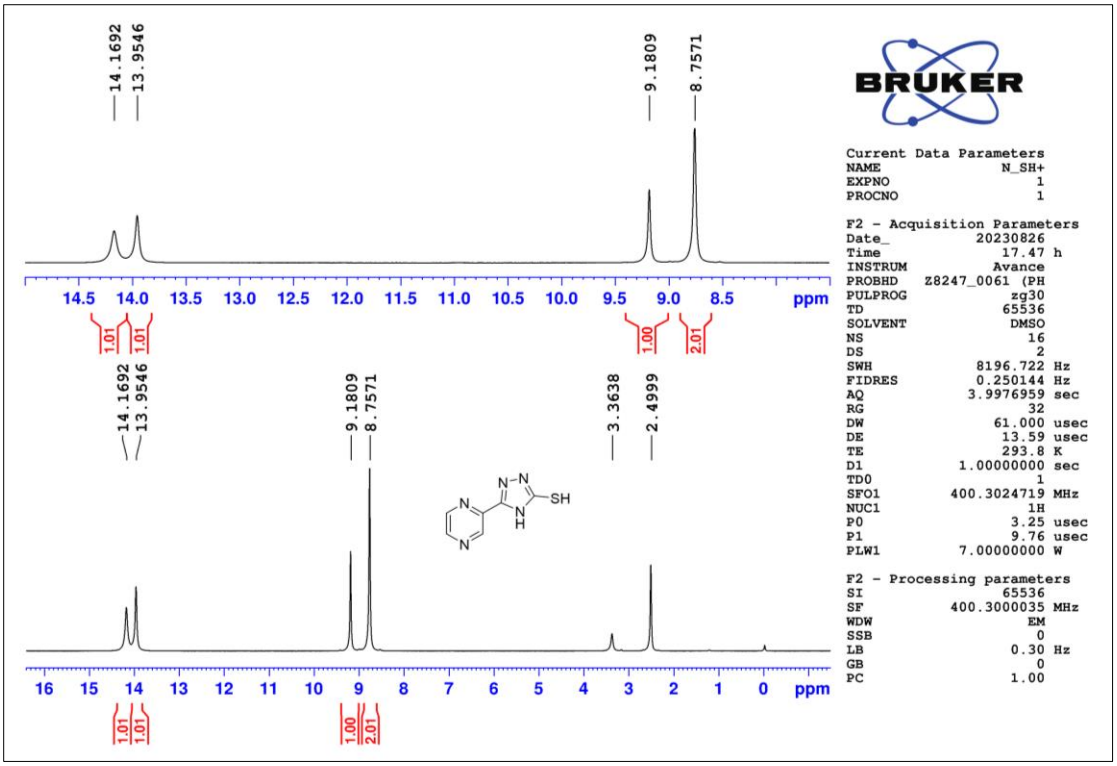

Figure 2.39 *^{1}H-NMR spectrum of compound **7***

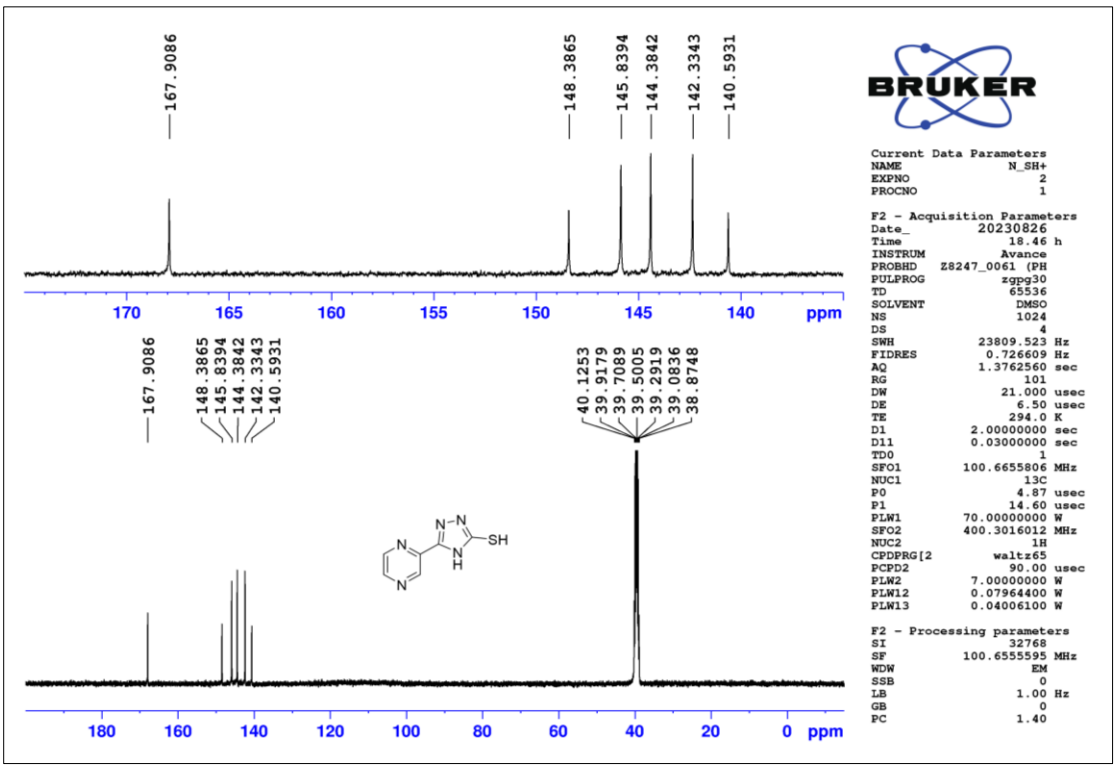

Figure 2.40 *^{13}C-NMR spectrum of compound **7***

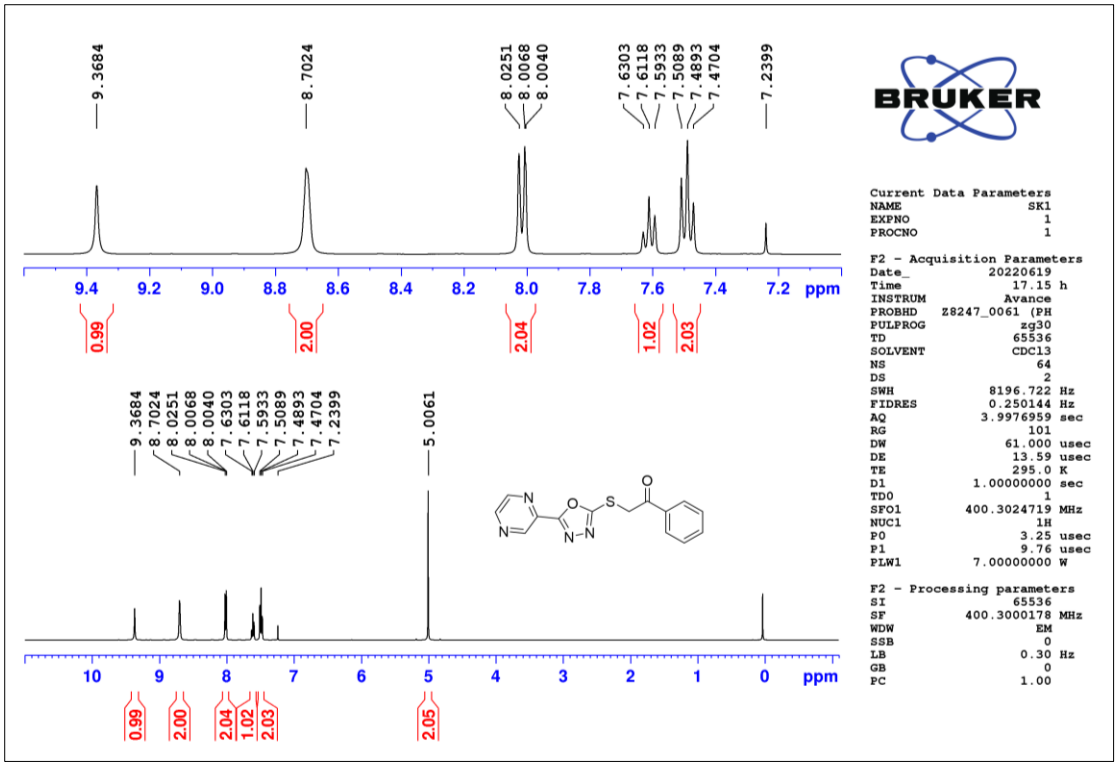

Figure 2.41 *^{1}H-NMR spectrum of compound* ***T1***

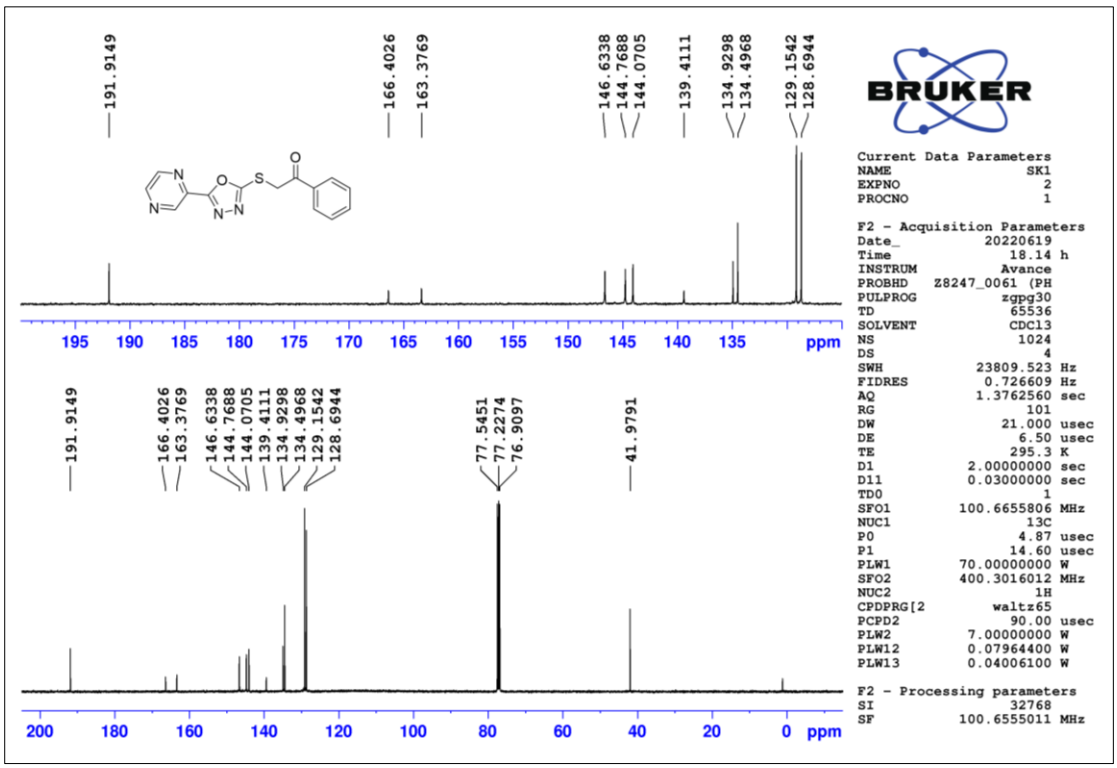

Figure 2.42 *^{13}C-NMR spectrum of compound* ***T1***

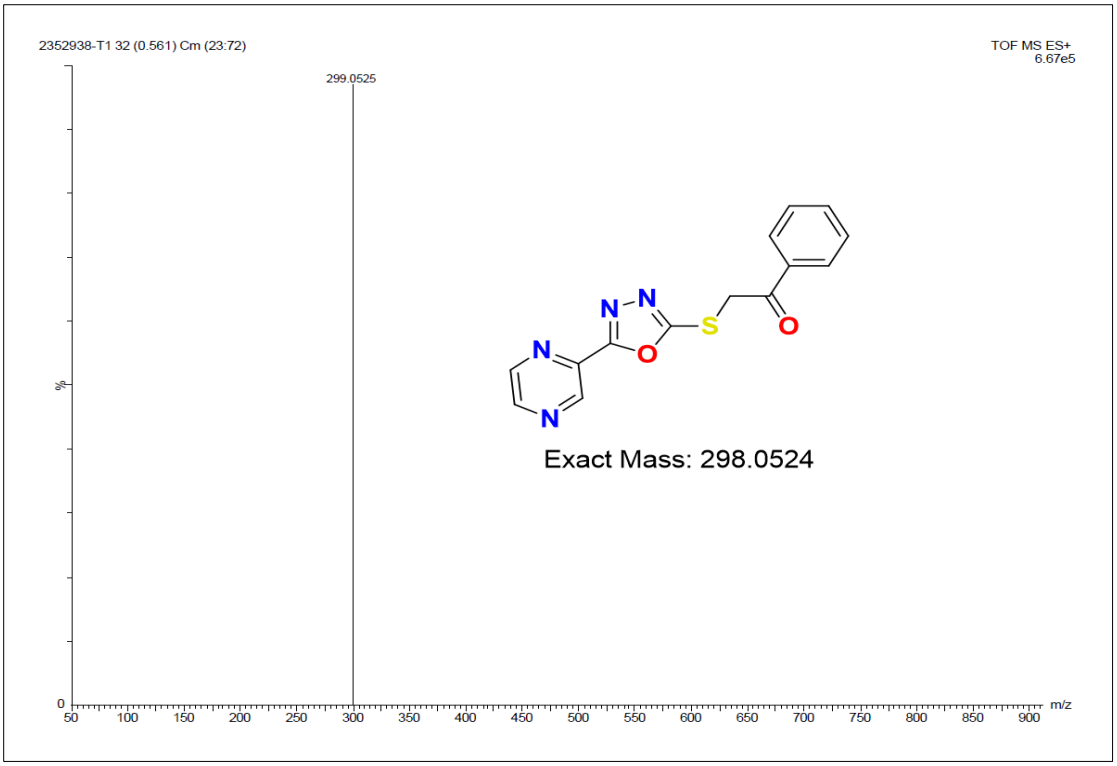

Figure 2.43 *HR-MS spectrum of compound* ***T1***

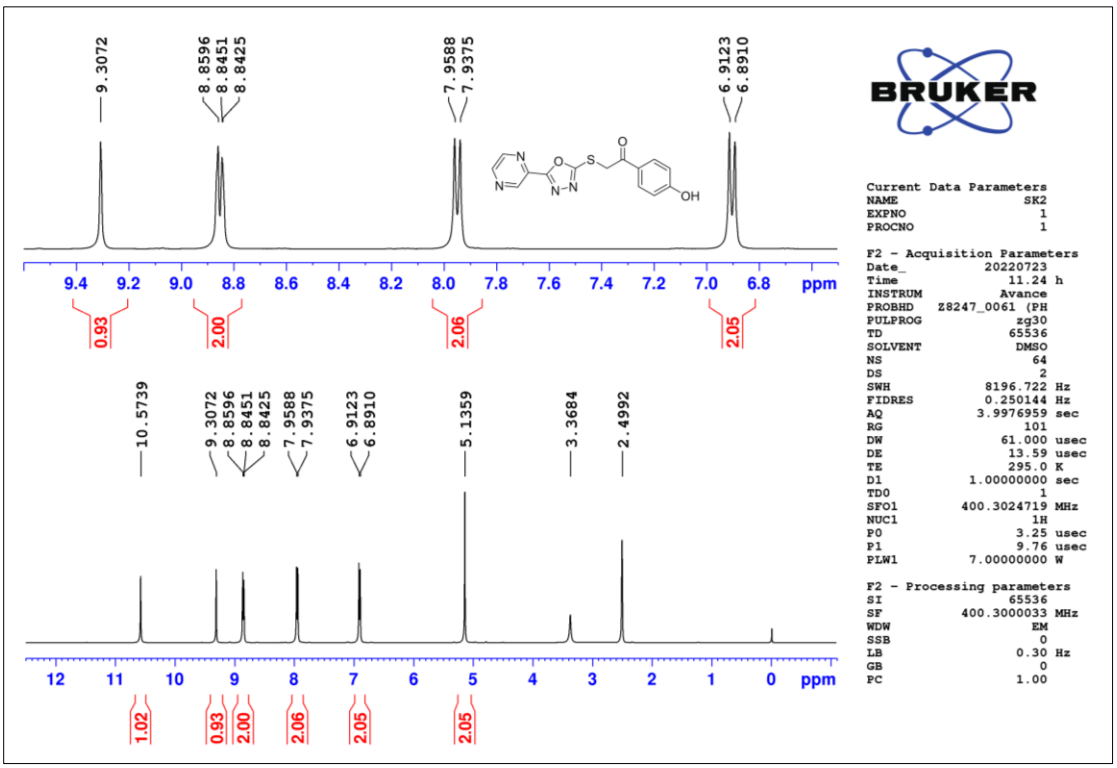

Figure 2.44 *^{1}H-NMR spectrum of compound* ***T2***

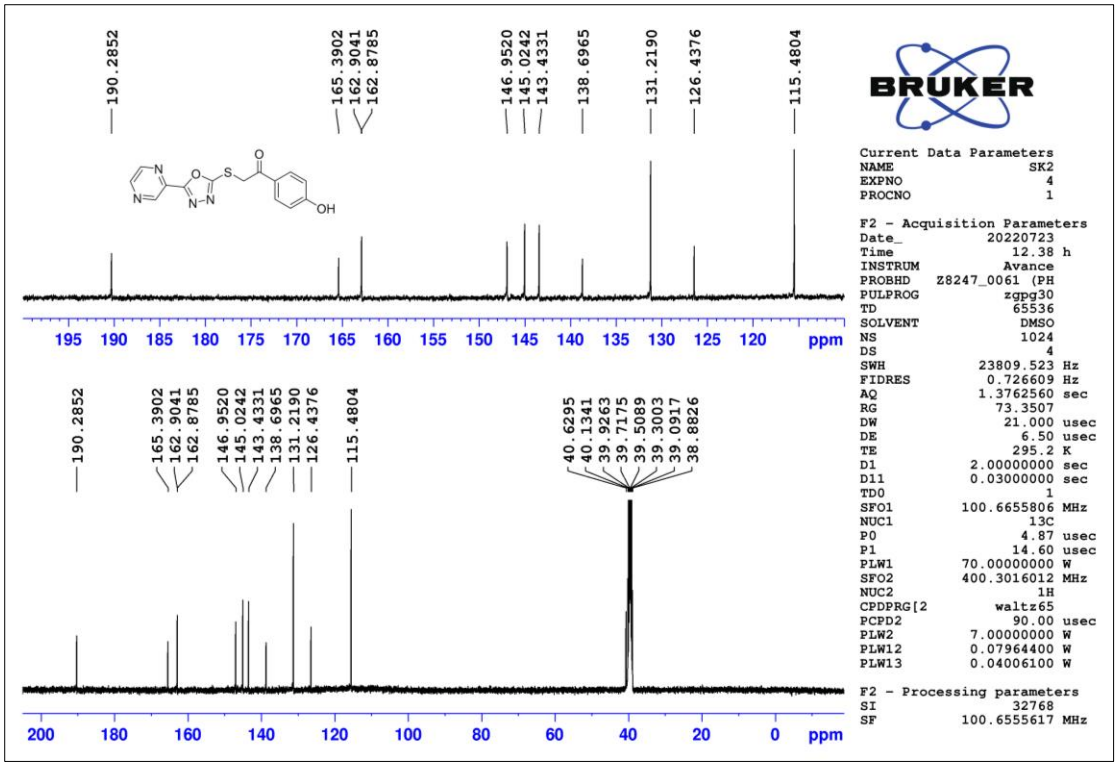

Figure 2.45 *^{13}C-NMR spectrum of compound* ***T2***

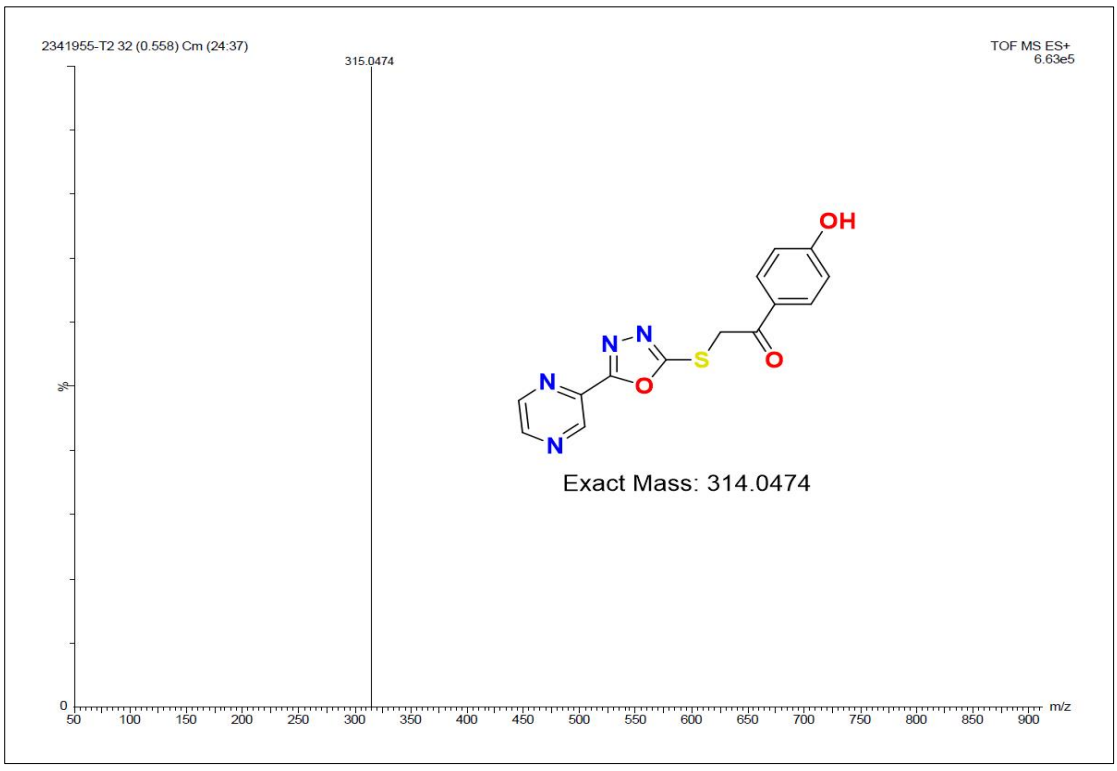

Figure 2.46 *HR-MS spectrum of compound* ***T2***

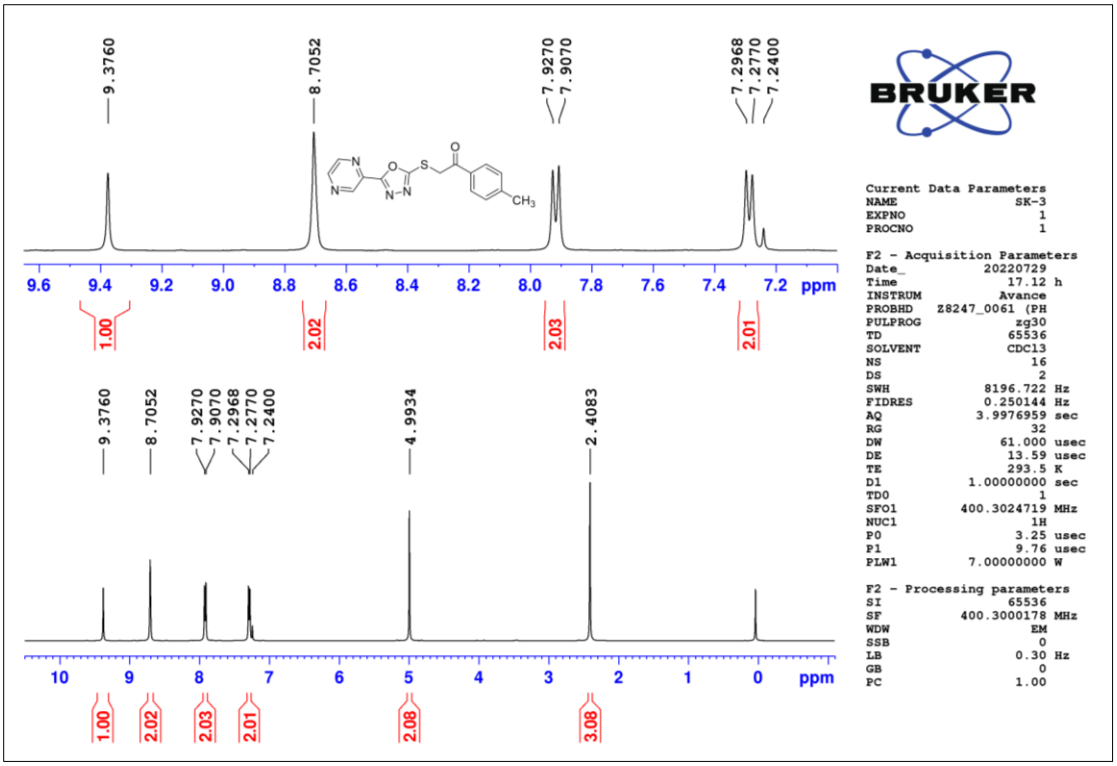

Figure 2.47 *^{1}H-NMR spectrum of compound* ***T3***

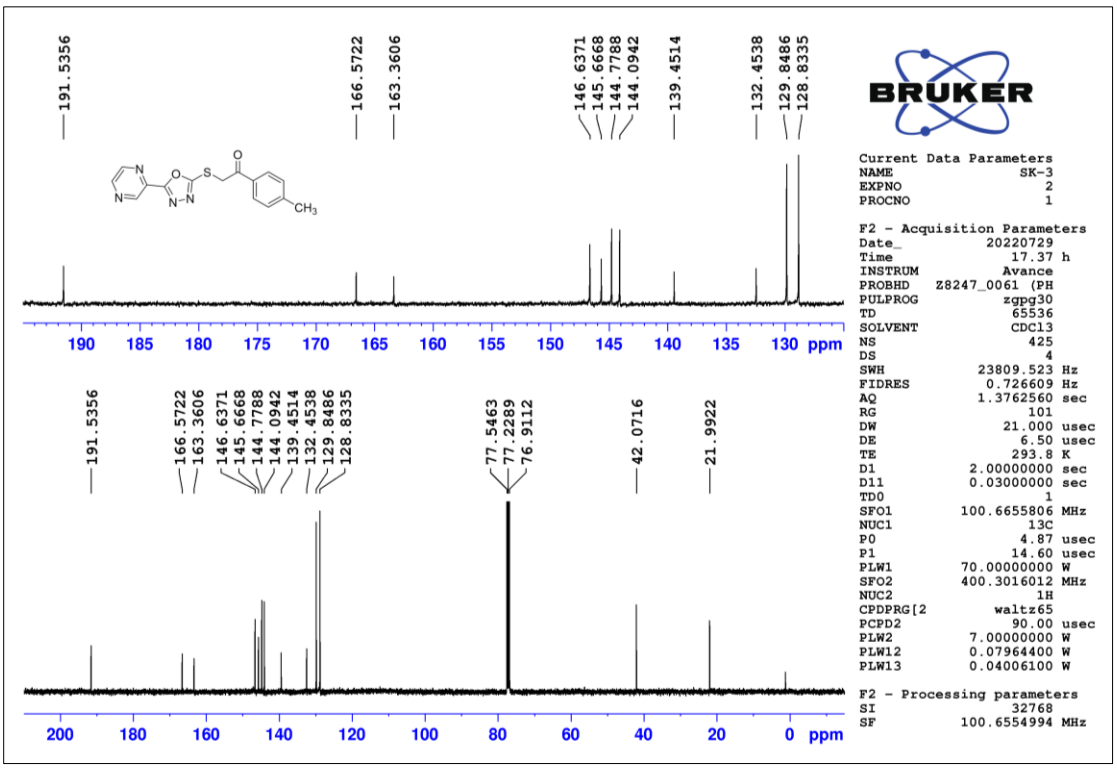

Figure 2.48 *^{13}C-NMR spectrum of compound* ***T3***

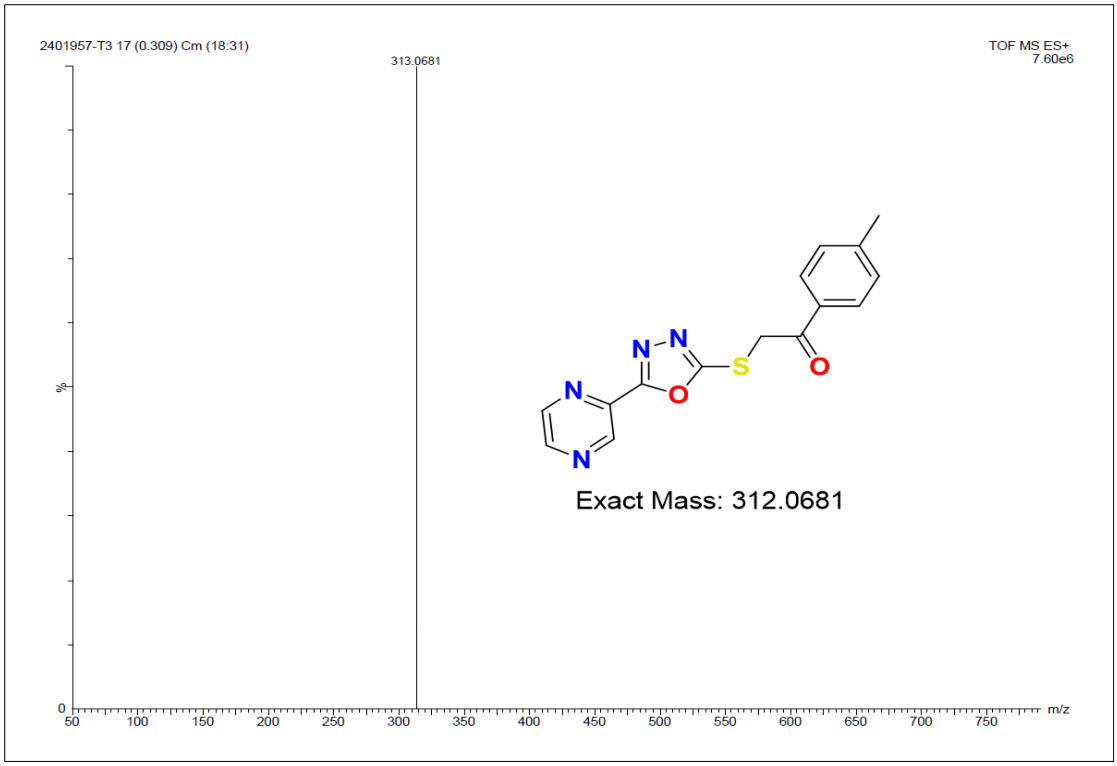

Figure 2.49 *HR-MS spectrum of compound* ***T3***

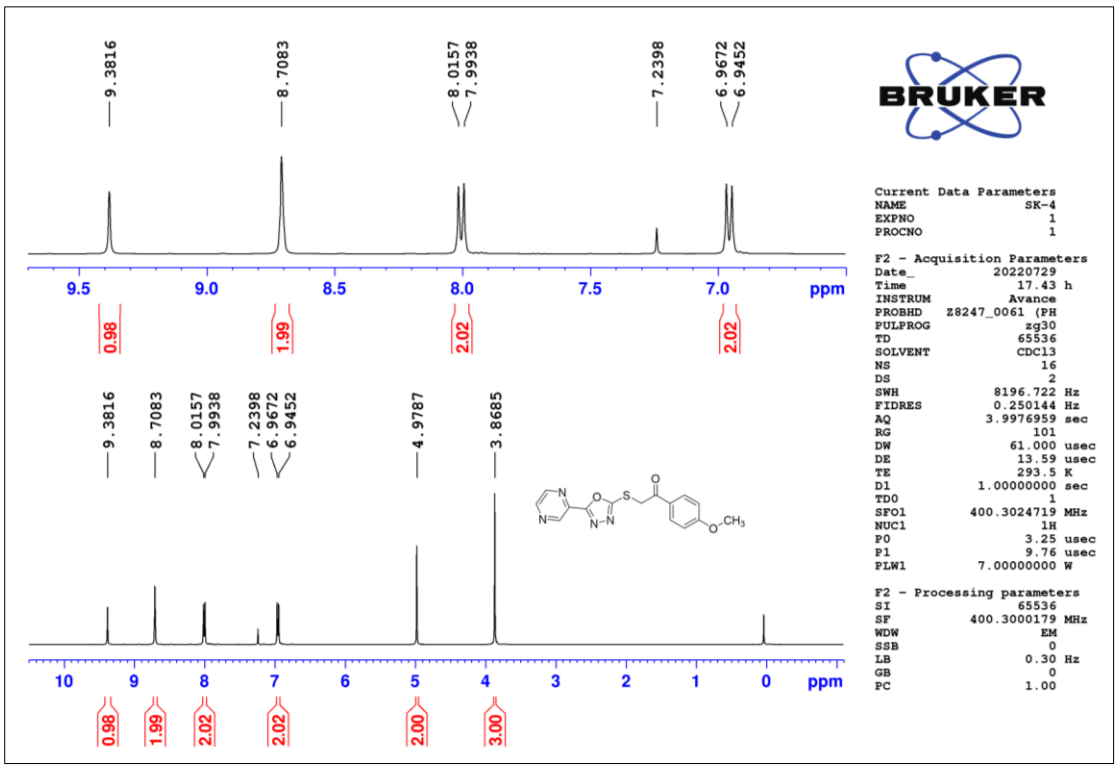

Figure 2.50 *^{1}H-NMR spectrum of compound* ***T4***

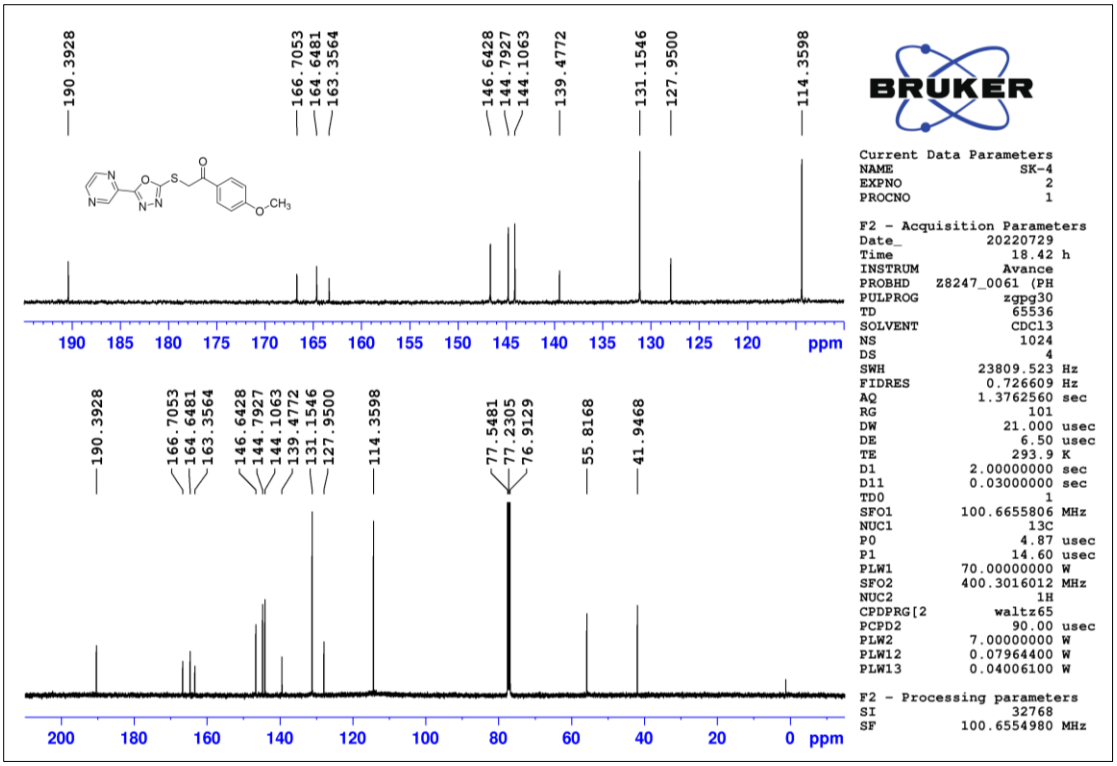

Figure 2.51 *^{13}C-NMR spectrum of compound* ***T4***

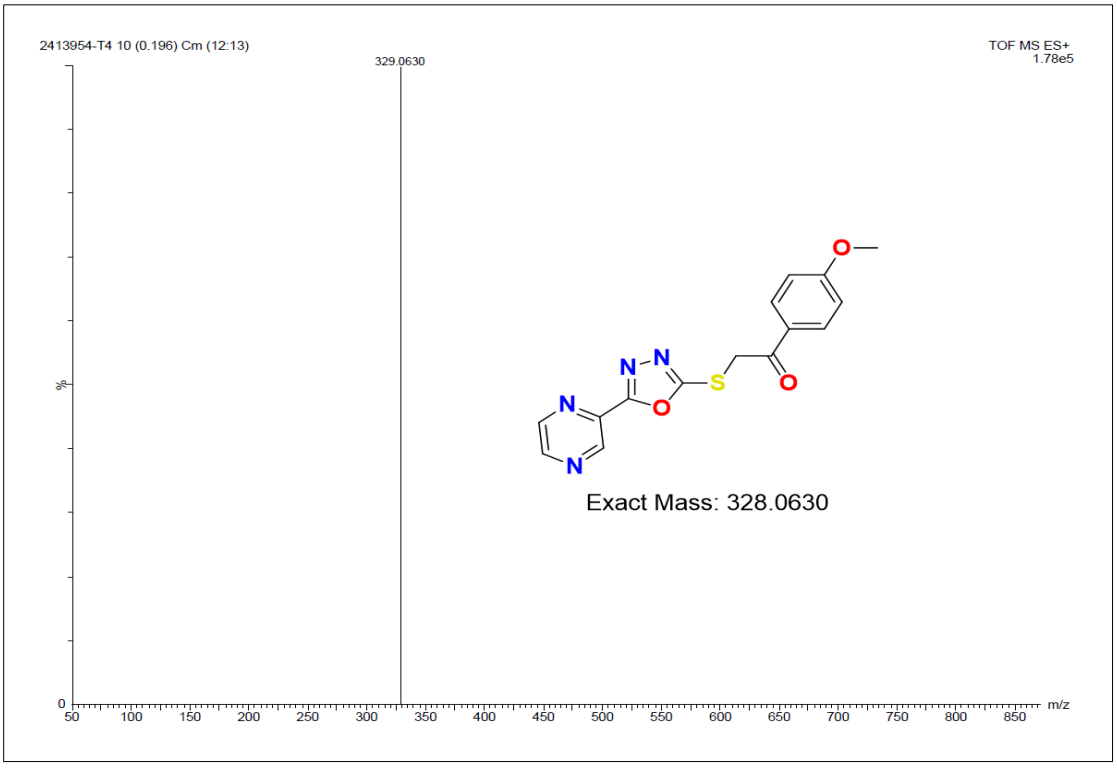

Figure 2.52 *HR-MS spectrum of compound* ***T4***

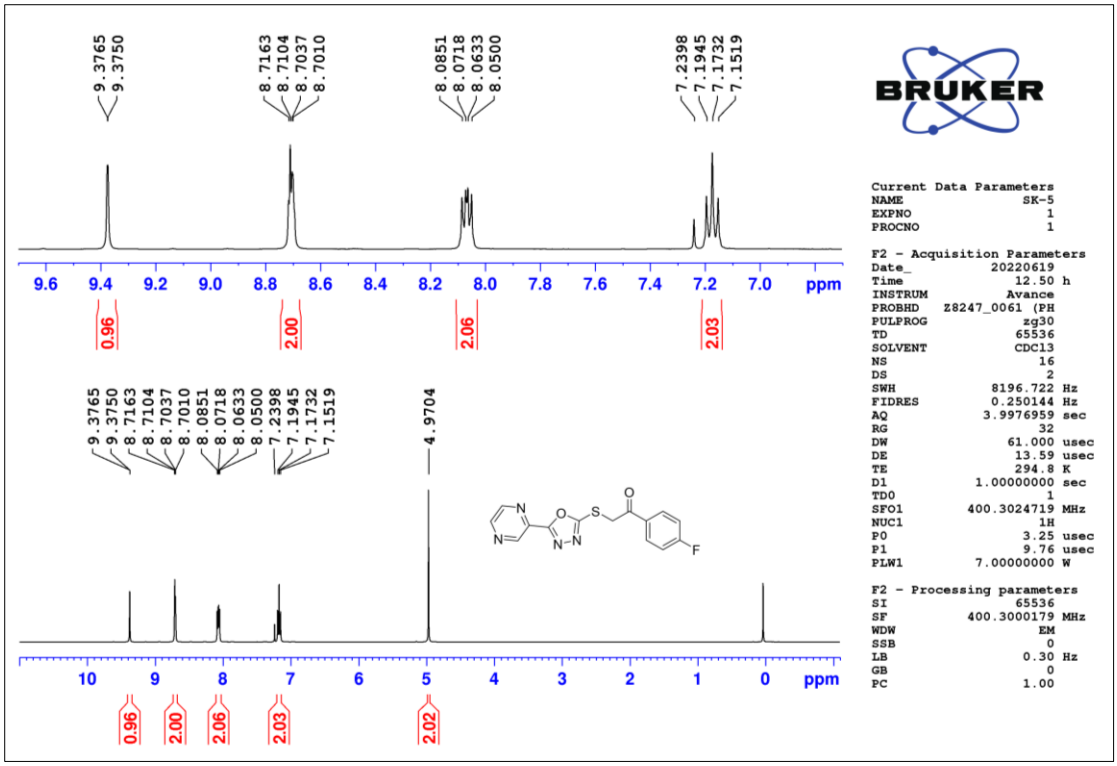

Figure 2.53 *^{1}H-NMR spectrum of compound* ***T5***

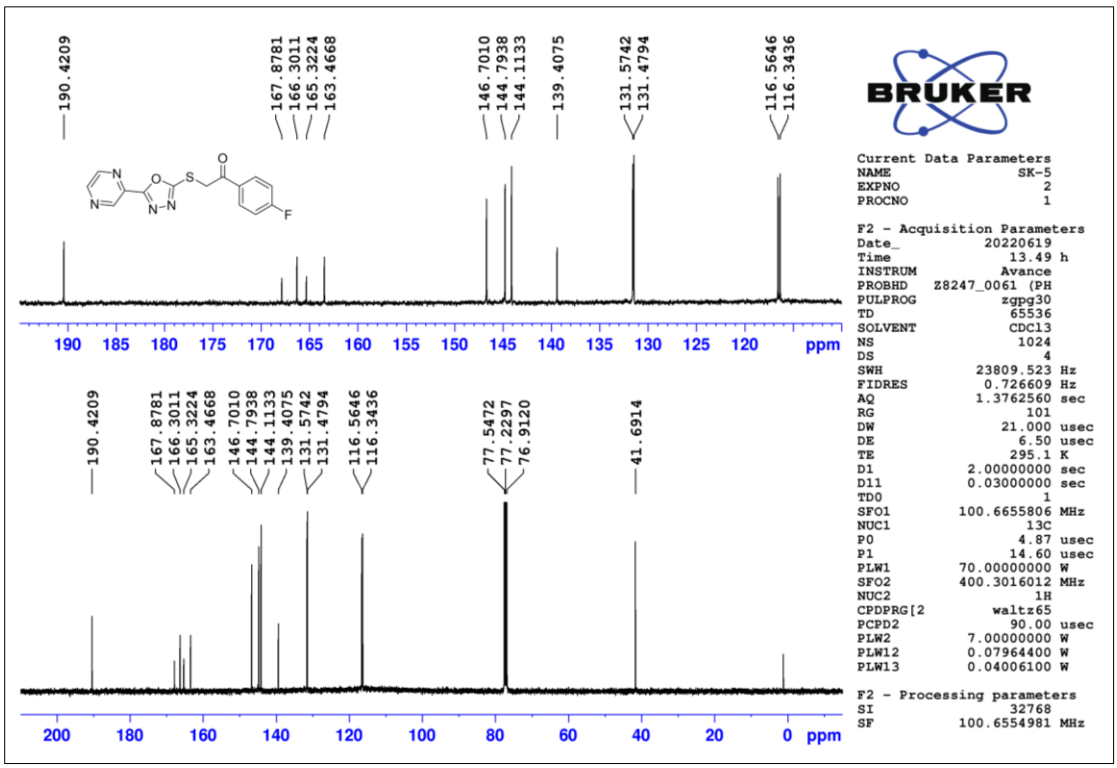

Figure 2.54 *^{13}C-NMR spectrum of compound* ***T5***

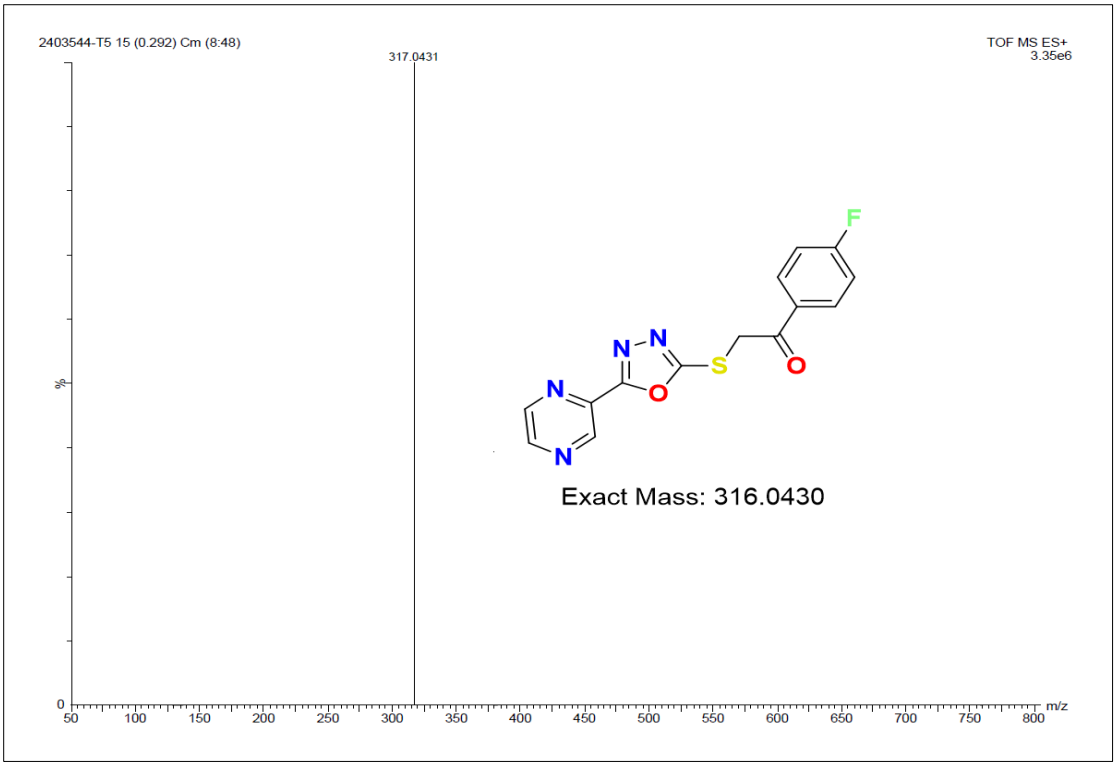

Figure 2.56 *HR-MS spectrum of compound* ***T5***

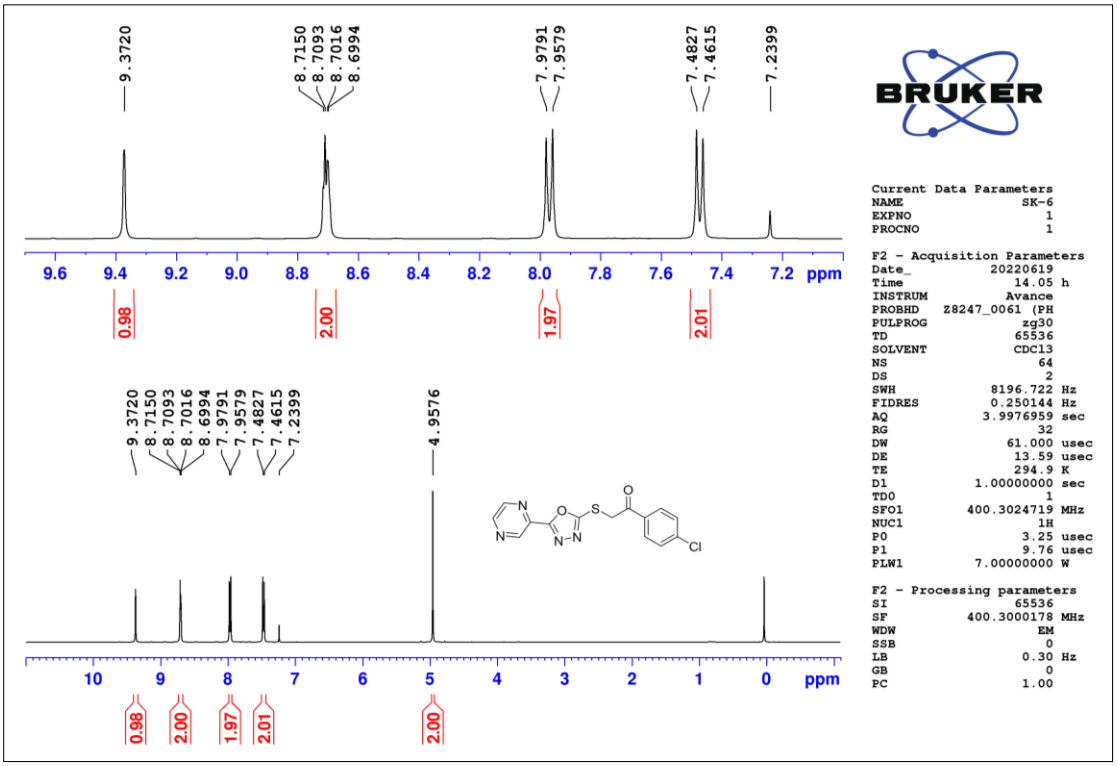

Figure 2.57 *^{1}H-NMR spectrum of compound* ***T6***

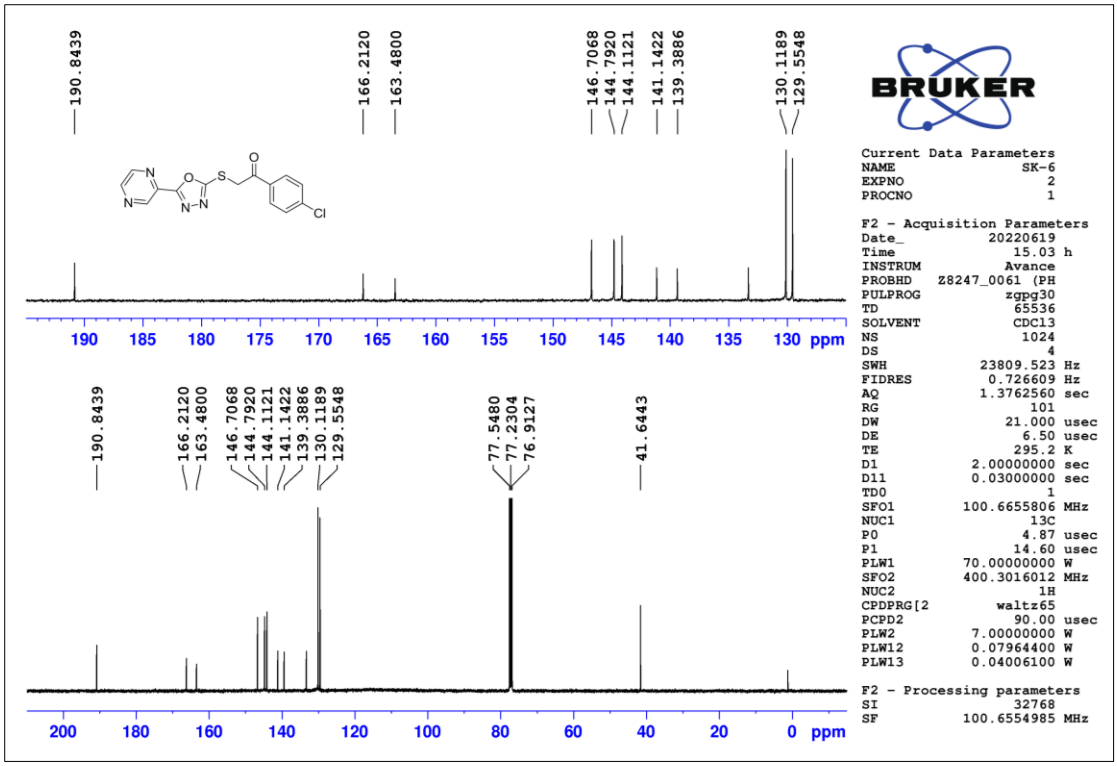

Figure 2.58 *^{13}C-NMR spectrum of compound* ***T6***

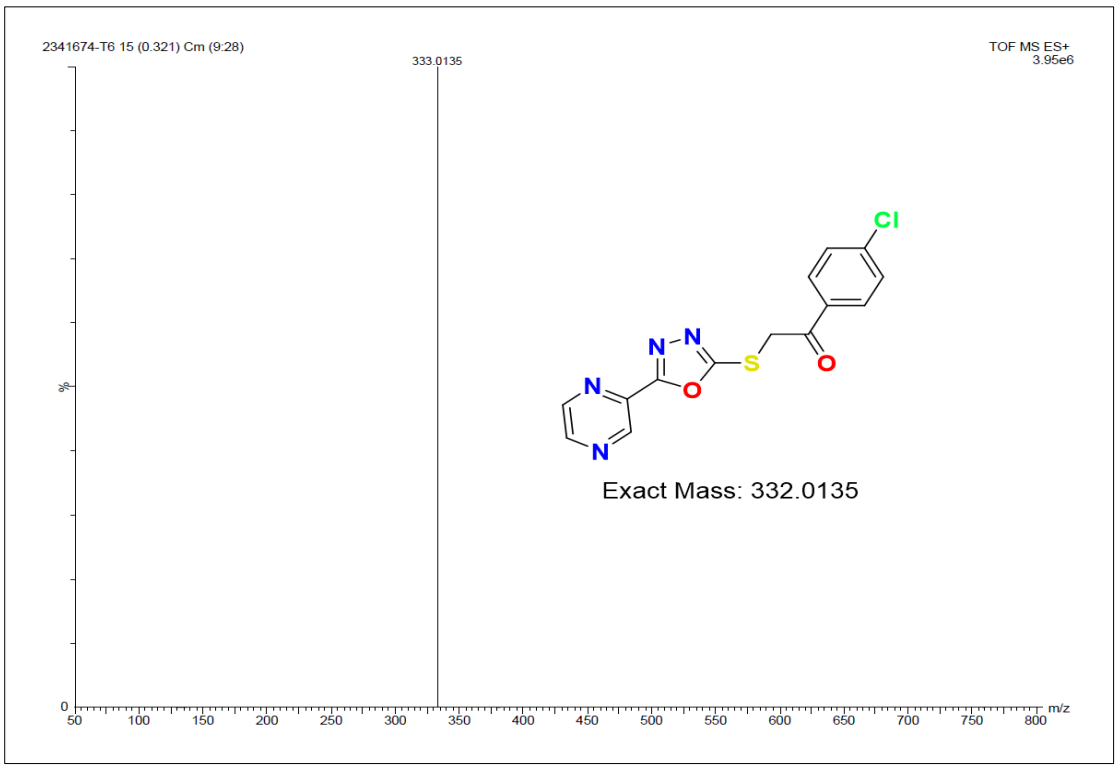

Figure 2.59 *HR-MS spectrum of compound* ***T6***

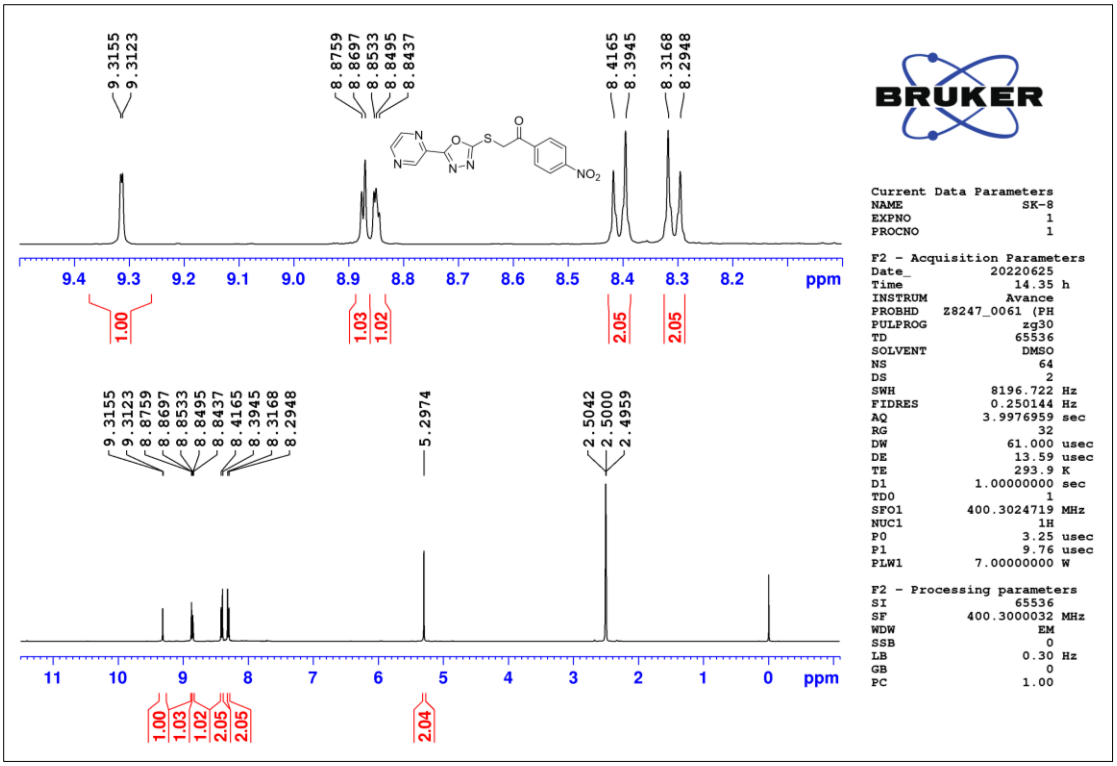

Figure 2.60 *^{1}H-NMR spectrum of compound* ***T8***

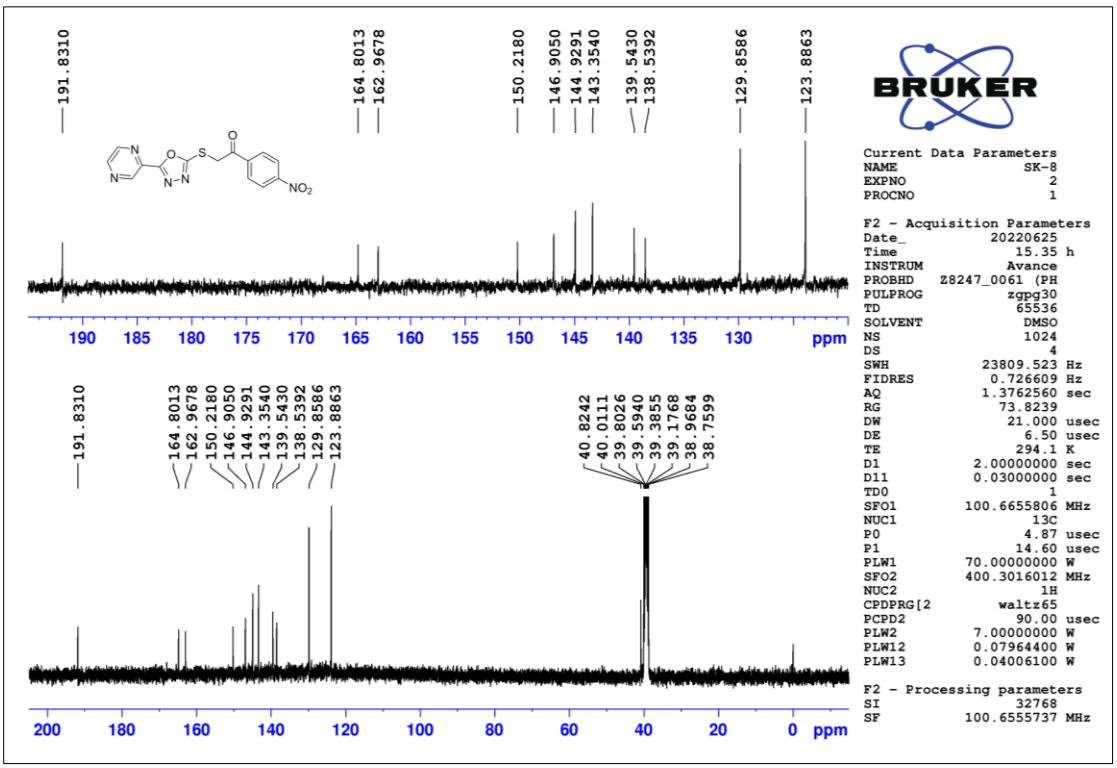

Figure 2.61 *^{13}C-NMR spectrum of compound* ***T8***

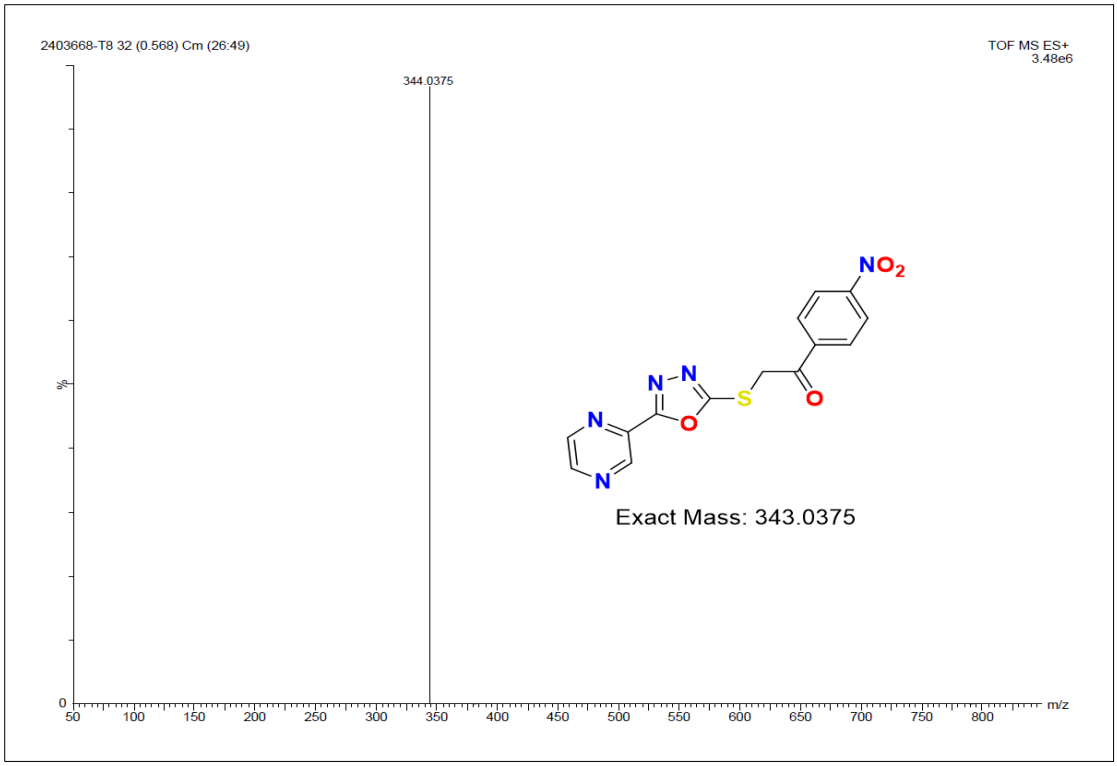

Figure 2.62 *HR-MS spectrum of compound* ***T8***

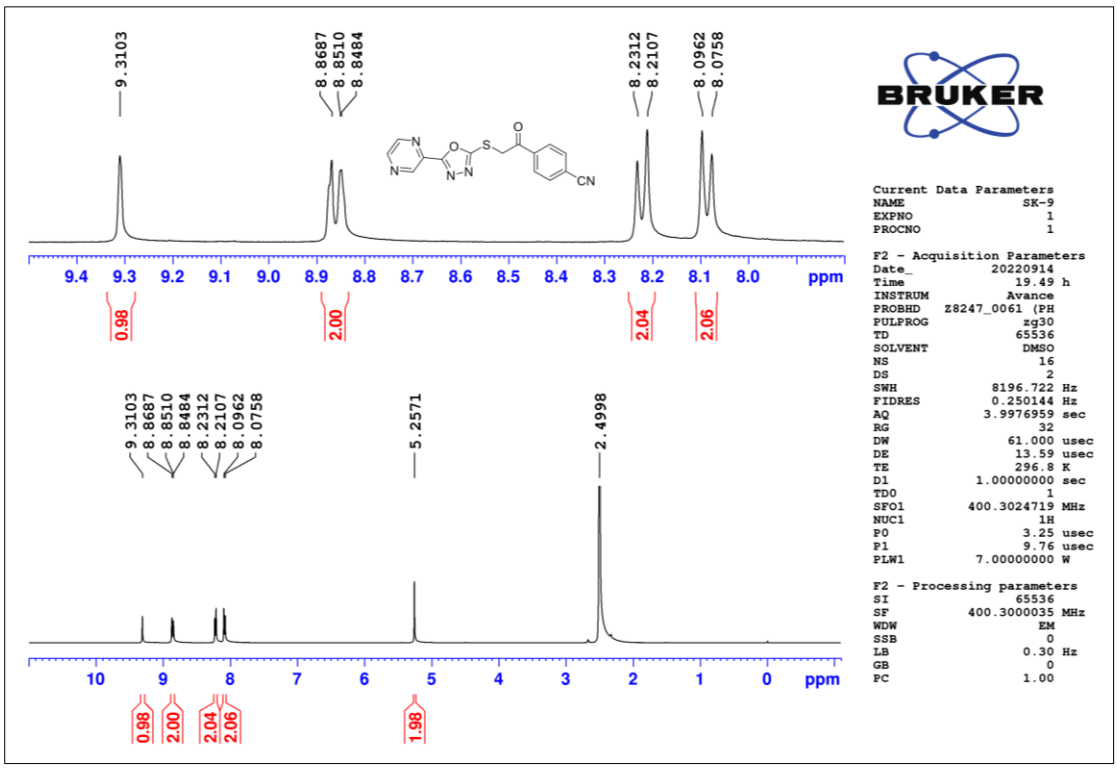

Figure 2.63 *^{1}H-NMR spectrum of compound* ***T9***

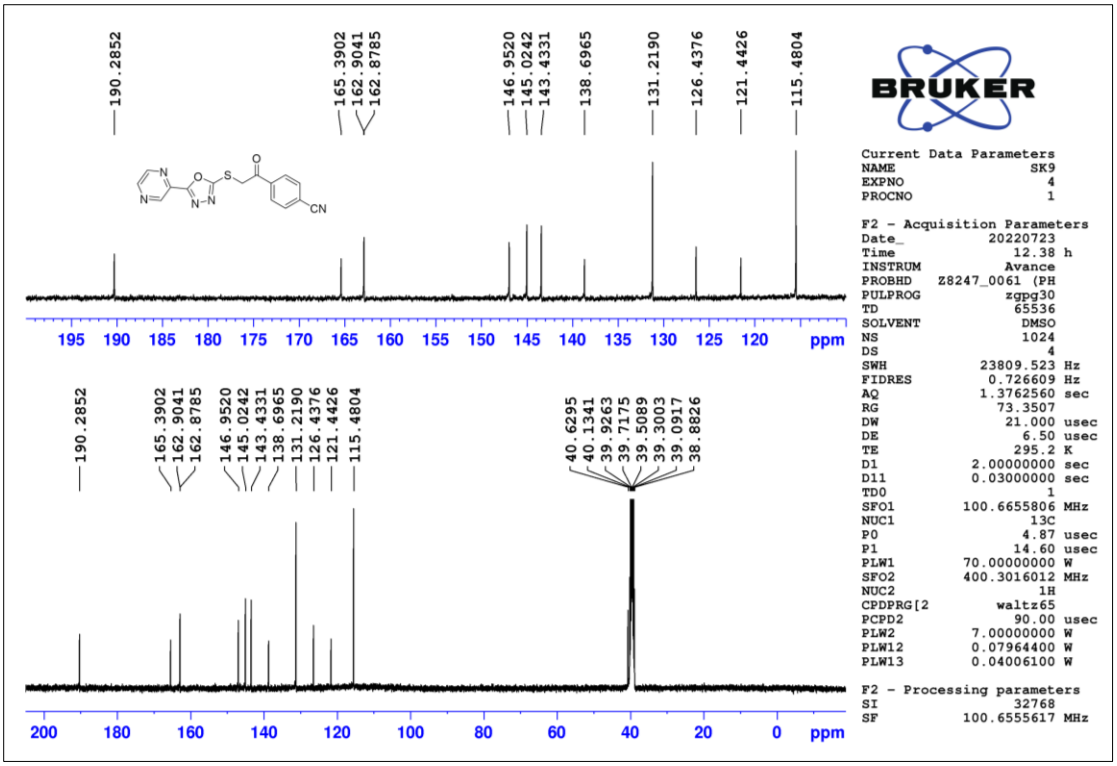

Figure 2.64 *^{13}C-NMR spectrum of compound* ***T9***

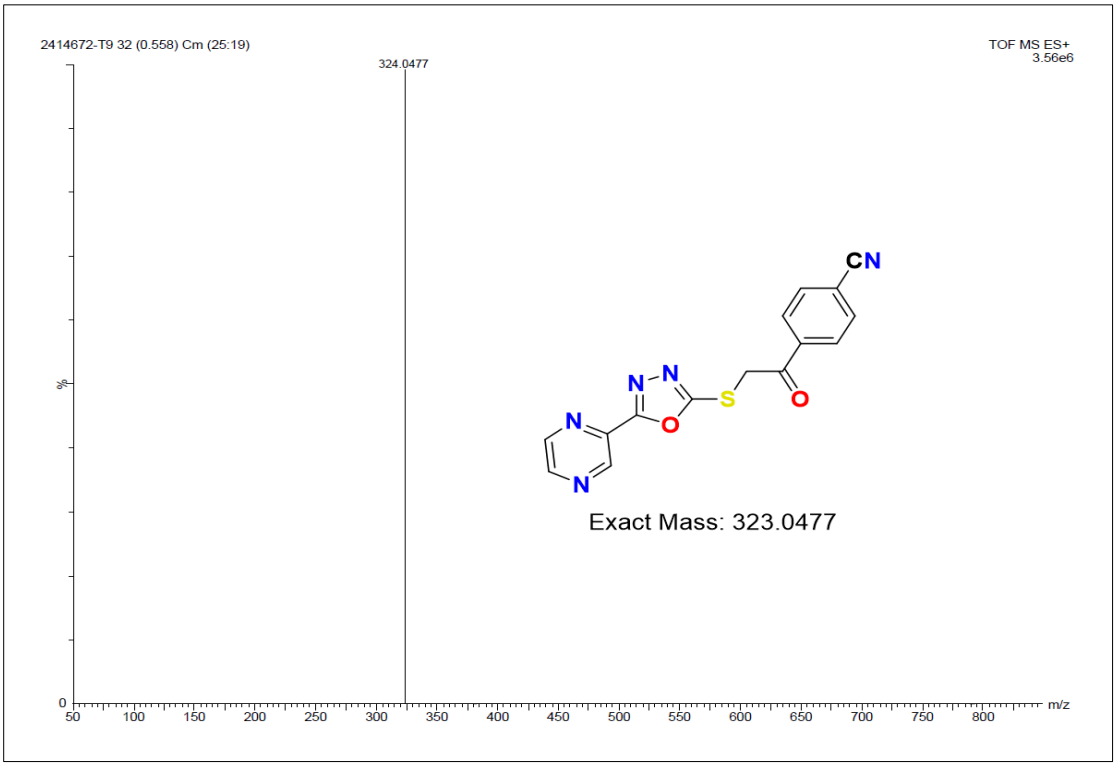

Figure 2.65 *HR-MS spectrum of compound* ***T9***

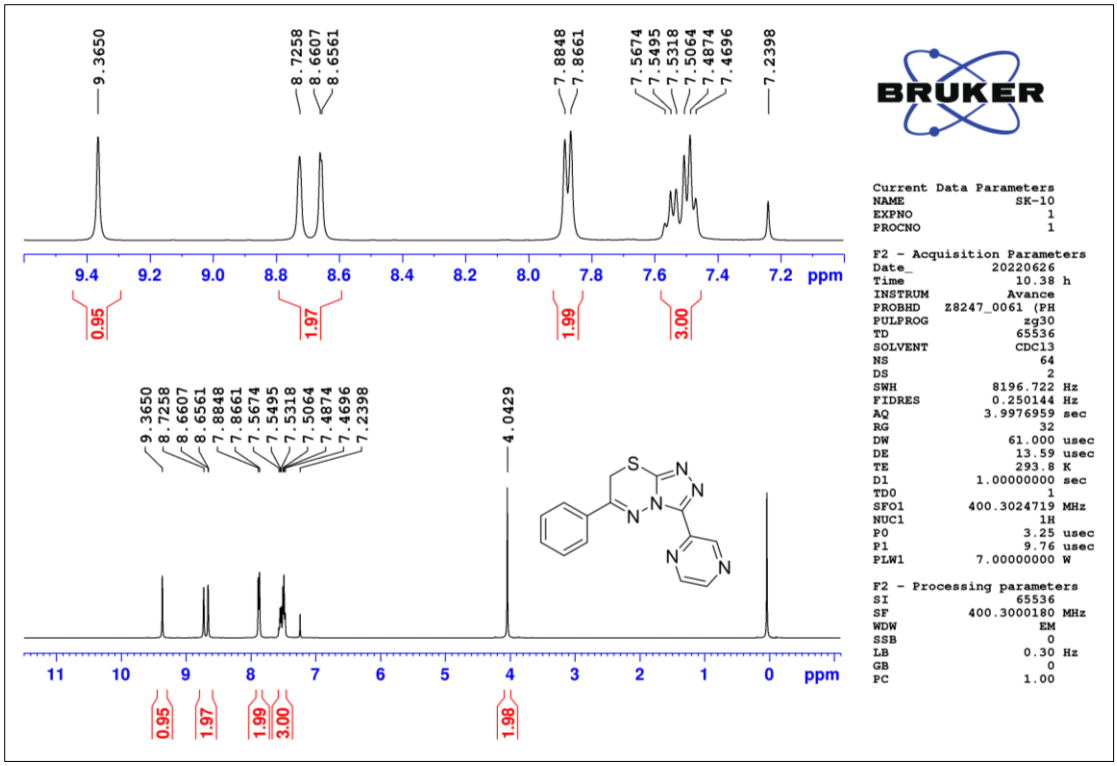

Figure 2.66 *^{1}H-NMR spectrum of compound* ***T10***

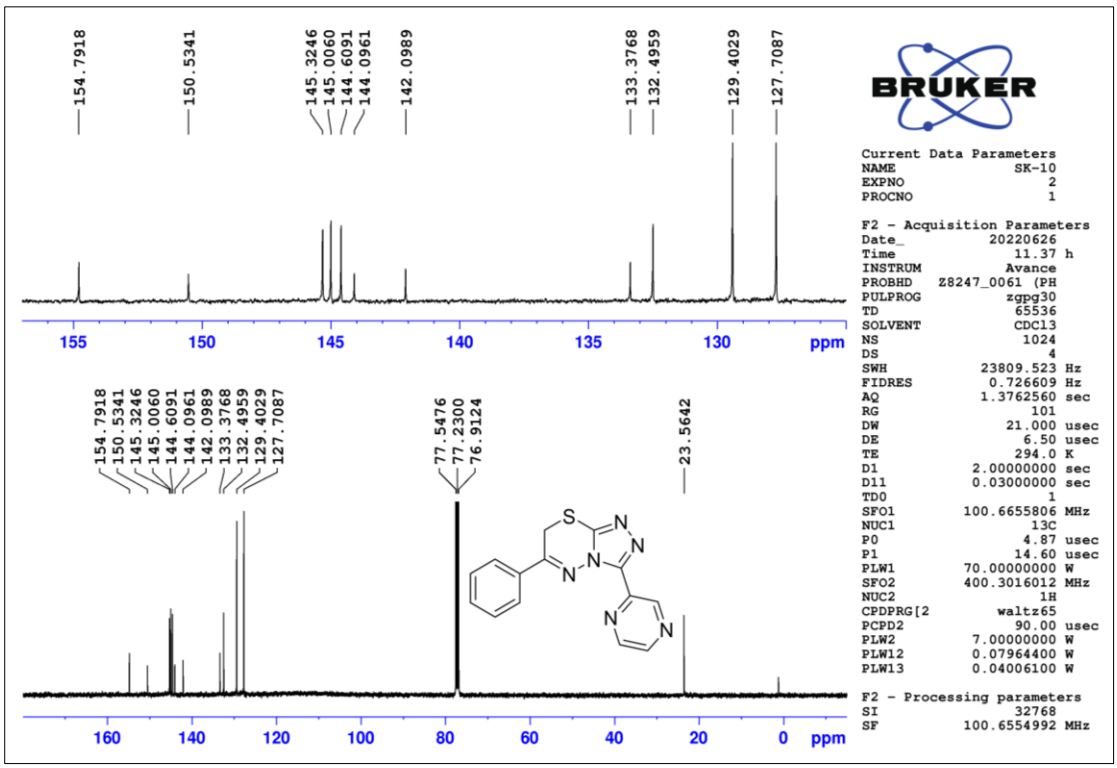

Figure 2.67 *^{13}C-NMR spectrum of compound* ***T10***

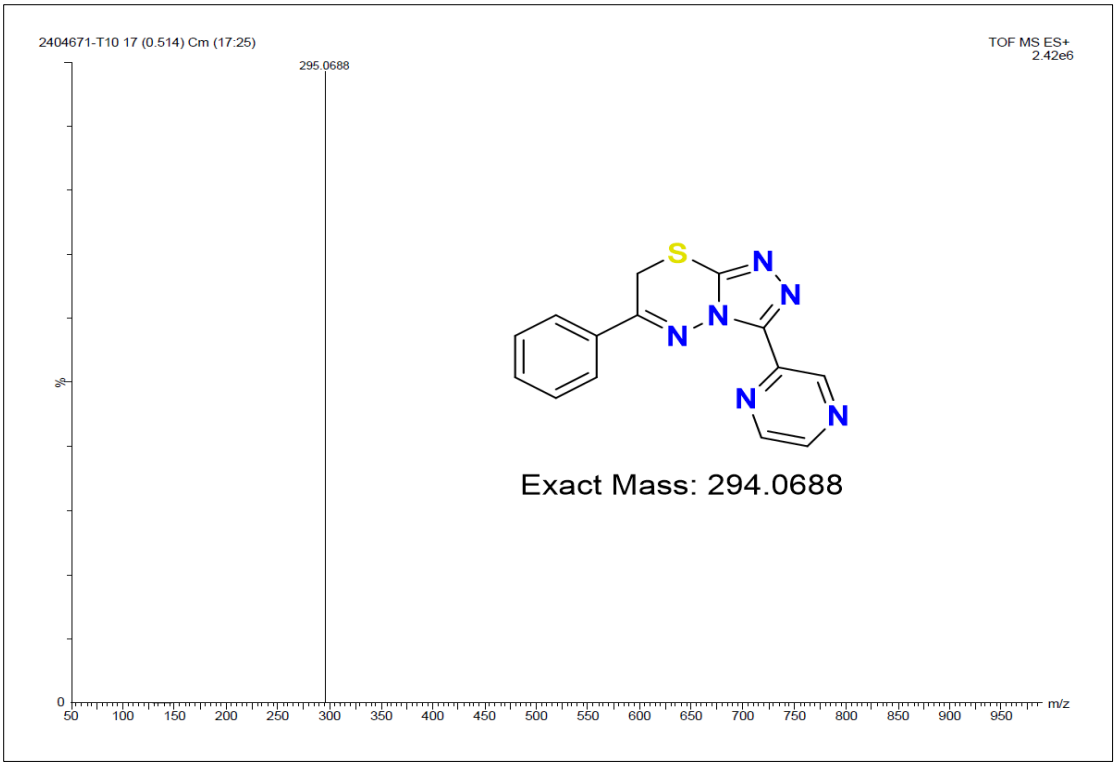

Figure 2.68 *HR-MS spectrum of compound* ***T10***

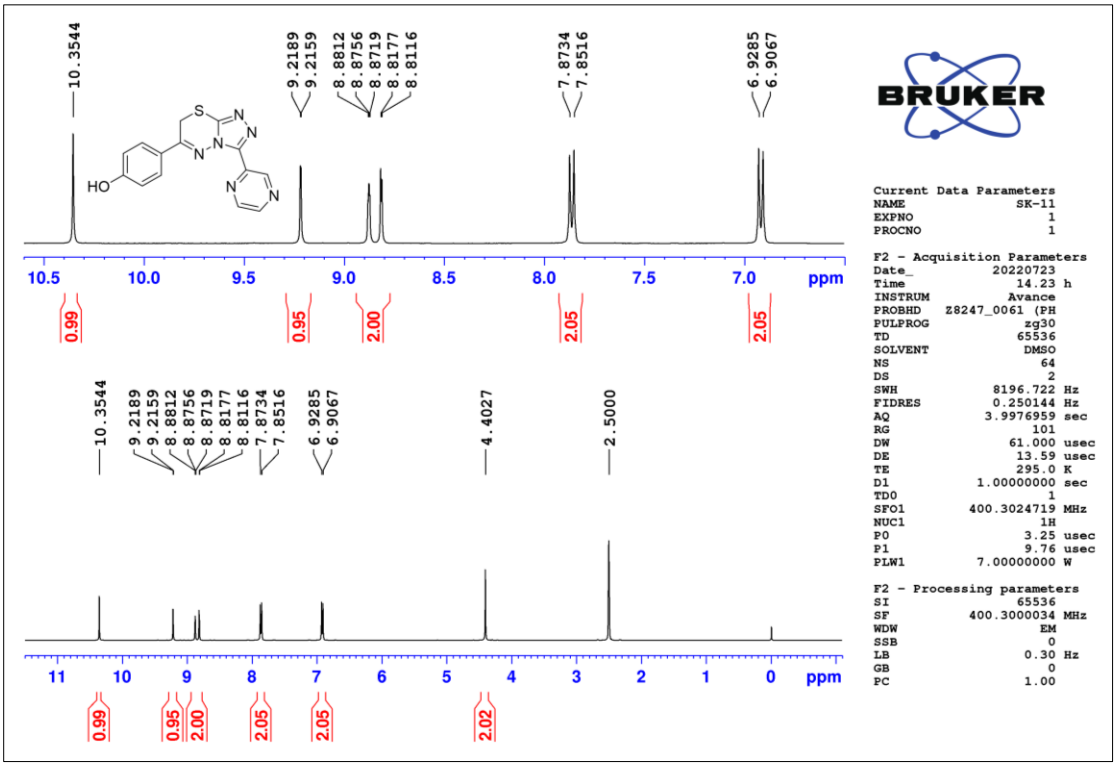

Figure 2.69 *^{1}H-NMR spectrum of compound* ***T11***

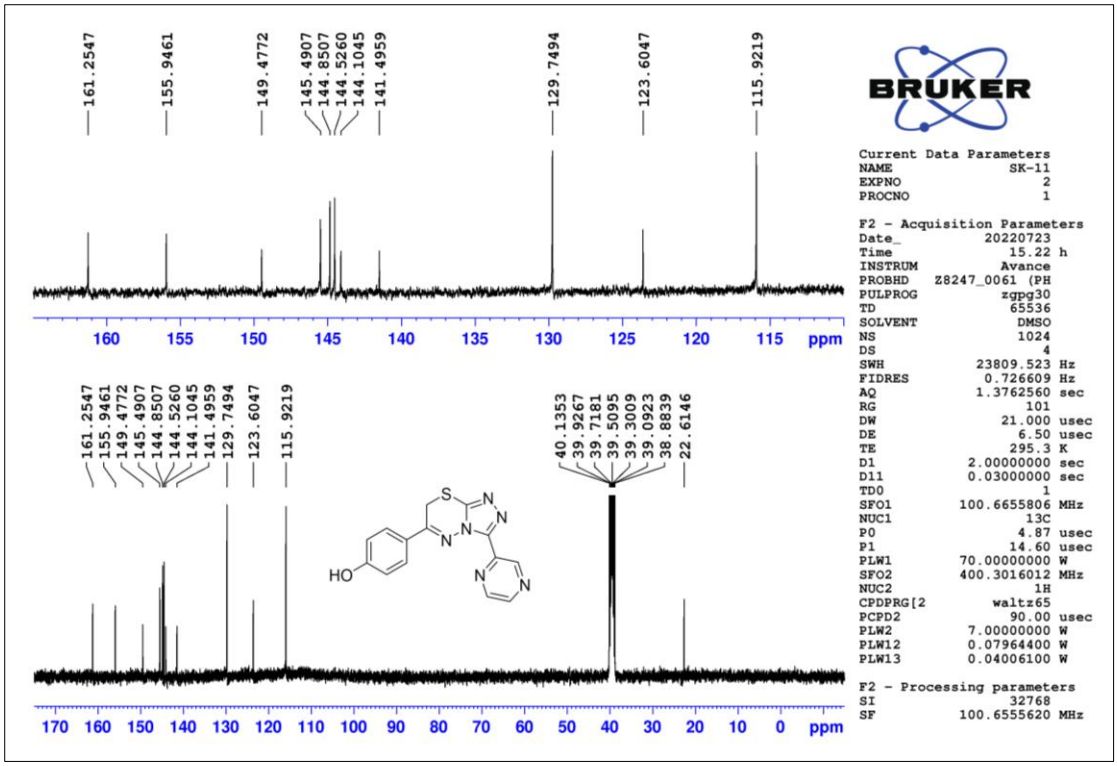

Figure 2.70 *^{13}C-NMR spectrum of compound* ***T11***

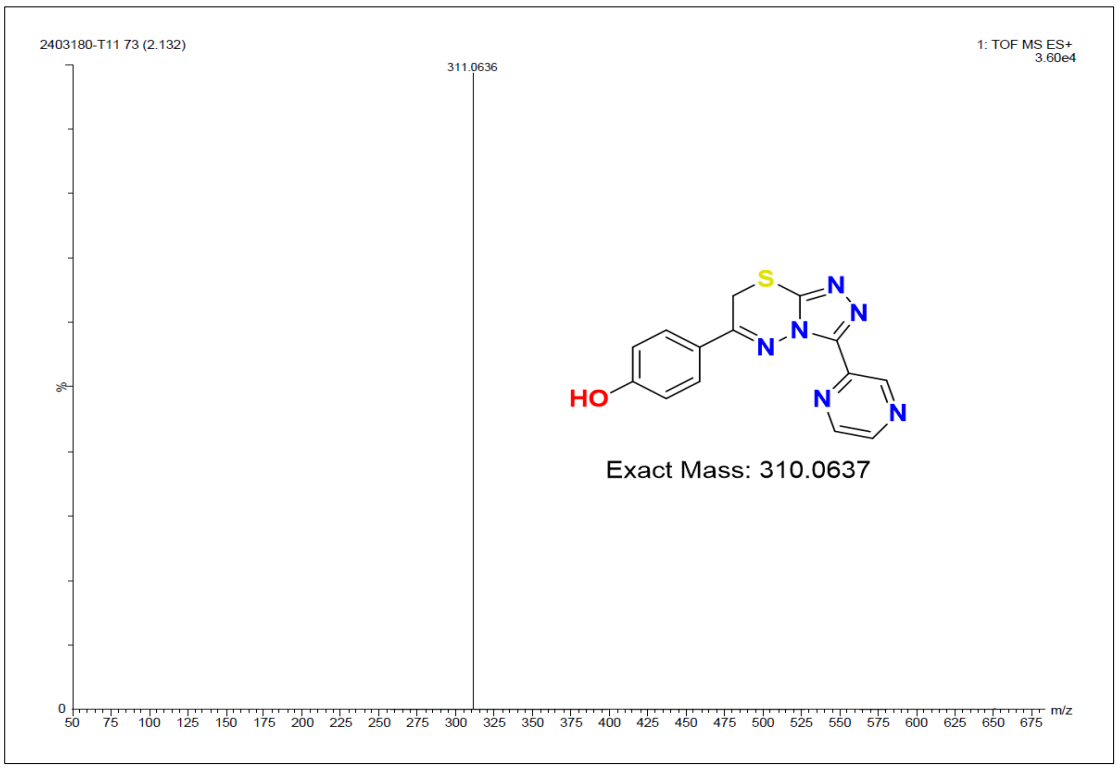

Figure 2.71 *HR-MS spectrum of compound* ***T11***

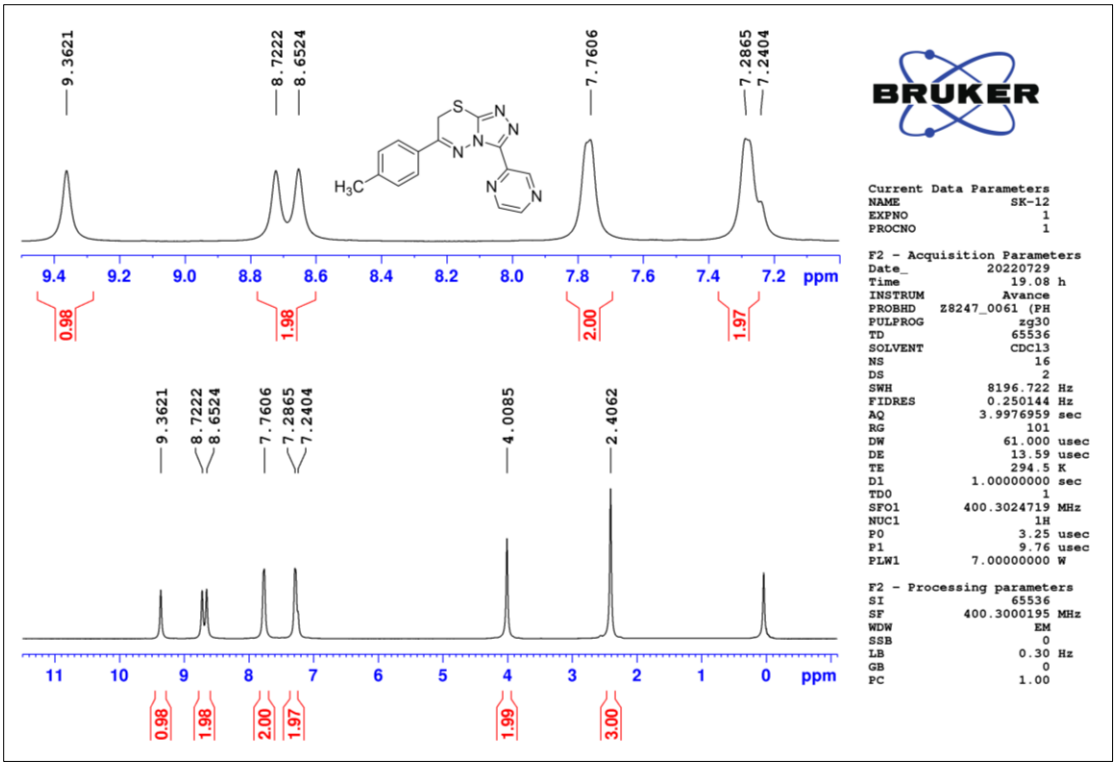

Figure 2.72 *^{1}H-NMR spectrum of compound* ***T12***

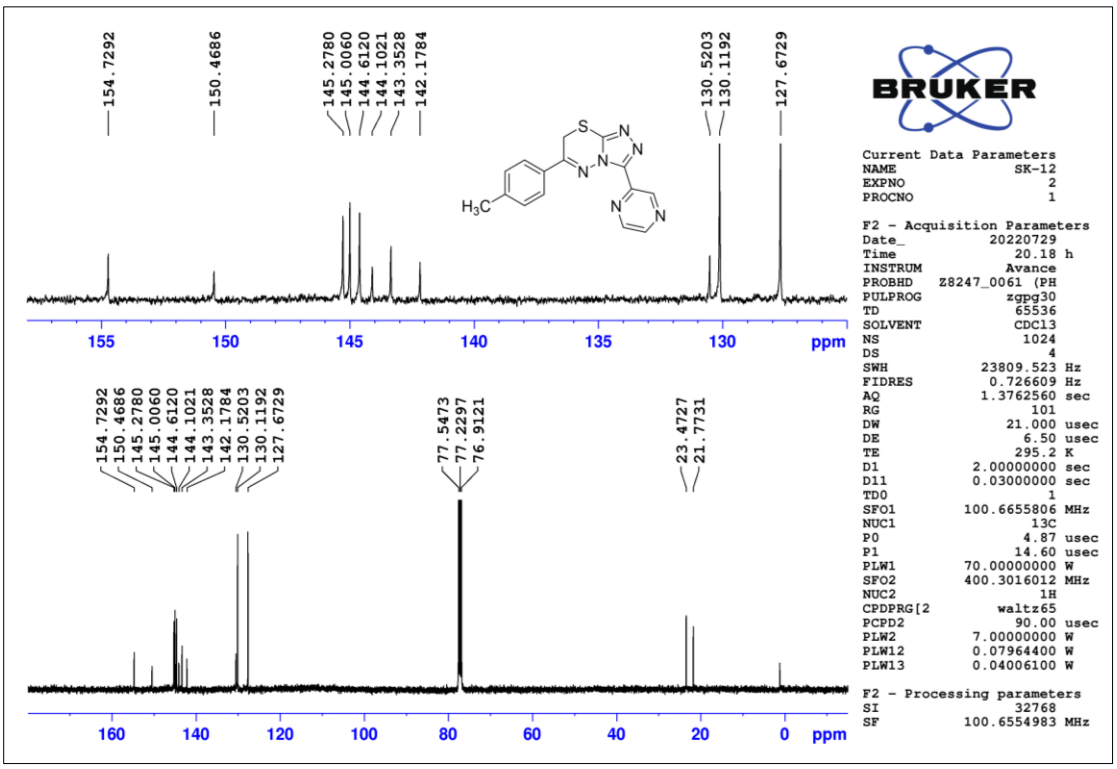

Figure 2.73 *^{13}C-NMR spectrum of compound* ***T12***

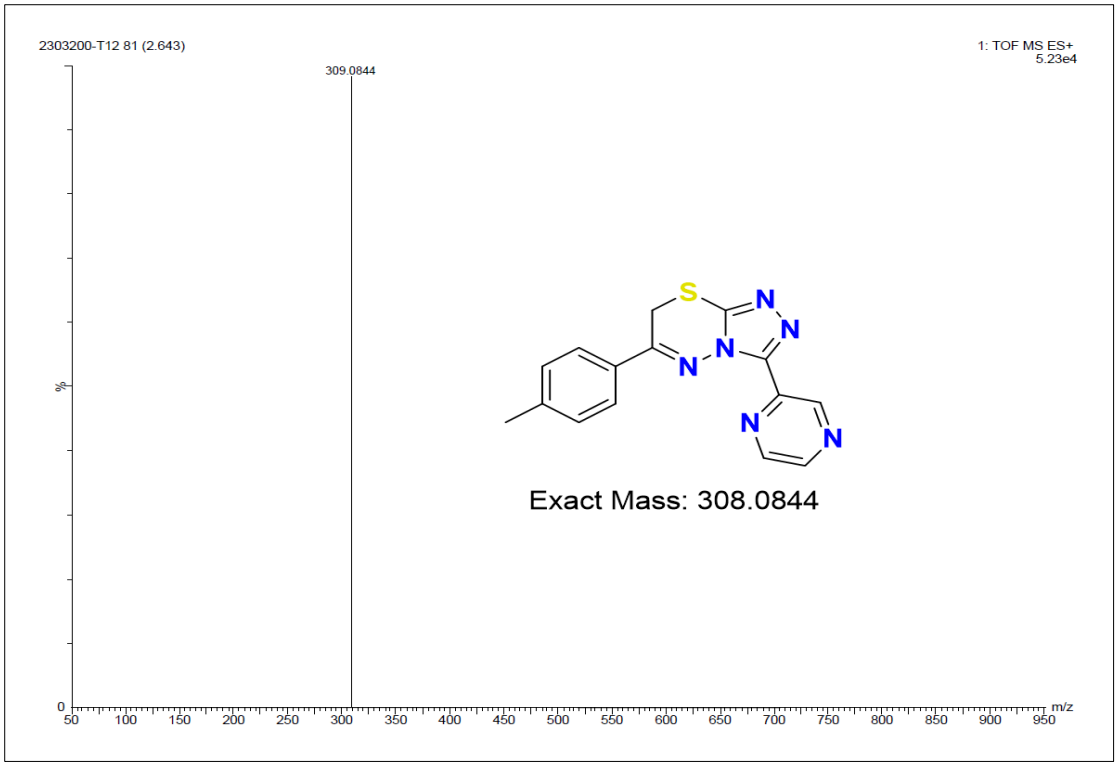

Figure 2.74 *HR-MS spectrum of compound* ***T12***

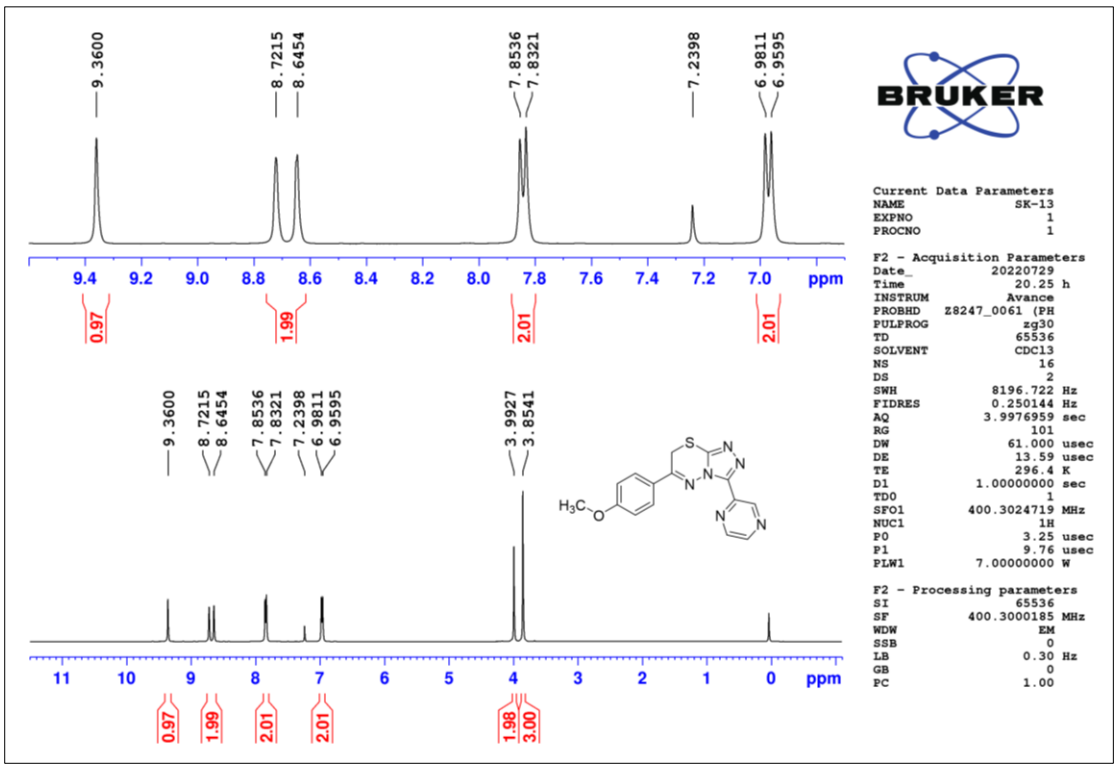

Figure 2.75 *^{1}H-NMR spectrum of compound* ***T13***

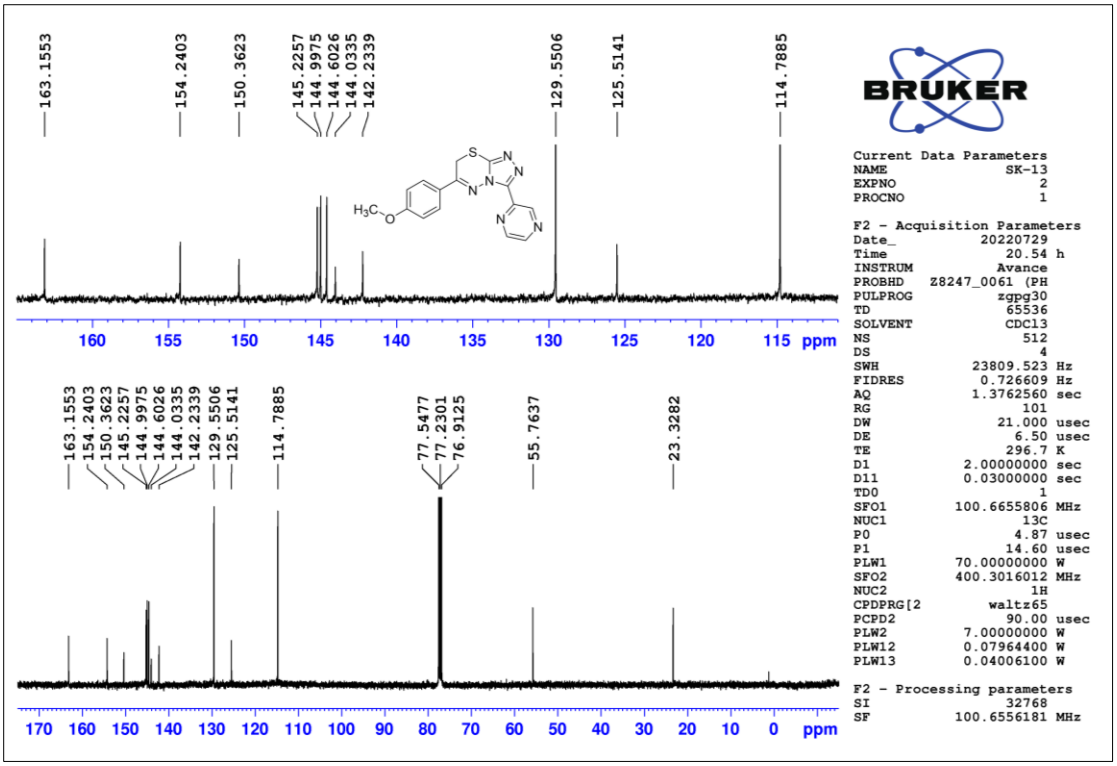

Figure 2.76 *^{13}C-NMR spectrum of compound* ***T13***

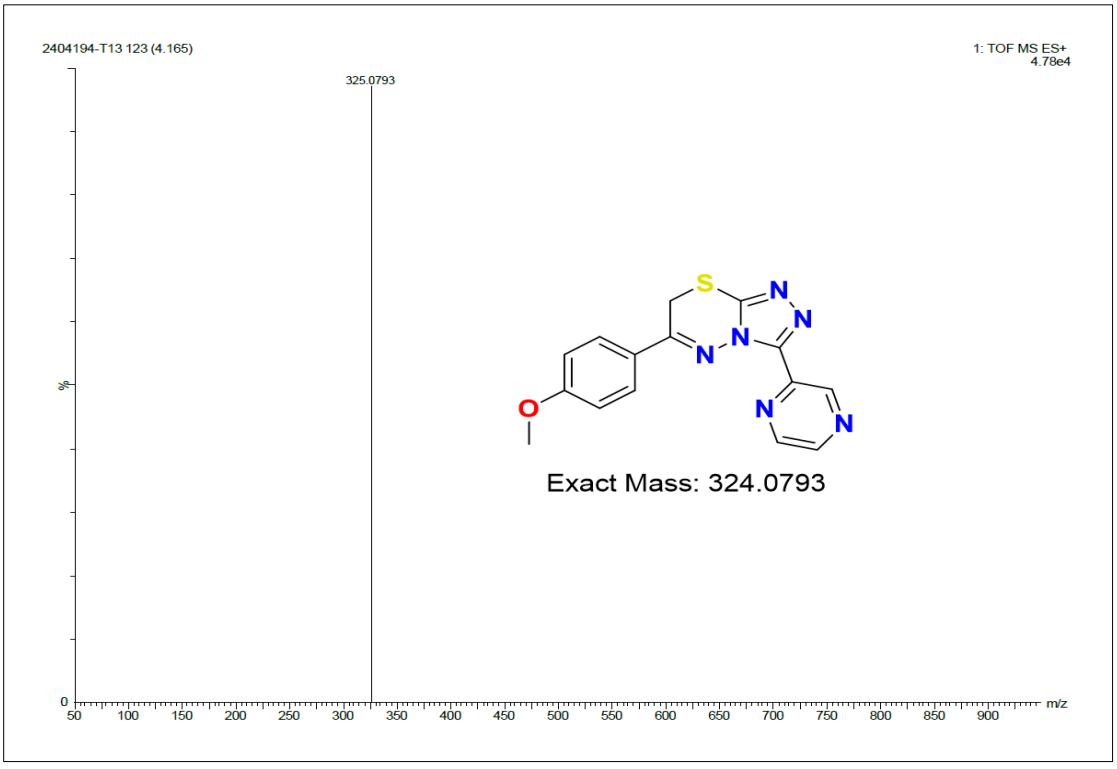

Figure 2.77 *HR-MS spectrum of compound* ***T13***

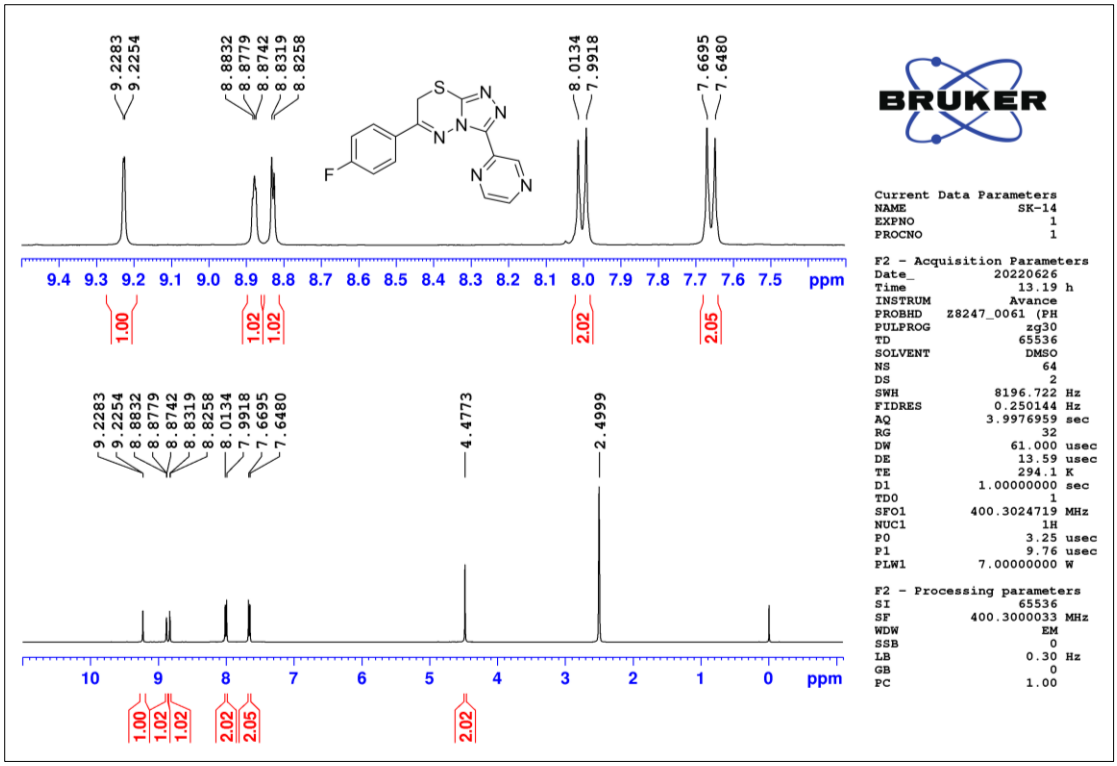

Figure 2.78 *[1]H-NMR spectrum of compound* ***T14***

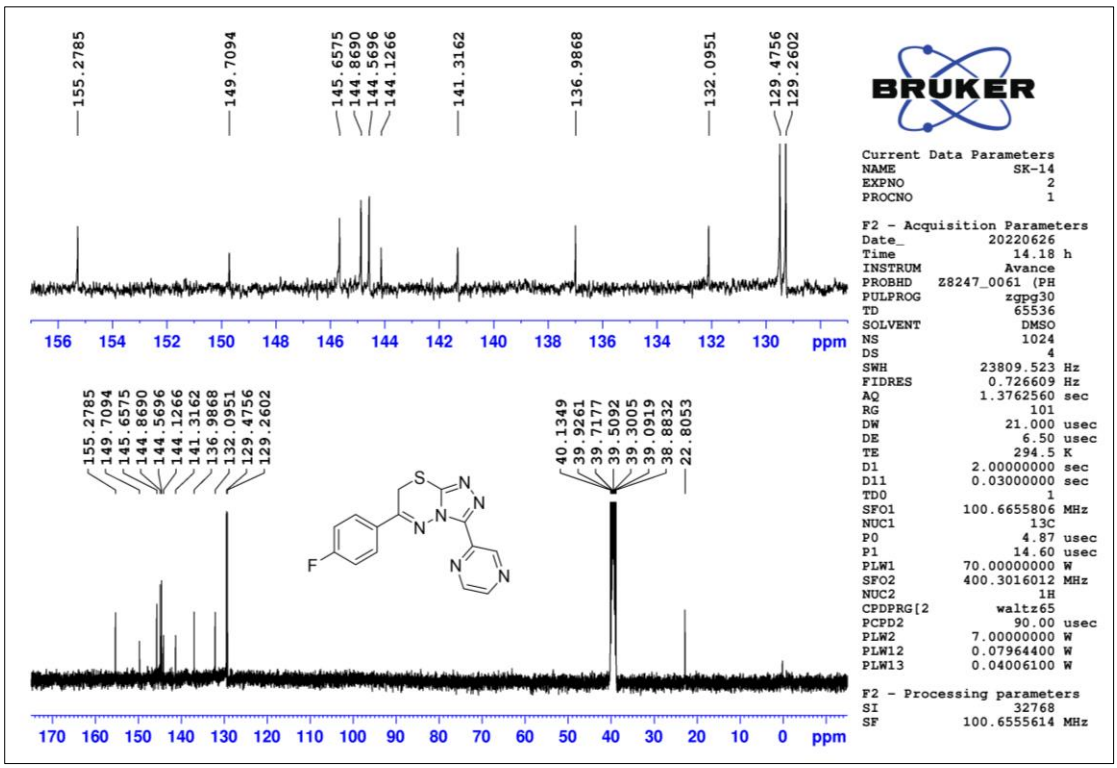

Figure 2.79 *[13]C-NMR spectrum of compound* ***T14***

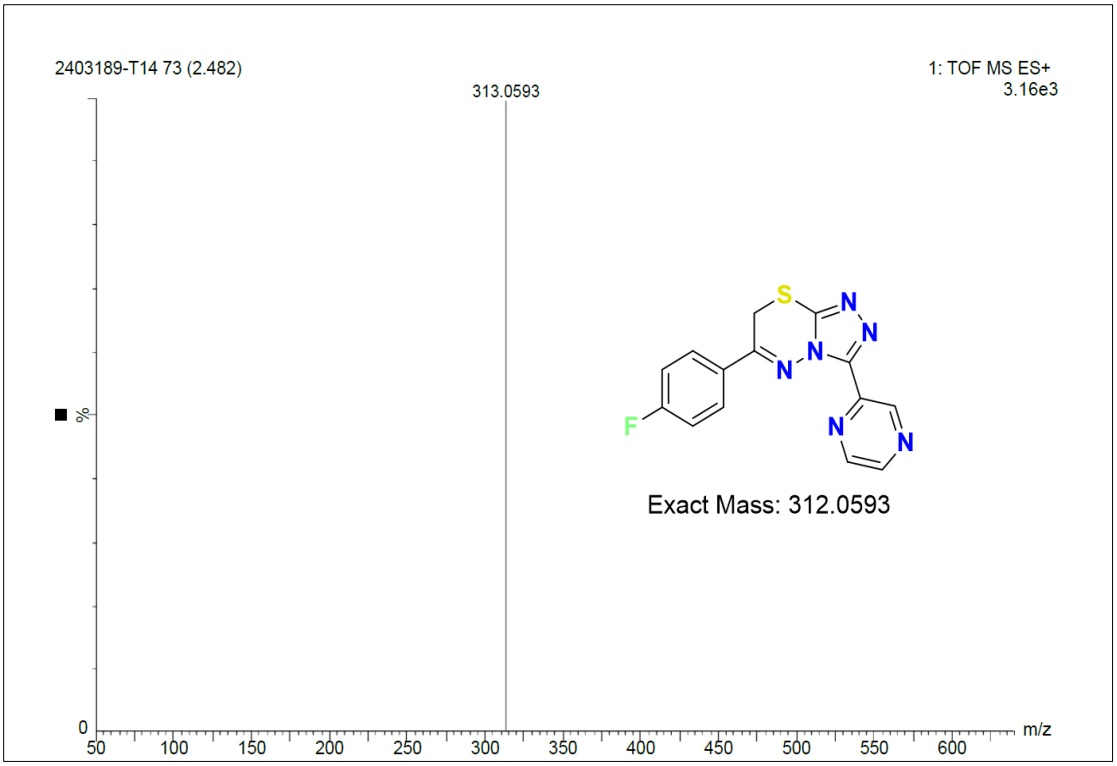

Figure 2.80 *HR-MS spectrum of compound* ***T14***

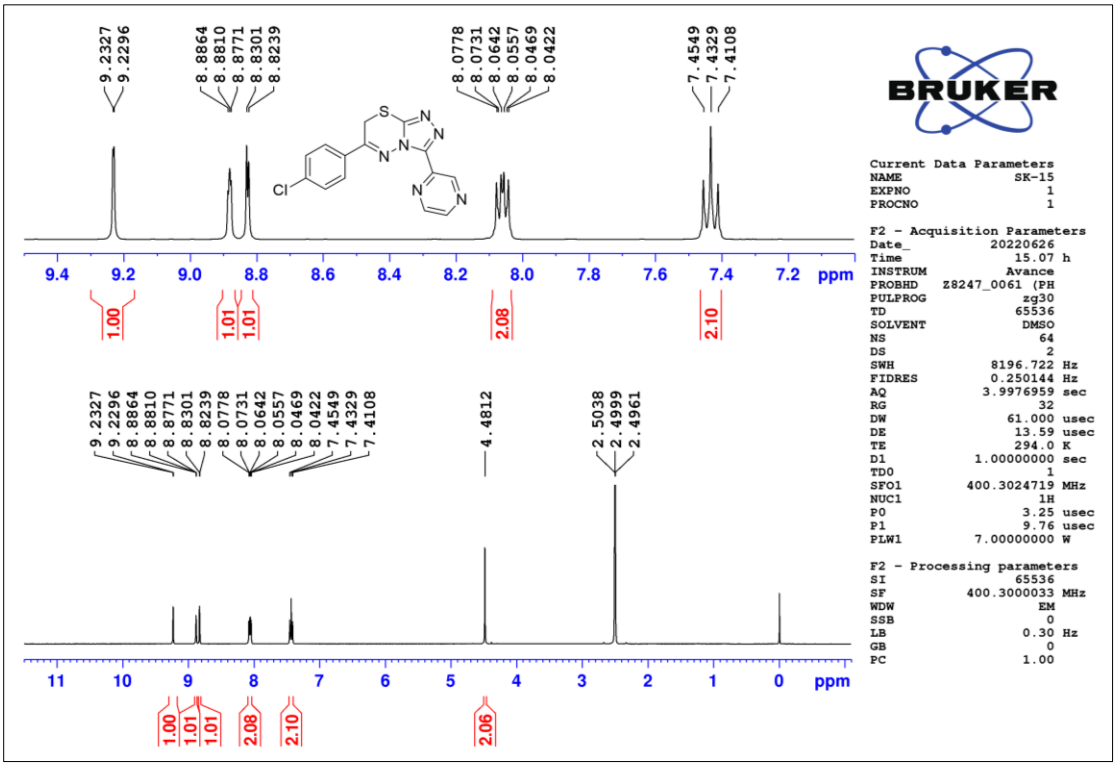

Figure 2.81 *^{1}H-NMR spectrum of compound* ***T15***

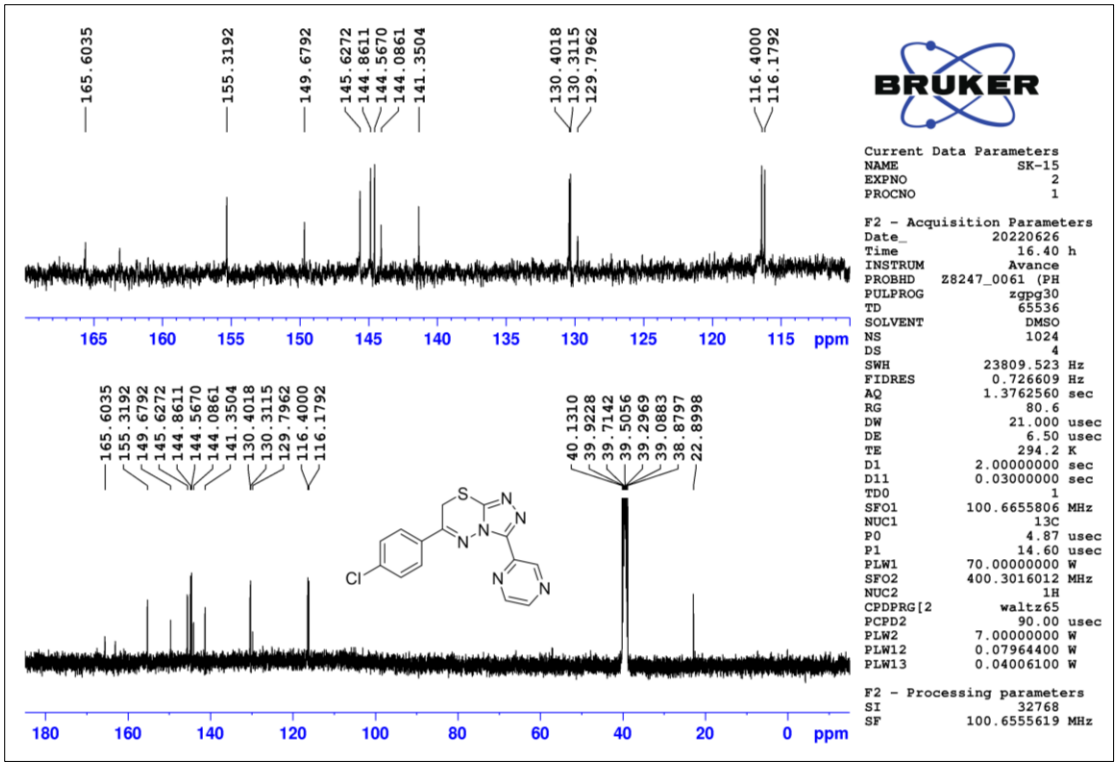

Figure 2.82 *^{13}C-NMR spectrum of compound* ***T15***

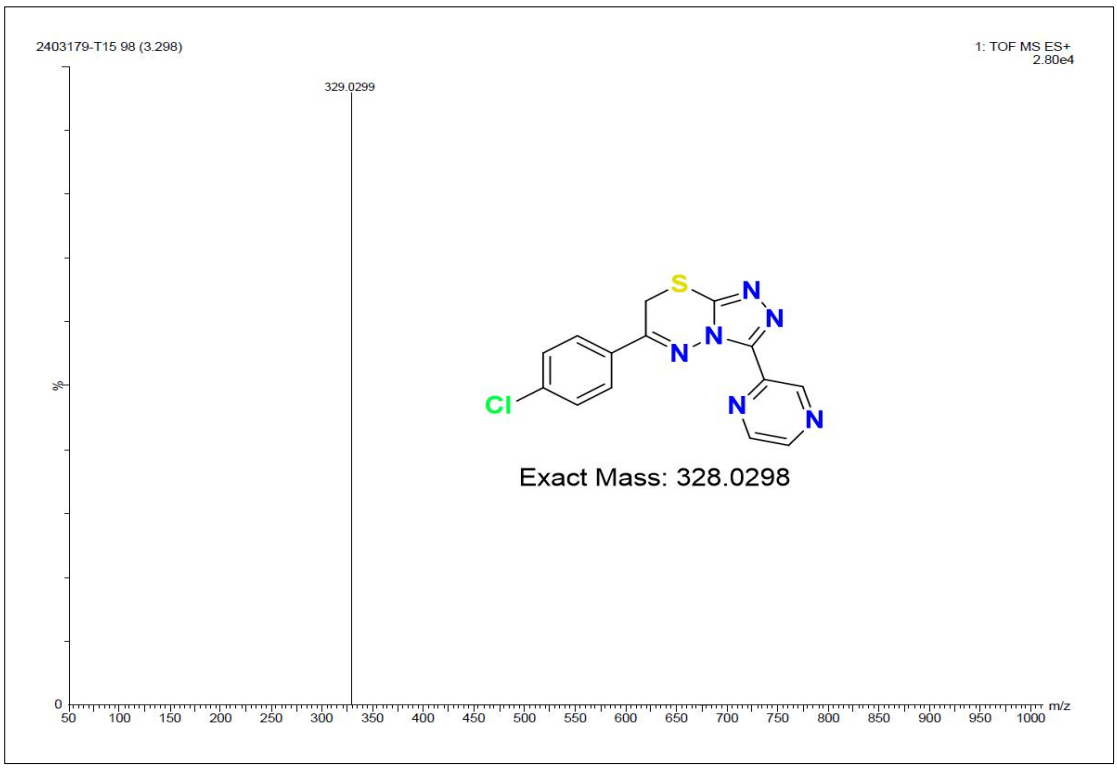

Figure 2.83 *HR-MS spectrum of compound* ***T15***

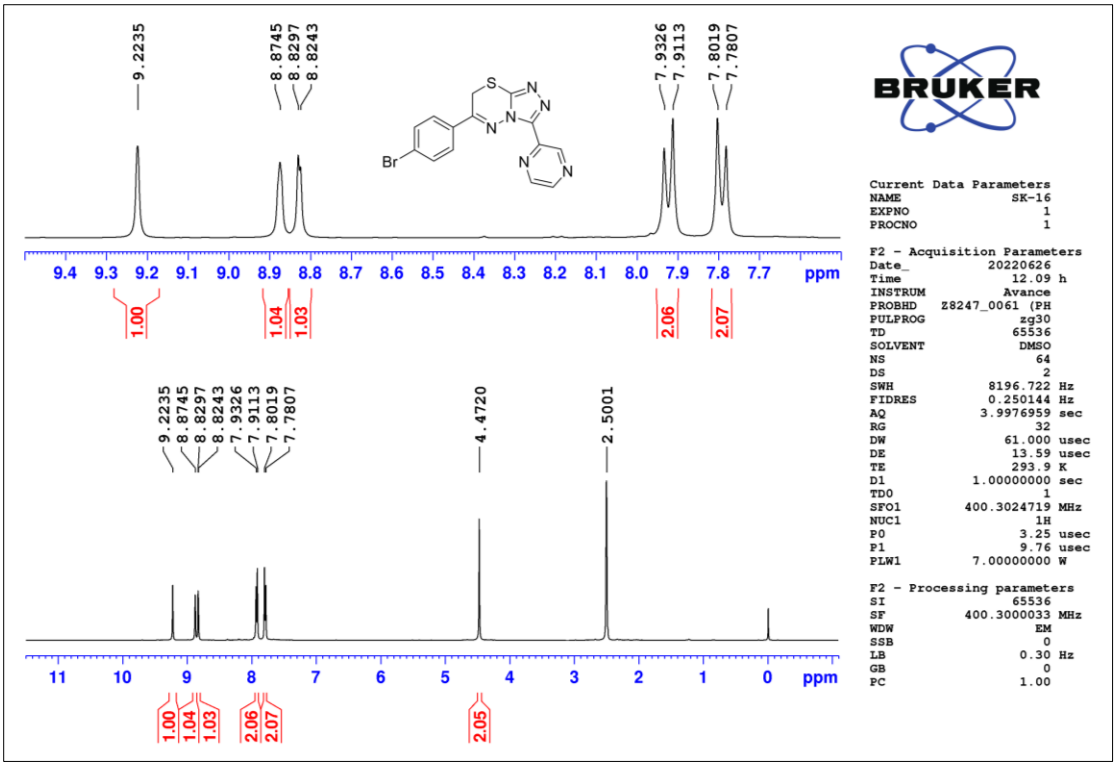

Figure 2.84 *[1]H-NMR spectrum of compound* ***T16***

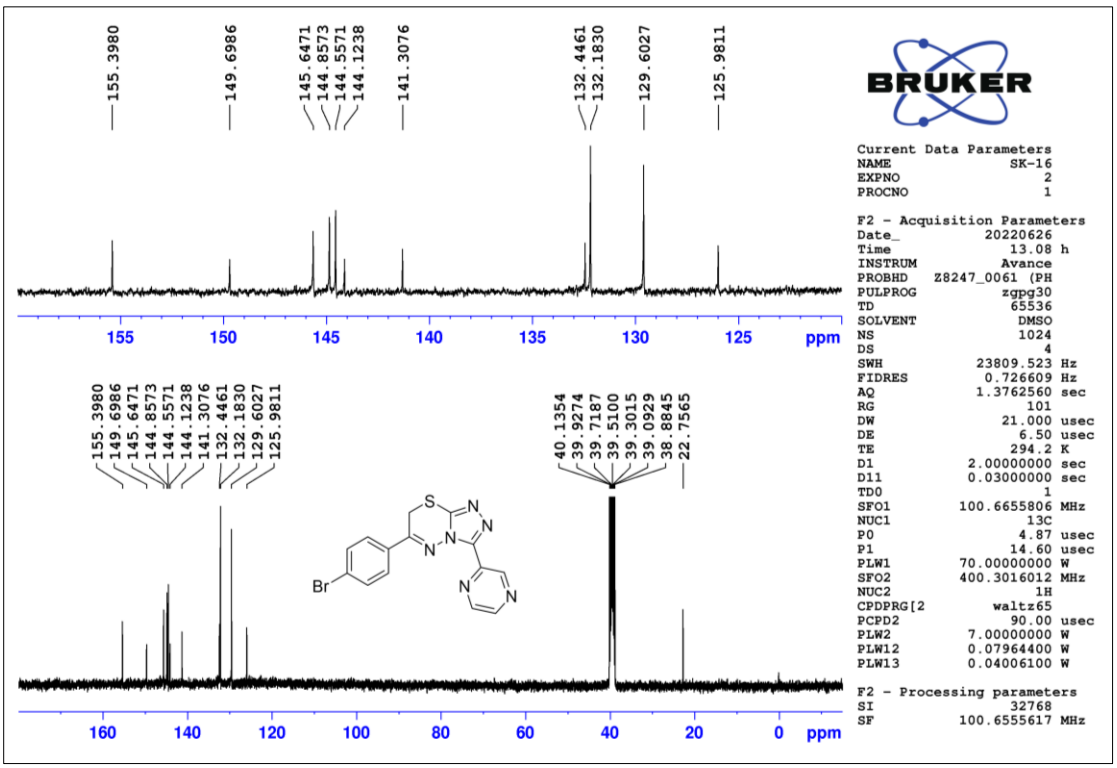

Figure 2.85 *[13]C-NMR spectrum of compound* ***T16***

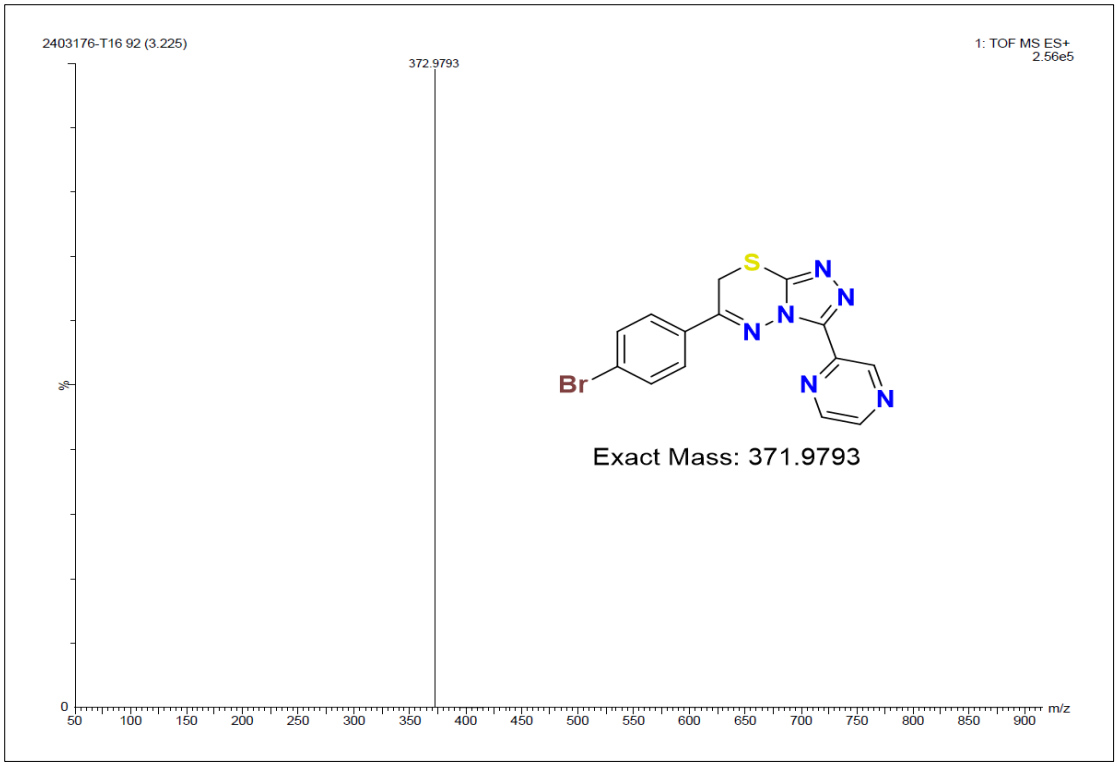

Figure 2.86 *HR-MS spectrum of compound* ***T16***

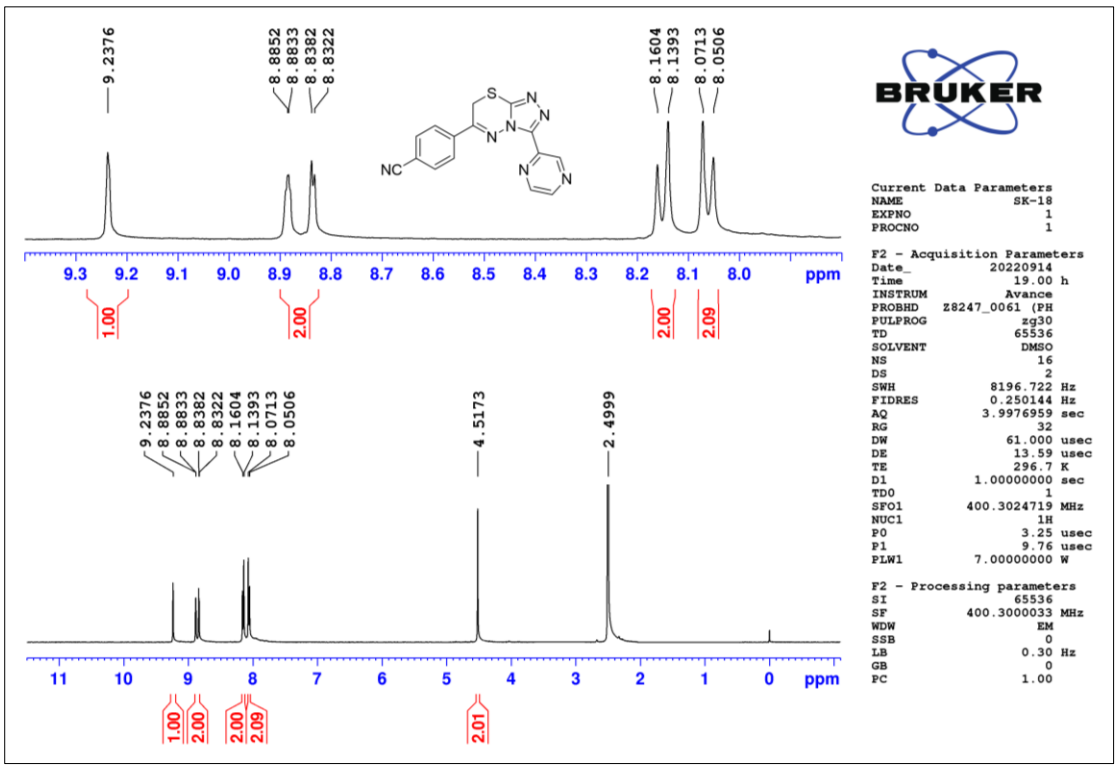

Figure 2.87 *^{1}H-NMR spectrum of compound* ***T18***

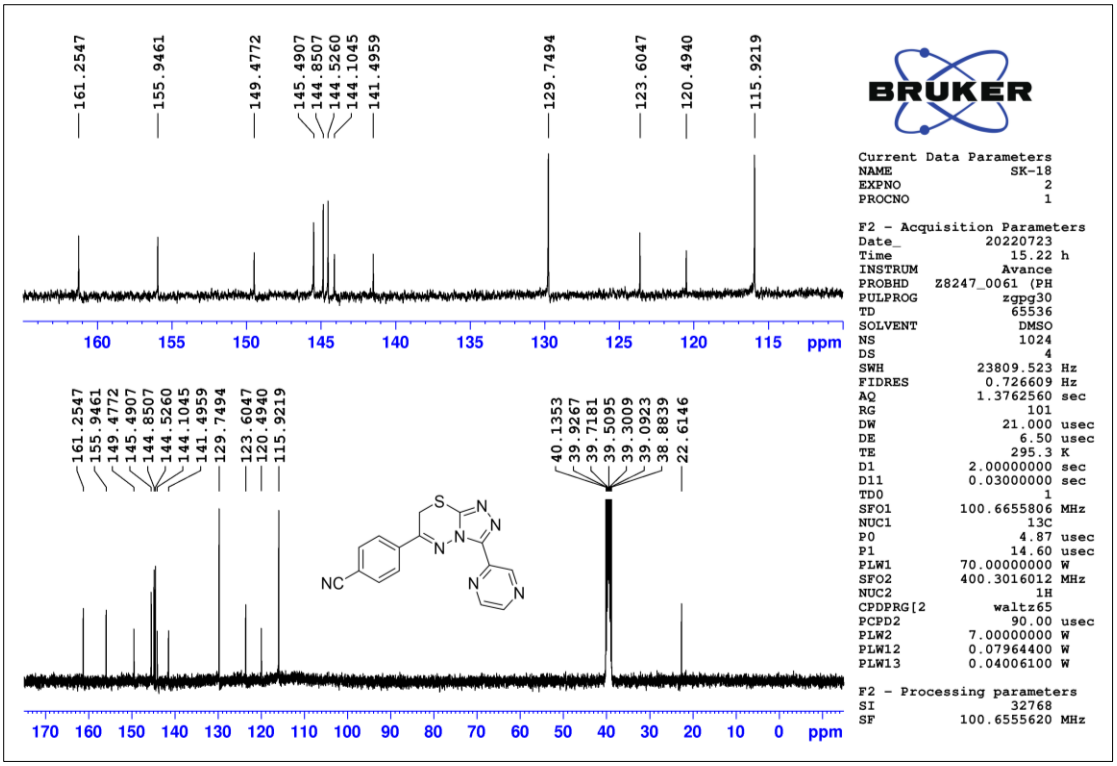

Figure 2.88 *^{13}C-NMR spectrum of compound* ***T18***

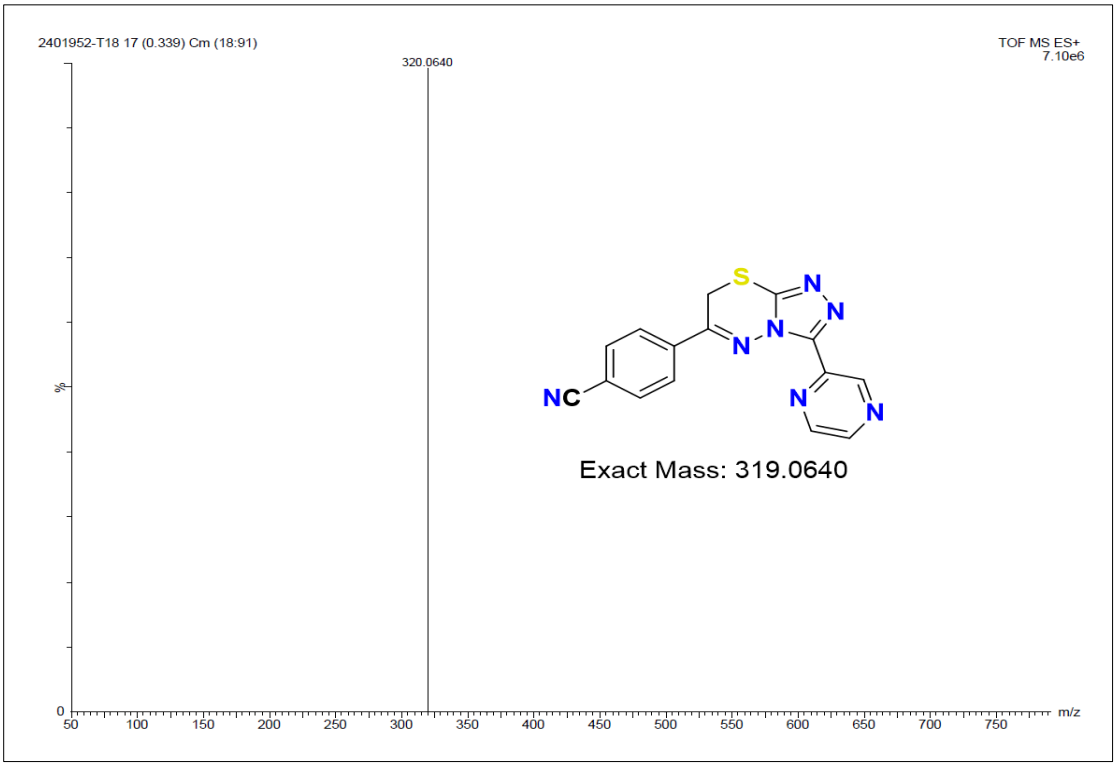

Figure 2.89 *HR-MS spectrum of compound* ***T18***

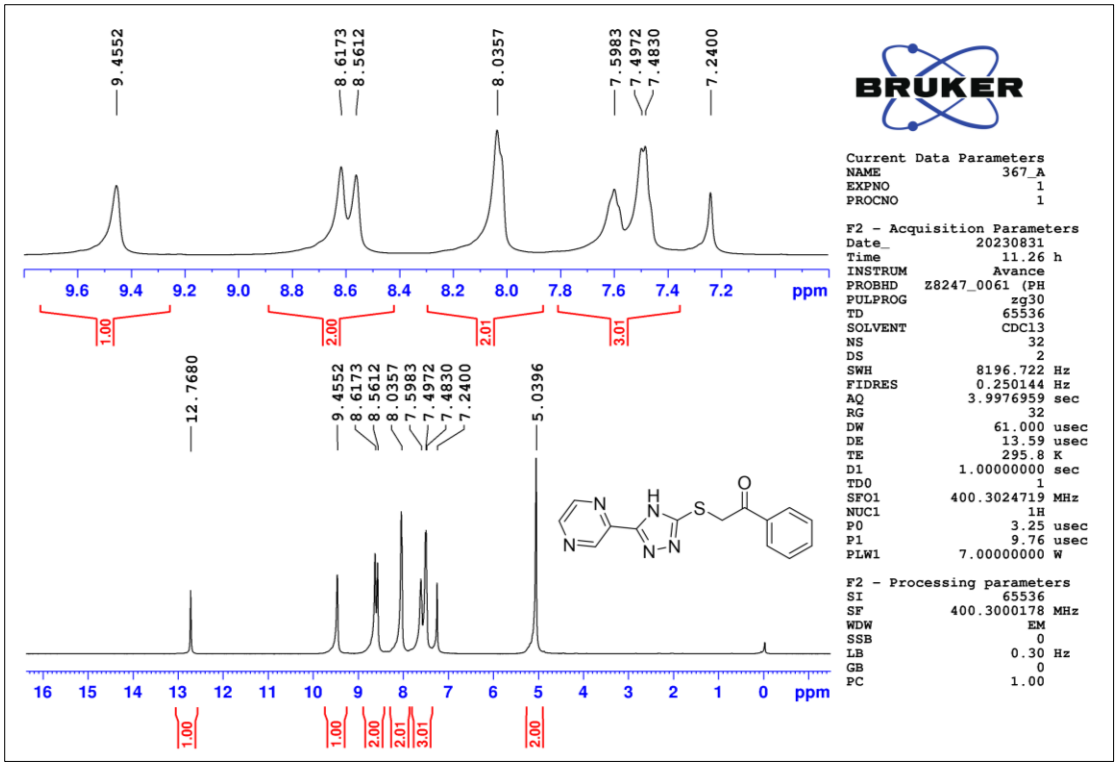

Figure 2.90 *[1]H-NMR spectrum of compound* ***T19***

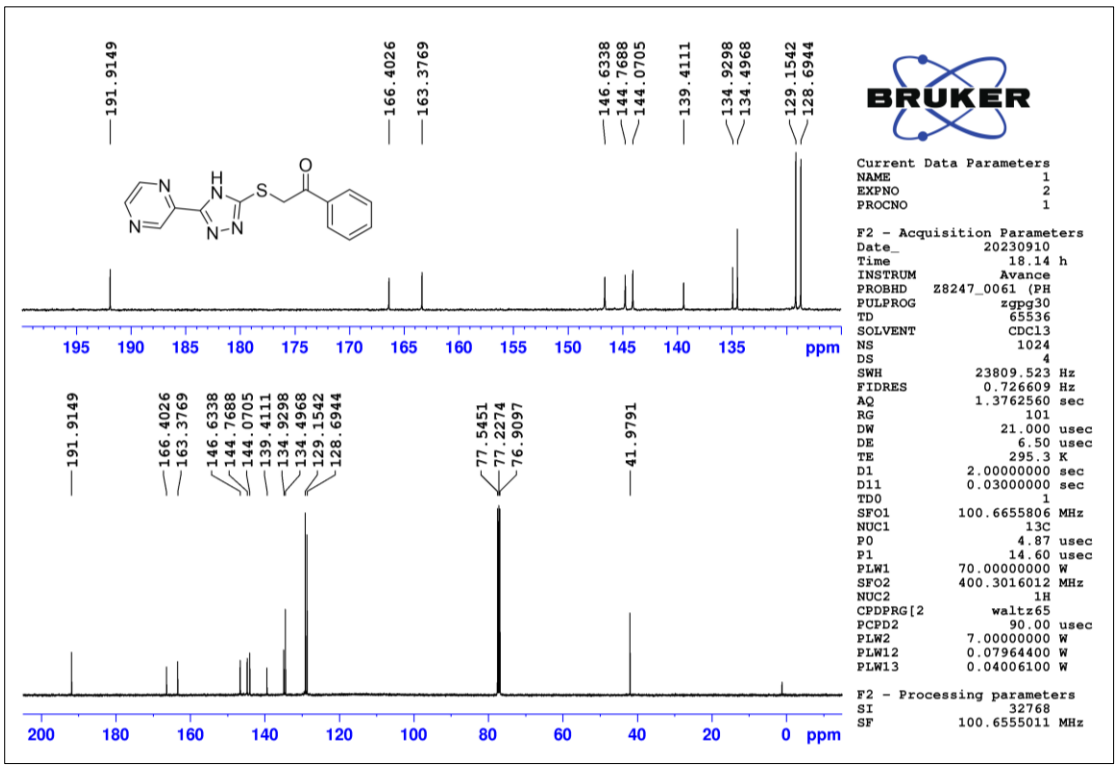

Figure 2.91 *[13]C-NMR spectrum of compound* ***T19***

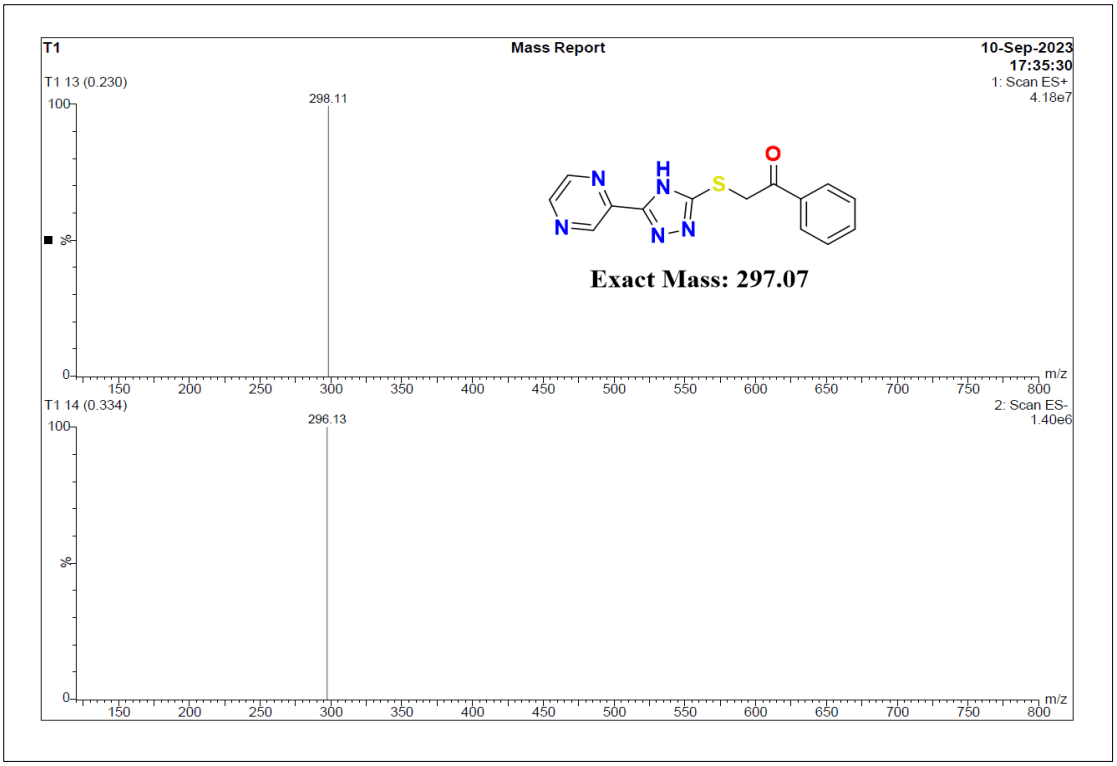

Figure 2.92 *ESI-MS spectrum of compound* ***T19***

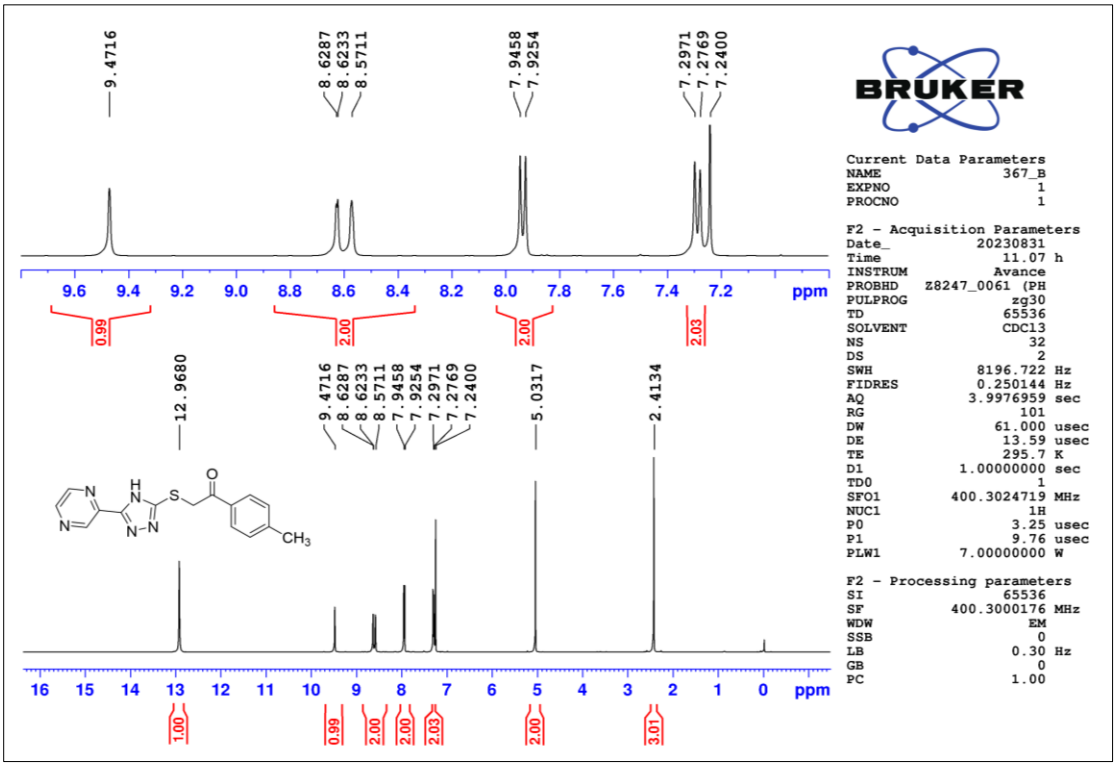

Figure 2.93 *^{1}H-NMR spectrum of compound* ***T20***

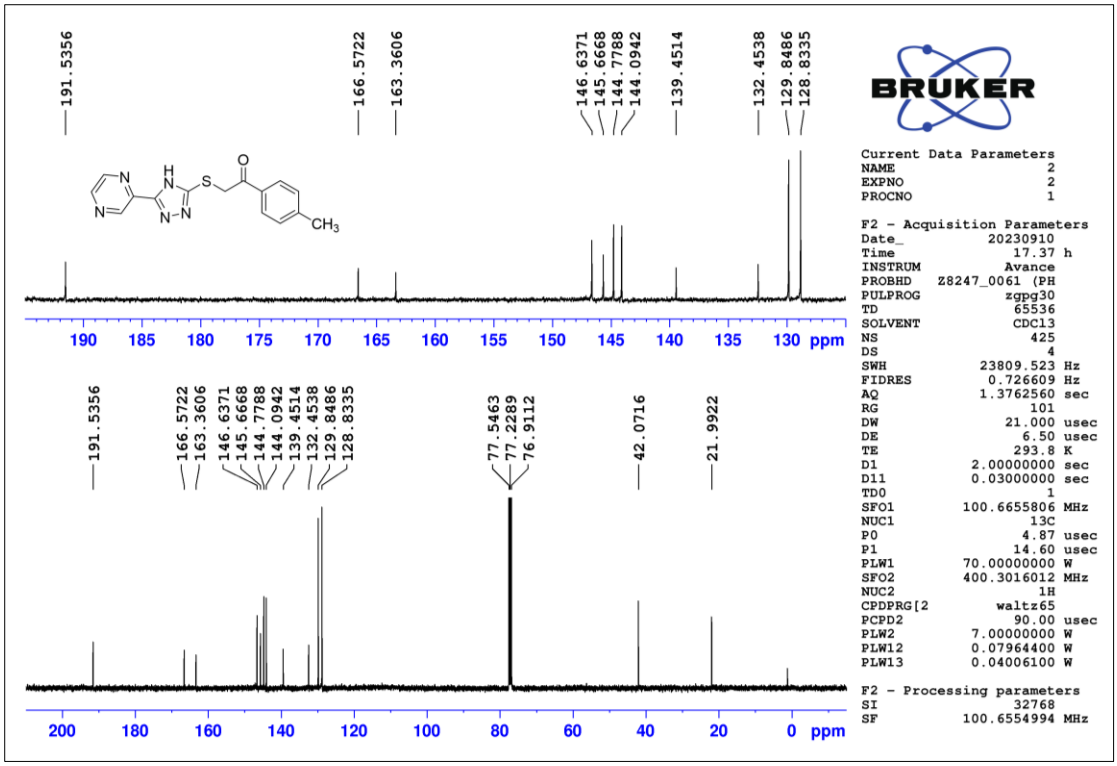

Figure 2.94 *^{13}C-NMR spectrum of compound* ***T20***

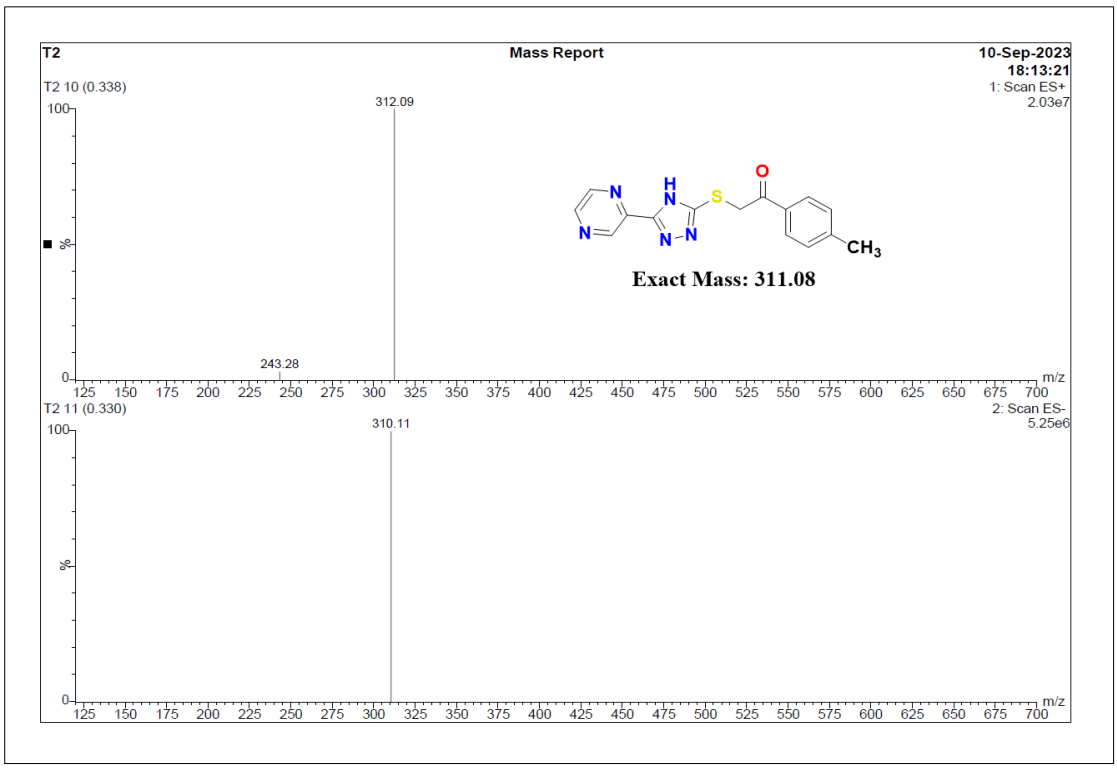

Figure 2.95 *ESI-MS spectrum of compound* ***T20***

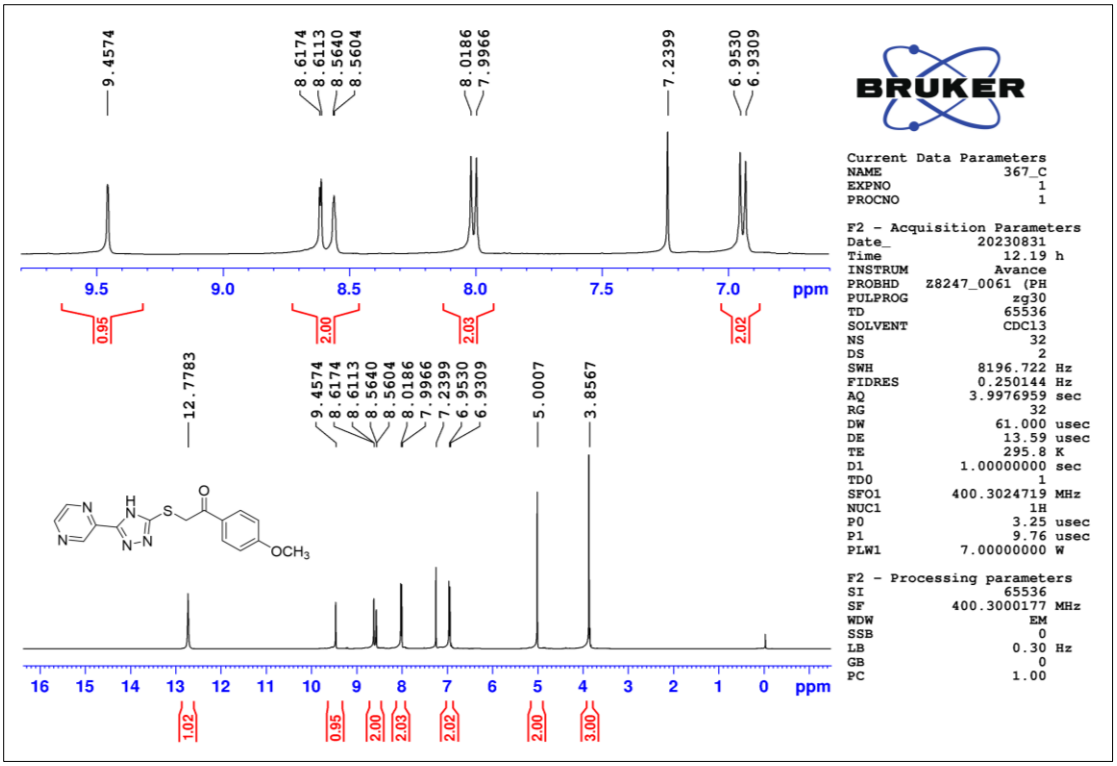

Figure 2.96 *^{1}H-NMR spectrum of compound* ***T21***

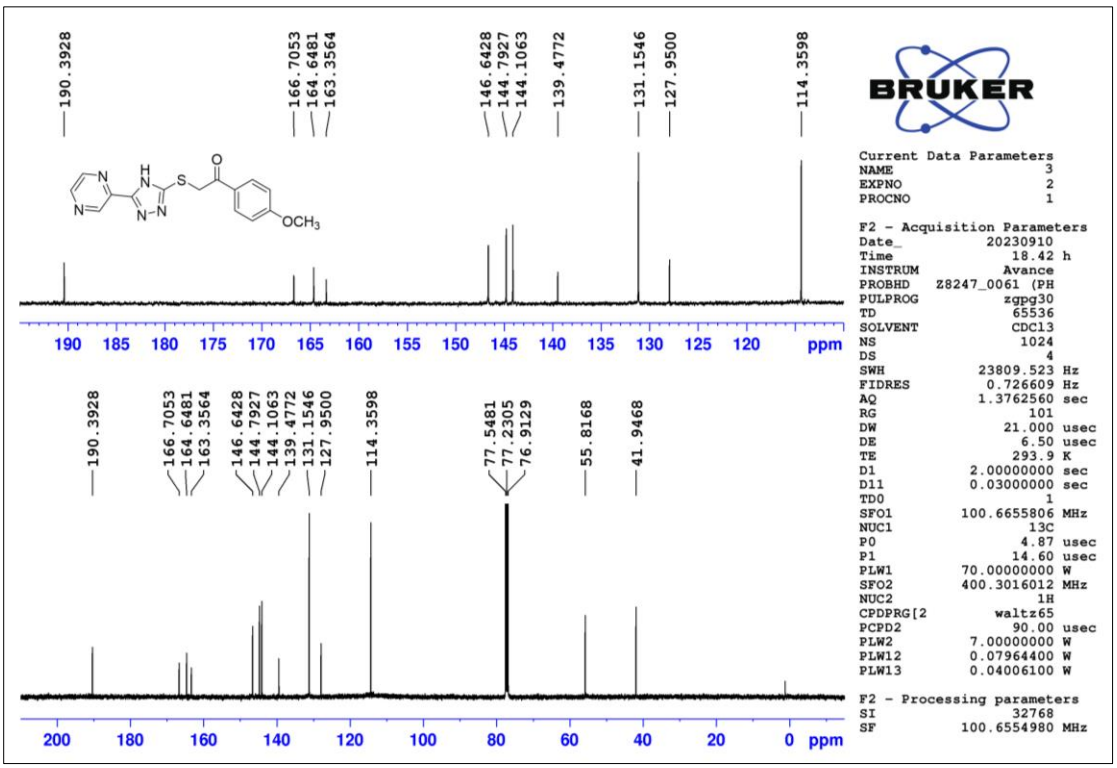

Figure 2.97 *^{13}C-NMR spectrum of compound* ***T21***

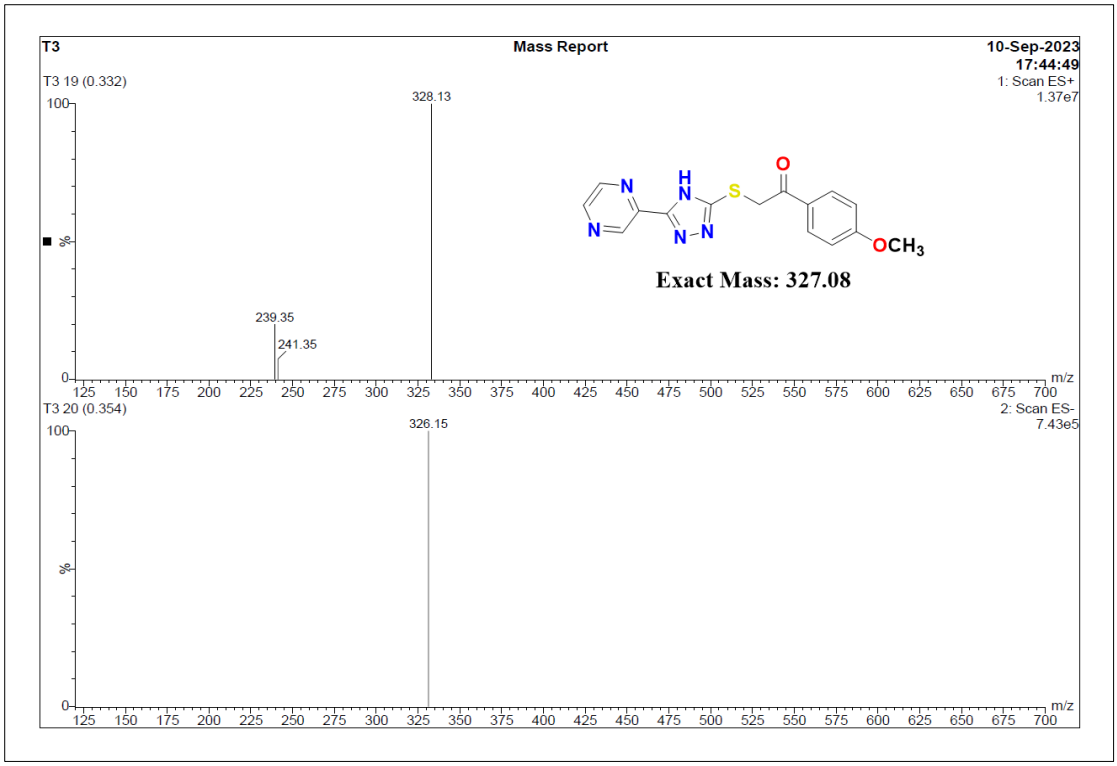

Figure 2.98 *ESI-MS spectrum of compound* ***T21***

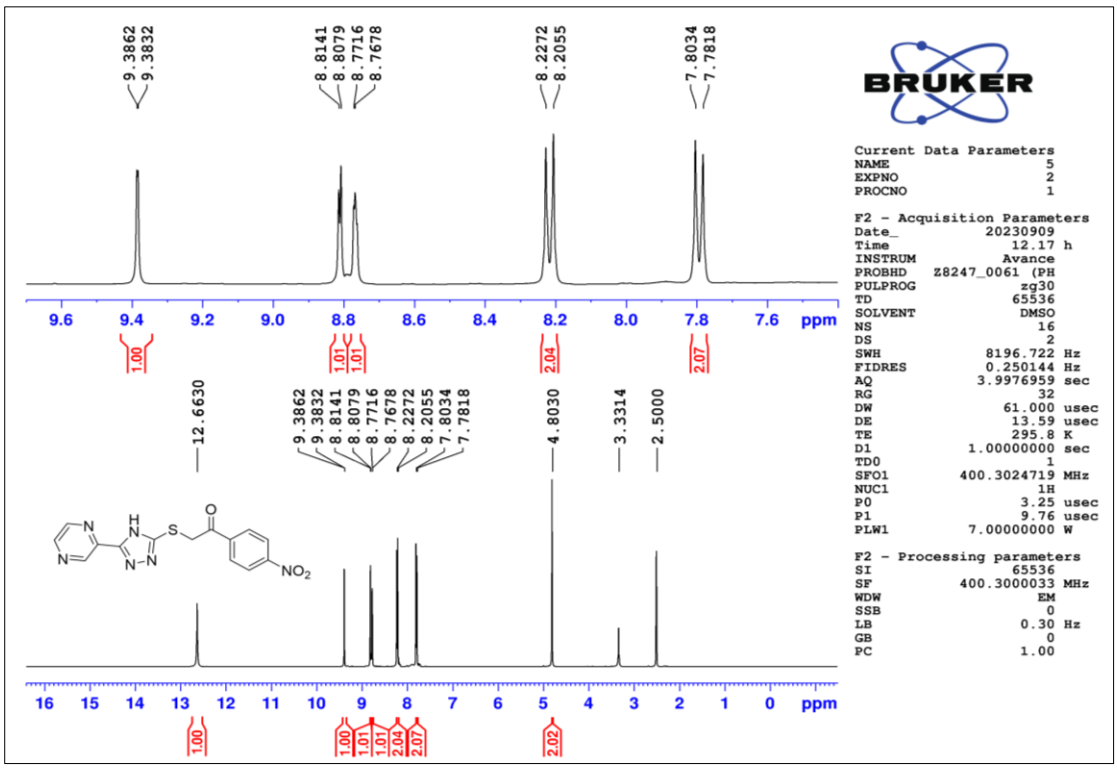

Figure 2.99 *^{1}H-NMR spectrum of compound* ***T23***

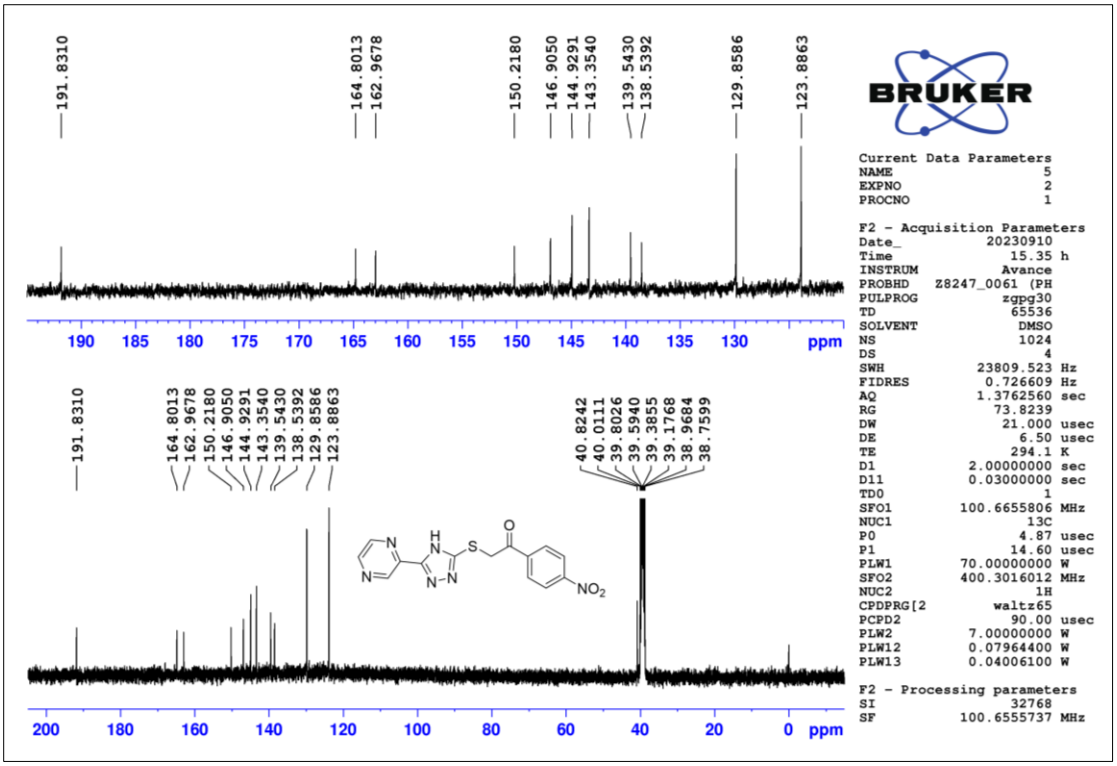

Figure 2.100 *^{13}C-NMR spectrum of compound* ***T23***

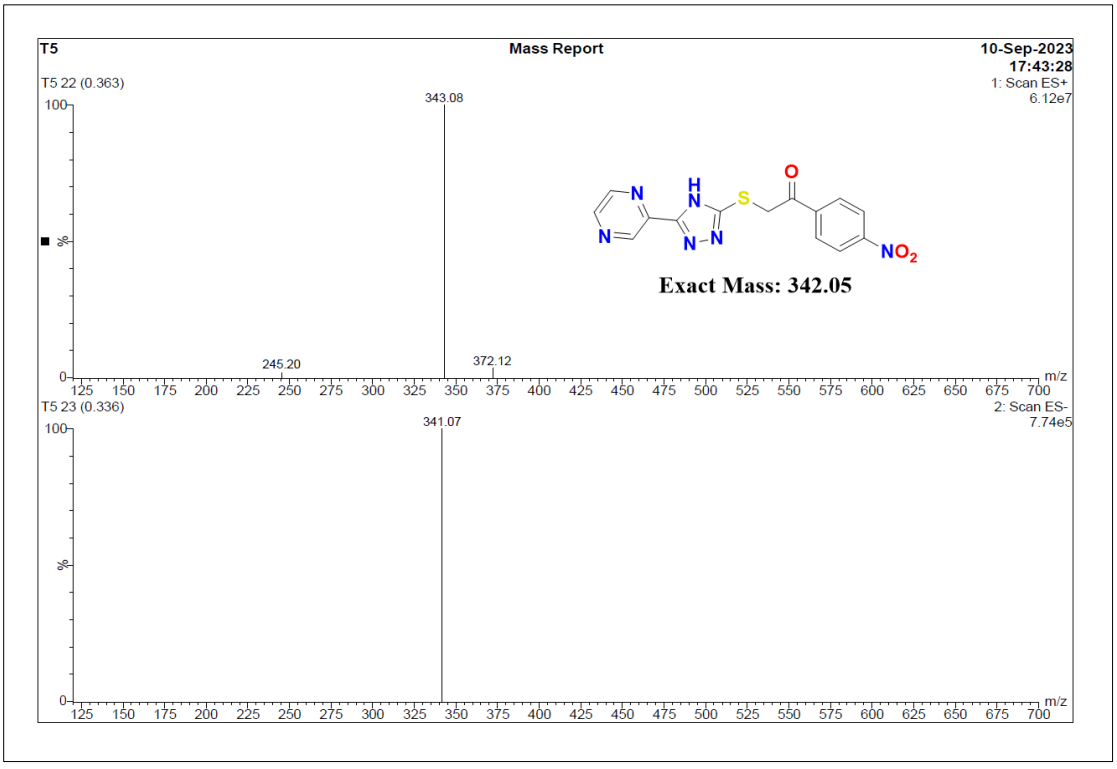

Figure 2.101 *ESI-MS spectrum of compound* ***T23***

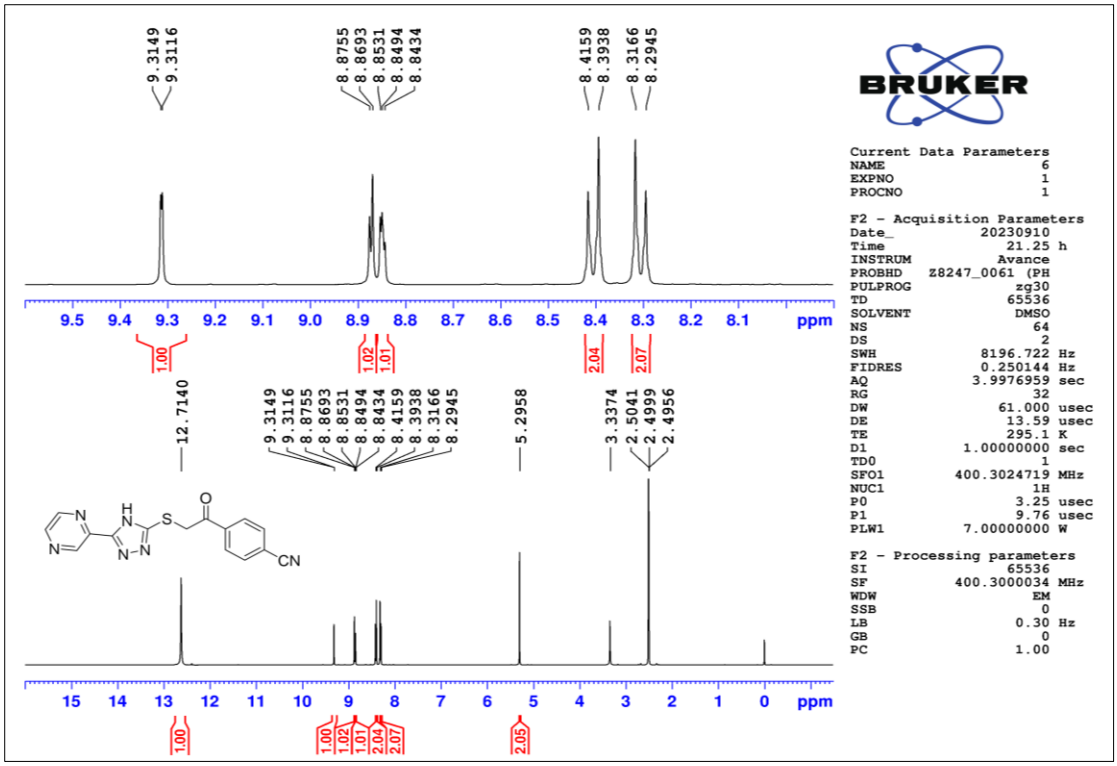

Figure 2.102 *^{1}H-NMR spectrum of compound* ***T24***

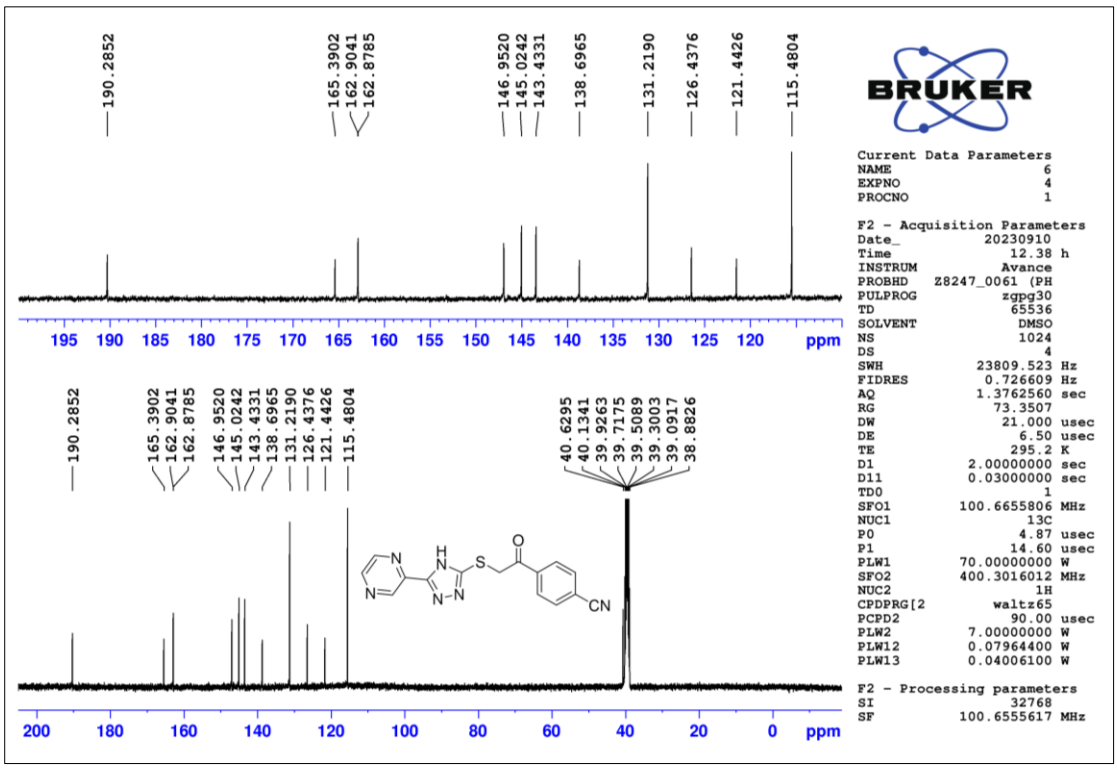

Figure 2.103 *^{13}C-NMR spectrum of compound* ***T24***

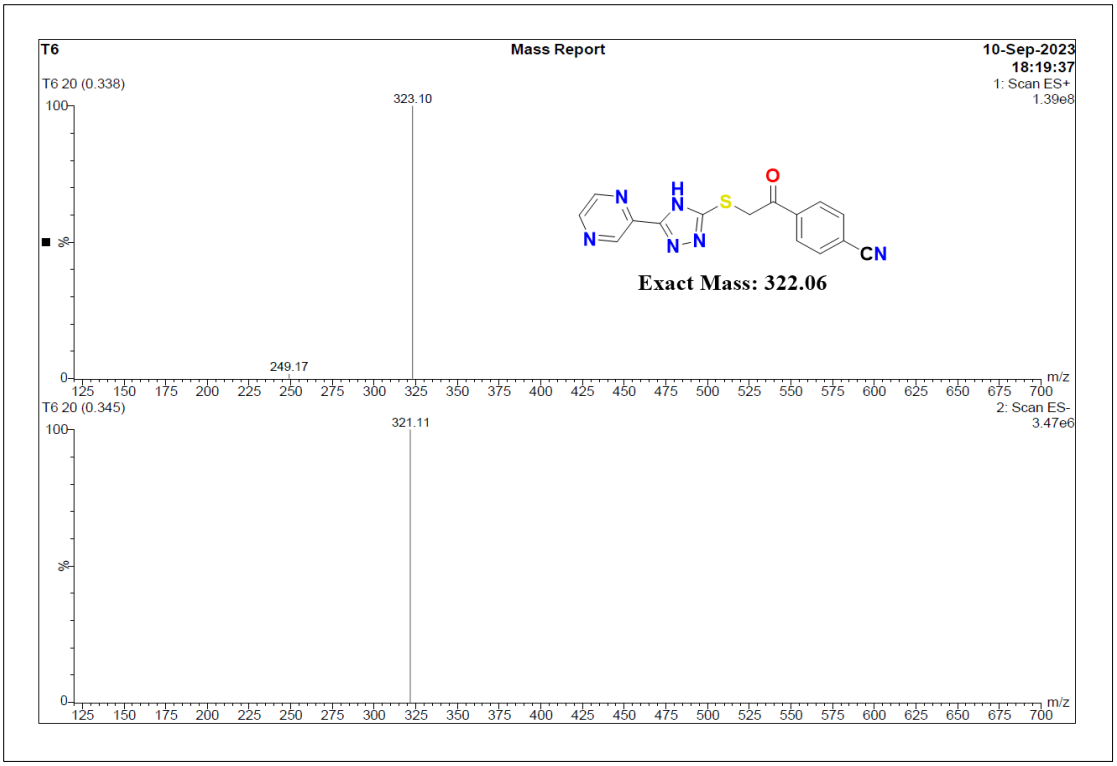

Figure 2.104 *ESI-MS spectrum of compound* ***T24***

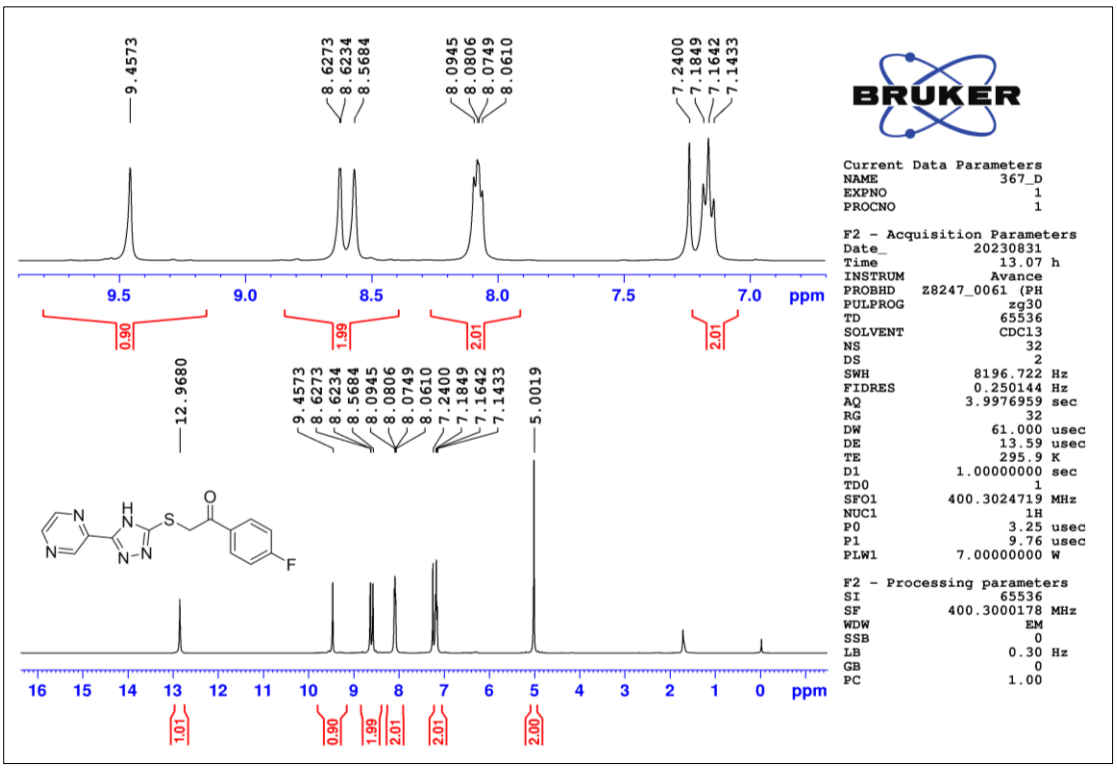

Figure 2.105 *^{1}H-NMR spectrum of compound* ***T25***

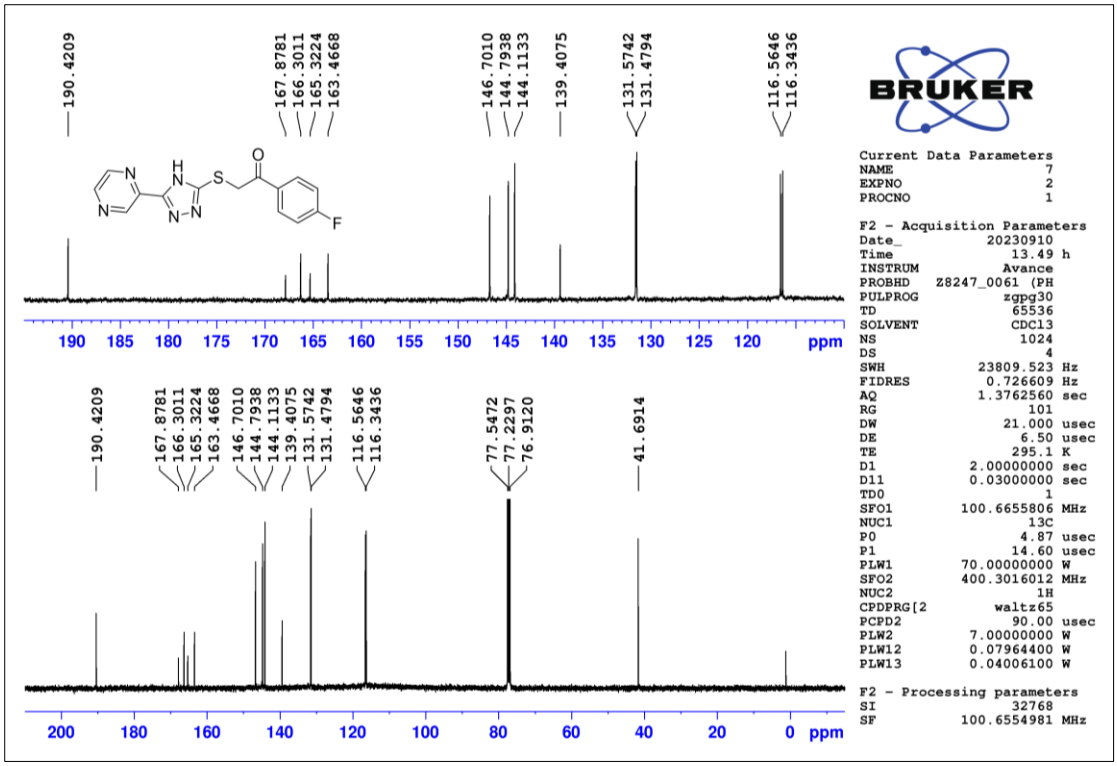

Figure 2.106 *^{13}C-NMR spectrum of compound* ***T25***

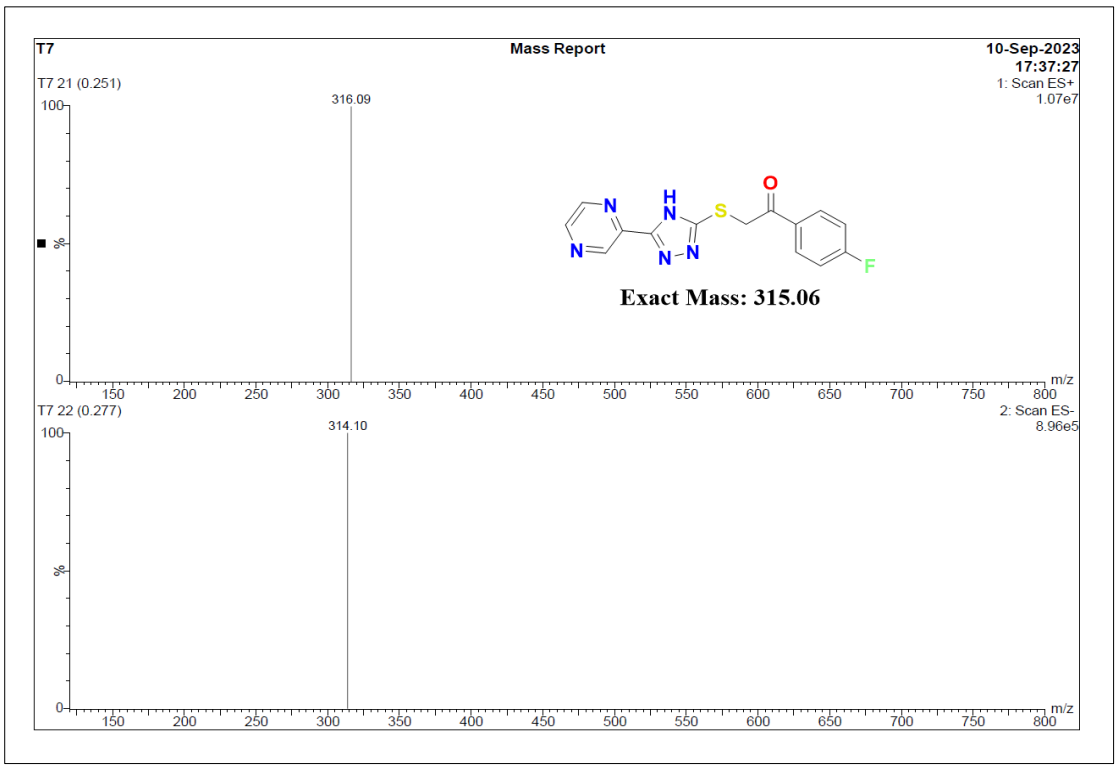

Figure 2.107 *ESI-MS spectrum of compound* ***T25***

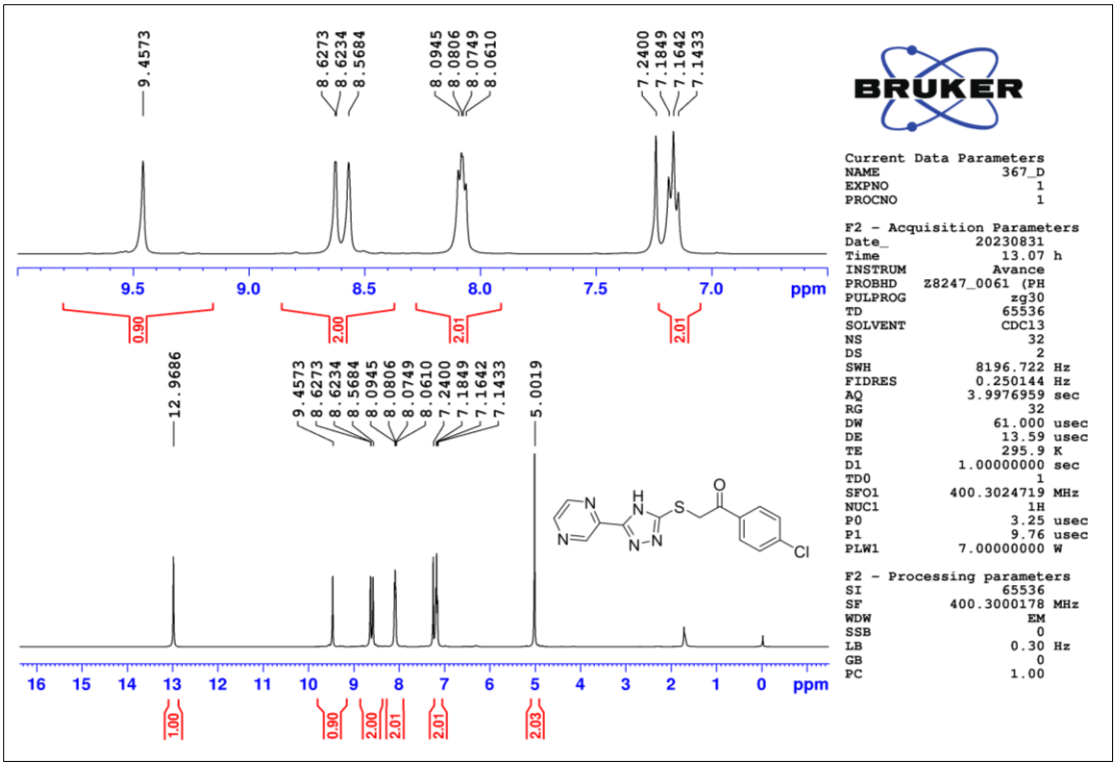

Figure 2.108 *^{1}H-NMR spectrum of compound* ***T26***

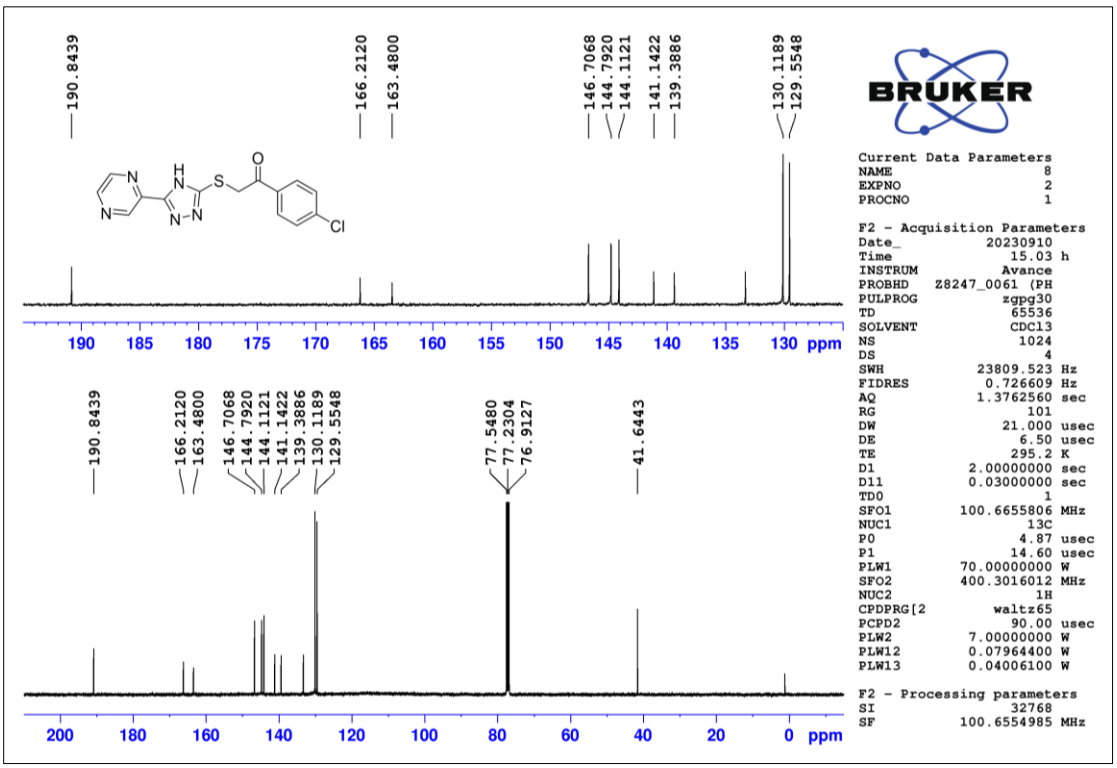

Figure 2.109 *^{13}C-NMR spectrum of compound* ***T26***

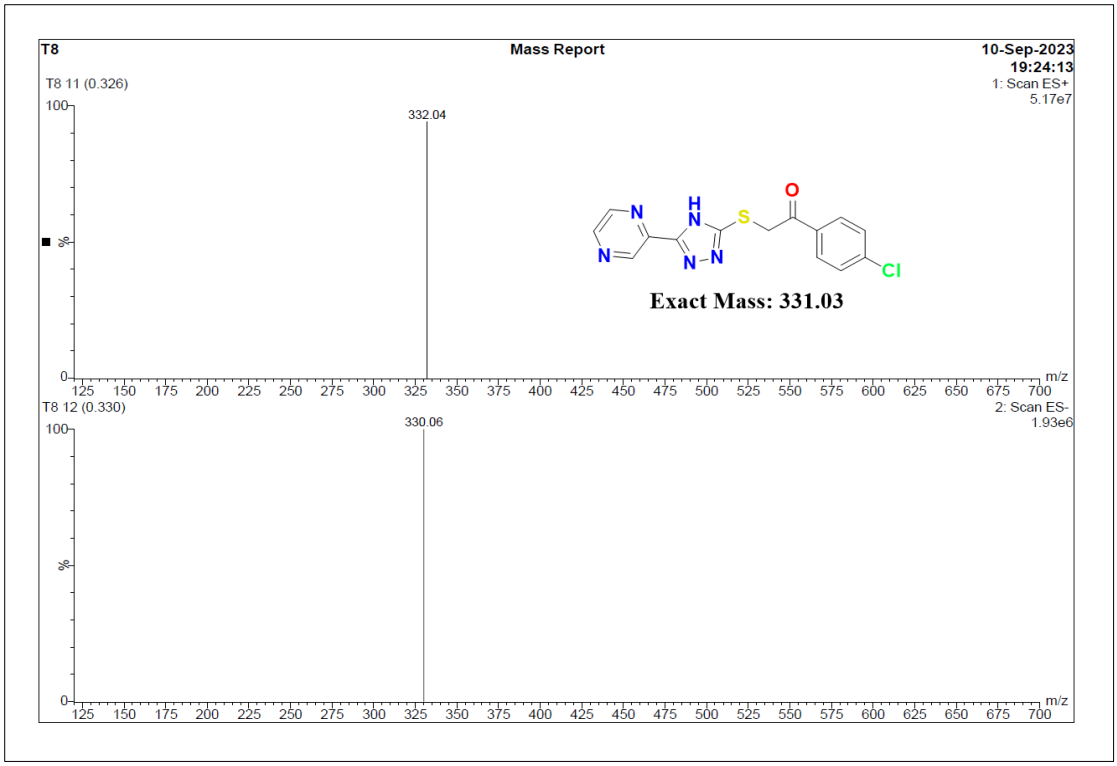

Figure 2.110 *ESI-MS spectrum of compound* ***T26***

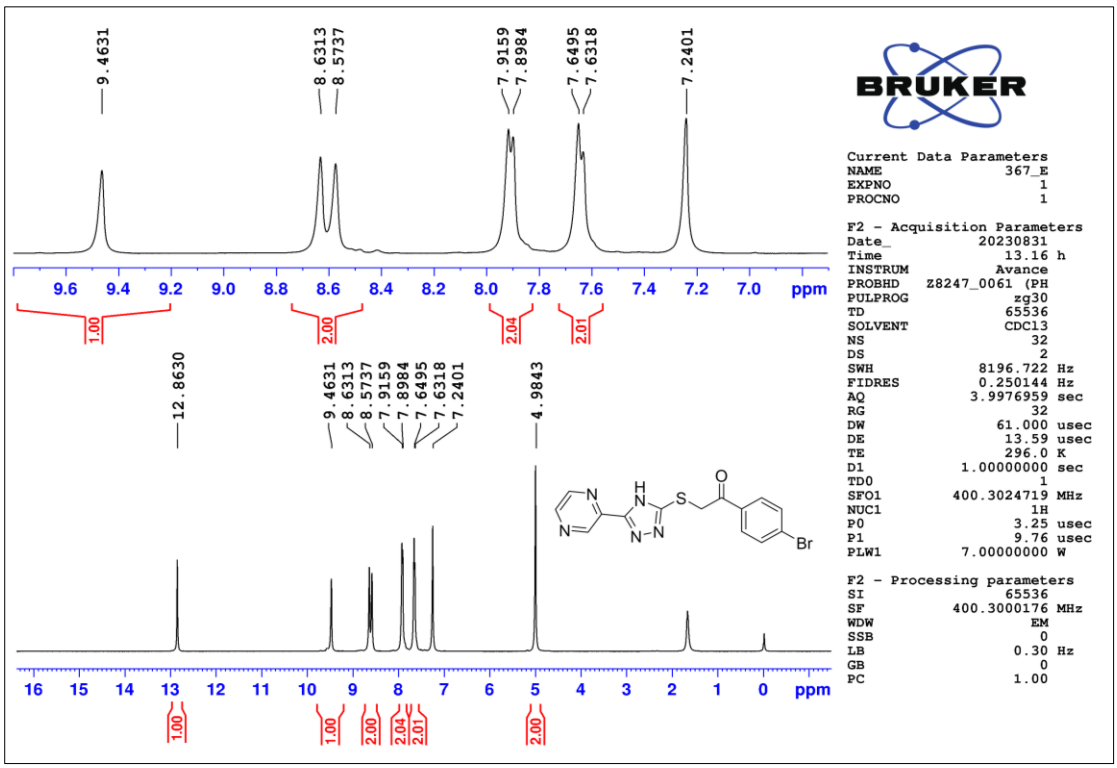

Figure 2.111 *[1]H-NMR spectrum of compound* ***T27***

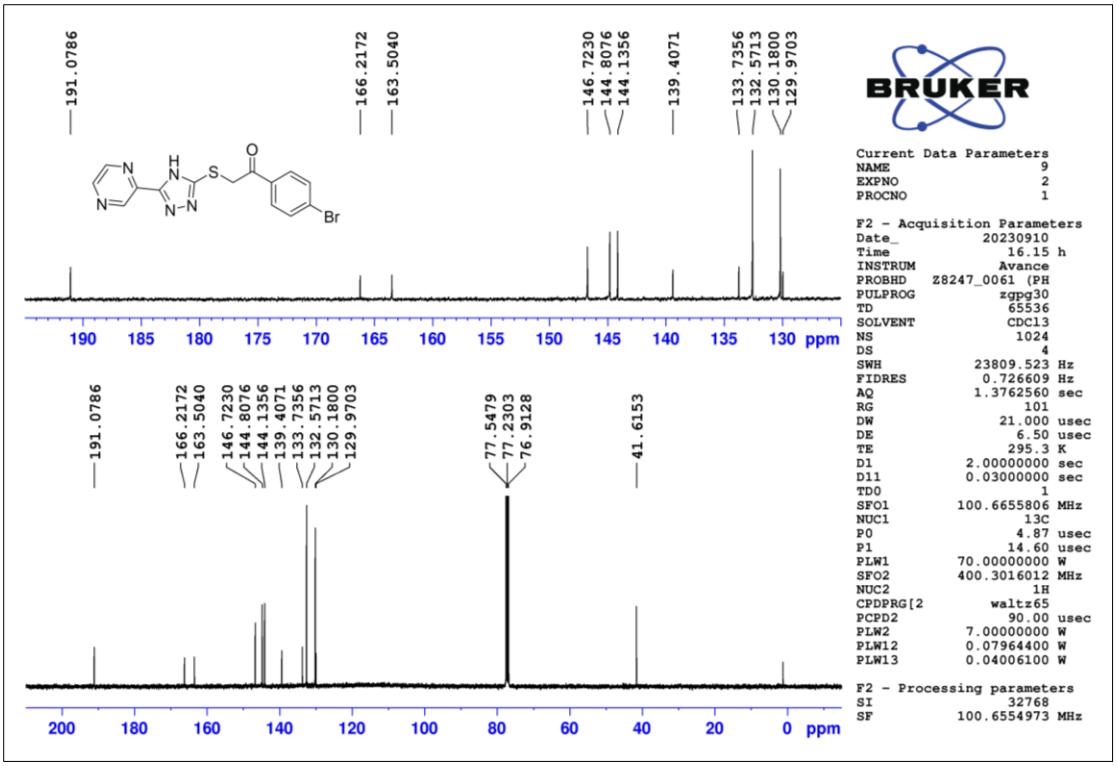

Figure 2.112 *^{13}C-NMR spectrum of compound* ***T27***

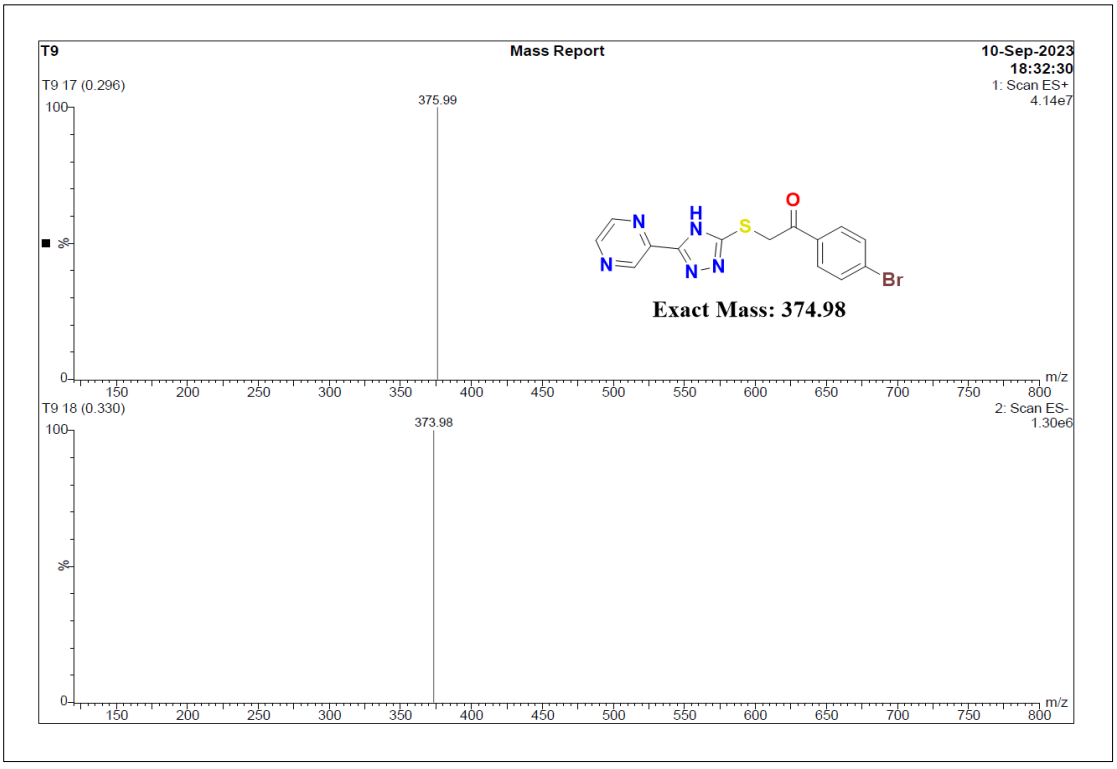

Figure 2.113 *ESI-MS spectrum of compound* ***T27***

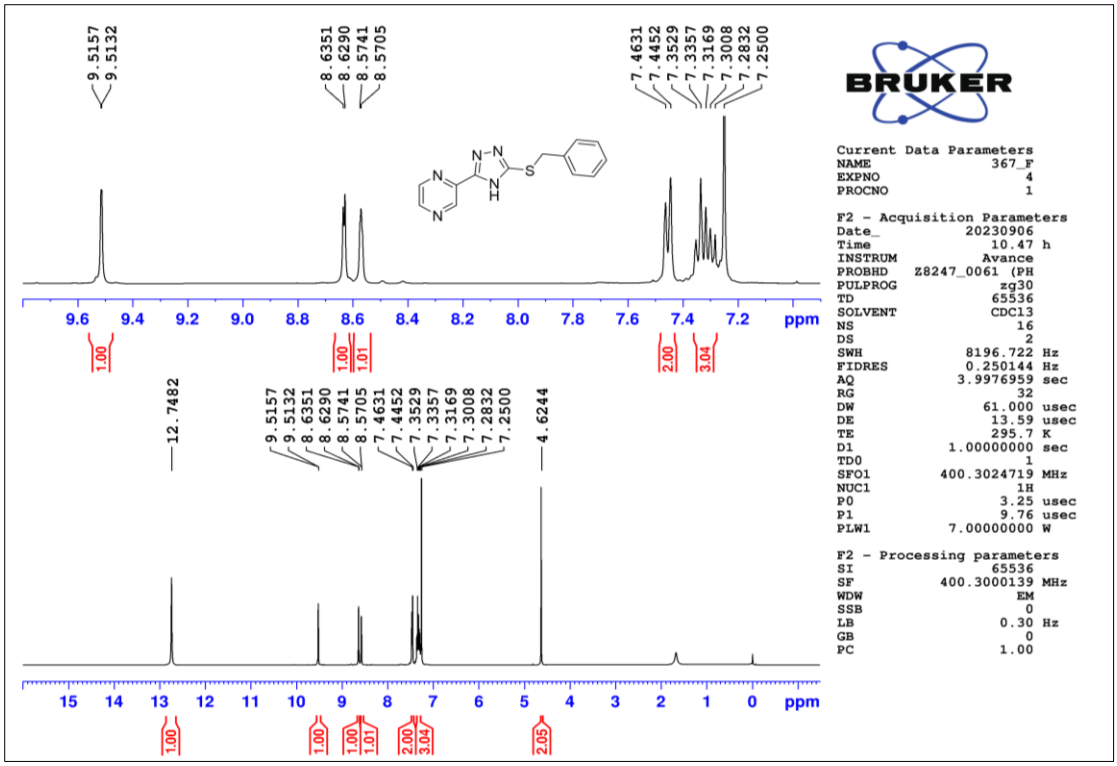

Figure 2.114 *[1]H-NMR spectrum of compound* ***T28***

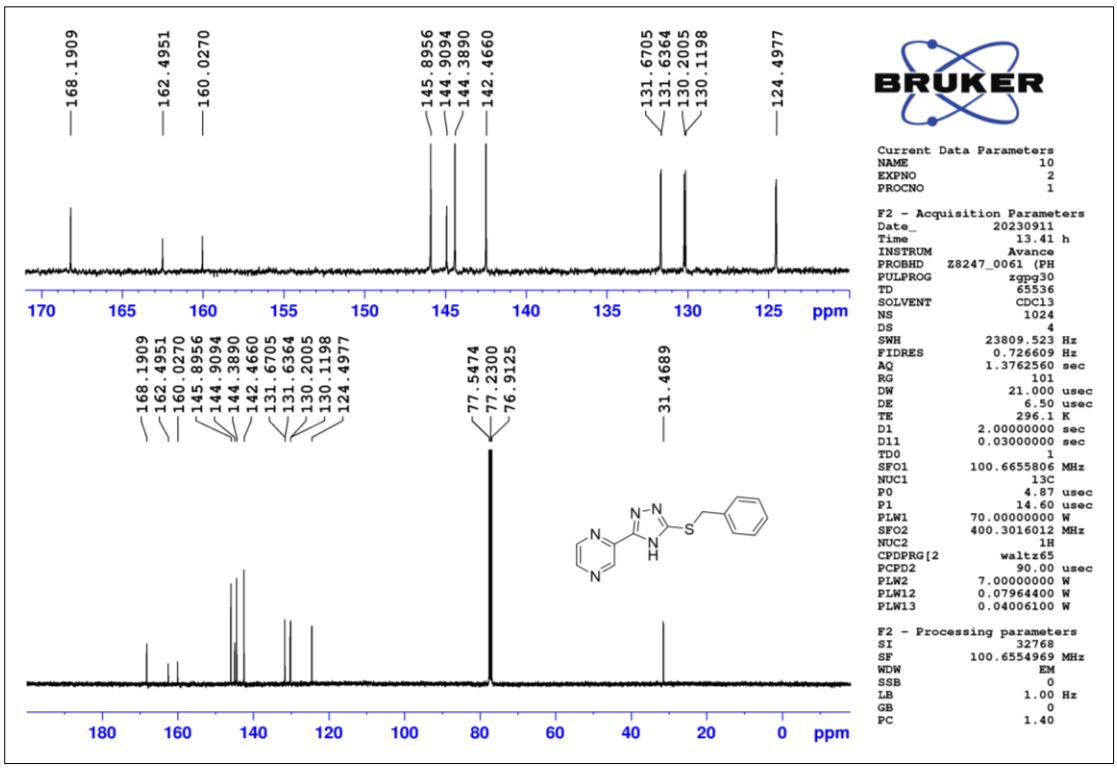

Figure 2.115 *[13]C-NMR spectrum of compound* ***T28***

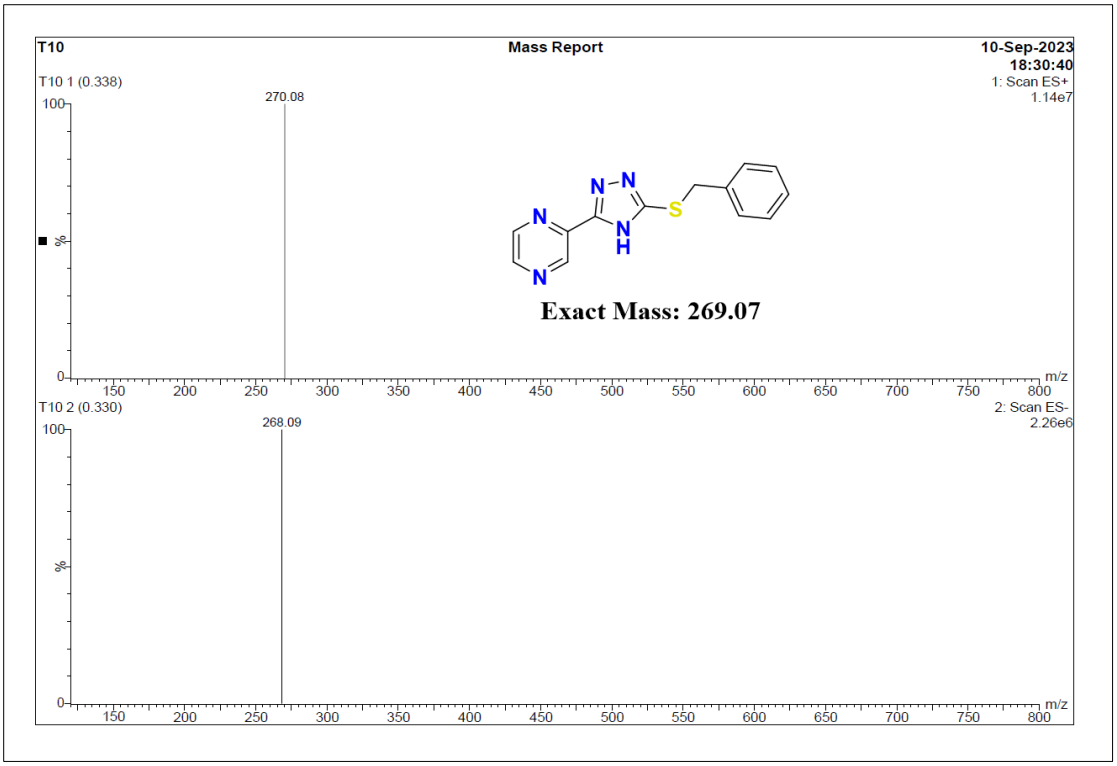

Figure 2.116 *ESI-MS spectrum of compound* ***T28***

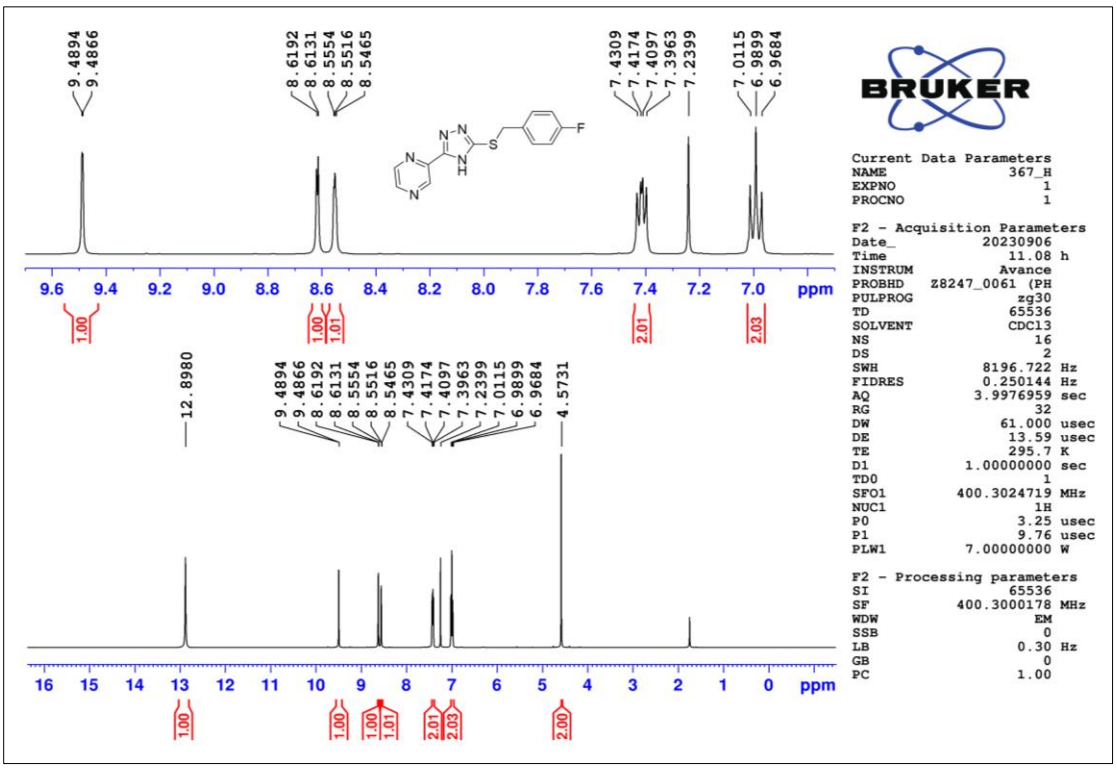

Figure 2.117 *^{1}H-NMR spectrum of compound* ***T30***

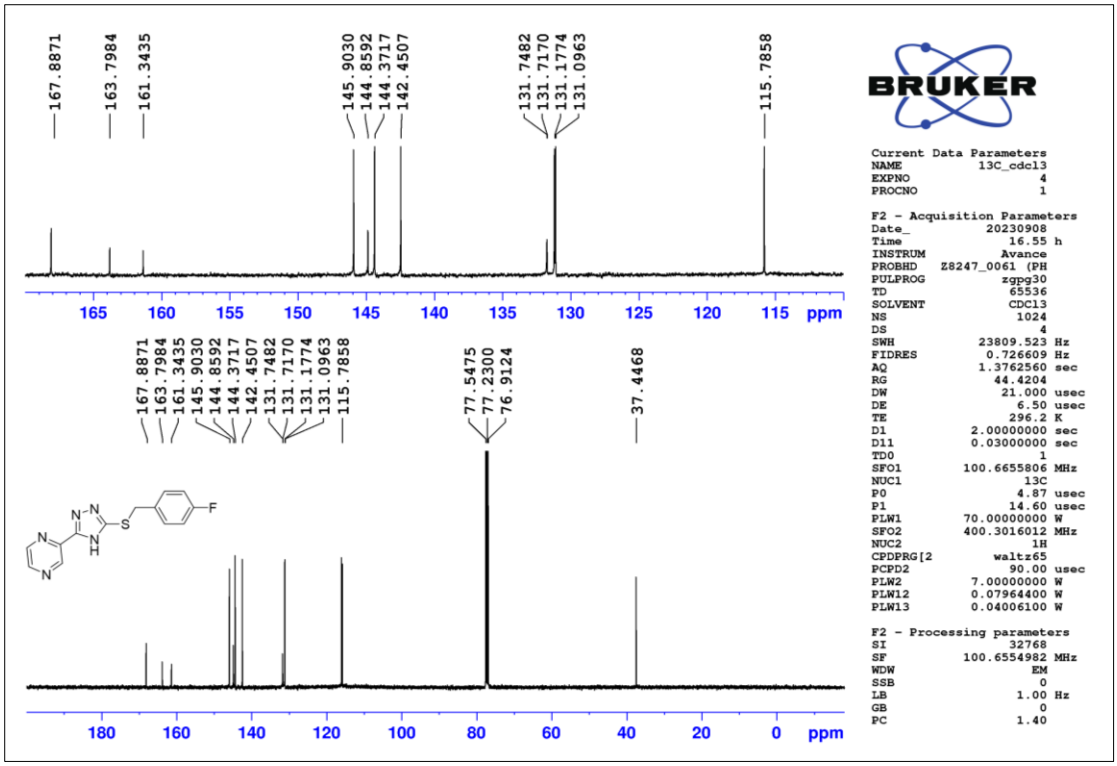

Figure 2.118 *^{13}C-NMR spectrum of compound* ***T30***

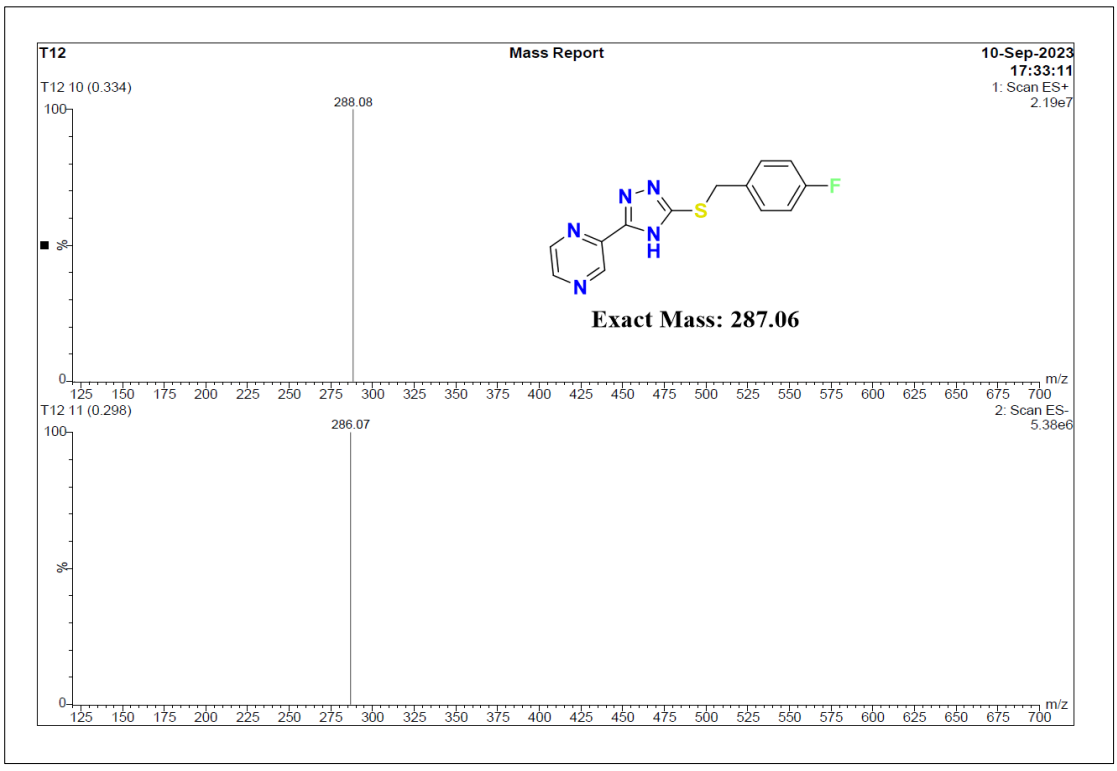

Figure 2.119 *ESI-MS spectrum of compound* ***T30***

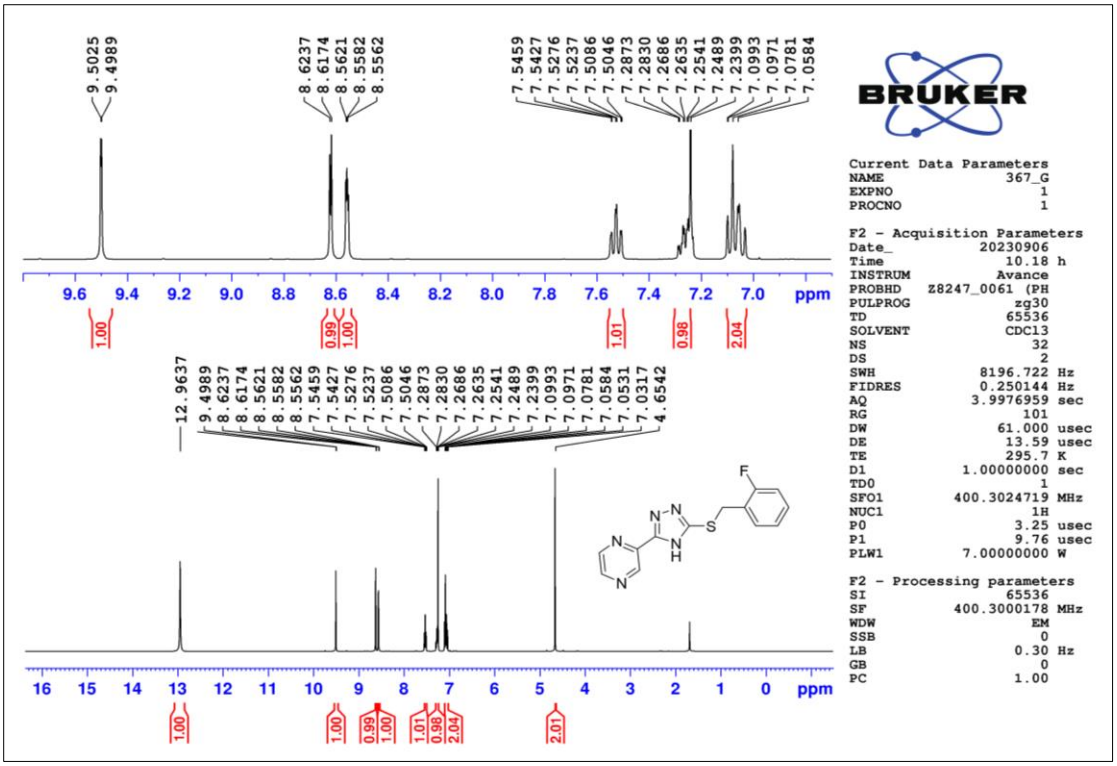

Figure 2.120 *^{1}H-NMR spectrum of compound* ***T31***

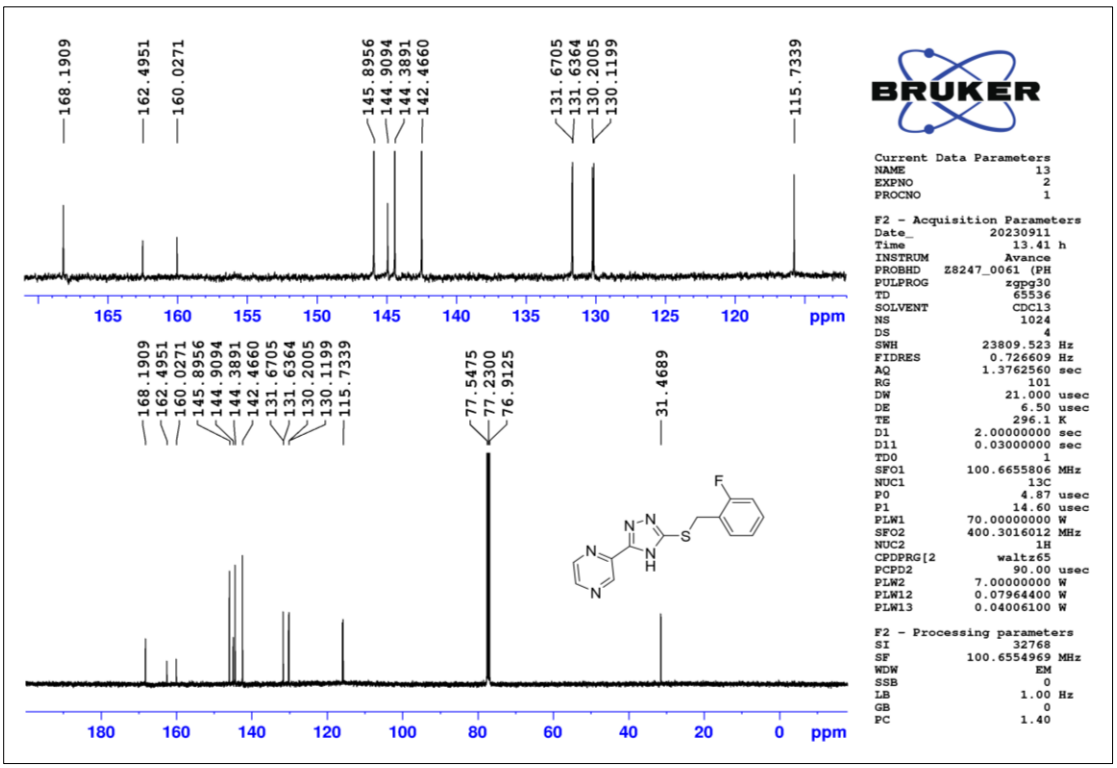

Figure 2.121 *^{13}C-NMR spectrum of compound* ***T31***

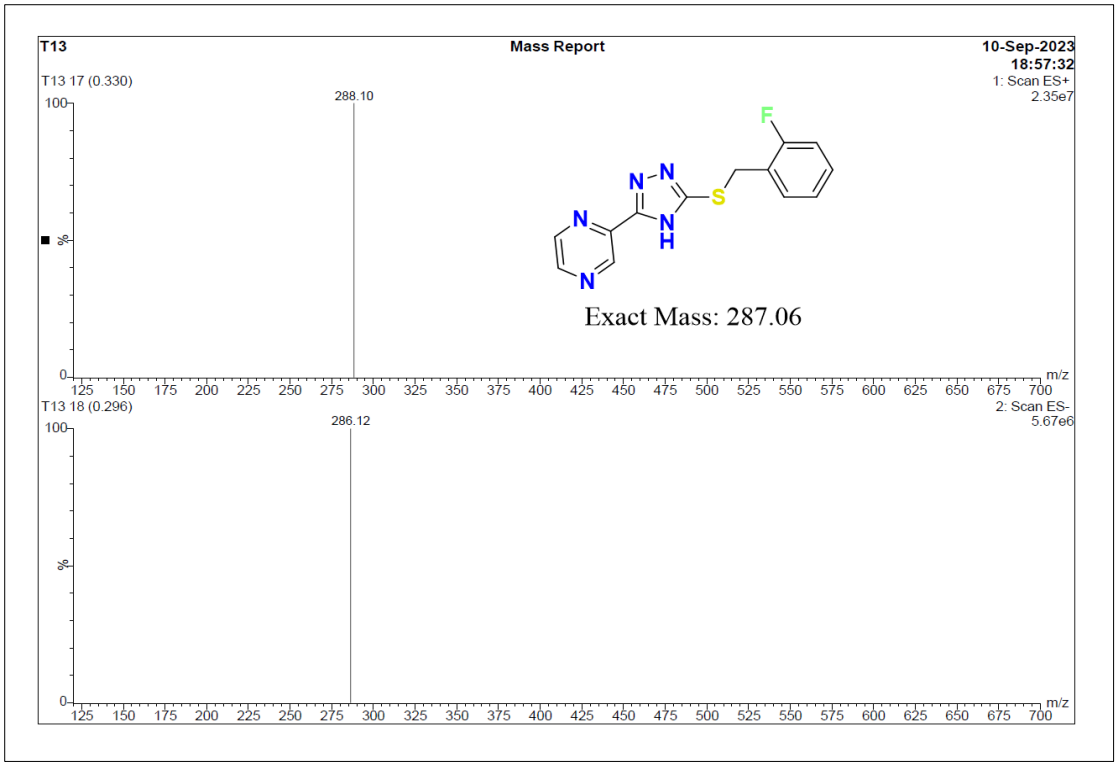

Figure 2.122 *ESI-MS spectrum of compound* ***T31***

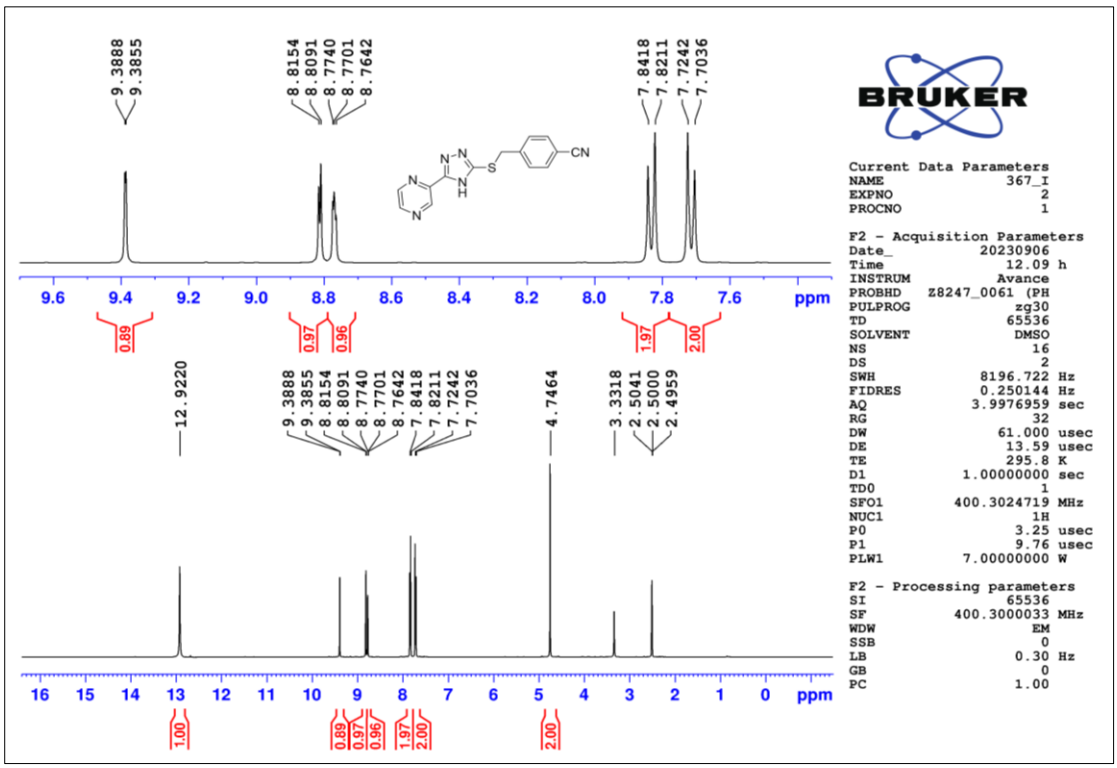

Figure 2.123 *[1]H-NMR spectrum of compound* ***T32***

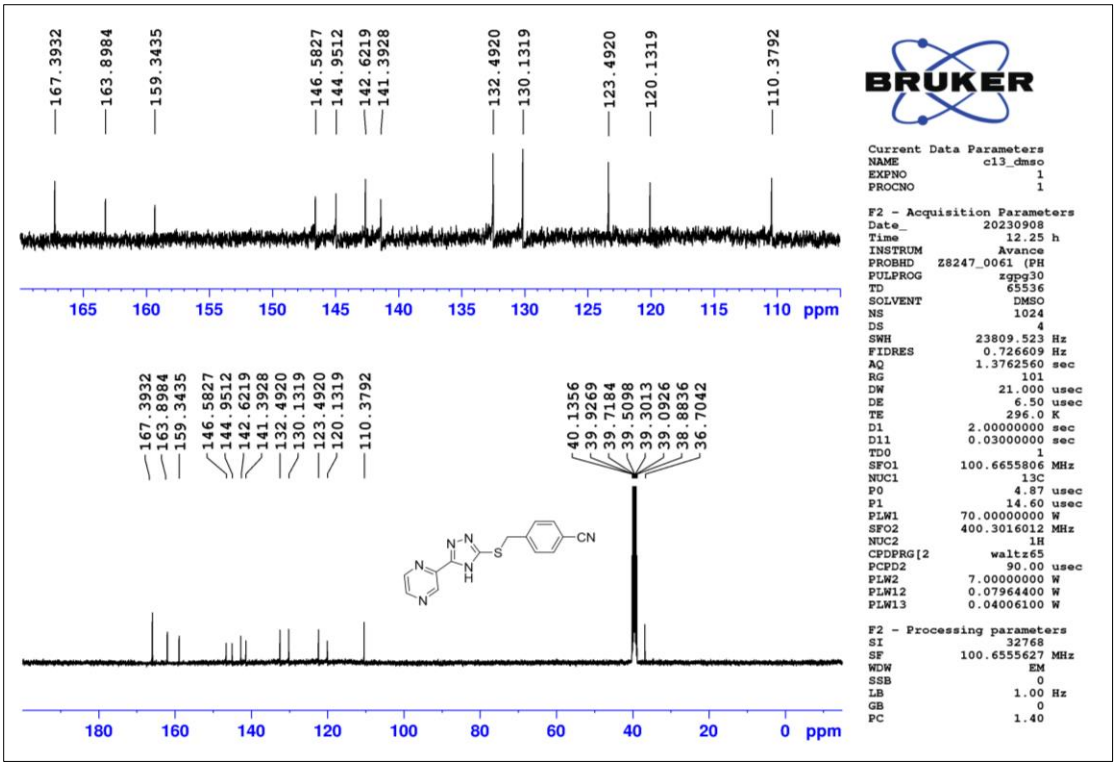

Figure 2.124 *^{13}C-NMR spectrum of compound* ***T32***

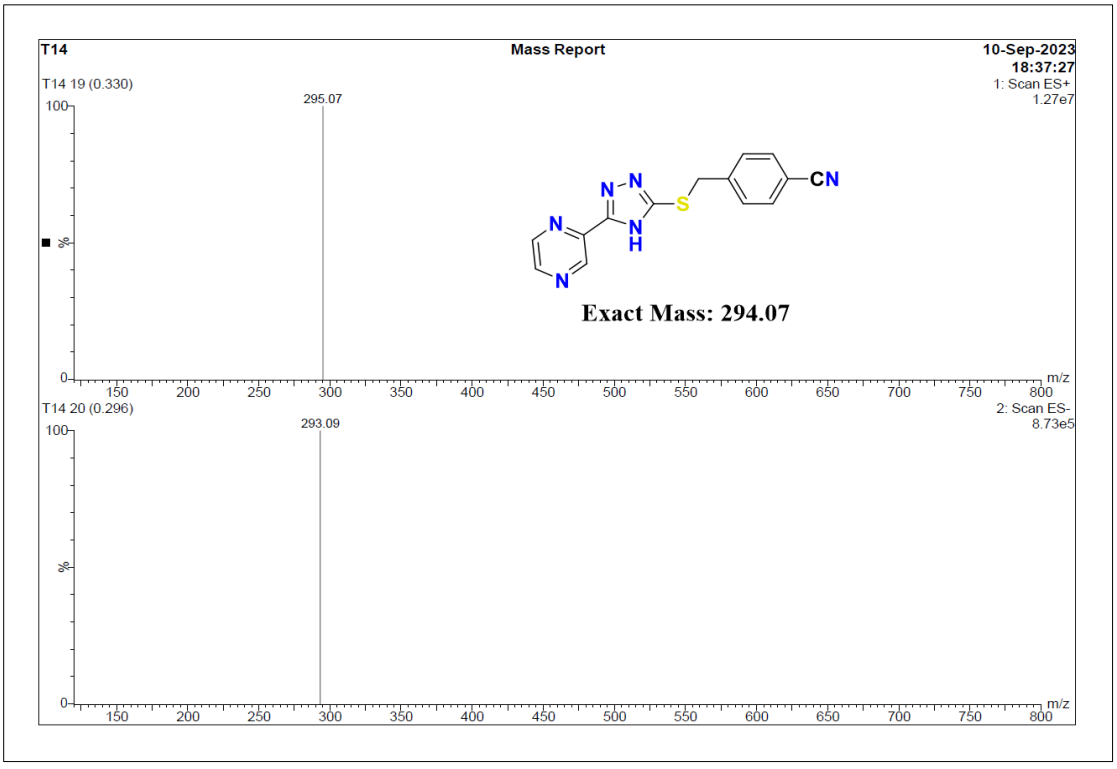

Figure 2.125 *ESI-MS spectrum of compound* ***T32***

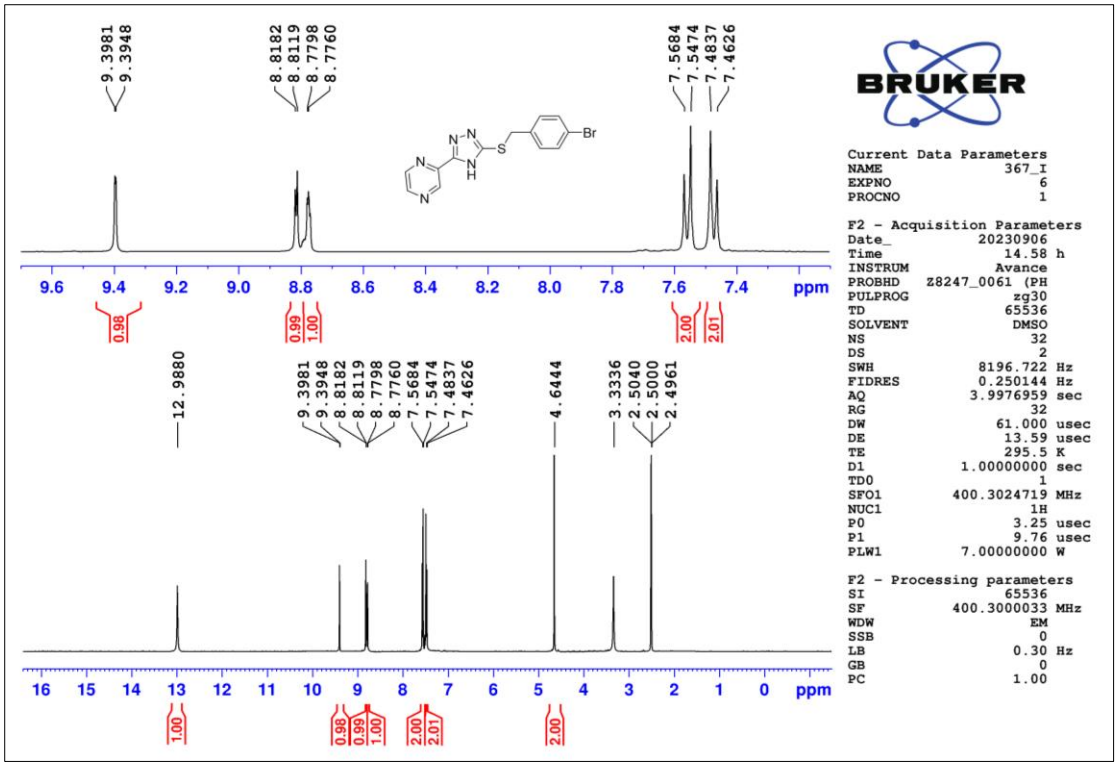

Figure 2.126 *^{1}H-NMR spectrum of compound* ***T33***

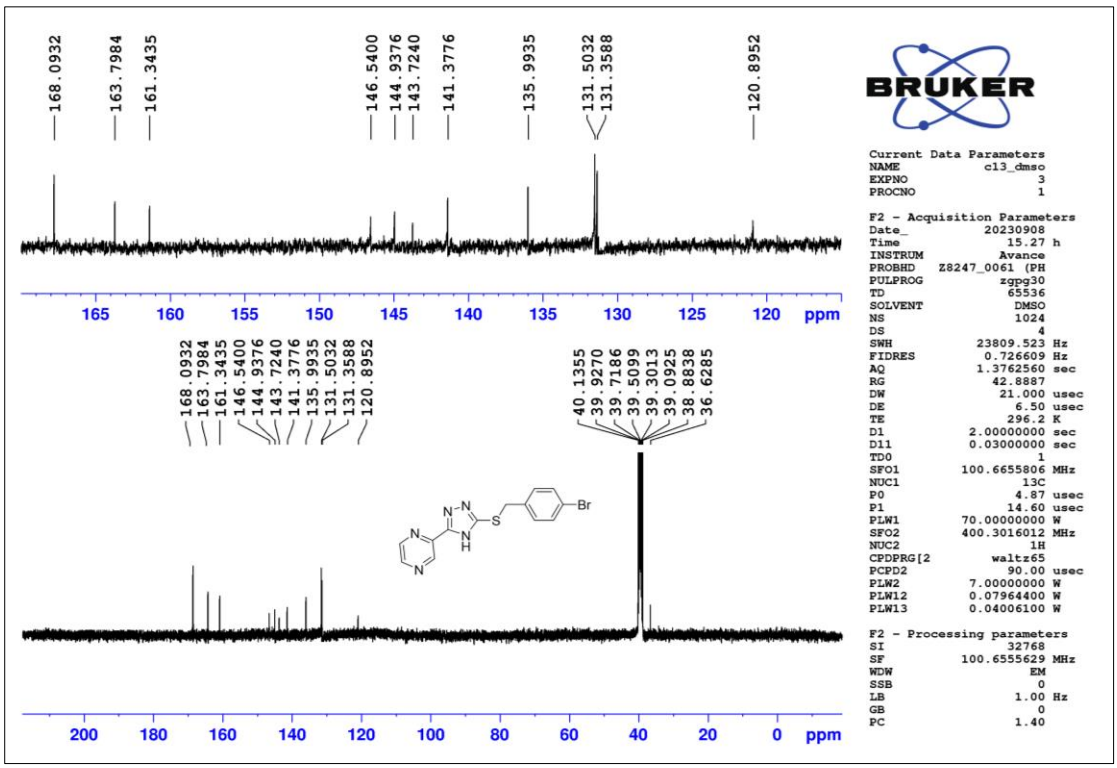

Figure 2.127 *^{13}C-NMR spectrum of compound* ***T33***

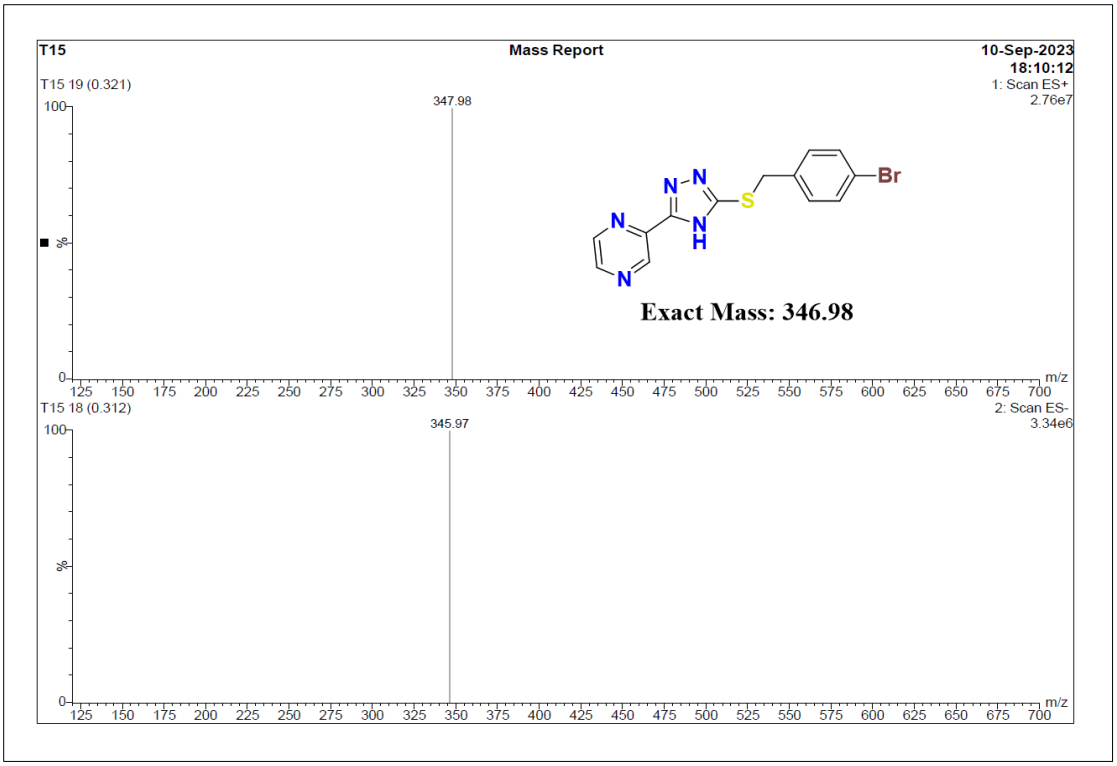

Figure 2.128 *ESI-MS spectrum of compound* ***T33***

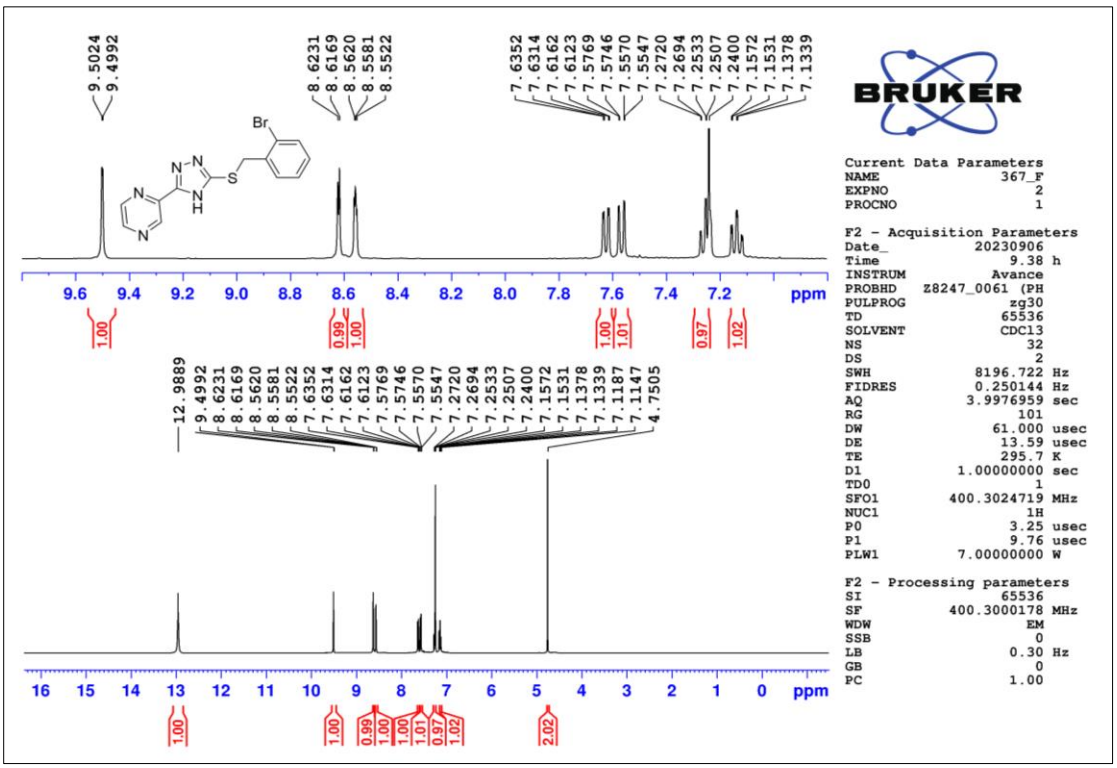

Figure 2.129 *^{1}H-NMR spectrum of compound* ***T34***

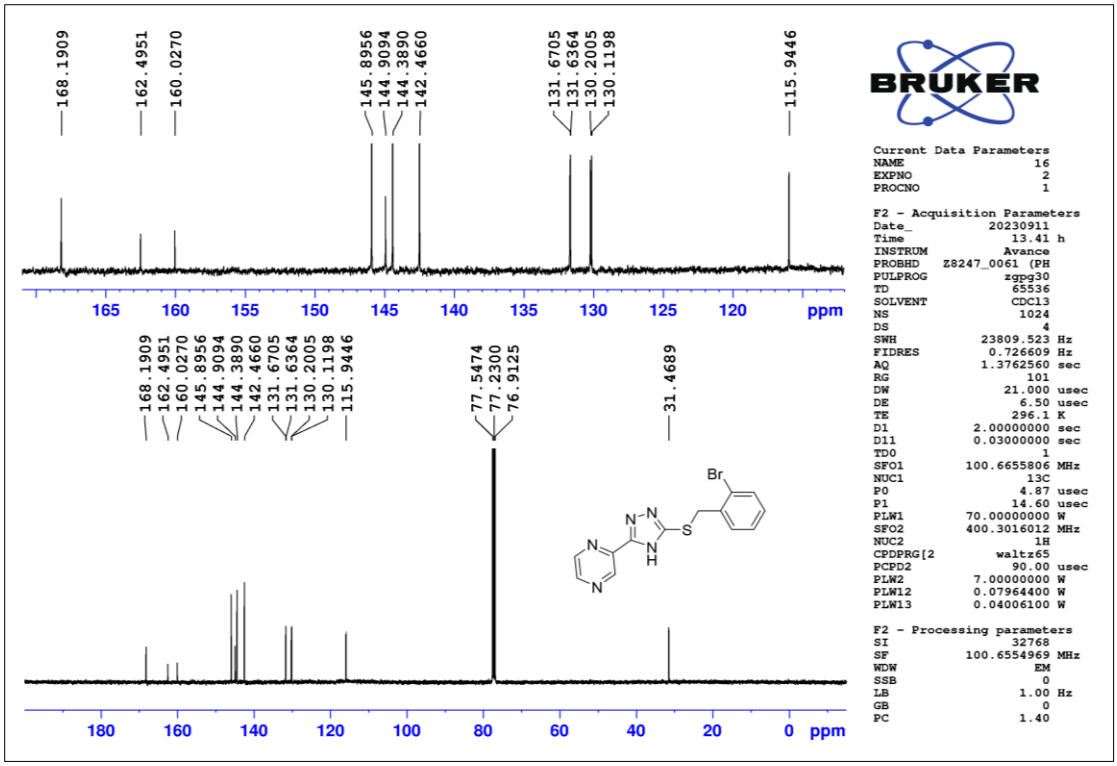

Figure 2.130 *^{13}C-NMR spectrum of compound* ***T34***

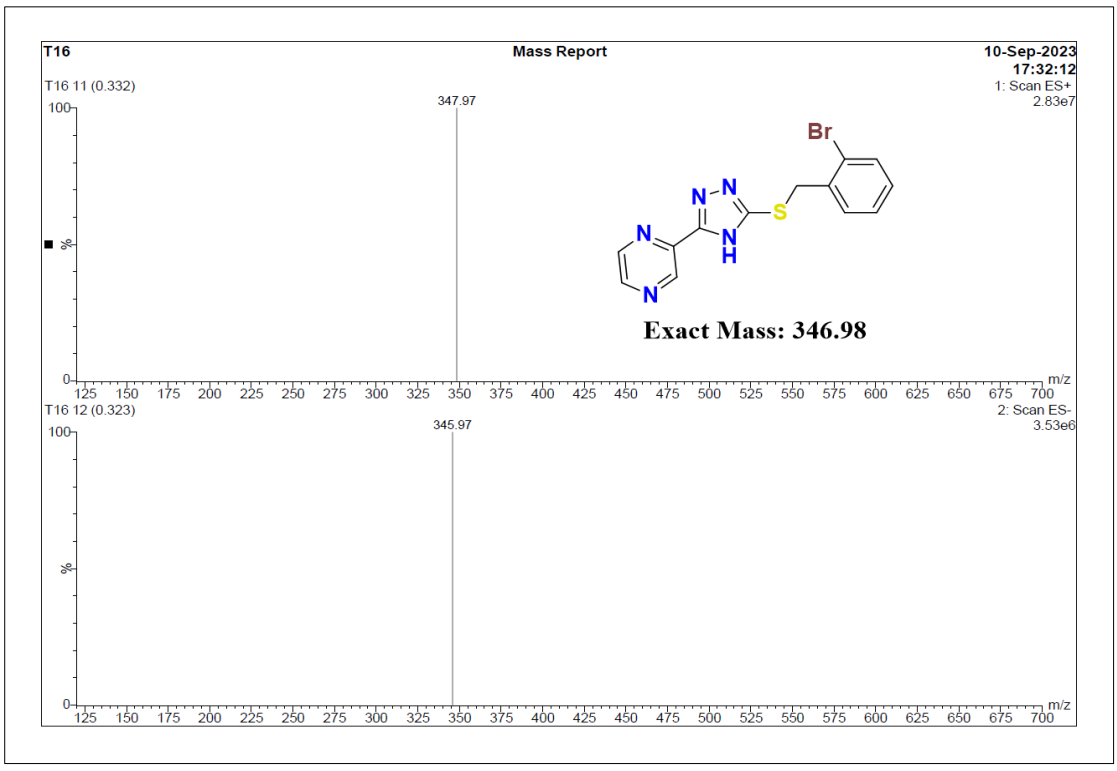

Figure 2.131 *ESI-MS spectrum of compound* ***T34***

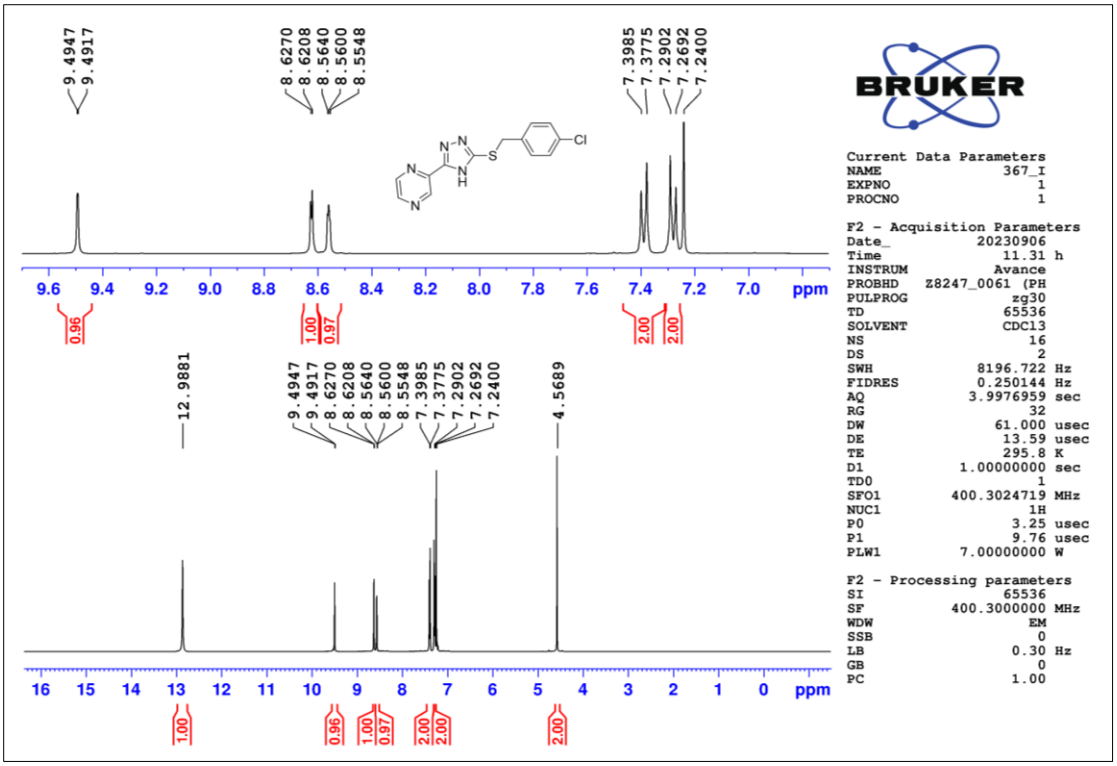

Figure 2.132 *^{1}H-NMR spectrum of compound* ***T35***

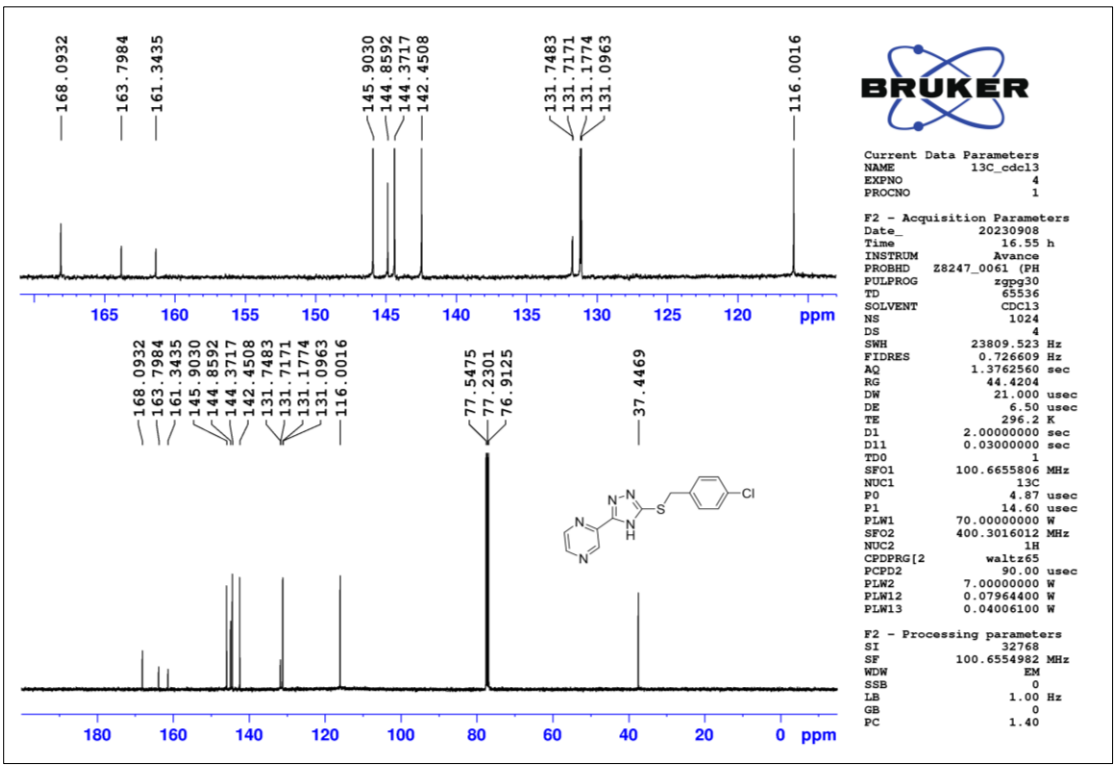

Figure 2.133 *^{13}C-NMR spectrum of compound* ***T35***

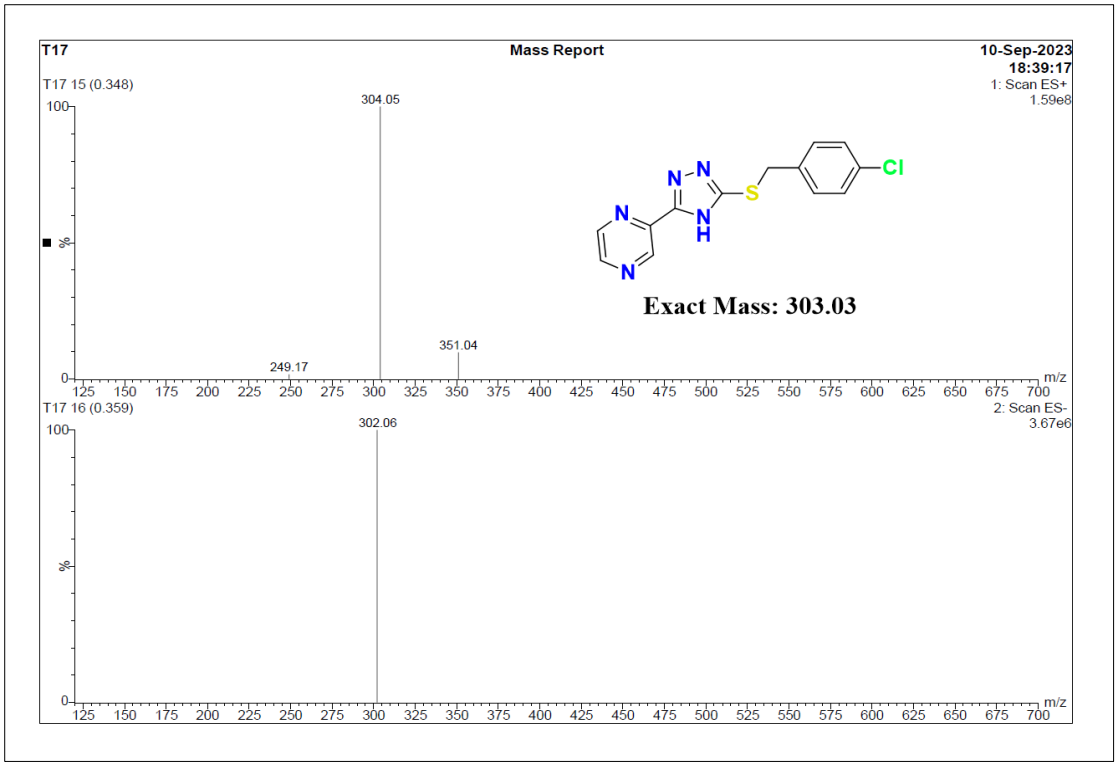

Figure 2.134 *ESI-MS spectrum of compound* ***T35***

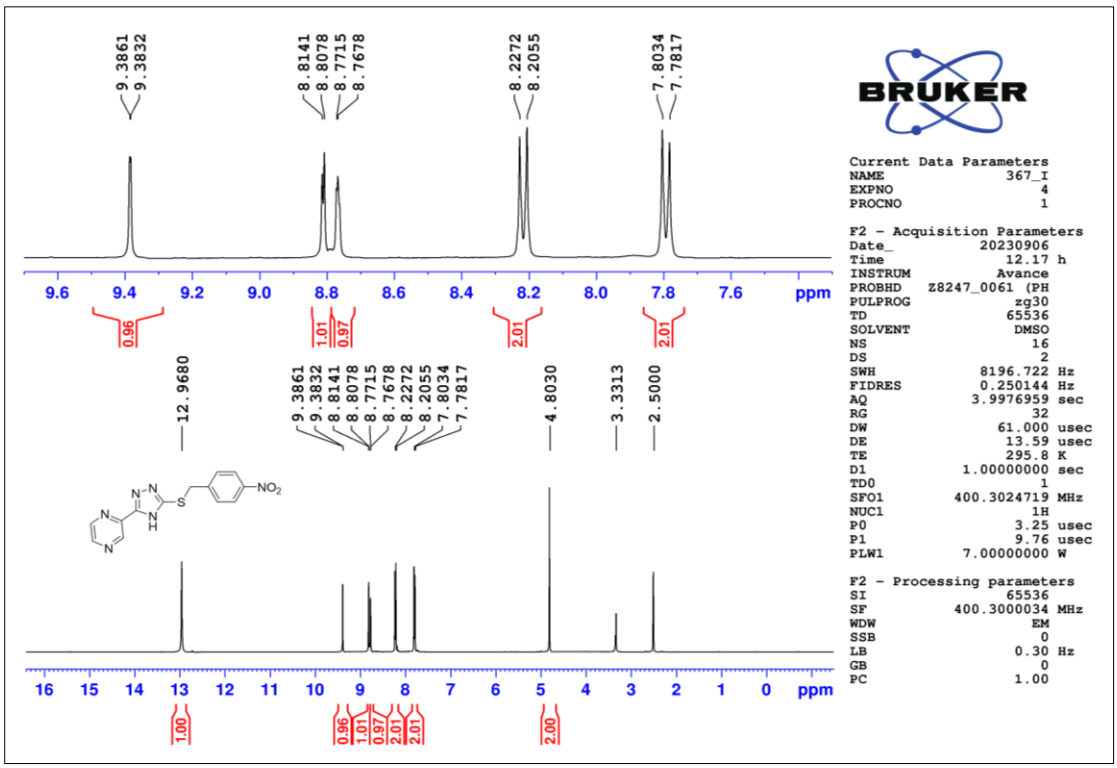

Figure 2.135 *^{1}H-NMR spectrum of compound* ***T36***

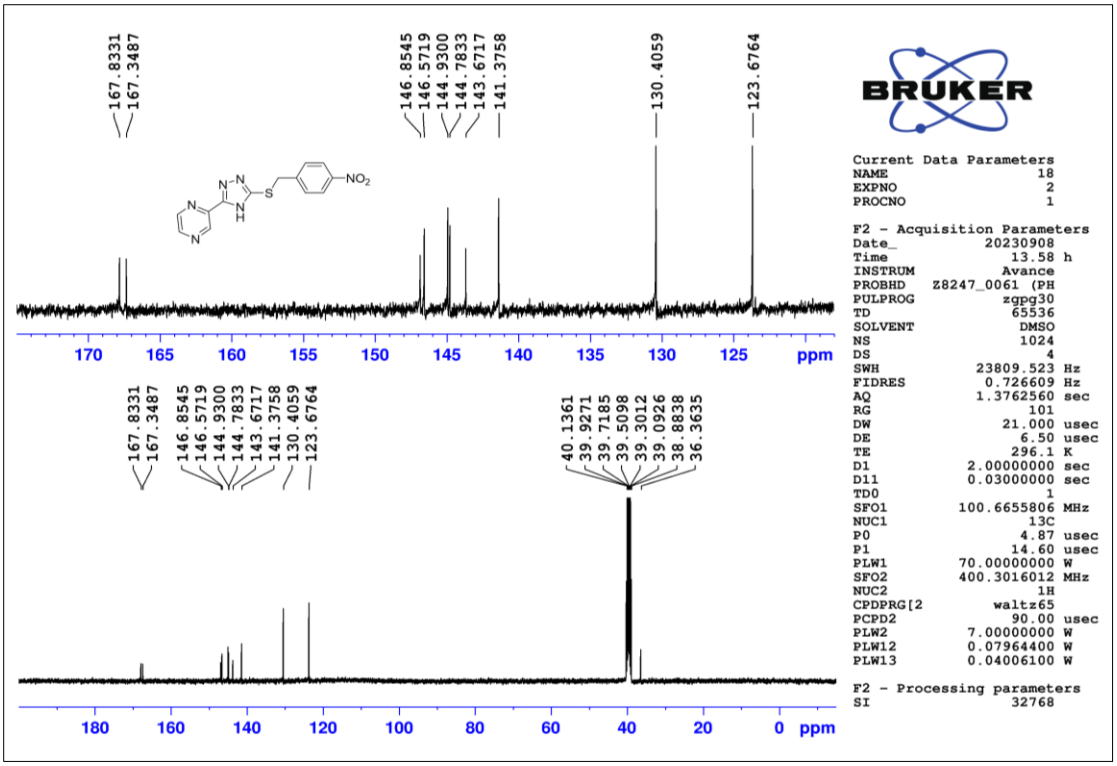

Figure 2.136 *^{13}C-NMR spectrum of compound* ***T36***

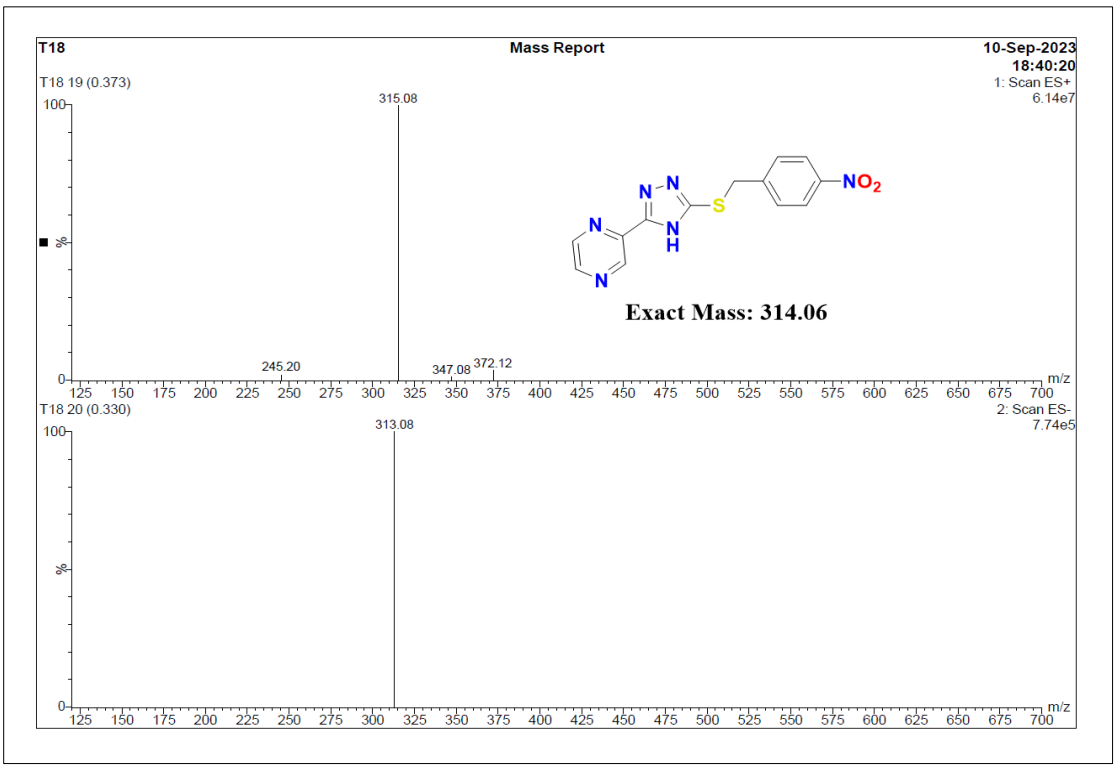

Figure 2.137 *ESI-MS spectrum of compound* ***T36***

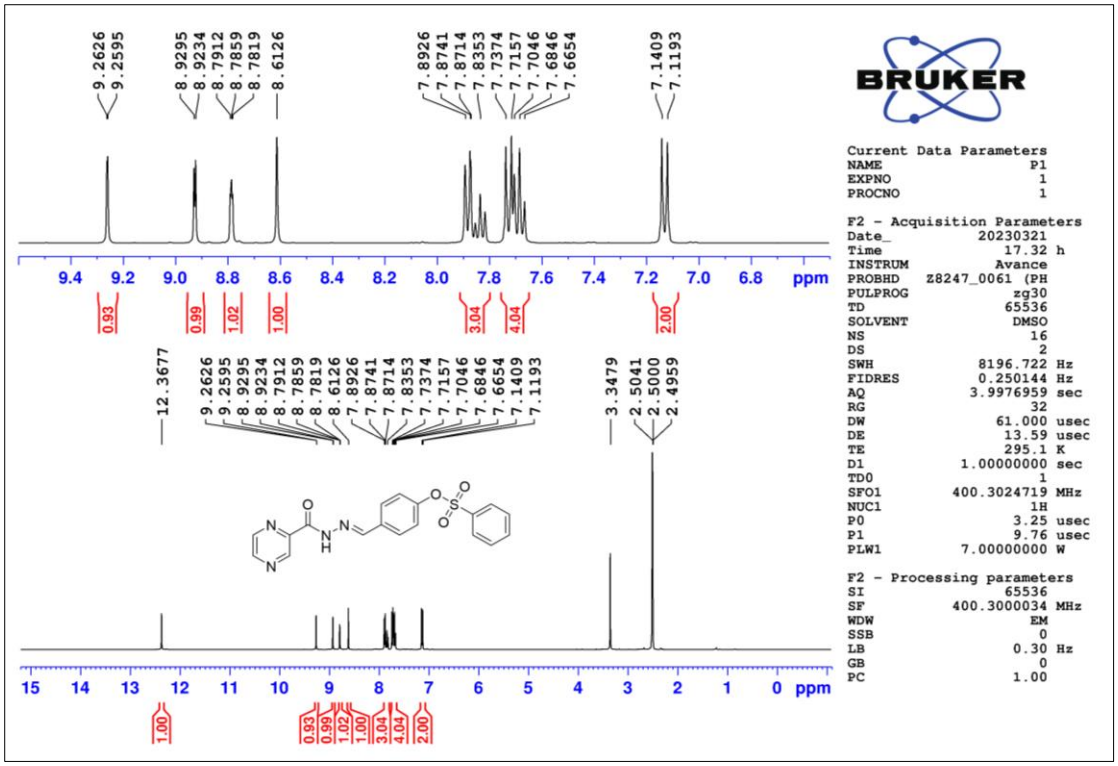

Figure 2.138 *^{1}H-NMR spectrum of compound* ***T37***

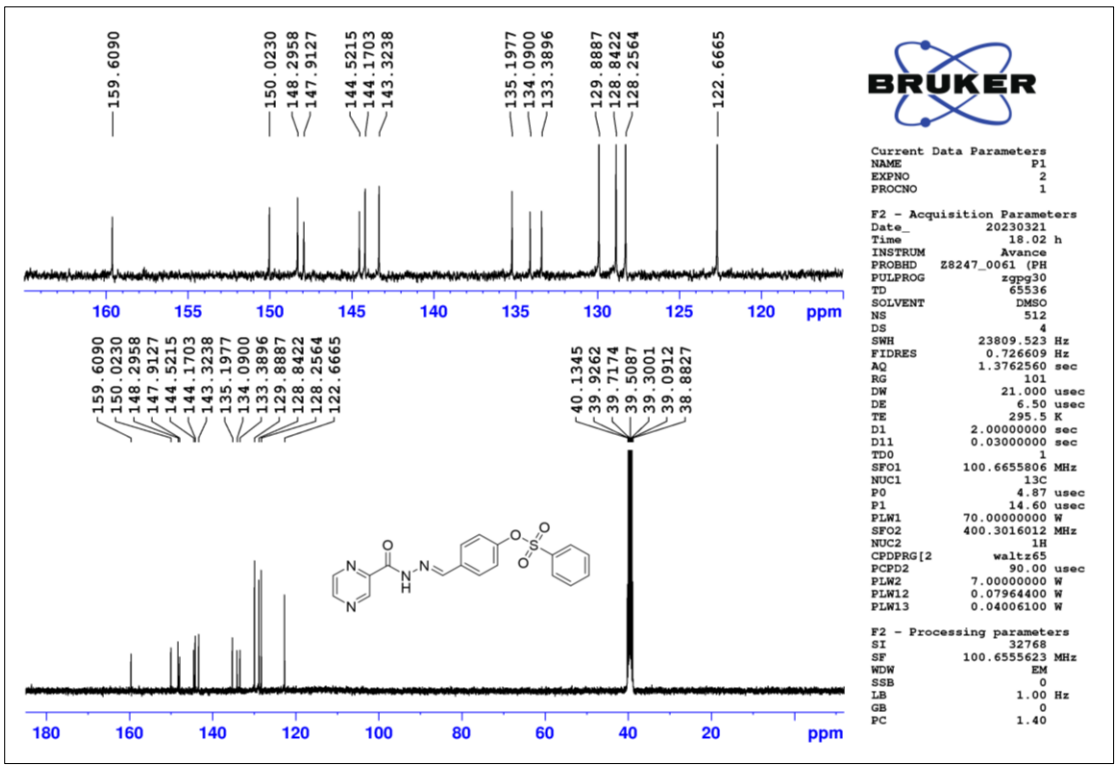

Figure 2.139 *^{13}C-NMR spectrum of compound* ***T37***

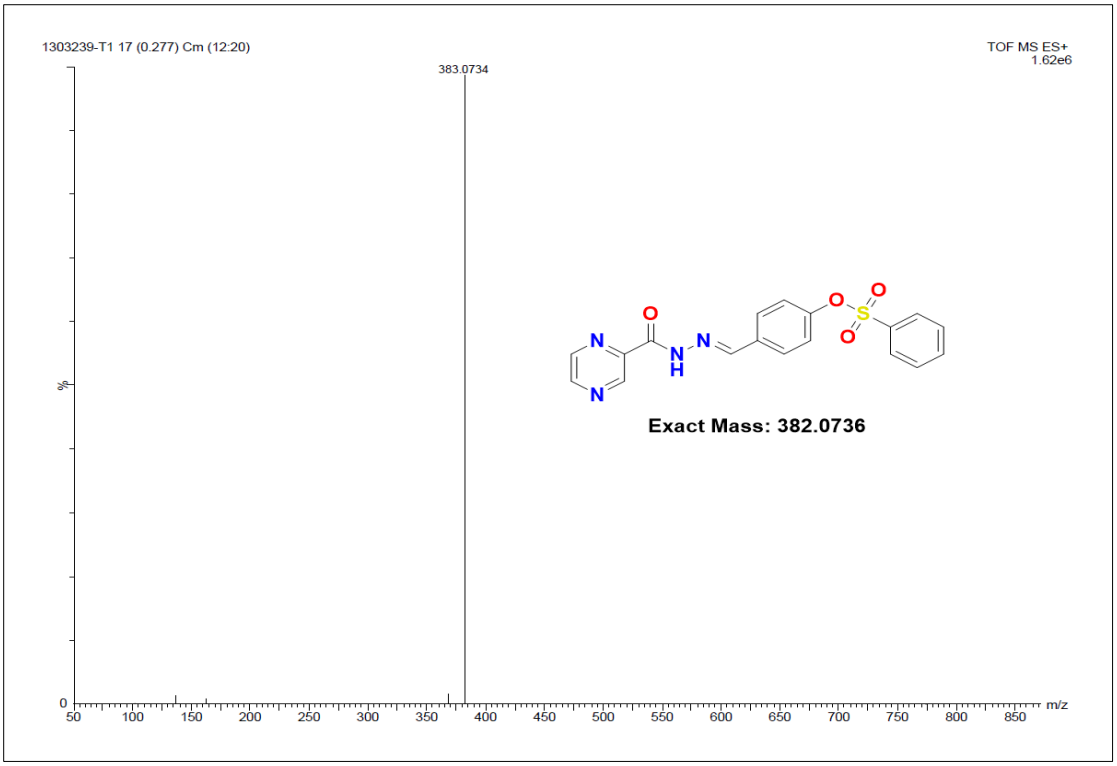

Figure 2.140 *HR-MS spectrum of compound* ***T37***

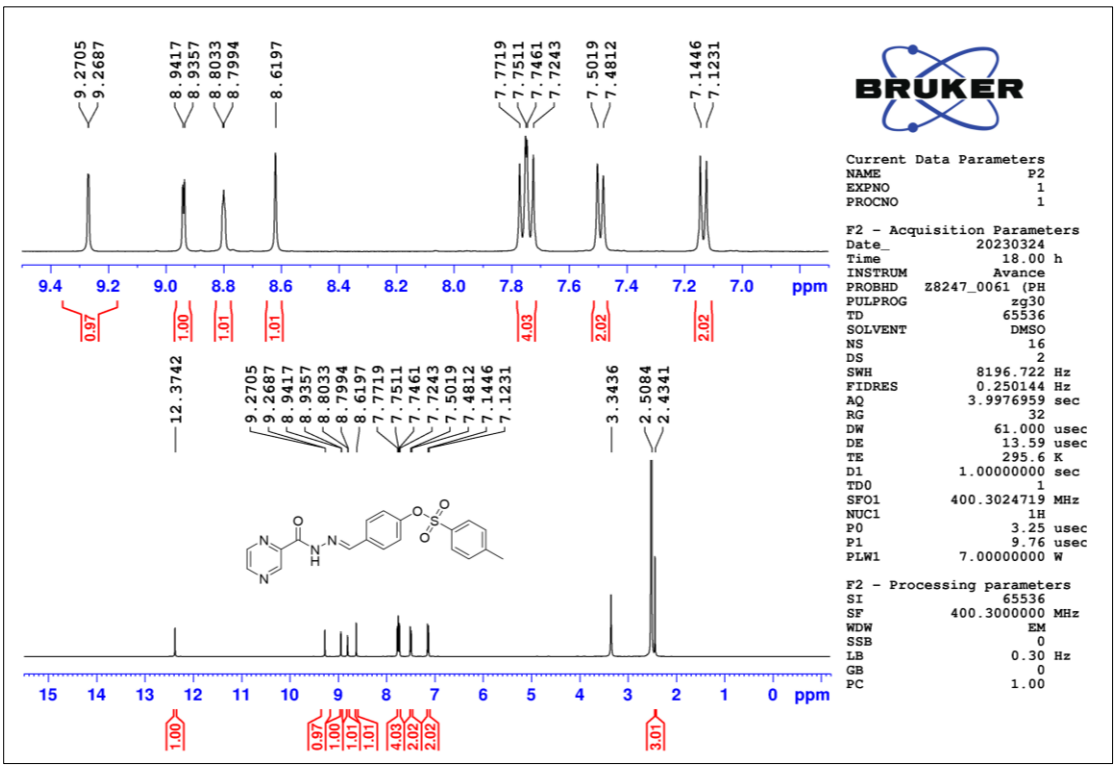

Figure 2.141 *^{1}H-NMR spectrum of compound* ***T38***

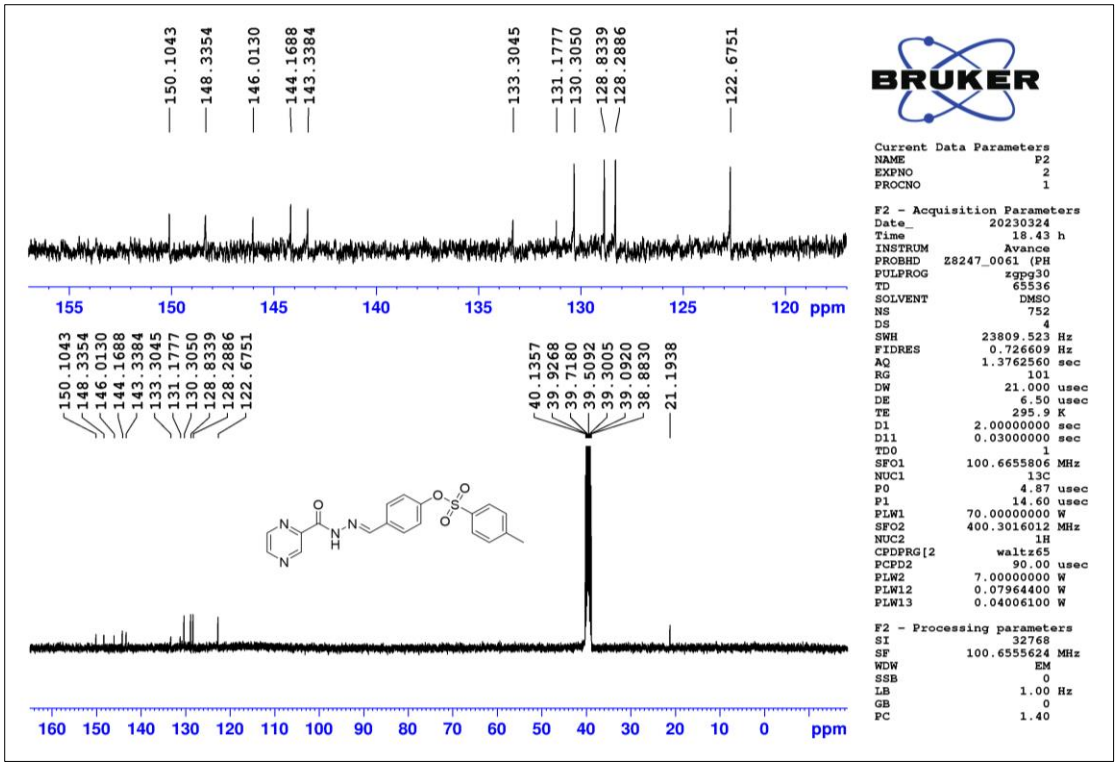

Figure 2.142 *^{13}C-NMR spectrum of compound* ***T38***

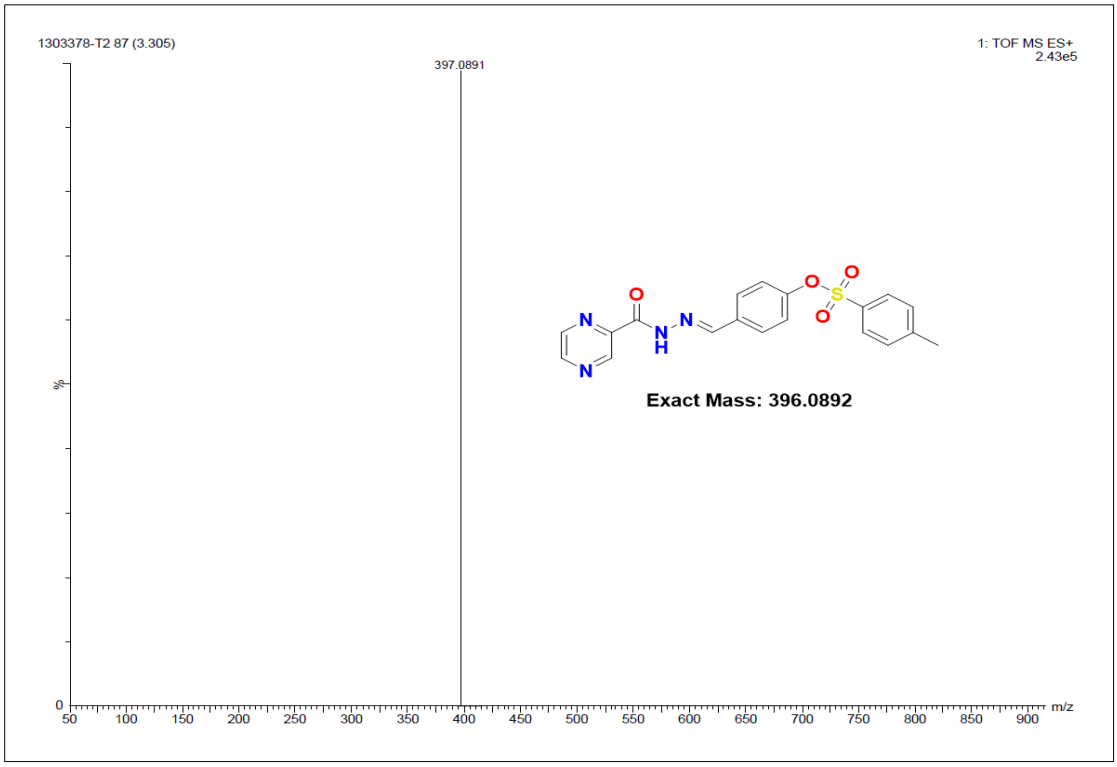

Figure 2.143 *HR-MS spectrum of compound* ***T38***

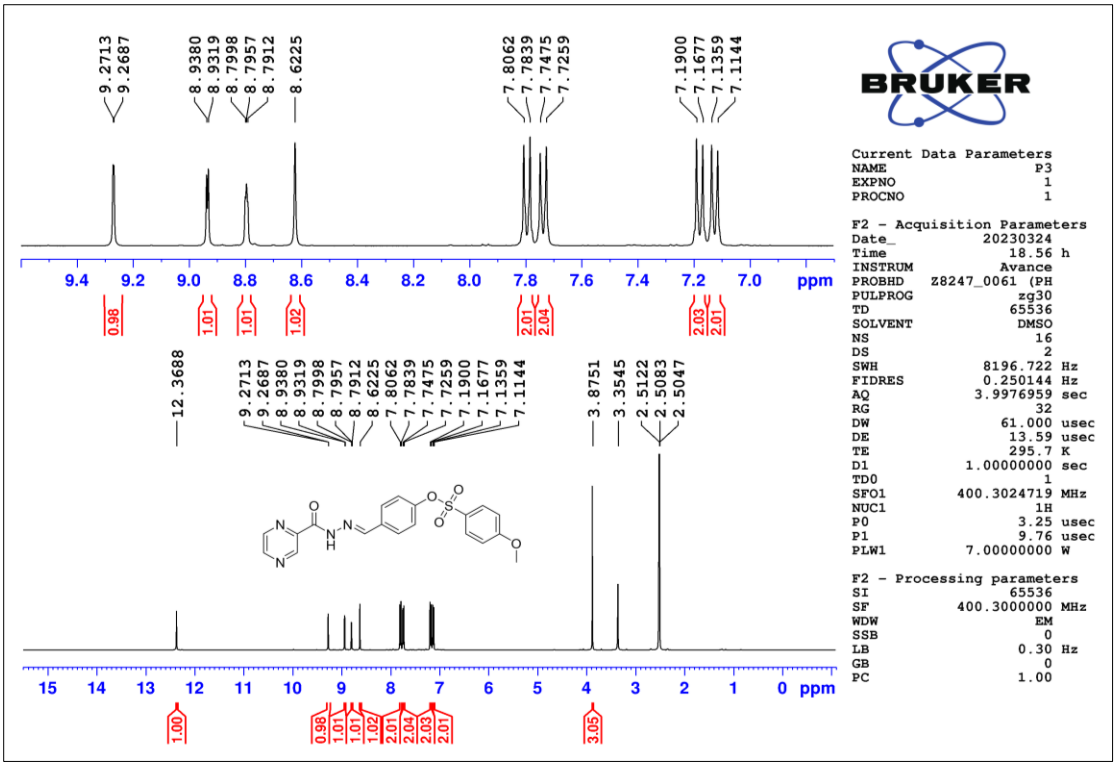

Figure 2.144 *^{1}H-NMR spectrum of compound* ***T39***

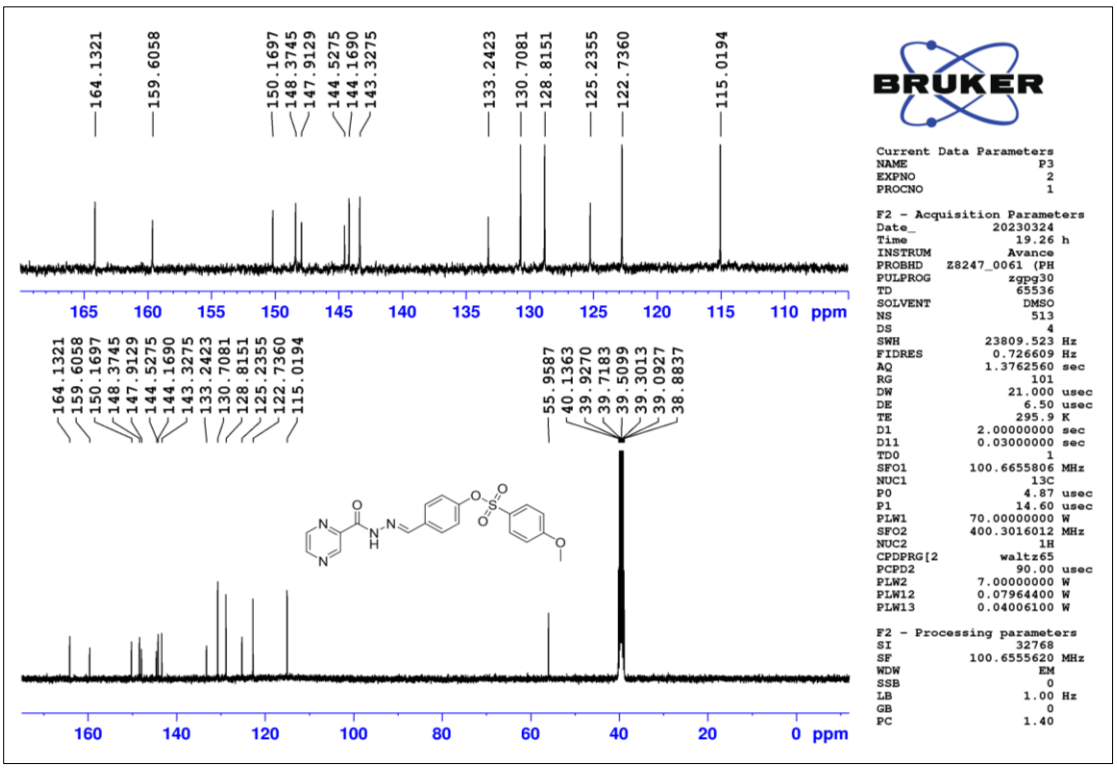

Figure 2.145 *^{13}C-NMR spectrum of compound* ***T39***

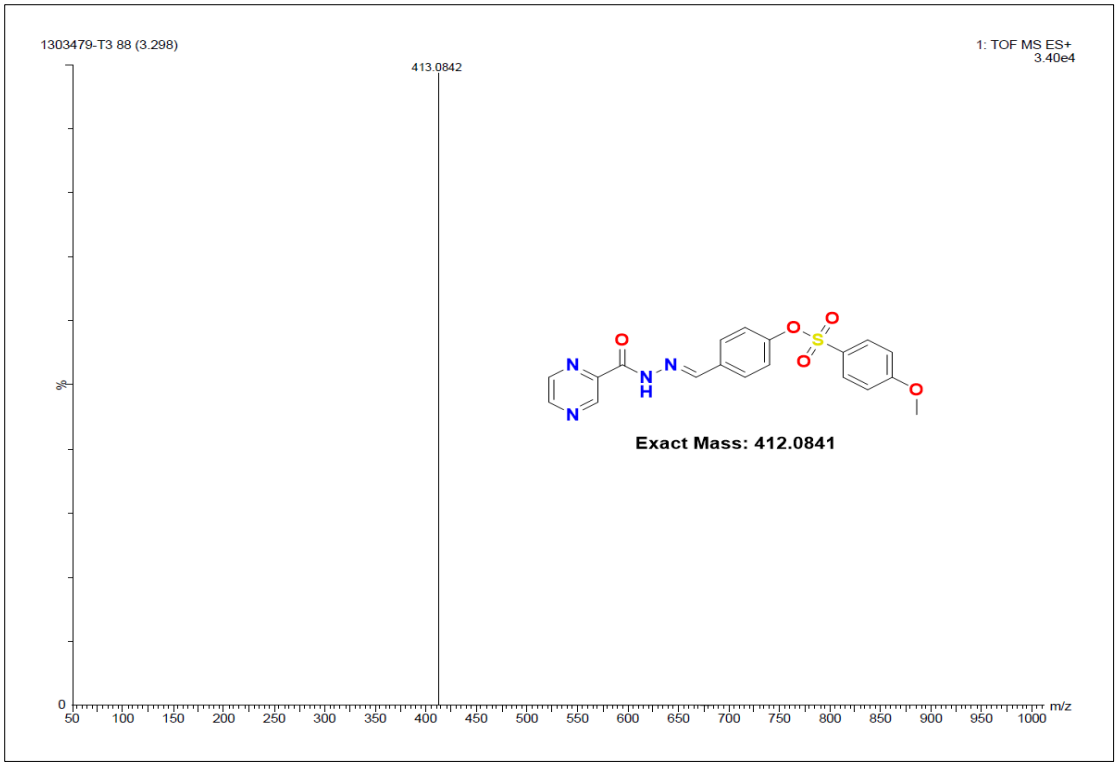

Figure 2.146 *HR-MS spectrum of compound* ***T39***

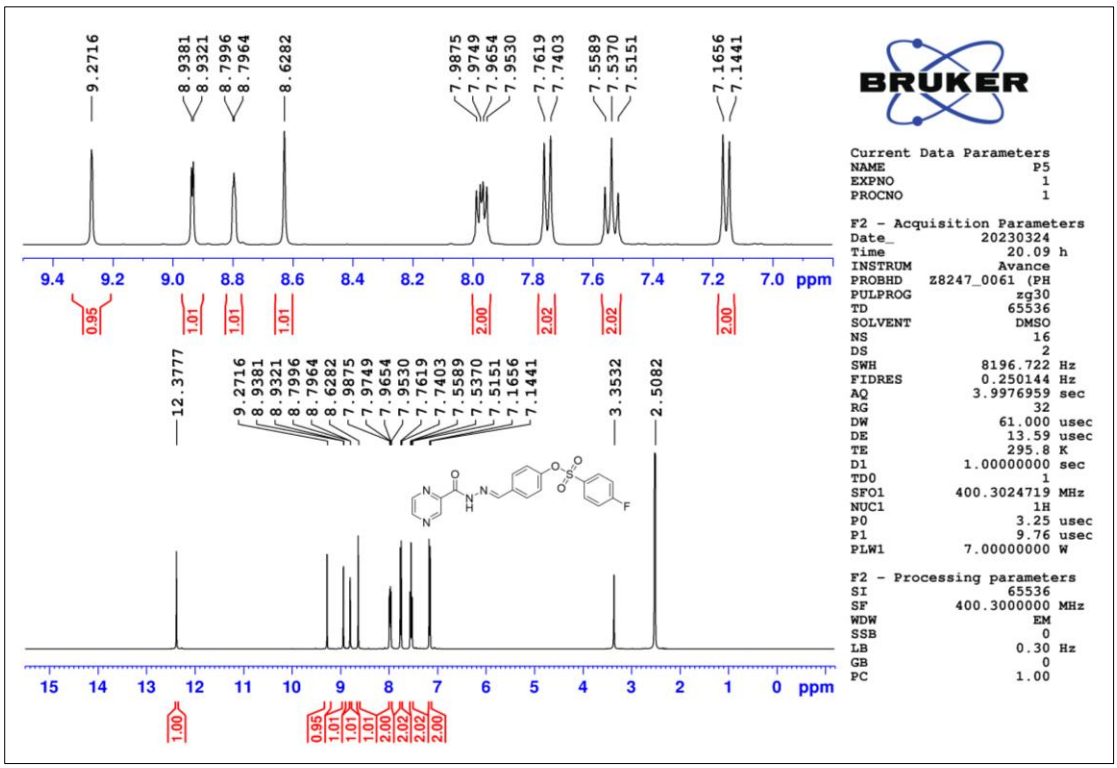

Figure 2.147 *^{1}H-NMR spectrum of compound* ***T41***

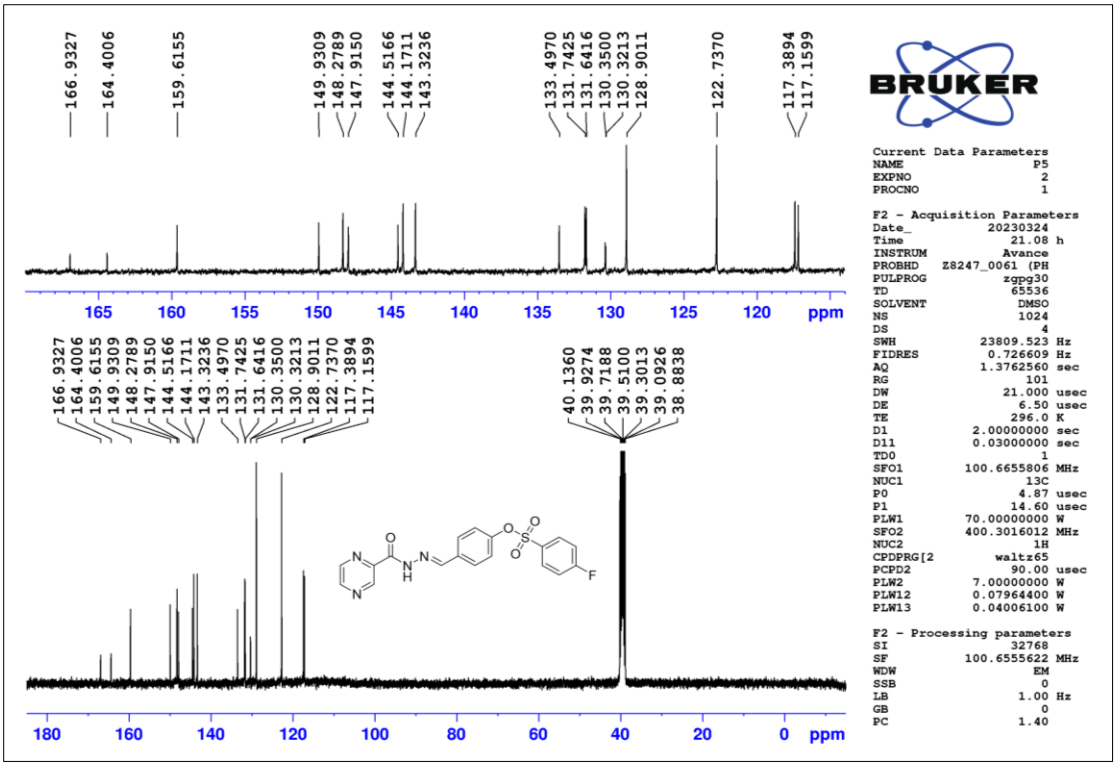

Figure 2.148 *^{13}C-NMR spectrum of compound* ***T41***

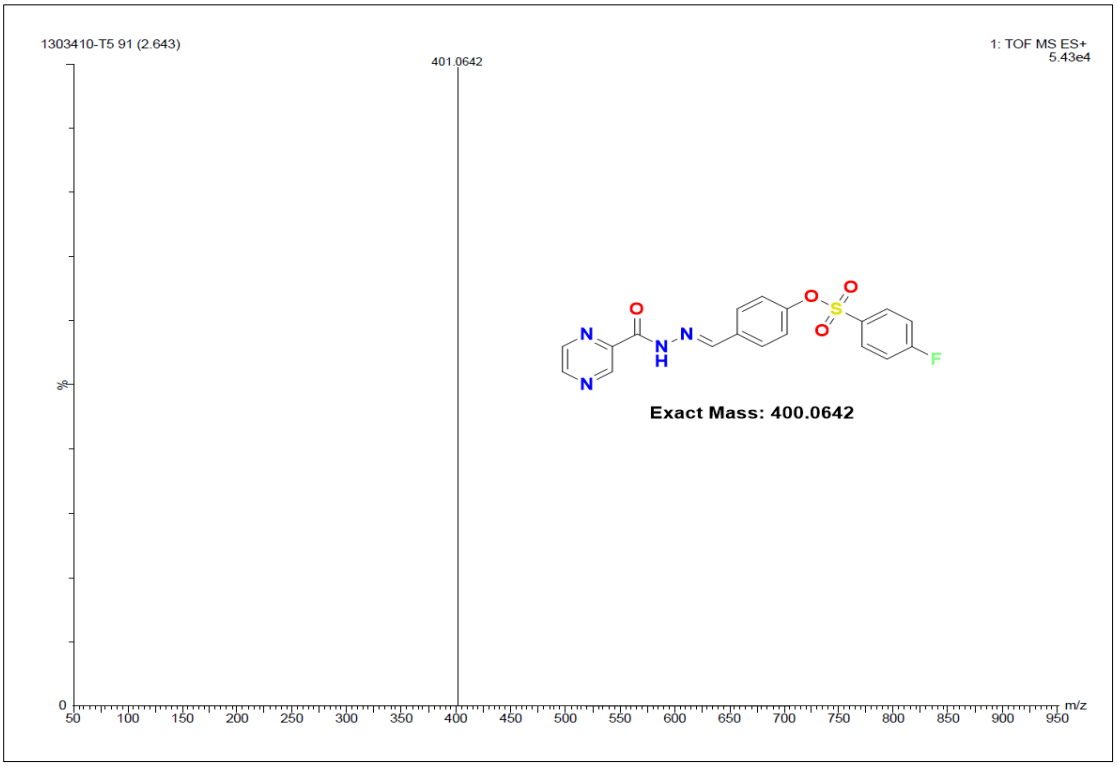

Figure 2.149 *HR-MS spectrum of compound* ***T41***

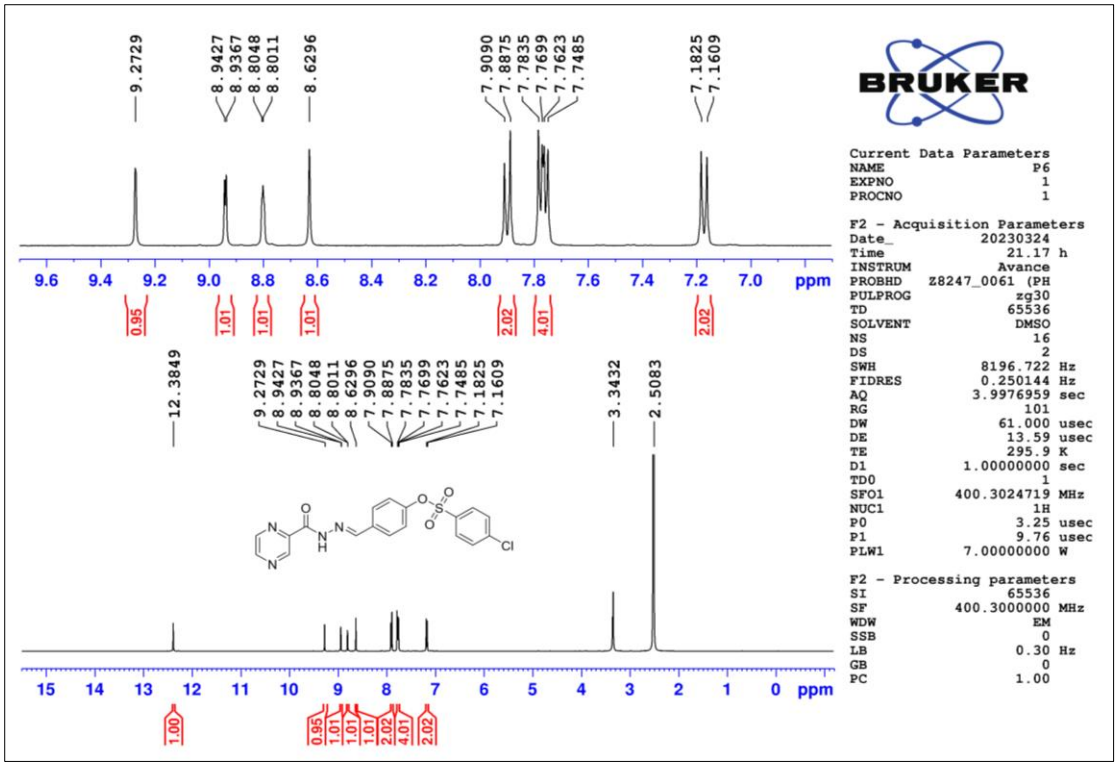

Figure 2.150 *^{1}H-NMR spectrum of compound* ***T42***

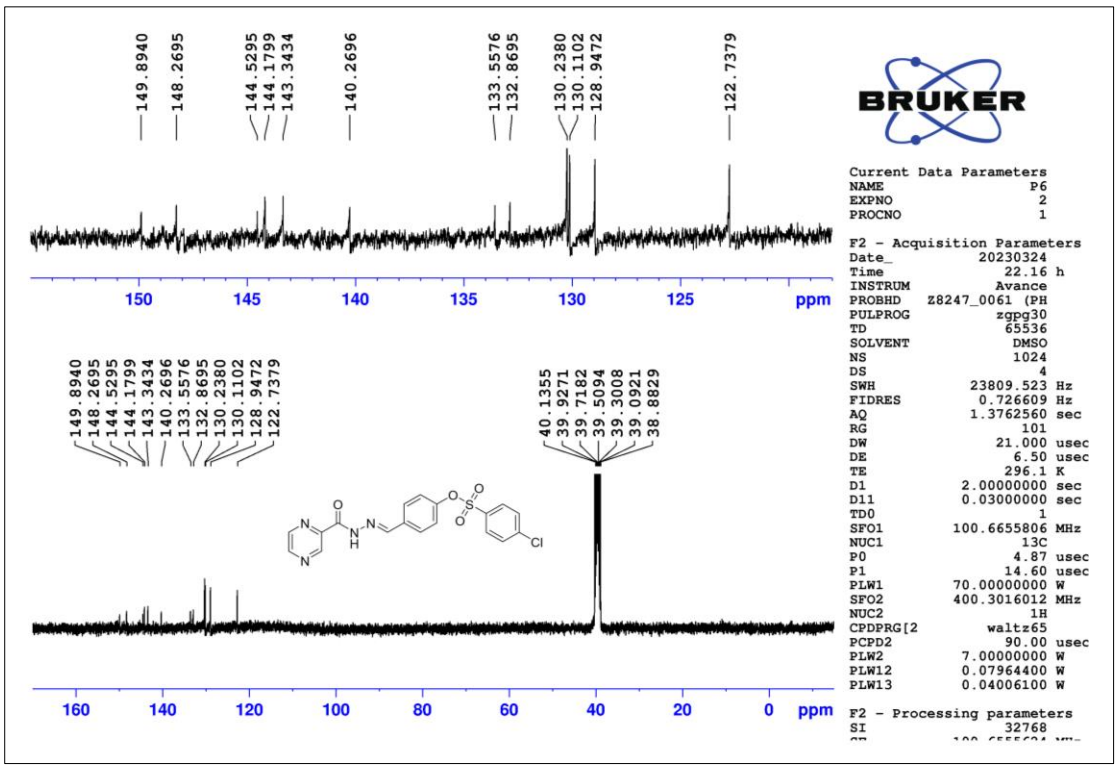

Figure 2.151 *^{13}C-NMR spectrum of compound* ***T42***

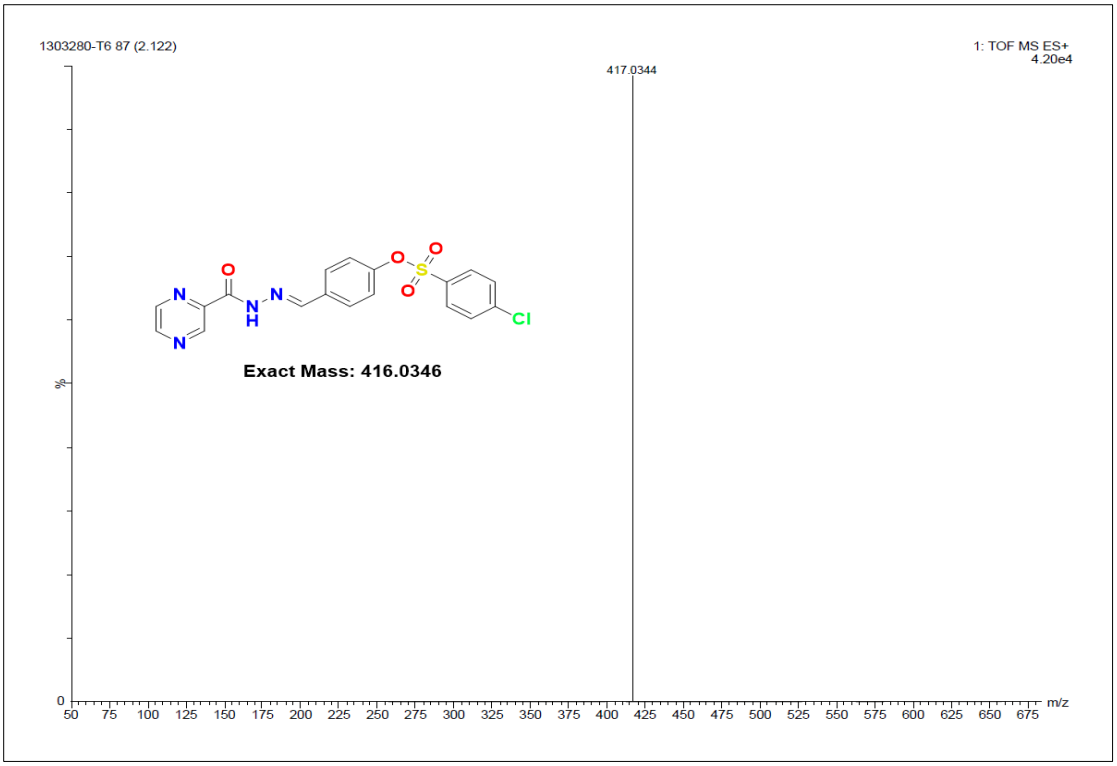

Figure 2.152 *HR-MS spectrum of compound* ***T42***

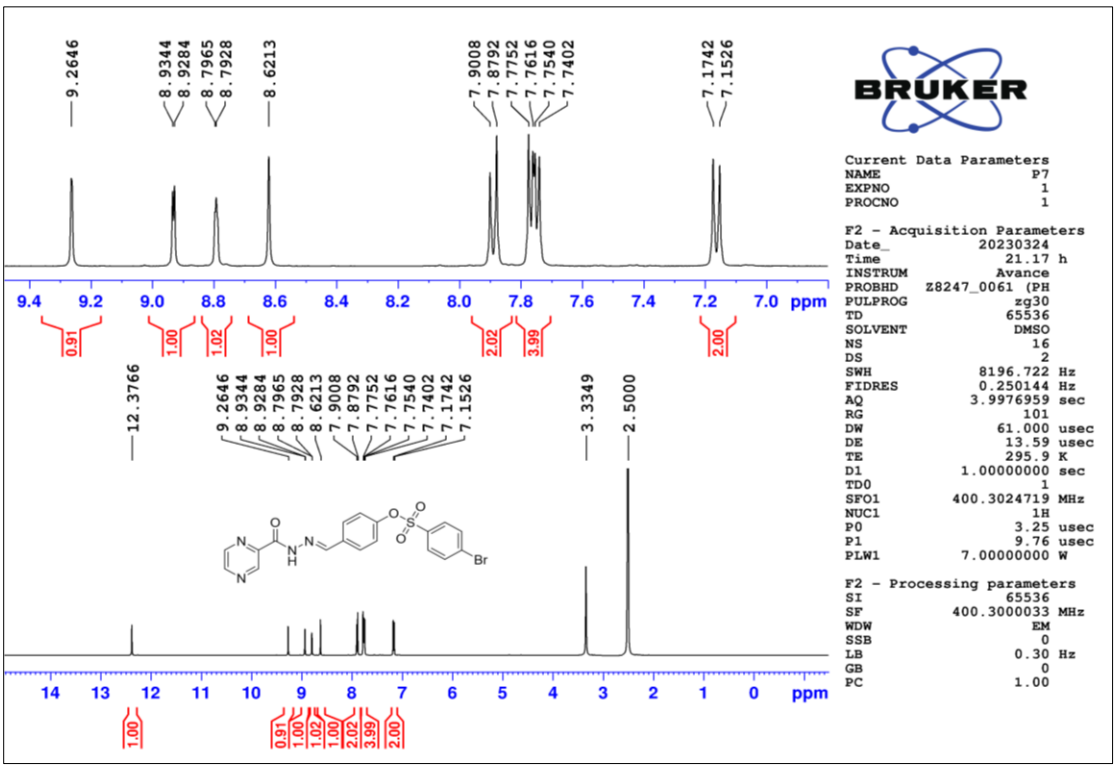

Figure 2.153 *^{1}H-NMR spectrum of compound* ***T43***

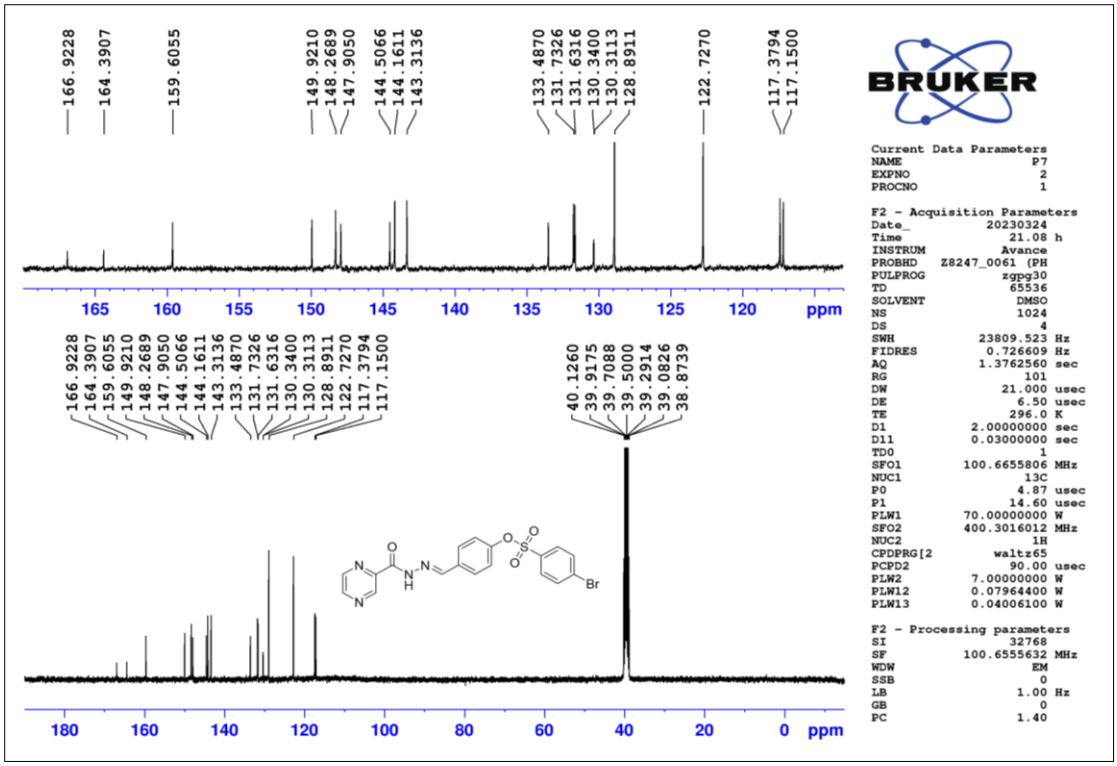

Figure 2.154 *^{13}C-NMR spectrum of compound* ***T43***

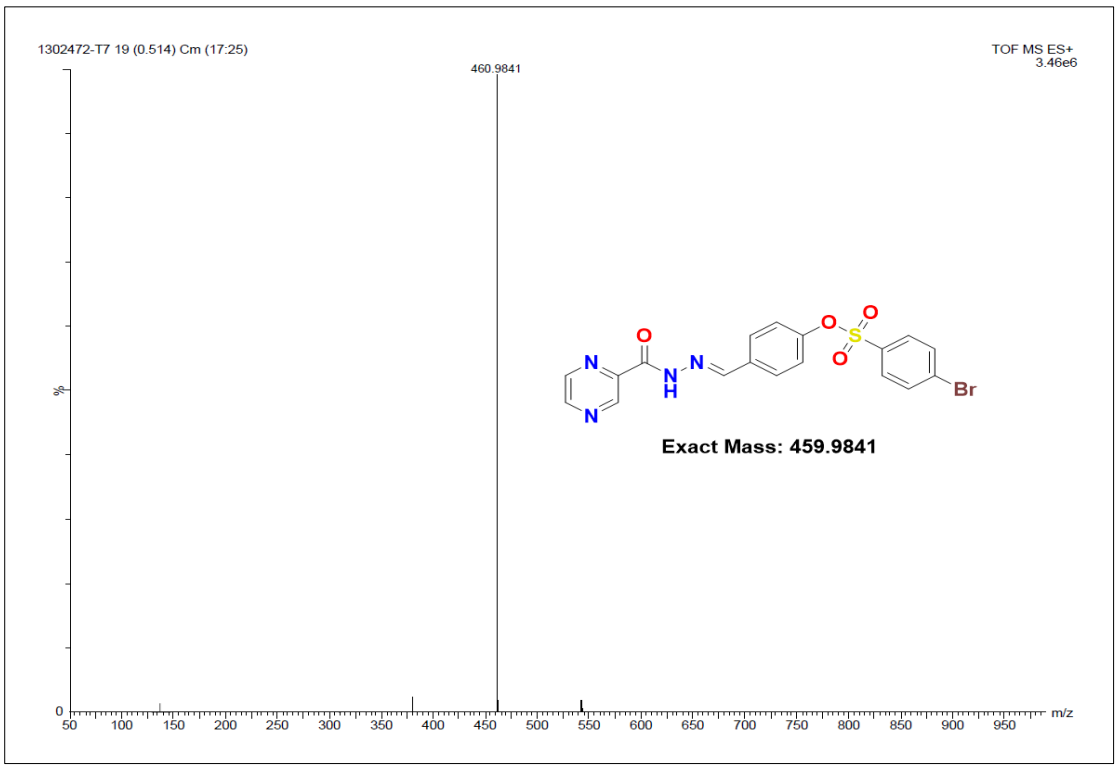

Figure 2.155 *HR-MS spectrum of compound* ***T43***

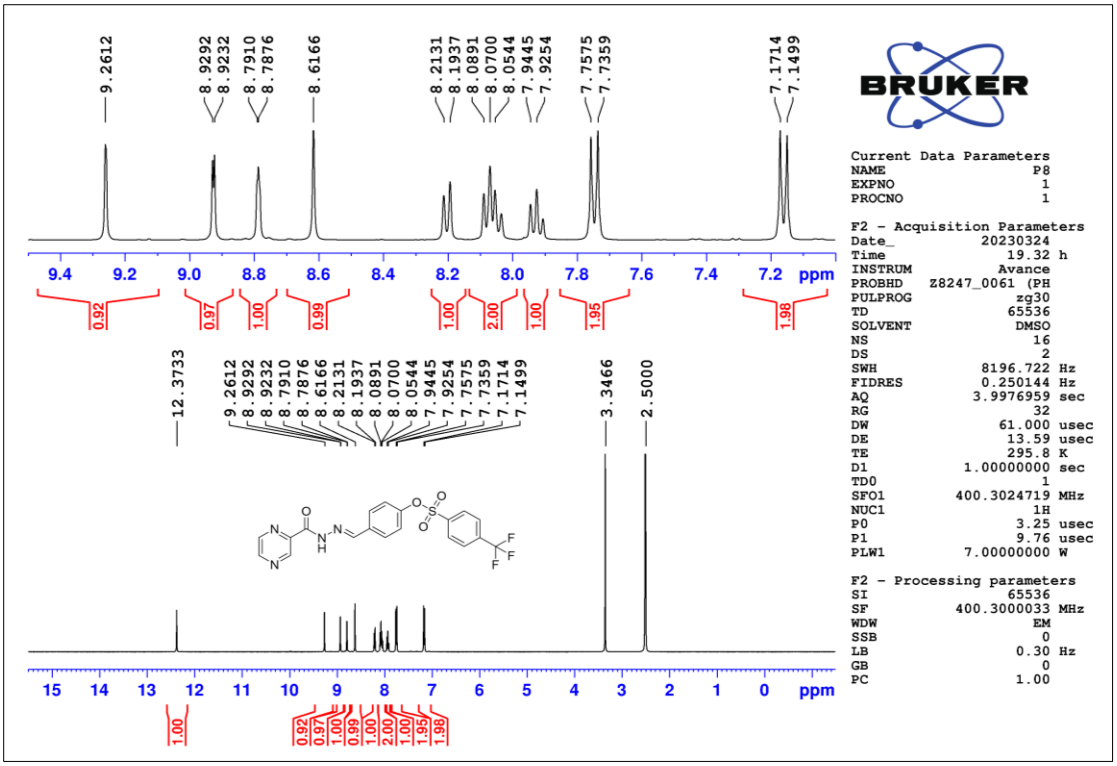

Figure 2.156 *[1]H-NMR spectrum of compound* ***T44***

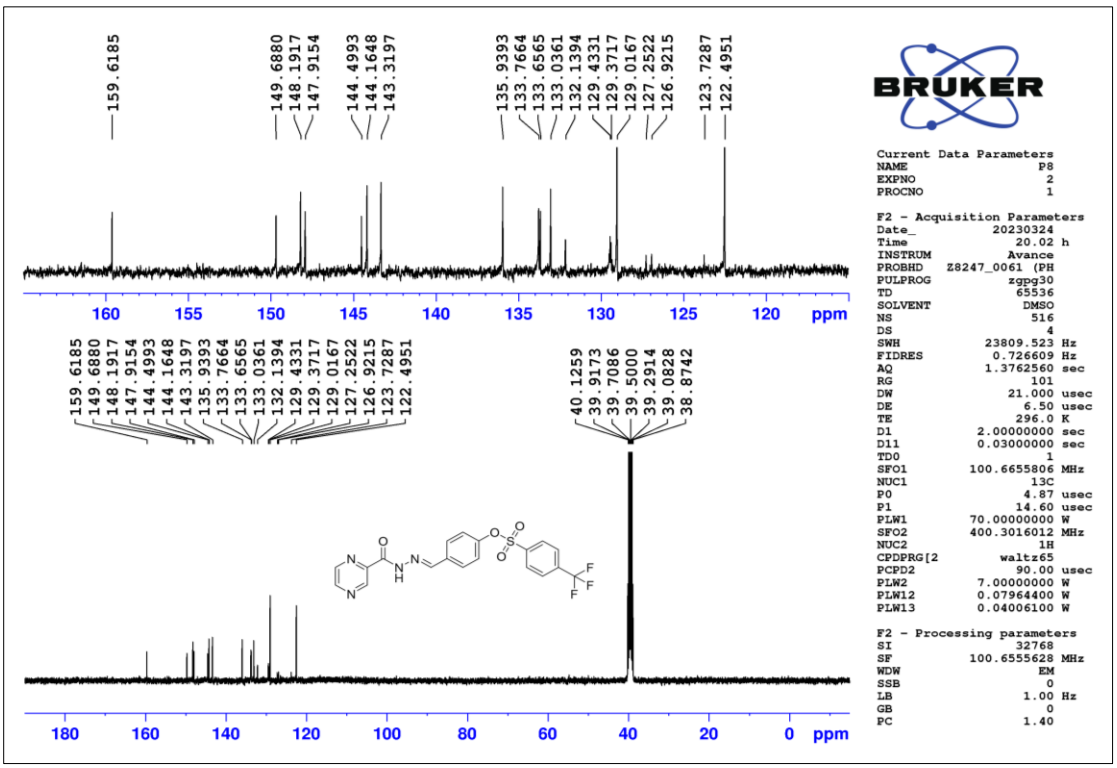

Figure 2.157 *[13]C-NMR spectrum of compound* ***T44***

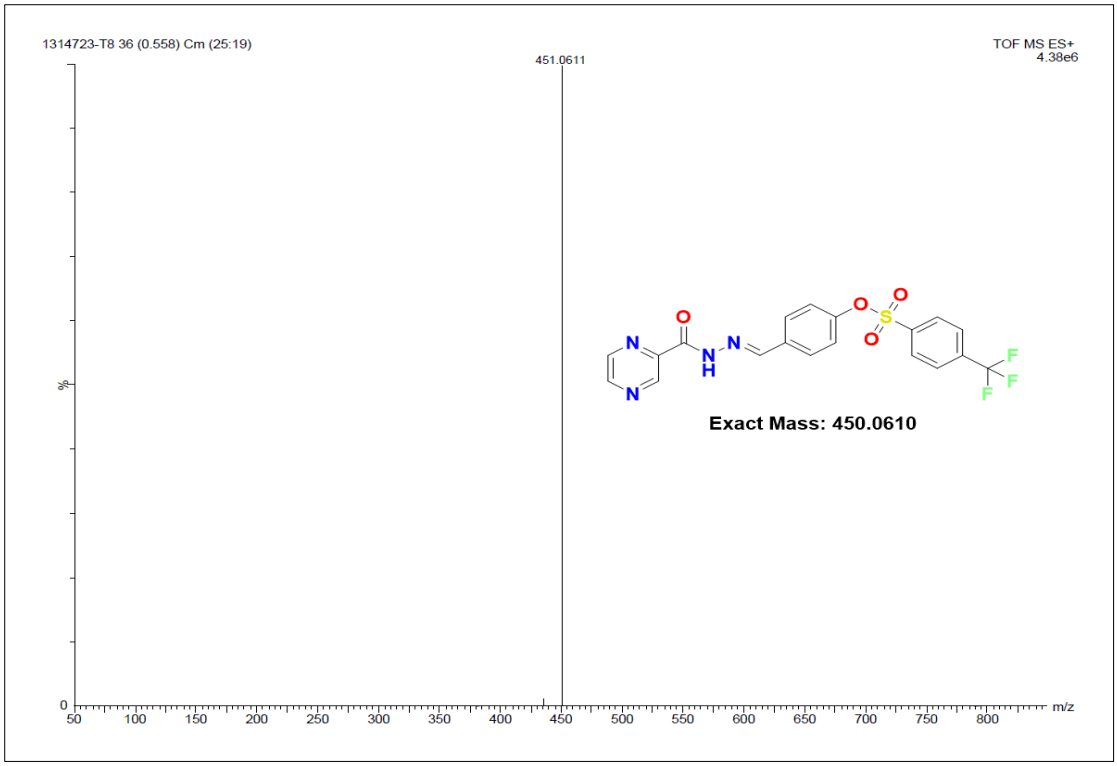

Figure 2.158 *HR-MS spectrum of compound* ***T44***

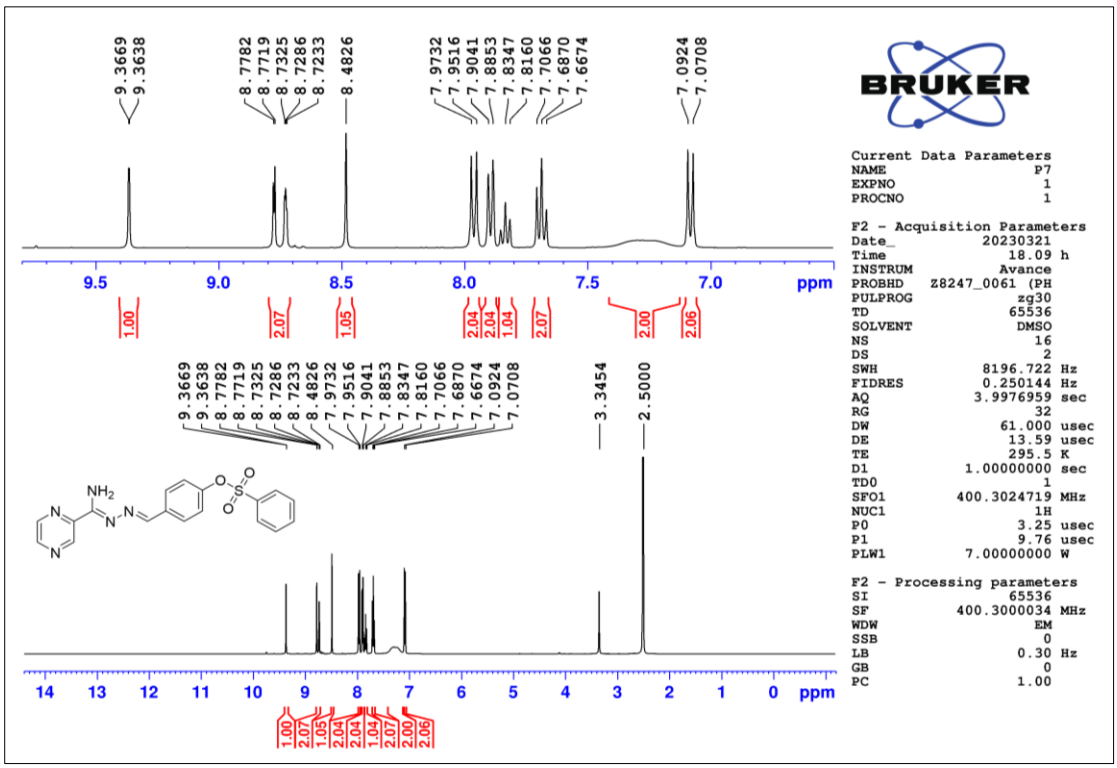

Figure 2.159 *^{1}H-NMR spectrum of compound* ***T45***

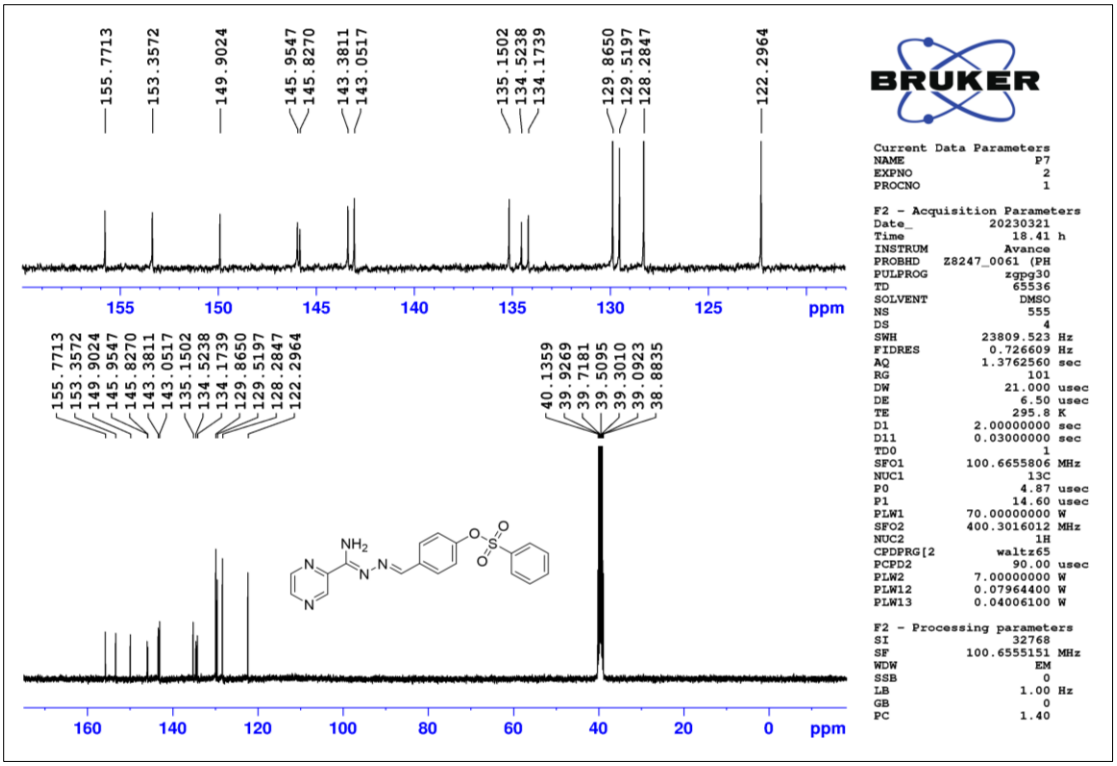

Figure 2.160 *^{13}C-NMR spectrum of compound* ***T45***

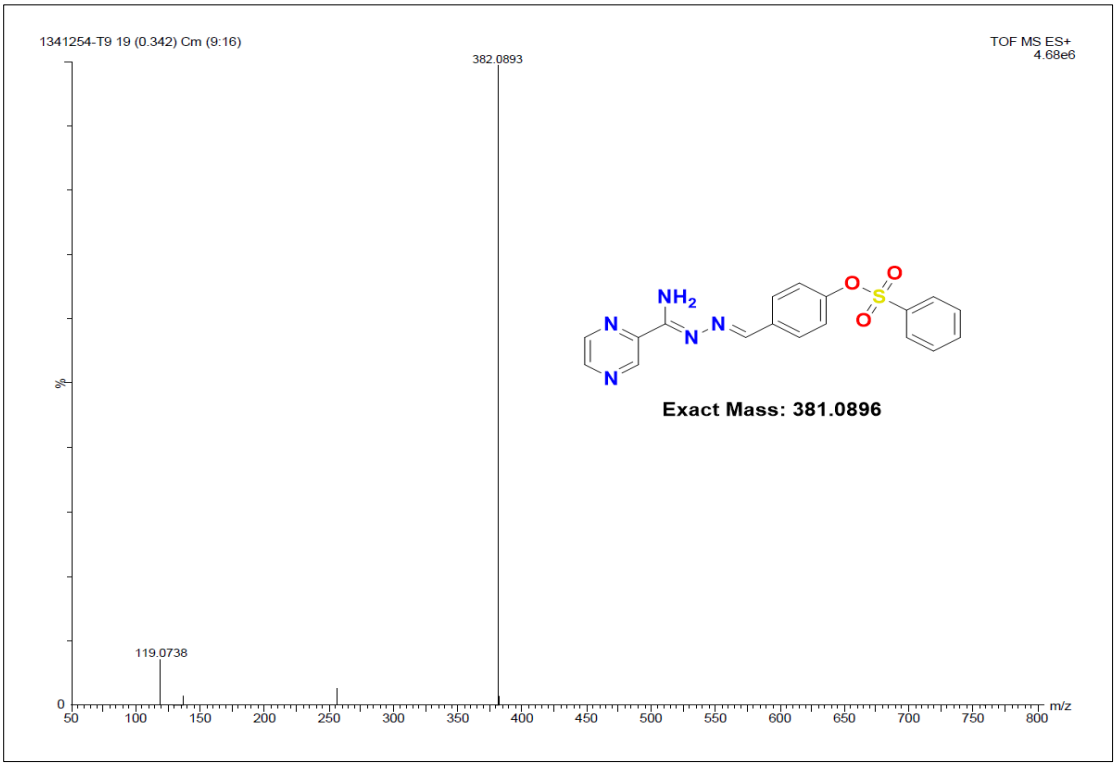

Figure 2.161 *HR-MS spectrum of compound* ***T45***

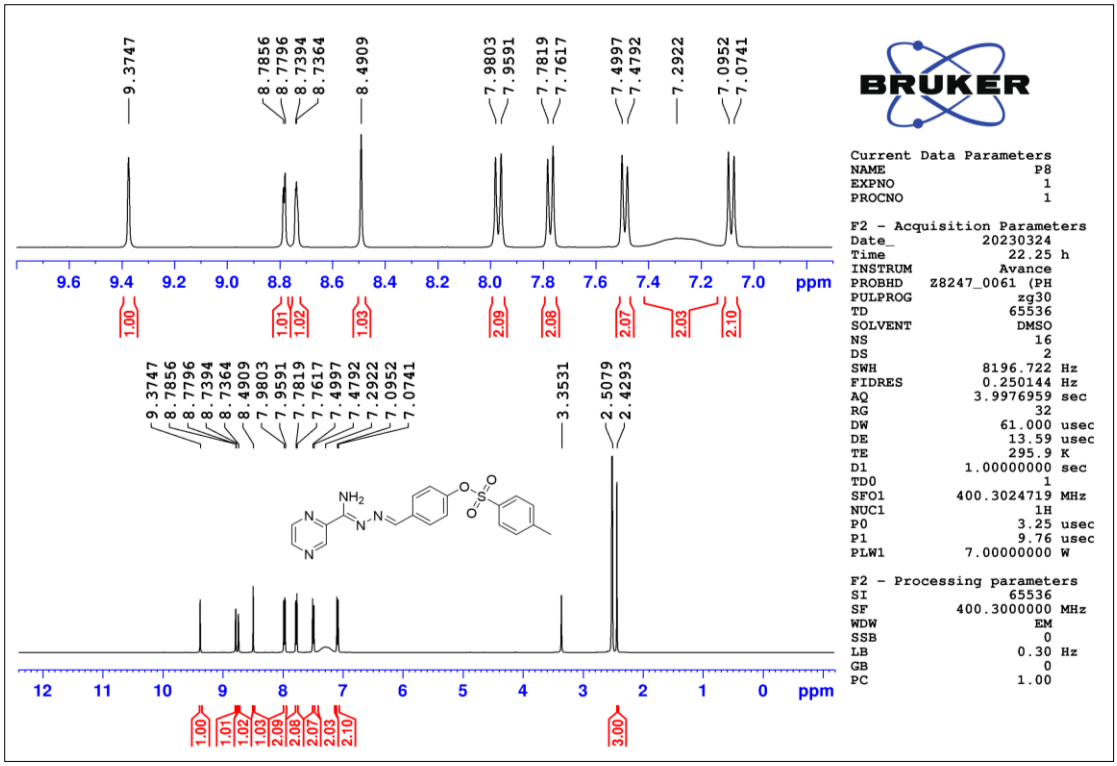

Figure 2.162 *^{1}H-NMR spectrum of compound* ***T46***

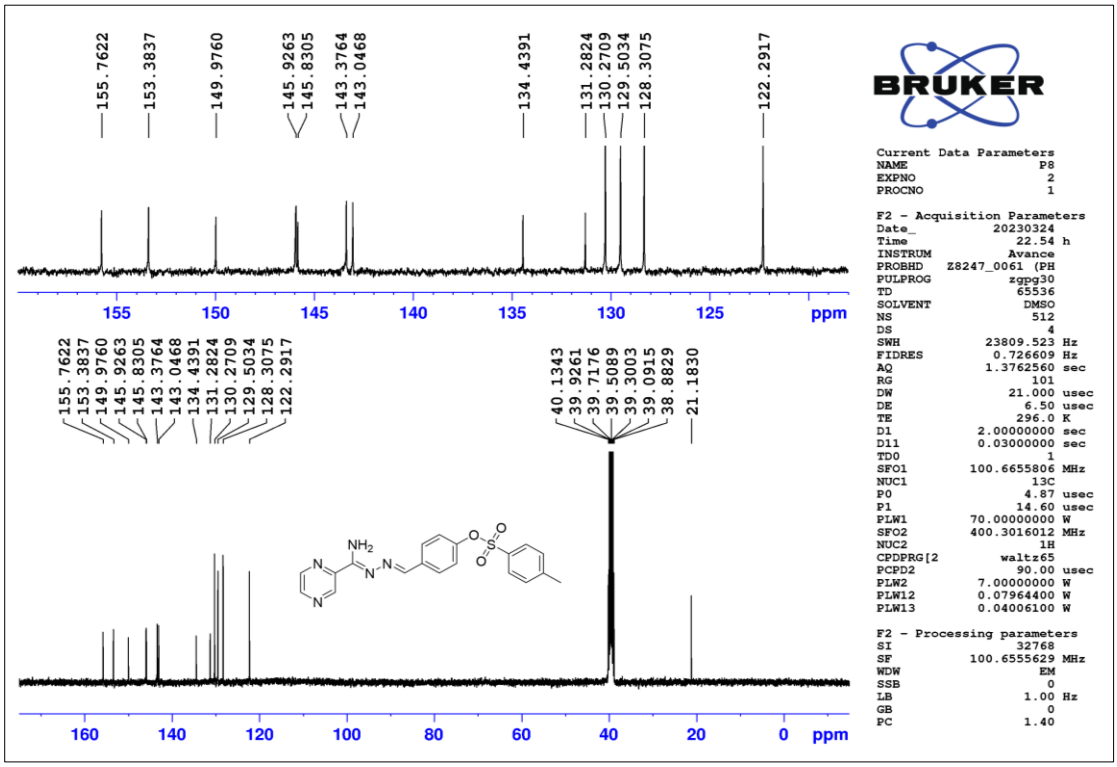

Figure 2.163 *^{13}C-NMR spectrum of compound* ***T46***

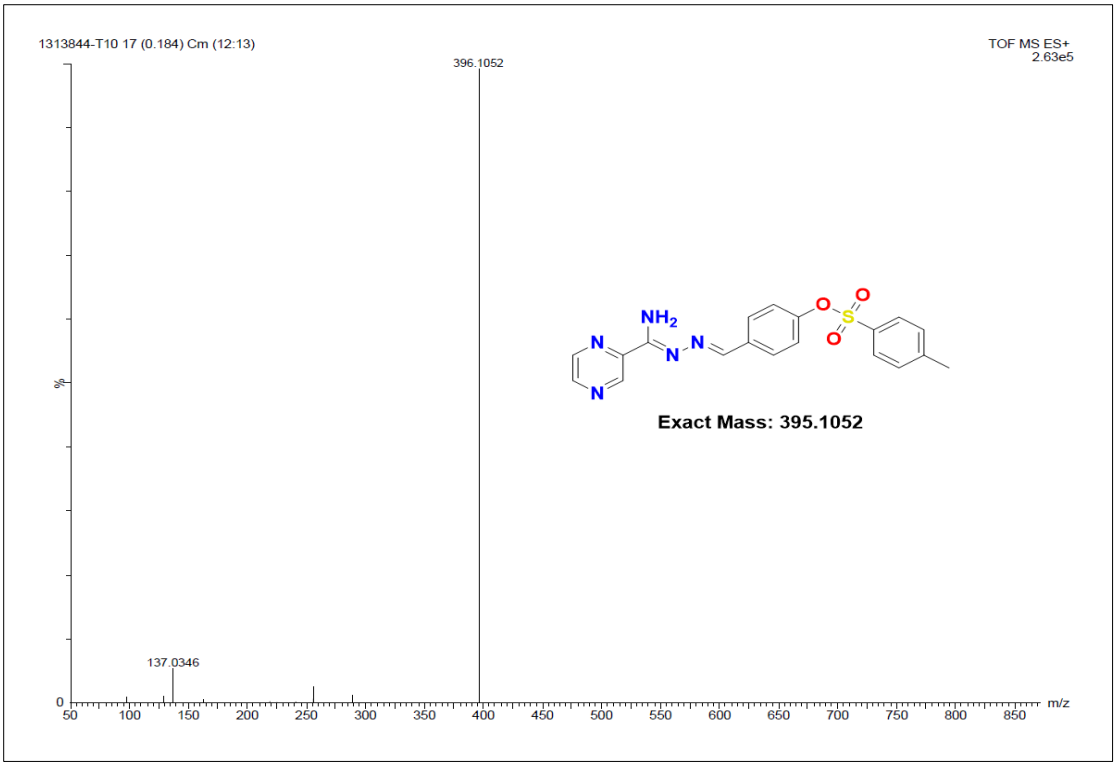

Figure 2.164 *HR-MS spectrum of compound* ***T46***

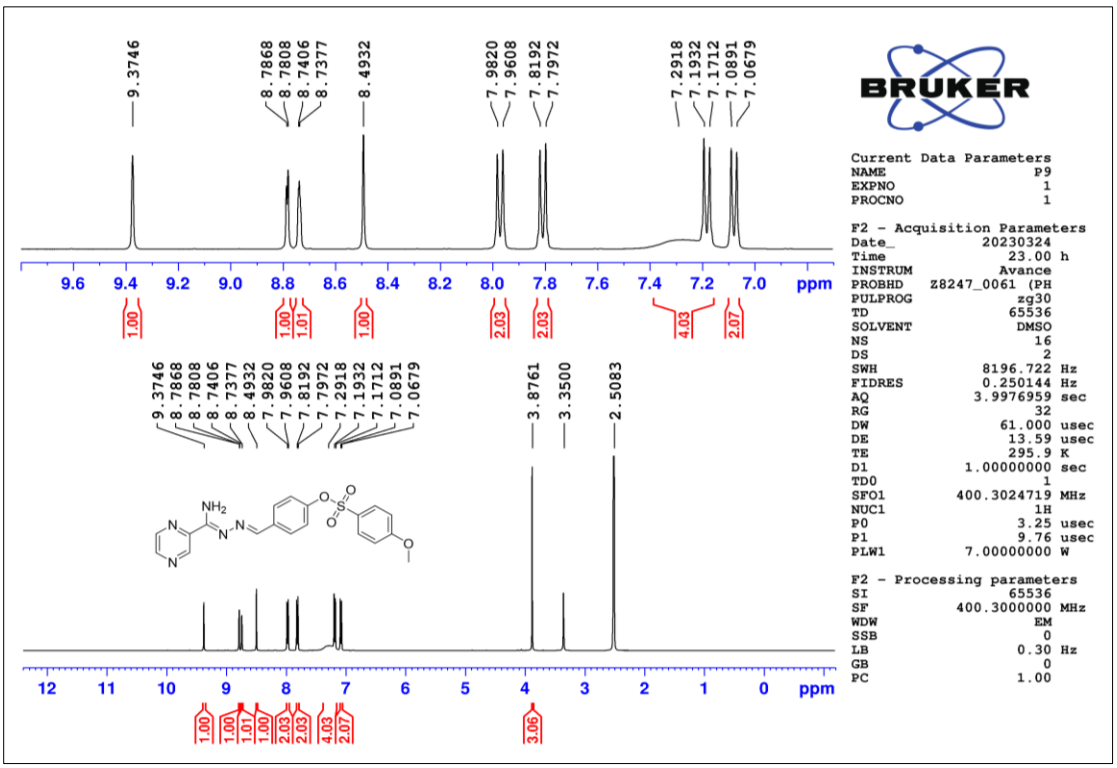

Figure 2.165 *^{1}H-NMR spectrum of compound* ***T47***

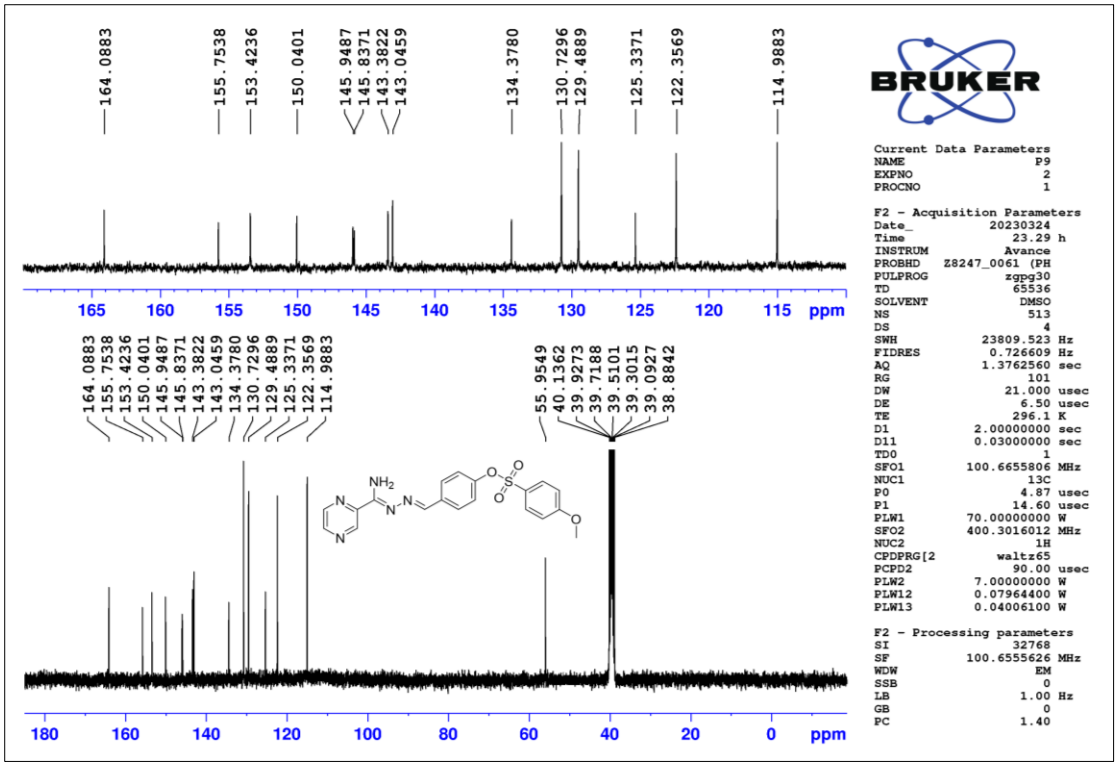

Figure 2.166 *^{13}C-NMR spectrum of compound* ***T47***

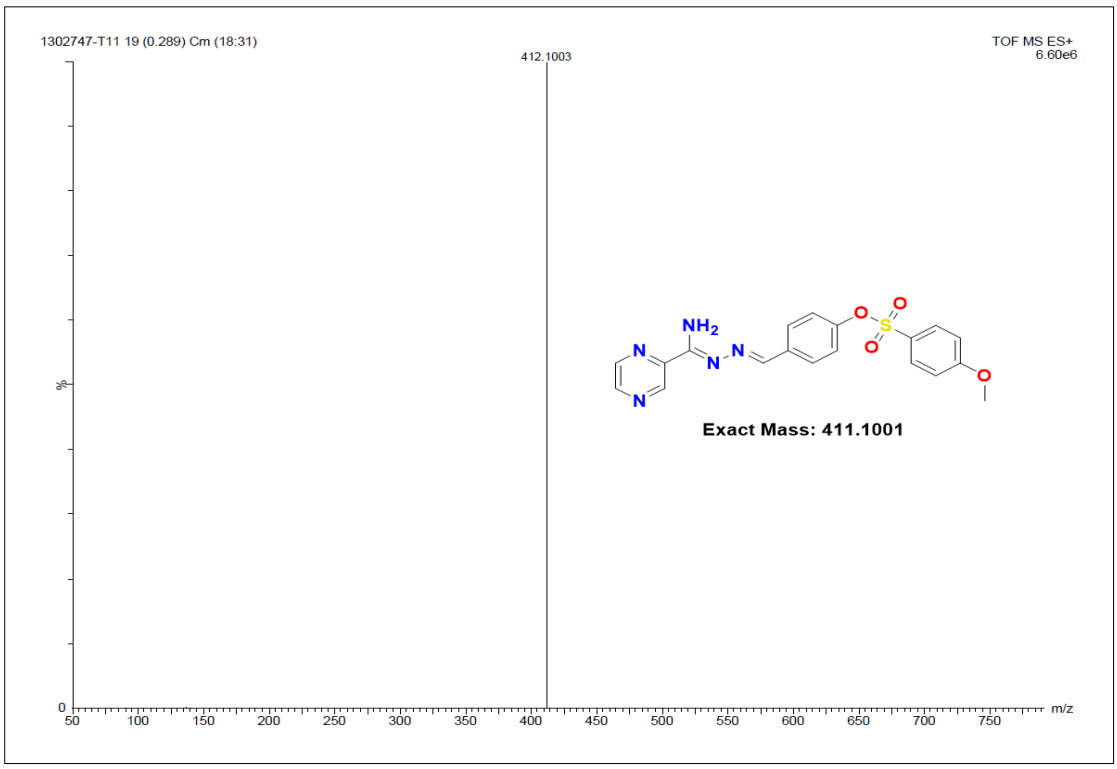

Figure 2.167 *HR-MS spectrum of compound* ***T47***

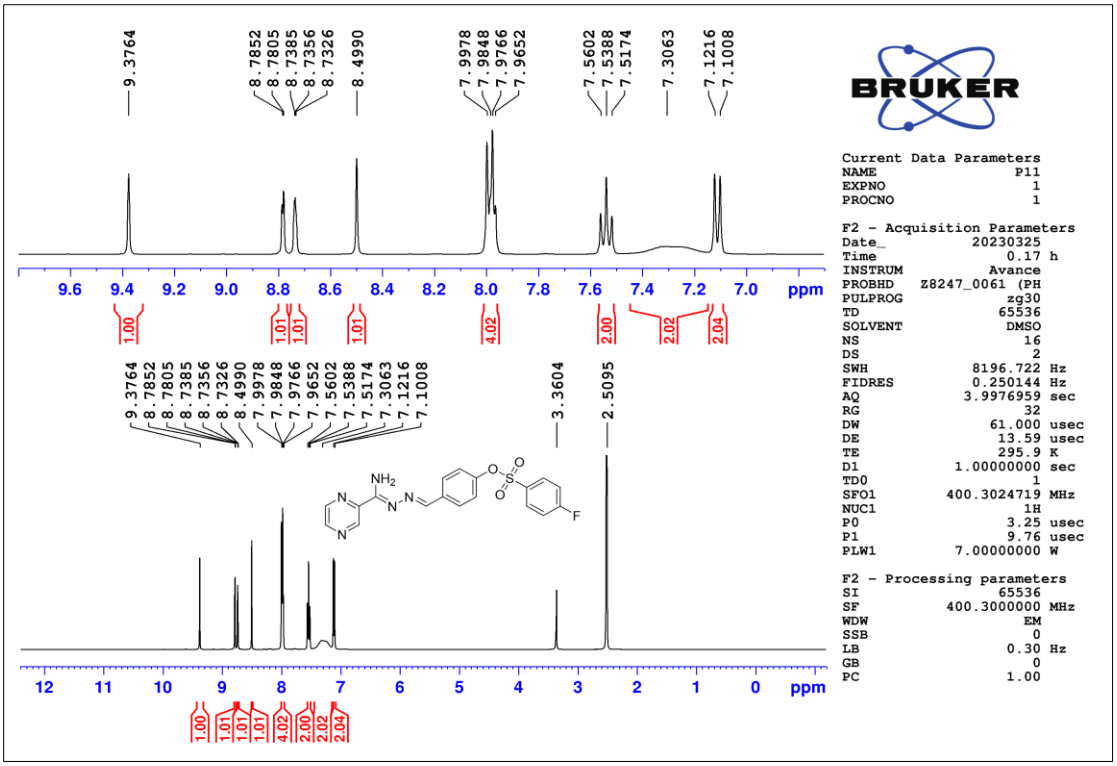

Figure 2.168 *^{1}H-NMR spectrum of compound* ***T49***

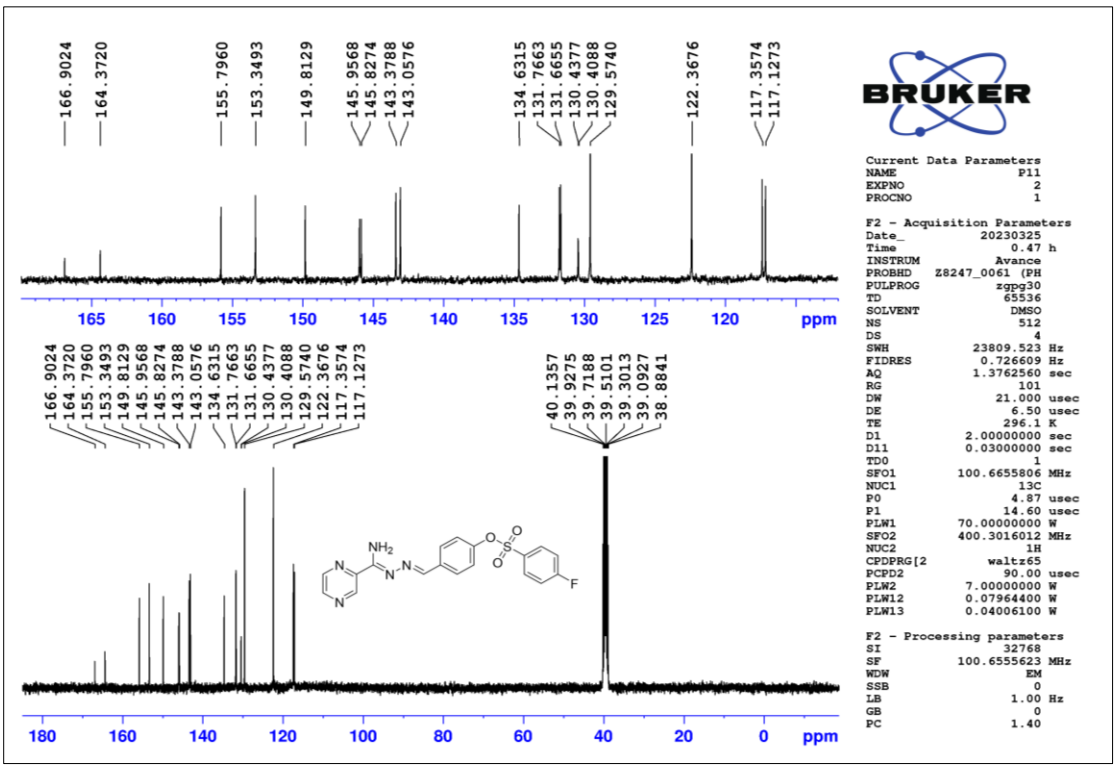

Figure 2.169 *^{13}C-NMR spectrum of compound* ***T49***

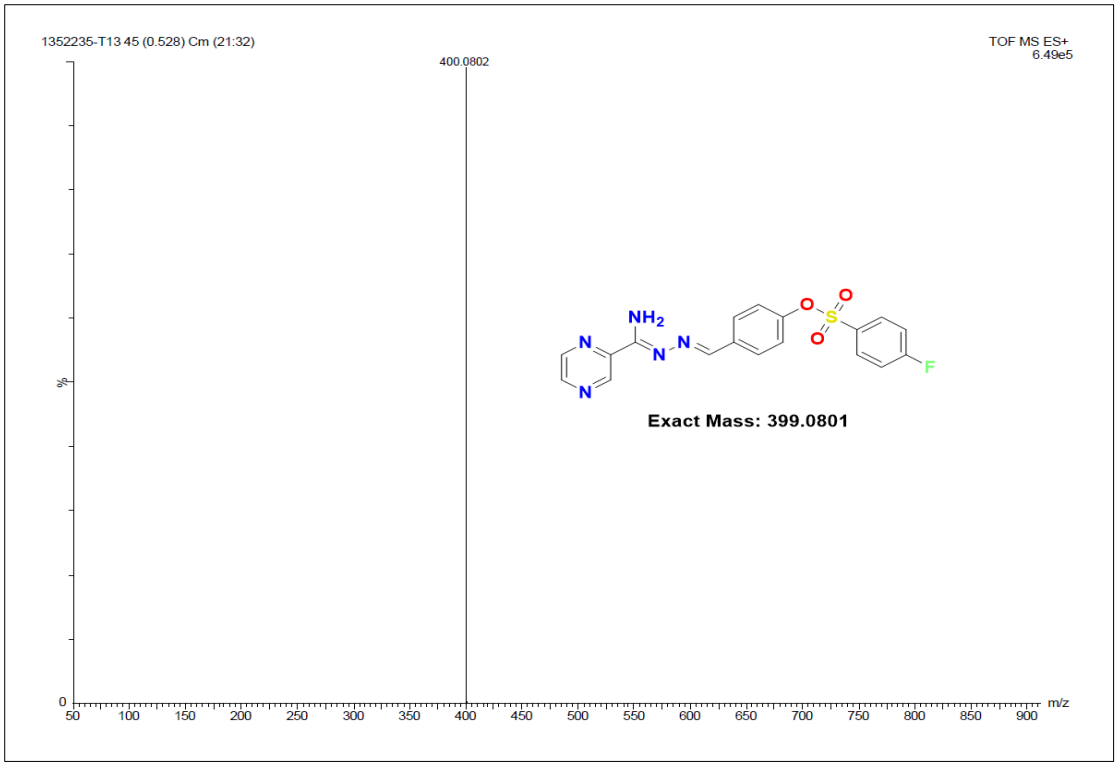

Figure 2.170 *HR-MS spectrum of compound* ***T49***

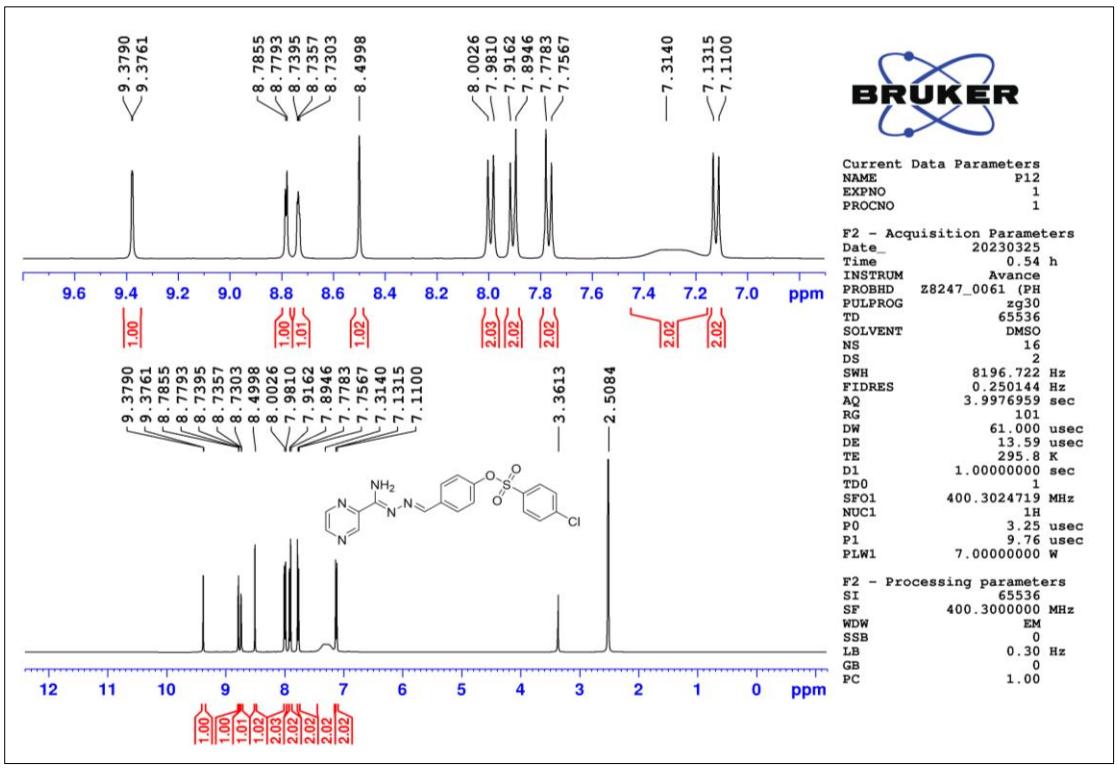

Figure 2.171 *[1]H-NMR spectrum of compound* ***T50***

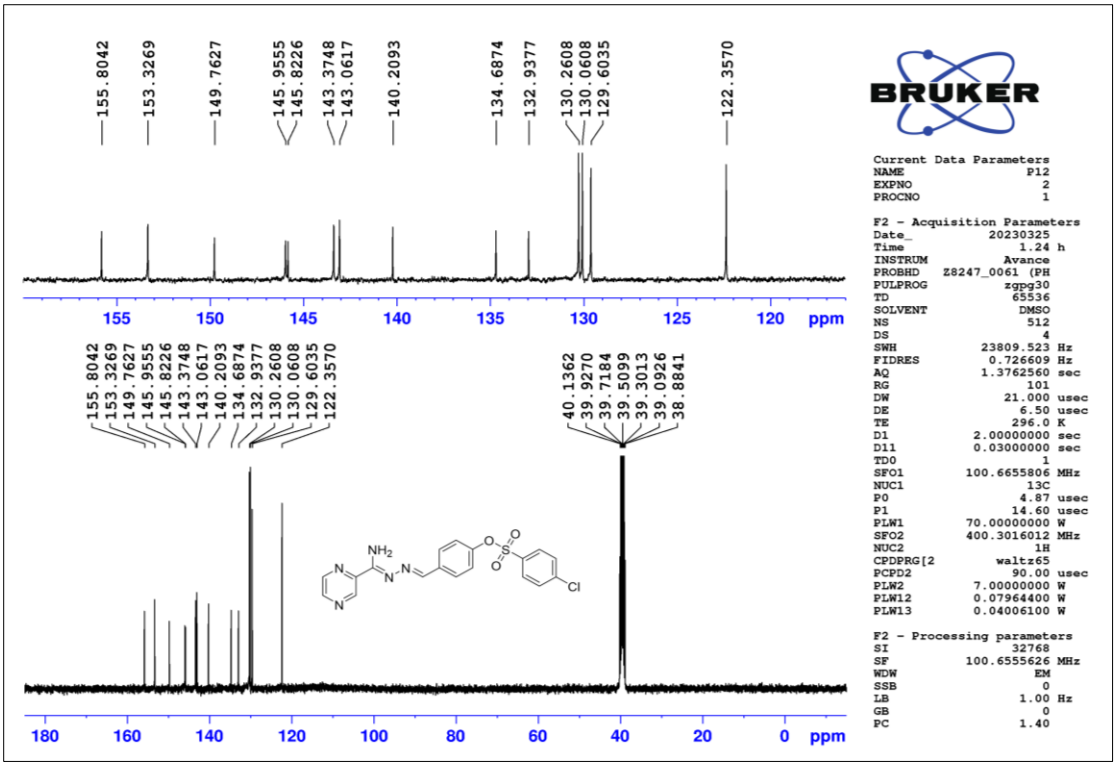

Figure 2.172 *^{13}C-NMR spectrum of compound* ***T50***

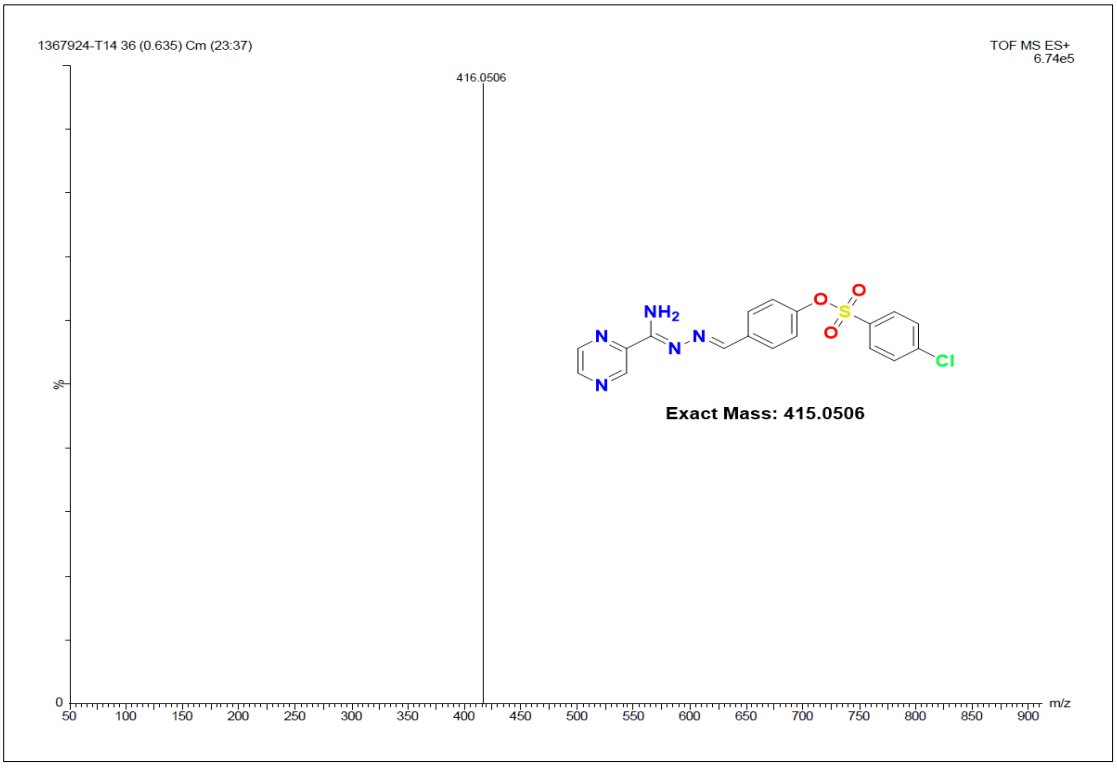

Figure 2.173 *HR-MS spectrum of compound* ***T50***

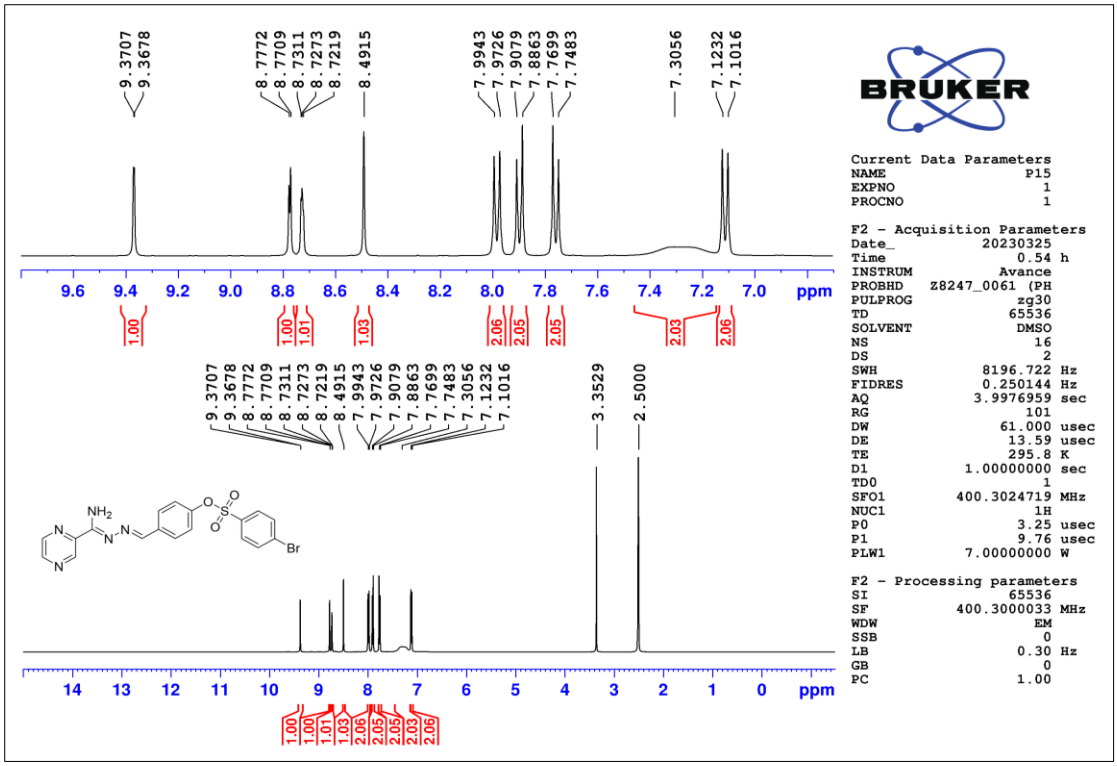

Figure 2.174 *^{1}H-NMR spectrum of compound* ***T51***

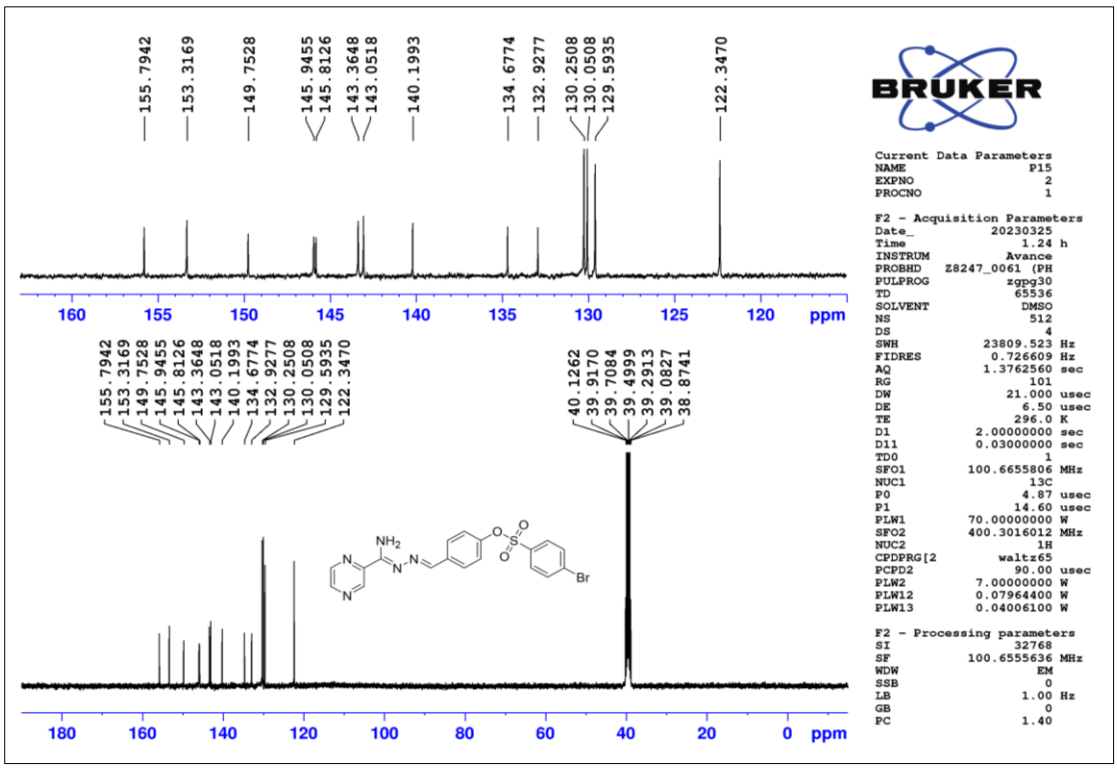

Figure 2.175 *^{13}C-NMR spectrum of compound* ***T51***

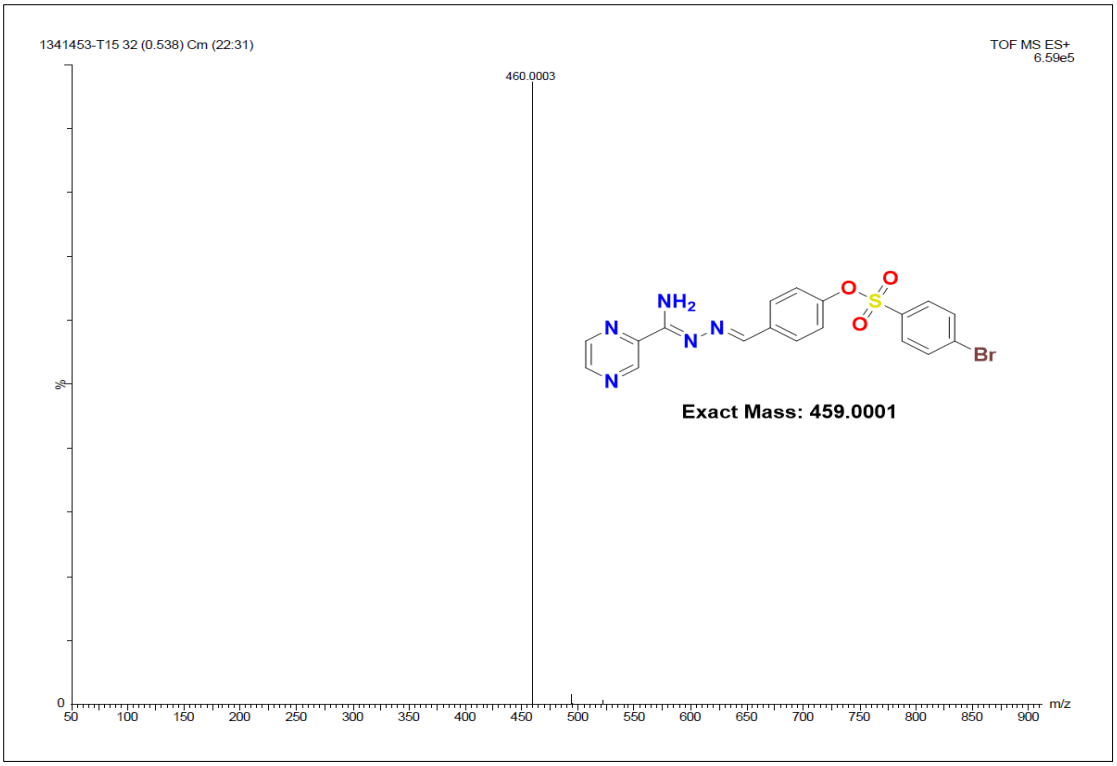

Figure 2.176 *HR-MS spectrum of compound* ***T51***

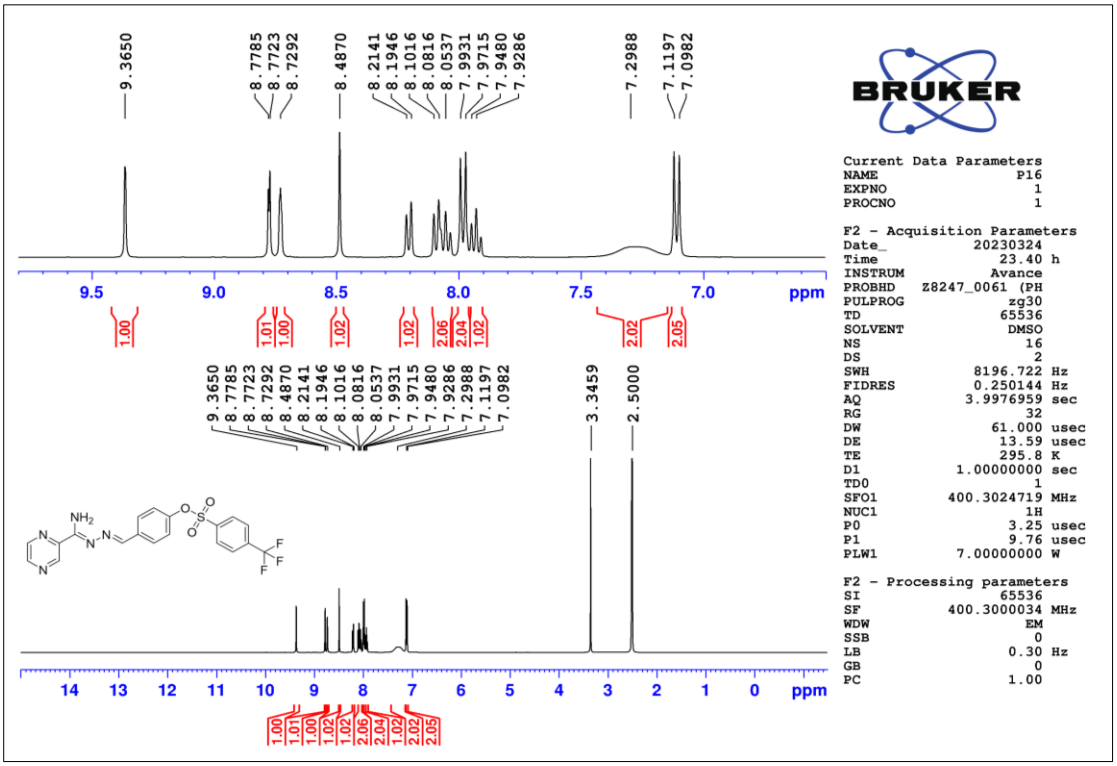

Figure 2.177 *^{1}H-NMR spectrum of compound* ***T52***

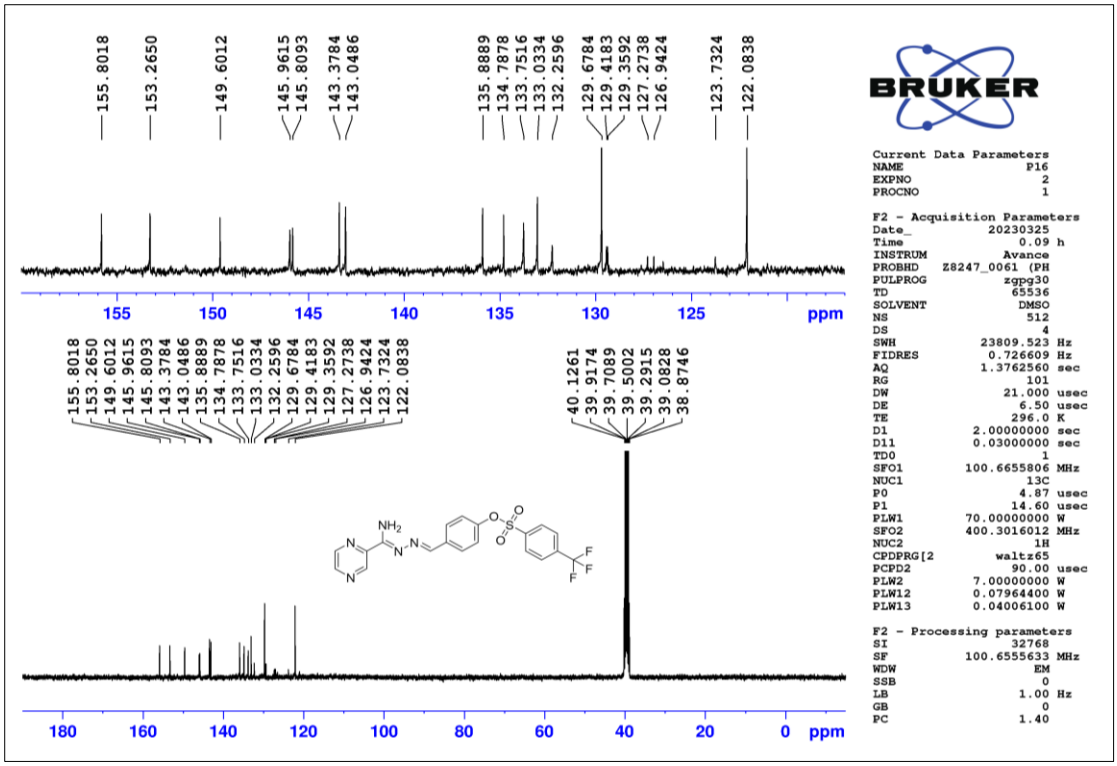

Figure 2.178 *^{13}C-NMR spectrum of compound* ***T52***

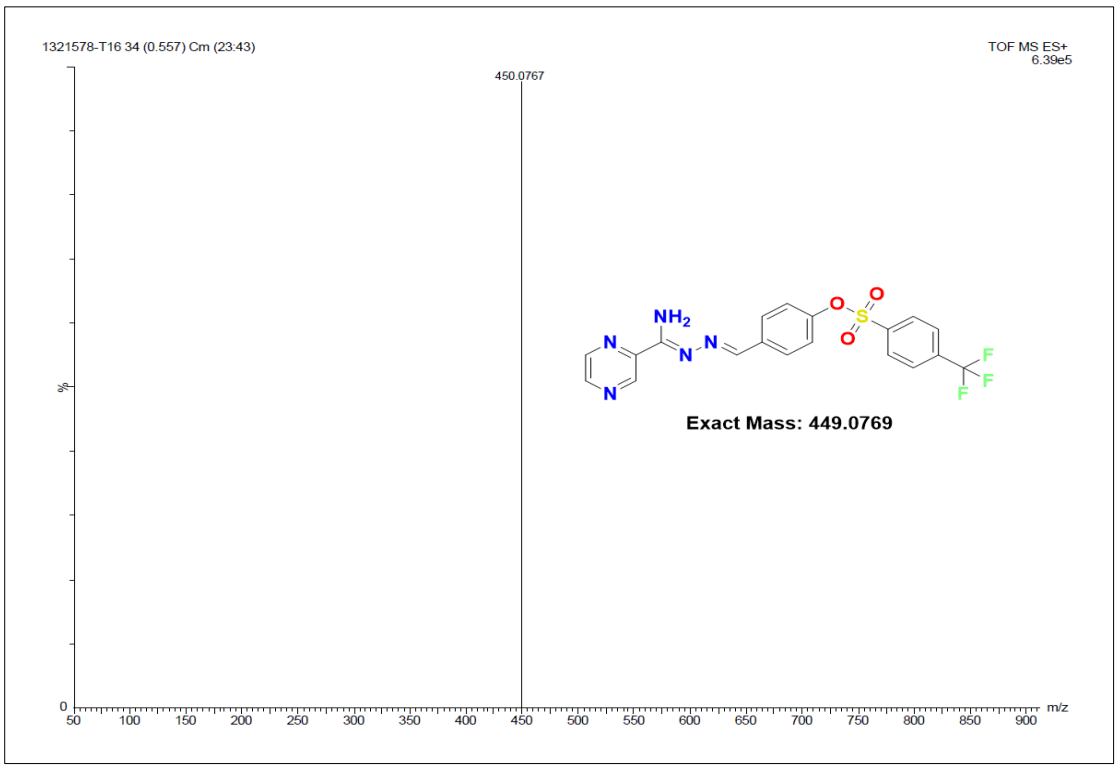

Figure 2.179 *HR-MS spectrum of compound* ***T52***

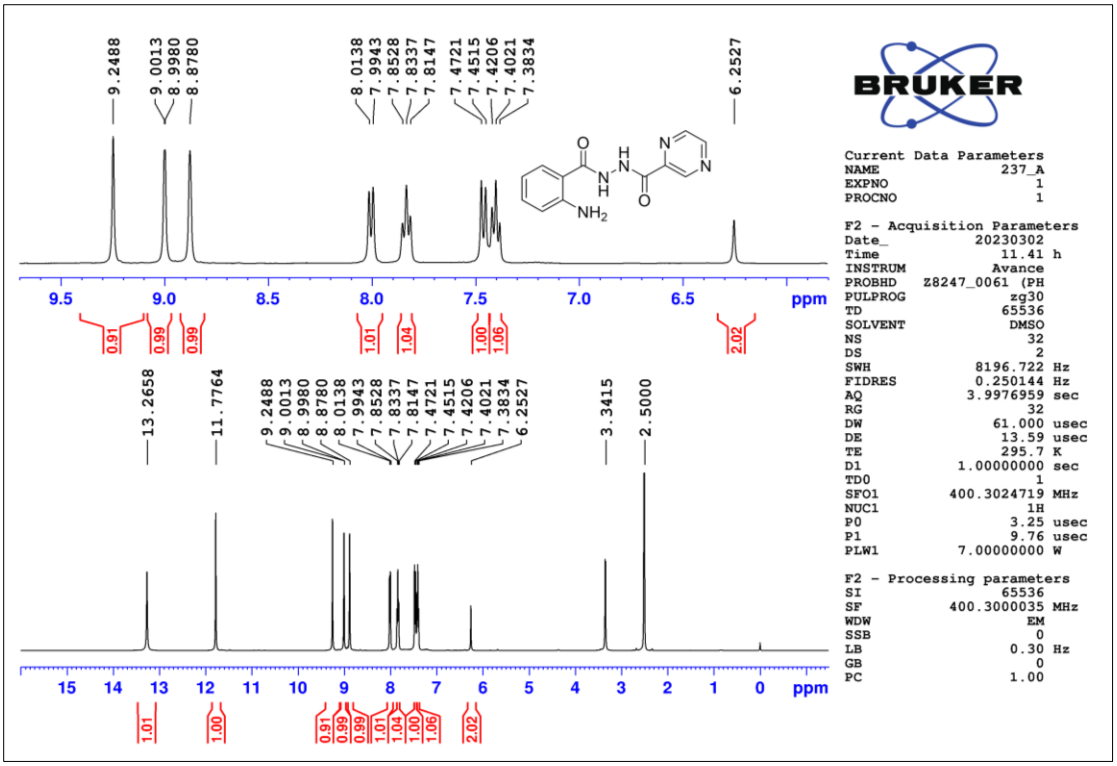

Figure 2.180 *[1]H-NMR spectrum of compound* ***T53***

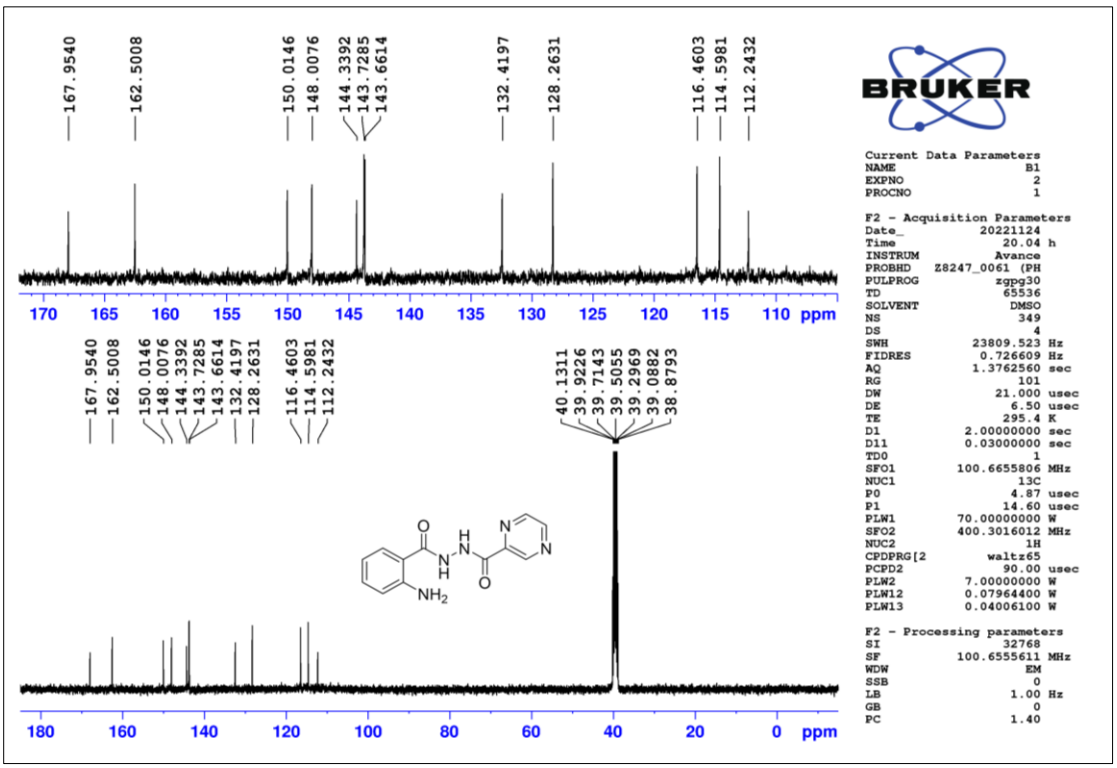

Figure 2.181 *[13]C-NMR spectrum of compound* ***T53***

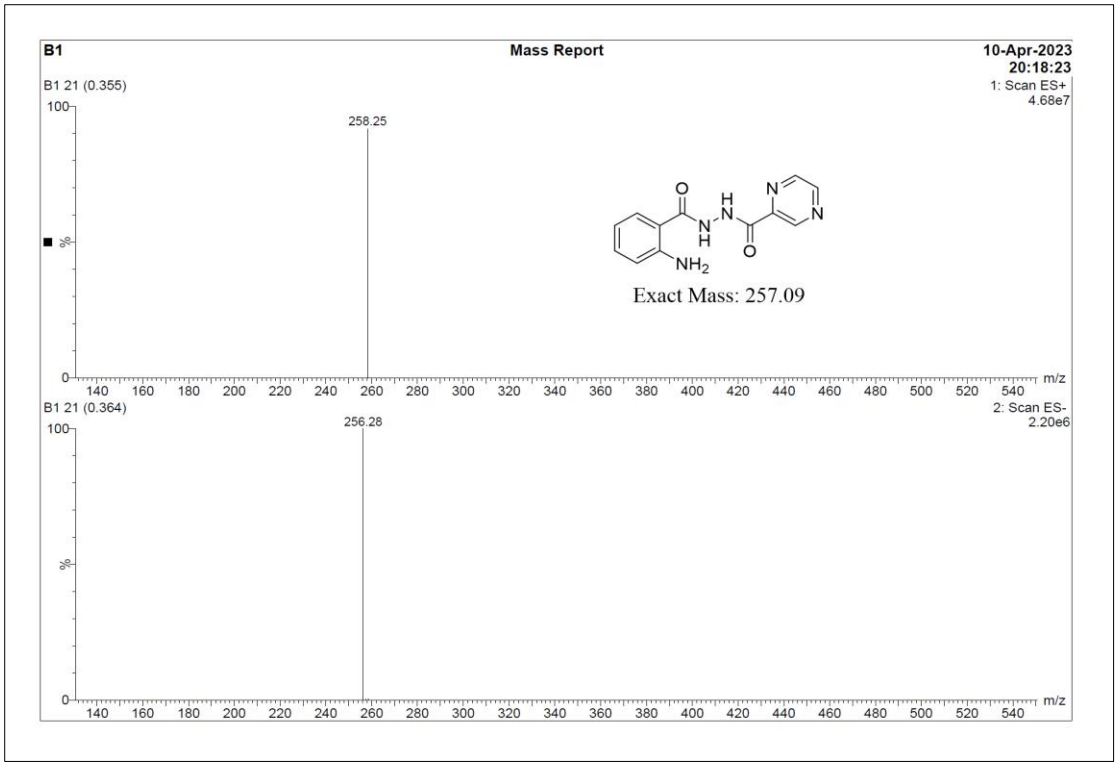

Figure 2.182 *ESI-MS spectrum of compound* ***T53***

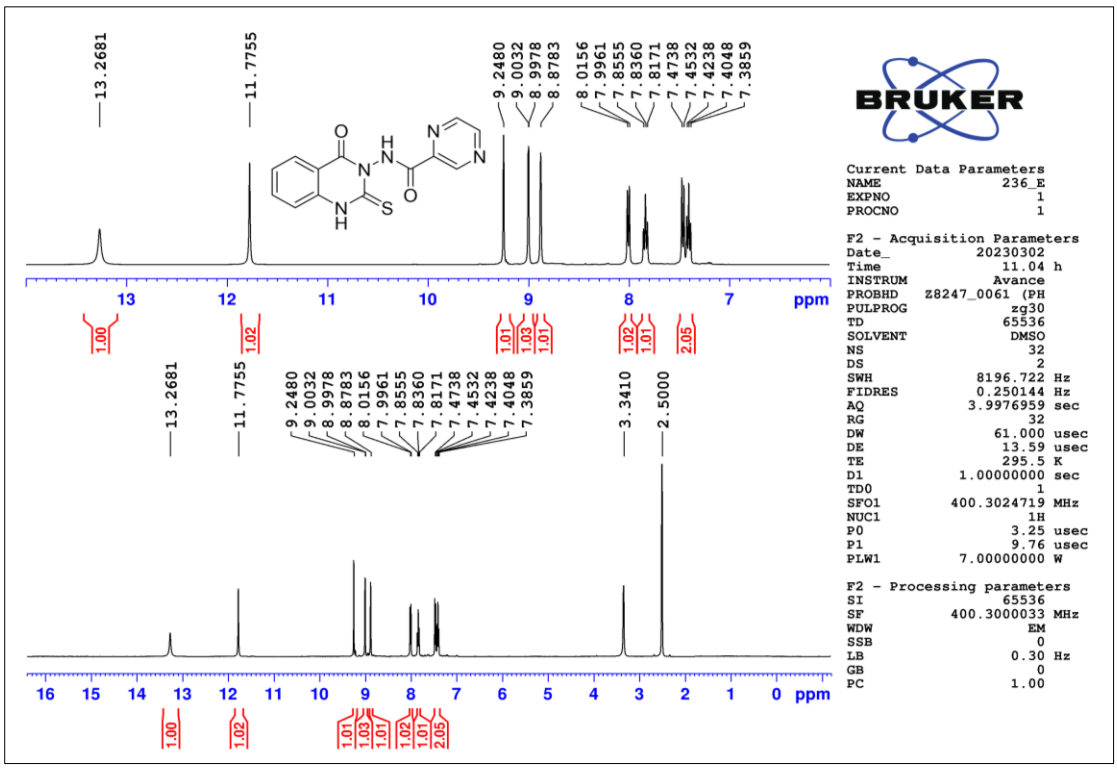

Figure 2.183 *[1]H-NMR spectrum of compound* ***T54***

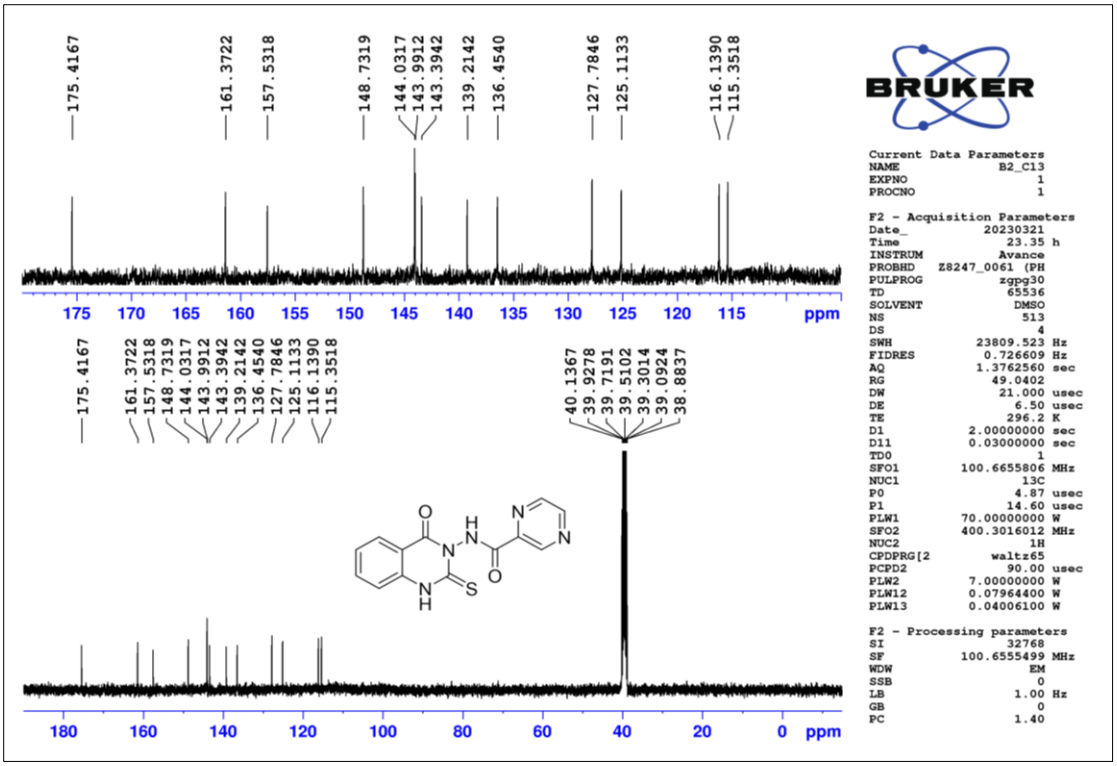

Figure 2.184 *^{13}C-NMR spectrum of compound* ***T54***

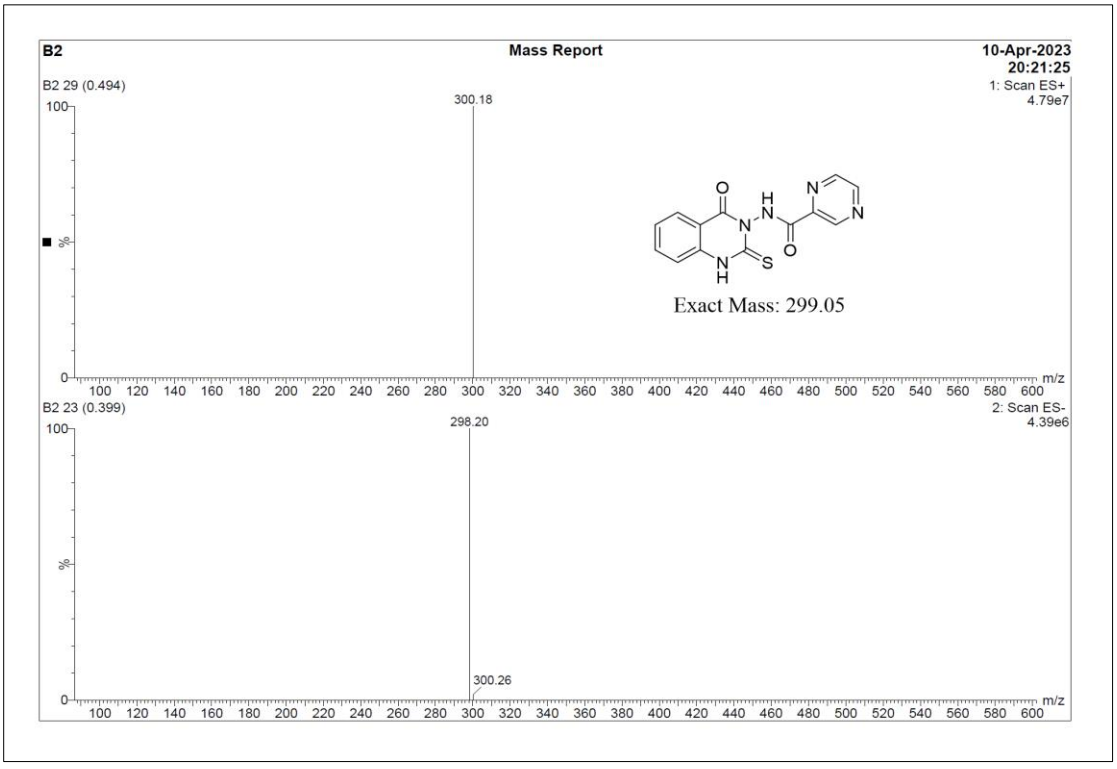

Figure 2.185 *ESI-MS spectrum of compound* ***T54***

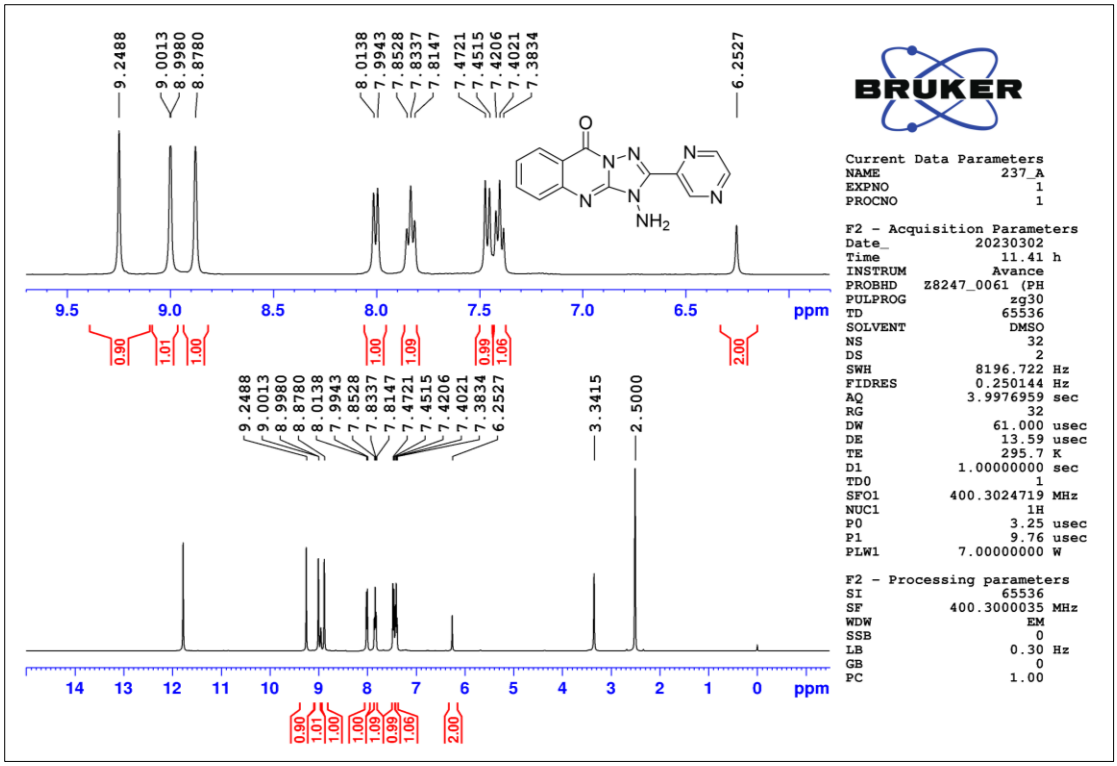

Figure 2.186 *^{1}H-NMR spectrum of compound* ***T55***

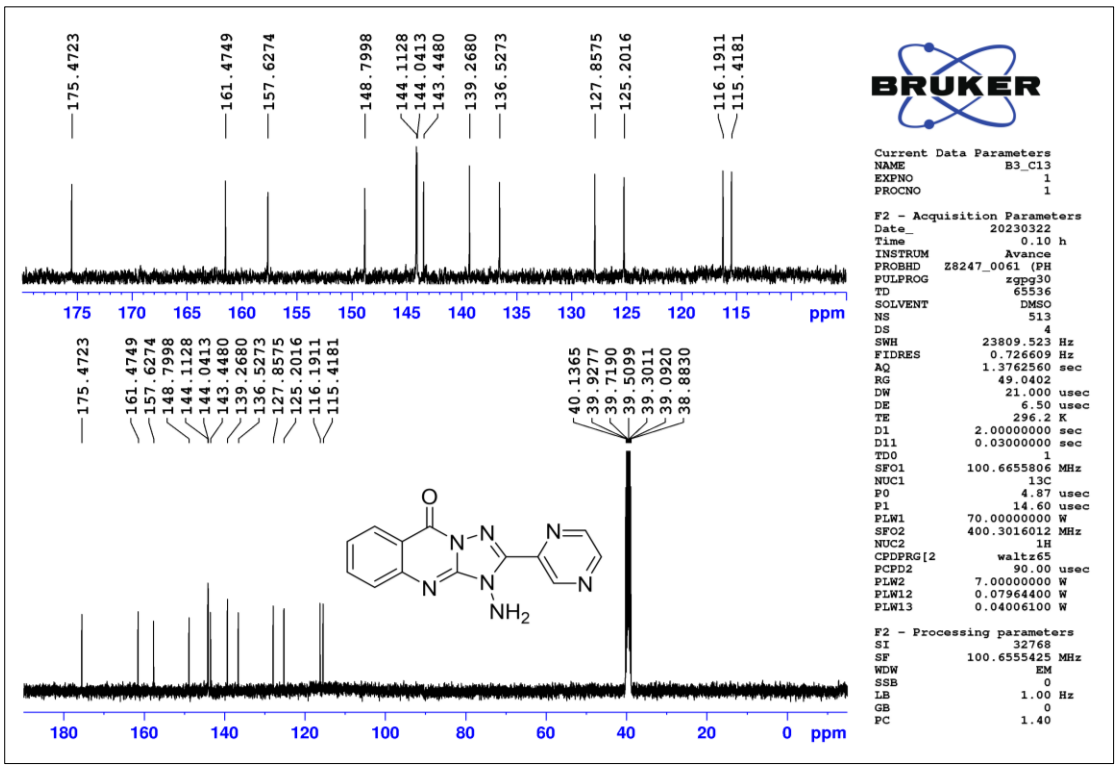

Figure 2.187 *^{13}C-NMR spectrum of compound* ***T55***

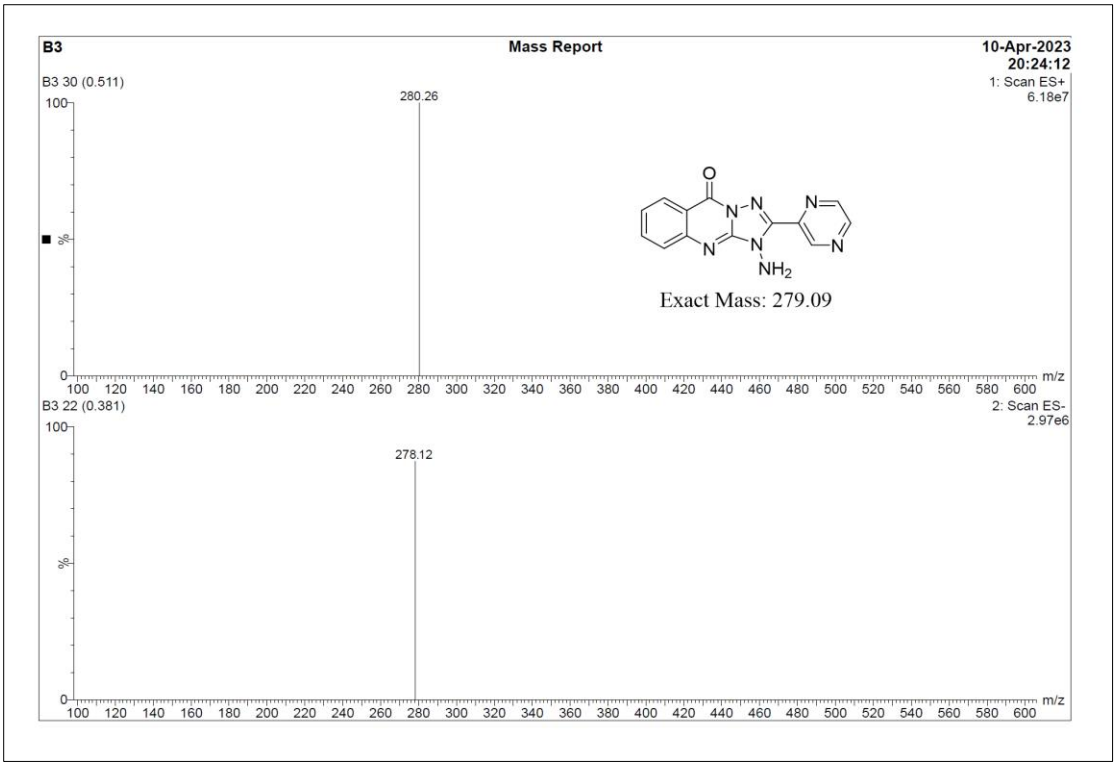

Figure 2.188 *ESI-MS spectrum of compound* ***T55***

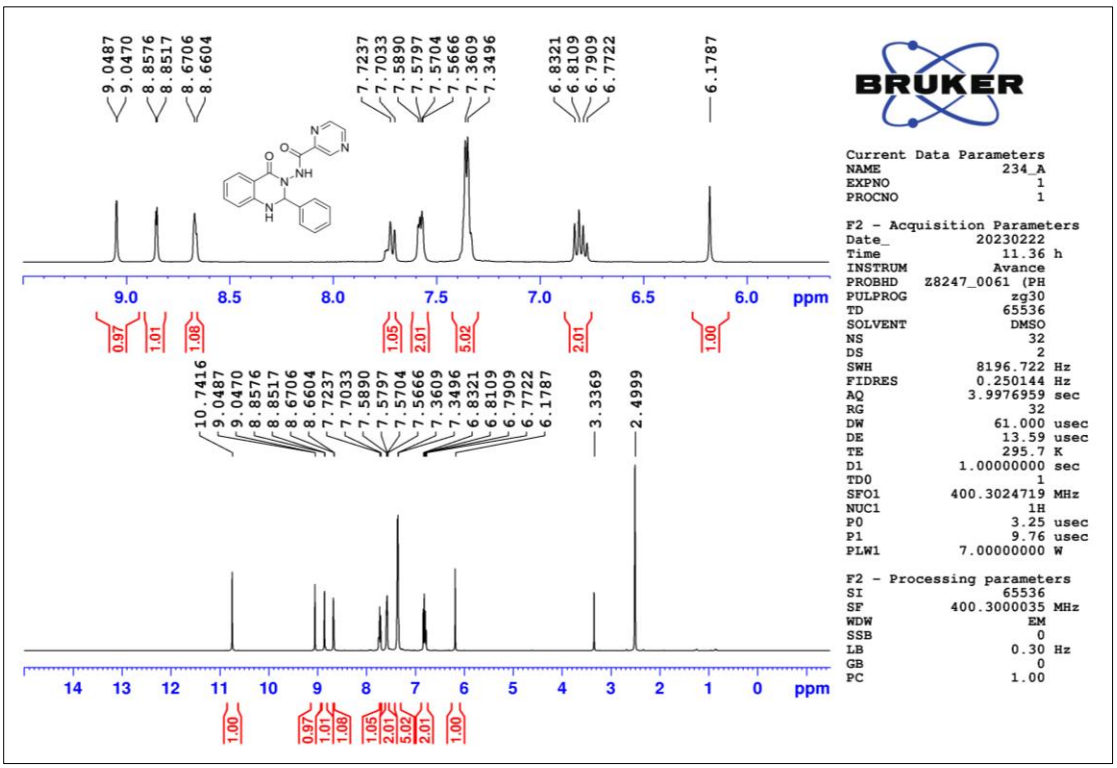

Figure 2.189 *^{1}H-NMR spectrum of compound* ***T56***

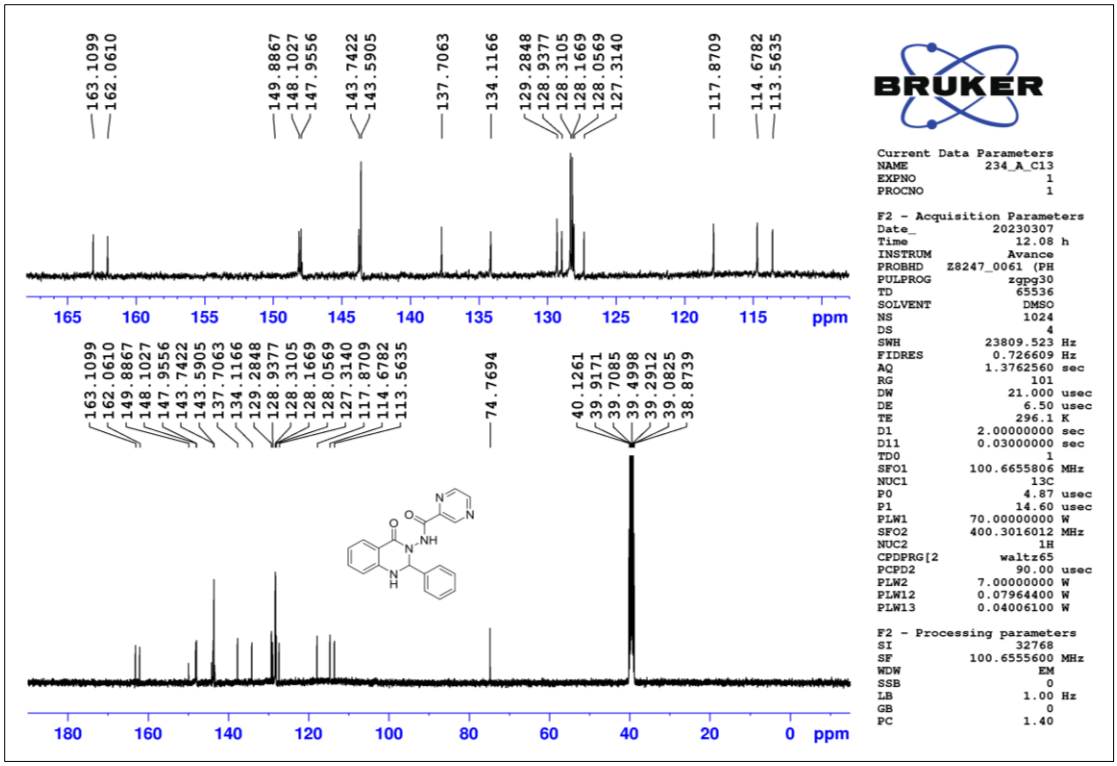

Figure 2.190 *^{13}C-NMR spectrum of compound* ***T56***

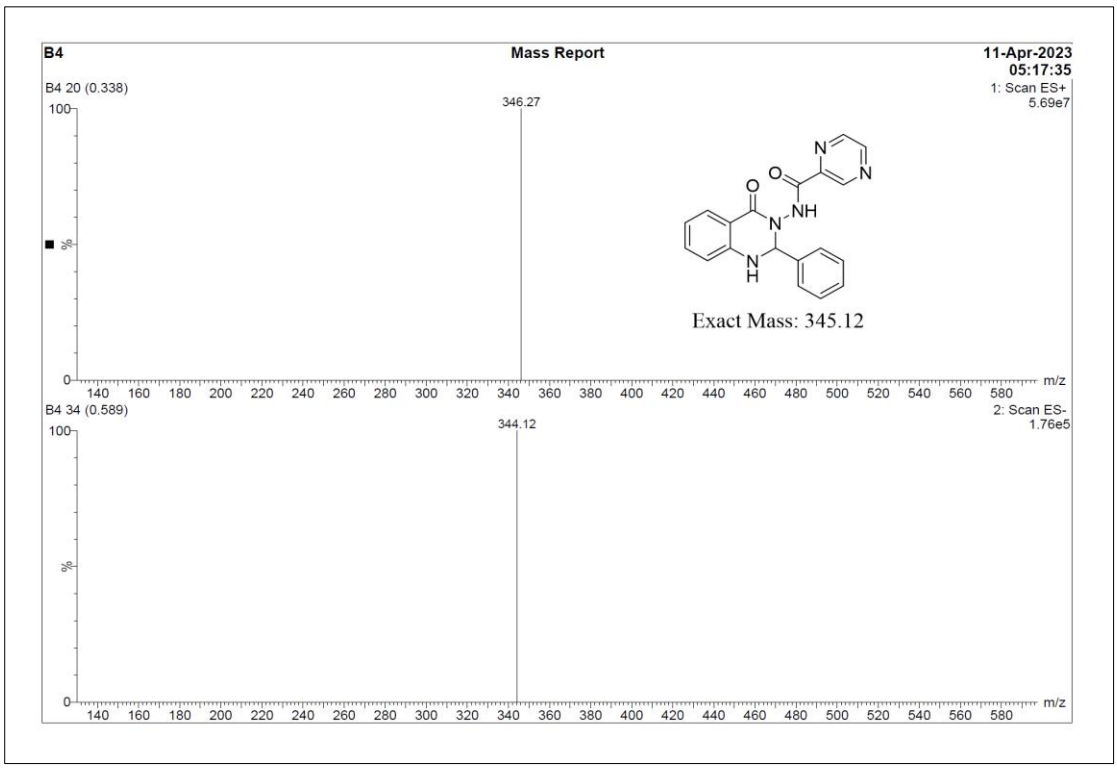

Figure 2.191 *ESI-MS spectrum of compound* ***T56***

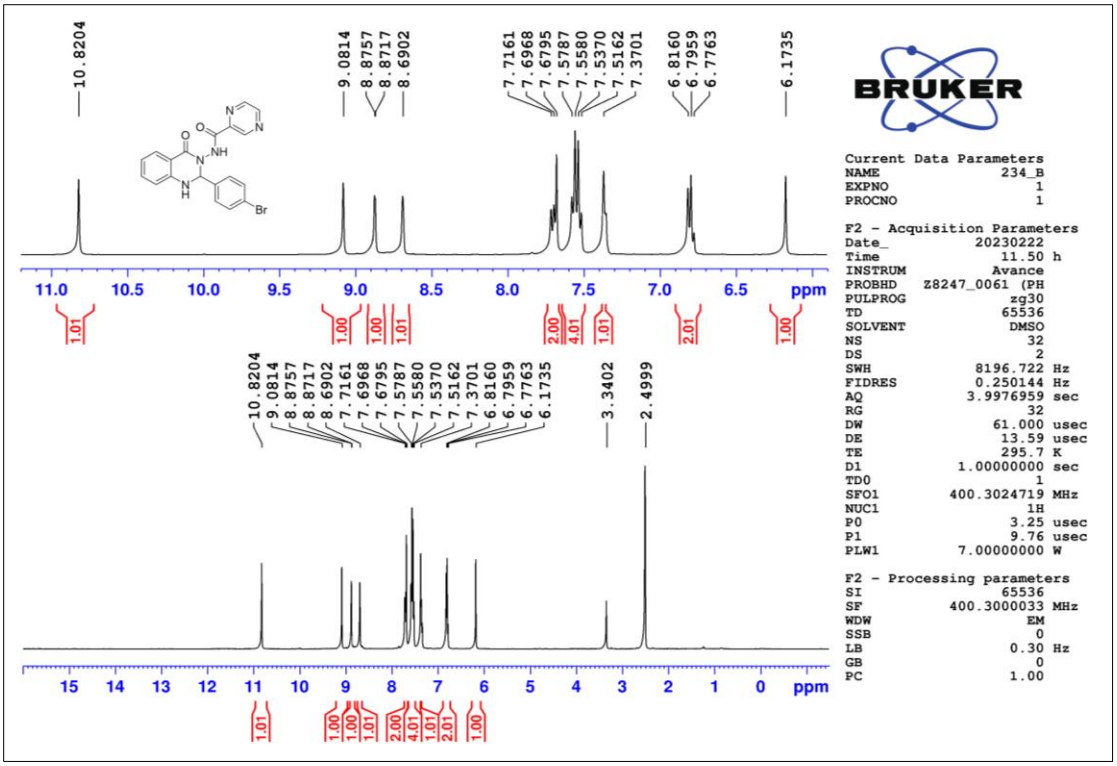

Figure 2.192 *^{1}H-NMR spectrum of compound* ***T57***

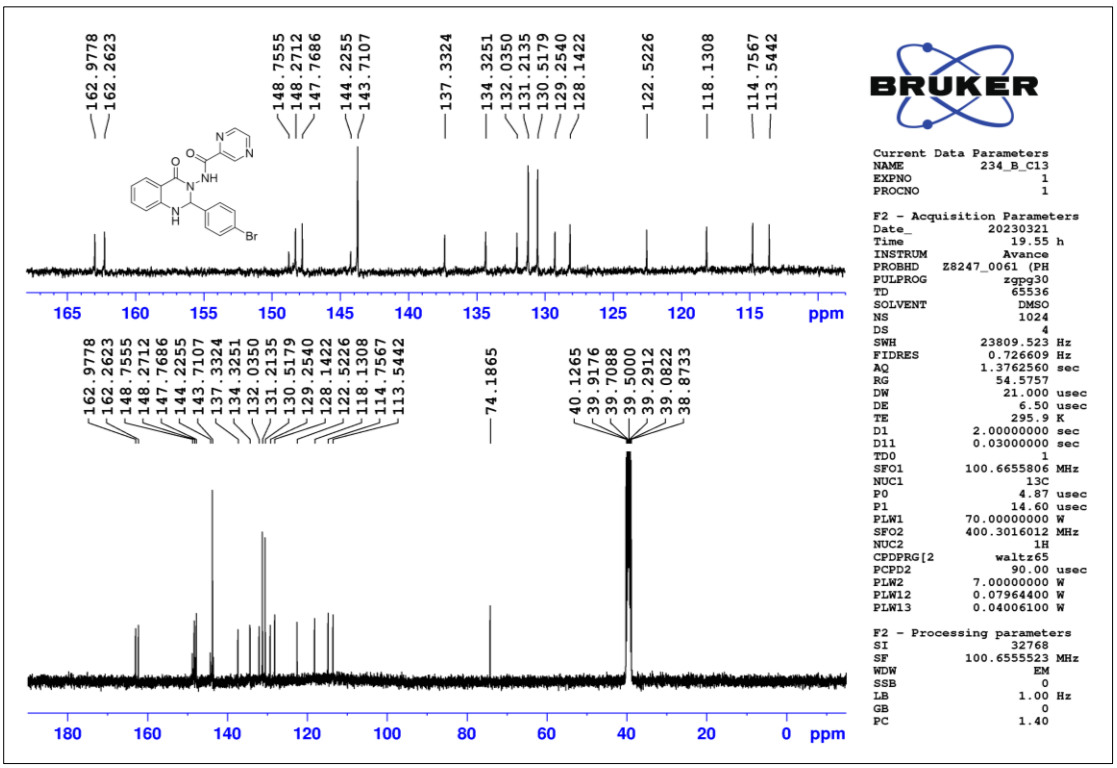

Figure 2.193 *^{13}C-NMR spectrum of compound* ***T57***

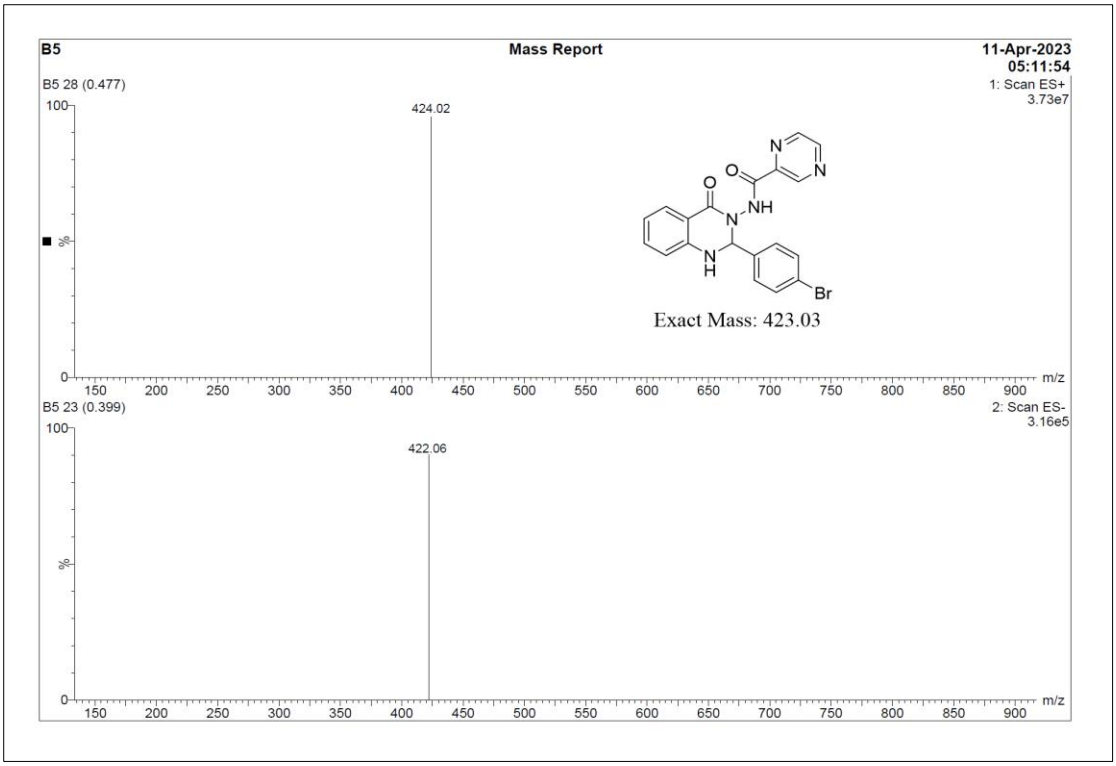

Figure 2.194 *ESI-MS spectrum of compound* ***T57***

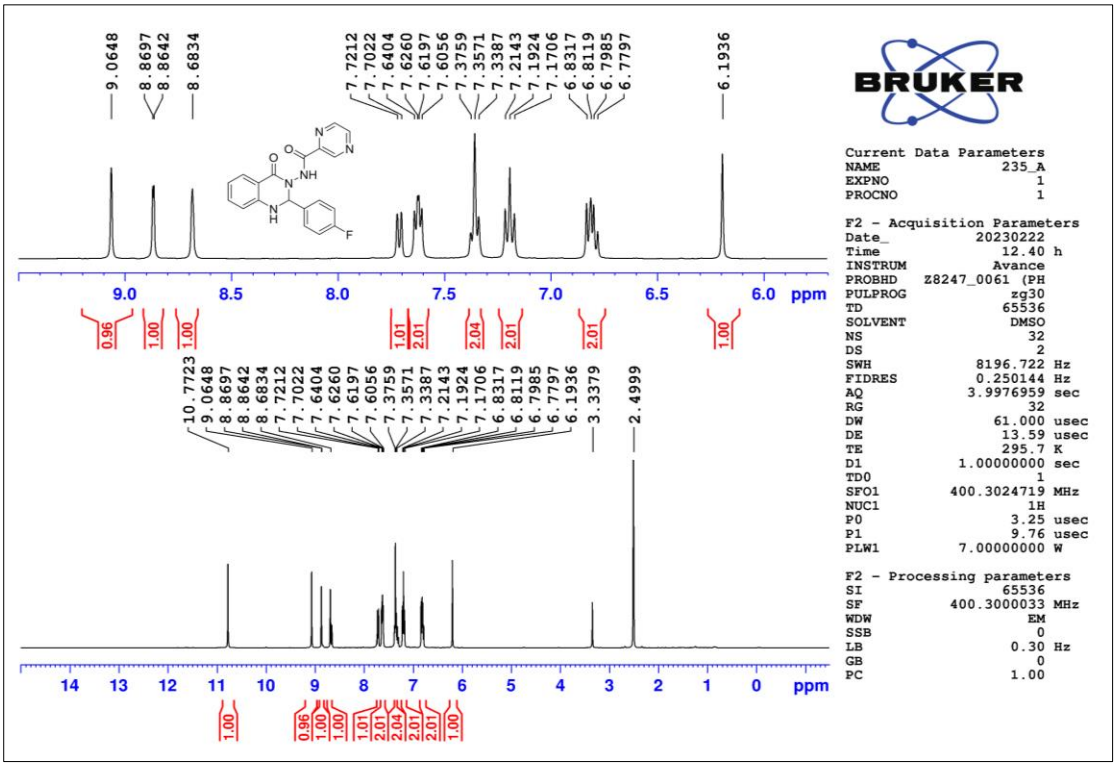

Figure 2.195 *[1]H-NMR spectrum of compound* ***T58***

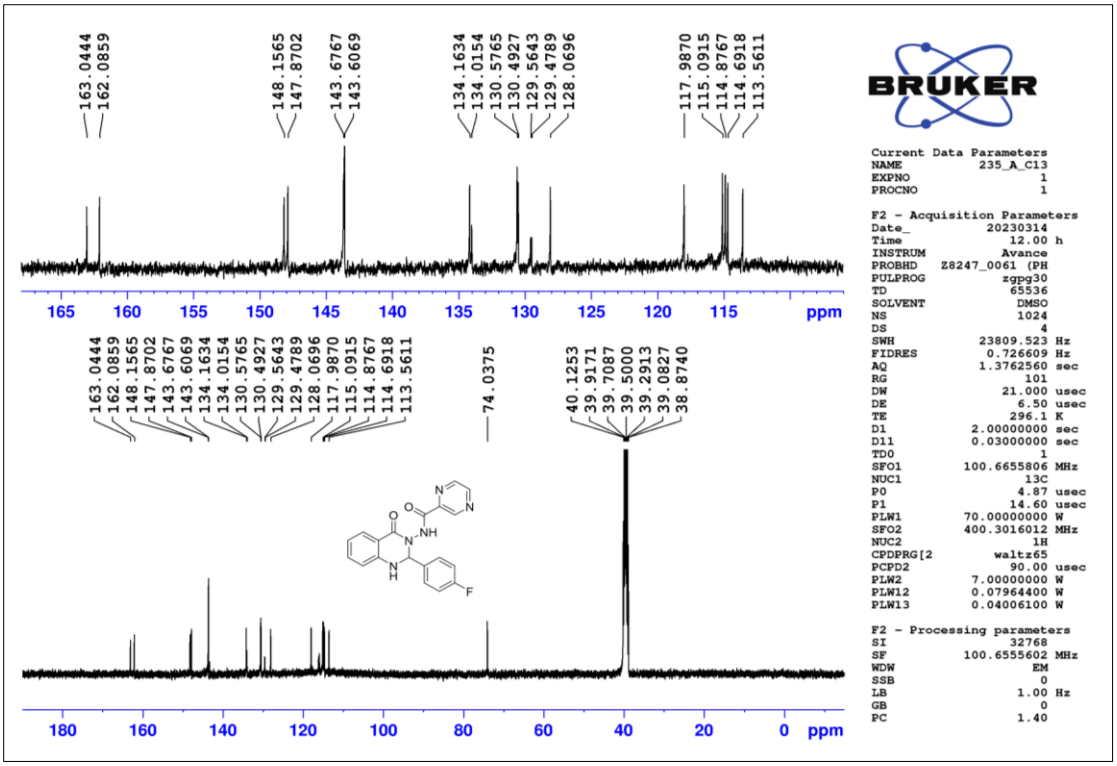

Figure 2.196 *^{13}C-NMR spectrum of compound* ***T58***

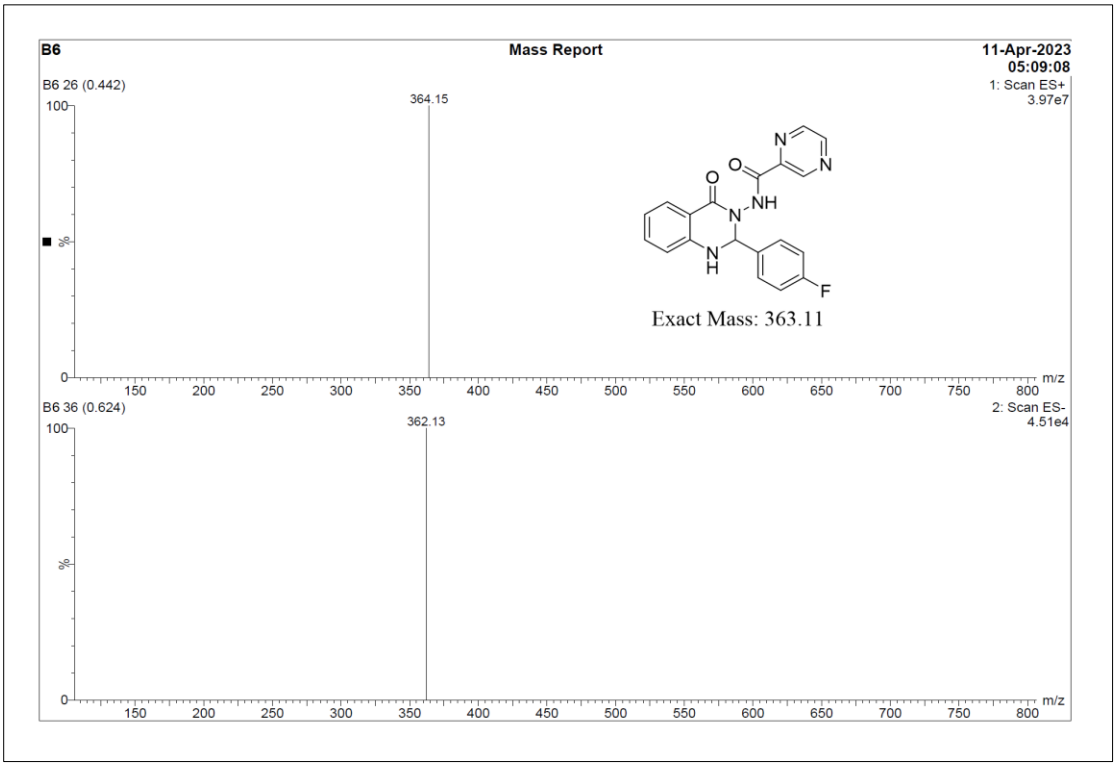

Figure 2.197 *ESI-MS spectrum of compound* ***T58***

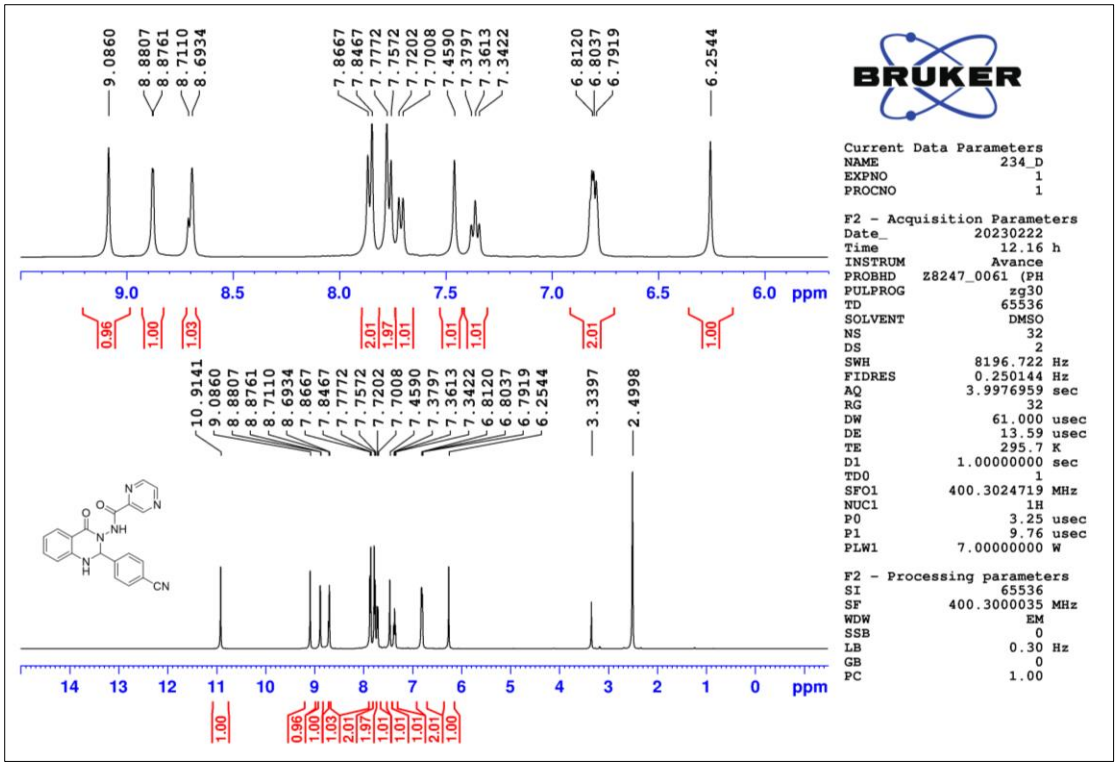

Figure 2.198 *[1]H-NMR spectrum of compound* ***T59***

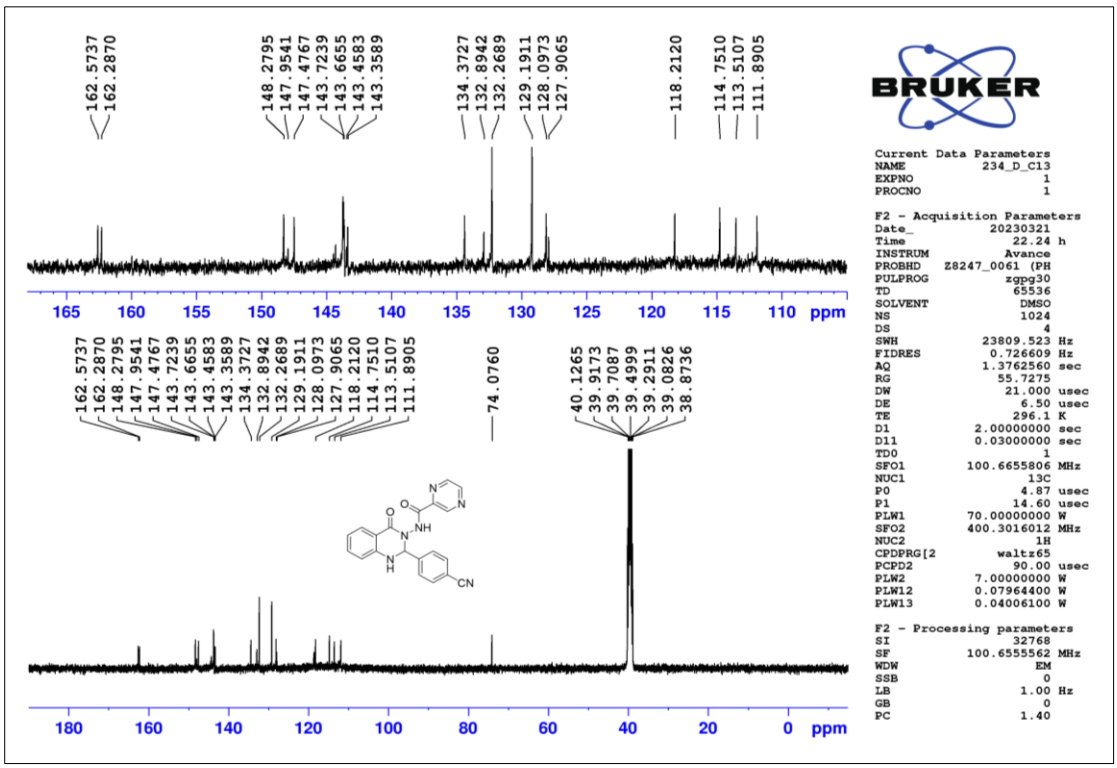

Figure 2.199 *[13]C-NMR spectrum of compound* ***T59***

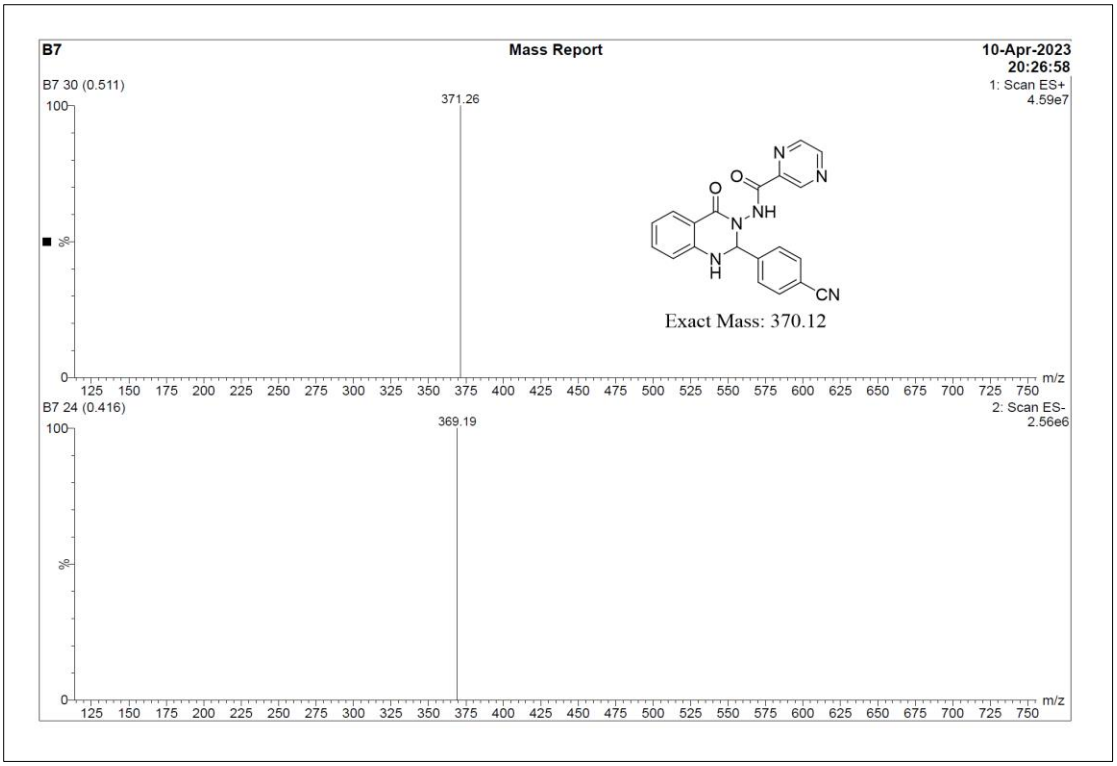

Figure 2.200 *ESI-MS spectrum of compound* ***T59***

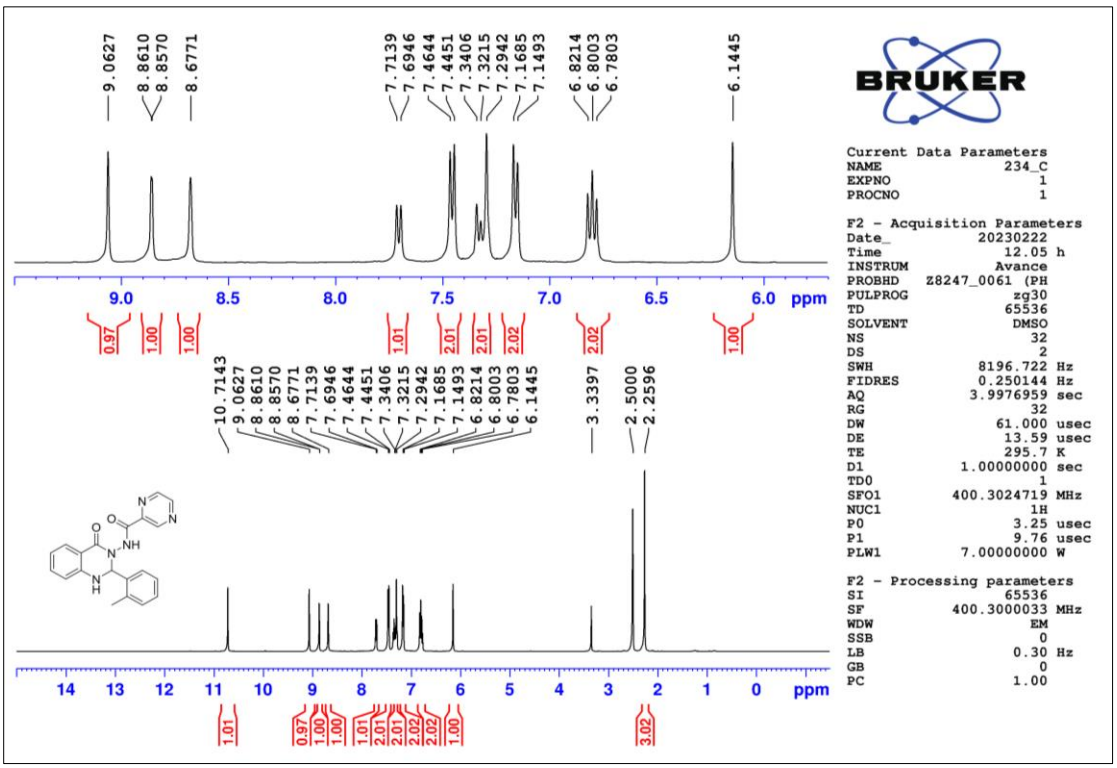

Figure 2.201 *^{1}H-NMR spectrum of compound* ***T61***

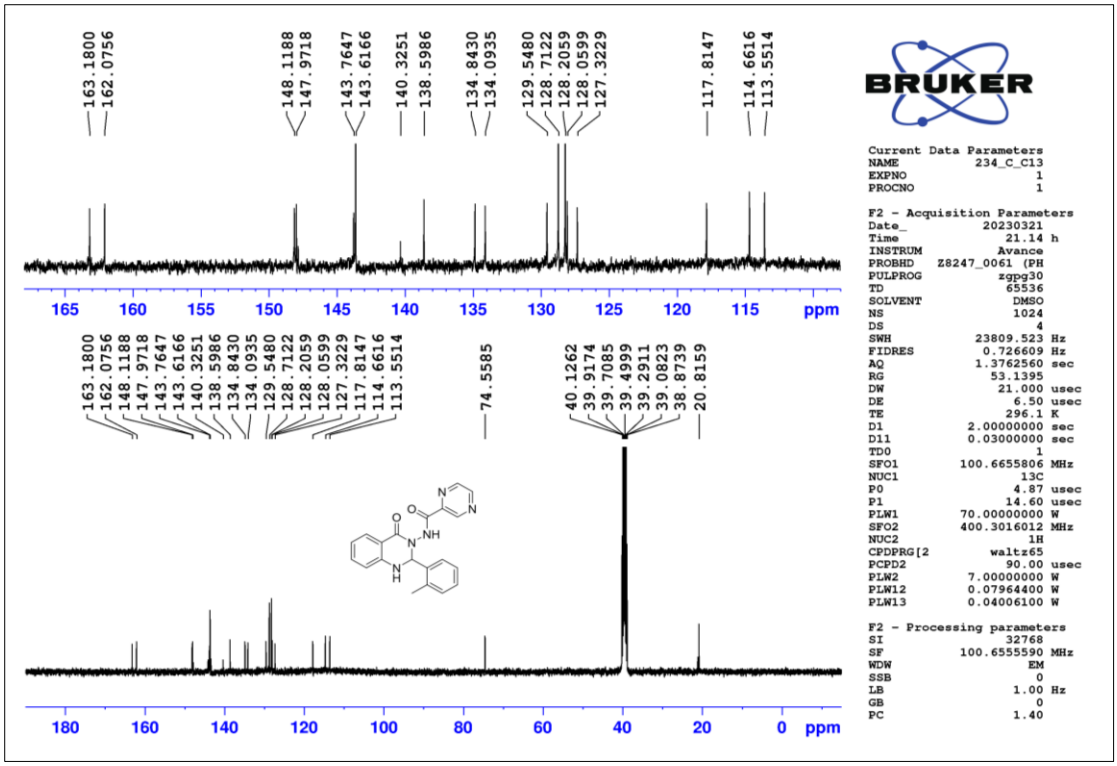

Figure 2.202 *^{13}C-NMR spectrum of compound* ***T61***

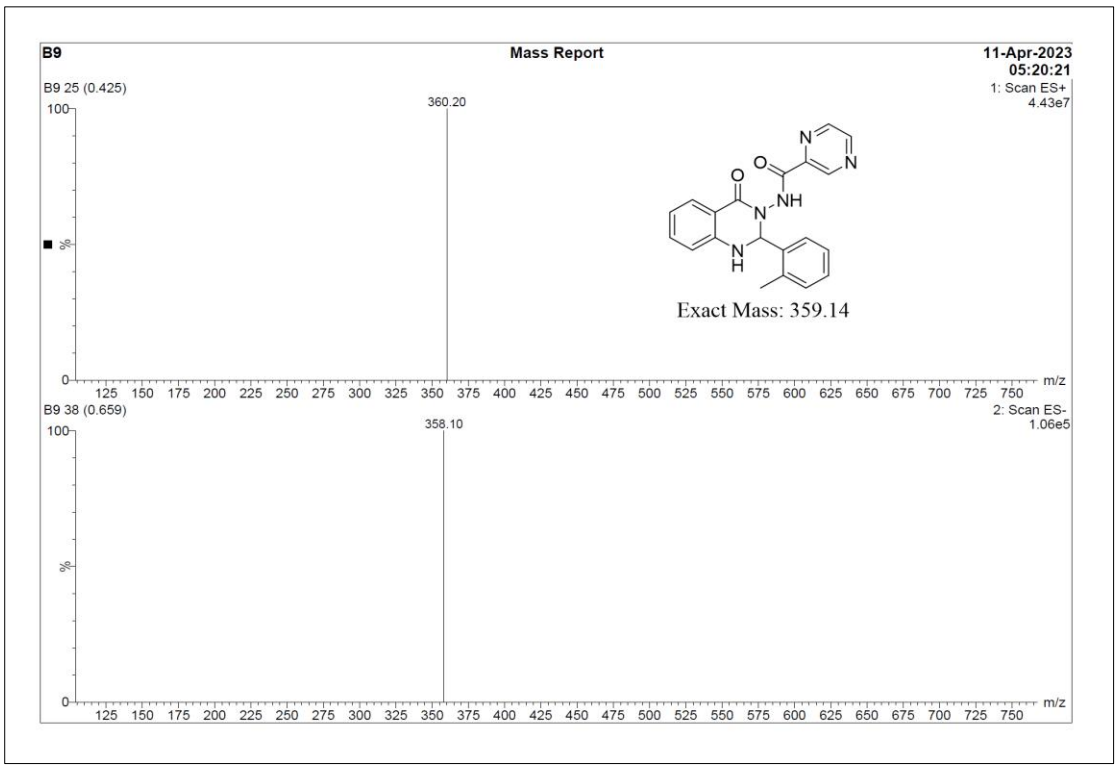

Figure 2.203 *ESI-MS spectrum of compound* ***T61***

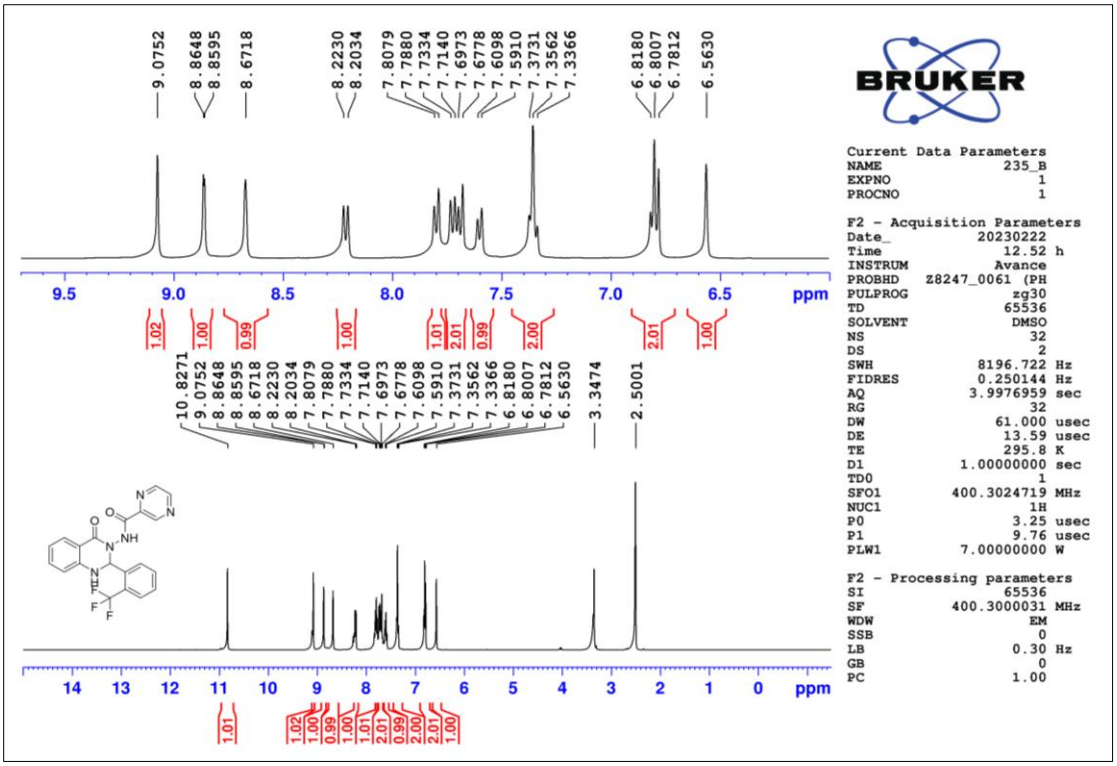

Figure 2.204 *^{1}H-NMR spectrum of compound* ***T62***

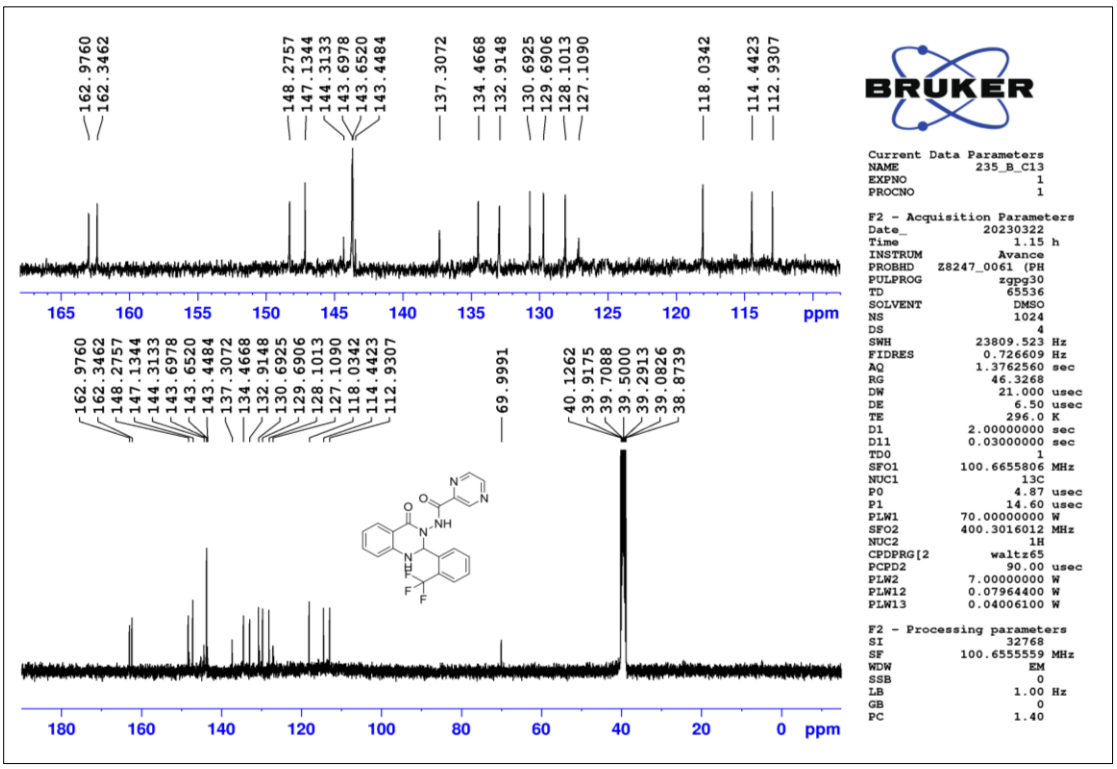

Figure 2.205 *^{13}C-NMR spectrum of compound* ***T62***

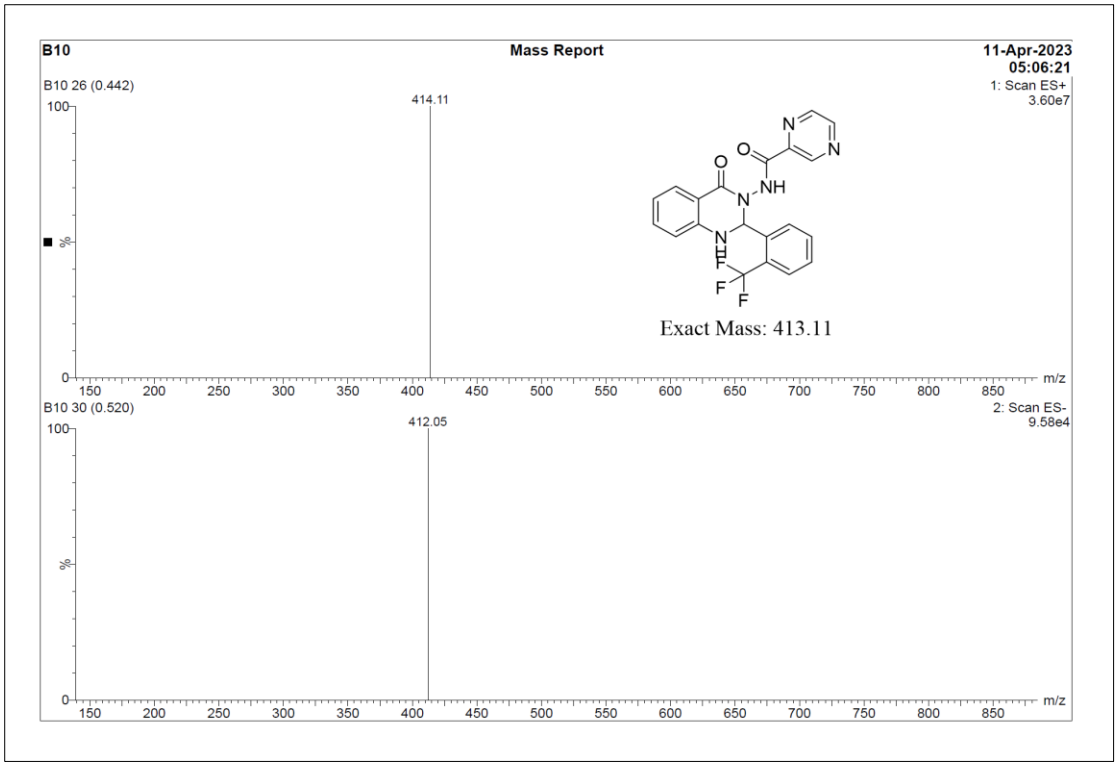

Figure 2.206 *ESI-MS spectrum of compound* ***T62***

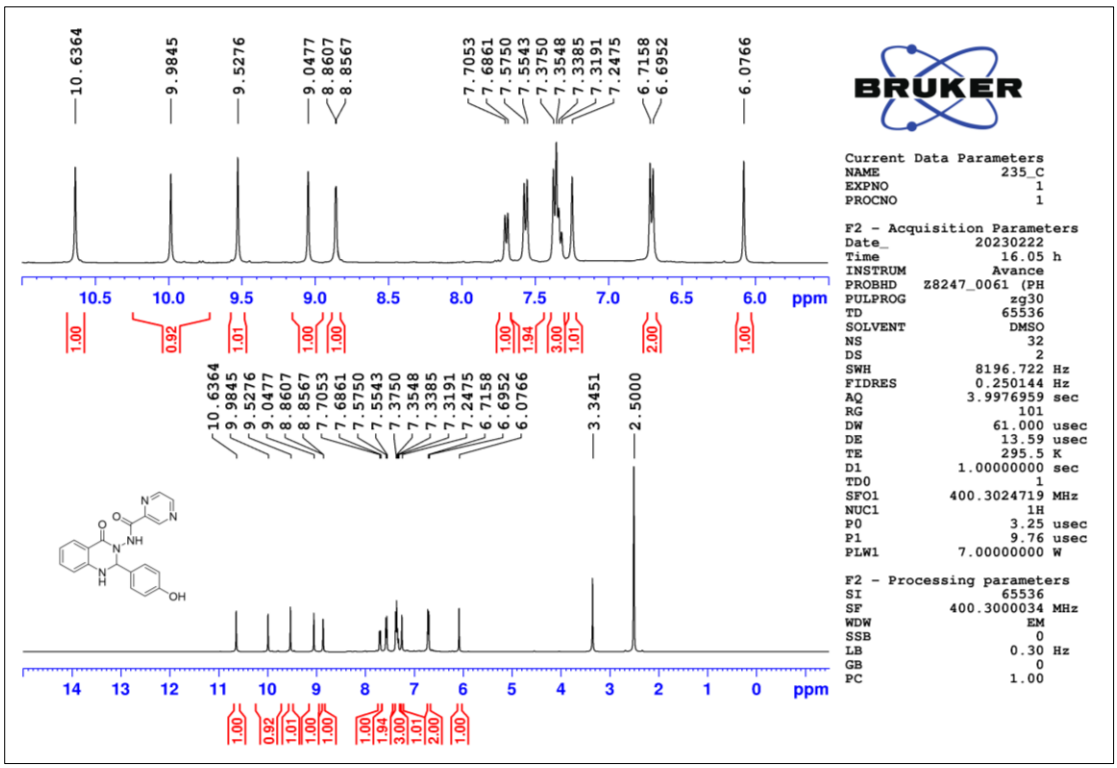

Figure 2.207 *^{1}H-NMR spectrum of compound* ***T63***

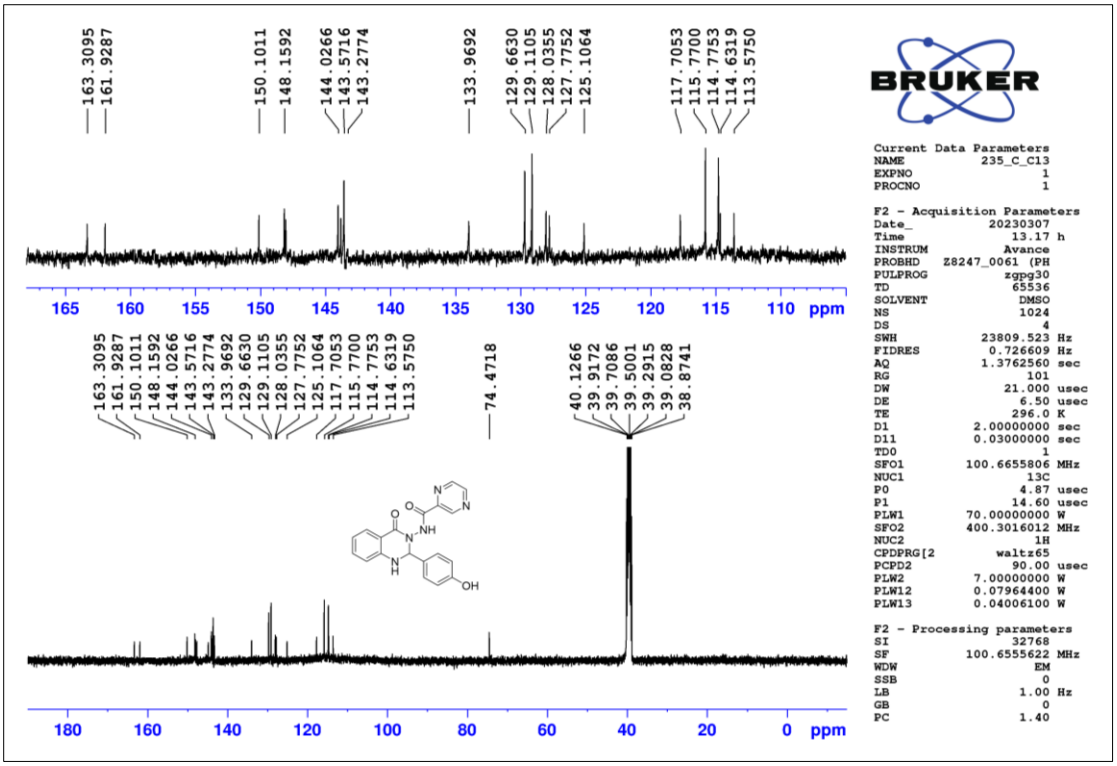

Figure 2.208 *^{13}C-NMR spectrum of compound* ***T63***

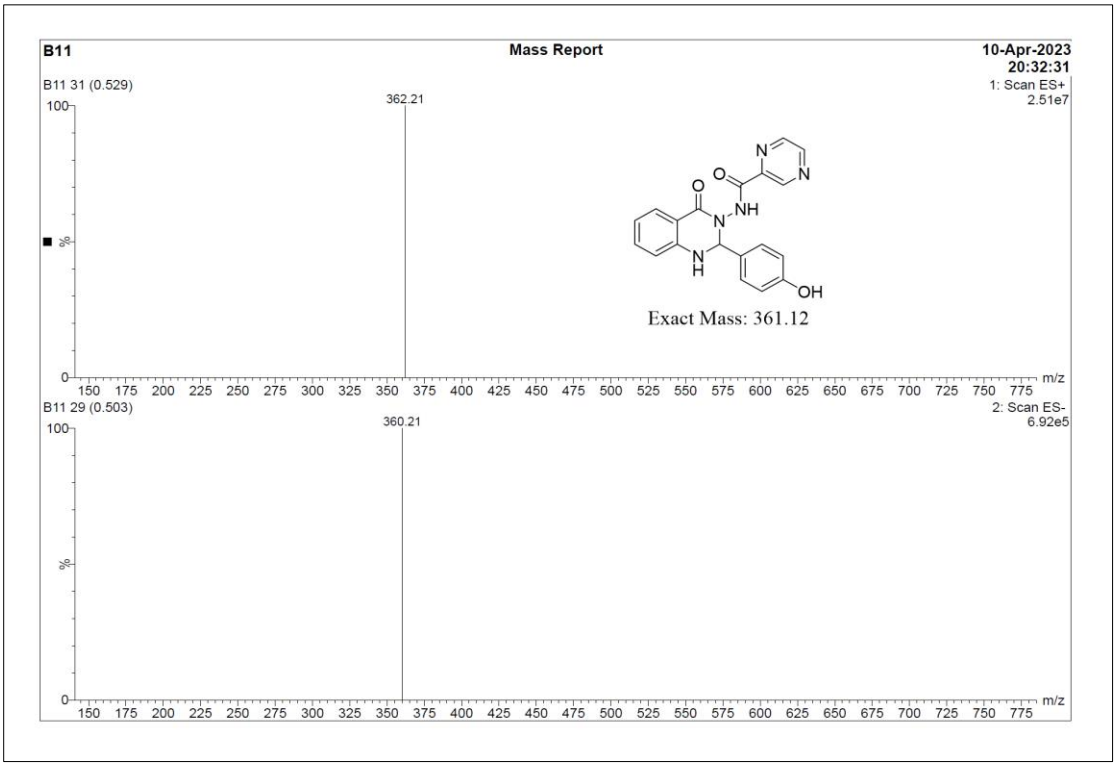

Figure 2.209 *ESI-MS spectrum of compound* ***T63***

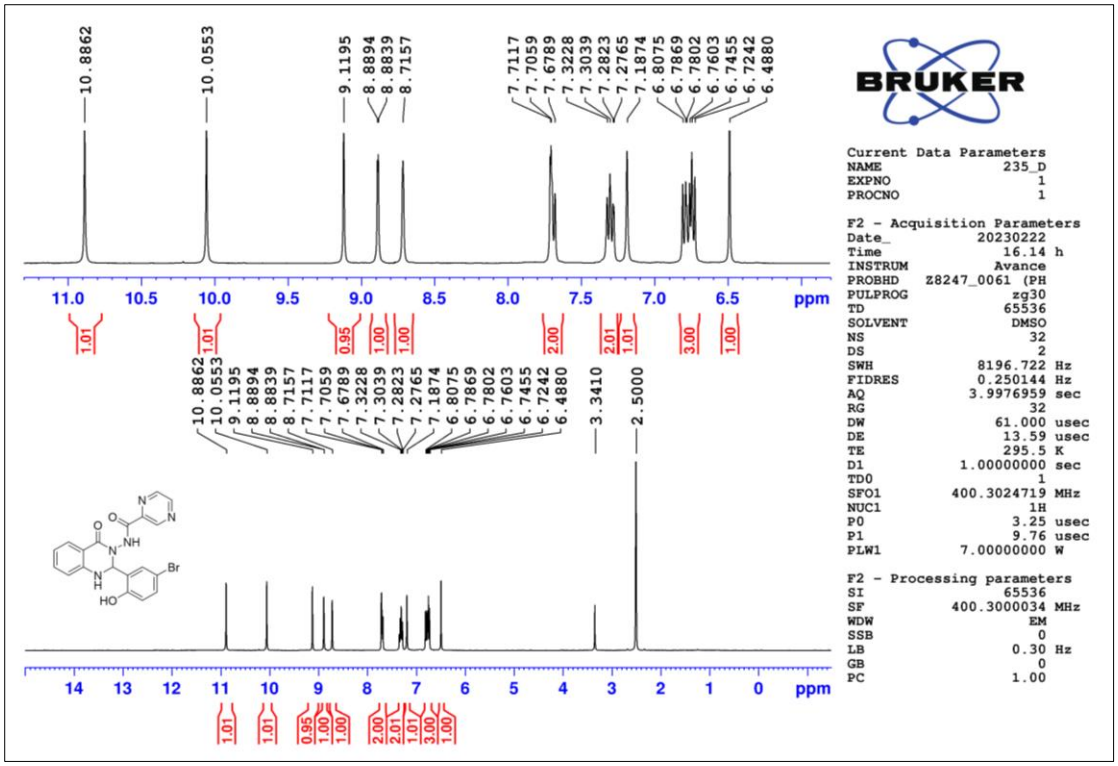

Figure 2.210 *^{1}H-NMR spectrum of compound* ***T64***

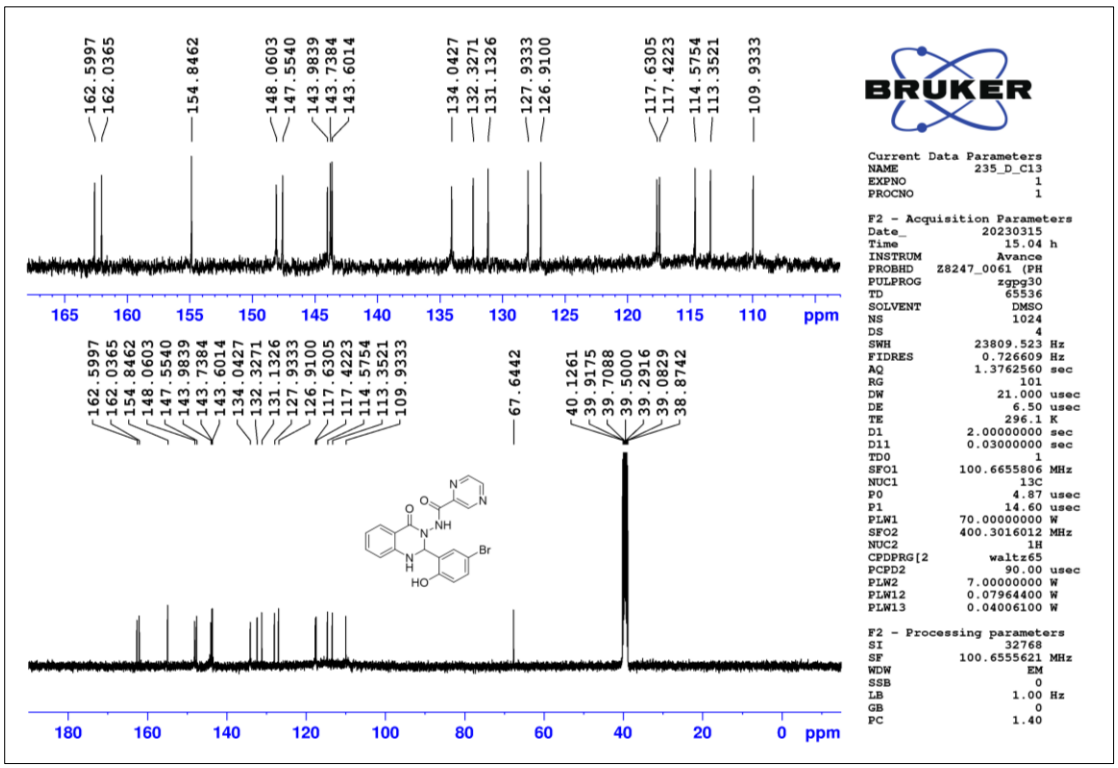

Figure 2.211 *^{13}C-NMR spectrum of compound* ***T64***

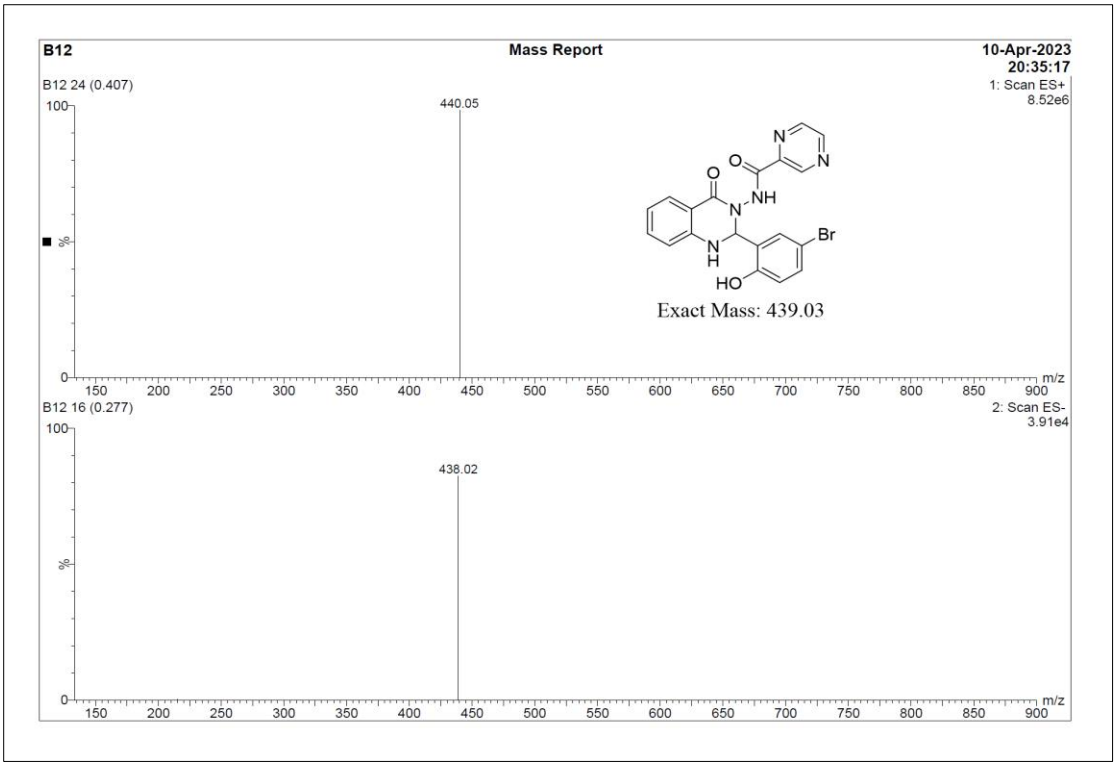

Figure 2.212 *ESI-MS spectrum of compound* ***T64***

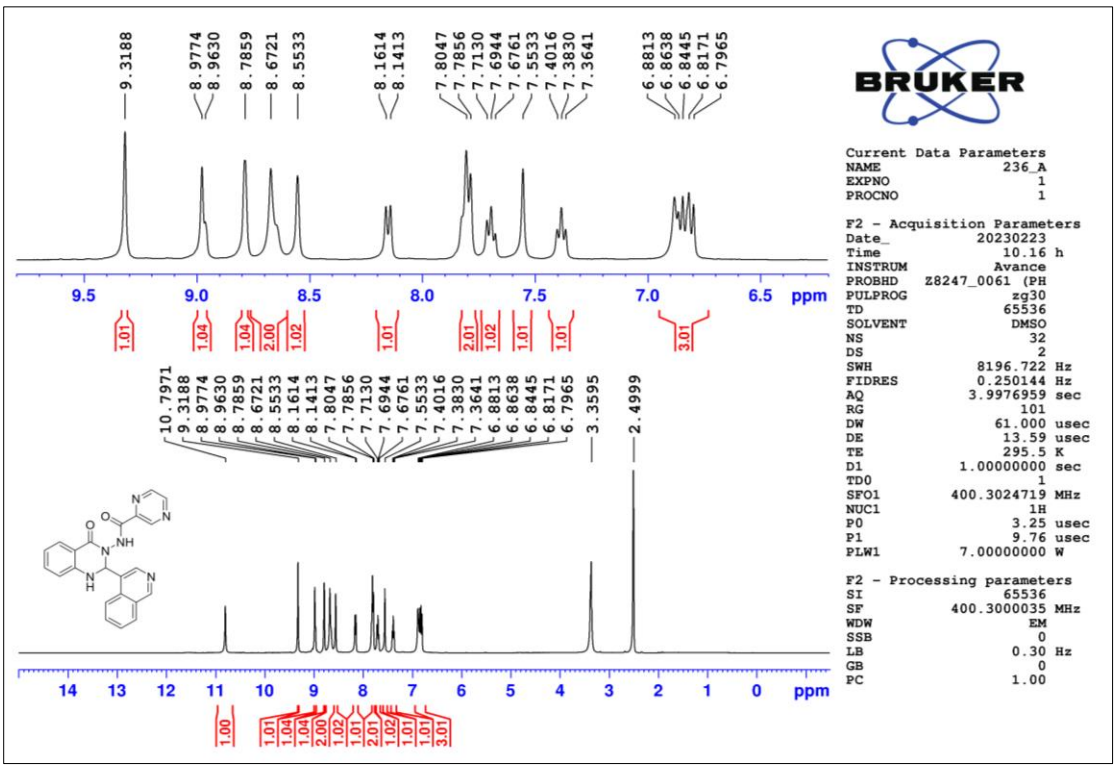

Figure 2.213 *^{1}H-NMR spectrum of compound* ***T66***

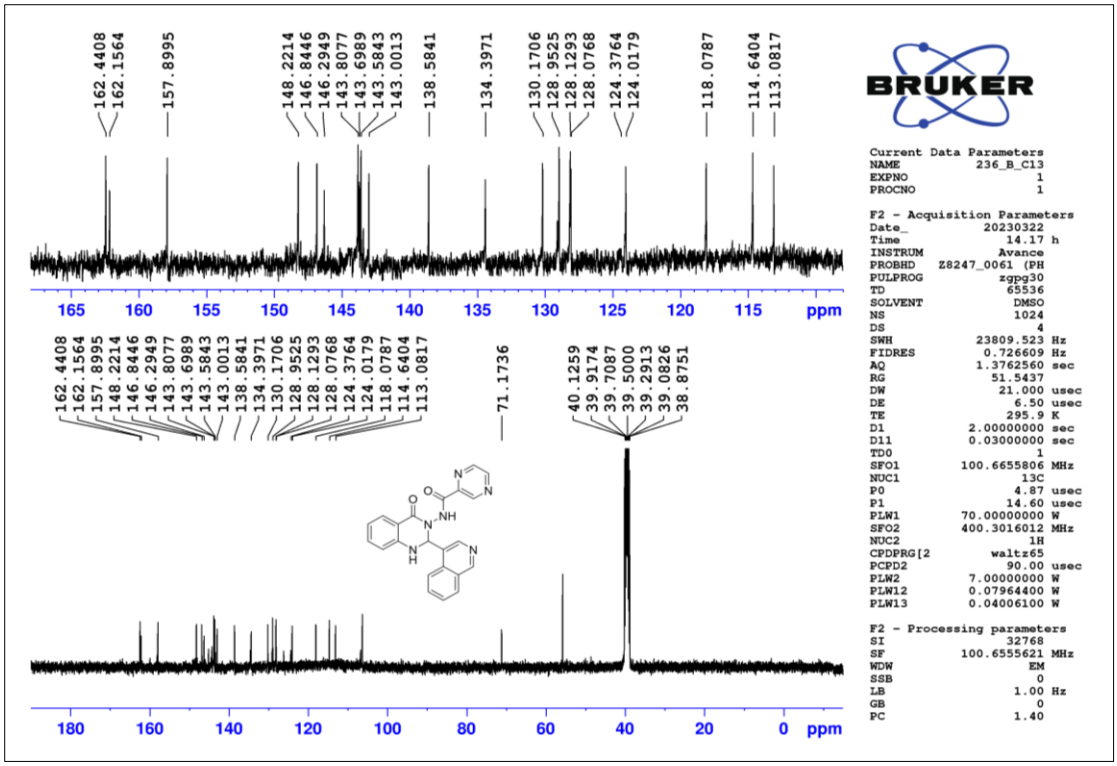

Figure 2.214 *^{13}C-NMR spectrum of compound* ***T66***

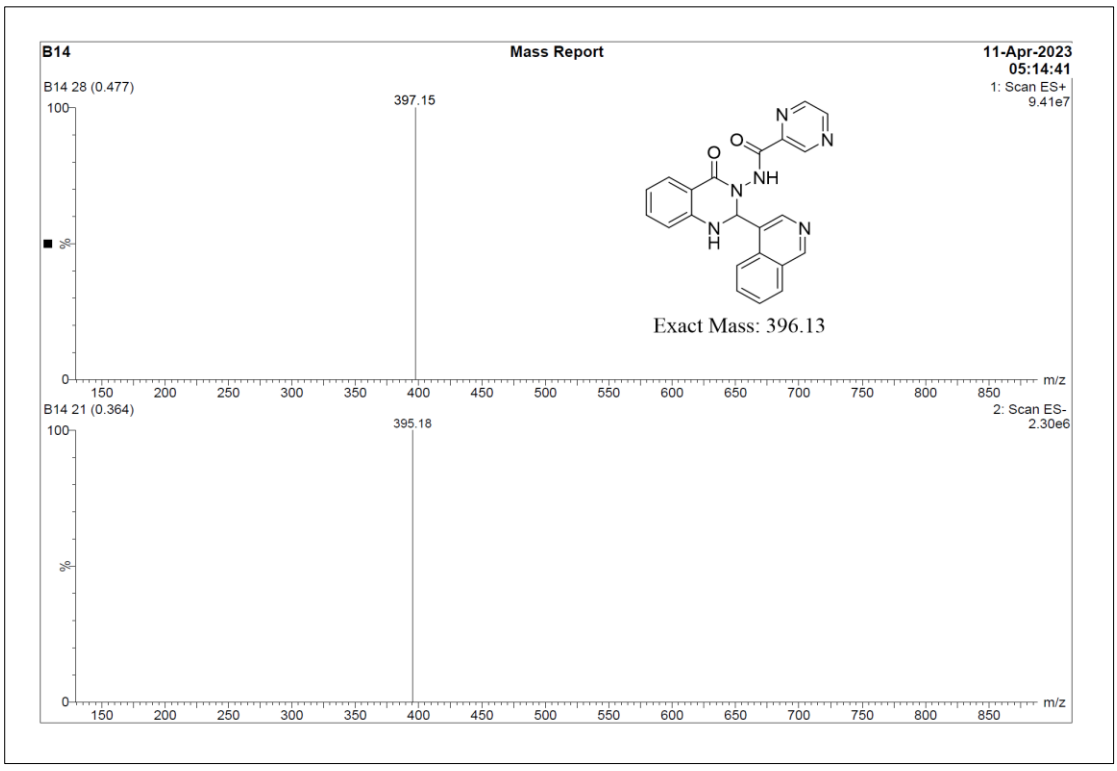

Figure 2.215 *ESI-MS spectrum of compound* ***T66***

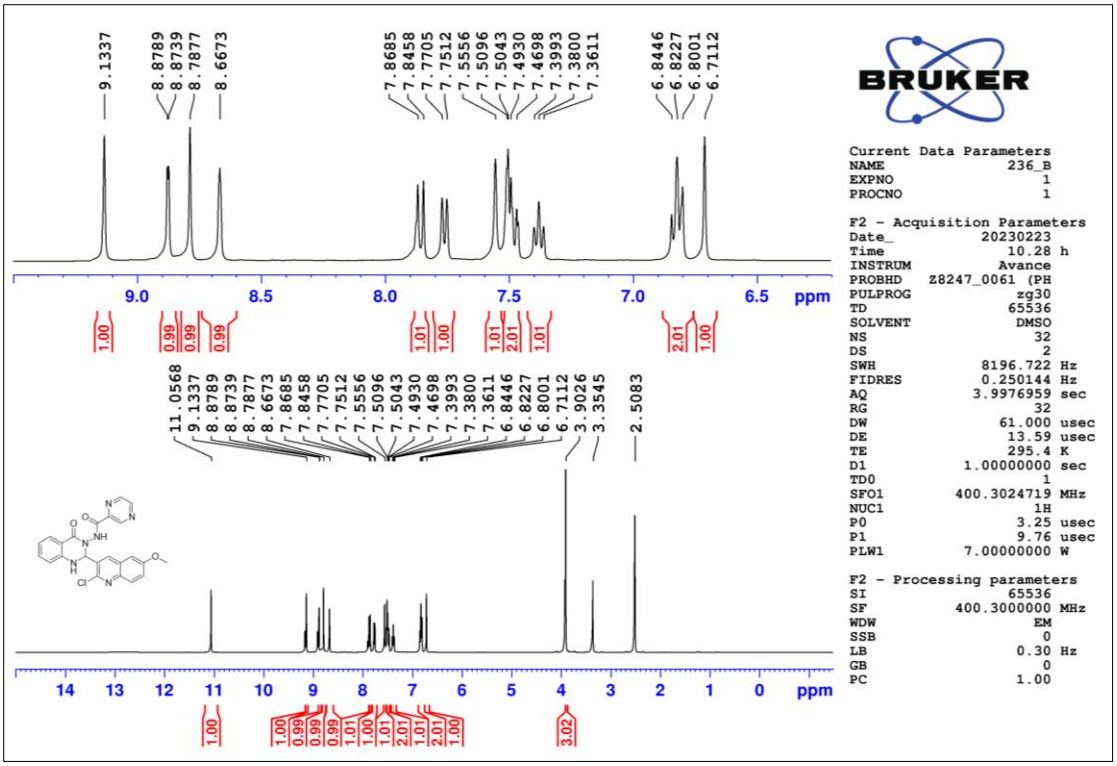

Figure 2.216 *[1]H-NMR spectrum of compound* ***T67***

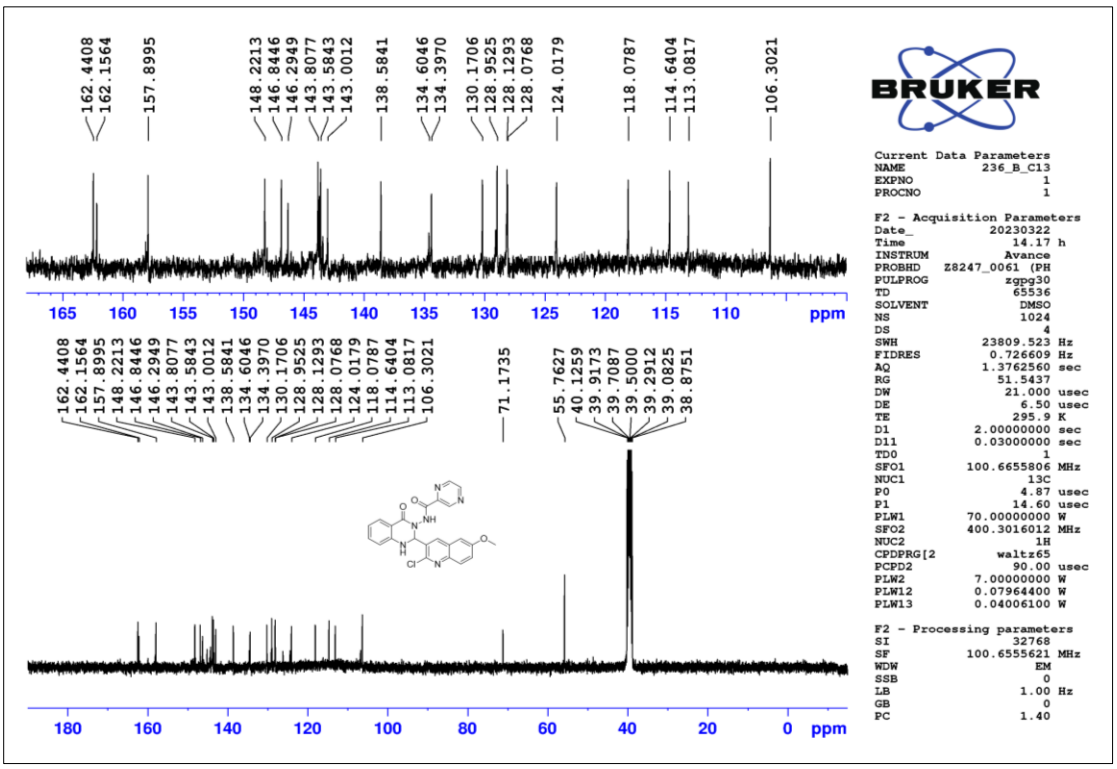

Figure 2.217 *[13]C-NMR spectrum of compound* ***T67***

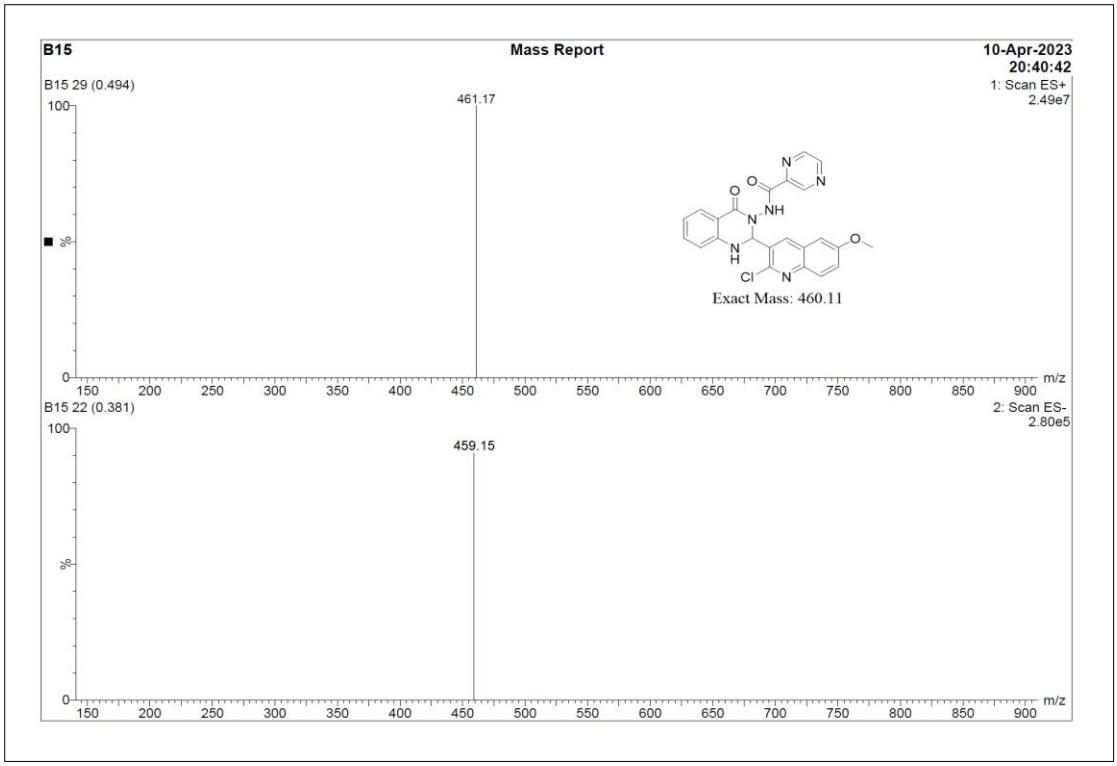

Figure 2.218 *ESI-MS spectrum of compound* ***T67***

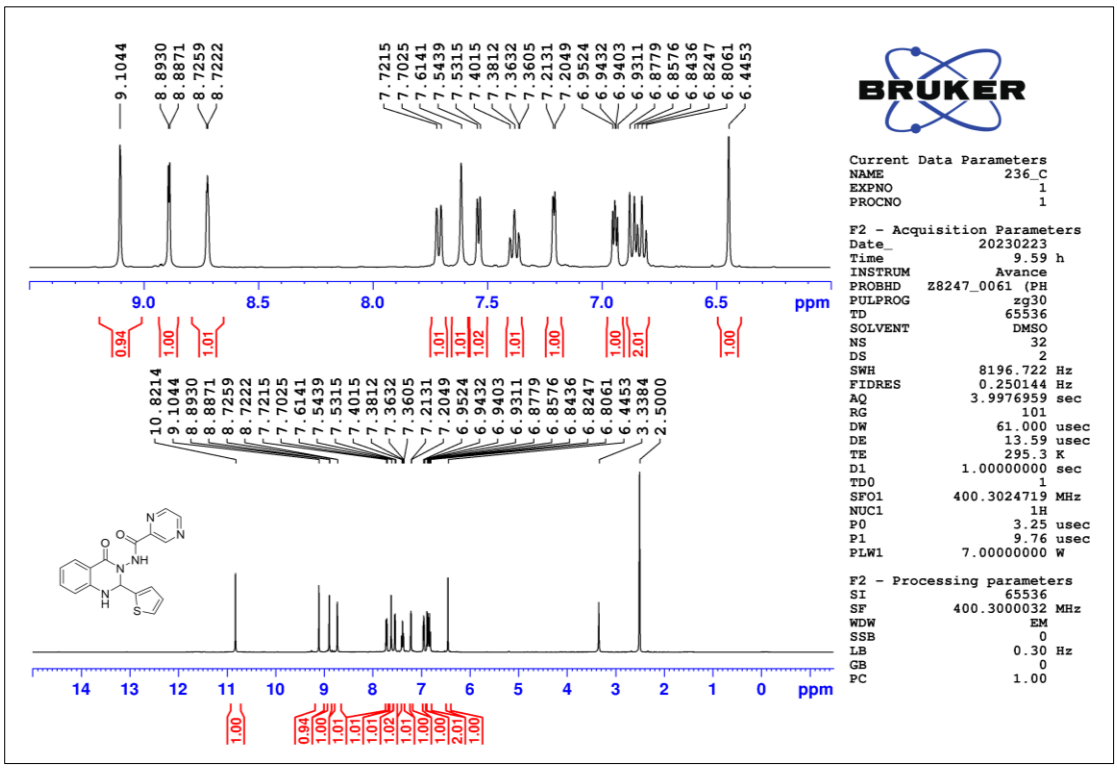

Figure 2.219 *^{1}H-NMR spectrum of compound* ***T68***

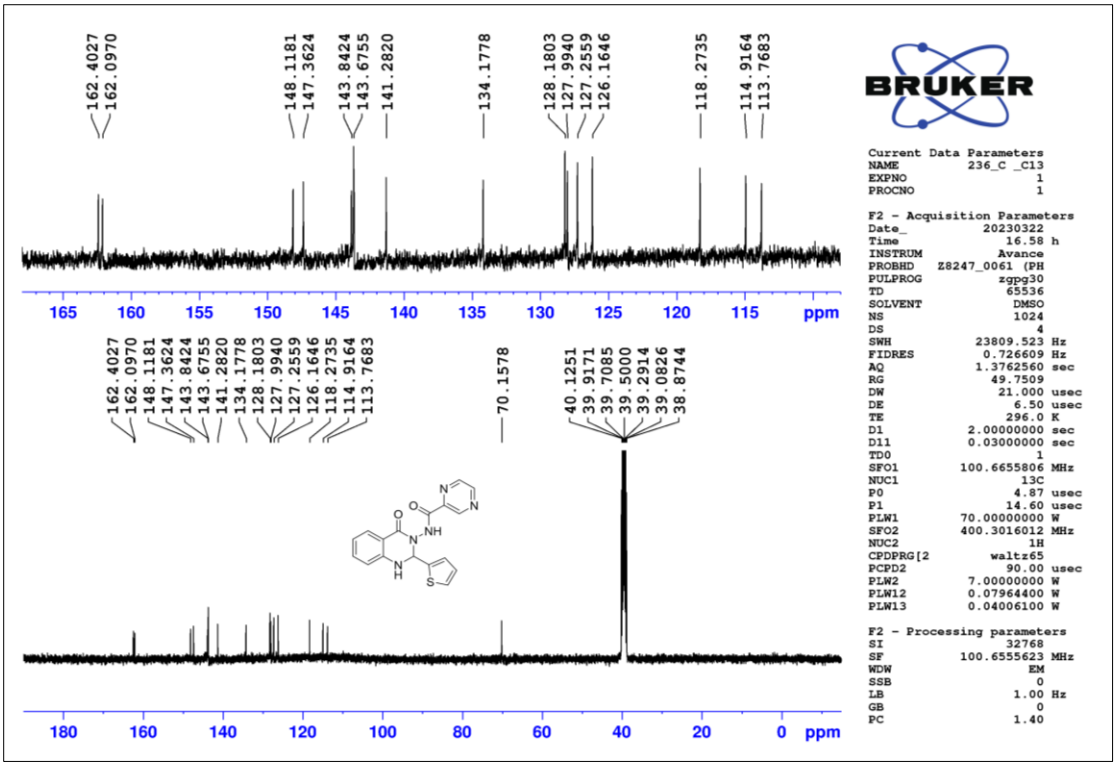

Figure 2.220 *^{13}C-NMR spectrum of compound* ***T68***

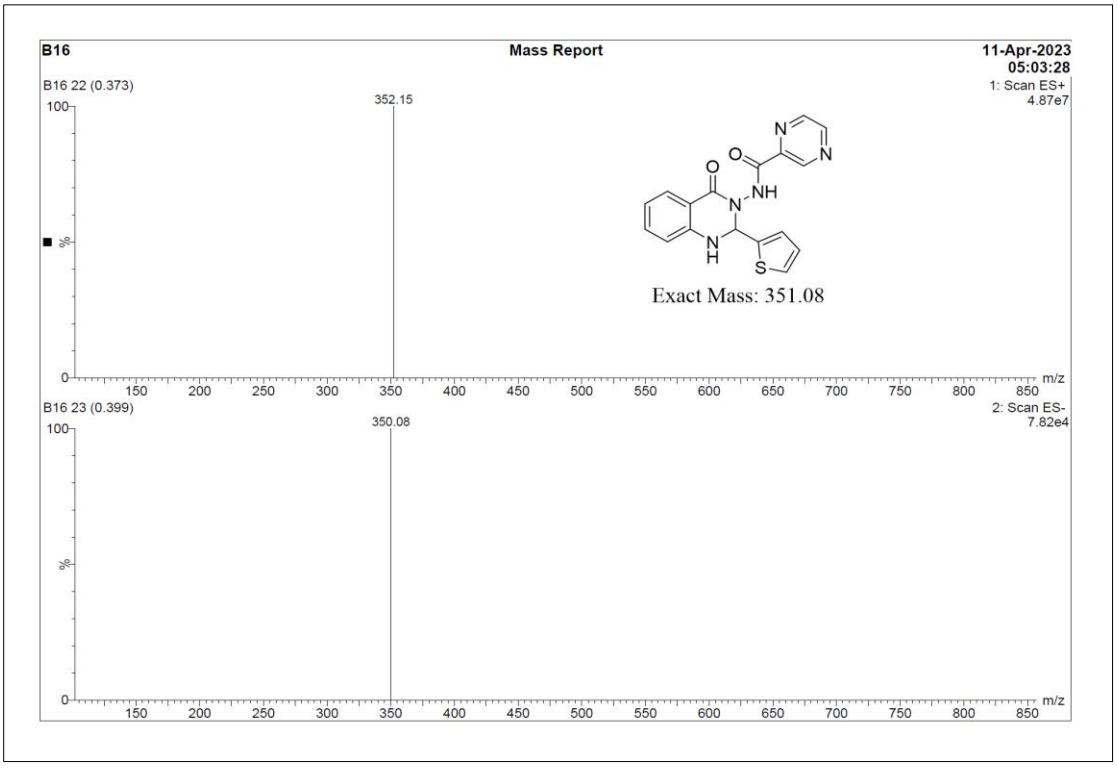

Figure 2.221 *ESI-MS spectrum of compound* ***T68***

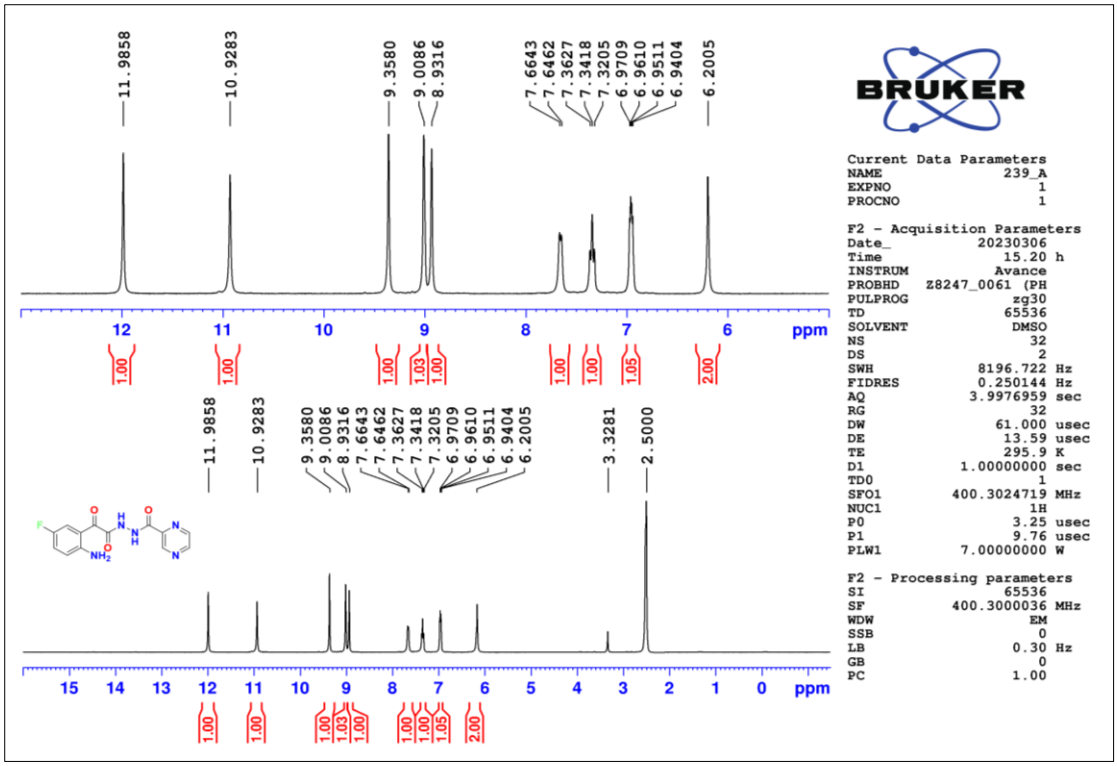

Figure 2.222 *^{1}H-NMR spectrum of compound* ***T70***

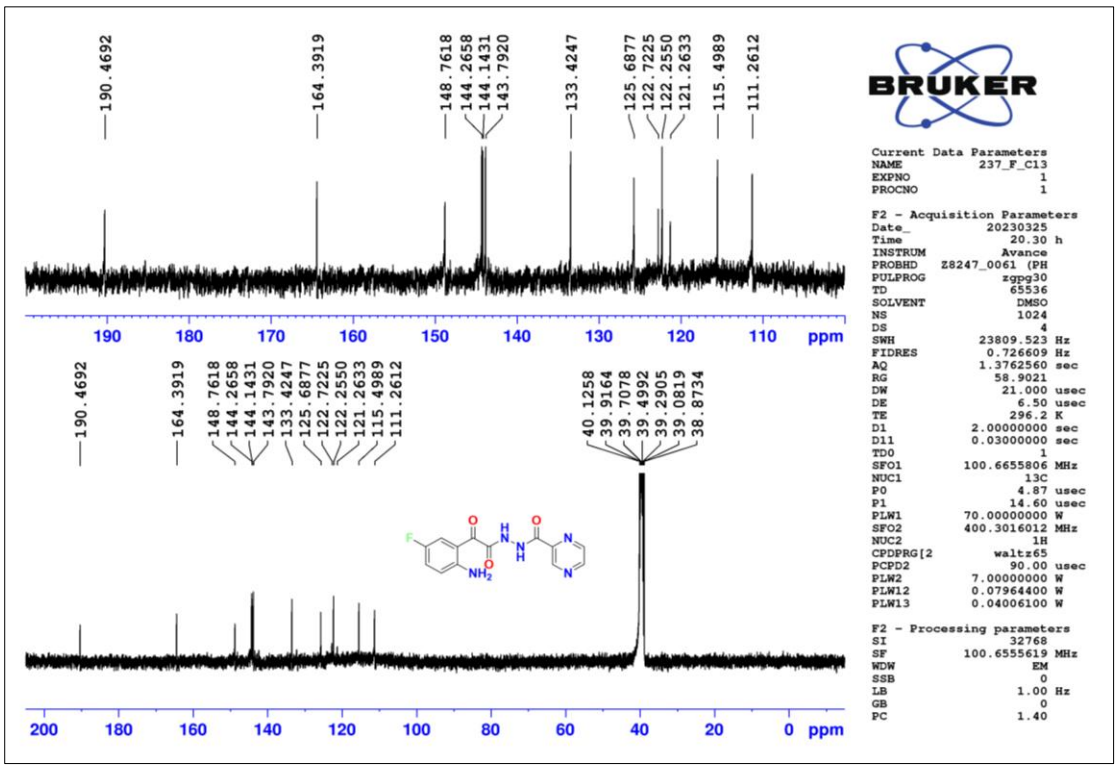

Figure 2.223 *^{13}C-NMR spectrum of compound* ***T70***

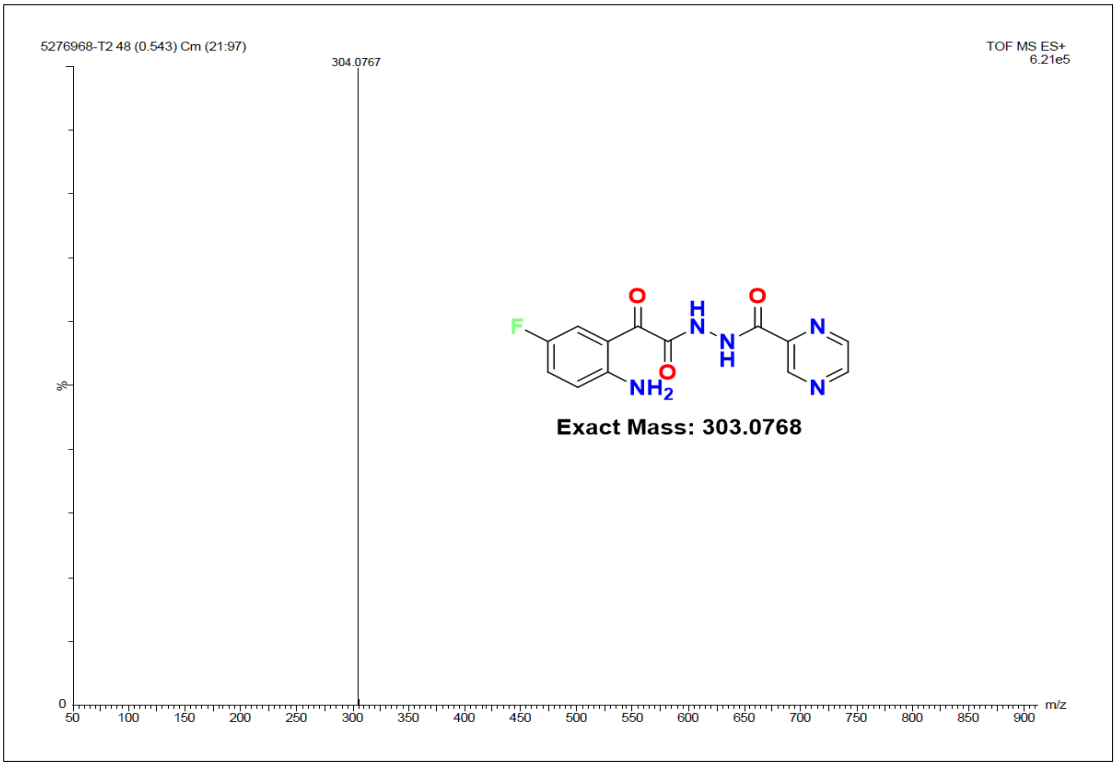

Figure 2.224 *HR-MS spectrum of compound* ***T70***

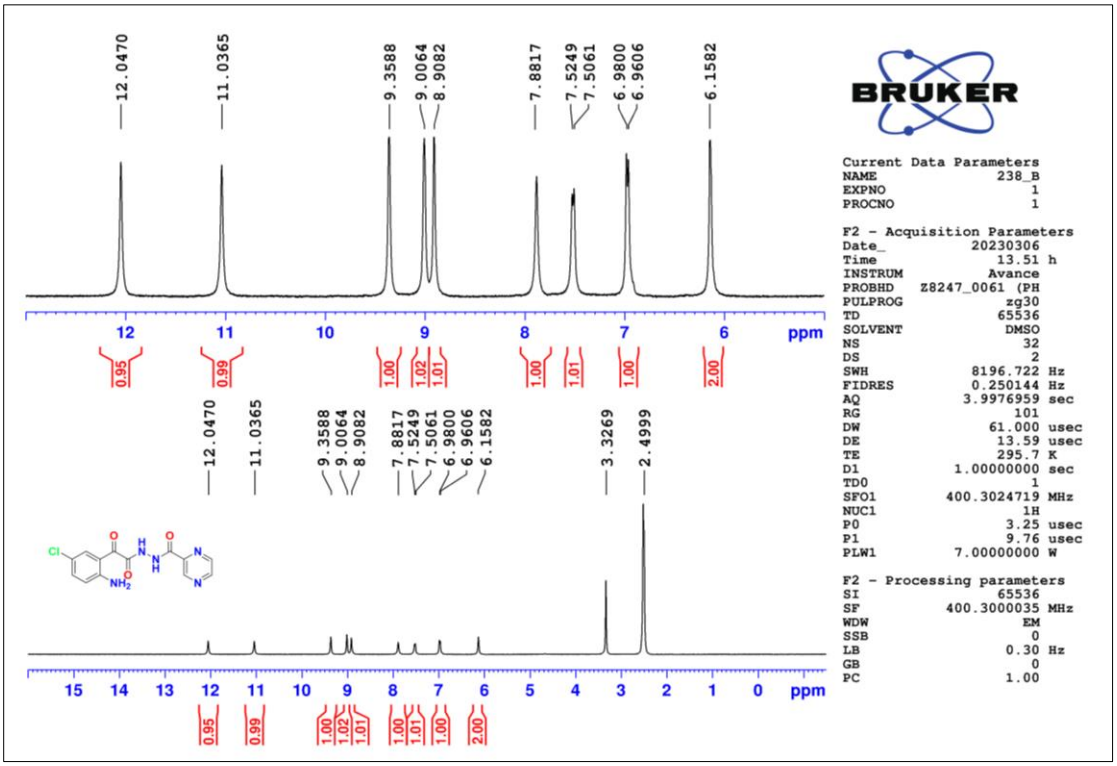

Figure 2.225 *^{1}H-NMR spectrum of compound* ***T71***

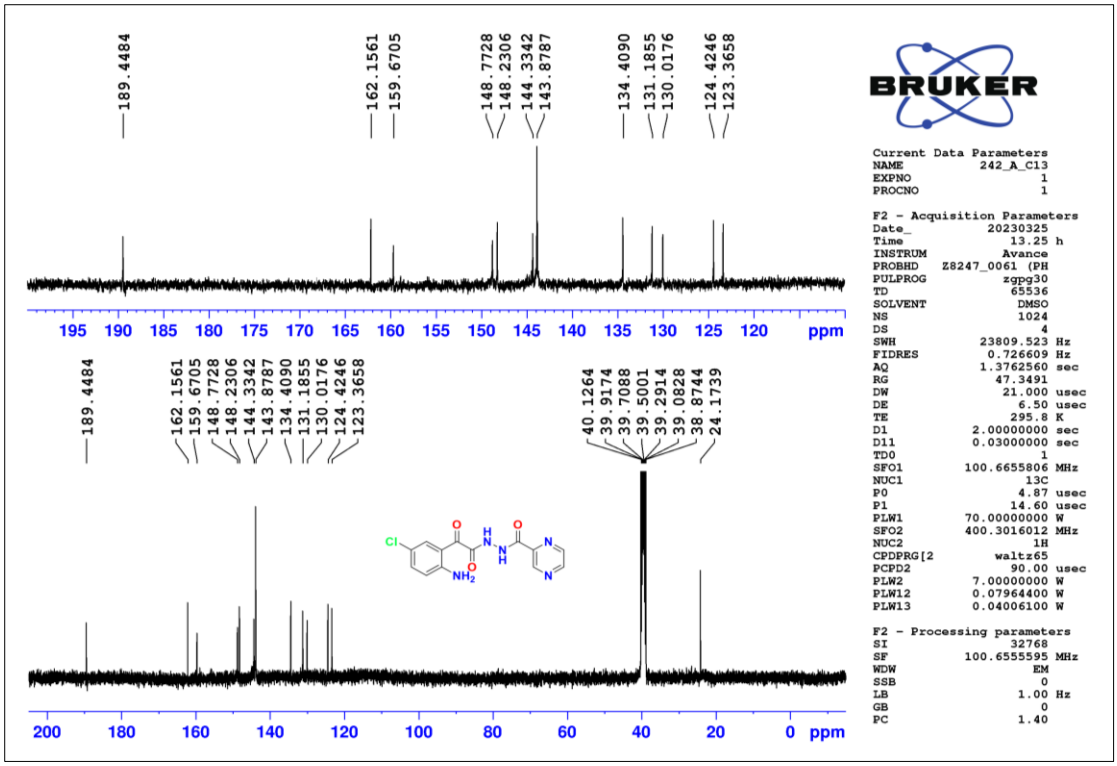

Figure 2.226 *^{13}C-NMR spectrum of compound* ***T71***

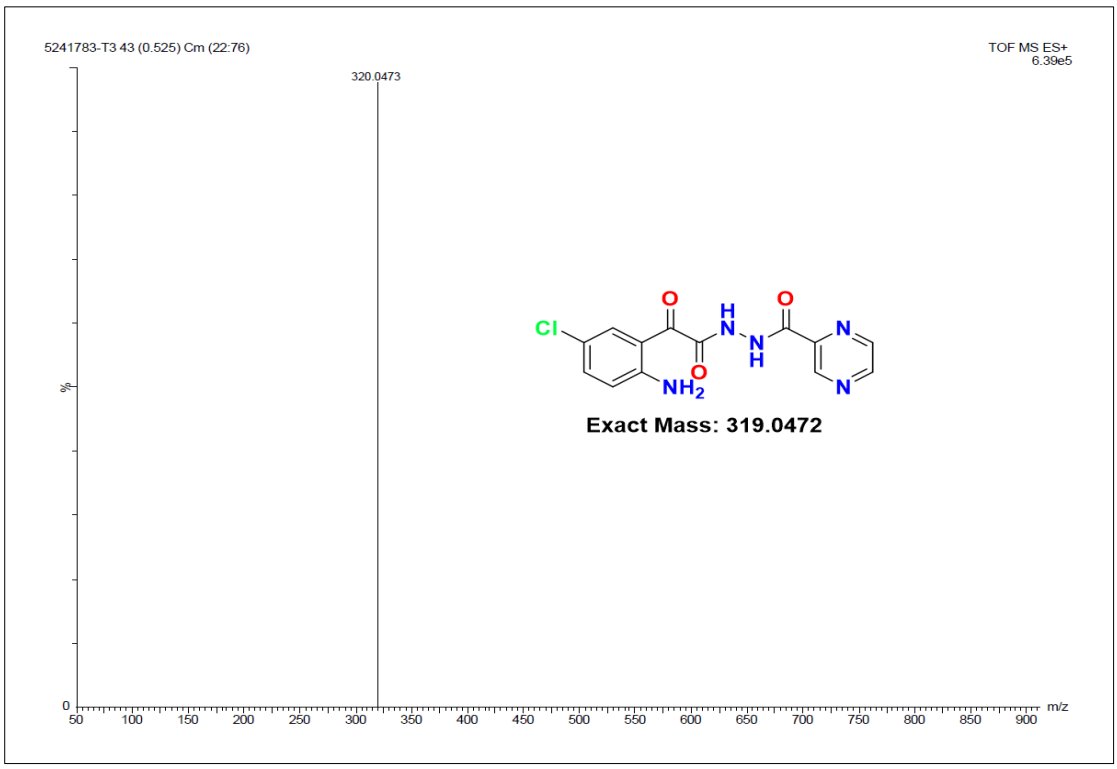

Figure 2.227 *HR-MS spectrum of compound* ***T71***

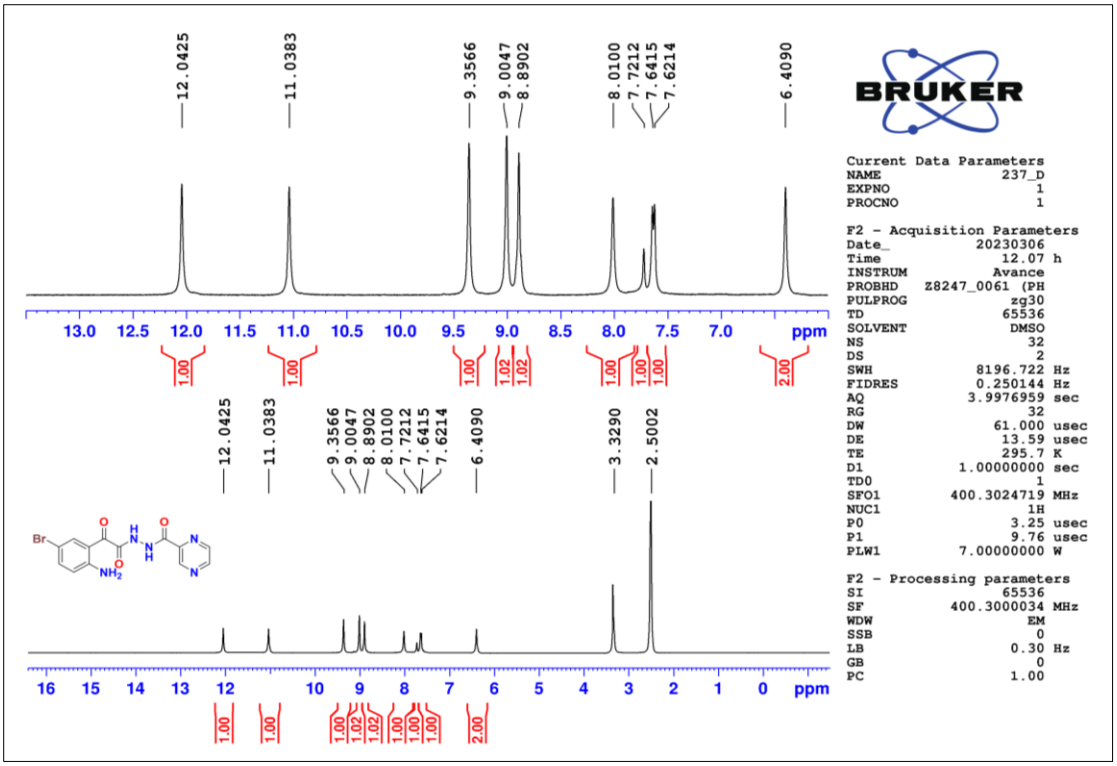

Figure 2.228 *^{1}H-NMR spectrum of compound* ***T72***

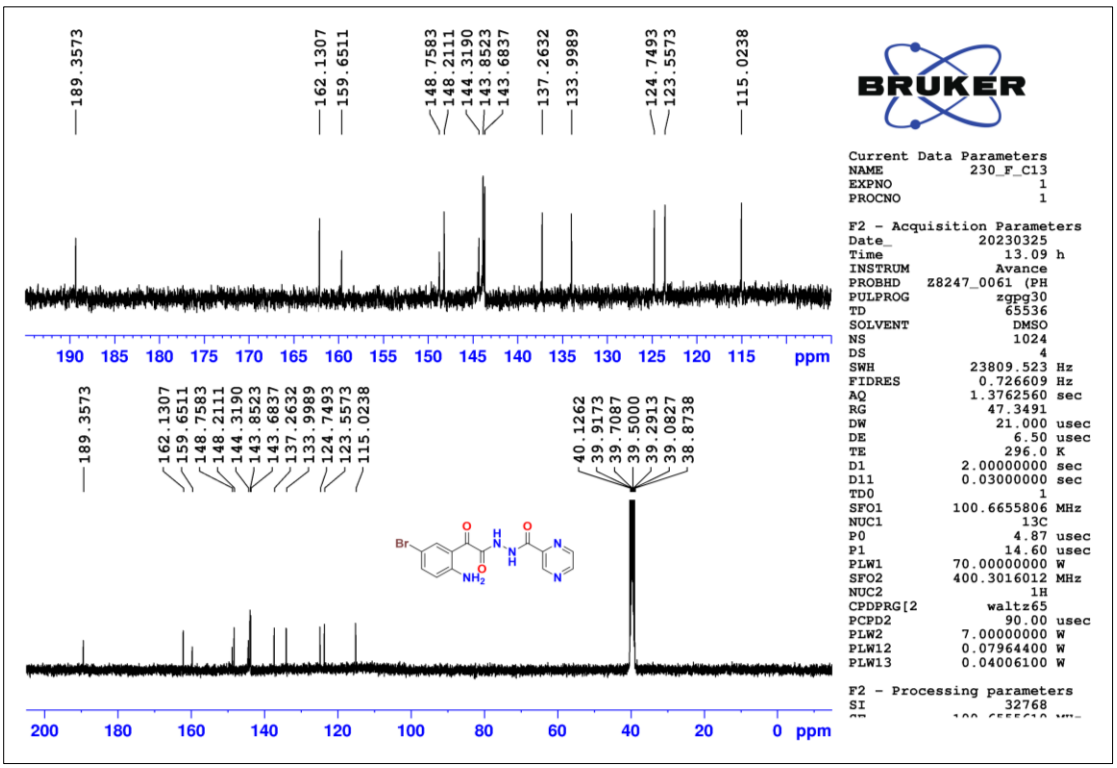

Figure 2.229 *^{13}C-NMR spectrum of compound* ***T72***

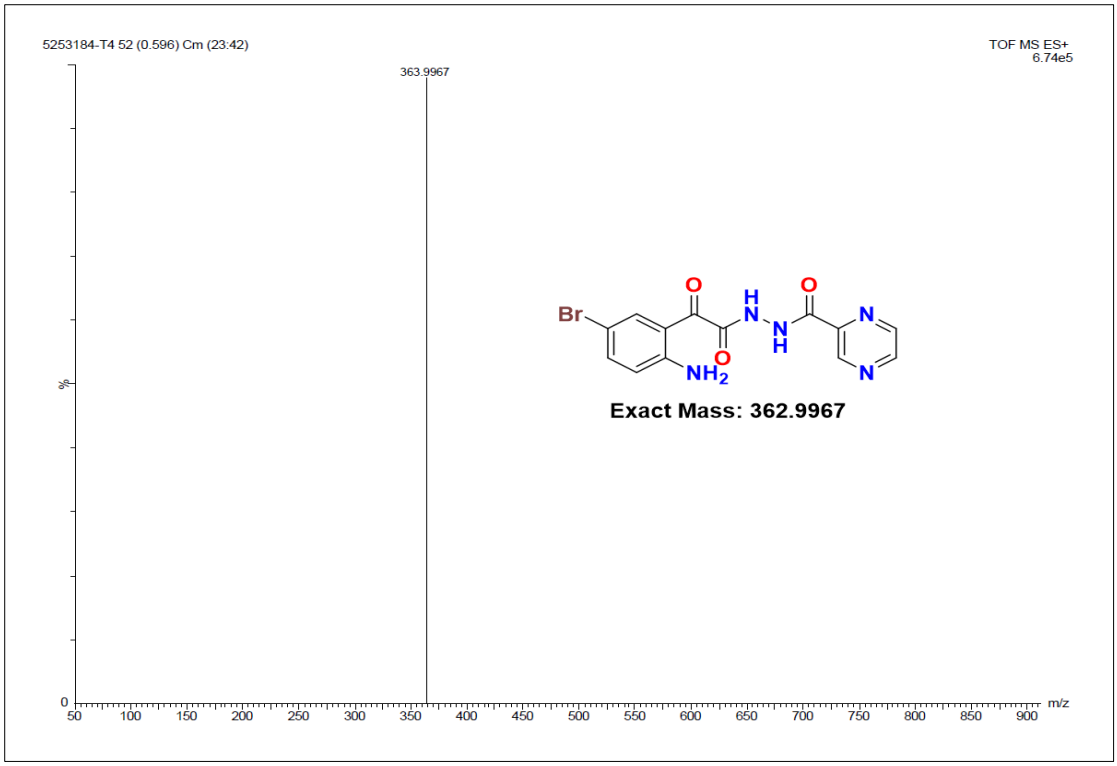

Figure 2.230 *HR-MS spectrum of compound* ***T72***

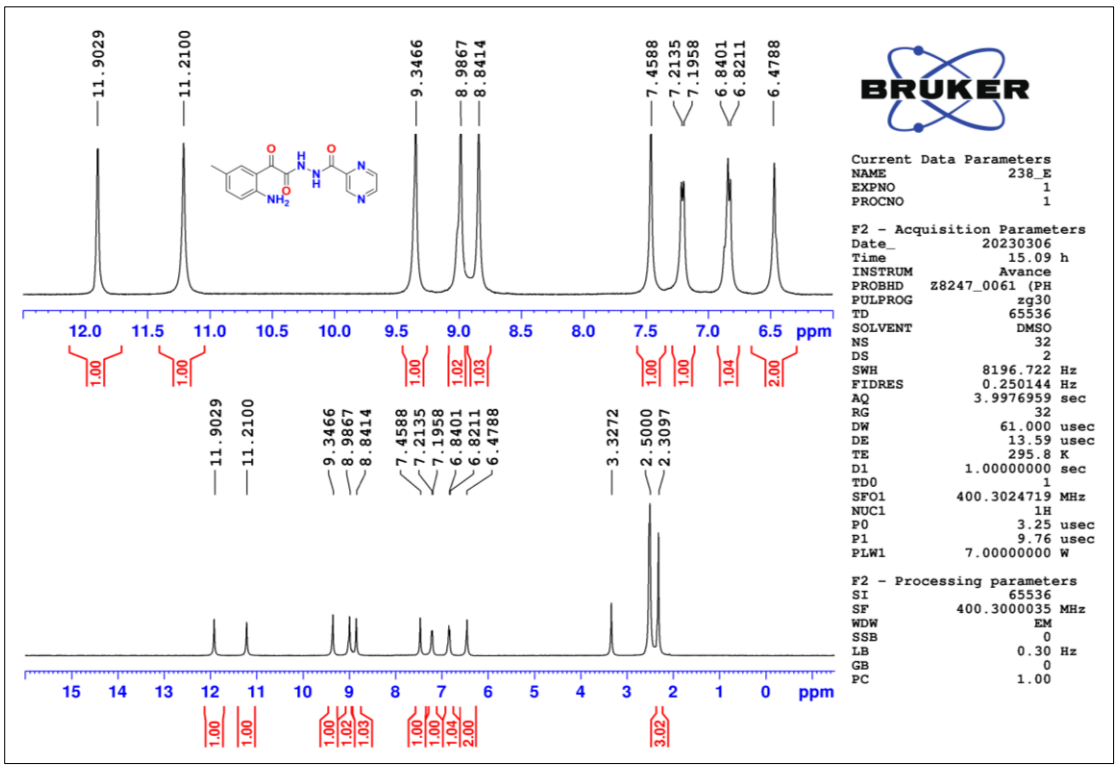

Figure 2.231 *^{1}H-NMR spectrum of compound* ***T73***

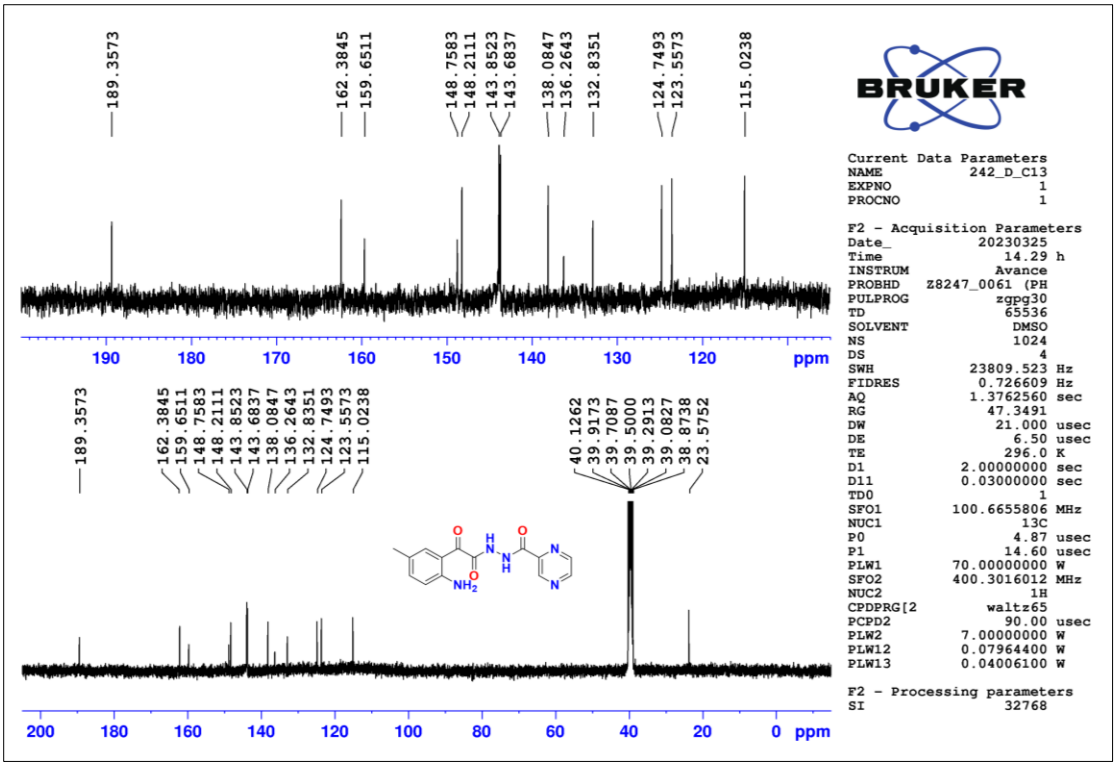

Figure 2.232 *^{13}C-NMR spectrum of compound* ***T73***

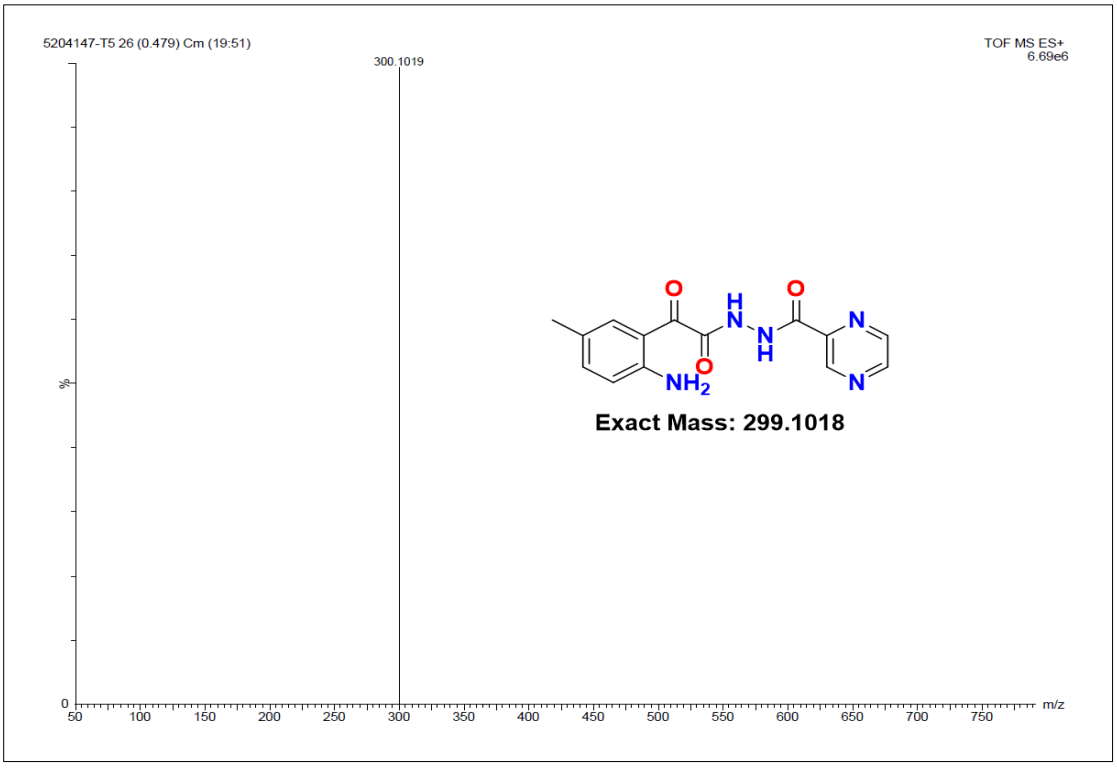

Figure 2.233 *HR-MS spectrum of compound* ***T73***

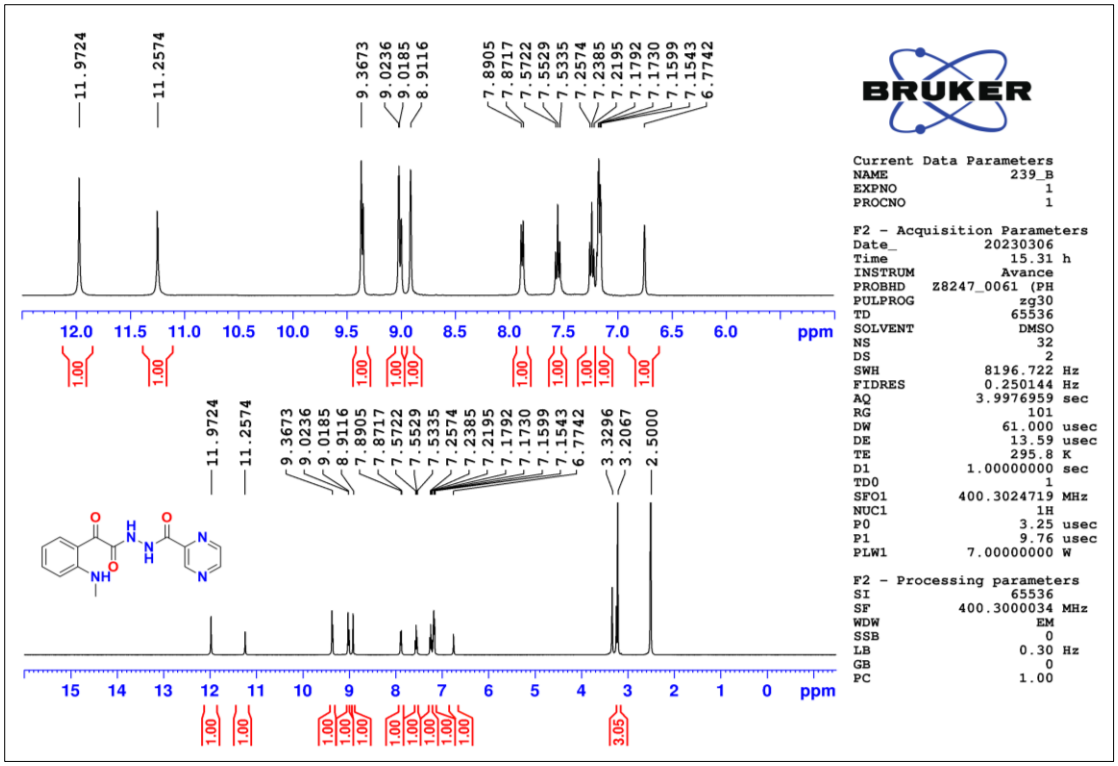

Figure 2.234 *^{1}H-NMR spectrum of compound* ***T74***

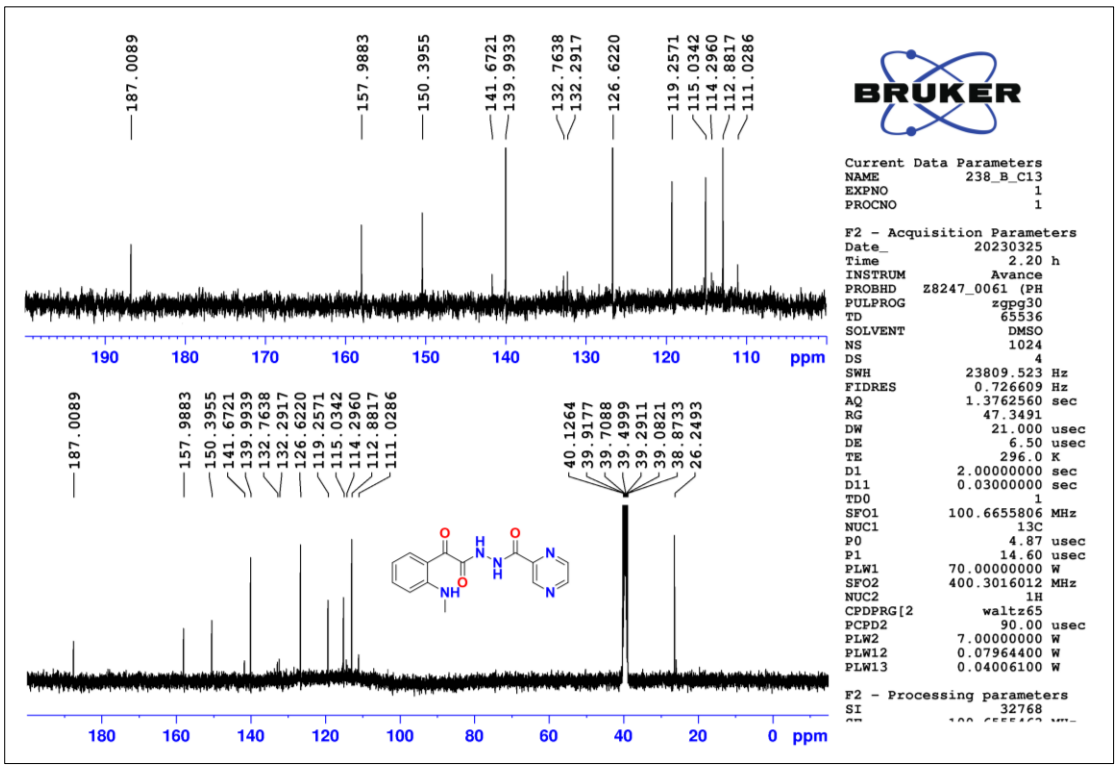

Figure 2.235 *^{13}C-NMR spectrum of compound* ***T74***

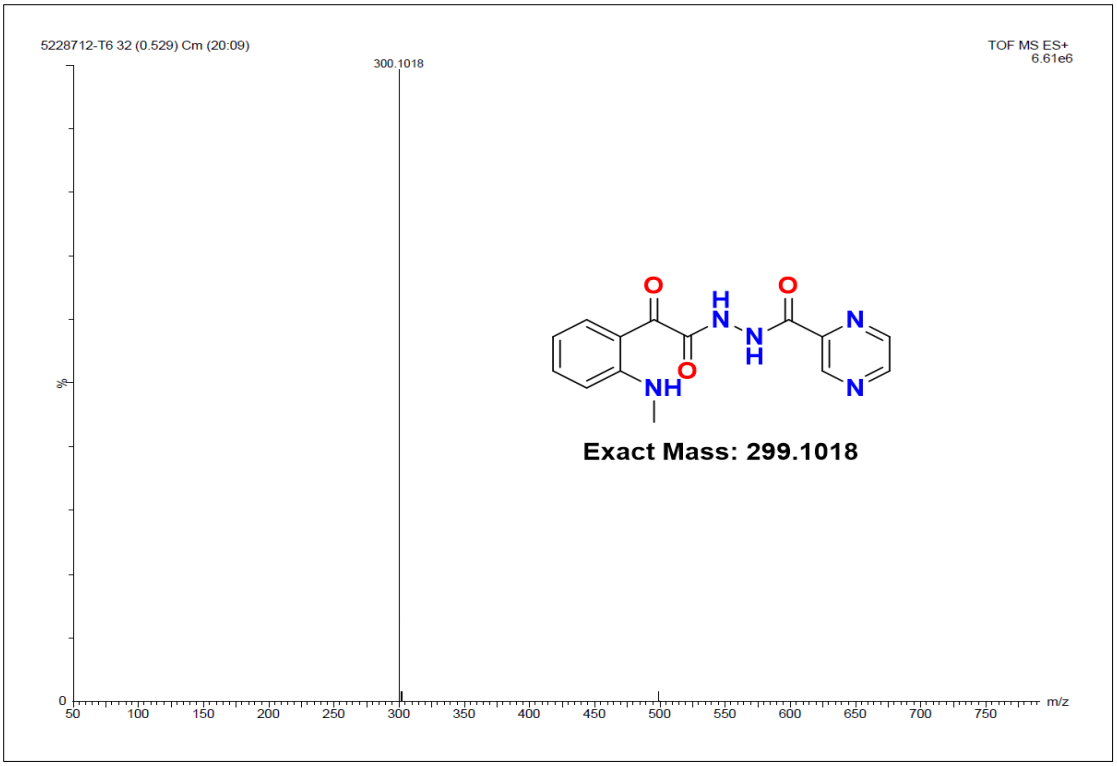

Figure 2.236 *HR-MS spectrum of compound* ***T74***

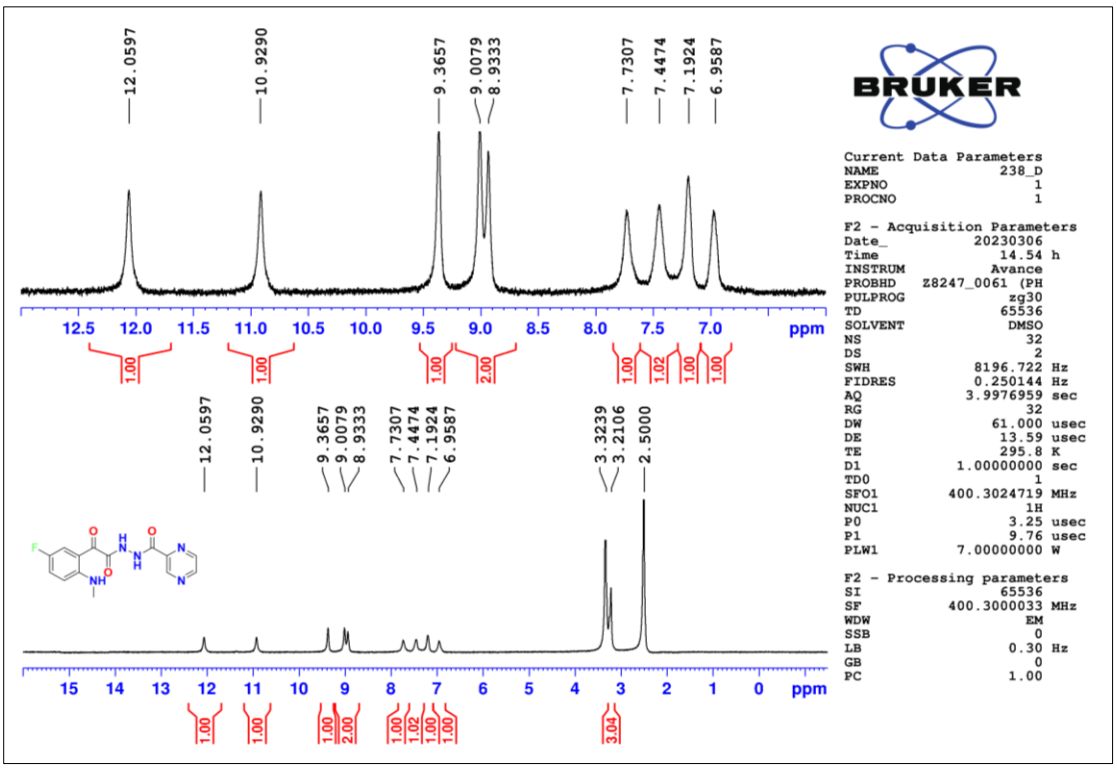

Figure 2.237 *^{1}H-NMR spectrum of compound* ***T75***

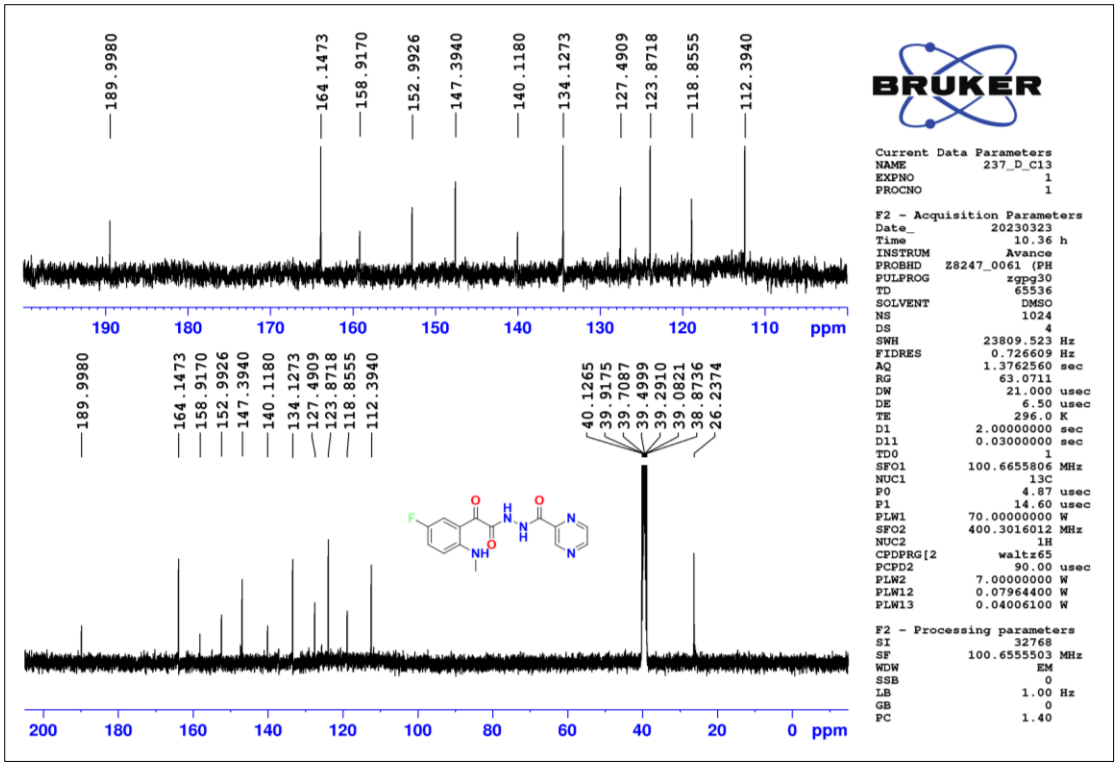

Figure 2.238 *^{13}C-NMR spectrum of compound* ***T75***

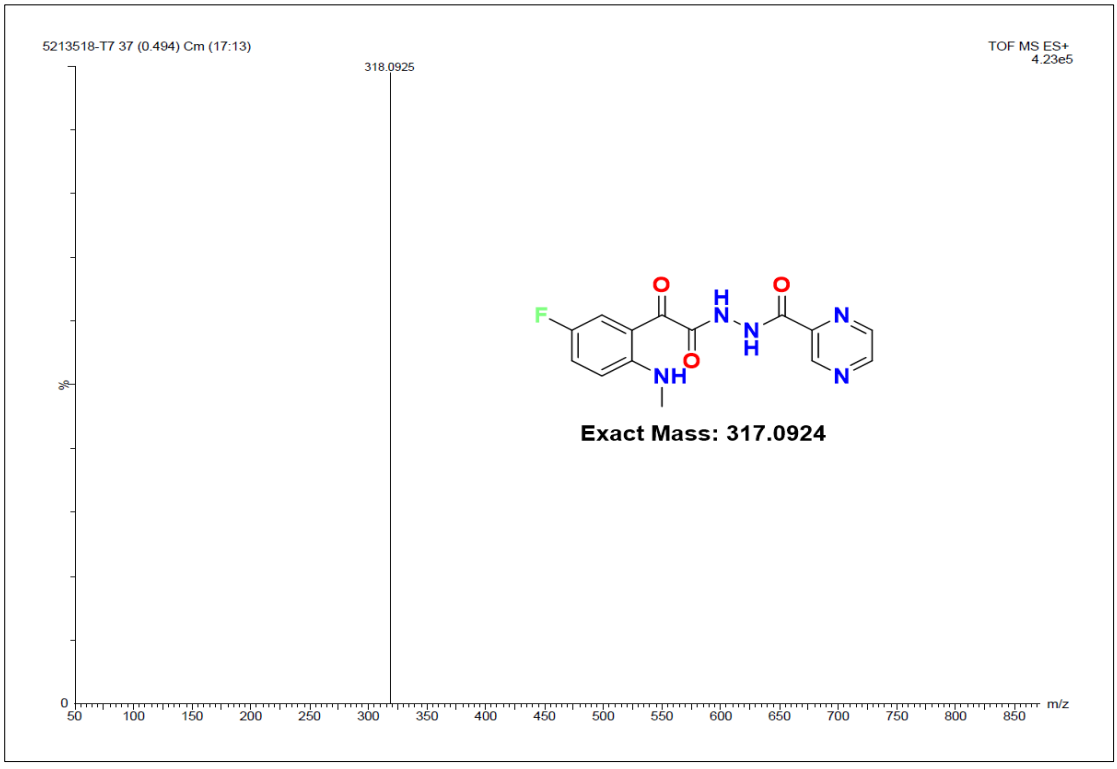

Figure 2.239 *HR-MS spectrum of compound* ***T75***

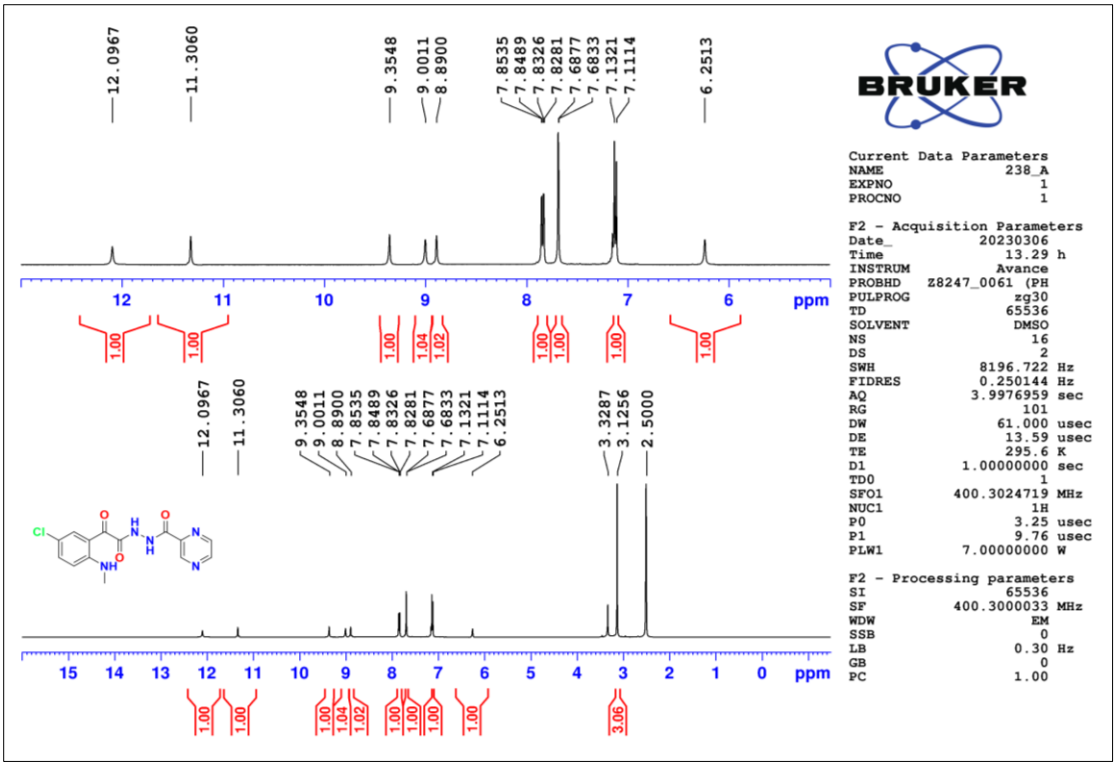

Figure 2.240 *^{1}H-NMR spectrum of compound* ***T76***

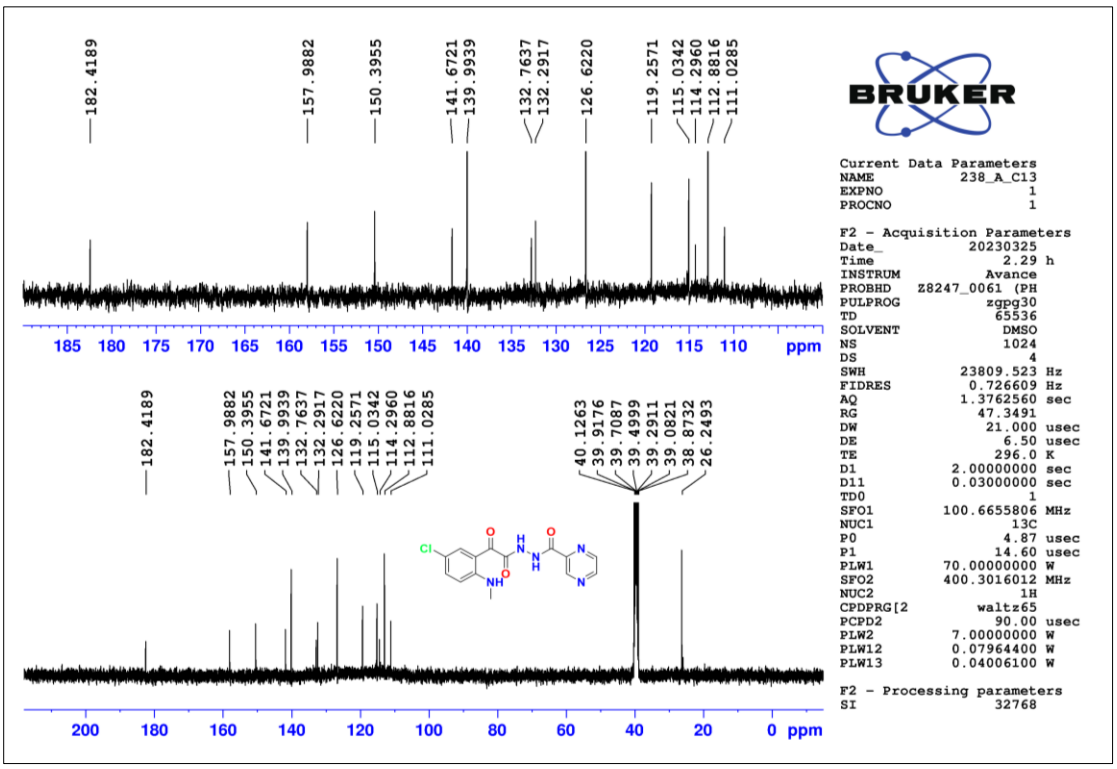

Figure 2.241 *^{13}C-NMR spectrum of compound* ***T76***

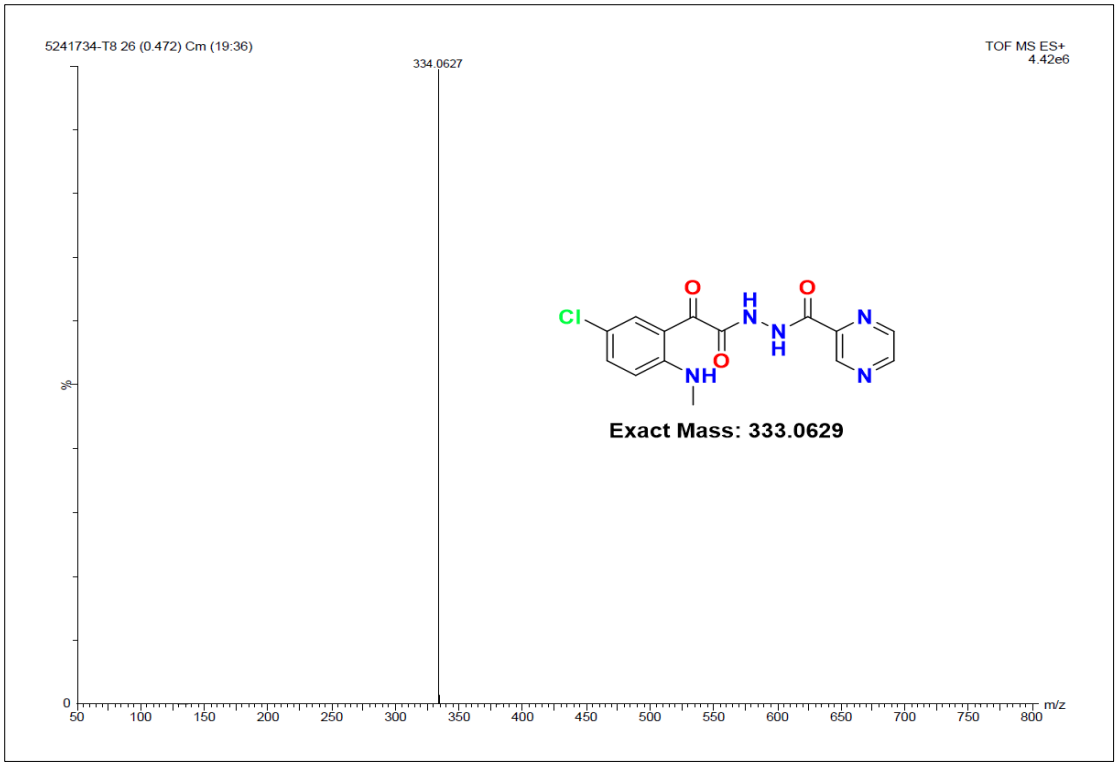

Figure 2.242 *HR-MS spectrum of compound* ***T76***

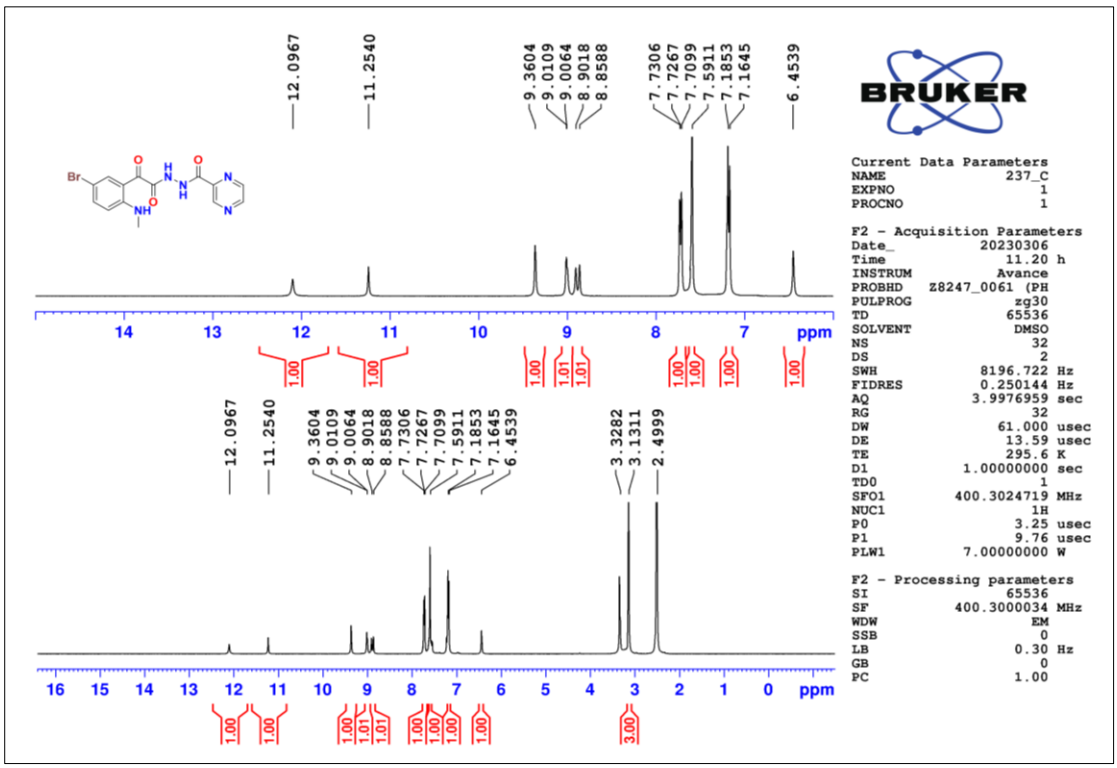

Figure 2.243 *^{1}H-NMR spectrum of compound* ***T77***

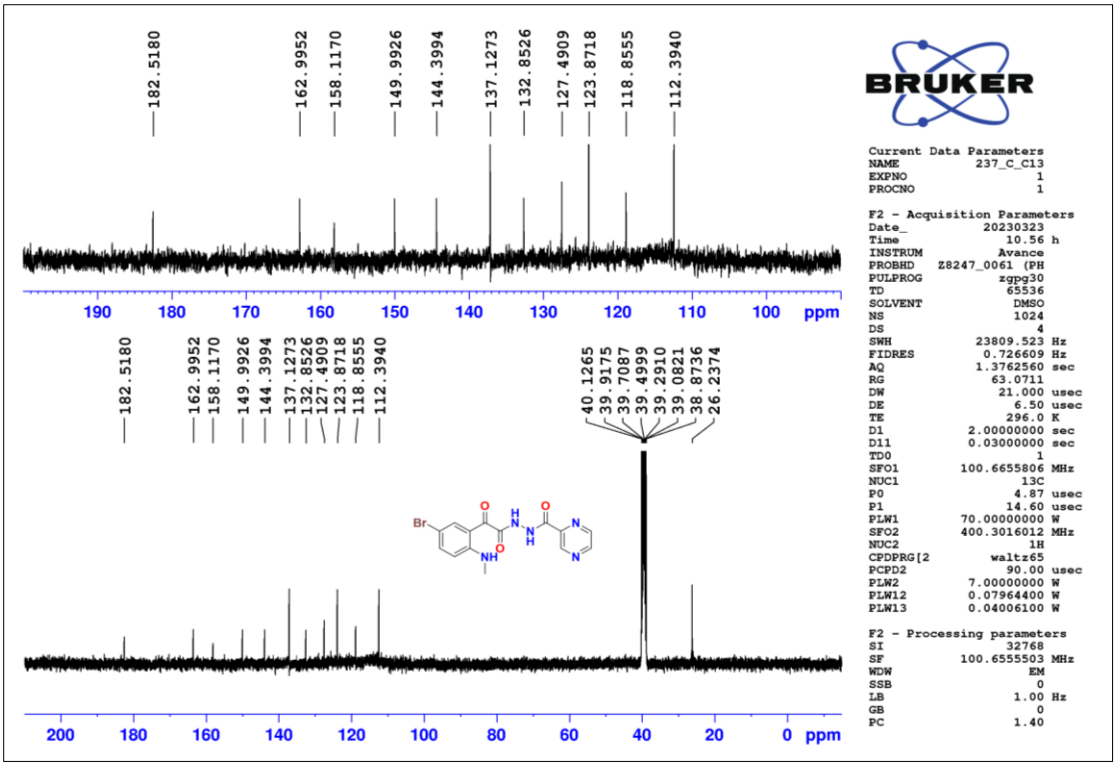

Figure 2.244 *^{13}C-NMR spectrum of compound* ***T77***

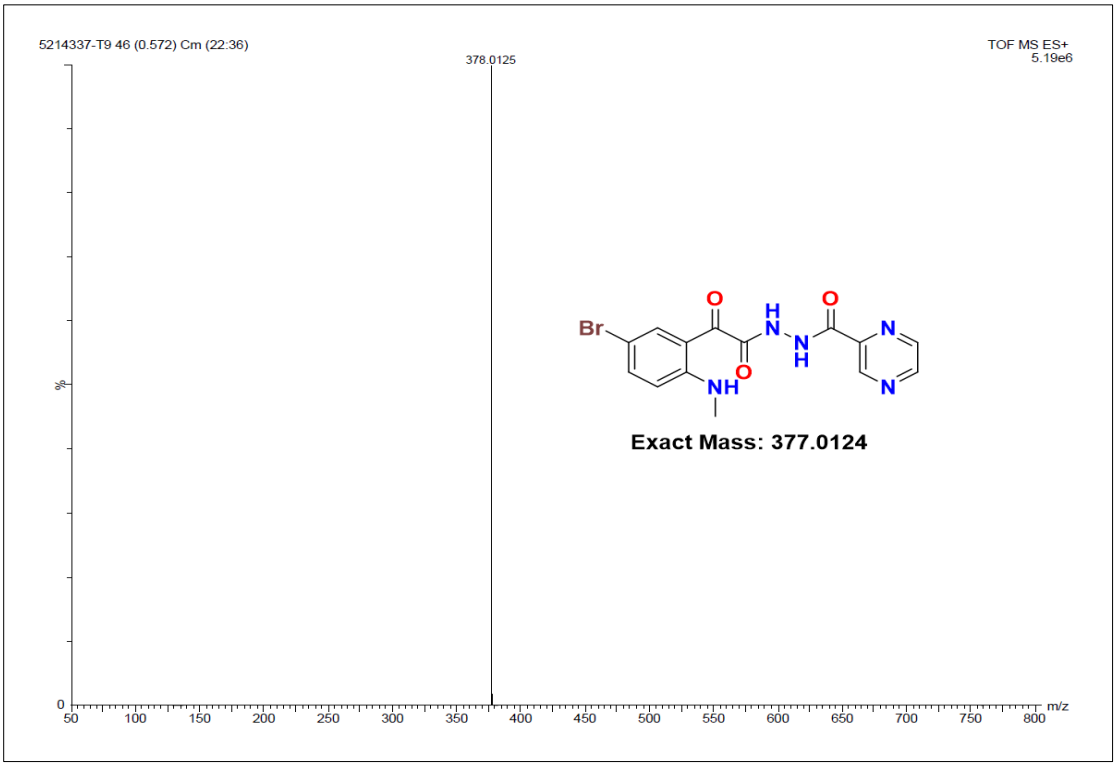

Figure 2.245 *HR-MS spectrum of compound* ***T77***

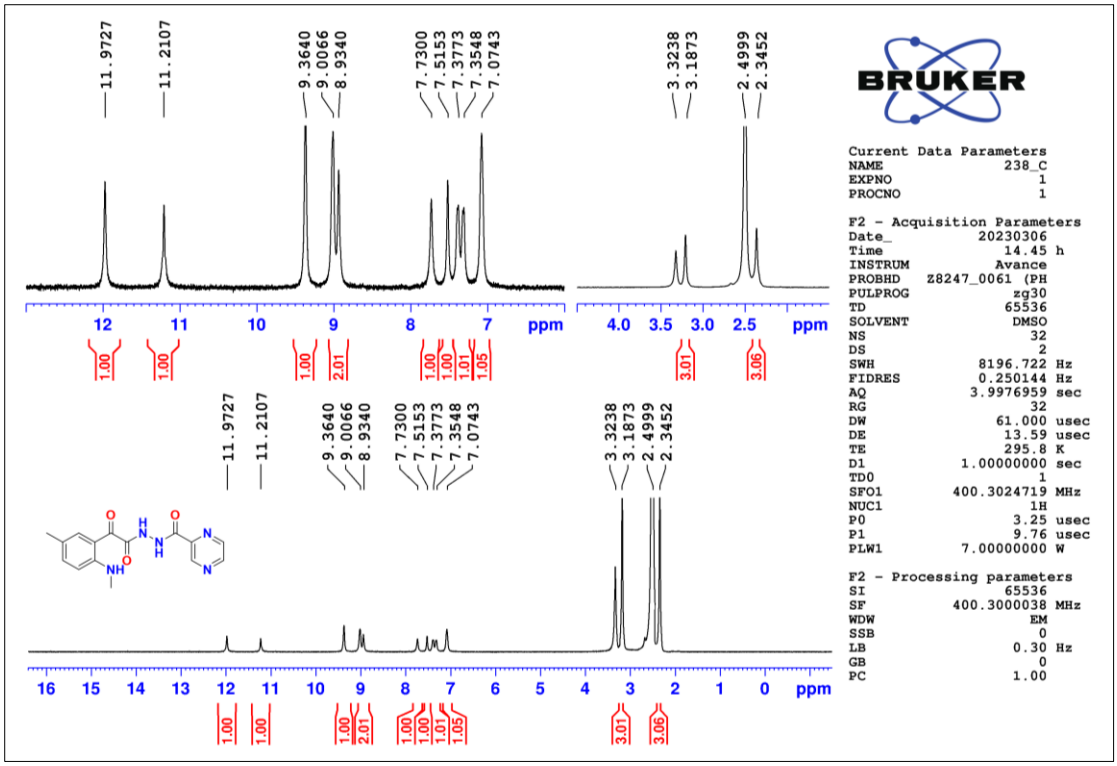

Figure 2.246 *^{1}H-NMR spectrum of compound* ***T78***

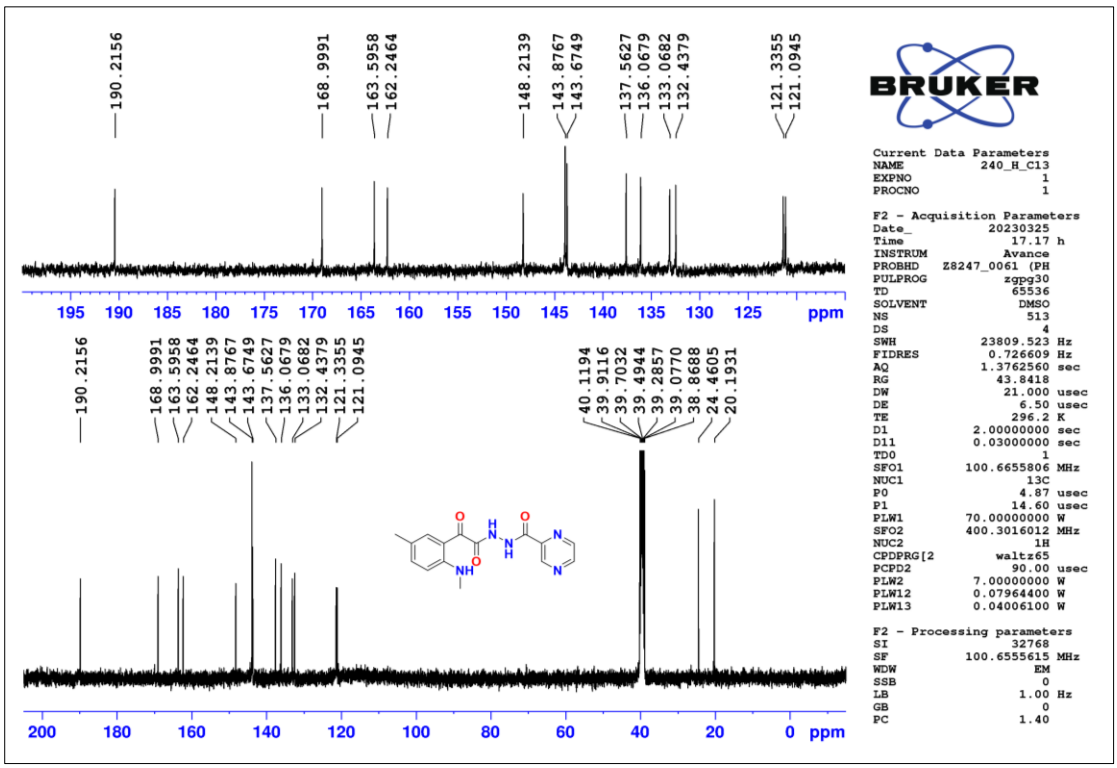

Figure 2.247 *^{13}C-NMR spectrum of compound* ***T78***

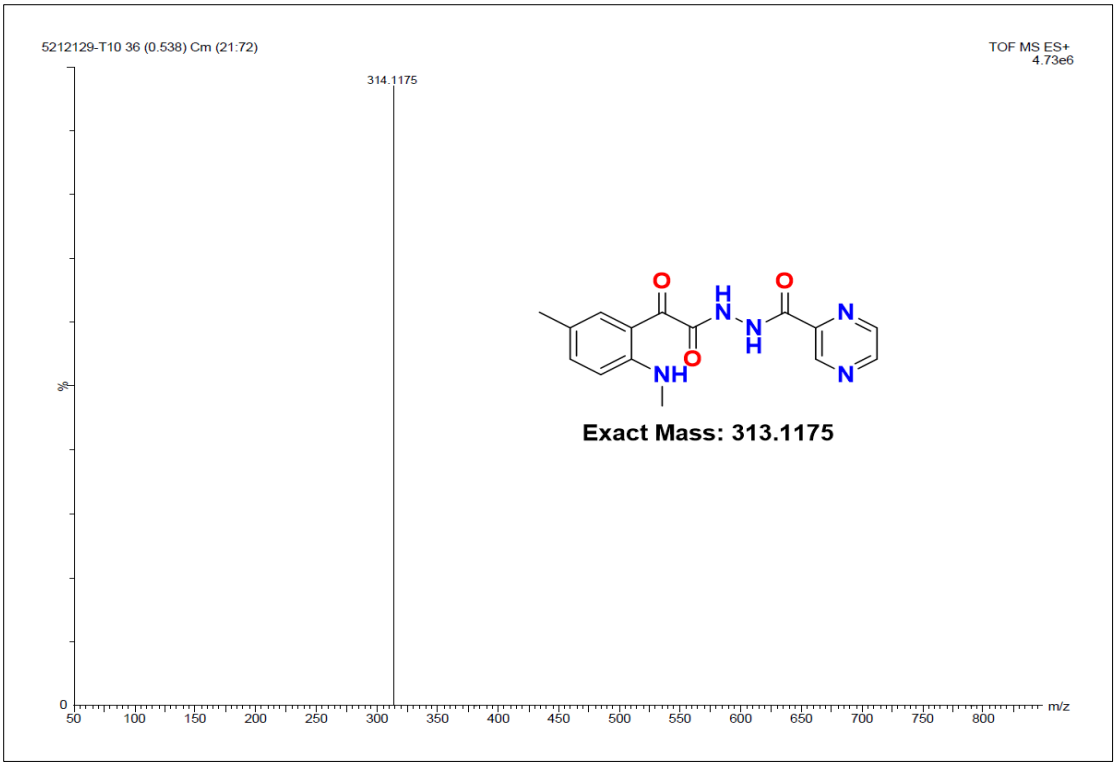

Figure 2.248 *HR-MS spectrum of compound* ***T78***

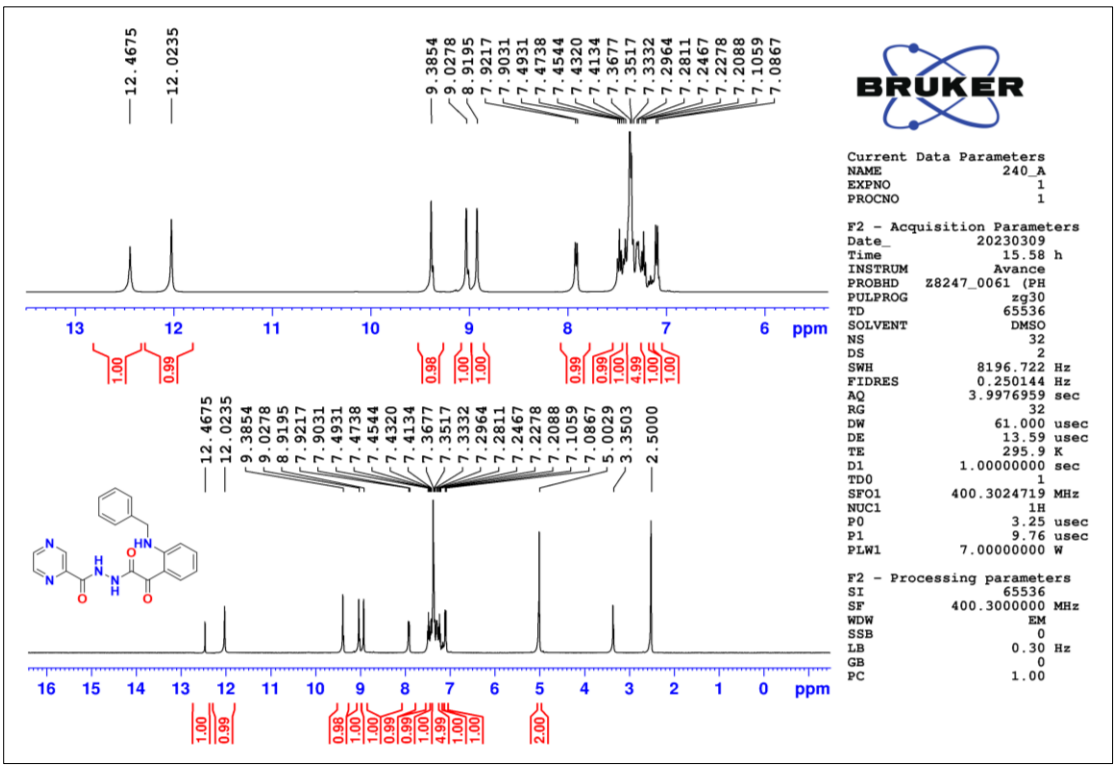

Figure 2.249 *^{1}H-NMR spectrum of compound* ***T79***

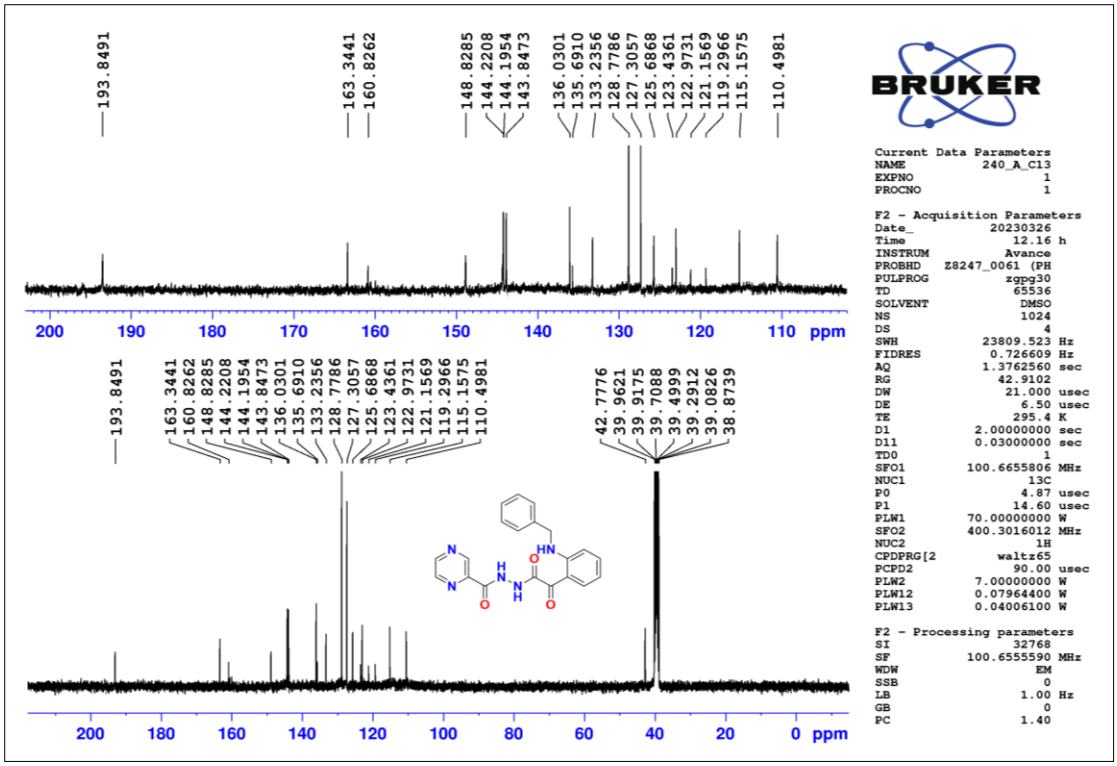

Figure 2.250 *^{13}C-NMR spectrum of compound* ***T79***

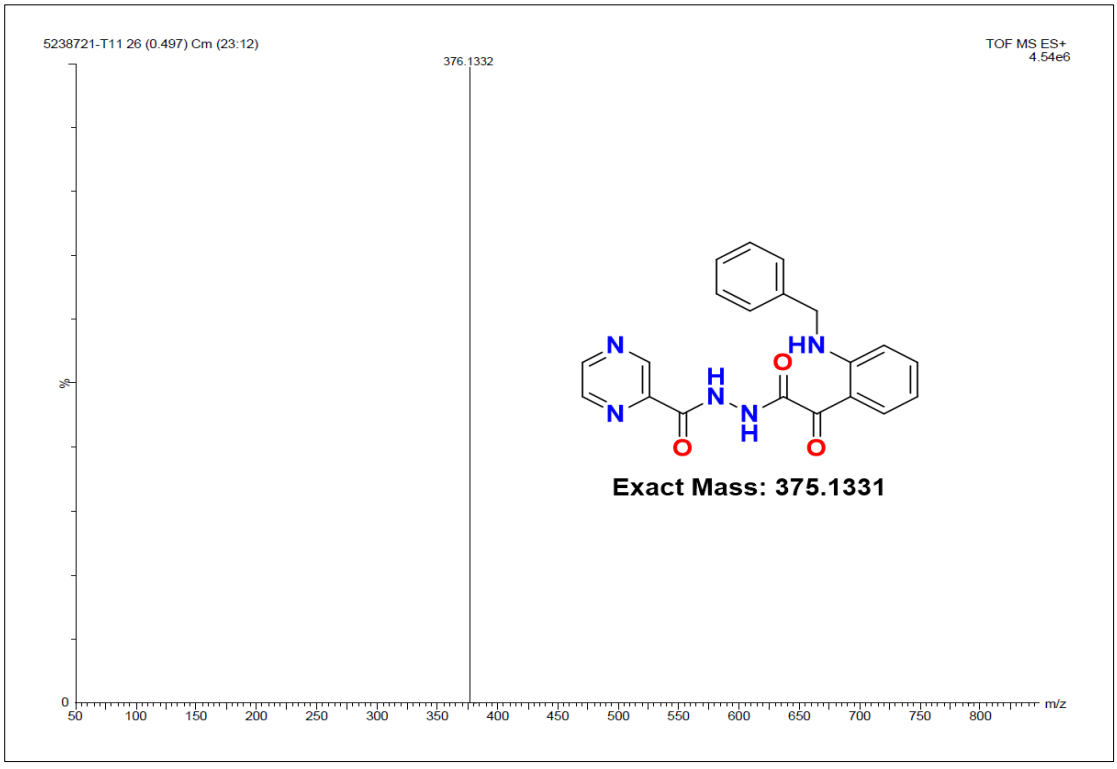

Figure 2.251 *HR-MS spectrum of compound* ***T79***

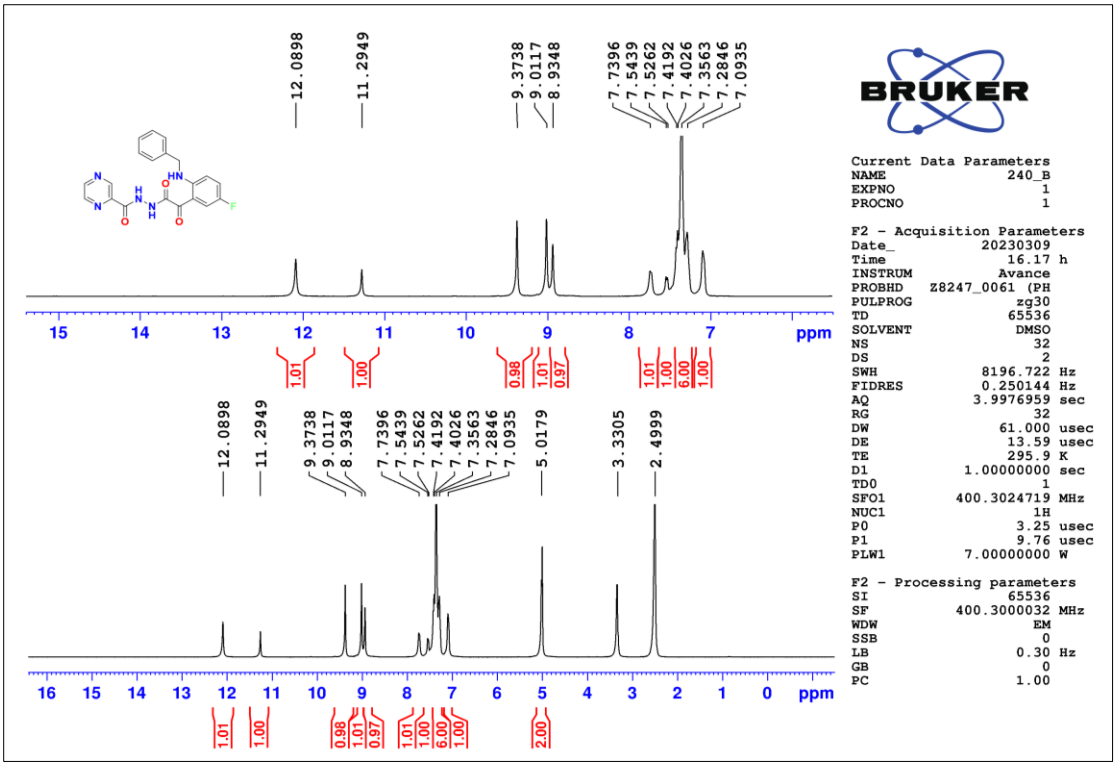

Figure 2.252 *[1]H-NMR spectrum of compound* ***T80***

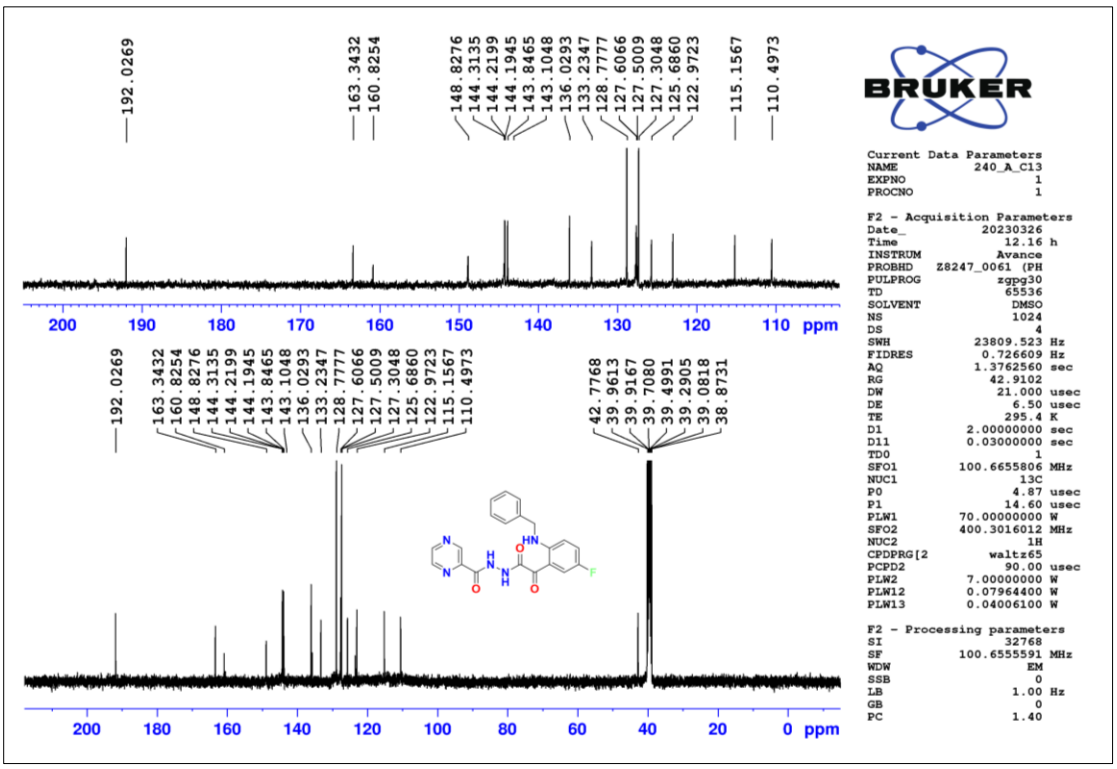

Figure 2.253 *[13]C-NMR spectrum of compound* ***T80***

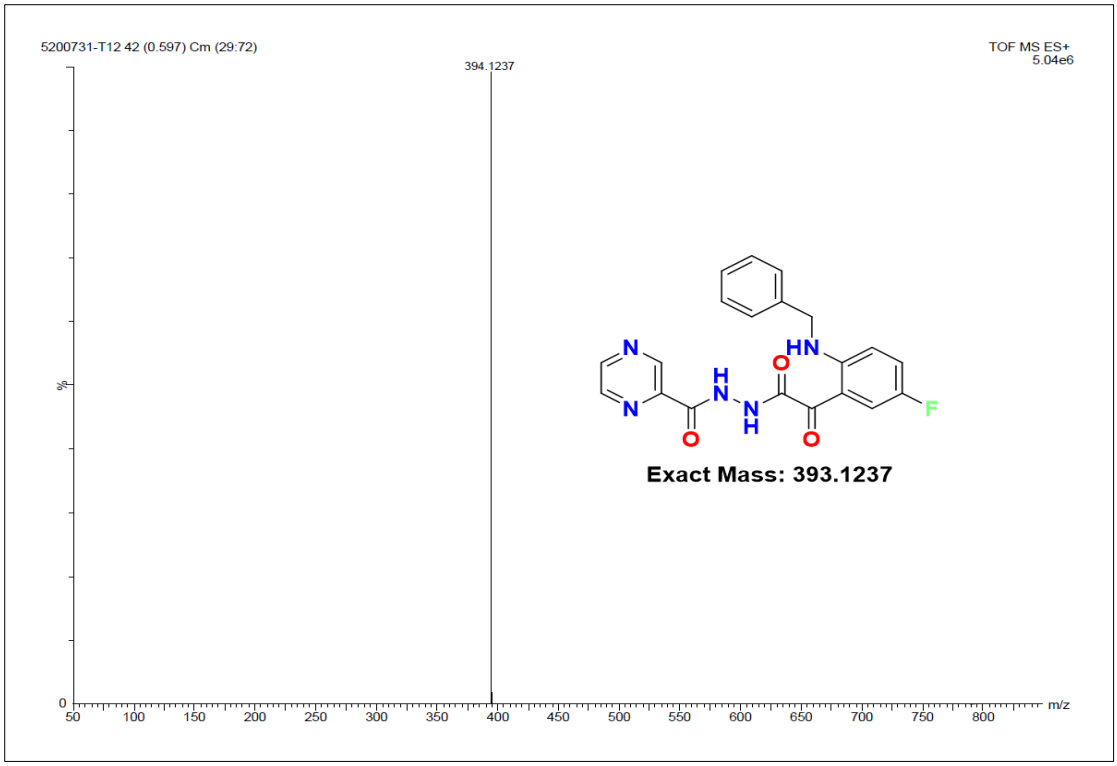

Figure 2.254 *HR-MS spectrum of compound* ***T80***

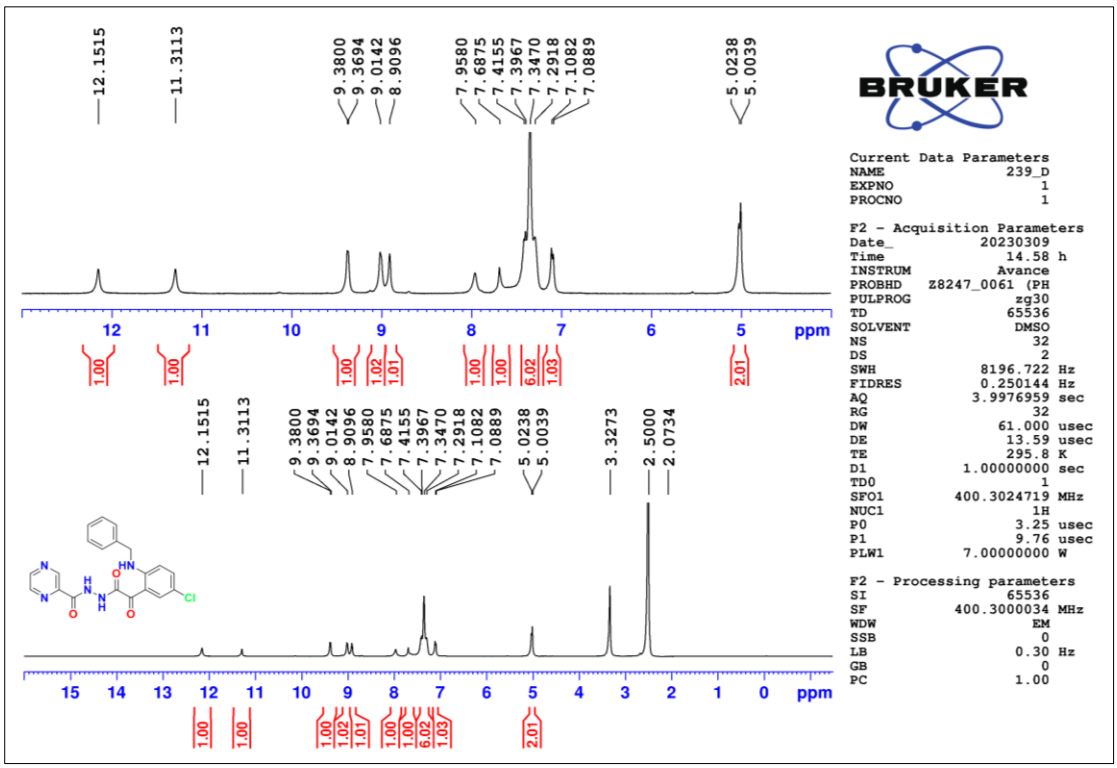

Figure 2.255 *^{1}H-NMR spectrum of compound* ***T81***

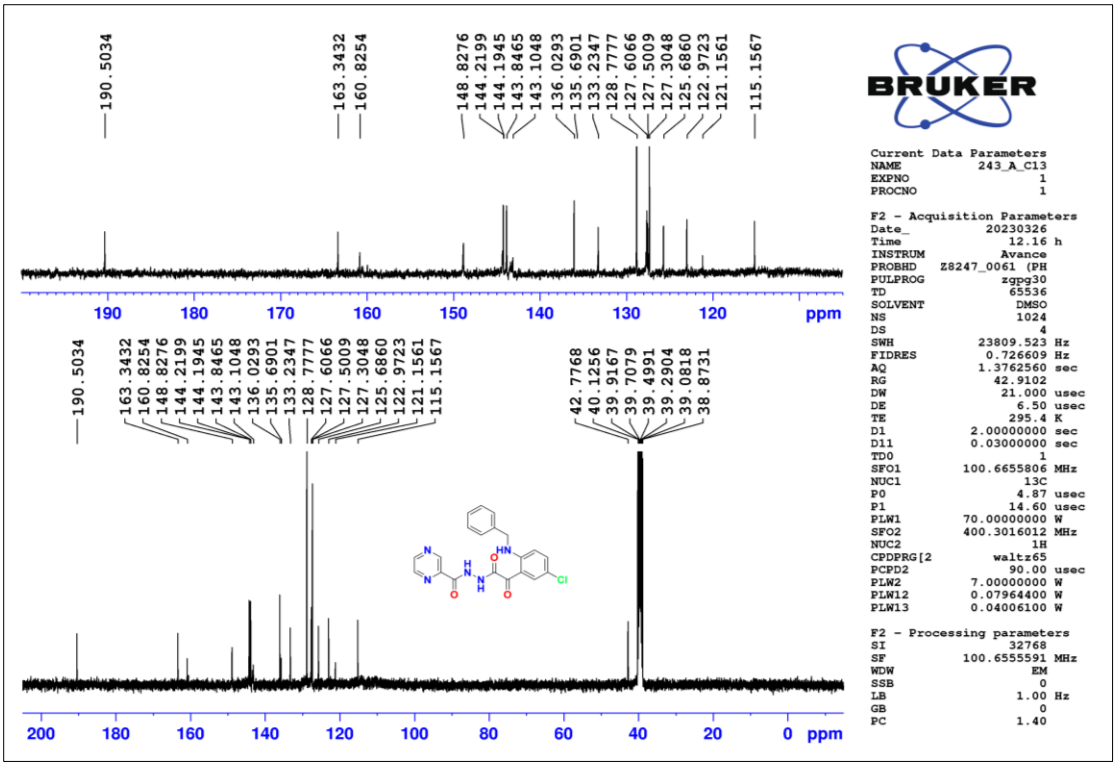

Figure 2.256 *^{13}C-NMR spectrum of compound* ***T81***

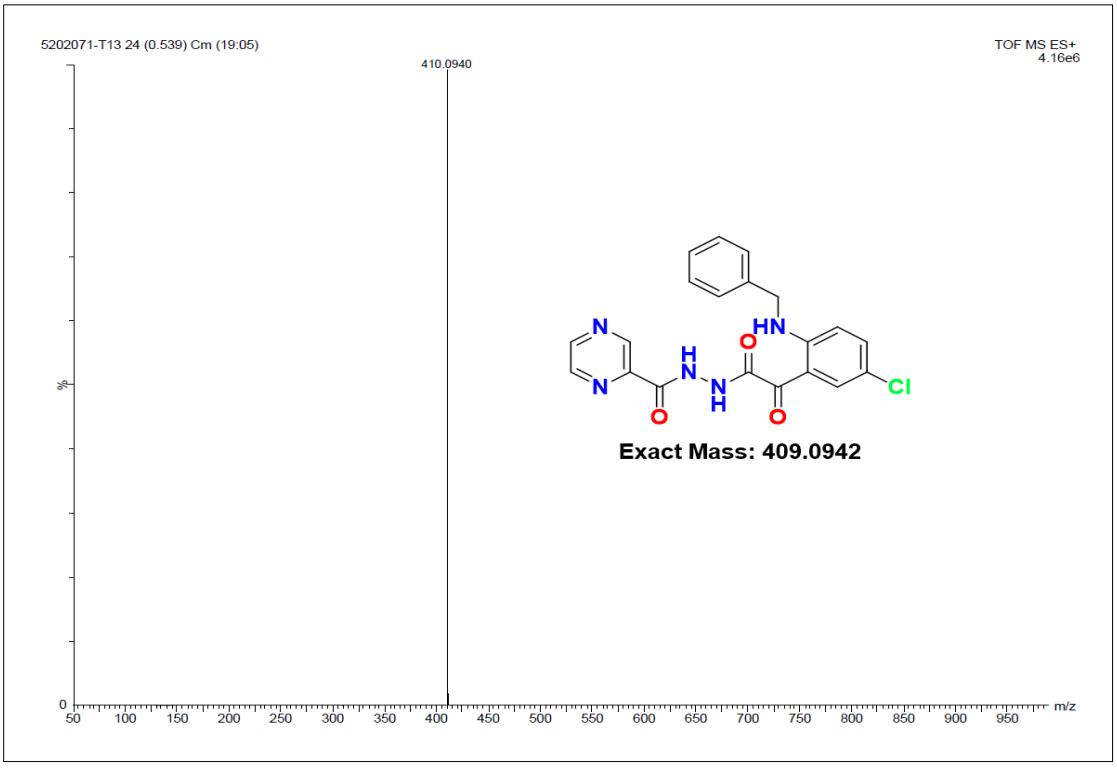

Figure 2.257 *HR-MS spectrum of compound* ***T81***

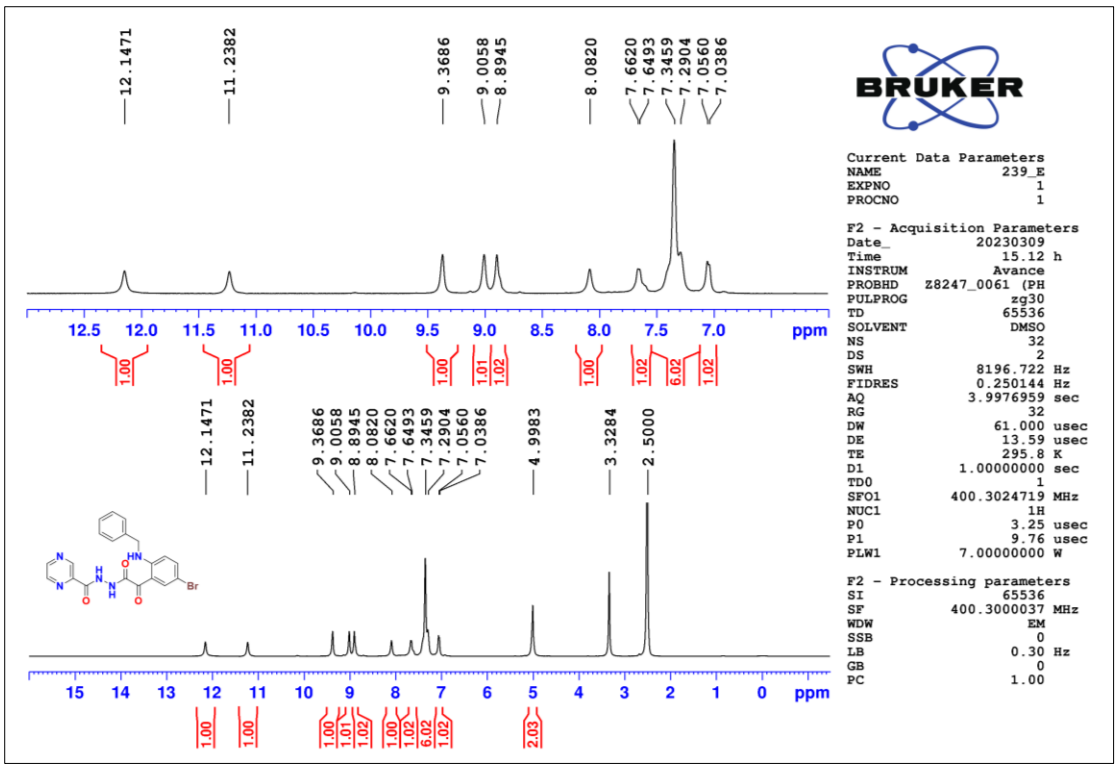

Figure 2.258 *^{1}H-NMR spectrum of compound* ***T82***

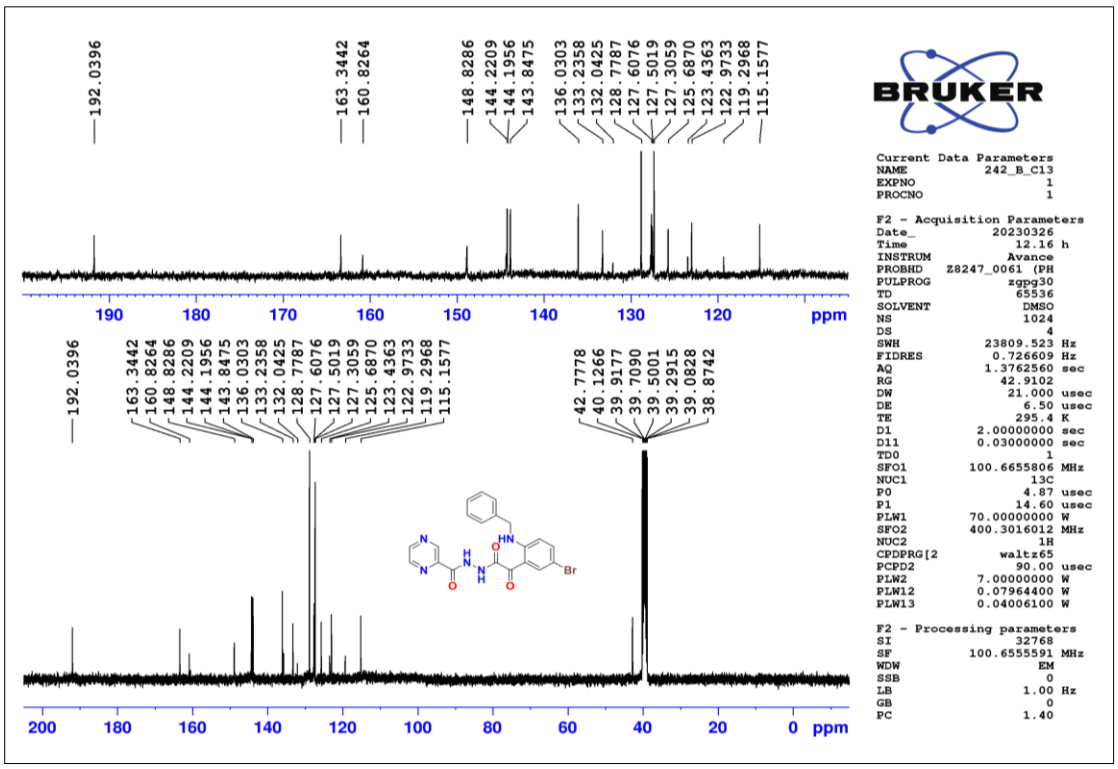

Figure 2.259 *^{13}C-NMR spectrum of compound* ***T82***

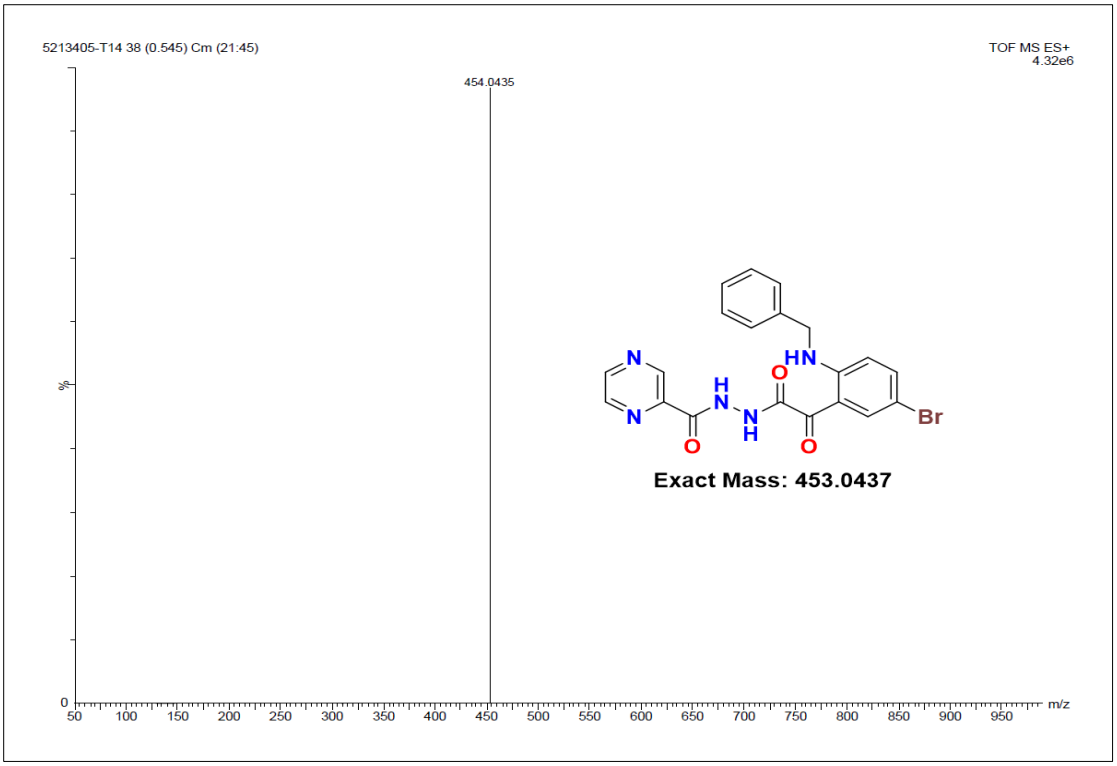

Figure 2.260 *HR-MS spectrum of compound* ***T82***

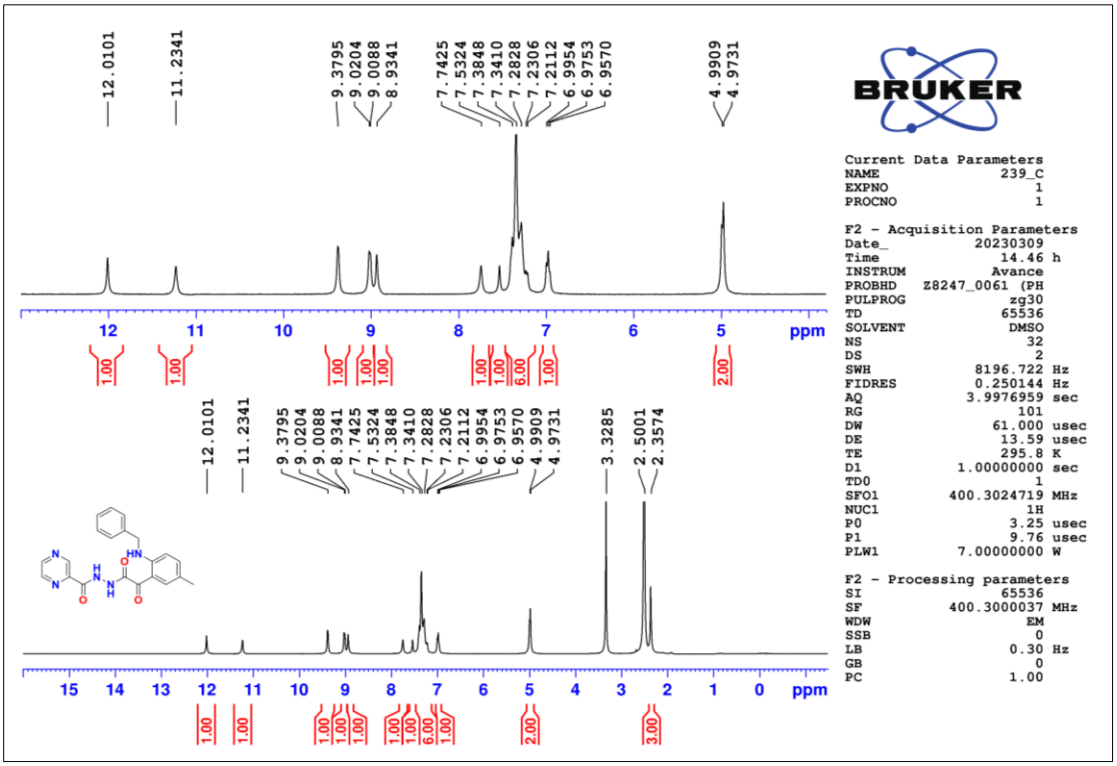

Figure 2.261 *^{1}H-NMR spectrum of compound* ***T83***

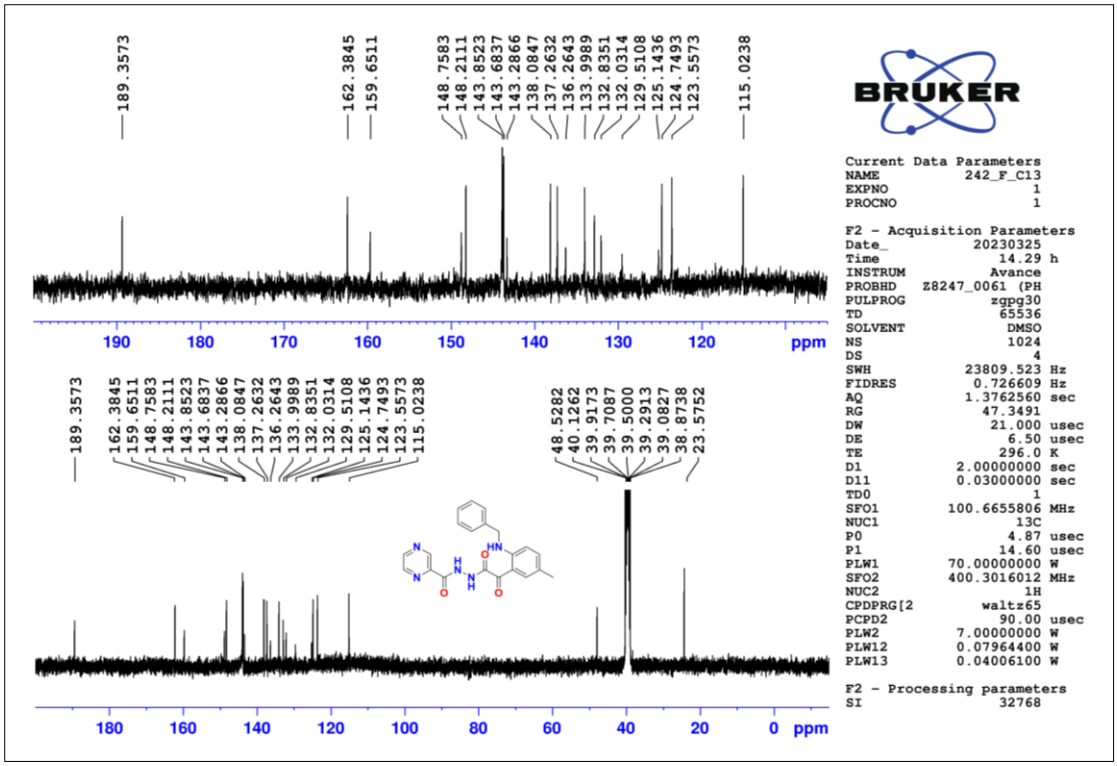

Figure 2.262 *^{13}C-NMR spectrum of compound* ***T83***

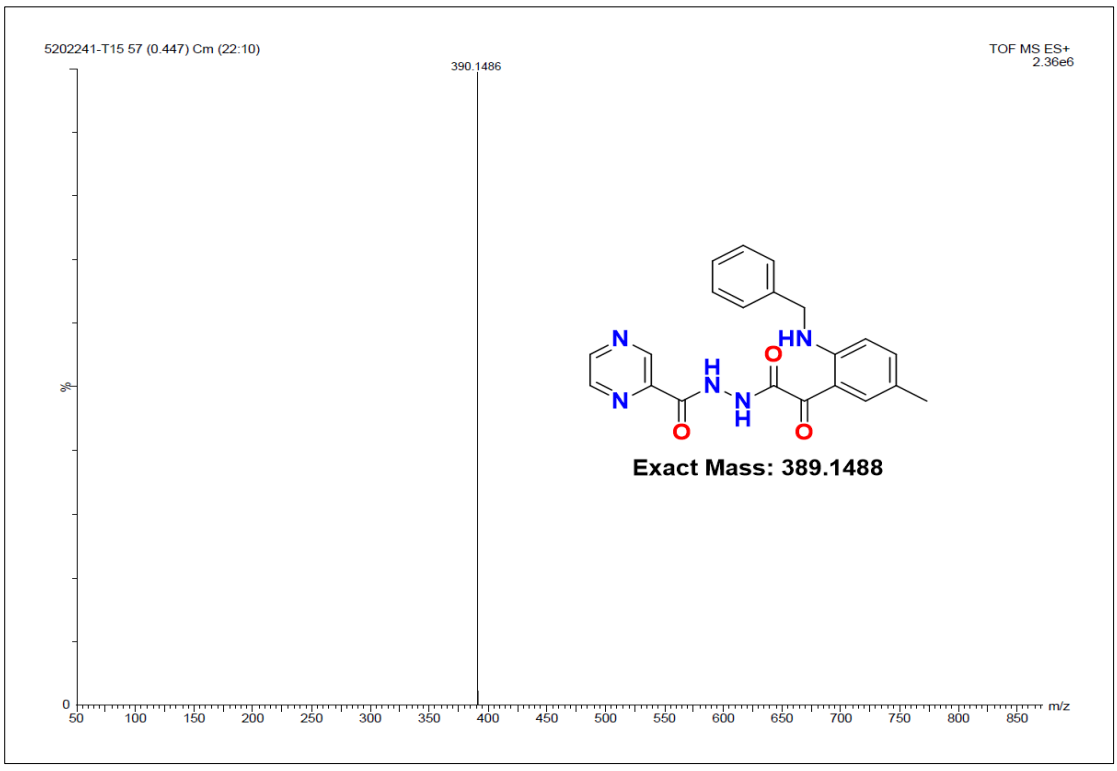

Figure 2.263 *HR-MS spectrum of compound* ***T83***

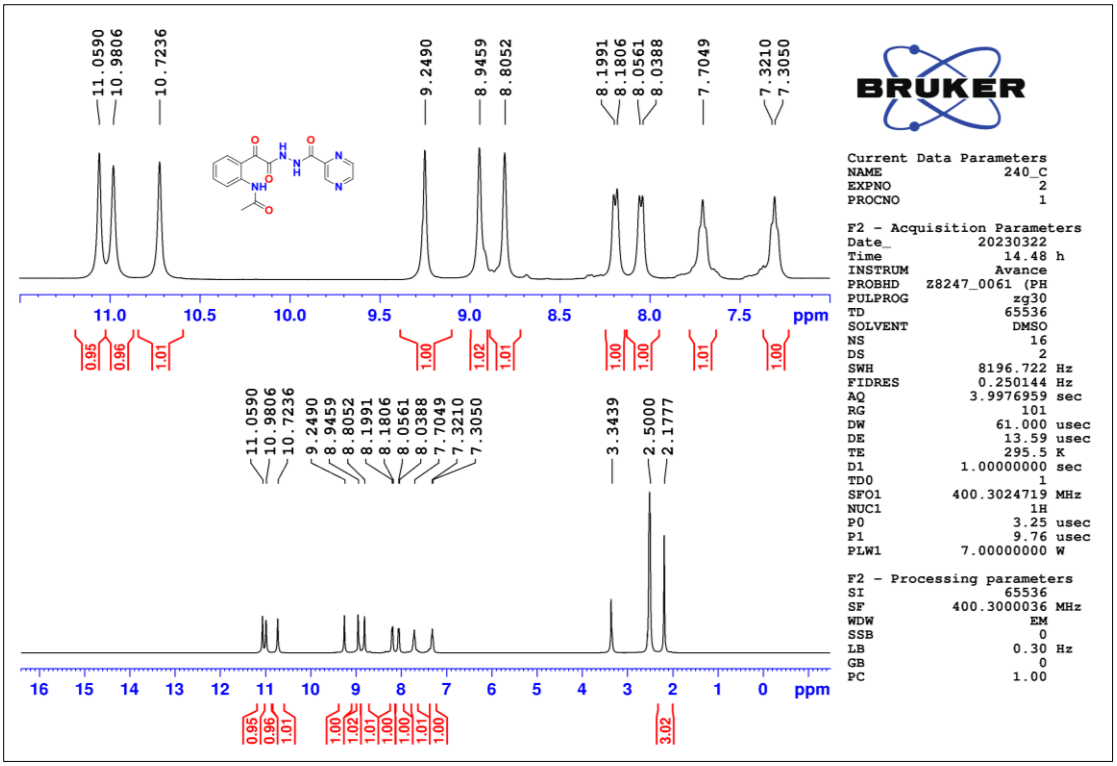

Figure 2.264 *[1]H-NMR spectrum of compound* ***T84***

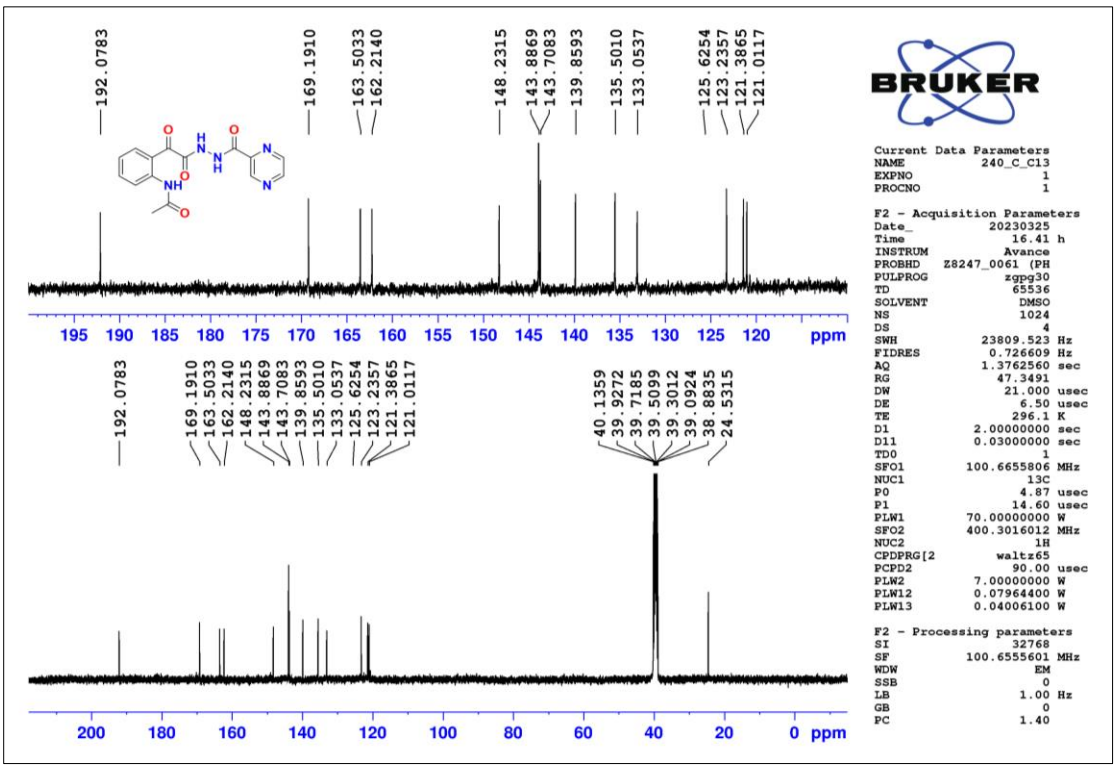

Figure 2.265 *[13]C-NMR spectrum of compound* ***T84***

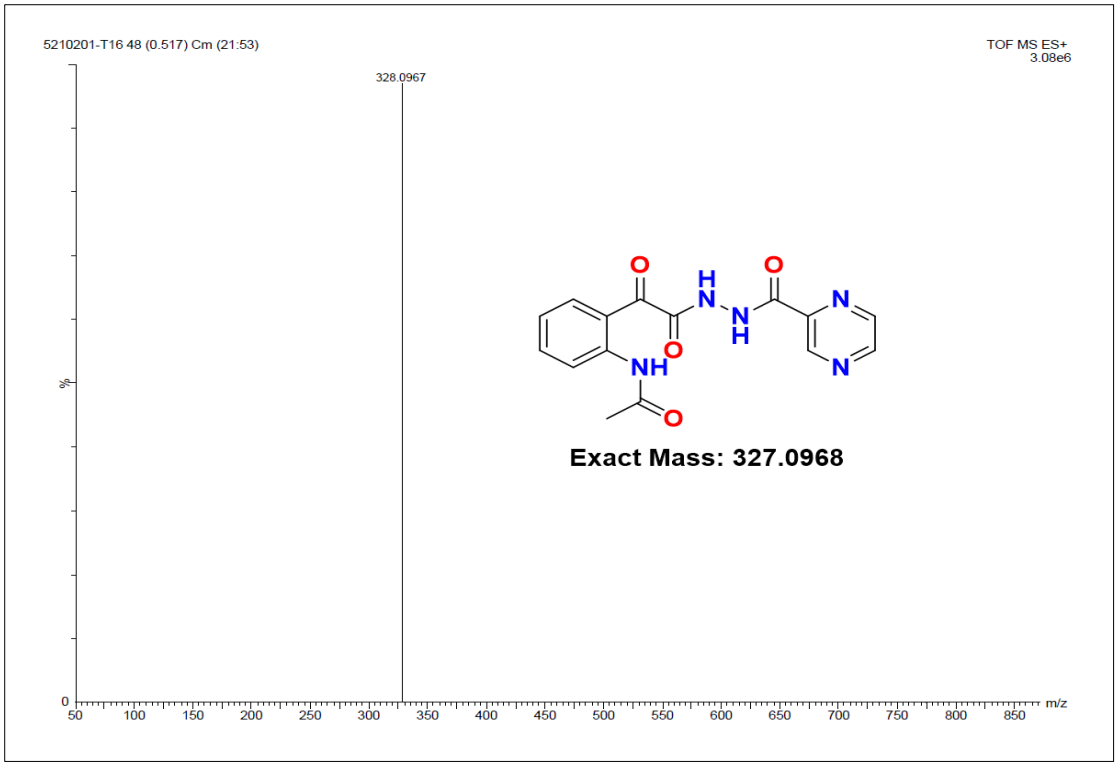

Figure 2.266 *HR-MS spectrum of compound* ***T84***

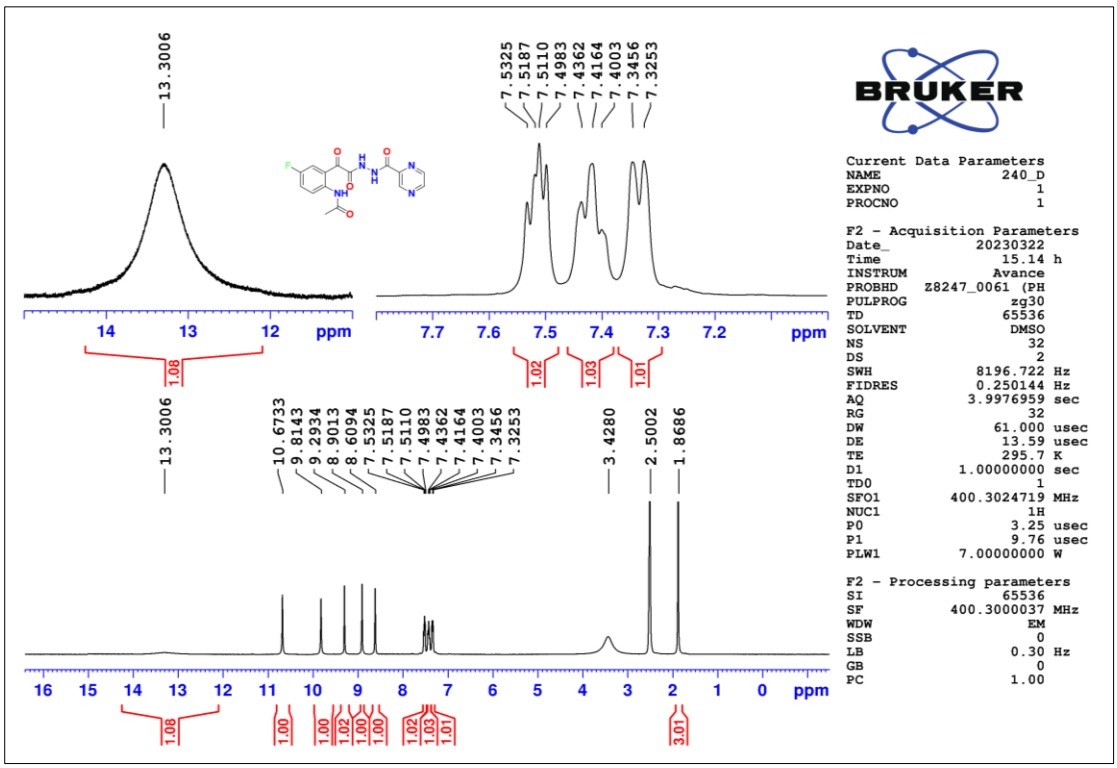

Figure 2.267 *^{1}H-NMR spectrum of compound* ***T85***

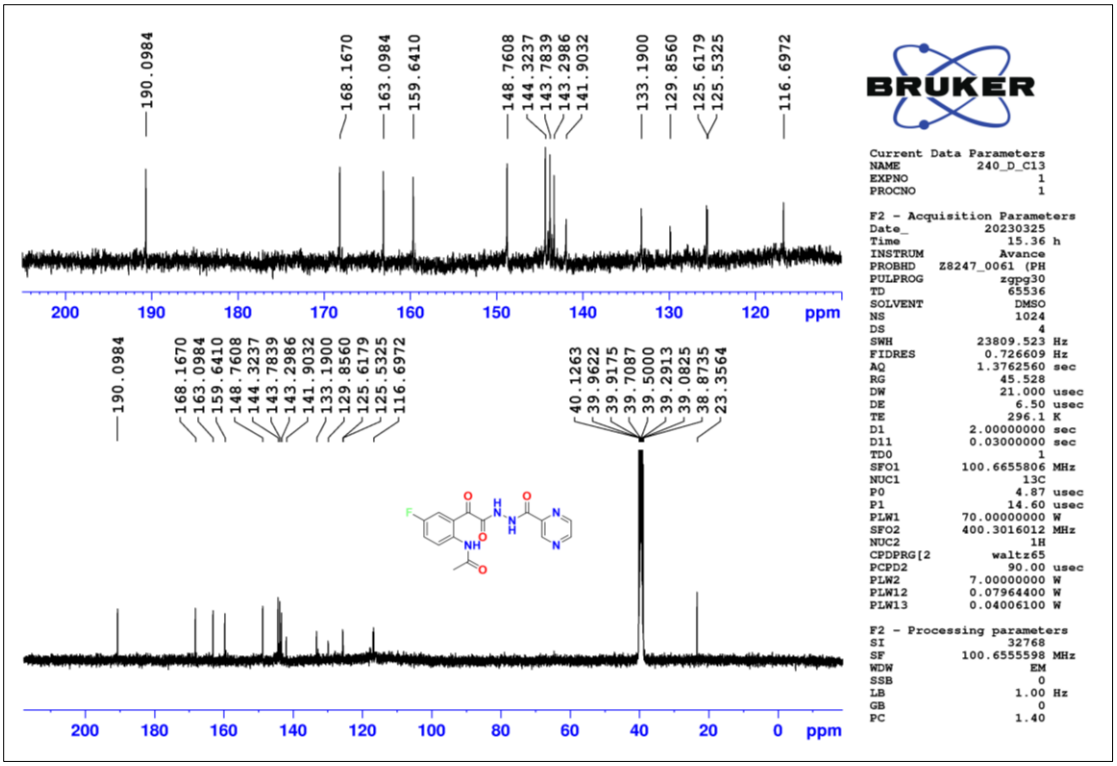

Figure 2.268 *^{13}C-NMR spectrum of compound* ***T85***

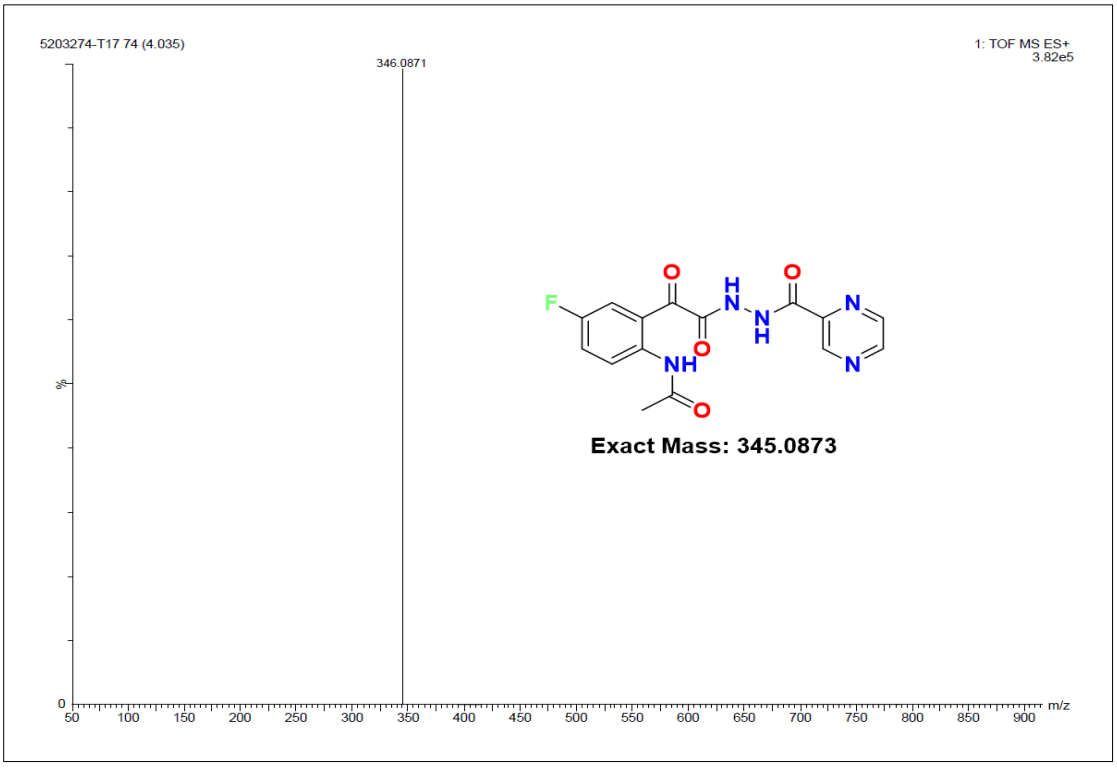

Figure 2.269 *HR-MS spectrum of compound* ***T85***

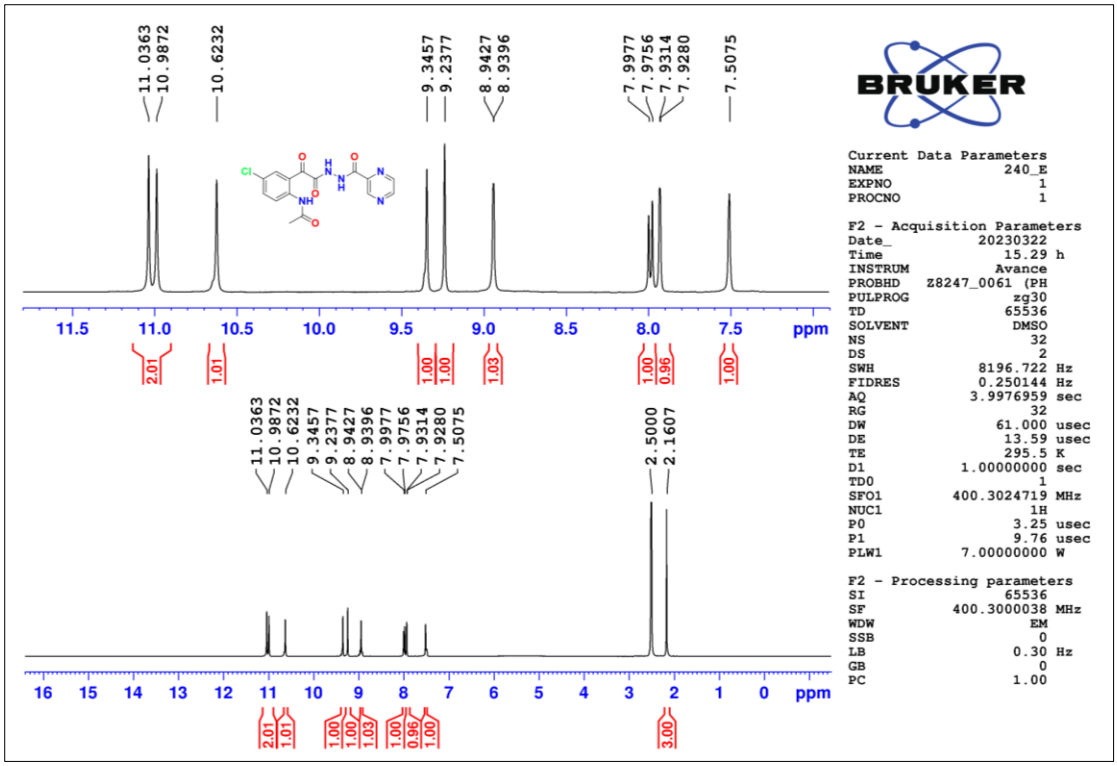

Figure 2.270 *^{1}H-NMR spectrum of compound* ***T86***

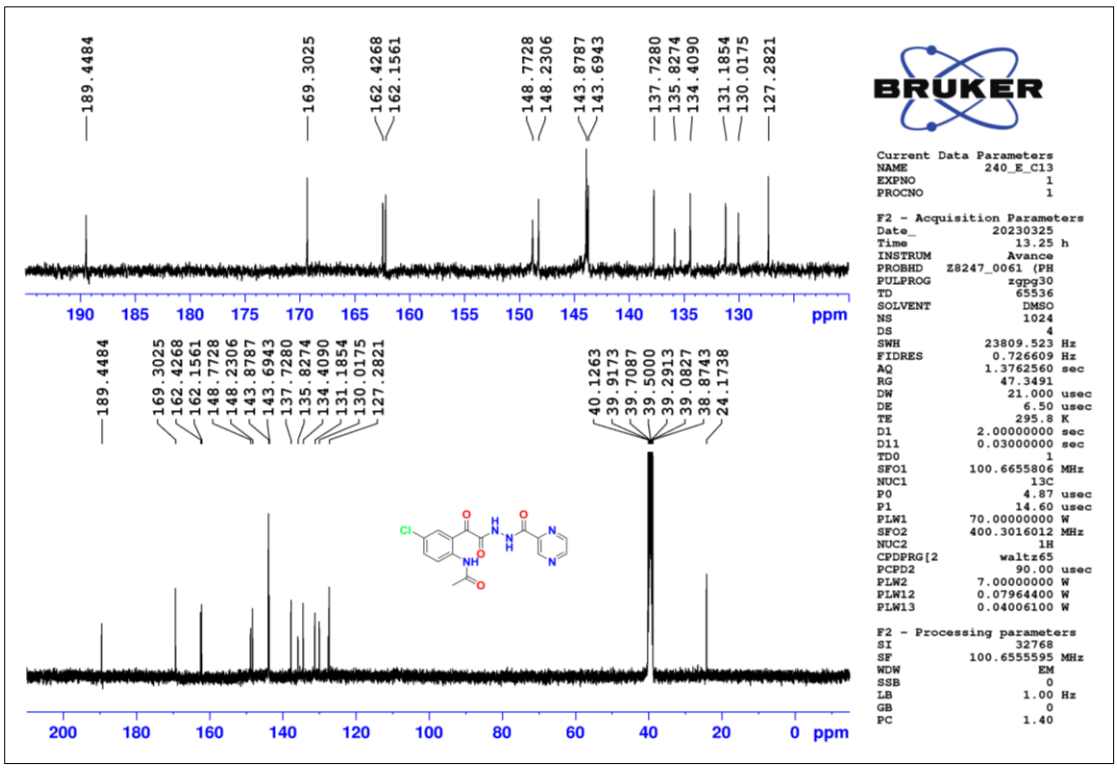

Figure 2.271 *^{13}C-NMR spectrum of compound* ***T86***

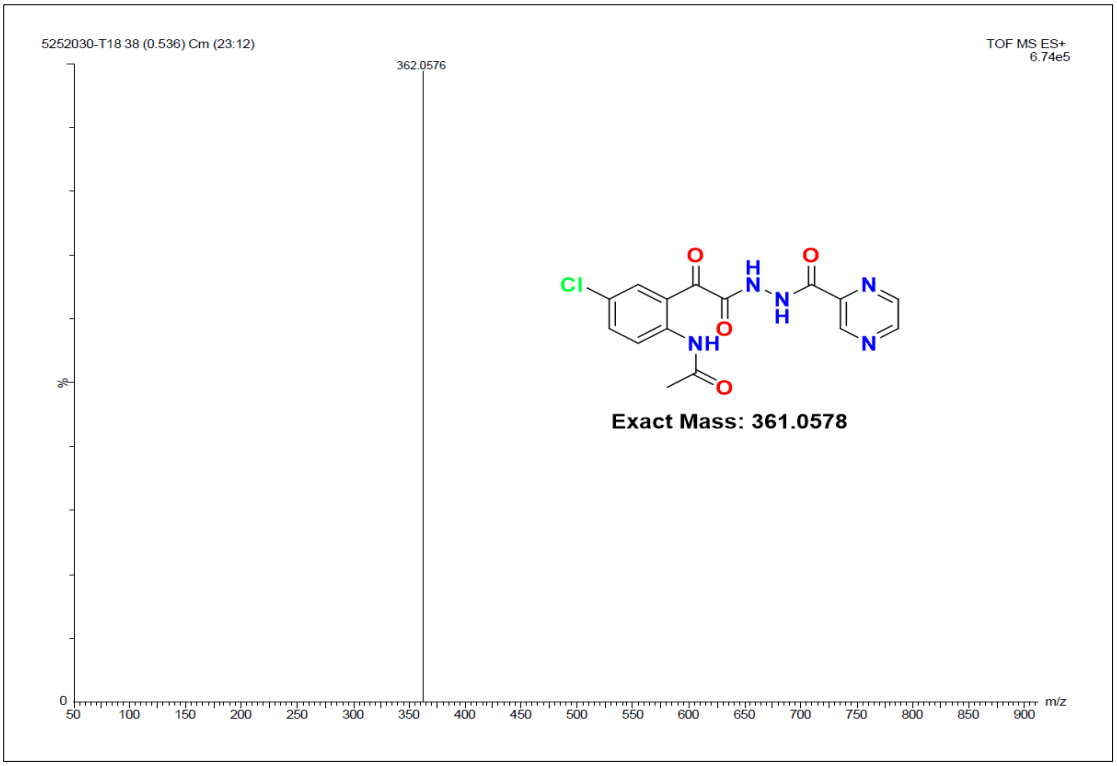

Figure 2.272 *HR-MS spectrum of compound* ***T86***

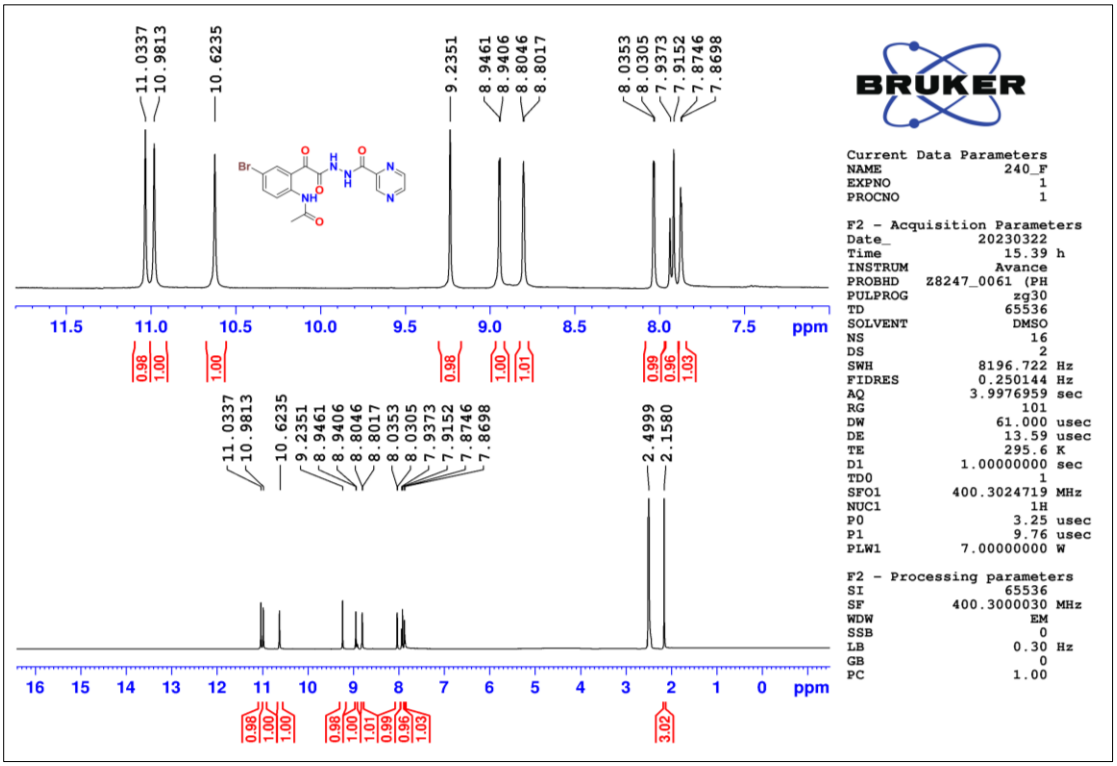

Figure 2.273 *^{1}H-NMR spectrum of compound* ***T87***

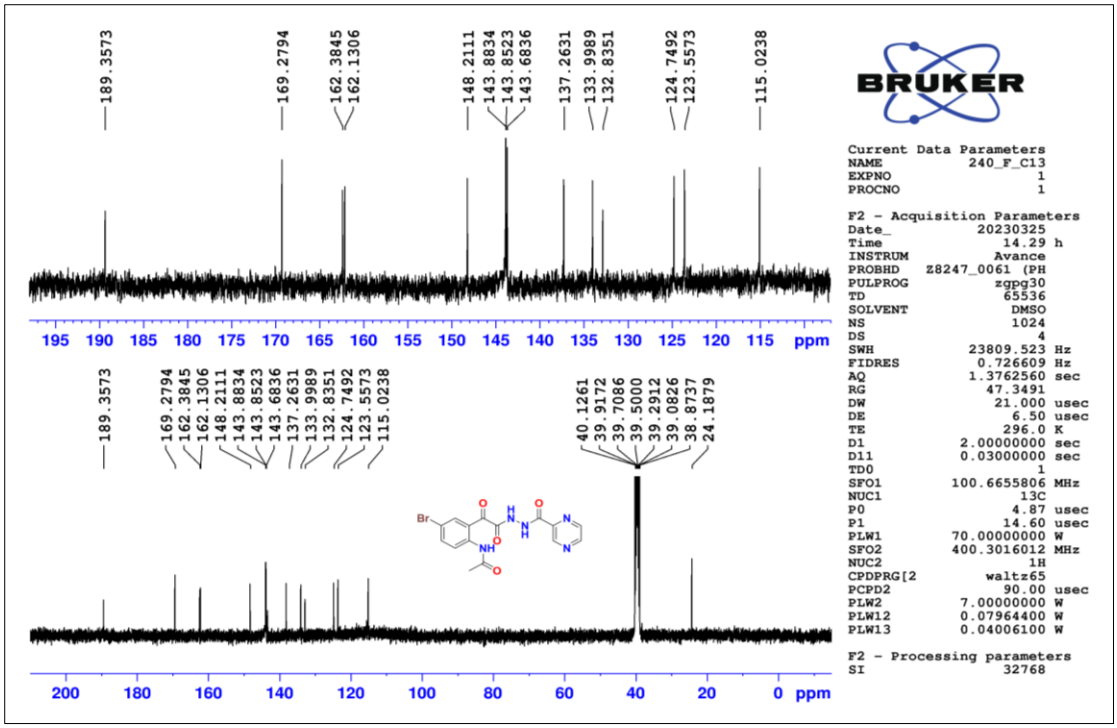

Figure 2.274 *^{13}C-NMR spectrum of compound* ***T87***

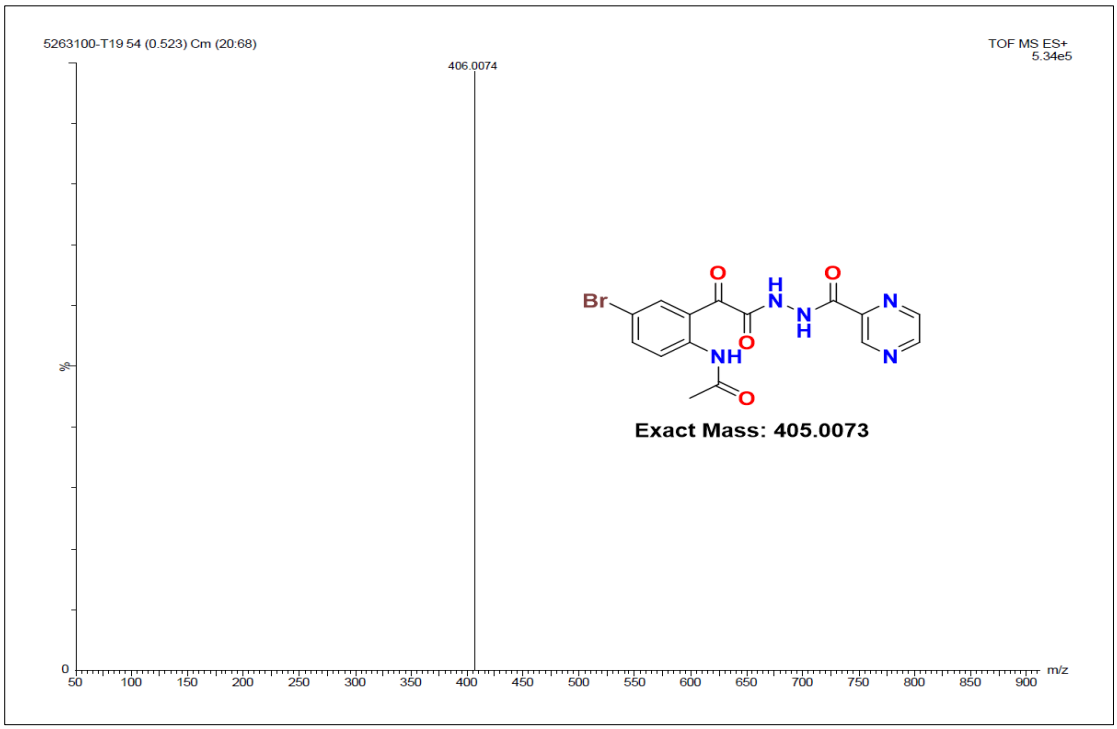

Figure 2.275 *HR-MS spectrum of compound* ***T87***

****

CHAPTER 3

BIOLOGICAL SCREENING: *IN VITRO* STUDIES ON ANTITUBERCULAR, ANTIBACTERIAL, ANTIFUNGAL ACTIVITY, AND CYTOTOXICITY

Abstract:

This chapter presents the biological evaluation of five new series of pyrazine-based compounds. It details the experimental procedures and results concerning the antitubercular, antibacterial, and antifungal activities, as well as the cytotoxicity, of the synthesized compounds.

3.1 Introduction

Microbes are minuscule living organisms, most of which can only be observed with the aid of a microscope due to their small size. They are incredibly abundant in nature, with just a teaspoon of soil containing over a million microbes. Similarly, the human body, both internally and externally, harbors vast populations of microorganisms. While over 95% of these microbes are harmless, some, known as pathogens, can cause diseases in humans and animals. Microbes occur in a variety of sizes and shapes and are mainly divided into six major types. They are bacteria, viruses, fungi, protozoa, algae, and archaea. The primary distinction between viruses and bacteria lies in their reproductive mechanisms. Viruses require a living host such as a plant or animal to reproduce, whereas most bacteria can grow on non-living surfaces. While certain bacteria have beneficial roles, all viruses are considered harmful. Bacteria typically exhibit three main shapes: spiral (spirilla), spherical (cocci), and rod-shaped (bacilli). Viruses, on the other hand, can vary in shape, appearing as rods, spheres, or multisided structures. Some viruses may resemble tadpoles. Various diseases are caused by microorganisms, some of which are significant and listed below in **Table 3.1**.

Table 3.1 *Some of the important diseases caused by microorganisms*

Infectious disease	A microbe that causes the disease	Type of microbe
Tuberculosis	*Mycobacterium tuberculosis*	Bacterium
Bubonic plague	*Yersinia pestis*	Bacterium
Whooping cough	*Bordatella pertussis*	Bacterium
Malaria	*Plasmodium falciparum*	Protozoan
COVID-19	*SARS-CoV-2*	Virus
Cold	*Rhinovirus*	Virus
Chickenpox	*Varicella zoster*	Virus
German measles	*Rubella*	Virus
AIDS	*Human immune deficiency virus*	Virus
Ringworm	*Trichophyton rubrum*	Fungus
Athlete's foot	*Trichophyton mentagrophytes*	Fungus

Antimicrobials are substances that either kill microorganisms or inhibit their growth. There are more than 15 distinct classes of antimicrobials, each differing in chemical structure and mode of action. Specific antimicrobials are required to effectively treat particular pathogens. Since their discovery, antimicrobials have played a crucial role in reducing the threat of infectious diseases. When used alongside advancements in sanitation, nutrition, housing, and widespread immunization programs, antimicrobial drugs have significantly decreased deaths from once prevalent, untreatable, and often fatal diseases. These medications have also contributed significantly to the increase in life expectancy by effectively controlling numerous serious infectious diseases. Consequently, they are often referred to as "wonder drugs" due to their remarkable impact on public health.

Antibacterial substances can be categorized into two types based on their effects on target cells. Those that actively kill microorganisms are known as "bactericidal," while those that merely hinder their growth are termed "bacteriostatic." Examples of bactericidal drugs include penicillin, cephalosporins, aminoglycosides, and quinolones. On the other hand, bacteriostatic drugs, such as tetracyclines, sulfonamides, and macrolides, only inhibit microbial growth. The choice between bactericidal or bacteriostatic drugs for treating an infection depends entirely on the nature of the infection. Also, based on their range of activity, antimicrobial drugs can be classified as (i) narrow-spectrum drugs, which are only active against a relatively small number of gram-positive organisms, (ii) moderate spectrum drugs, which are effective against gram-positive and the most systemic, enteric and urinary tract gram-negative pathogens, (iii) narrow and moderate spectrum drugs like beta-lactam antibiotics, (iv) broad-spectrum drugs which are active against all prokaryotes with two exceptions, *Mycobacteria* and *Pseudomonas* and (v) drugs which are effective against *Mycobacteria* only.

3.1.1 Mode of action of antimicrobials

Antimicrobial agents work by targeting different components within microbial cells, such as their cell walls, plasma membranes, nucleic acids, and protein synthesis machinery. While the exact mechanisms of action are not fully understood, proposed views suggest how these agents may function. Below is a schematic representation (**Figure 3.1**) illustrating the potential mechanisms of action of antimicrobial agents.

- **Inhibition of cell wall synthesis**: β-Lactam antibiotics are bacteria-killing agents that work by blocking the production of the peptidoglycan layer within bacterial cell walls. This layer is crucial for maintaining the structural strength of the cell wall, particularly in Gram-positive bacteria, where it serves as the outermost and most essential component. The last step in peptidoglycan synthesis, called transpeptidation, is facilitated by enzymes known as Penicillin-binding proteins.
- **Inhibition of protein synthesis**: A protein synthesis inhibitor is a substance that hinders the growth or reproduction of cells by interfering with the processes

directly involved in creating new proteins. Various antimicrobial agents, such as chloramphenicol, erythromycin, streptomycin, and tetracyclines, function by impeding protein synthesis. Because ribosomes in prokaryotic cells have slight structural differences compared to those in eukaryotes, they can be targeted by these inhibitors.

- **Injury to the plasma membrane**: Certain antibacterial and antifungal agents operate by targeting specific mechanisms within microbial cells. Antifungal medications primarily act on fungus cell membranes, exploiting the presence of ergosterol instead of cholesterol. Despite their efficacy against microbial pathogens, these antimicrobials can pose significant toxicity risks to the host. Examples of such agents include polymixins (antibacterial), amphotericin B, miconazole, and ketoconazole (antifungals).
- **Inhibition of nucleic acid synthesis**: There are two main types of antibacterial agents that work by preventing the production of nucleic acids: DNA inhibitors and RNA inhibitors. DNA inhibitors, like quinolines, target DNA gyrase, while RNA inhibitors, such as rifampicin, target RNA-dependent RNA polymerase.
- **Inhibition of the synthesis of essential metabolites**: Sulfa drugs and trimethoprim typically operate through this mechanism. They disrupt the pathway bacteria use to synthesize folic acid. Because humans produce folic acid through a distinct pathway, these drugs have minimal impact on human cells.

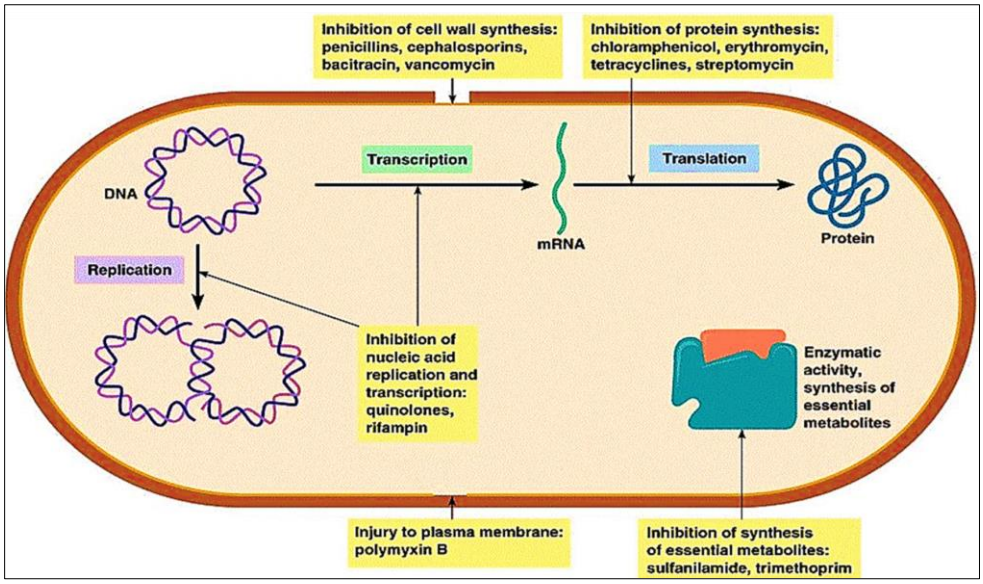

Figure 3.1 *Schematic representation of the mechanism of action on the bacterial cell* (Source:http://classes.midlandstech.edu/carterp/Courses/bio225/chap20/lecture2.htm)

3.1.2 Antimicrobial screening

Various methods are employed to investigate the antimicrobial activity of compounds, encompassing both *in vitro* and *in vivo* approaches. *In vitro* methods are commonly utilized for the initial assessment of antibacterial, antifungal, and antitubercular activities. Conversely, *in vivo* studies on animal models of human conditions are essential for understanding antimicrobial mechanisms and developing effective drugs to combat pathogenic microbes. Additionally, toxicity studies, typically conducted on non-cancerous cells to determine IC_{50} values, are crucial before advancing substances to clinical trials. Over the past few decades, the Clinical and Laboratory Standards Institute (CLSI) has developed various experimental procedures for Antimicrobial Susceptibility Testing (AST). These procedures set standards for conducting tests to assess the effectiveness of antimicrobial agents against microbes. AST methods are crucial for determining the molecular potency of antimicrobials. Typically, *in vitro* antimicrobial susceptibility testing methods fall into three main categories: (i) diffusion, (ii) dilution, and (iii) combined diffusion and dilution methods. Below, we'll discuss some significant antimicrobial testing methods in detail.

3.1.2.1 Diffusion method

The diffusion method encompasses two significant techniques: the Stokes method and the Kirby-Bauer method. These techniques are commonly employed for antimicrobial susceptibility testing, a practice strongly endorsed by the National Committee for Clinical Laboratory Standards (NCCLS).

Stokes method: In this method, a known quantity of bacteria is cultured on agar plates alongside thin wafers containing standard antibiotics. If the bacteria are vulnerable to a specific antimicrobial, an area of clearing forms around the wafer where bacteria cannot grow, known as a zone of inhibition. Additionally, the rates of antimicrobial diffusion are measured, helping to estimate the bacteria's sensitivity to that particular antimicrobial agent. Generally, larger zones indicate lower concentrations of test compounds required to inhibit the microorganism. This data aids in selecting suitable antimicrobials to treat a specific infection.

Kirby-Bauer method: This method, also known as the disk diffusion method, is widely used to test bacterial susceptibility to antibiotics. It helps determine the most effective antibiotics for a particular infection. In this test, a culture medium like Mueller-Hinton agar is spread uniformly with the bacteria. Then, paper discs soaked in specific concentrations of antibiotics are placed on the agar. As the bacteria grow, the antibiotics work to inhibit their growth. If the bacteria are susceptible to a particular antibiotic, no growth will occur around the antibiotic disc. This creates a visible zone of inhibition, which can be measured to determine the bacteria's susceptibility to that antibiotic.

3.1.2.2 Dilution method

Dilution methods primarily consist of the minimum inhibitory concentration (MIC) method. This method can be further categorized into broth dilution and agar dilution methods.

Minimum inhibitory concentration method: The MIC method is commonly employed to determine the lowest concentration of an antimicrobial required to completely inhibit or kill microorganisms. This is typically accomplished by diluting

the antimicrobial solution in either agar or broth media. The dilutions are typically expressed in log2 serial dilutions, which means each dilution is two-fold weaker than the previous one. In this method, the pure culture of a single microorganism is first grown in an appropriate broth. This culture is then standardized using standard microbiological techniques, aiming for a concentration of around 1 million cells per milliliter. The compound being tested is then diluted multiple times, usually in a 1:1 ratio, using a sterile diluent. After dilution, a volume of the standardized inoculum equivalent to the volume of the diluted compound is added to each dilution vessel, ensuring a microbial concentration of approximately 500,000 cells per milliliter. The inoculated, serially diluted antimicrobial agent is then incubated. Following incubation, the dilution vessels are examined for microbial growth, typically indicated by turbidity or color change. The last tube in the dilution series that shows no growth corresponds to the MIC of the antimicrobial agent.

Broth dilution method: The Broth dilution method is a straightforward approach used for testing isolates, even if there's only one. Here's how it works: the antimicrobial agent is gradually diluted in a liquid medium. Then, a standardized number of organisms is added, and the mixture is left to incubate for a set period. The lowest concentration of antibiotics preventing the appearance of turbidity is considered to be the minimal inhibitory concentration. An additional advantage of this method is that the same tubes can be used to determine Minimum Bactericidal Concentrations (MBC) as well.

Agar dilution method: In this method, the compounds being tested are diluted using log2 dilution intervals. Each petri dish contains a solution with 50 percent of the concentration of the compound in the previous dilution. After dilution, the solution is mixed into agar medium by gently rotating it and then poured into a petri dish. Additionally, a control plate without any antimicrobial agent is used alongside each compound to monitor the growth of both the test and control strains. Readings are taken after the Petri dishes have been incubated. One key advantage of this method is its ability to test multiple organisms on the same plate.

3.1.2.3 Dilution and Diffusion Method

The dilution and diffusion method, also known as the E-test, is a convenient way to assess the susceptibility of substances to antimicrobial agents. This method involves creating a gradient of antimicrobial concentration on a carrier strip, which is then placed on an agar plate inoculated with bacteria. After incubation, a symmetrical zone of inhibition forms, and the point where this zone intersects the strip indicates the MIC of the antimicrobial agent. The E-test is straightforward, reliable, and provides MIC values over a wide concentration range with precision. It is particularly useful for organisms like *H. influenzae*, but its cost and limited availability can be drawbacks. Another cutting-edge approach for detecting antimicrobial resistance is genotypic testing, which involves identifying specific resistance genes in bacteria. Various DNA-based assays are being developed for this purpose, offering increased sensitivity, specificity, and speed compared to traditional methods. When used alongside phenotypic analysis, these genotypic techniques enhance the accuracy and efficiency of antimicrobial susceptibility testing (AST).

3.2 Materials and Methods

3.2.1 Antitubercular activity

The antitubercular activity of the synthesized compounds against *M. tuberculosis* was performed using the microplate alamar blue assay (MABA) method, which is non-toxic and uses a thermally stable cell permeable reagent such as resazurin (Franzblau et al. 1998). To reduce the medium evaporation in the test wells while incubation 200 µL of sterile deionized water was added to all test wells of sterile 96-well plates. The synthesized compounds and standard drugs were prepared in two-fold dilutions (50.0, 25.0, 12.5, 6.25, 3.13, 1.56, and 0.78 µg/mL) by dissolving in DMSO. 100 µL of the Middlebrook 7H9 broth with 0.2% glycerol and 10% oleate-albumin dextrose-catalase (OADC), 100 µL of *M. tuberculosis* H37Rv (ATCC27294) inoculum was supplemented into 7H9 broth wells containing ten-fold serial dilutions of drugs per mL. Plates were covered with parafilm and incubated at 37 ℃ for five days. After this, a freshly prepared 1:1 mixture of Alamar blue reagent and 10% tween 80 was added to the wells and incubated for 24 hours at 37 ℃. The color of the wells was recorded. The

pink color represents the growth of bacteria whereas, the blue color represents the inhibition of bacteria. The minimum inhibition concentration is defined as the minimum concentration of a compound required to inhibit the growth of bacteria. Pyrazinamide (PZA), Ciprofloxacin (INN), and Streptomycin (STM) were used as reference drugs for comparison.

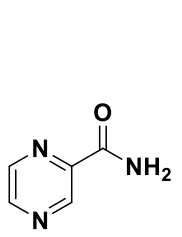

Pyrazinamide

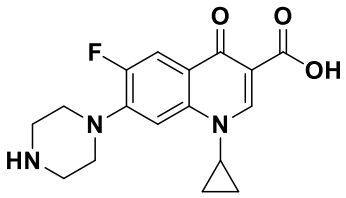

Ciprofloxacin

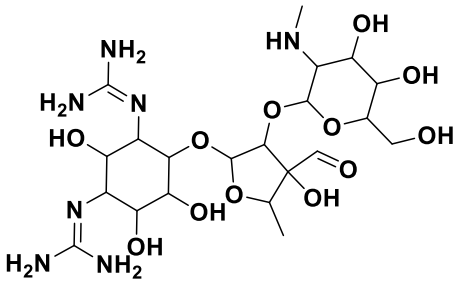

Streptomycin

3.2.2 Antibacterial activity

The antibacterial activities of newly synthesized compounds were determined by the broth microdilution method. Overnight-cultured pure strains of two Gram-positive bacteria (*Staphylococcus aureus, Streptococcus mutans*) and two Gram-negative bacteria (*Escherichia coli, Salmonella* Typhi) were introduced into Mueller Hinton Broth (MHB) and permitted to proliferate at 37 °C until reaching a density akin to 0.5 McFarland unit. A 96-well microtiter plate was employed, with 95 µl of MHB added uniformly across all wells. Initially, 100 µl of the compound was introduced into the initial well and thoroughly amalgamated through pipetting. Sequentially, 100µl from the initial well was transposed to the subsequent well, and this process continued up to the ninth well, while the suspension from the ninth well was discarded. Subsequently, 5 µl of the respective bacterial cultures was added to all wells. The tenth well functioned as a compound control, containing 95 µl of MHB and 5 µl of the compound. The eleventh was well-acted as a culture control, harboring 95 µl of MHB and 5 µl of the bacterial culture. Finally, the twelfth well operated as a media control, containing solely 95 µl of MHB. Streptomycin (STM) and Chloramphenicol (CHL) were used as antibacterial standards (Heatley 1943).

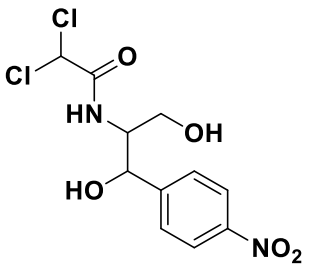

Chloramphenicol

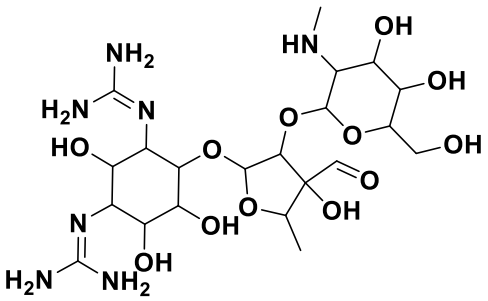

Streptomycin

3.2.3 Antifungal activity

The antifungal activity of newly synthesized compounds was carried out by the broth microdilution method. The pure fungal culture of *Aspergillus niger*, cultivated overnight, was strategically applied in small doses onto Potato Dextrose Agar (PDA) plates. These plates underwent an incubation period at 30 °C lasting 3 to 4 days, fostering the proliferation of an extensive layer of fungal spores. Subsequently, these spores were meticulously harvested using sterilized cotton swabs and then suspended within PDB. A 96-well microtiter plate was meticulously prepared, with each well receiving 95 µl of MHB. Initially, 100 µl of a particular compound was added to the first well, thoroughly blending it using precise pipetting techniques. This process of transferring 100 µl from each well to the subsequent one was rigorously executed until reaching the ninth well, after which the resultant suspension was carefully discarded. At this stage, 5 µl of the previously prepared fungal spore suspension was uniformly introduced into all wells, except for the tenth well, designated as the compound control, containing 95 µl of MHB and 5 µl of the compound. The eleventh well served as a control for the culture, comprising 95µl of MHB and 5µl of fungal spores. Finally, the twelfth well functioned as the media control, solely containing 95µl of MHB without any additional components. Amphotericin B (AmB) was used as an antifungal standard (Heatley 1943).

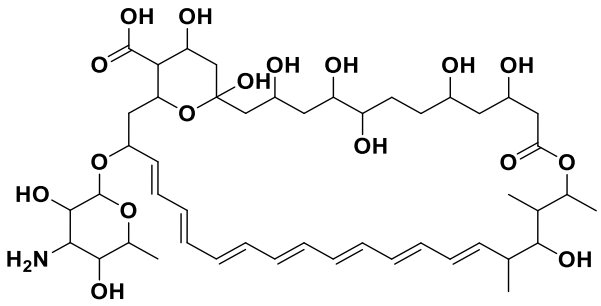

Amphotericin B

3.2.4 Cytotoxicity Studies

The cytotoxicity of the active compounds was determined using MTT assay. The VERO cell line (African green monkey kidney: Cat. no. 11965-092) was procured from the National Center for Cell Sciences (NCCS), Pune, India. The cell lines were seeded in 96 well flat-bottom microtiter plates accommodating DMEM media which was supplemented with 10% heat-inactivated fetal calf serum (FBS) and added 1% Antibiotic-Antimycotic 100X solution (Espíndola et al. 2022). The cells were incubated at 37 ℃ (95% humidity and 5% CO_2) for 24 hours. The target compounds were prepared in different concentrations (100, 75, 50, and 25 µg/mL) by dissolving them in distilled DMSO. The cells were then treated to different drug concentrations and incubated for another 72 hours. The cells in the well were washed twice with phosphate buffer solution, then a stock solution of MTT (20 µL, 5mg/mL in sterile PBS) was added to each well, and cells were incubated for another 4 hours at 5% CO_2 atmosphere. After the supernatant was flicked off from the incubator, 100 µL of DMSO was added to dissolve the formed crystals. The absorbance of wells containing cells and blanks was recorded at 570 nm using a microplate reader. The percentage of growth inhibition was calculated using the equation: % Growth Inhibition = (Mean OD of target compound/Mean OD of Negative control) x 100.

3.3 Results and Discussions

3.3.1 Antitubercular, antibacterial, and antifungal activity of 1,3,4-oxadiazole/[1,2,4] triazolo[3,4-*b*][1,3,4]thiadiazine incorporated pyrazine derivatives (T1-T18)

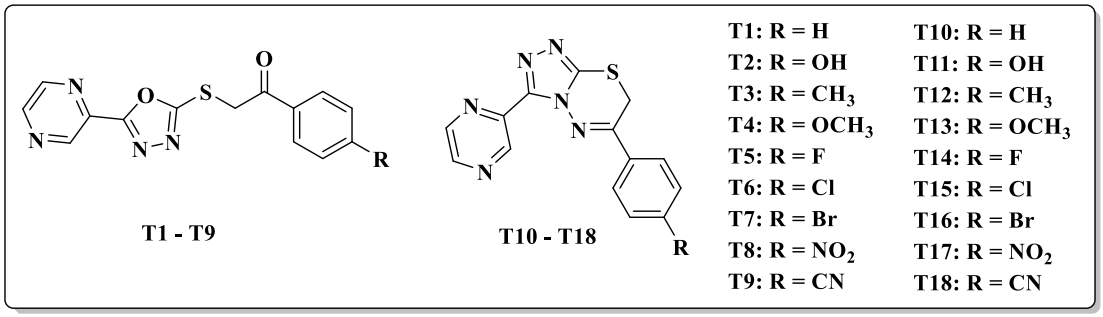

In this series 18 compounds were synthesized. The newly synthesized compounds (**T1-T18**) were screened for their *in vitro* antitubercular activity against *mycobacterium tuberculosis* H37Rv (ATCC27294) using PZA, INN, and STM as standard by the MABA method, and their MIC values (µg/mL) were determined, as shown in **Table 3.2**. The antitubercular screening revealed that few of the tested compounds showed good inhibition against the tested strain compared to the standard drugs. Among the synthesized compounds, **T7**, **T8**, and **T17** exhibited the highest potency among the series, with an MIC of 1.56 µg/mL. These compounds are twice as potent as the standard TB drugs PZA and INN and four times more effective than STM in terms of the MIC value. Additionally, compounds **T2, T3, T4, T9,** and **T16,** demonstrated equivalent antitubercular activity with a MIC of 3.12 µg/mL, matching the effectiveness of PZA and INN and surpassing STM by a factor of two. In contrast, compounds **T1, T5, T6, T10, T11, T12, T13, T14, T15,** and **T18** exhibited lower antitubercular activity, with a MIC of 6.25 µg/mL. This performance was inferior to PZA and INN but on par with STM. The synthesized compounds were screened for their *in vitro* antibacterial activity using the broth microdilution method and the MIC values were measured in mg/mL. All the synthesized compounds were screened against two gram-positive bacterial strains (*S. aureus* and *S. mutans),* and two gram-negative bacterial strains (*E. coli and S.* Typhi*)* using Streptomycin (STM) and Chloramphenicol (CHL) as the standard drugs. The MIC values of the target compounds along with those of standard drugs for comparison are presented in **Table 3.3**. Among the screened compounds, **T5** demonstrated significant inhibition activity against *S. aureus,* whereas compounds **T3**, **T7, T11,** and **T13** were active against *S. mutans*. Compounds **T11** and **T13** were potent against *S.* Typhi. Compounds **T7, T8, T11,** and **T12** showed moderate

inhibition against *E. coli.* The synthesized compounds were also screened for their *in vitro* antifungal activity using the broth microdilution method and the MIC values were measured in mg/mL. All the synthesized compounds were screened against the fungal strain *A. niger* using Amphotericin B (AmB) as a standard drug. The MIC values of the target compounds along with the standard drugs for comparison are presented in **Table 3.4**. Among the screened compounds **T4, T7, T16,** and **T17** showed significant inhibition activity against *A. niger*. Compounds **T1, T2, T3, T6, T8, T10, T12, T14,** and **T18** demonstrated moderate inhibition activity against the tested strain.

Table 3.2 *Antitubercular activity of the compounds* ***T1-T18*** *with M. tuberculosis H37Rv*

Comp.	*M. tuberculosis* H37Rv		Comp.	*M. tuberculosis* H37Rv	
	MIC (µg/mL)	MIC (µM)		MIC (µg/mL)	MIC (µM)
T1	6.25	20.89	**T12**	6.25	20.22
T2	3.12	9.90	**T13**	6.25	19.22
T3	3.12	9.96	**T14**	6.25	19.96
T4	3.12	9.48	**T15**	6.25	18.99
T5	6.25	19.71	**T16**	3.12	8.36
T6	6.25	18.76	**T17**	1.56	4.58
T7	1.56	4.13	**T18**	6.25	19.52
T8	1.56	4.53	**PZA**	3.12	25.34
T9	3.12	9.62	**STM**	6.25	10.74
T10	6.25	21.18	**INN**	3.12	9.41
T11	6.25	20.09			

Comp.: Compound, PZA: Pyrazinamide, STM: Streptomycin, INN: Ciprofloxacin

Table 3.3 *Antibacterial activity (MIC in mg/mL) of the target compounds (****T1-T18****)*

Comp.	MIC (mg/mL)			
	S. aureus	***S. mutants***	***E. coli***	***S.* Typhi**
T1	2.5	> 5.0	> 5.0	2.5
T2	2.5	> 5.0	> 5.0	2.5

T3	2.5	0.3125	> 5.0	> 5.0
T4	> 5.0	> 5.0	> 5.0	5.0
T5	1.25	5.0	> 5.0	5.0
T6	5.0	1.25	> 5.0	5.0
T7	5.0	0.01953	5.0	> 5.0
T8	5.0	> 5.0	5.0	> 5.0
T9	5.0	> 5.0	> 5.0	> 5.0
T10	5.0	2.5	> 5.0	> 5.0
T11	> 5.0	0.625	5.0	0.625
T12	5.0	2.5	5.0	5.0
T13	> 5.0	0.625	> 5.0	0.01953
T14	> 5.0	> 5.0	> 5.0	> 5.0
T15	5.0	5.0	> 5.0	> 5.0
T16	> 5.0	> 5.0	> 5.0	> 5.0
T17	5.0	> 5.0	> 5.0	5.0
T 18	> 5.0	> 5.0	> 5.0	5.0
STM	0.012	0.010	0.010	0.011
CHL	0.010	0.010	0.012	0.010
Control	00	00	00	00

Comp.: Compound, STM: Streptomycin, CHL: Chloramphenicol, Control: DMSO

Table 3.4 *Antifungal activity (MIC in mg/mL) of the target compounds (**T1-T18**)*

Comp.	**MIC (mg/mL)**	**Comp.**	**MIC (mg/mL)**
	A. niger		***A. niger***
T1	5.0	**T11**	> 5.0
T2	5.0	**T12**	5.0
T3	5.0	**T13**	> 5.0
T4	2.5	**T14**	5.0
T5	> 5.0	**T15**	> 5.0
T6	5.0	**T16**	2.5

T7	2.5	**T17**	2.5
T8	5.0	**T 18**	5.0
T9	> 5.0	**AmB**	0.004
T10	5.0	**Control**	00

Comp.: Compound, AmB: Amphotericin B, Control: DMSO

3.3.2 Antitubercular, antibacterial, and antifungal activity of 1,2,4-triazole incorporated pyrazine derivatives (T19-T36)

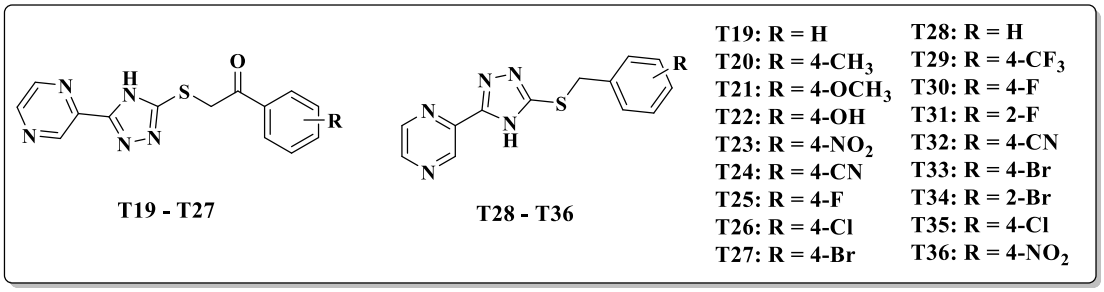

In this series, a total of 18 compounds (**T19-T36**) were prepared. The synthesized compounds underwent screening for their antitubercular activity. The MIC values (µg/mL) of the tested compounds are tabulated in **Table 3.5**. The antitubercular screening revealed that few of the tested compounds showed good inhibition against the tested strain compared to the standard drugs. Among the synthesized compounds, **T29** exhibited the highest potency displaying a MIC of 3.12 µg/mL which is comparable to the effectiveness of PZA and INN, and surpasses STM by a factor of two in terms of MIC. Furthermore, compounds **T22, T23, T24, T32, T33, T34,** and **T36** demonstrated promising antitubercular activity with MIC value 6.25 µg/mL. While not as potent as PZA and INN, they exhibited effectiveness comparable to that of STM. The remaining compounds exhibited moderate antitubercular activity, with a MIC value of 12.5 µg/mL. The *in vitro* antibacterial activity of the synthesized compounds (**T19-T36**) was tested using the broth microdilution method and the MIC values were measured in mg/mL. All the synthesized compounds were screened against two gram-positive bacterial strains (*S. aureus* and *S. mutans),* and two gram-negative bacterial strains (*E. coli and S.* Typhi*)* using Streptomycin (STM) and Chloramphenicol (CHL)

as the standard drugs. The MIC values of the target compounds along with those of standard drugs for comparison are presented in **Table 3.6**. Among the screened compounds, **T27, T28, T34,** and **T36** demonstrated significant inhibition activity against *S. aureus,* whereas compound **T34** was active against *S. mutans*. Compounds **T22**, and **T34** were potent against both *E. coli*. None of the compounds showed notable inhibition activity against *S.* Typhi. The *in vitro* antifungal activity of the synthesized compounds (**T19-T36**) was also screened using the broth microdilution method and the MIC values were measured in mg/mL. All the synthesized compounds were screened against the fungal strain *A. niger* using Amphotericin B (AmB) as a standard drug. The MIC values of the target compounds along with the standard drugs for comparison are presented in **Table 3.7**. Among the screened compounds **T30** and **T32** showed significant inhibition activity against *A. niger*. Compounds **T29** and **T33** demonstrated moderate inhibition activity against the tested strain.

Table 3.5 *Antitubercular activity of the compounds* ***T19-T36*** *with M. tuberculosis H37Rv*

Comp.	*M. tuberculosis* H37Rv		Comp.	*M. tuberculosis* H37Rv	
	MIC (µg/mL)	MIC (µM)		MIC (µg/mL)	MIC (µM)
T19	12.5	42.07	**T30**	12.5	43.54
T20	12.5	40.18	**T31**	12.5	43.54
T21	12.5	38.21	**T32**	6.25	21.25
T22	6.25	19.96	**T33**	6.25	18.01
T23	6.25	18.27	**T34**	6.25	18.01
T24	6.25	19.40	**T35**	12.5	41.25
T25	12.5	39.67	**T36**	6.25	19.90
T26	12.5	37.76	**PZA**	3.12	25.34
T27	12.5	33.33	**STM**	6.25	10.74
T28	12.5	46.45	**INN**	3.12	9.41
T29	3.12	9.25			

Comp.: Compound, PZA: Pyrazinamide, STM: Streptomycin, INN: Ciprofloxacin

Table 3.6 *Antibacterial activity (MIC in mg/mL) of the target compounds (**T19-T36**)*

Comp.	MIC (mg/mL)			
	S. aureus	***S. mutans***	***E. coli***	***S.* Typhi**
T19	2.5	> 5.0	5.0	> 5.0
T20	2.5	> 5.0	5.0	> 5.0
T21	5.0	5.0	5.0	> 5.0
T22	2.5	1.25	0.625	> 5.0
T23	1.25	> 5.0	> 5.0	> 5.0
T24	5.0	> 5.0	> 5.0	> 5.0
T25	2.5	> 5.0	5.0	> 5.0
T26	5.0	5.0	5.0	> 5.0
T27	0.01953	1.25	> 5.0	1.25
T28	0.625	2.5	5.0	> 5.0
T29	5.0	5.0	1.26	5.0
T30	2.5	5.0	5.0	5.0
T31	2.5	5.0	5.0	5.0
T32	2.5	> 5.0	> 5.0	> 5.0
T33	2.5	5.0	2.5	> 5.0
T34	0.01953	0.01953	0.625	2.5
T35	2.5	> 5.0	> 5.0	5.0
T36	0.625	> 5.0	1.25	5.0
STM	0.012	0.010	0.010	0.011
CHL	0.010	0.010	0.012	0.010
Control	00	00	00	00

Comp.: Compound, STM: Streptomycin, CHL: Chloramphenicol, Control: DMSO

Table 3.7 *Antifungal activity (MIC in mg/mL) of the target compounds (**T19-T36**)*

Comp.	MIC (mg/mL)	Comp.	MIC (mg/mL)
	A. niger		***A. niger***
T19	2.5	**T29**	1.25

T20	5.0	**T30**	0.625
T21	5.0	**T31**	5.0
T22	5.0	**T32**	0.625
T23	5.0	**T33**	1.25
T24	5.0	**T34**	2.5
T25	5.0	**T35**	5.0
T26	2.5	**T36**	5.0
T27	5.0	**AmB**	0.004
T28	5.0	**Control**	00

Comp.: Compound, AmB: Amphotericin B, Control: DMSO

3.3.3 Antitubercular, antibacterial, and antifungal activity of pyrazine hydrazinylidene derivatives containing benzenesulfonate scaffold (T37-T52)

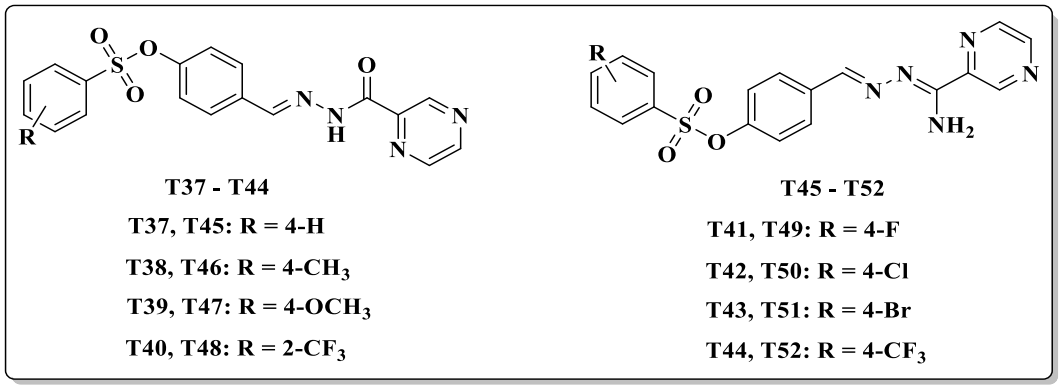

In this series 16 derivatives were synthesized and evaluated their antitubercular activity. The MIC (µg/mL**)** values are listed in **Table 3.8**. The antitubercular screening revealed that few of the tested compounds showed good inhibition against the tested strain compared to the standard drugs. Among the synthesized compounds **T40, T43,** and **T48** displayed the highest potency within this group, with an MIC of 1.56 µg/mL. These compounds are twice as effective as the standard tuberculosis drugs PZA and INN and four times more potent than STM in terms of MIC. Furthermore, compounds **T39, T41, T42, T44, T47, T49, T50, T51,** and **T52** exhibited comparable antitubercular activity with an MIC of 3.12 µg/mL, matching the effectiveness of PZA

and INN and surpassing STM by a factor of two. On the other hand, compounds **T37, T38, T45,** and **T46** demonstrated lower antitubercular activity, with an MIC of 6.25 µg/mL. This performance was less effective than PZA and INN but equivalent to STM. The antibacterial activity of the synthesized compounds (**T37-T52**) was assessed *in vitro* using the broth microdilution method, and their minimum inhibitory concentration values were measured in mg/mL. These compounds were tested against two gram-positive bacterial strains (*S. aureus* and *S. mutans*) and two gram-negative bacterial strains (*E. coli* and *S.* Typhi), with Streptomycin (STM) and Chloramphenicol (CHL), used as standard drugs for comparison. The MIC values of the compounds, along with those of the standard drugs, are summarized in **Table 3.9**. Among the tested compounds, **T38, T42,** and **T50** displayed significant inhibitory activity against *E. coli*. Additionally, compounds **T42** and **T50** showed notable inhibitory effects against *S.* Typhi. However, none of the compounds exhibited substantial inhibitory activity against *S. aureus* and *S. mutans*. The antifungal activity of synthesized compounds (**T37-T52**) was also evaluated *in vitro* using the broth microdilution method, with minimum inhibitory concentration values measured in mg/mL. These compounds were tested against the fungal strain *A. niger*, with Amphotericin B (AmB) employed as the standard drug for comparison. The MIC values of the compounds, along with those of the standard drug, are presented in **Table 3.10**. Among the screened compounds, **T42** exhibited significant inhibitory activity against *A. niger*. Compounds **T41, T43,** and **T50** showed moderate inhibition activity against the tested strain.

Table 3.8 *Antitubercular activity of the compounds* ***T37-T52*** *with M. tuberculosis H37Rv*

Comp.	*M. tuberculosis* H37Rv		Comp.	*M. tuberculosis* H37Rv	
	MIC (µg/mL)	MIC (µM)		MIC (µg/mL)	MIC (µM)
T37	6.25	16.31	**T47**	3.12	7.57
T38	6.25	15.73	**T48**	1.56	3.46
T39	3.12	7.55	**T49**	3.12	7.79
T40	1.56	3.45	**T50**	3.12	7.49

T41	3.12	7.77	**T51**	3.12	6.78
T42	3.12	7.48	**T52**	3.12	6.93
T43	1.56	3.38	**PZA**	3.12	25.34
T44	3.12	6.91	**STM**	6.25	10.74
T45	6.25	16.35	**INN**	3.12	9.41
T46	6.25	15.77			

Comp.: Compound, PZA: Pyrazinamide, STM: Streptomycin, INN: Ciprofloxacin

Table 3.9 *Antibacterial activity (MIC in mg/mL) of the target compounds (**T37-T52**)*

Comp.	**MIC (mg/mL)**			
	S. aureus	***S. mutans***	***E. coli***	***S.* Typhi**
T37	> 5.0	> 5.0	0.625	> 5.0
T38	> 5.0	> 5.0	0.01925	0.625
T39	> 5.0	> 5.0	2.5	> 5.0
T40	> 5.0	> 5.0	2.5	2.5
T41	> 5.0	> 5.0	2.5	2.5
T42	2.5	5.0	0.01925	0.01925
T43	5.0	> 5.0	0.3125	2.5
T44	> 5.0	> 5.0	0.625	2.5
T45	> 5.0	> 5.0	2.5	> 5.0
T46	> 5.0	> 5.0	0.625	0.625
T47	> 5.0	> 5.0	0.625	> 5.0
T48	> 5.0	> 5.0	2.5	> 5.0
T49	> 5.0	> 5.0	0.625	2.5
T50	5.0	5.0	0.01925	0.01925
T51	> 5.0	> 5.0	0.625	2.5
T52	> 5.0	> 5.0	0.3125	2.5
STM	0.012	0.010	0.010	0.011
CHL	0.010	0.010	0.012	0.010
Control	00	00	00	00

Comp.: Compound, STM: Streptomycin, CHL: Chloramphenicol, Control: DMSO

Table 3.10 *Antifungal activity (MIC in mg/mL) of the target compounds (**T37-T52**)*

Comp.	MIC (mg/mL) *A. niger*	Comp.	MIC (mg/mL) *A. niger*
T37	> 5.0	**T46**	> 5.0
T38	5.0	**T47**	> 5.0
T39	> 5.0	**T48**	5.0
T40	5.0	**T49**	5.0
T41	2.5	**T50**	2.5
T42	0.3125	**T51**	5.0
T43	2.5	**T52**	5.0
T44	5.0	**AmB**	0.004
T45	> 5.0	**Control**	00

Comp.: Compound, AmB: Amphotericin B, Control: DMSO

3.3.4 Antitubercular, antibacterial, and antifungal activity of 4-quinazolinone incorporated pyrazine derivatives (T53-T68)

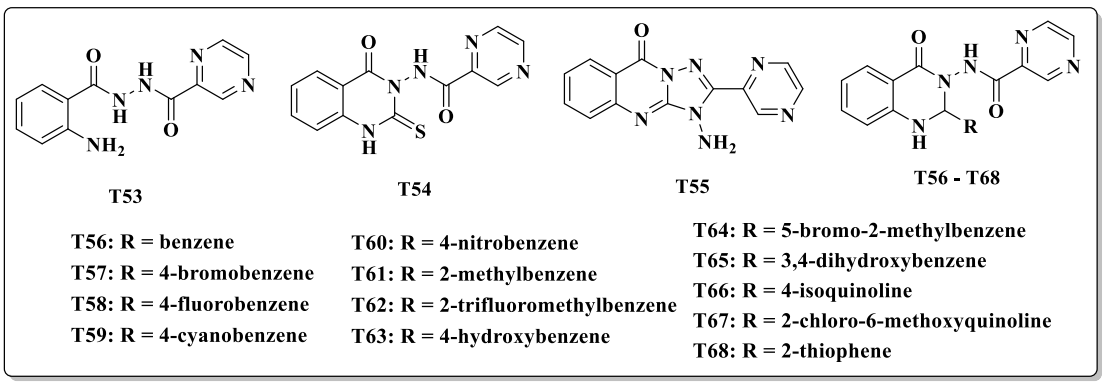

In this series, 16 compounds (**T53-T68**) were synthesized and assessed for their effectiveness in inhibiting the growth of *Mycobacterium tuberculosis* H37Rv. The MIC values (µg/mL) were determined and are presented in **Table 3.11**. The results of the screening indicated that some of the synthesized compounds exhibited promising inhibition against the tested strain compared to the standard drugs. Notably, compounds **T60** and **T65** showed the highest potency, with MIC values of 3.12 µg/mL, which were

comparable to the efficacy of PZA and INN and were twice as potent as STM. Additionally, compounds **T61, T64, T66,** and **T67** demonstrated significant antitubercular activity, with MIC values of 6.25 µg/mL. Although their potency was lower than that of PZA and INN, it was on par with STM. The remaining compounds showed moderate antitubercular activity, with MIC values ranging from 12.5 to 25 µg/mL. The antibacterial activity of the synthesized compounds (**T53-T68**) was assessed *in vitro* using the broth microdilution method, and their minimum inhibitory concentration values were measured in mg/mL. These compounds were tested against two gram-positive bacterial strains (*S. aureus* and *S. mutans*) and two gram-negative bacterial strains (*E. coli* and *S.* Typhi), with Streptomycin (STM) and Chloramphenicol (CHL), used as standard drugs for comparison. The MIC values of the compounds, along with those of the standard drugs, are summarized in **Table 3.12**. Among the screened compounds, **T54, T55,** and **T64** displayed significant inhibitory activity against all the tested strains. The antifungal activity of synthesized compounds (**T53-T68**) was also evaluated *in vitro* using the broth microdilution method, with minimum inhibitory concentration values measured in mg/mL. These compounds were tested against the fungal strain *A. niger*, with Amphotericin B (AmB) employed as the standard drug for comparison. The MIC values of the compounds, along with those of the standard drug, are presented in **Table 3.13**. Among the screened compounds, **T64** and **T65** demonstrated commendable inhibitory activity against the tested fungal strain.

Table 3.11 *Antitubercular activity of the compounds* ***T53-T68*** *with M. tuberculosis H37Rv*

Comp.	*M. tuberculosis* H37Rv		Comp.	*M. tuberculosis* H37Rv	
	MIC (µg/mL)	MIC (µM)		MIC (µg/mL)	MIC (µM)
T53	25	97.24	**T63**	12.5	34.61
T54	25	83.59	**T64**	6.25	14.23
T55	25	89.57	**T65**	3.12	8.27
T56	12.5	36.21	**T66**	6.25	15.77
T57	12.5	29.54	**T67**	6.25	13.58

T58	12.5	34.42	**T68**	12.5	35.60
T59	12.5	33.77	**PZA**	3.12	25.34
T60	3.12	7.99	**STM**	6.25	10.74
T61	6.25	17.40	**INN**	3.12	9.41
T62	12.5	30.25			

Comp.: Compound, PZA: Pyrazinamide, STM: Streptomycin, INN: Ciprofloxacin

Table 3.12 *Antibacterial activity (MIC in mg/mL) of the target compounds (**T53-T68**)*

Comp.	**MIC (mg/mL)**			
	S. aureus	***S. mutans***	***E. coli***	***S.* Typhi**
T53	> 5.0	> 5.0	0.625	2.5
T54	0.01925	0.01925	0.3125	0.625
T55	0.01925	0.01925	0.01925	> 5.0
T56	> 5.0	> 5.0	> 5.0	> 5.0
T57	> 5.0	> 5.0	> 5.0	> 5.0
T58	> 5.0	> 5.0	> 5.0	> 5.0
T59	> 5.0	> 5.0	> 5.0	> 5.0
T60	> 5.0	> 5.0	> 5.0	> 5.0
T61	> 5.0	> 5.0	> 5.0	> 5.0
T62	> 5.0	> 5.0	> 5.0	> 5.0
T63	> 5.0	0.3125	0.625	2.5
T64	0.01925	0.01925	0.01925	0.01925
T65	0.625	> 5.0	0.625	> 5.0
T66	2.5	> 5.0	5.0	> 5.0
T67	5.0	> 5.0	5.0	> 5.0
T68	2.5	2.5	5.0	> 5.0
STM	0.012	0.010	0.010	0.011
CHL	0.010	0.010	0.012	0.010
Control	00	00	00	00

Comp.: Compound, STM: Streptomycin, CHL: Chloramphenicol, Control: DMSO

Table 3.13 *Antifungal activity (MIC in mg/mL) of the target compounds (**T53-T68**)*

Comp.	MIC (mg/mL) *A. niger*	Comp.	MIC (mg/mL) *A. niger*
T53	> 5.0	**T62**	> 5.0
T54	> 5.0	**T63**	> 5.0
T55	> 5.0	**T64**	0.625
T56	> 5.0	**T65**	0.3125
T57	> 5.0	**T66**	5.0
T58	> 5.0	**T67**	5.0
T59	> 5.0	**T68**	> 5.0
T60	5.0	**AmB**	0.004
T61	5.0	**Control**	00

Comp.: Compound, AmB: Amphotericin B, Control: DMSO

3.3.5 Antitubercular, antibacterial, and antifungal activity of 2-aminophenyl and 2-oxoacetyl incorporated pyrazine-2-carbohydrazide derivatives (T69-T88)

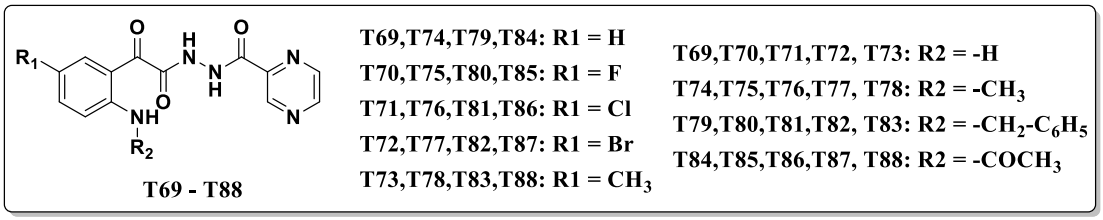

In this series 20 molecules were synthesized and tested for their ability to combat tuberculosis *in vitro* and their MIC values (µg/mL) were determined, as shown in **Table 3.14**. The antitubercular screening revealed that some of the tested compounds showed good inhibition against the tested strain compared to the standard drugs. Among the tested compounds, **T84** and **T87** displayed the highest potency, with a MIC value of 1.56 µg/mL. These compounds showed twice the effectiveness of the standard tuberculosis drugs PZA and INN, and four times more potency than STM based on MIC values. Additionally**, T81, T82,** and **T83** demonstrated comparable antitubercular activity, with a MIC value of 3.12 µg/mL, matching the effectiveness of PZA and INN,

and surpassing STM by a factor of two. On the other hand, **T85, T86,** and **T88** exhibited moderate antitubercular activity, with a MIC value of 6.25 µg/mL. Although less effective than PZA and INN, these compounds performed equally to STM. The remaining compounds showed lower antitubercular activity, with MIC values ranging from 12.5 to 25 µg/mL. The *in vitro* antibacterial activity of the synthesized compounds (**T69-T88**) was tested using the broth microdilution method and the MIC values were measured in mg/mL. All the synthesized compounds were screened against two gram-positive bacterial strains (*S. aureus* and *S. mutans),* and two gram-negative bacterial strains (*E. coli and S.* Typhi*)* using Streptomycin (STM) and Chloramphenicol (CHL) as the standard drugs. The MIC values of the target compounds along with those of standard drugs for comparison are presented in **Table 3.15**. Among the screened compounds, **T72, T76, T77,** and **T87** demonstrated significant inhibitory activity against *S. aureus,* whereas compounds **T76, T77,** and **T87** were active against *S. mutans*. Compounds **T76, T77, T84,** and **T87** were potent against both *E. coli.* and *S.* Typhi. The *in vitro* antifungal activity of the synthesized compounds (**T69-T88**) was screened using the broth microdilution method and the MIC values were measured in mg/mL. All the synthesized compounds were screened against the fungal strain *A. niger* using Amphotericin B (AmB) as a standard drug. The MIC values of the target compounds along with the standard drugs for comparison are presented in **Table 3.16**. Among the screened compounds **T72, T77, T84, T85, T86,** and **T87** showed significant inhibition activity against *A. niger*. The rest of the compounds showed moderate inhibition activity against the tested strain.

Table 3.14 *Antitubercular activity of the compounds* ***T69-T88*** *with M. tuberculosis H37Rv*

Comp.	*M. tuberculosis* H37Rv		Comp.	*M. tuberculosis* H37Rv	
	MIC (µg/mL)	MIC (µM)		MIC (µg/mL)	MIC (µM)
T69	25	87.69	**T81**	3.12	7.62
T70	25	82.48	**T82**	3.12	6.88
T71	25	78.36	**T83**	3.12	8.01

T72	25	68.87	**T84**	1.56	4.76
T73	25	83.58	**T85**	6.25	18.11
T74	12.5	41.79	**T 86**	6.25	17.31
T75	12.5	39.42	**T87**	1.56	3.85
T76	12.5	37.53	**T88**	6.25	18.32
T77	12.5	33.15	**PZA**	3.12	25.34
T78	12.5	39.92	**STM**	6.25	10.74
T79	6.25	16.66	**INN**	3.12	9.41
T80	6.25	15.89			

Comp.: Compound, PZA: Pyrazinamide, STM: Streptomycin, INN: Ciprofloxacin

Table 3.15 *Antibacterial activity (MIC in mg/mL) of the target compounds (**T69-T88**)*

Comp.	**MIC (mg/mL)**			
	S. aureus	***S. mutants***	***E. coli***	***S.* Typhi**
T69	2.5	5.0	2.5	2.5
T70	2.5	5.0	5.0	2.5
T71	2.5	5.0	2.5	5.0
T72	0.625	1.25	2.5	5.0
T73	2.5	5.0	5.0	2.5
T74	5.0	1.25	5.0	5.0
T75	5.0	2.5	5.0	> 5.0
T76	0.3125	0.01953	0.3125	0.625
T77	0.01953	0.01953	0.3125	0.3125
T78	5.0	2.5	> 5.0	> 5.0
T79	2.5	5.0	5.0	1.25
T80	5.0	2.5	5.0	5.0
T81	5.0	5.0	5.0	1.25
T82	5.0	> 5.0	2.5	2.5
T83	5.0	5.0	2.5	2.5
T84	2.5	2.5	0.625	0.3125

T85	5.0	2.5	> 5.0	5.0
T 86	5.0	2.5	5.0	5.0
T87	0.625	0.3125	0.01953	0.3125
T88	5.0	5.0	2.5	2.5
STM	0.012	0.010	0.010	0.011
CHL	0.010	0.010	0.012	0.010
Control	00	00	00	00

Comp.: Compound, STM: Streptomycin, CHL: Chloramphenicol, Control: DMSO

***Table 3.16** Antifungal activity (MIC in mg/mL) of the target compounds (**T69-T88**)*

Comp.	MIC (mg/mL)	Comp.	MIC (mg/mL)
	A. niger		***A. niger***
T69	5.0	**T80**	2.5
T70	2.5	**T81**	2.5
T71	2.5	**T82**	1.25
T72	0.625	**T83**	5.0
T73	5.0	**T84**	0.625
T74	5.0	**T85**	0.625
T75	2.5	**T 86**	0.625
T76	2.5	**T87**	0.3125
T77	0.625	**T88**	2.5
T78	5.0	**AmB**	0.004
T79	2.5	**Control**	00

Comp.: Compound, AmB: Amphotericin B, Control: DMSO

3.3.6 *In vitro* cytotoxicity of the active compounds

The MTT assay was utilized to assess the cytotoxicity of the efficacious compounds (with a MIC ≤ 3.12 µg/mL in antitubercular screening) against the Vero cell line (African green monkey kidney, Catalog No. 11965-092). **Table 3.17** shows the cellular growth inhibition for these efficacious compounds across four discrete

concentrations: 25, 50, 75, and 100 µM. Interestingly, we found that all the active compounds we studied showed no significant toxicity, as indicated by IC_{50} values greater than 350 µM, as shown in **Table 3.18**. Importantly, none of these compounds had harmful effects on normal cells, indicating an overall lack of toxicity to healthy cellular entities.

Table 3.17 *Cell growth inhibition of active compounds against Vero cell line*

Compound	% of inhibition			
	25 µM	**50 µM**	**75 µM**	**100 µM**
T2	2.42 ± 0.47	4.27 ± 0.48	7.06 ± 0.32	10.74 ± 0.46
T3	1.93 ± 0.76	3.96 ± 0.54	5.68 ± 0.41	9.36 ± 0.35
T4	2.57 ± 0.46	4.34 ± 0.73	7.14 ± 0.36	11.16 ± 0.92
T7	1.76 ± 0.72	3.37 ± 0.22	5.17 ± 0.37	8.43 ± 0.47
T8	1.43 ± 0.57	3.49 ± 0.34	5.37 ± 0.27	8.61 ± 0.39
T9	2.64 ± 0.63	4.56 ± 0.39	7.43 ± 0.79	12.20 ± 0.83
T16	2.37 ± 0.37	4.03 ± 0.56	6.91 ± 0.95	10.20 ± 0.32
T17	1.54 ± 0.65	3.87 ± 0.69	5.52 ± 0.79	8.70 ± 0.58
T22	3.21 ± 0.34	6.46 ± 0.21	9.61 ± 0.18	12.92 ± 0.26
T23	3.05 ± 0.23	6.38 ± 0.17	9.53 ± 0.15	12.87 ± 0.19
T24	3.14 ± 0.27	6.35 ± 0.32	9.89 ± 0.23	13.05 ± 0.23
T29	2.97 ± 0.15	6.03 ± 0.22	9.08 ± 0.27	12.10 ± 0.14
T32	3.02 ± 0.18	6.24 ± 0.31	9.63 ± 0.20	13.09 ± 0.17
T33	2.99 ± 0.31	6.12 ± 0.19	9.74 ± 0.38	12.64 ± 0.27
T34	3.04 ± 0.25	6.16 ± 0.27	9.37 ± 0.16	12.35 ± 0.22
T36	3. 17 ± 0.23	6.38 ± 0.22	9.71 ± 0.21	12.59 ± 0.25
T37	3.12 ± 0.17	6.02 ± 0. 35	8.96 ± 0.47	12.74 ± 0.42
T38	2.93 ± 0.47	6.23 ± 0.27	9.38 ± 0.35	12.36 ± 0.55
T39	3.07 ± 0.63	5.92 ± 0.46	8.14 ± 0.76	11.16 ± 0.39
T40	2.16 ± 0.83	4.94 ± 0.57	7.37 ± 0.25	9.83 ± 0.79
T41	2.83 ± 0.58	5.27 ± 0.42	8.17 ± 0.15	11.61 ± 0.58

T42	2.94 ± 0.62	5.19 ± 0.51	8.51 ± 0.46	11.81 ± 0.41
T43	2.21 ± 0.27	5.62 ± 0.68	8.16 ± 0.37	10.47 ± 0.36
T44	3.19 ± 0.35	6.32 ± 0.25	9.15 ± 0.68	12.59 ± 0.67
T45	3.02 ± 0.26	6.08 ± 0.43	9.02 ± 0.53	12.61 ± 0.25
T46	3.47 ± 0.41	6.19 ± 0.78	9.47 ± 0.35	12.82 ± 0.36
T47	2.78 ± 0.25	5.95 ± 0.58	8.80 ± 0.52	11.07 ± 0.57
T48	2.14 ± 0.33	4.83 ± 0.61	7.89 ± 0.58	10.72 ± 0.63
T49	2.90 ± 0.26	5.47 ± 0.48	8.46 ± 0.61	11.27 ± 0.57
T50	3.03 ± 0.34	5.79 ± 0.58	8.67 ± 0.54	10.93 ± 0.49
T51	2.74 ± 0.18	5.91 ± 0.63	8.24 ± 0.39	10.82 ± 0.90
T52	2.93 ± 0.31	5.62 ± 0.68	8.40 ± 0.72	11.02 ± 0.81
T60	2.31 ± 0.26	5.68 ± 0.53	8.09 ± 0.49	11.91 ± 0.84
T61	3.18 ± 0.27	6.45 ± 0.56	9.70 ± 0.75	13.02 ± 0.59
T64	3.27 ± 0.54	6.09 ± 0.64	9.05 ± 0.39	12.67 ± 0.88
T65	2.43 ± 0.41	5.75 ± 0.39	8.47 ± 0.47	11.83 ± 0.37
T66	3.08 ± 0.87	6.58 ± 0.98	9.42 ± 1.21	13.23 ± 0.73
T67	3.22 ± 0.23	6.64 ± 1.02	9.60 ± 1.04	13.41 ± 1.61
T81	3.87 ± 0.98	7.93 ± 0.47	10.05 ± 0.99	13.05 ± 1.26
T82	4.12 ± 0.67	8.39 ± 0.78	12.48 ± 0.73	16.27 ± 0.99
T83	3.74 ± 0.72	7.41 ± 0.93	10.63 ± 0.86	13.45 ± 0.95
T84	3.08 ± 0.91	6.32 ± 0.86	9.41 ± 0.94	12.37 ± 1.02
T87	3.13 ± 0.67	6.47 ± 0.79	9.73 ± 0.99	12.69 ± 1.25

The values represent the mean ± standard error of the mean obtained from three separate determinations after 72 hours of exposure.

Table 3.18 *IC_{50} values of active compounds obtained through an MTT assay against Vero cell line*

Compound	IC_{50} (µM)	Compound	IC_{50} (µM)
T2	475.35 ± 10.11	**T43**	463.88 ± 10.84

T3	552.75 ± 11.32	**T44**	401.10 ± 11.93
T4	461.56 ± 12.35	**T45**	399.53 ± 9.85
T7	612.72 ± 10.44	**T46**	394.45 ± 10.29
T8	585.67 ± 10.53	**T47**	443.26 ± 11.37
T9	424.04 ± 10.38	**T48**	457.03 ± 11.48
T16	498.13 ± 10.43	**T49**	444.84 ± 11.59
T17	580.70 ± 11.46	**T50**	452.87 ± 11.40
T22	387.53 ± 10.15	**T51**	459.35 ± 10.27
T23	387.29 ± 12.03	**T52**	453.70 ± 10.38
T24	379.88 ± 10.49	**T60**	419.57 ± 10.28
T29	412.32 ± 11.63	**T61**	383.70 ± 10.53
T32	379.86 ± 11.47	**T64**	401.54 ± 10.76
T33	389.47 ± 10.73	**T65**	418.82 ± 10.56
T34	402.72 ± 13.48	**T66**	380.35 ± 9.59
T36	393.80 ± 12.44	**T67**	376.00 ± 10.21
T37	398.27 ± 10.53	**T81**	383.23 ± 11.23
T38	400.53 ± 11.26	**T82**	305.18 ± 10.86
T39	454.56 ± 11.09	**T83**	367.69 ± 10.24
T40	501.36 ± 10.64	**T84**	402.07 ± 10.60
T41	436.63 ± 11.25	**T87**	390.86 ± 10.45
T42	426.81 ± 10.71		

The IC_{50} values represent the concentration of a substance required to inhibit 50% of cell viability calculated after a 72-hour exposure.

3.4 Structure-activity relationship

3.4.1 Structure-activity relationship of 1,3,4-oxadiazole/[1,2,4] triazolo[3,4-*b*][1,3,4]thiadiazine incorporated pyrazine derivatives (T1-T18)

The antitubercular and antimicrobial activities of synthesized compounds (**T1-T18**) reveals specific structure-activity relationships (SAR). Among the series, compounds **T7, T8,** and **T17**, featuring 4-Br, 4-NO_2, and 4-NO_2 substituents on the phenyl ring respectively, showed the highest potency with an MIC of 1.56 µg/mL. Compounds **T2, T3, T4, T9,** and **T16,** containing 4-OH, 4-CH_3, 4-OCH_3, 4-CN, and 4-Br substituents on the phenyl ring respectively, demonstrated equivalent antitubercular activity with an MIC of 3.12 µg/mL. However, compounds **T1, T5, T6, T10, T11, T12, T13, T14, T15,** and **T18**, which incorporate 4-H, 4-F, 4-Cl, 4-H, 4-OH, 4-CH_3, 4-OCH_3, 4-F, 4-Cl, and 4-CN substituents on the phenyl ring respectively, exhibited lower antitubercular activity, with an MIC of 6.25 µg/mL. The analysis of structure-activity relationships suggests that the presence of a nitro group or halogens at position 4 of the phenyl ring is more favorable for enhancing antitubercular and antimicrobial properties.

3.4.2 Structure-activity relationship of 1,2,4-triazole incorporated pyrazine derivatives (T19-T36)

The effectiveness of the synthesized compounds (**T19-T36**) in terms of their antitubercular and antimicrobial properties reveals specific structure-activity relationships (SAR). The introduction of substituents that enhance the aromaticity and electron density within the pyrazine or 1,2,4-triazole ring resulted in improved antitubercular activity. Both 1-phenyl-2-((5-(pyrazin-2-yl)-4*H*-1,2,4-triazol-3-yl)thio)ethan-1-one (**T19-T27**) and 2-(5-(benzylthio)-4*H*-1,2,4-triazol-3-yl)pyrazine derivatives (**T28-T36**) exhibited superior activity when equipped with electron-withdrawing groups. For instance, **T23** and **T36** with a nitro group as well as **T24** and **T32** with a cyano group are equipotent (MIC of 6.25 µg/mL). The introduction of a -CF_3 (trifluoromethyl) group (**T29**) into the active pharmacophore further improved the antimycobacterial activity (MIC of 3.12 µg/mL). This improvement is attributed to the small size of fluorine, which closely resembles hydrogen and can meet the steric requirements for interaction with the receptor enzyme. Additionally, it enhances lipid

solubility, thereby improving the absorption rate. Fluorinated analogues also offer increased thermal and oxidative stability to the compounds, as the carbon-fluorine (C-F) bond exhibits greater bond strength relative to the carbon-hydrogen (C-H) bond. Furthermore, the fluorine substituent can form hydrogen bonds with target enzymes. The substitution of the -CF_3 group is more favorable than the -F group, as it is more lipophilic. Hence it can be concluded that compound **T29** exhibited the highest potency among the tested compounds primarily due to the presence of the -CF_3 substituent.

3.4.3 Structure-activity relationship of pyrazine hydrazinylidene derivatives containing benzenesulfonate scaffold (T37-T52)

The biological activity of the synthesized compounds (**T37-T52**) reveals specific structure-activity relationships (SAR) for their antitubercular and antimicrobial properties. In terms of antitubercular activity, compounds with an electron-withdrawing group outperformed those with an electron-donating group. In particular, (*E*)-4-((2-(pyrazine-2-carbonyl)hydrazineylidene)methyl)phenyl benzenesulfonate and 4-((*E*)-(((*Z*)-amino(pyrazin-2-yl)methylene)hydrazineylidene)methyl)phenyl benzenesulfonate derivatives with electron-withdrawing groups showed superior activity. Enhanced antitubercular activity against *M. tuberculosis* H37Rv was observed with stronger electron-withdrawing substituents, following the order: CF_3 > Br > Cl > F > OCH_3 > CH_3 > H. Additionally, having a 2-CF_3 group in the ortho position of the benzenesulfonate moiety (**T40** and **T48**) was more favorable than its presence in the para position (**T44** and **T52**). In case of antimicrobial activity, compounds featuring (*E*)-4-((2-(pyrazine-2-carbonyl)hydrazineylidene)methyl)phenyl benzenesulfonate showed better performance than 4-((*E*)-(((*Z*)-amino(pyrazin-2-yl)methylene)hydrazineylidene)methyl)phenyl benzene sulfonate derivatives. Furthermore, the presence of a chlorine (-Cl) group in the para position of the benzenesulfonate enhanced their effectiveness against various tested bacterial and fungal strains.

3.4.4 Structure-activity relationship of 4-quinazolinone incorporated pyrazine derivatives (T53-T68)

The biological efficacy of the target compounds (**T53-T68**) unveils particular structure-activity correlations (SAR) (**Figure 3.2**) concerning their antitubercular and antimicrobial characteristics. The core constituent 4-oxo-1,4-dihydroquinazolinylpyrazine-2-carboxamide exhibits an aryl or heteroaryl substitution at the fourth position. Compounds **T60** (*N*-(2-(4-nitrophenyl)-4-oxo-1,4-dihydroquinazolin-3(2*H*)-yl)pyrazine-2-carboxamide) and **T65** (*N*-(2-(3,4-dihydroxyphenyl)-4-oxo-1,4-dihydroquinazolin-3(2*H*)-yl)pyrazine-2-carboxamide) with 4-NO_2 phenyl and 3,4-dihydroxy phenyl at the fourth position of the central moiety manifest themselves as the most potent antitubercular agents, with a minimum inhibitory concentration of 3.12 µg/mL. Compounds featuring 2-CH_3 phenyl, 5-Br-2-CH_3 phenyl, 4-isoquinoline, and 2-Cl-6-OCH_3-quinoline at the fourth position of the central moiety exhibit commendable antitubercular activity, characterized by an MIC of 6.25 µg/mL. On the other hand, compounds harboring phenyl, 4-Br phenyl, 4-F phenyl, 4-CN phenyl, 2-CF_3 phenyl, 4-OH phenyl, and 2-thiophene at the fourth position of the central moiety demonstrate a moderate antitubercular activity, denoting a MIC of ≥ 12.5 µg/mL. Compounds **T53, T54,** and **T55**, devoid of any aryl or heteroaryl substitutions, exhibited attenuated antitubercular efficacy, yet paradoxically displayed superior antibacterial potency in contrast to their counterparts. In a general context, the presence of a phenyl ring at the fourth position of the central moiety, augmented by electron-donating groups, yields superior activity compared to a phenyl ring adorned with electron-withdrawing groups. Furthermore, the inclusion of a heterocyclic ring, such as quinoline and isoquinoline, at the fourth position of the central moiety outperforms the phenyl ring in terms of activity.

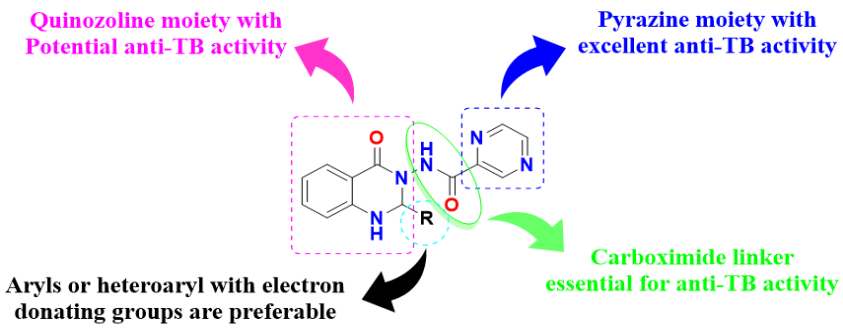

Figure 3.2 *Structure-activity relationship of the target molecules (**T53-T68**)*

3.4.5 Structure-activity relationship of 2-aminophenyl and 2-oxoacetyl incorporated pyrazine-2-carbohydrazide derivatives (T69-T88)

In this series, we have synthesized four distinct set of compounds, namely *N*'-(2-(2-aminophenyl)-2-oxoacetyl)pyrazine-2-carbohydrazides (**T69-T73**), *N*'-(2-(2-(methyl amino)phenyl)-2-oxoacetyl)pyrazine-2-carbohydrazides (**T74-T78**), *N*'-(2-(2-(benzylamino) phenyl)-2-oxoacetyl) pyrazine-2-carbohydrazides (**T79-T83**), and *N*-(2-(2-oxo-2-(2-(pyrazine-2-carbonyl)hydrazineyl)acetyl)phenyl)acetamides (**T84-T88**) which were subsequently examined for their antimicrobial efficacy. The effectiveness of these compounds reveals specific relationships between their structure and activity concerning their antimicrobial effects. All compounds share a crucial pyrazine core, which is vital for their ability to combat tuberculosis. In all the four series, the pyrazine core is intricately linked to the phenyl component through a dipeptide bioactive linker. This connection enhances antimicrobial strength, while reducing potential toxicity. In terms of their effectiveness against tuberculosis, derivatives with an amino group show activity with a minimum inhibitory concentration of 25 µg/mL. Those with a methyl group exhibit activity with an MIC of 12.5 µg/mL, while derivatives containing a benzyl group demonstrate activity within the range of 3.12 to 6.25 µg/mL. Compounds with an acyl group show activity within the range of 1.56 to 6.25 µg/mL. The presence of the acyl group significantly enhances activity, with approximately 16-fold, 8-fold, and 4-fold increases compared to compounds with amino, methyl, and benzyl groups, respectively. Additionally, introducing halogens at the 5-position of the phenyl ring enhances the compound's activity. **Figure 3.3** provides a comprehensive summary of the structure-activity relationships in the various compound series mentioned above.

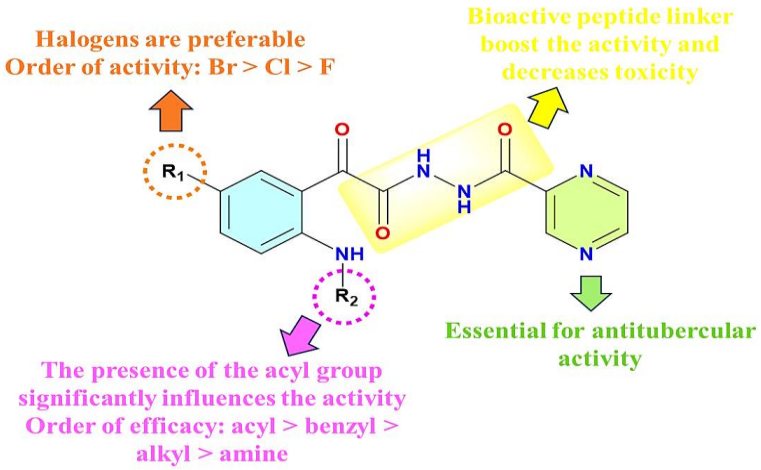

Figure 3.3 *Structure-activity relationship of the target molecules (**T69-T88**)*

3.5 Conclusions

A total of 88 synthesized compounds (**T1-T88**), underwent screening to assess their potential effectiveness against *Mycobacterium tuberculosis* H37Rv strain using the MABA method. Furthermore, their antibacterial and antifungal activities were evaluated using the broth microdilution method. Among these compounds, 8 displayed the highest potency against the *M. tuberculosis* H37Rv strain, with a Minimum Inhibitory Concentration of 1.56 µg/mL. Additionally, 20 compounds exhibited promising activity against the same strain, with an MIC of 3.12 µg/mL. The remaining compounds demonstrated moderate activity. In terms of antibacterial and antifungal activity, 12 compounds demonstrated notable antibacterial activity against the tested strains, while 6 compounds exhibited promising antifungal activity. Furthermore, the cytotoxicity of the active compounds was evaluated using the MTT assay, which indicated minimal toxicity as all compounds showed IC_{50} values greater than 350 µM. To understand the drug-likeness and potential action mechanisms of the synthesized compounds, *in silico* studies were conducted and discussed in Chapter 4.

****

CHAPTER 4

IN SILICO STUDIES: A COMPREHENSIVE EXPLORATION OF ADMET, DFT, AND MOLECULAR DOCKING OF PYRAZINE-BAESD DERIVATIVES

Abstract:

This chapter presents the in silico studies of five new series of pyrazine-based compounds. It details the computational methodology and results related to the pharmacokinetics, physicochemical properties, DFT studies, and molecular docking studies of the synthesized compounds.

4.1 Introduction

In the quest for novel therapeutics to combat diseases, drug discovery stands at the forefront of scientific innovation. Historically, drug development has been a costly and time-consuming process, fraught with challenges ranging from target identification to clinical trials. However, with the advent of computational methods and advances in technology, a paradigm shift has occurred in the field of drug discovery. Among these innovations, *in silico* methods have emerged as indispensable tools, revolutionizing the way researchers approach the identification and optimization of potential drug candidates. The term "*in silico*" refers to computational methods that simulate biological processes and chemical interactions in a virtual environment. These methods encompass a wide array of techniques, including molecular modeling, virtual screening, and quantitative structure-activity relationship (QSAR) modeling, among others. Unlike traditional experimental approaches, which rely heavily on trial and error, *in silico* methods offer a rational and systematic means of understanding molecular mechanisms and predicting the behavior of molecules in biological systems. One of the primary roles of *in silico* methods in drug discovery is target identification and

validation. Before the onset of *in silico* techniques, target identification often relied on laborious experimental screening. However, computational approaches enable researchers to sift through vast datasets and predict potential drug targets based on their biological relevance and druggability. By analyzing genomic, proteomic, and metabolomic data, *in silico* methods facilitate the identification of key molecular targets involved in disease pathways, thereby accelerating the drug discovery process. Furthermore, *in silico* methods play a crucial role in lead identification and optimization. Once a potential target has been identified, researchers employ virtual screening techniques to sift through large chemical libraries and identify molecules with the desired pharmacological properties. In the dynamic landscape of drug discovery, the quest for novel therapeutics demands a multi-faceted approach that integrates various disciplines, methodologies, and technologies. Among the crucial aspects shaping this field are the evaluation of Absorption, Distribution, Metabolism, Excretion, and Toxicity (ADMET), Density Functional Theory (DFT) studies, and Molecular Docking. These methodologies have emerged as indispensable tools, offering insights into the pharmacokinetic, pharmacodynamic, and molecular interactions that underpin the development of efficacious and safe drugs.

ADMET, as an acronym, encapsulates the fundamental processes governing a drug's fate within the biological system. Understanding how a drug is absorbed, distributed, metabolized, excreted, and its potential toxicity profile is quintessential in the early stages of drug development. ADMET studies enable researchers to anticipate and mitigate potential risks associated with candidate compounds, thereby streamlining the drug discovery process. By employing various *in vitro* and *in silico* models, researchers can predict ADMET properties, such as bioavailability, protein binding, metabolism pathways, and potential adverse effects, facilitating informed decision-making in lead optimization and candidate selection.

Complementing ADMET studies, Density Functional Theory (DFT) has emerged as a powerful computational tool for elucidating the molecular properties and behaviors of drug molecules. DFT, a quantum mechanical modeling approach, offers a

detailed understanding of molecular structures, electronic properties, and reactivity, facilitating the rational design of drugs with enhanced efficacy and reduced toxicity. Through DFT studies, researchers can explore the energetics of molecular transformations, investigate reaction mechanisms, and predict key physicochemical properties, providing valuable insights into the structure-activity relationships (SAR) crucial for drug optimization.

Moreover, Molecular Docking serves as a cornerstone in structure-based drug design, facilitating the exploration of ligand-receptor interactions at the atomic level. By simulating the binding of small molecules (ligands) to target proteins (receptors), molecular docking enables the prediction of binding affinities, identification of putative binding sites, and elucidation of binding modes. This information is pivotal in guiding the design and optimization of lead compounds, enabling the development of drugs with high specificity and potency. Molecular docking also plays a pivotal role in virtual screening, wherein vast libraries of compounds are screened computationally to identify potential drug candidates, expediting the hit-to-lead optimization process. In essence, the integration of ADMET studies, DFT calculations, and Molecular Docking represents a synergistic approach to drug discovery, leveraging experimental and computational methodologies to expedite the identification and optimization of novel therapeutics.

4.2 Materials and Methods

4.2.1 Pharmacokinetic and Physicochemical Studies

Absorption, distribution, metabolism, and excretion (ADME) are the internal processes that describe how a drug moves throughout the body (Vrbanac and Slauter 2016). Understanding the ADME properties of a drug is essential to the development of safe and effective drug entities. The qikprop program of Schrodinger (Beard et al. 2013) was used to predict the pharmacokinetic and pharmacodynamic parameters of the synthesized compounds.

4.2.2 DFT Studies

The molecular geometry of the synthesized compounds was optimized using ab initio methods such as density functional theory (DFT) in association with 6-31G++ (d, p) basis set, and Beck's three-parameter exchange function along with the Lee-Yang-Parr nonlocal correlation functional (B3LYP) which is executed in Schrodinger material science package (Tirado-Rives and Jorgensen 2008). Frontier Molecular Orbital (FMO) analysis was done to find out the charge transfer and difference in energy between the orbitals. From the calculation of the energy of HOMO and LUMO orbitals, chemical reactivity parameters were determined to know the stability and reactivity of the synthesized compounds.

4.2.3 *In silico* Molecular Docking Studies

In silico molecular docking was performed to analyze the interaction between the receptor and ligand molecules. *In silico* molecular docking of the synthesized compounds was done using the software Auto Dock-Vina 1.1.2 (Eberhardt et al. 2021; Trott and Olson 2009). The chemical structures of the ligands were drawn in the software ChemDraw Professional 20.1.1 and their three-dimensional structures were energy-minimized using the software Chem3D 20.1.1 (Cousins 2005). The crystal structure of the receptor was retrieved from the protein data bank (PDB ID: 4P8N). The missing residues and atoms of the receptor were fixed using the tool Modeller (Fiser et al. 2000). Before docking all the non-protein components such as cofactors, bound ligands, water molecules, and hetero atoms were removed from the protein's three-dimensional structure. After that polar hydrogens and Kollman charges were added. The active site of the receptor was determined using an online server COACH (Yang et al. 2013). After that, the configuration file was generated by setting the boundary of the docking by creating the cubical grid box of dimensions 100 x 100 x 105 with -0.389 Å, -3.917 Å, and 4.861 Å spacing along the x, y, and z directions respectively. Then the docking was performed using the software Vina by keeping the value of exhaustiveness to 16.

4.3 Results and Discussions

4.3.1 Pharmacokinetic and Physicochemical Studies

4.3.1.1 Pharmacokinetic and Physicochemical studies of 1,3,4-oxadiazole/[1,2,4] triazolo[3,4-*b*][1,3,4]thiadiazine incorporated pyrazine derivatives (T1-T18)

Table 4.1 provides a comprehensive insight into the pharmacokinetic and pharmacodynamic properties of the synthesized molecules (**T1-T18**), affirming their potential as promising candidates for further drug development. These compounds have demonstrated strict adherence to Lipinski's Rule of Five, a fundamental criterion for oral bioavailability, thereby instilling confidence in their suitability for oral administration. The assessment of polar surface area, an essential parameter for drug absorption, reveals values well within the optimal range (**63.54 - 134.33 Å**). Additionally, the favorable Caco-2 cell permeability (QPPCaco) and aqua solubility parameter (QPlogS) values (ranging from **54.25** to **1026.32 nm/s** and **-4.21** to **-2.55**, respectively) further bolster the prospect of exceptional intestinal absorption. Crucially, the blood/brain partition coefficient (QPlogBB) values are found to be within the acceptable range (**-2.02 to -0.08**), signifying the potential of these compounds to traverse the blood-brain barrier a vital attribute for drugs targeting the central nervous system. Furthermore, the Human serum albumin binding coefficient (QPlogKhsa) is well within the desired range (ranging from **-0.99 to -0.11**), emphasizing the compound's ability to bind effectively to human serum albumin, a key factor in drug distribution. Most notably, the percentage of human oral absorption for the majority of these compounds is greater than **80%**, a strong indicator of their outstanding oral bioavailability. In summary, the results of rigorous *in silico* ADME predictions strongly support the progression of these compounds as promising drug candidates.

Table 4.1 *Pharmacokinetic and Physicochemical parameters of the synthesized compounds (**T1-T18**)*

Comp.	MW (≤500 Da)	HBD (≤5)	HBA (≤10)	QPlog P (o/w) (≤5)	QPlog S (≤0.5)	nRB (0-15)	PSA (≤140 Å)	QPPCaco (<25nm/s is low; >500nm/s is high	QPlog Khsa (-1.5 to 1.5)	QPlog BB (-3.0 to 1.2)	%OA (>80% is high: <25% is low)

T1	298.32	0	7	1.49	-2.55	4	89.99	446.15	-0.74	-0.95	83.14
T2	314.32	1	7.75	1.16	-3.20	5	112.65	134.62	-0.50	-1.56	71.86
T3	312.34	0	7	1.81	-3.15	4	89.99	446.15	-0.56	-0.99	85.00
T4	328.34	0	7.75	1.52	-2.55	5	97.25	500.24	-0.79	-0.97	84.19
T5	316.31	0	7	1.73	-2.93	4	89.98	446.50	-0.69	-0.85	84.55
T6	332.76	0	7	2.00	-3.32	4	89.98	446.44	-0.61	-0.80	86.10
T7	377.21	0	7	2.08	-3.44	4	89.96	447.08	-0.58	-0.80	86.60
T8	343.32	0	8	0.73	-2.56	5	134.33	54.25	-0.84	-2.02	62.28
T9	323.33	0	8.5	0.66	-3.34	5	115.78	92.37	-0.99	-1.80	66.01
T10	294.33	0	5.5	2.23	-3.31	0	63.55	1025.86	-0.28	-0.24	93.93
T11	310.33	1	6.25	1.81	-3.78	1	86.21	309.54	-0.13	-0.81	82.16
T12	308.36	0	5.5	2.55	-3.91	0	63.55	1025.86	-0.11	-0.27	95.79
T13	324.36	0	6.25	2.24	-3.36	1	72.02	1025.86	-0.33	-0.32	93.98
T14	312.32	0	5.5	2.47	-3.69	0	63.54	1026.09	-0.23	-0.13	95.33
T15	328.78	0	5.5	2.74	-4.08	0	63.54	1026.07	-0.15	-0.09	96.89
T16	373.23	0	5.5	2.82	-4.21	0	63.55	1026.32	-0.13	-0.08	100
T17	339.33	0	6.5	1.47	-3.33	1	107.90	124.75	-0.39	-1.22	73.07
T18	319.34	0	7	1.40	-4.10	1	89.35	212.40	-0.53	-1.02	76.80

Comp.: *Compound****, MW:*** *Molecular Weight,* ***HBD:*** *Number of hydrogen bond donors,* ***HBA:*** *Number of hydrogen bond acceptors,* ***QPlogP (o/w):*** *Logarithm of partition coefficient between n-octanol and water,* ***QPlogS:*** *Aqua solubility parameter,* ***nRB:*** *Number of rotatable bonds,* ***PSA:*** *Polar Surface Area,* ***QPPCaco:*** *Caco-2 Cell permeability,* ***QPlogKhsa:*** *Human serum albumin binding co-efficient,* ***QPlogBB:*** *Blood/Brain partition co-efficient,* ***%OA:*** *Percentage of oral absorption.*

4.3.1.2 Pharmacokinetic and Physicochemical Studies of 1,2,4-triazole incorporated pyrazine derivatives (T19-T36)

The comprehensive summary of the pharmacokinetic and physicochemical characteristics of the synthesized molecules (**T19-T36**) is outlined in **Table 4.2**, outlining their potential as promising candidates for advancing drug development. Adhering closely to Lipinski's rule of five, a well-established standard for assessing a compound's suitability for oral administration ensures that all target compounds possess favorable pharmaceutical attributes. Compounds that violate more than one of these criteria often face challenges related to permeability or solubility and are considered less suitable for pharmaceutical advancement. In the scope of this study, all the

synthesized compounds adhere to Lipinski's rule of five, thereby confirming their suitability for oral delivery. The evaluation of a drug's safety profile heavily relies on the parameters associated with Absorption, Distribution, Metabolism, and Excretion. All of the target compounds exhibit favorable ADME characteristics. When examining the polar surface area, a crucial factor in how well a drug is absorbed, we found that the values comfortably fall within the optimal range (ranging from **60.70** to **131.85 Å**). Moreover, the favorable values for Caco-2 cell permeability (QPPCaco) and the aqueous solubility parameter (QPlogS) (ranging from **54.31** to **1128.37 nm/s** and **-5.25** to **-3.38**, respectively) further enhance the potential for efficient absorption in the intestines. Significantly, the blood-brain partition coefficient (QPlogBB) values are within an acceptable range (**-2.02** to **-0.24**), indicating that these compounds can cross the blood-brain barrier. Furthermore, the Human serum albumin binding coefficient (QPlogKhsa) falls comfortably within the desired range (ranging from **-0.50** to **0.20**), underscoring the potential of these compounds to effectively bind to human serum albumin, a critical factor in how drugs are distributed in the body. Notably, a majority of these compounds demonstrate a human oral absorption rate greater than **85%**, which is a strong indicator of their outstanding oral bioavailability. In summary, the comprehensive *in silico* ADME predictions provide strong support for advancing these compounds as promising candidates for further development in drug discovery.

Table 4.2 *Pharmacokinetic and Physicochemical parameters of the synthesized compounds (**T19-T36**)*

Comp.	MW (≤500 Da)	HBD (≤5)	HBA (≤10)	QPlogP (o/w) (≤5)	QPlogS (≤0.5)	nRB (0-15)	PSA (≤140 Å)	QPPCaco (<25nm/s is low; >500nm/s is high	QPlogKhsa (-1.5 to 1.5)	QPlogBB (-3.0 to 1.2)	%OA (>80% is high: <25% is low)
T19	297.33	1	6.5	1.84	-3.49	4	87.14	454.69	-0.32	-0.95	85.31
T20	311.36	1	6.5	2.10	-4.03	4	87.16	454.22	-0.17	-0.99	86.83
T21	327.36	1	7.25	1.95	-3.73	5	95.37	453.58	-0.32	-1.05	85.90
T22	313.33	2	7.25	1.21	-3.38	5	109.73	137.55	-0.40	-1.57	72.31
T23	342.33	1	7.5	1.13	-3.60	5	131.86	54.32	-0.39	-2.03	64.61
T24	322.34	1	8	1.08	-4.41	5	112.94	96.13	-0.51	-1.78	68.78
T25	315.32	1	6.5	2.02	-3.78	4	87.15	454.64	-0.28	-0.85	86.31
T26	331.78	1	6.5	2.35	-4.23	4	87.14	454.89	-0.22	-0.81	88.27
T27	376.23	1	6.5	2.42	-4.33	4	87.14	454.87	-0.20	-0.80	88.70

T28	269.32	1	4.5	2.61	-3.85	3	60.78	1109.17	-0.05	-0.48	96.73
T29	337.32	1	4.5	3.58	-5.26	3	60.78	1109.04	0.20	-0.24	100
T30	287.31	1	4.5	2.83	-4.19	3	60.78	1109.26	-0.01	-0.38	100
T31	287.31	1	4.5	2.78	-4.08	3	60.77	1109.81	-0.02	-0.40	100
T32	294.33	1	6	1.83	-4.78	4	86.58	234.64	-0.22	-1.29	80.10
T33	348.22	1	4.5	3.17	-4.68	3	60.78	1109.31	0.09	-0.32	100
T34	348.22	1	4.5	3.08	-4.48	3	60.70	1128.37	0.06	-0.33	100
T35	303.77	1	4.5	3.09	-4.57	3	60.78	1109.50	0.06	-0.33	100
T36	314.32	1	5.5	1.88	-3.99	4	105.46	132.99	-0.10	-1.54	75.99

Comp.: *Compound,* ***MW:*** *Molecular Weight,* ***HBD:*** *Number of hydrogen bond donors,* ***HBA:*** *Number of hydrogen bond acceptors,* ***QPlogP (o/w):*** *Logarithm of partition coefficient between n-octanol and water,* ***QPlogS:*** *Aqua solubility parameter,* ***nRB:*** *Number of rotatable bonds,* ***PSA:*** *Polar Surface Area,* ***QPPCaco:*** *Caco-2 Cell permeability,* ***QPlogKhsa:*** *Human serum albumin binding co-efficient,* ***QPlogBB:*** *Blood/Brain partition co-efficient,* ***%OA:*** *Percentage of oral absorption.*

4.3.1.3 Pharmacokinetic and Physicochemical Studies of pyrazine hydrazinylidene derivatives containing benzenesulfonate scaffold (T37-T52)

Table 4.3 provides a detailed overview of the pharmacokinetic and pharmacodynamic properties of the synthesized compounds (**T37-T52**), highlighting their potential as promising candidates for further drug development. All the synthesized compounds meet Lipinski's rule of five, ensuring their drug-like properties. The ADME parameters play a crucial role in assessing the safety profile of a drug. All the synthesized compounds exhibit favorable ADME properties. The evaluation of the polar surface area, an important factor in drug absorption, reveals values well within the optimal range (ranging from **104.09** to **127.91 Å**). Additionally, the favorable values for Caco-2 cell permeability (QPPCaco) and aqueous solubility parameter (QPlogS) (ranging from **179.31** to **301.84 nm/s** and **-5.59** to **-3.99**, respectively) further enhance the prospect of excellent intestinal absorption. Crucially, the blood-brain partition coefficient (QPlogBB) values fall within the acceptable range (**-1.97** to **-1.43**), indicating that these compounds have the potential to cross the blood-brain barrier, which is essential for drugs targeting the central nervous system. Furthermore, the Human serum albumin binding coefficient (QPlogKhsa) is well within the desired range

(ranging from **-0.49** to **-0.24**), emphasizing the potential of these compounds to effectively bind to human serum albumin, a key factor in drug distribution. Most notably, the majority of these compounds exhibit a human oral absorption rate greater than **80%**, which is a strong indicator of their exceptional oral bioavailability.

Table 4.3 *Pharmacokinetic and Physicochemical parameters of the synthesized compounds (**T37-T52**)*

Comp.	MW (≤500 Da)	HBD (≤5)	HBA (≤10)	QPlogP (o/w) (≤5)	QPlogS (≤0.5)	nRB (0-15)	PSA (≤140 Å)	QPPCaco (<25nm/s is low; >500nm/s is high	QPlog Khsa (-1.5 to 1.5)	QPlog BB (-3.0 to 1.2)	%OA (>80% is high: <25% is low)
T37	382.39	1	9.5	1.93	-4.185	7	119.44	179.31	-0.40	-1.88	78.58
T38	396.42	1	9.5	2.22	-4.721	7	119.44	179.31	-0.26	-1.93	80.28
T39	412.41	1	10	1.95	-4.278	8	127.91	179.31	-0.43	-1.97	78.74
T40	450.39	1	9.5	2.52	-4.74	7	112.61	208.28	-0.27	-1.58	83.23
T41	400.38	1	9.5	2.16	-4.543	7	119.42	179.35	-0.36	-1.78	79.94
T42	416.83	1	9.5	2.41	-4.90	7	119.43	179.35	-0.298	-1.75	81.43
T43	381.40	2	10	1.75	-3.99	8	112.66	209.83	-0.47	-1.85	78.75
T44	461.28	1	9.5	2.49	-5.02	7	119.40	179.32	-0.275	-1.74	81.88
T45	450.39	1	9.5	2.89	-5.59	7	119.44	179.31	-0.165	-1.67	84.22
T46	395.43	2	10	2.02	-4.49	8	112.66	209.83	-0.338	-1.89	80.38
T47	411.43	2	10	1.78	-4.09	9	121.14	209.83	-0.491	-1.94	78.95
T48	449.40	2	10	2.48	-4.63	8	104.09	301.84	-0.323	-1.43	85.87
T49	399.39	2	10	1.97	-4.34	8	112.65	209.88	-0.434	-1.75	80.09
T50	415.85	2	10	2.22	-4.69	8	112.65	209.88	-0.371	-1.71	81.54
T51	460.30	2	10	2.30	-4.80	8	112.63	209.84	-0.35	-1.70	81.98
T52	449.40	2	10	2.69	-5.35	8	112.66	209.83	-0.249	-1.64	84.27

Comp.: *Compound,* ***MW:*** *Molecular Weight,* ***HBD:*** *Number of hydrogen bond donors,* ***HBA:*** *Number of hydrogen bond acceptors,* ***QPlogP (o/w):*** *Logarithm of partition coefficient between n-octanol and water,* ***QPlogS:*** *Aqua solubility parameter,* ***nRB:*** *Number of rotatable bonds,* ***PSA:*** *Polar Surface Area,* ***QPPCaco:*** *Caco-2 Cell permeability,* ***QPlogKhsa:*** *Human serum albumin binding co-efficient,* ***QPlogBB:*** *Blood/Brain partition co-efficient,* ***%OA:*** *Percentage of oral absorption.*

4.3.1.4 Pharmacokinetic and Physicochemical Studies of 4-quinazolinone incorporated pyrazine derivatives (T53-T68)

Table 4.4 furnishes an intricate synopsis of the pharmacokinetic and pharmacodynamic characteristics of the synthesized compounds (**T53-T68**), delineating their potential as favourable options for advancing drug development. All the synthesized compounds align with Lipinski's rule of five, thus corroborating their aptitude for oral dispensation. Each of the synthesized compounds evinces propitious ADME characteristics. Scrutiny of the polar surface area, a pivotal determinant in drug absorptiveness, discloses values comfortably situated well within the optimal range (ranging from **93.30** to **138.28 Å**). Additionally, the favorable values for Caco-2 cell permeability (QPPCaco) and the aqueous solubility parameter (QPlogS) (ranging from **52.00** to **907.52 nm/s** and **-5.30** to **-1.43**, respectively) further augments the potential for superlative intestinal assimilation. Importantly, the blood-brain partition coefficient (QPlogBB) values fall within the acceptable range (**-1.83** to **-0.39**), indicating that these compounds possess the capability to traverse the blood-brain barrier. Furthermore, the Human serum albumin binding coefficient (QPlogKhsa) is well within the desired range (ranging from **-0.01** to **-0.65**), underscoring the potential of these compounds to effectively bind to human serum albumin, a key factor in drug distribution. Most notably, the majority of these compounds exhibit a human oral absorption rate surpassing **80%**, a strong indicator of their exceptional oral bioavailability.

Table 4.4 *Pharmacokinetic and Physicochemical parameters of the synthesized compounds* ***(T53-T68)***

Comp.	MW (≤500 Da)	HBD (≤5)	HBA (≤10)	QPlog P (o/w) (≤5)	QPlog S (≤0.5)	nRB (0-15)	PSA (≤140 Å)	QPPCaco (<25nm/s is low; >500nm/s is high	QPlog Khsa (-1.5 to 1.5)	QPlogBB (-3.0 to 1.2)	%OA (>80% is high: <25% is low)
T53	257.25	1.5	6	0.95	-2.86	4	124.11	122.68	-0.39	-1.56	69.90
T54	299.30	1.25	7.25	1.43	-3.30	2	103.04	487.68	-0.43	-0.68	83.43
T55	279.26	2	9	-0.41	-1.43	1	110.65	52.00	-0.65	-0.71	55.22
T56	345.36	1.25	7.75	2.29	-3.98	2	93.94	709.18	-0.11	-0.69	91.40
T57	424.25	1.25	7.75	2.85	-4.79	2	93.88	713.96	0.01	-0.53	94.71
T58	363.35	1.25	7.75	2.52	-4.33	2	93.91	711.51	-0.07	-0.58	92.77
T59	370.37	1.25	9.25	1.53	-4.94	3	119.73	146.83	-0.28	-1.51	74.73
T60	390.35	1.25	8.75	1.56	-4.08	3	138.28	86.24	-0.17	-1.73	70.78
T61	359.38	1.25	7.75	2.55	-4.27	2	94.48	842.44	-0.01	-0.62	94.26
T62	413.35	1.25	7.75	3.04	-4.84	2	93.30	907.52	0.04	-0.39	100
T63	361.35	2.25	8.5	1.63	-3.90	3	116.59	213.98	-0.19	-1.29	78.24

T64	440.25	2.25	8.5	2.28	-4.63	3	116.01	305.31	-0.08	-0.98	84.77
T65	377.35	3.25	9.25	1.01	-3.79	4	138.02	75.33	-0.29	-1.83	66.50
T66	396.40	1.25	9.25	2.23	-4.42	2	108.08	399.94	-0.12	-1.00	86.62
T67	460.87	1.25	9.5	3.05	-5.30	3	112.72	548.11	0.07	-0.83	93.84
T68	351.38	1.25	7.75	2.24	-3.96	2	94.69	694.10	-0.16	-0.59	90.92

Comp.: *Compound****, MW:*** *Molecular Weight,* ***HBD:*** *Number of hydrogen bond donors,* ***HBA:*** *Number of hydrogen bond acceptors,* ***QPlogP (o/w):*** *Logarithm of partition coefficient between n-octanol and water,* ***QPlogS:*** *Aqua solubility parameter,* ***nRB:*** *Number of rotatable bonds,* ***PSA:*** *Polar Surface Area,* ***QPPCaco:*** *Caco-2 Cell permeability,* ***QPlogKhsa:*** *Human serum albumin binding co-efficient,* ***QPlogBB:*** *Blood/Brain partition co-efficient,* ***%OA:*** *Percentage of oral absorption.*

4.3.1.5 Pharmacokinetic and Physicochemical Studies of 2-aminophenyl and 2-oxoacetyl incorporated pyrazine-2-carbohydrazide derivatives (T69-T88)

Table 4.5 provides a detailed summary of how well the synthesized compounds (**T69-T88**) move through the body, indicating their potential as promising options for developing drugs. All the synthesized compounds of the series meet Lipinski's rule of five, confirming their potential for oral delivery. All the compounds display favorable ADME characteristics. Examination of the polar surface area, a critical factor in drug absorption, reveals values comfortably within the optimal range (ranging from **133.70** to **159.50 Å**). Moreover, the advantageous values for Caco-2 cell permeability (QPPCaco) and the aqueous solubility parameter (QPlogS) (ranging from **139.34** to **223.57 nm/s** and **-5.81** to **-2.91**, respectively) further enhance the potential for excellent absorption in the intestines. Significantly, the blood-brain partition coefficient (QPlogBB) values fall within the acceptable range (**-2.41** to **-1.82**), suggesting that these compounds can cross the blood-brain barrier. Additionally, the Human serum albumin binding coefficient (QPlogKhsa) is well within the desired range (ranging from **-0.01** to **-0.80**), highlighting the ability of these compounds to effectively bind to human serum albumin, a critical factor in drug distribution. Most notably, a majority of these compounds exhibit a human oral absorption rate greater than **80%**, indicating exceptional oral bioavailability. To summarize, the comprehensive *in silico* ADME

predictions strongly advocate for the advancement of these compounds as promising candidates for further development in drug discovery.

Table 4.5 *Pharmacokinetic and Physicochemical parameters of the synthesized compounds (**T69-T88**)*

Comp.	MW (≤ 500 Da)	HBD (≤ 5)	HBA (≤ 10)	QPlogP (o/w) (≤ 5)	QPlogS (≤ 0.5)	nRB (0-15)	PSA (≤ 140Å)	QPPCaco (<25nm/s is low; >500nm/s is high	QPlogKhsa (-1.5 to 1.5)	QPlogBB (-3.0 to 1.2)	%OA (>80% is high: <25% is low)
T69	285.26	1.25	7.75	0.33	-2.91	5	148.38	139.54	-0.59	-2.27	77.51
T70	303.25	1.25	7.75	0.56	-3.26	5	148.54	139.34	-0.56	-2.18	78.80
T71	319.70	1.25	7.75	0.81	-3.62	5	148.53	139.34	-0.49	-2.15	70.26
T72	364.15	1.25	7.75	0.89	-3.72	5	148.41	139.58	-0.47	-2.15	70.75
T73	299.28	1.25	7.75	0.61	-3.42	5	148.38	139.54	-0.46	-2.34	79.14
T74	299.28	0.25	7.75	0.89	-3.05	5	135.89	191.15	-0.62	-1.95	77.26
T75	317.27	0.25	7.75	1.13	-3.42	5	136.06	190.6	-0.57	-1.86	78.59
T76	333.7	0.25	7.75	1.39	-3.80	5	136.05	190.60	-0.50	-1.82	80.11
T77	378.18	0.25	7.75	1.46	-3.91	5	135.94	191.12	-0.47	-1.82	80.62
T78	313.31	0.25	7.75	1.19	-3.61	5	135.89	191.15	-0.46	-2.01	79.03
T79	375.38	0.25	7.75	2.72	-4.94	7	133.75	223.57	-0.06	-2.11	80.34
T80	393.37	0.25	7.75	2.96	-5.32	7	133.91	222.83	-0.01	-2.02	81.69
T81	409.83	0.25	7.75	3.22	-5.70	7	133.90	222.83	0.05	-1.98	83.21
T82	454.28	0.25	7.75	3.30	-5.81	7	133.8	223.54	0.08	-1.98	83.72
T83	389.41	0.25	7.75	2.79	-5.16	7	133.90	206.97	0.03	-2.17	79.60
T84	327.29	0.25	9.25	0.37	-2.95	5	159.36	144.34	-0.80	-2.35	88.62
T85	345.28	0.25	9.25	0.61	-3.32	5	159.50	144.11	-0.76	-2.26	89.97
T86	361.74	0.25	9.25	0.87	-3.70	5	159.49	144.11	-0.68	-2.23	81.48
T87	406.19	0.25	9.25	0.95	-3.81	5	159.37	144.40	-0.66	-2.22	82.99
T88	341.32	0.25	9.25	0.67	-3.51	5	159.36	144.34	-0.64	-2.41	80.39

Comp.: *Compound,* ***MW:*** *Molecular Weight,* ***HBD:*** *Number of hydrogen bond donors,* ***HBA:*** *Number of hydrogen bond acceptors,* ***QPlogP (o/w):*** *Logarithm of partition coefficient between n-octanol and water,* ***QPlogS:*** *Aqua solubility parameter,* ***nRB:*** *Number of rotatable bonds,* ***PSA:*** *Polar Surface Area,* ***QPPCaco:*** *Caco-2 Cell permeability,* ***QPlogKhsa:*** *Human serum albumin binding co-efficient,* ***QPlogBB:*** *Blood/Brain partition co-efficient,* ***%OA:*** *Percentage of oral absorption.*

4.3.2 DFT studies

4.3.2.1 DFT studies of 1,3,4-oxadiazole/[1,2,4] triazolo[3,4-*b*][1,3,4]thiadiazine incorporated pyrazine derivatives (T1-T18)

The geometry of the synthesized compounds (**T1-T18**) was optimized using ab initio methods, such as density functional theory (DFT), along with a 6-31G++ (d, p) basis set and the B3LYP functional. In this context, the HOMO (highest occupied molecular orbital) and LUMO (lowest unoccupied molecular orbital) are significant as they are referred to as the frontier molecular orbitals (FMOs). The HOMO represents an electron-rich orbital, while the LUMO is an electron-poor orbital. These FMOs play a crucial role in dictating how a molecule interacts with its target. Generally, a compound's binding capacity tends to decrease as its HOMO energy decreases and its LUMO energy increases. **Table 4.6** presents the energies of the HOMO and LUMO for the synthesized compounds (**T1-T18**) determined using the DFT method. **Figures 4.1a** and **4.2a** display the FMOs for the active compounds **T7** and **T17** respectively. From the DFT analysis, it is observed that the HOMO electron cloud is distributed across the pyrazine and 1,3,4-oxadiazole ring, as well as the sulfur atom attached to the 1,3,4-oxadiazole ring. Conversely, the LUMO electron cloud extends over the benzene ring and the carbonyl group attached to it. The energy difference between the HOMO and LUMO reflects the reactivity, hardness, and softness of the compound. A smaller energy difference indicates higher chemical reactivity and more potential intermolecular interactions, making the molecule soft. Conversely, molecules with a larger energy difference possess greater thermal stability and fewer intermolecular interactions, classifying them as hard molecules.

Understanding global chemical reactivity descriptors is crucial for establishing connections between a molecule's structure, stability, and reactivity**.** These descriptors, which include Ionization Potential (IP), Electron Affinity (EA), Chemical Hardness (η), Chemical Softness (σ), Chemical Potential (μ), Electrophilicity Index (ω), and Electronegativity (χ), were calculated based on the HOMO and LUMO energy levels of the molecules, and their values are provided in **Table 4.6**. The higher the chemical

softness value, the stronger the binding affinity to the receptor, whereas a higher chemical hardness value indicates a weaker binding affinity. All the synthesized compounds exhibit greater chemical softness and lower chemical hardness compared to standard drugs. The interaction between the ligand and receptor becomes more pronounced as the chemical potential increases, and all the target compounds have higher chemical potential values compared to standard drugs. Electrophilicity index and electronegativity are metrics used to gauge a molecule's ability to attract electrons from its surroundings. Molecules with higher electrophilicity index and electronegativity values tend to form more interactions with receptors. All of the synthesized compounds exhibit higher electronegativity values than standard drugs, and their electrophilicity index values are similar to those of standard drugs. Ionization potential and electron affinity are used to assess a molecule's tendency to gain or lose electrons to its surroundings. **Figures 4.1b** and **4.2b** represent the electron density surface of the compounds **T7** and **T17** respectively. Toxicity tends to increase as IP and EA values decrease. FDA-approved drugs typically have EA values ranging from -3 to 7 eV and IP values ranging from 4 to 15 eV. All the target compounds in question have IP and EA values within this specified range. To validate the reactivity of these molecules, we employed molecular electrostatic potential surface (MEP) calculations. This approach is crucial for predicting the relationships between the physical and chemical properties of these target molecules. Furthermore, it helps us understand their propensity to engage in electrophilic and nucleophilic reactions. Using DFT we computed the MEP of the target compounds. The MEPs of the compounds **T7** and **T17** are depicted in **Figures 4.1c** and **4.2c** respectively. The MEP surface is color-coded for clarity. Blue regions signify positive electrostatic potential, while red regions indicate negative electrostatic potential. White regions denote neutral electrostatic potential. Across all these molecules, the areas with negative electrostatic potential tend to be concentrated around oxygen, nitrogen, and sulfur atoms. Conversely, the regions displaying positive electrostatic potential are primarily located near hydrogen atoms and a phenyl ring.

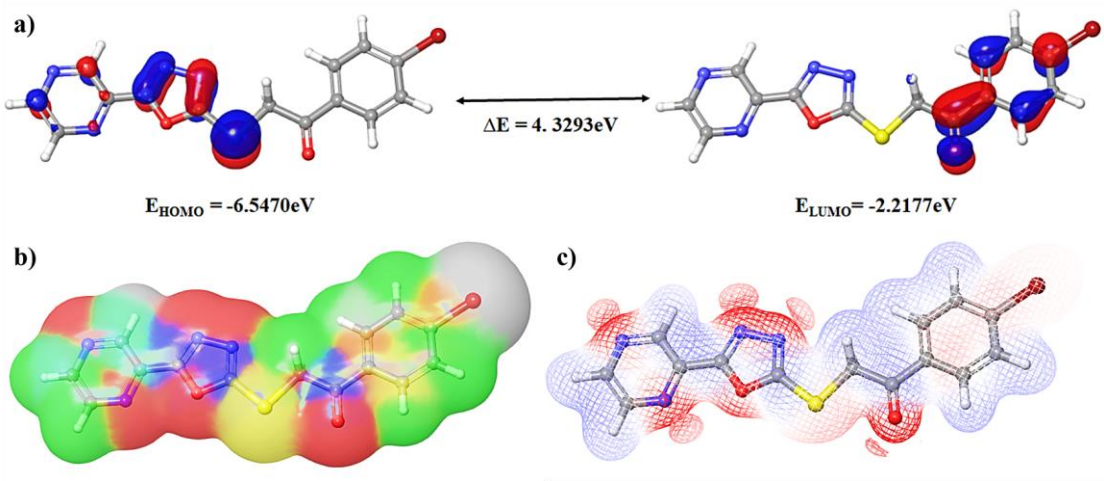

Figure 4.1 *a) Frontier Molecular Orbitals; b) Electron density surface; and c) Electrostatic potential of compound T7*

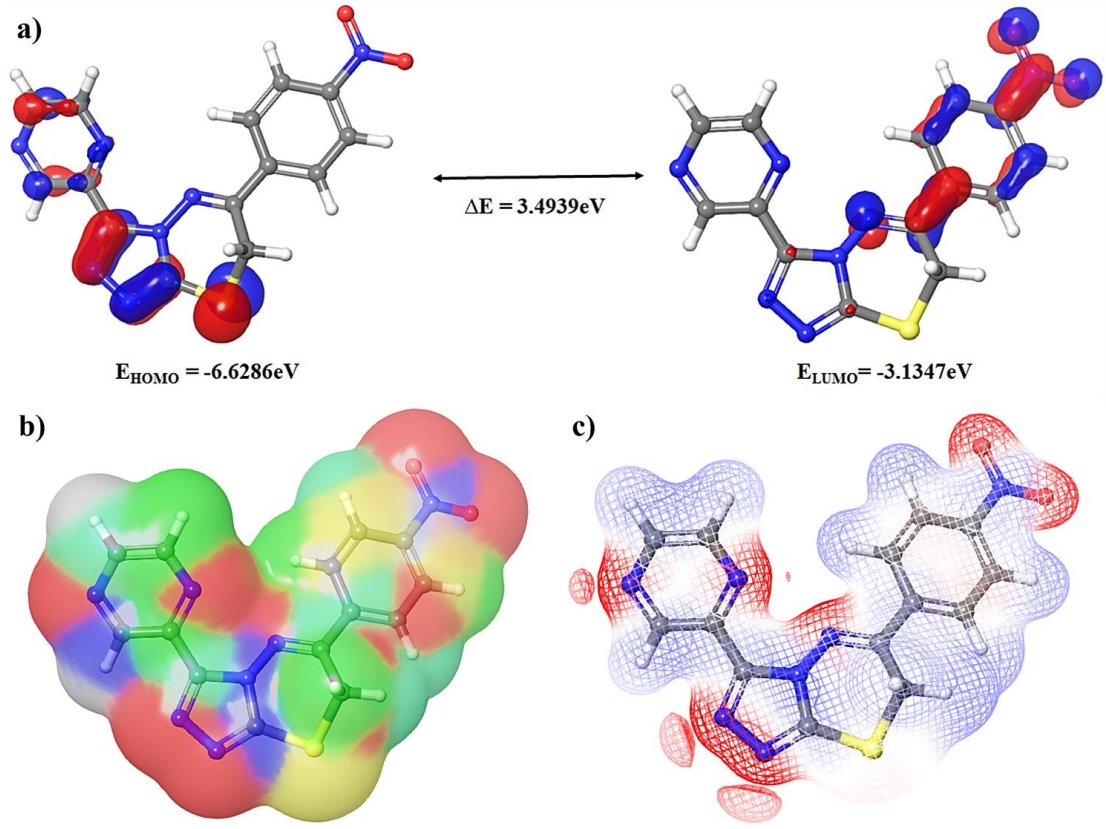

Figure 4.2 *a) Frontier Molecular Orbitals; b) Electron density surface; and c) Electrostatic potential of compound T17*

Table 4.6 *Global reactivity parameters of the synthesized compounds (**T1-T18**)*

Comp.	E_{HOMO} (eV)	E_{LUMO} (eV)	ΔE (eV)	IP (eV)	EA (eV)	η (eV)	σ (eV)	μ (eV)	ω (eV)	χ (eV)
T1	-6.4572	-2.0571	4.4001	6.4572	2.0571	2.2000	0.2273	-2.2000	1.1000	4.2571
T2	-6.3783	-2.0163	4.3620	6.3783	2.0163	2.1810	0.2292	-2.1810	1.0905	4.1973
T3	-6.4082	-2.0299	4.3783	6.4082	2.0299	2.1891	0.2284	-2.1891	1.0945	4.2190
T4	-6.3484	-2.0109	4.3375	6.3484	2.0109	2.1687	0.2305	-2.1687	1.0843	4.1796
T5	-6.5062	-2.0925	4.4137	6.5062	2.0925	2.2068	0.2266	-2.2068	1.1034	4.2993
T6	-6.5416	-2.1959	4.3457	6.5416	2.1959	2.1728	0.2301	-2.1728	1.0864	4.3687
T7	-6.5470	-2.2177	4.3293	6.5470	2.2177	2.1646	0.2310	-2.1646	1.0823	4.3823
T8	-6.6967	-3.2109	3.4858	6.6967	3.2109	1.7429	0.2869	-1.7429	0.8714	4.9538
T9	-6.6722	-2.7728	3.8994	6.6722	2.7728	1.9497	0.2564	-1.9497	0.9748	4.7225
T10	-6.3212	-2.1578	4.1634	6.3212	2.1578	2.0817	0.2402	-2.0817	1.0408	4.2395
T11	-6.2368	-2.0408	4.1960	6.2368	2.0408	2.0980	0.2383	-2.0980	1.0490	4.1388
T12	-6.2722	-2.0871	4.1851	6.2722	2.0871	2.0925	0.2390	-2.0925	1.0462	4.1796
T13	-6.1824	-2.0027	4.1797	6.1824	2.0027	2.0898	0.2392	-2.0898	1.0449	4.0925
T14	-6.3756	-2.2095	4.1661	6.3756	2.2095	2.0830	0.2400	-2.0830	1.0415	4.2925
T15	-6.4273	-2.3429	4.0844	6.4273	2.3429	2.0422	0.2448	-2.0422	1.0211	4.3851
T16	-6.4327	-2.3537	4.0790	6.4327	2.3537	2.0395	0.2451	-2.0395	1.0197	4.3932
T17	-6.6286	-3.1347	3.4939	6.6286	3.1347	1.7469	0.2862	-1.7469	0.8734	4.8816
T18	-6.5878	-2.7728	3.8150	6.5878	2.7728	1.9075	0.2621	-1.9075	0.9537	4.6803
PZA	-6.7838	-1.9347	4.8491	6.7838	1.9347	2.4246	0.2062	-2.4246	1.2123	4.3592
INN	-5.7007	-1.2027	4.4980	5.7007	1.2027	2.2490	0.2223	-2.2490	1.1245	3.4517

Comp.: *Compound, Bandgap (*ΔE*)* = E_{HOMO} - E_{LUMO}*, Ionization potential (**IP**) = -* E_{HOMO}*, Electron affinity (**EA**) = -* E_{LUMO}*, Chemical hardness (**η**) = (**IP-EA**)/2, Chemical softness (**σ**) = 1/2 **η**, Chemical potential (**μ**) = - **η**, electrophilicity index (**ω**) = **η** /2, electronegativity (**χ**) = (**IP** + **EA**)/2.*

4.3.2.2 DFT studies of 1,2,4-triazole incorporated pyrazine derivatives (T19-T36)

The synthesized compounds (**T19-T36**) were subjected to DFT calculations to optimize their geometry and determine the energy of the frontier molecular orbitals. **Table 4.7** summarizes the HOMO and LUMO energy values for these compounds. **Figure 4.3a** provides visual representations of the FMOs for the potent molecule **T29**. Through DFT analysis, it was observed that in compound **T29**, the electron cloud of the HOMO is mainly localized across the 1,2,4-triazole ring and the accompanying sulfur atom. Conversely, the LUMO exhibits a broader distribution of its electron cloud across the Pyrazine ring. Chemical reactivity descriptors were derived from the evaluation of the HOMO and LUMO energy levels, as detailed in **Table 4.7**. Notably,

All the synthesized compounds exhibit greater chemical softness and lower chemical hardness compared to standard drugs. Also, all the synthesized compounds display higher chemical potential values compared to standard pharmaceuticals. Additionally, their electronegativity and electrophilicity index values are similar to those of the reference drugs. **Figure 4.3c** illustrates the electron density surface of compound **T29**. It's worth noting that all investigated compounds fall within the specified range of ionization potential and electron affinity values typical of FDA-approved pharmaceuticals, with EA values ranging from -3 to 7 eV and IP values from 4 to 15 eV. To assess the reactivity of these compounds, Molecular Electrostatic Potential computations were conducted. In **Figure 4.3b**, the MEP of compound **T29** was depicted with detailed color coding for clarity. Throughout the molecules, regions with a negative electrostatic potential are primarily located near nitrogen, sulfur, and fluorine atoms, while regions with a positive electrostatic potential are predominantly found near hydrogen atoms and a complex phenyl ring structure.

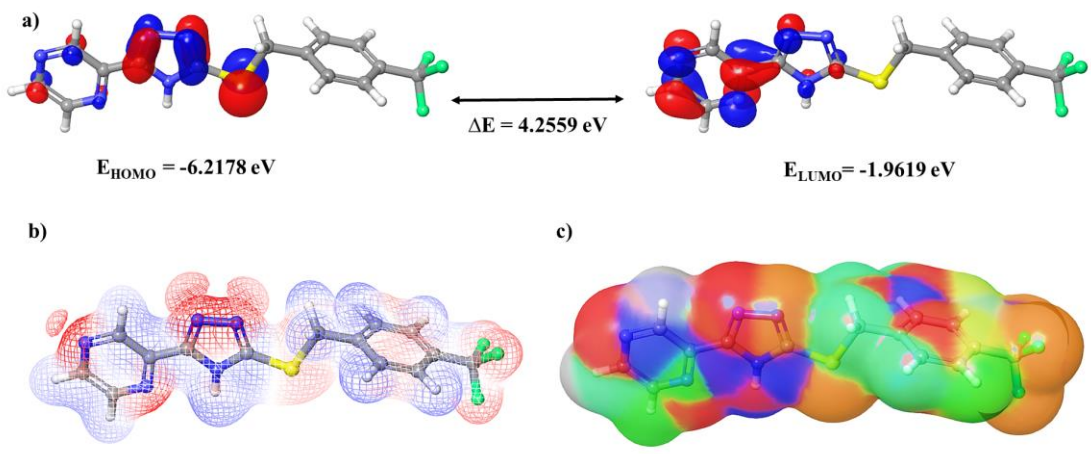

Figure 4.3 *a) Frontier Molecular Orbitals, b) Molecular electrostatic potentials, and c) Electron density surface of compound T29*

Table 4.7 *Global reactivity parameters of the synthesized compounds (**T19-T36**)*

Comp.	E_{HOMO} (eV)	E_{LUMO} (eV)	ΔE (eV)	IP (eV)	EA (eV)	η (eV)	σ (eV)	μ (eV)	ω (eV)	χ (eV)
T19	-6.0954	-1.8858	4.2096	6.0954	1.8858	2.1048	0.2376	-2.1048	1.0524	3.9906
T20	-6.0437	-1.8531	4.1906	6.0437	1.8531	2.0953	0.2386	-2.0953	1.0476	3.9484

T21	-6.0518	-1.7905	4.2613	6.0518	1.7905	2.1307	0.2347	-2.1307	1.0653	3.9212
T22	-6.0300	-1.8449	4.1851	6.0300	1.8449	2.0926	0.2389	-2.0926	1.0463	3.9375
T23	-6.3212	-3.1266	3.1946	6.3212	3.1266	1.5973	0.3130	-1.5973	0.7987	4.7239
T24	-6.3049	-2.6694	3.6354	6.3049	2.6694	1.8177	0.2751	-1.8177	0.9089	4.4872
T25	-6.1362	-1.9184	4.2178	6.1362	1.9184	2.1089	0.2371	-2.1089	1.0544	4.0273
T26	-6.1743	-2.0871	4.0872	6.1743	2.0871	2.0436	0.2447	-2.0436	1.0218	4.1307
T27	-6.1824	-2.1034	4.0790	6.1824	2.1034	2.0395	0.2452	-2.0395	1.0197	4.1429
T28	-6.0437	-1.8585	4.1851	6.0437	1.8585	2.0926	0.2389	-2.0926	1.0463	3.9511
T29	-6.2178	-1.9619	4.2559	6.2178	1.9619	2.1279	0.2350	-2.1279	1.0640	4.0899
T30	-6.1144	-1.8994	4.2150	6.1144	1.8994	2.1075	0.2372	-2.1075	1.0538	4.0069
T31	-6.0573	-1.8558	4.2014	6.0573	1.8558	2.1007	0.2380	-2.1007	1.0504	3.9565
T32	-6.3130	-2.0218	4.2912	6.3130	2.0218	2.1456	0.2330	-2.1456	1.0728	4.1674
T33	-6.1688	-1.9347	4.2341	6.1688	1.9347	2.1170	0.2362	-2.1170	1.0585	4.0518
T34	-6.0709	-1.8613	4.2096	6.0709	1.8613	2.1048	0.2376	-2.1048	1.0524	3.9661
T35	-6.1661	-1.9293	4.2368	6.1661	1.9293	2.1184	0.2360	-2.1184	1.0592	4.0477
T36	-6.3457	-2.6096	3.7361	6.3457	2.6096	1.8681	0.2677	-1.8681	0.9340	4.4776
PZA	-6.7838	-1.9347	4.8491	6.7838	1.9347	2.4246	0.2062	-2.4246	1.2123	4.3592
INN	-5.7007	-1.2027	4.4980	5.7007	1.2027	2.2490	0.2223	-2.2490	1.1245	3.4517

Comp.: *Compound, Bandgap (*ΔE*)* = E_{HOMO} - E_{LUMO}*, Ionization potential* ***(IP)*** = - E_{HOMO}*, Electron affinity* ***(EA)*** = - E_{LUMO}*, Chemical hardness* (η) = ***(IP-EA)/2****, Chemical softness* (σ) = ***1/2*** η*, Chemical potential* (μ) = - η*, electrophilicity index* (ω) = η */2****, electronegativity*** (χ) = ***(IP + EA)/2****.*

4.3.2.3 DFT studies of pyrazine hydrazinylidene derivatives containing benzenesulfonate scaffold (T37-T52)

The synthesized compounds (**T37-T52**) underwent DFT calculations to optimize their geometry and determine the energy levels of the frontier molecular orbitals. **Table 4.8** presents the HOMO and LUMO energy values obtained for these synthesized compounds through DFT calculations. **Figures 4.4a**, **4.4b**, and **4.4c** depict the Frontier Molecular Orbitals for the active compounds **T40**, **T43**, and **T48**, respectively. The DFT analysis reveals that the electron cloud of the HOMO is distributed across both the phenyl ring and the hydrazinylidene linker attached to the pyrazine and phenyl ring. Conversely, the electron cloud of the LUMO extends over the pyrazine ring and the carbonyl group attached to it. Understanding global chemical reactivity descriptors is essential for establishing connections between a molecule's

structure, stability, and reactivity. These descriptors were determined based on the HOMO and LUMO energy levels of the molecules, and their values are detailed in **Table 4.8**. A higher chemical softness value indicates a stronger binding affinity to the receptor, whereas a higher chemical hardness value suggests a weaker binding affinity. Notably, all the target compounds exhibit greater chemical softness and lower chemical hardness compared to reference drugs. The interaction between the ligand and receptor becomes more prominent as the chemical potential increases, and all the target compounds have higher chemical potential values compared to reference drugs. It is worth noting that all the synthesized compounds display values of electronegativity and electrophilicity index similar to those of reference drugs. It's noteworthy that all the compounds have IP and EA values falling within the specified range for FDA-approved drugs, with EA values ranging from -3 to 7 eV and IP values ranging from 4 to 15 eV. To validate the reactivity of these molecules, we performed molecular electrostatic potential surface calculations. The MEP of compounds **T40, T43,** and **T48** were visually represented in **Figures 4.5d**, **4.5e**, and **4.5f**, respectively. In these figures, the MEP surface is color-coded for clarity. Across all these molecules, the regions with negative electrostatic potential are predominantly concentrated and around oxygen, nitrogen, and sulfur atoms, while regions with positive electrostatic potential are primarily found near hydrogen atoms and a phenyl ring.

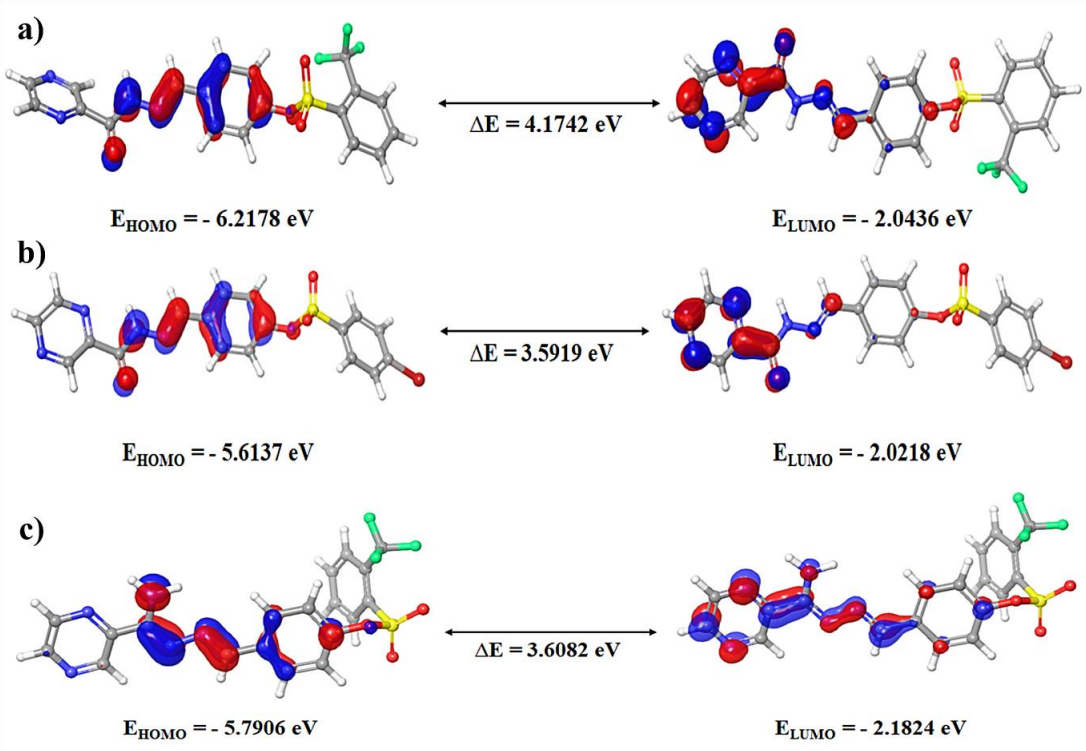

Figure 4.4 *Frontier Molecular Orbitals of the compounds a) T40 b) T43 and c) T48*

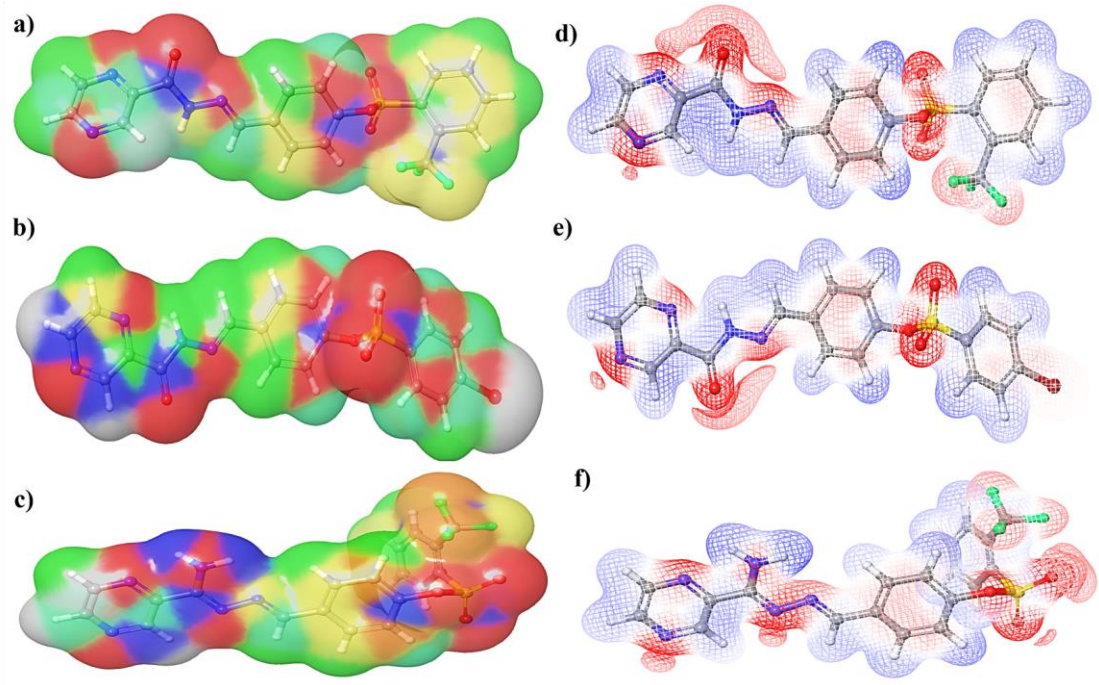

Figure 4.5 *Electron density surface of the compounds a) T40, b) T43, and c) T48 and electrostatic potential of the compounds d) T40, e) T43, and f) T48*

Table 4.8 *Global reactivity parameters of the synthesized compounds (**T37-T52**)*

Comp.	E_{HOMO} (eV)	E_{LUMO} (eV)	ΔE (eV)	IP (eV)	EA (eV)	η (eV)	σ (eV)	μ (eV)	ω (eV)	χ (eV)
T37	-6.0817	-2.1769	3.9048	6.0817	2.1769	1.9524	0.2561	-1.9524	0.9762	4.1293
T38	-6.0491	-2.1606	3.8885	6.0491	2.1606	1.9443	0.2572	-1.9443	0.9721	4.1048
T39	-6.0246	-2.1388	3.8858	6.0246	2.1388	1.9429	0.2573	-1.9429	0.9714	4.0817
T40	-6.2178	-2.0436	4.1742	6.2178	2.0436	2.0871	0.2396	-2.0871	1.0436	4.1307
T41	-6.1307	-2.2041	3.9266	6.1307	2.2041	1.9633	0.2547	-1.9633	0.9817	4.1674
T42	-6.1552	-2.2232	3.9320	6.1552	2.2232	1.9660	0.2543	-1.9660	0.9830	4.1892
T43	-5.6137	-2.0218	3.5919	5.6137	2.0218	1.7960	0.2784	-1.7960	0.8980	3.8178
T44	-6.1471	-2.2177	3.9293	6.1471	2.2177	1.9647	0.2545	-1.9647	0.9823	4.1824
T45	-6.1960	-2.2531	3.9429	6.1960	2.2531	1.9715	0.2536	-1.9715	0.9857	4.2246
T46	-5.5865	-2.0000	3.5865	5.5865	2.0000	1.7932	0.2788	-1.7932	0.8966	3.7933
T47	-5.5566	-1.9728	3.5837	5.5566	1.9728	1.7919	0.2790	-1.7919	0.8959	3.7647
T48	-5.7906	-2.1824	3.6082	5.7906	2.1824	1.8041	0.2771	-1.8041	0.9021	3.9865
T49	-5.6464	-2.0517	3.5946	5.6464	2.0517	1.7973	0.2782	-1.7973	0.8987	3.8491
T50	-5.6763	-2.0762	3.6001	5.6763	2.0762	1.8000	0.2778	-1.8000	0.9000	3.8763
T51	-5.6681	-2.0790	3.5892	5.6681	2.0790	1.7946	0.2786	-1.7946	0.8973	3.8735
T52	-5.7008	-2.1089	3.5919	5.7008	2.1089	1.7960	0.2784	-1.7960	0.8980	3.9048
PZA	-6.7838	-1.9347	4.8491	6.7838	1.9347	2.4246	0.2062	-2.4246	1.2123	4.3592
INN	-5.7007	-1.2027	4.4980	5.7007	1.2027	2.2490	0.2223	-2.2490	1.1245	3.4517

Comp.: *Compound, Bandgap (**ΔE**) = **E_{HOMO} - E_{LUMO}**, Ionization potential (**IP**) = - **E_{HOMO}**, Electron affinity (**EA**) = - **E_{LUMO}**, Chemical hardness (**η**) = **(IP-EA)/2**, Chemical softness (**σ**) = **1/2 η**, Chemical potential (**μ**) = - **η**, electrophilicity index (**ω**) = **η /2**, electronegativity (**χ**) = **(IP + EA)/2**.*

4.3.2.4 DFT studies of 4-quinazolinone incorporated pyrazine derivatives (T53-T68)

DFT calculations were conducted on the synthesized compounds (**T53-T68**) to optimize their geometry and assess the energy levels of the frontier molecular orbitals. **Table 4.9** presents the energy values of the HOMO and LUMO for these molecules. **Figures 4.6a** and **4.6b** illustrate visual representations of the FMOs for the active molecules **T60** and **T65**, respectively. According to the DFT analysis, compound **T60** exhibits a HOMO with its electron cloud mainly distributed across the quinazoline ring, while the LUMO extends its electron cloud over the benzene ring and the attached nitro group. Conversely, in compound **T65**, the electron density of the HOMO is dispersed

over both the quinazoline ring and the connected 3,4-dihydroxybenzene ring, while the LUMO electron density is expansive over the pyrazine ring. Understanding global chemical reactivity descriptors is essential for establishing connections between a molecule's structural characteristics, stability, and reactivity. These descriptors have been ascertained through the evaluation of the HOMO and LUMO energy levels of the molecules, with their numerical values delineated in **Table 4.9**. A higher chemical softness value indicates a stronger tendency for binding to the receptor, while an increased chemical hardness value suggests a reduced affinity for binding. It's important to note that all the synthesized compounds show superior chemical softness and reduced chemical hardness compared to the reference drugs. The interaction between the ligand and the receptor becomes more pronounced as the chemical potential increases, and all the target compounds exhibit elevated chemical potential values in contrast to the reference drugs. Electrophilicity index and electronegativity are metrics used to evaluate a molecule's ability to attract electrons from its surroundings. **Figures 4.7a** and **4.7b** represents the electron density surface of the compound **T60** and **T65** respectively. Molecules with higher electrophilicity index and electronegativity values are more likely to form interactions with receptors. It's noteworthy that all the synthesized compounds display electronegativity and electrophilicity index values similar to those of the reference drugs. All the compounds under investigation fall within the specified IP and EA value range characteristic of FDA-approved pharmaceuticals, with EA values ranging from -3 to 7 eV and IP values spanning from 4 to 15 eV. To assess the reactivity of these molecules, we conducted molecular electrostatic potential surface computations. **Figures 4.8a** and **4.8b** intricately illustrate the MEPs of compounds **T60** and **T65**, respectively, with the MEP surface meticulously color-coded for clarity. Across the entire spectrum of these molecules, the regions displaying a negative electrostatic potential are predominantly clustered near oxygen and nitrogen atoms, while zones with a positive electrostatic potential are mainly situated close to hydrogen atoms and an intricately structured phenyl ring.

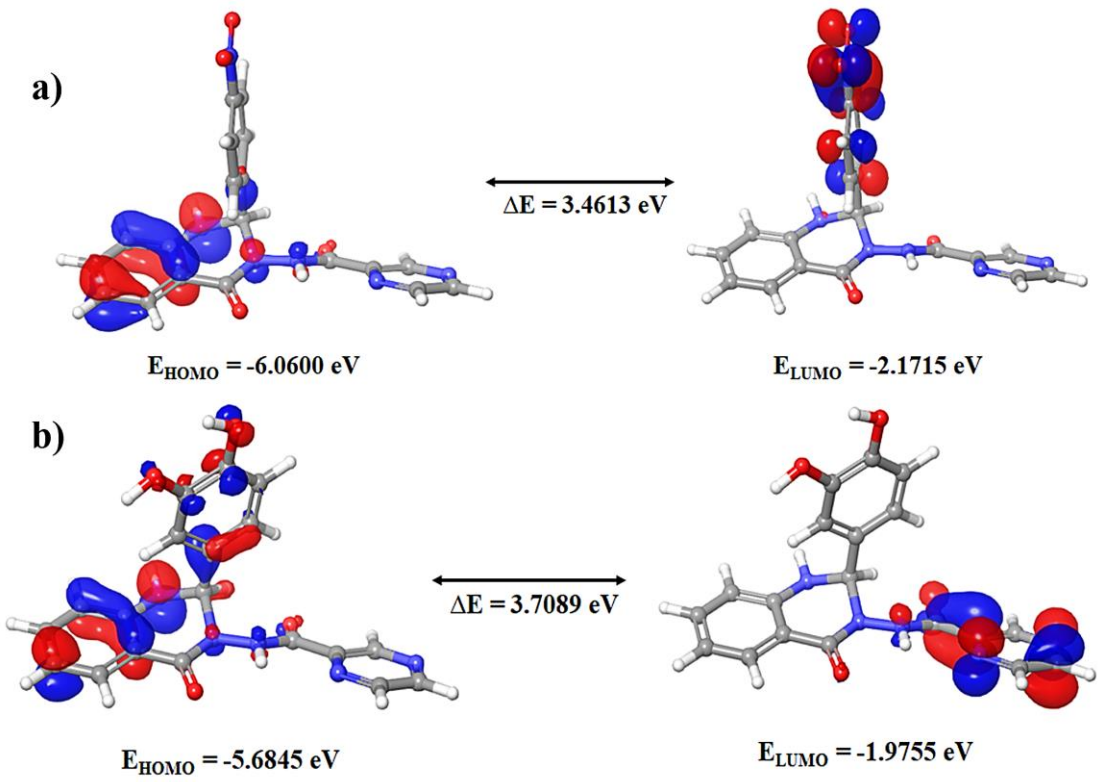

Figure 4.6 *Frontier Molecular Orbitals of the compounds a) T60 and b) T65*

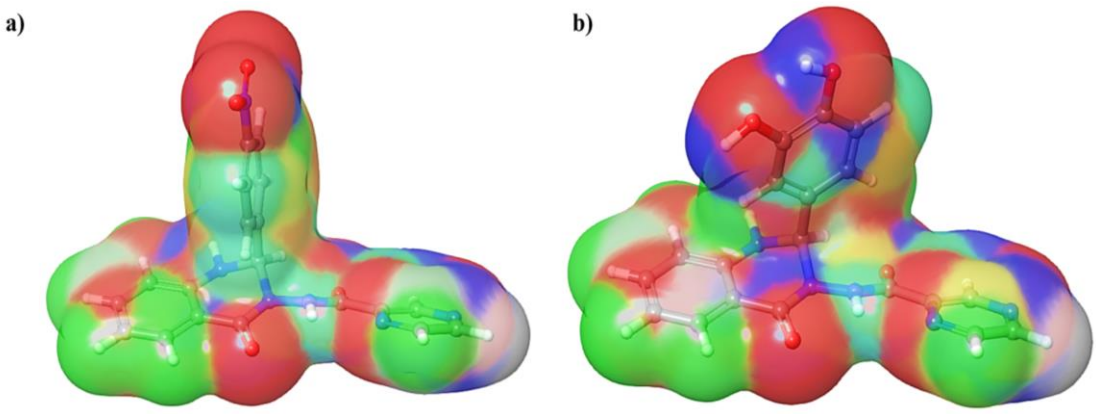

Figure 4.7 *Electron density surface of the compounds a) T60 and b) T65*

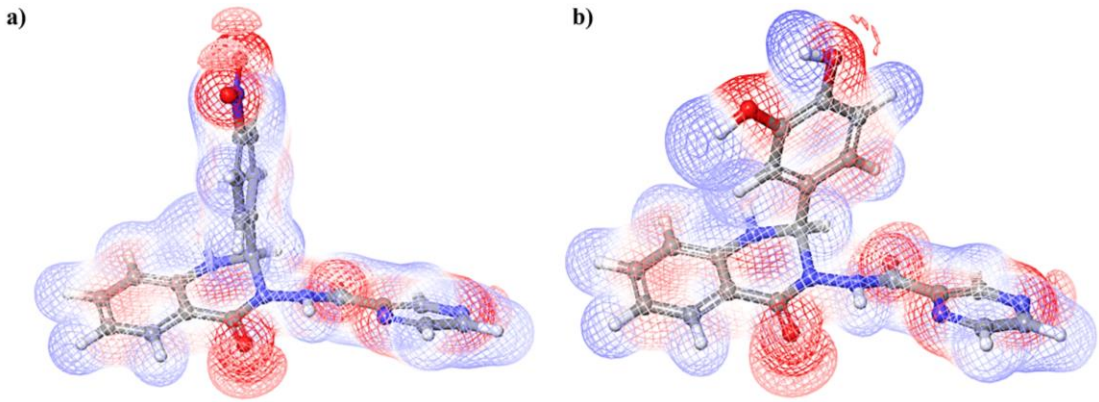

Figure 4.8 *Electrostatic potential of the compounds a) T60 and b) T65*

Table 4.9 *Global reactivity parameters of the synthesized compounds (**T53-T68**)*

Comp.	E_{HOMO} (eV)	E_{LUMO} (eV)	ΔE (eV)	IP (eV)	EA (eV)	η (eV)	σ (eV)	μ (eV)	ω (eV)	χ (eV)
T53	-5.5647	-2.0599	3.5048	5.5647	2.0599	1.7524	0.2853	-1.7524	0.8762	3.8123
T54	-6.1334	-2.0191	4.1144	6.1334	2.0191	2.0572	0.2431	-2.0572	1.0286	4.0763
T55	-5.6953	-2.2749	3.4205	5.6953	2.2749	1.7102	0.2924	-1.7102	0.8551	3.9851
T56	-5.6926	-1.9946	3.6980	5.6926	1.9946	1.8490	0.2704	-1.8490	0.9245	3.8436
T57	-5.8287	-2.0762	3.7525	5.8287	2.0762	1.8762	0.2665	-1.8762	0.9381	3.9525
T58	-5.7715	-2.0517	3.7198	5.7715	2.0517	1.8599	0.2688	-1.8599	0.9299	3.9116
T59	-6.0164	-2.1715	3.8450	6.0164	2.1715	1.9225	0.2601	-1.9225	0.9612	4.0940
T60	-6.0600	-2.5987	3.4613	6.0600	2.5987	1.7306	0.2889	-1.7306	0.8653	4.3293
T61	-5.6409	-2.0164	3.6246	5.6409	2.0164	1.8123	0.2759	-1.8123	0.9061	3.8286
T62	-5.7362	-2.0272	3.7089	5.7362	2.0272	1.8545	0.2696	-1.8545	0.9272	3.8817
T63	-5.6382	-1.9946	3.6436	5.6382	1.9946	1.8218	0.2745	-1.8218	0.9109	3.8164
T64	-5.7144	-2.0000	3.7144	5.7144	2.0000	1.8572	0.2692	-1.8572	0.9286	3.8572
T65	-5.6845	-1.9755	3.7089	5.6845	1.9755	1.8545	0.2696	-1.8545	0.9272	3.8300
T66	-5.7797	-2.0327	3.7470	5.7797	2.0327	1.8735	0.2669	-1.8735	0.9368	3.9062
T67	-5.8205	-2.1062	3.7144	5.8205	2.1062	1.8572	0.2692	-1.8572	0.9286	3.9633
T68	-5.8260	-2.0164	3.8096	5.8260	2.0164	1.9048	0.2625	-1.9048	0.9524	3.9212
PZA	-6.7838	-1.9347	4.8491	6.7838	1.9347	2.4246	0.2062	-2.4246	1.2123	4.3592
INN	-5.7007	-1.2027	4.4980	5.7007	1.2027	2.2490	0.2223	-2.2490	1.1245	3.4517

Comp.: *Compound, Bandgap (**ΔE**) = **E_{HOMO} - E_{LUMO}**, Ionization potential (**IP**) = - **E_{HOMO}**, Electron affinity (**EA**) = - **E_{LUMO}**, Chemical hardness (**η**) = **(IP-EA)/2**, Chemical softness (**σ**) = **1/2 η**, Chemical potential (**μ**) = - **η**, electrophilicity index (**ω**) = **η /2**, electronegativity (**χ**) = **(IP + EA)/2**.*

4.3.2.5 DFT studies of 2-aminophenyl and 2-oxoacetyl incorporated pyrazine-2-carbohydrazide derivatives (T69-T88)

The synthesized compounds (**T69-T88**) were subjected to DFT calculations to refine their geometry and evaluate the energy levels of the frontier molecular orbitals. **Table 4.10** provides the energy values of the HOMO and LUMO for the synthesized compounds. **Figures 4.9a** and **4.9b** elucidate the visual representations of the FMOs for the active molecules **T84** and **T87**, respectively. The DFT studies reveals that in compound **T84**, the HOMO predominantly allocates its electron cloud across the phenyl ring and the attached amide group, while the LUMO extends its electron cloud over the carbonyl groups linked to the phenyl ring. Similarly, concerning compound **T87**, the electron density of the HOMO disperses diffusely over the benzene structure, the bromo and carboxamide group affixed to the phenyl ring, while the LUMO's electron density expands over the carbonyl groups bonded to the benzene ring. The chemical reactivity descriptors are derived from assessing the HOMO and LUMO energy levels of molecules, with their specific values detailed in **Table 4.10**. A higher chemical softness value indicates a stronger tendency to bind to the receptor, whereas an increased chemical hardness value implies a reduced affinity for binding. It's noteworthy that all the synthesized compounds exhibit superior chemical softness and decreased chemical hardness compared to the reference drugs. As the chemical potential rises, the interaction between the ligand and the receptor becomes more apparent, with all synthesized compounds demonstrating higher chemical potential values compared to the reference drugs. All the synthesized compounds display electronegativity and electrophilicity index values similar to those of the reference drugs. **Figures 4.10a** and **4.10b** illustrate the electron density surface of compounds **T84** and **T87**, respectively. Ionization potential and electron affinity are used to assess a molecule's inclination to gain or lose electrons to its surroundings. Typically, as the values of IP and EA decrease, there tends to be an increase in toxicity. Notably, all the compounds examined here fall within the specified IP and EA value range characteristic of FDA-approved drugs, with EA values ranging from -3 to 7 eV and IP values spanning from 4 to 15 eV. To understand how these molecules react, we used a method called

molecular electrostatic potential surface computations. **Figures 4.11a** and **4.11b** intricately portray the MEPs of compounds **T84** and **T87**, respectively, with the MEP surface color-coded for enhanced lucidity. Across the entire spectrum of these molecules, the areas exhibiting a negative electrostatic potential are predominantly clustered proximate to oxygen and nitrogen atoms, while zones with a positive electrostatic potential are predominantly situated in proximity to hydrogen atoms and an intricately structured phenyl ring.

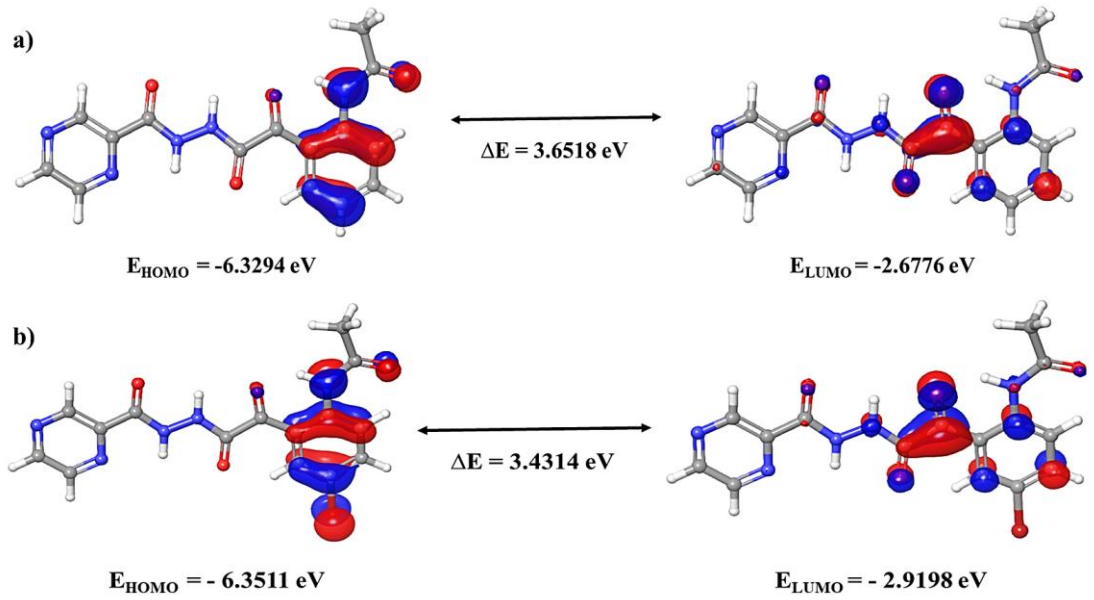

Figure 4.9 *Frontier Molecular Orbitals of the compounds a) T84 and b) T87*

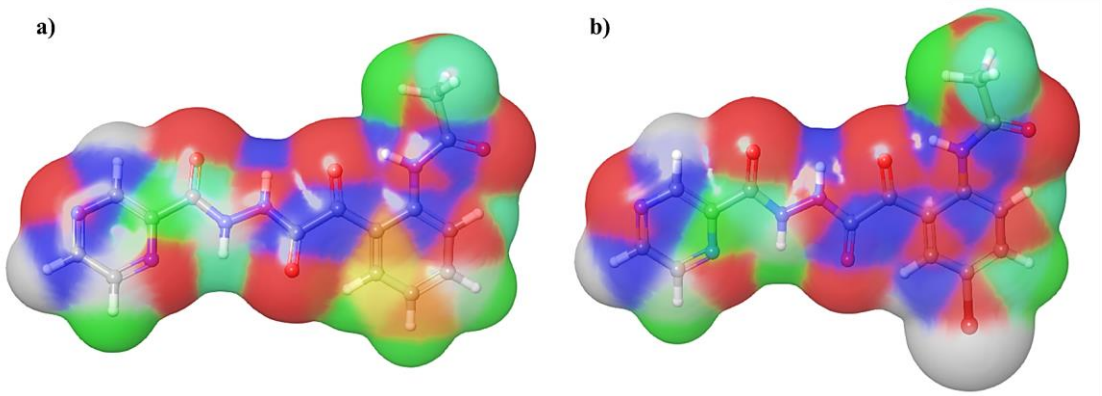

Figure 4.10 *Electron density surface of the compounds a) T84 and b) T87*

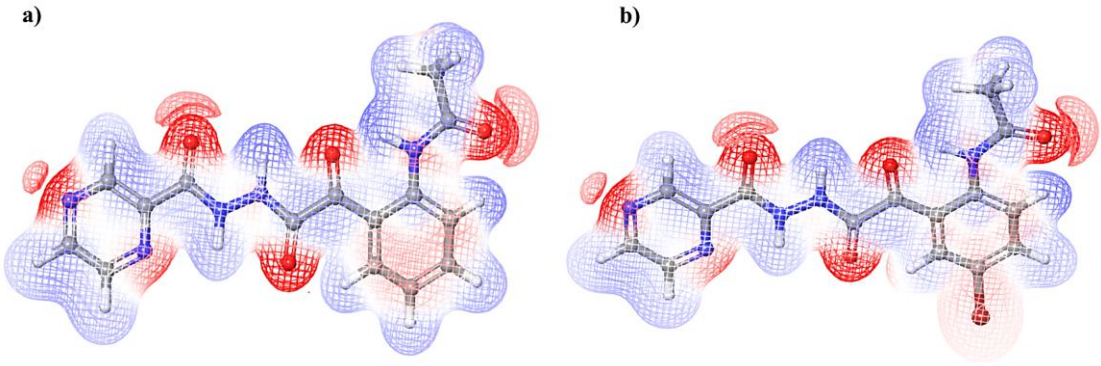

Figure 4.11 *Electrostatic potentials of the compounds a) T84 and b) T87*

Table 4.10 *Global reactivity parameters of the synthesized compounds (**T69-T88**)*

Comp.	E_{HOMO} (eV)	E_{LUMO} (eV)	ΔE (eV)	IP (eV)	EA (eV)	η (eV)	σ (eV)	μ (eV)	ω (eV)	χ (eV)
T69	-5.7525	-2.2722	3.4803	5.7525	2.2722	1.7402	0.2873	-1.7402	0.8701	4.0123
T70	-5.7307	-2.4164	3.3143	5.7307	2.4164	1.6572	0.3017	-1.6572	0.8286	4.0735
T71	-5.8613	-2.4790	3.3824	5.8613	2.4790	1.6912	0.2957	-1.6912	0.8456	4.1701
T72	-5.8613	-2.4926	3.3688	5.8613	2.4926	1.6844	0.2968	-1.6844	0.8422	4.1769
T73	-5.5783	-2.2341	3.3443	5.5783	2.2341	1.6721	0.2990	-1.6721	0.8361	3.9062
T74	-5.6083	-2.2640	3.3443	5.6083	2.2640	1.6721	0.2990	-1.6721	0.8361	3.9361
T75	-5.6001	-2.4082	3.1919	5.6001	2.4082	1.5959	0.3133	-1.5959	0.7980	4.0042
T76	-5.7280	-2.4654	3.2626	5.7280	2.4654	1.6313	0.3065	-1.6313	0.8157	4.0967
T77	-5.7334	-2.4817	3.2518	5.7334	2.4817	1.6259	0.3075	-1.6259	0.8129	4.1076
T78	-5.4532	-2.2259	3.2273	5.4532	2.2259	1.6136	0.3099	-1.6136	0.8068	3.8395
T79	-5.6001	-2.2531	3.3470	5.6001	2.2531	1.6735	0.2988	-1.6735	0.8368	3.9266
T80	-5.5865	-2.3919	3.1946	5.5865	2.3919	1.5973	0.3130	-1.5973	0.7987	3.9892
T81	-5.7062	-2.4409	3.2654	5.7062	2.4409	1.6327	0.3062	-1.6327	0.8163	4.0735
T82	-5.7144	-2.4626	3.2518	5.7144	2.4626	1.6259	0.3075	-1.6259	0.8129	4.0885
T83	-5.4913	-2.2477	3.2436	5.4913	2.2477	1.6218	0.3083	-1.6218	0.8109	3.8695
T84	-6.3294	-2.6776	3.6518	6.3294	2.6776	1.8259	0.2738	-1.8259	0.9129	4.5035
T85	-6.2886	-2.8545	3.4341	6.2886	2.8545	1.7170	0.2912	-1.7170	0.8585	4.5715
T86	-6.3729	-2.8980	3.4749	6.3729	2.8980	1.7374	0.2878	-1.7374	0.8687	4.6355
T87	-6.3511	-2.9198	3.4314	6.3511	2.9198	1.7157	0.2914	-1.7157	0.8578	4.6355
T88	-6.1443	-2.6232	3.5212	6.1443	2.6232	1.7606	0.2840	-1.7606	0.8803	4.3838
PZA	-6.7838	-1.9347	4.8491	6.7838	1.9347	2.4246	0.2062	-2.4246	1.2123	4.3592
INN	-5.7007	-1.2027	4.4980	5.7007	1.2027	2.2490	0.2223	-2.2490	1.1245	3.4517

Comp.: *Compound, Bandgap (**ΔE**) = E_{HOMO} - E_{LUMO}, Ionization potential (**IP**) = - E_{HOMO}, Electron affinity (**EA**) = - E_{LUMO}, Chemical hardness (**η**) = **(IP-EA)/2**, Chemical softness (**σ**) = **1/2 η**, Chemical potential (**μ**) = - **η**, electrophilicity index (**ω**) = **η /2**, electronegativity (**χ**) = **(IP + EA)/2**.*

4.3.3 *In silico* Molecular Docking studies

4.3.3.1 *In silico* Molecular Docking studies of 1,3,4-oxadiazole/[1,2,4] triazolo[3,4-*b*][1,3,4]thiadiazine incorporated pyrazine derivatives (T1-T18)

In silico molecular docking was performed to determine the binding interactions of all synthesized compounds (**T1-T18**) with the receptor. The synthesized molecules were docked within the active site of decaprenylphosphoryl-D-ribose oxidase of *Mycobacterium tuberculosis* (PDB ID: 4P8N) using the software Auto Dock-Vina 1.1.2. The ligands from the crystal structure of the enzyme-ligand complexes were rebuilt and redocked to validate the docking procedure. DprE1 enzyme plays a crucial role in the biosynthesis of the cell wall of *M. tuberculosis* which is essential for its survival. It contains complex lipids and glycolipids, including mycolic acids. The biosynthesis of mycolic acids is a multi-step process, and DprE1 is involved in one of these steps, known as epimerization. All the synthesized compounds showed interactions with active amino acid residues and exhibited higher binding energy values than the reference drugs (PZA, INN, and STM). Compound **T7** docked within the active site of the DprE1 with the binding energy of -10.10 kcal/mol and showed hydrogen bond interaction with Gly76 and Thr141 and showed *π-σ* and *π-alkyl* interaction with Ala72, and Ala147 respectively (**Figure 4.12**). Compound **T17** with a binding energy of -10.92 kcal/mol showed hydrogen bond interactions with Thr141 and Ile203 and exhibited *π-σ* and *π-alkyl* interactions with Ala72, and Ala147 respectively (**Figure 4.13**). The binding energy and interacting amino acid residues of all the synthesized compounds and reference compounds are presented in **Table 4.11**.

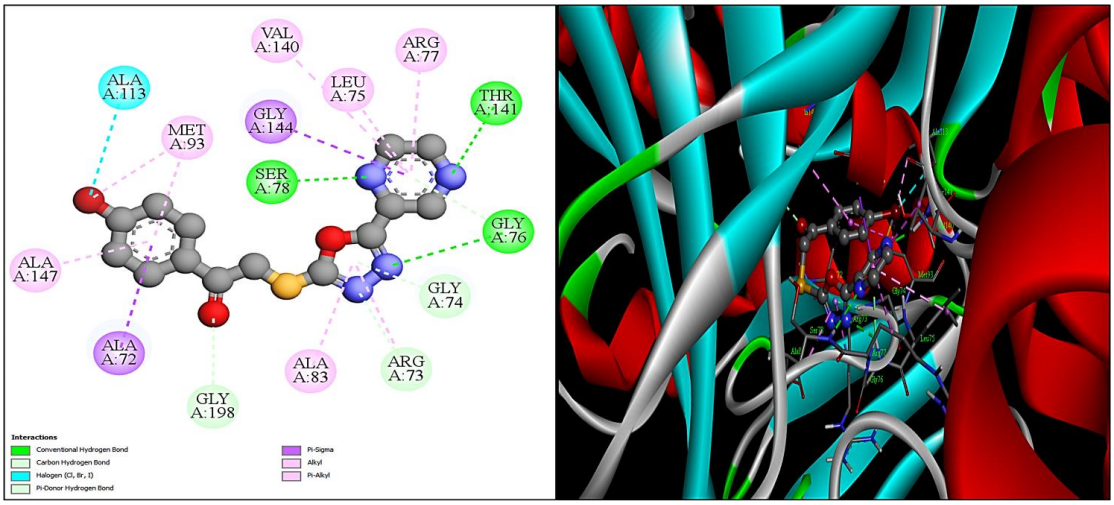

Figure 4.12 *The 2D (left) and 3D (right) docking poses of compound T7 with the receptor 4P8N*

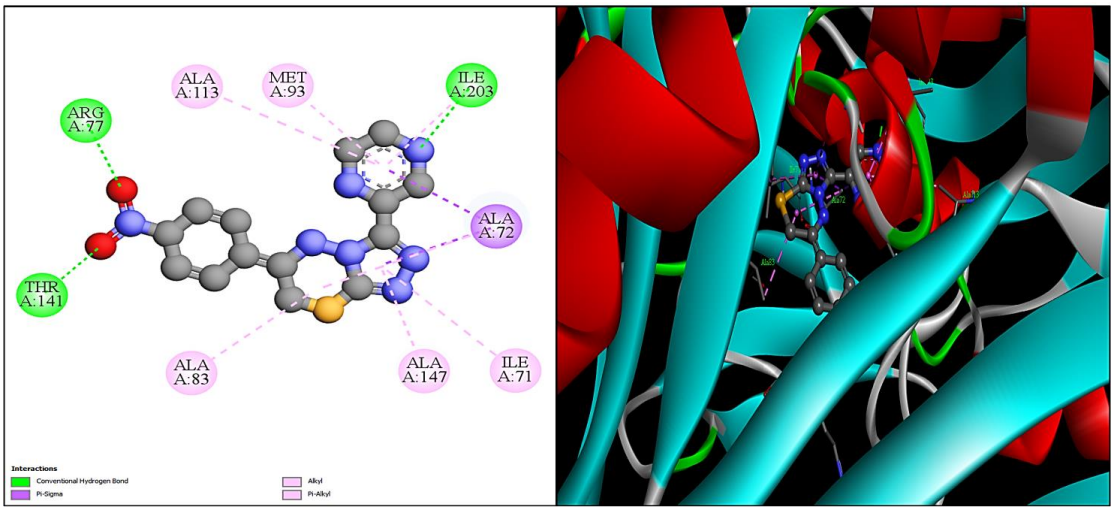

Figure 4.13 *The 2D (left) and 3D (right) docking poses of compound T17 with the receptor 4P8N*

Table 4.11 *Binding energy and interactions of synthesized compounds (**T1-T18**) with receptor 4P8N*

Comp.	Binding energy (kcal/mol)	Inhibition constant (K_i) (nM)	No. of H-bonds	Interacting amino acid residues
T1	-9.41	126.04	03	ALA72, GLY76, SER78, THR141
T2	-9.66	82.43	04	ALA72, GLY76, THR141

T3	-9.64	86.14	03	ALA72, GLY74, SER78, THR141, GLY143
T4	-8.93	286.34	05	LEU75, GLY76, ARG77, SER78, THR141
T5	-9.02	245.47	03	ALA72, GLY74, SER78, THR141, GLY143
T6	-9.32	147.91	03	ALA72, LEU75, VAL140, THR141, HIS151
T7	-10.01	45.66	03	ALA72, GLY76, SER78, THR141, GLY144
T8	-10.59	17.37	04	TRP35, LEU75, GLY76, VAL140, THR141
T9	-9.67	81.25	04	ALA72, ARG77, SER78, ALA83, THR141
T10	-9.42	124.80	04	LEU75, SER78, ASN82, GLY143
T11	-9.49	111.08	02	ALA72, ASN82, ALA83, GLY143, ILE203
T12	-9.87	58.65	03	ALA72, GLY74, SER78, ALA83, GLY143
T13	-9.36	137.09	02	ALA72, GLY74, SER78, ALA83, GLY143
T14	-9.38	133.28	03	LEU75, SER78, ASN82, ALA83, GLY143
T15	-9.87	58.66	02	ALA72, GLY74, SER78, ALA83, GLY143
T16	-9.92	53.26	02	ALA72, GLY74, SER78, ALA83, GLY143
T17	-10.92	9.85	03	ALA72, ARG77, THR141, ILE203
T18	-9.43	122.61	02	ALA72, GLY74, LEU75, ALA83, GLY143
PZA	-5.3	21.74µM	04	LEU56, GLY57, ARG58, SER59, GLY125
INN	-8.2	17.93µM	04	ALA53, ARG54, THR122, GLY125, ILE184
STM	-9.1	201.09	06	GLY117, HIS132, SER228, GLN336, TYR415

Comp.: Compound, PZA: Pyrazinamide, INN: Ciprofloxacin, STM: Streptomycin

4.3.3.2 *In silico* Molecular Docking studies of 1,2,4-triazole incorporated pyrazine derivatives (T19-T36)

In silico molecular docking was performed to uncover the binding interactions between the synthesized compounds (**T19-T36**) and the receptor, decaprenylphosphoryl-D-ribose oxidase of *Mycobacterium tuberculosis* (PDB ID: 4P8N). DprE1, a vital enzyme in the synthesis of the *M. tuberculosis* cell wall. The computational tool Auto Dock-Vina 1.1.2 was utilized for this purpose. The crucial amino acid residues situated in the active site of DprE1, including Arg58, Ser59, Ala64, Ala72, Gly76, Gly125, His132, Gly136, Thr141, Ala147, Cys148, Ile203, Cys387, Tyr434, and Tyr415, play a significant role. Most of the synthesized compounds demonstrated interactions with these amino acid residues and exhibited higher binding energy values compared to the reference drugs (PZA, INN, and STM). Compound **T29**

docked within the active site of DprE1 with a binding energy of -10.10 kcal/mol and formed five hydrogen bond interactions with Arg58, Ser59, Gly125, His132, and Tyr415 amino acid residues. It also showed *π-σ* interaction with Ala64 and Ile131 and *π-alkyl* interaction with Cys129 and Ala417 (**Figure 4.14**). **Table 4.12** provides a comprehensive summary of the binding energies and the amino acid residues engaged by both the synthesized compounds and reference compounds.

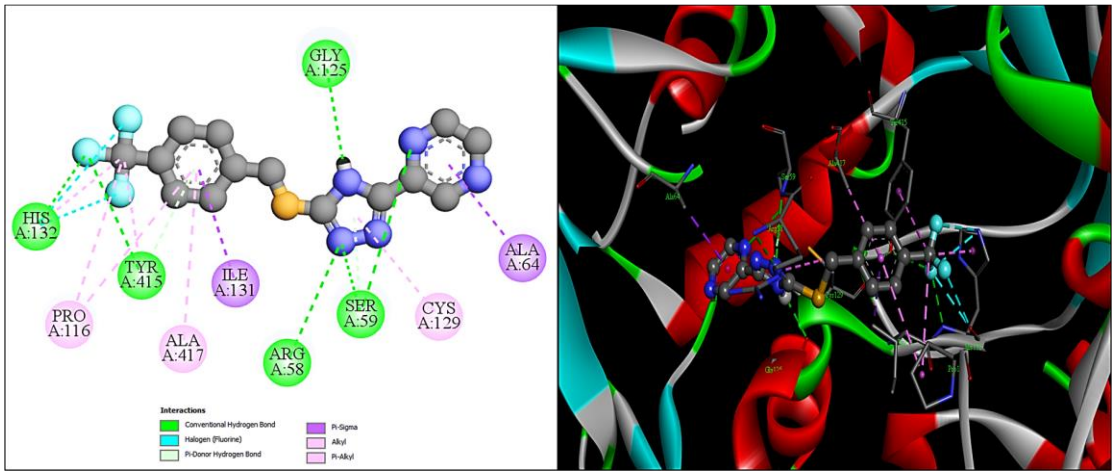

Figure 4.14 *The 2D (left) and 3D (right) docking poses of compound T29 with the receptor 4P8N*

Table 4.12 *Binding energy and interactions of synthesized compounds (**T19-T36**) with receptor 4P8N*

Comp.	Binding energy (kcal/mol)	Inhibition constant (K_i) (nM)	No. of H-bonds	Interacting amino acid residues
T19	-8.3	393.27	03	GLY57, ARG58, SER59, CYS129
T20	-9.4	125.14	04	GLY55, GLY57, ARG58, SER59, CYS129
T21	-9.1	156.21	02	ARG58, SER59, TYR60, ALA64
T22	-9.4	125.38	03	ALA53, ARG58, SER59, GLY125
T23	-8.8	277.76	04	SER59, GLY117, THR118, LYS134, GLN336
T24	-9.7	79.26	04	ARG58, SER59, CYS129, ASN63
T25	-9.3	149.61	03	ARG58, SER59, CYS129, ASN63
T26	-8.8	277.93	02	ALA53, SER59, GLY124, GLY125
T27	-8.9	281.47	02	ALA53, SER59, GLY124, GLY125, VAL121

T28	-9.0	243.35	02	SER59, ALA64, VAL121, GLY125, CYS129
T29	-10.1	39.47	05	ARG58, SER59, GLY125, HIS132, TYR415
T30	-9.2	151.87	02	SER59, ALA64, GLY125, CYS129
T31	-9.3	149.82	02	SER59, ALA64, GLY125, CYS129
T32	-9.7	74.65	04	SER59, ALA64, GLY117, GLY125, CYS129
T33	-9.3	149.47	05	SER59, GLY117, THR118, LYS134, TYR415
T34	-9.1	156.07	02	SER59, ALA64, GLY125, CYS129, LYS418
T35	-9.1	156.03	02	SER59, ALA64, GLY125, CYS129
T36	-9.8	69.08	04	ARG58, SER59, ALA64, HIS132, TYR415
PZA	-5.3	21.74µM	04	GLY57, ARG58, SER59, GLY125, CYS129
INN	-8.2	17.93µM	04	ALA53, ARG54, THR122, GLY125, ILE184
STM	-9.1	201.09	06	GLY117, HIS132, SER228, GLN336, TYR415

Comp.: Compound, PZA: Pyrazinamide, INN: Ciprofloxacin, STM: Streptomycin

4.3.3.3 *In silico* Molecular Docking studies of pyrazine hydrazinylidene derivatives containing benzenesulfonate scaffold (T37-T52)

Using the software AutoDock-Vina 1.1.2, *in silico* molecular docking was conducted to examine the binding interactions between the synthesized compounds (**T37-T52**) and the receptor. These molecules were docked into the active site of decaprenylphosphoryl-D-ribose oxidase. From the docking studies, it is found that the active molecules inhibit the flavoenzyme DprE1 through the formation of a noncovalent adduct with the amino acid Cys387. Most of the target compounds showed interactions with Cys387 and exhibited higher binding energy values than the reference drugs (PZA, INN, & STM). Compounds **T40**, **T43**, and **T48** docked within the active site of the DprE1 enzyme with the binding energy -11.15, -11.10, and 10.98 kcal/mol respectively, showed hydrogen bond interaction with Cys387 (**Figures 4.14**, **4.15**, and **4.16** respectively). The binding energy and interacting amino acid residues of all synthesized compounds and reference compounds are presented in **Table 4.13**.

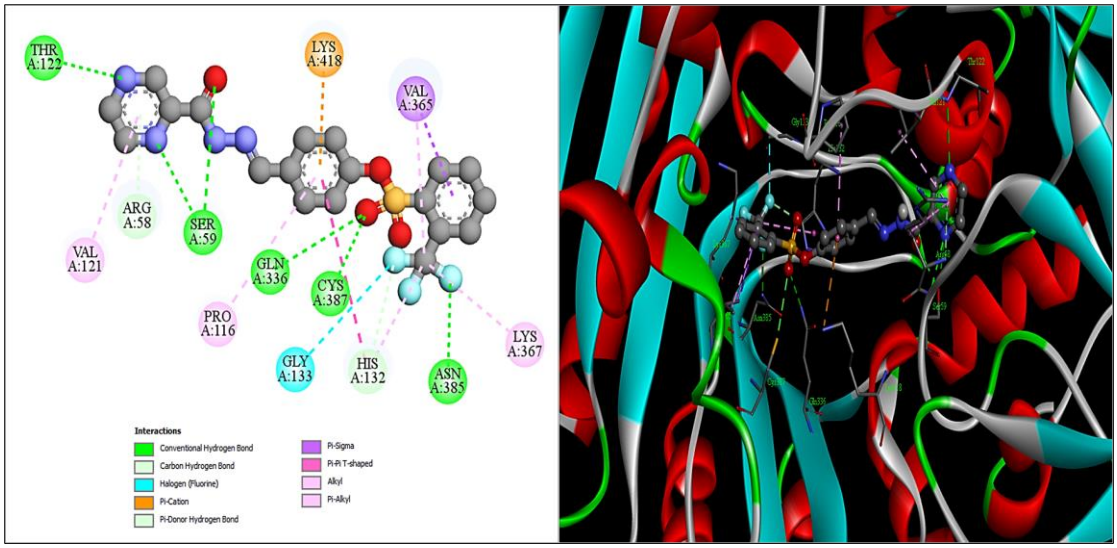

Figure 4.14 *The 2D (left) and 3D (right) docking poses of compound T40 with the receptor 4P8N*

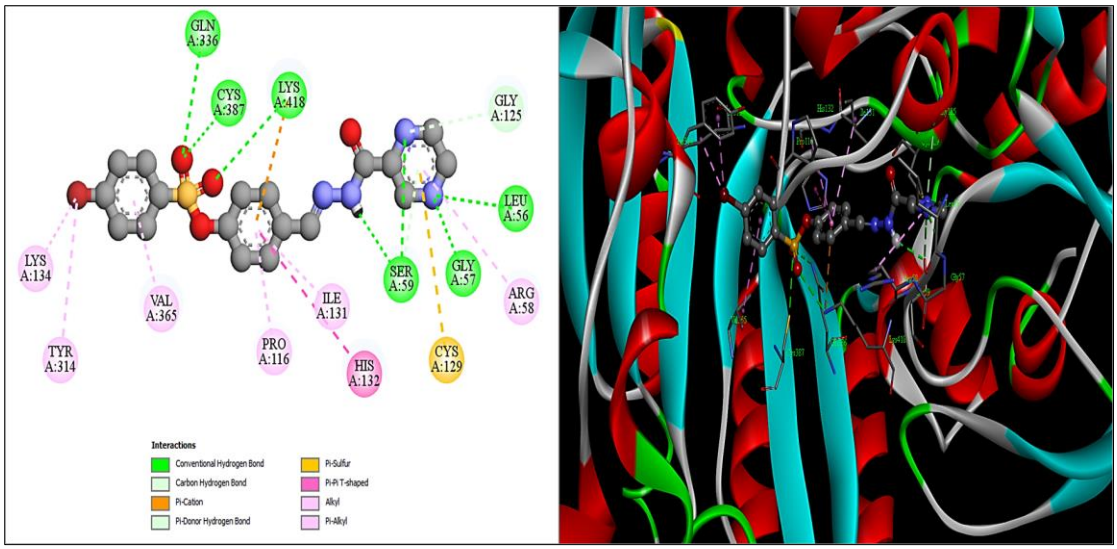

Figure 4.15 *The 2D (left) and 3D (right) docking poses of compound T43 with the receptor 4P8N*

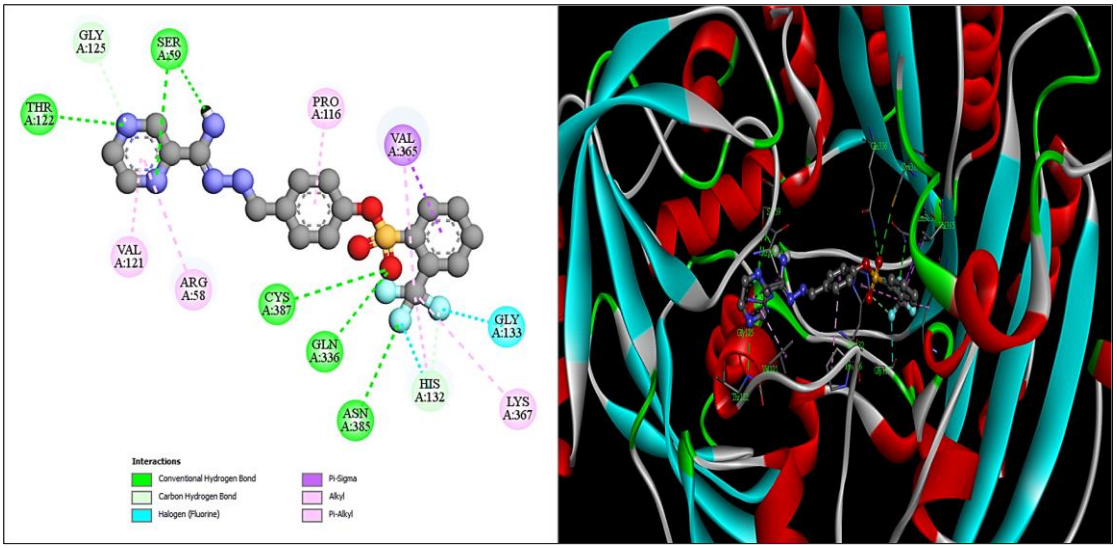

Figure 4.16 *The 2D (left) and 3D (right) docking poses of compound T48 with the receptor 4P8N*

Table 4.13 *Binding energy and interactions of synthesized compounds (**T37-T52**) with receptor 4P8N*

Comp.	Binding energy (kcal/mol)	Inhibition constant (K_i) (nM)	No. of H-bonds	Interacting amino acid residues
T37	-10.67	15.04	02	ARG58, CYS129, GLN336, LYS367, LYS418
T38	-11.02	8.33	03	HIS132, LYS134, SER228, GLN336, LYS418
T39	-10.65	15.71	05	ARG58, ALA64, HIS132, CYS387, TYR415
T40	-11.15	6.75	05	GLY133, GLN336, CYS387, ASN385, LYS418
T41	-10.68	14.80	04	GLY57, SER59, GLY133, CYS387, LYS418
T42	-11.07	7.69	05	GLY57, ARG58, ALA64, HIS132, CYS387
T43	-11.10	7.58	05	GLY57, HIS132, GLN336, CYS387, LYS418
T44	-11.04	7.19	04	HIS132, LYS134, SER228, GLN336, TYR415
T45	-10.11	39.02	03	GLY57, SER59, HIS132, CYS387, LYS418
T46	-10.42	22.91	03	GLY57, SER59, HIS132, CYS387, LYS418
T47	-10.30	27.96	05	GLT57, SER59, GLY125, GLN336, LYS418
T48	-10.98	8.80	05	SER59, GLY133, GLY365, GLN336, CYS387
T49	-10.49	19.90	04	GLY57, SER59, HIS132, CYS387, LYS418
T50	-10.72	13.92	04	GLY57, SER59, HIS132, CYS387, LYS418
T51	-11.00	8.62	05	GLY57, SER59, CYS129, GLN336, LYS418

T52	-10.85	11.62	03	GLY57, SER59, HIS132, CYS129, LYS418
PZA	-5.3	21.74μM	04	LEU56, GLY57, ARG58, SER59, GLY125
INN	-8.2	17.93μM	04	ALA53, ARG54, THR122, GLY125, ILE184
STM	-9.1	201.09	06	GLY117, HIS132, SER228, GLN336, TYR415

Comp.: Compound, PZA: Pyrazinamide, INN: Ciprofloxacin, STM: Streptomycin

4.3.3.4 *In silico* Molecular Docking studies of 4-quinazolinone incorporated pyrazine derivatives (T53-T68)

In silico molecular docking was conducted to elucidate the binding interactions between the target molecules (**T53-T68**) and the receptor, DprE1 of *Mycobacterium tuberculosis* (PDB ID: 4P8N). The outcome of these docking studies divulged that the active compounds exerted inhibitory effects on the flavoenzyme DprE1 through the formation of noncovalent adducts with the amino acid Cys387. A majority of the target compounds manifested interactions with Cys387, displaying notably superior binding energy values when compared with the benchmark drugs (PZA, INN, and STM). Notably, compounds **T60** and **T65**, with binding energies of -10.65 and 10.93 kcal/mol, respectively, were observed to dock effectively within the active site of the DprE1 enzyme. Additionally, these compounds formed hydrogen bond interactions with Cys387, as depicted in **Figures 4.17** and **4.18**, respectively. **Table 4.14** furnishes a comprehensive compendium of information about the binding energies and the amino acid residues with which both the synthesized compounds and reference compounds have engaged.

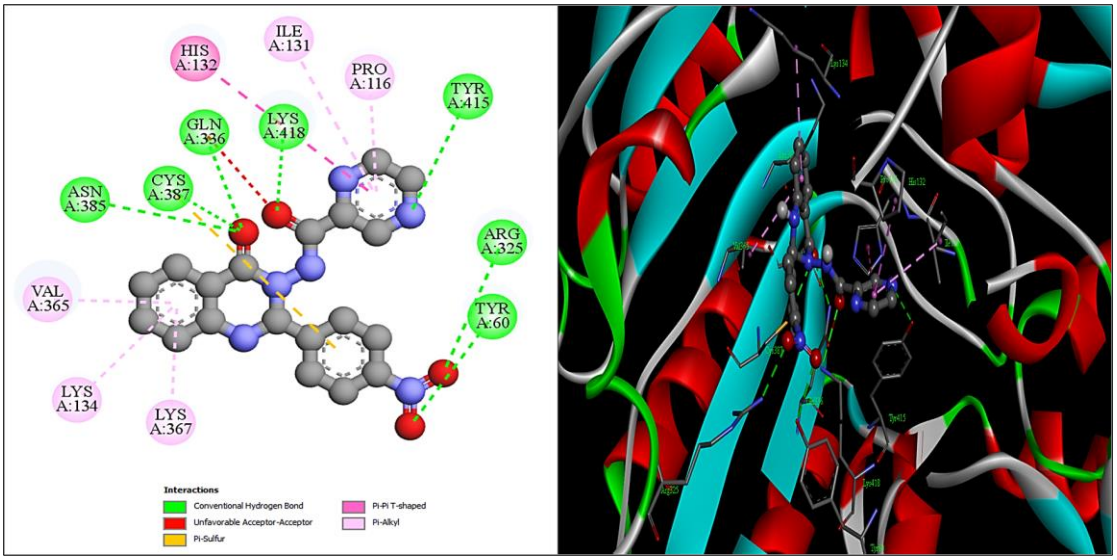

Figure 4.17 *The 2D (left) and 3D (right) docking poses of compound T60 with the receptor 4P8N*

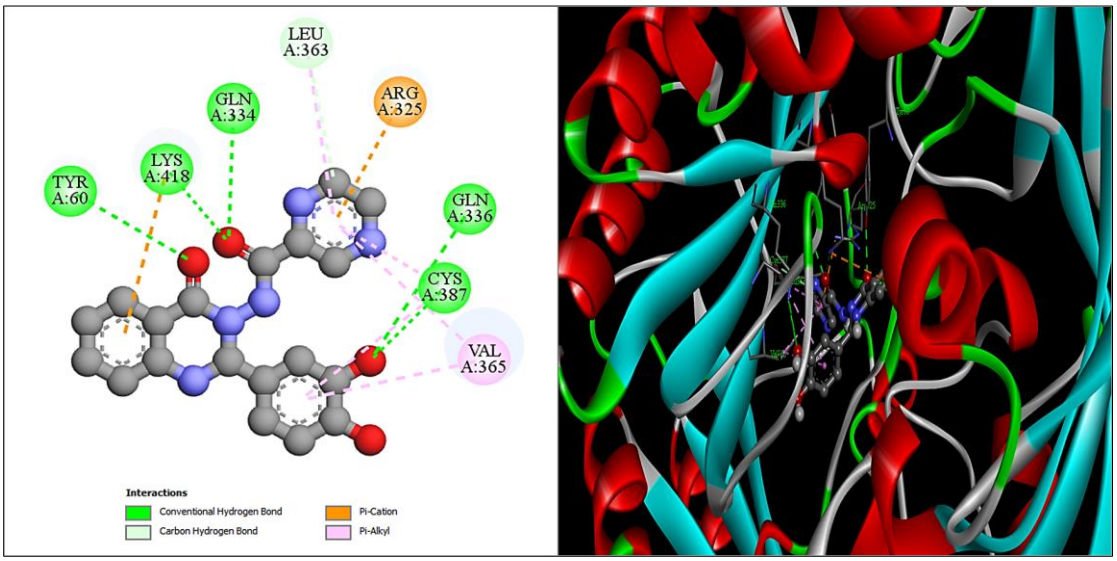

Figure 4.18 *The 2D (left) and 3D (right) docking poses of compound T65 with the receptor 4P8N*

Table 4.14 *Binding energy and interactions of synthesized compounds (**T53-T68**) with receptor 4P8N*

Comp.	Binding energy (kcal/mol)	Inhibition constant (K_i) (nM)	No. of H-bonds	Interacting amino acid residues

T53	-8.40	468.73	03	LEU56, GLY57, ARG58, CYS129, HIS132
T54	-8.50	414.59	02	HIS132, CYS387, TYR415, ALA417, LYS418
T55	-8.90	365.57	03	LYS134, SER228, TYR314, LEU317, VAL365
T56	-9.00	193.18	03	HIS 132, AGR325, GLN334, CYS387, LYS418
T57	-9.57	96.74	01	LYS134, SER228, PRO316, LEU317, VAL365
T58	-9.60	94.88	03	GLY117, LYS134, SER228, PRO316, LEU317
T59	-10.23	37.60	02	LYS134, SER228, PRO316, LEU317, ARG325
T60	-10.65	14.53	06	TYR60, HIS132, GLN336, CYS387, LYS418
T61	-10.00	46.66	01	LYS134, TYR314, PRO316, LYS367, CYS387
T62	-9.56	98.91	02	SER228, ALA229, LEU317, VAL365, LYS367
T63	-9.44	108.84	02	GLY117, LYS134, SER228, ALA244, PRO316
T64	-9.81	64.48	02	GLY117, SER228, VAL365, LYS367, CYS387
T65	-10.93	14.68	05	TYR60, ARG325, GLN336, CYS387, LYS418
T66	-10.49	12.48	03	LYS134, SER228, ALA229, LEU317, VAL365
T67	-10.34	26.56	03	ARG58, TYR60, THR118, GLN334, LYS418
T68	-9.15	282.97	01	PRO116, GLY117, ARG325, VAL365, LYS367
PZA	-5.3	21.74µM	04	LEU56, GLY57, ARG58, SER59, GLY125
INN	-8.2	17.93µM	04	ALA53, ARG54, THR122, GLY125, ILE184
STM	-9.1	201.09	06	GLY117, HIS132, SER228, GLN336, TYR415

Comp.: Compound, PZA: Pyrazinamide, INN: Ciprofloxacin, STM: Streptomycin

4.3.3.5 *In silico* Molecular Docking studies of 2-aminophenyl and 2-oxoacetyl incorporated pyrazine-2-carbohydrazide derivatives (T69-T88)

In silico molecular docking was undertaken to understand the binding interactions between the synthesized compounds (**T69-T88**) and the receptor, decaprenylphosphoryl-D-ribose oxidase of *Mycobacterium tuberculosis* (PDB ID: 4P8N). The results of the docking investigations showed that the active compounds in this study had inhibitory effects on the flavoenzyme DprE1. They achieved this by forming a noncovalent interaction with the amino acid Cys387. Most of the synthesized compounds showed interactions with Cys387, indicating significantly better binding energy values compared to standard drugs (PZA, INN, and STM). Notably, compounds **T84** and **T87** demonstrated efficient docking within the active site of the DprE1

enzyme, with binding energies of -10.32 and -10.44 kcal/mol, respectively. Additionally, these compounds formed hydrogen bond interactions with Cys387, as illustrated in **Figures 4.19** and **4.20,** respectively. **Table 4.15** provides a comprehensive overview of the binding energies and the amino acid residues involved for both the synthesized compounds and reference compounds.

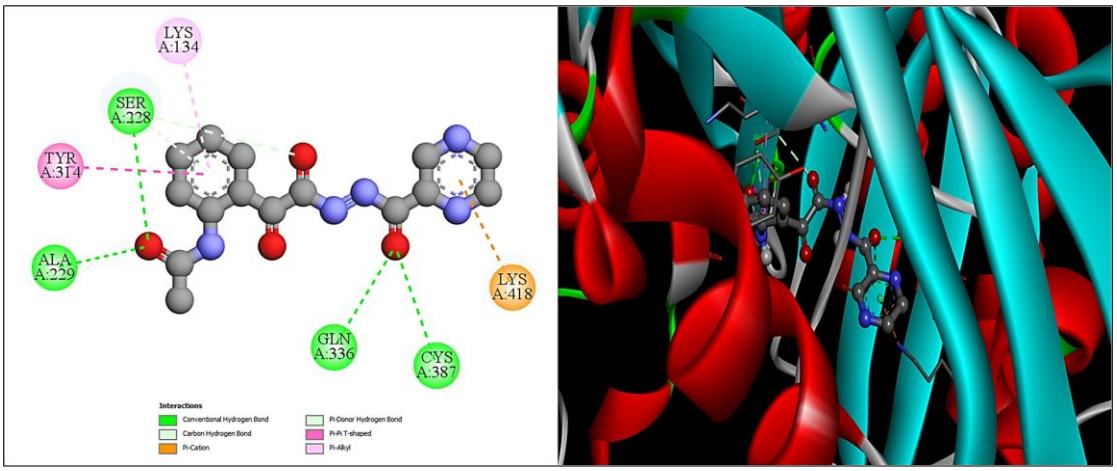

Figure 4.19 *The 2D (left) and 3D (right) docking poses of compound T84 with the receptor 4P8N*

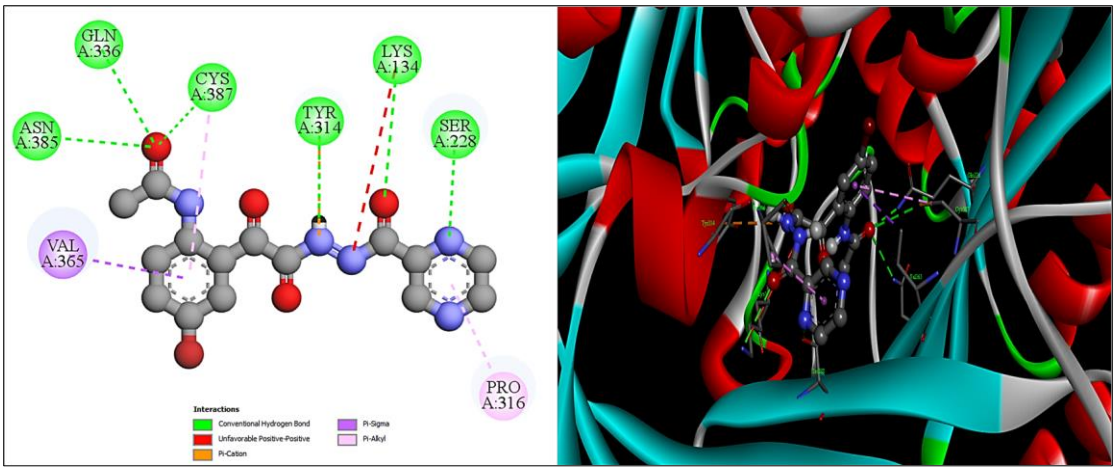

Figure 4.20 *The 2D (left) and 3D (right) docking poses of compound T87 with the receptor 4P8N*

Table 4.15 *Binding energy and interactions of synthesized compounds (**T69-T88**) with receptor 4P8N*

Comp.	Binding energy (kcal/mol)	Inhibition constant (K_i) (nM)	No. of H-bonds	Interacting amino acid residues
T69	-8.50	354.53	03	GLY55, SER59, ALA64, PRO116, CYS129
T70	-9.50	112.57	04	GLY55, SER59, ASN63, GLY124, CYS129
T71	-9.17	188.85	03	GLY57, SER59, ARG58, ALA64, CYS129
T72	-9.11	209.68	04	GLY55, SER59, ARG58, ALA64, CYS129
T73	-8.68	505.79	04	HIS132, LYS134, SER228, TYR314, TYR415
T74	-9.04	360.95	03	ARG58, SER59, ALA64, GLY125, HIS132
T75	-9.57	102.17	04	ARG58, SER59, ASN63, ALA64, THR122
T76	-9.20	197.33	05	GLY55, ARG58, SER59, ALA64, GLY125
T77	-9.36	137.33	05	GLY55, SER59, ASN63, ALA64, CYS129
T78	-8.63	516.45	04	ARG58, SER59, THR118, CYS129, TYR415
T79	-9.88	57.55	03	GLY57, SER59, THR118, CYS129, HIS132
T80	-10.18	25.67	05	GLY55, SER59, THR118, CYS129, HIS132
T81	-10.20	24.61	03	GLY55, SER59, THR118, CYS129, CYS387
T82	-10.21	23.58	03	GLY55, SER59, THR118, CYS129, CYS387
T83	-10.11	38.47	03	GLY55, SER59, ALA64, CYS129, CYS387
T84	-10.32	21.45	03	SER228, ALA229, GLN336, CYS387, LYS418
T85	-10.03	40.73	05	ARG58, SER59, THR118, TYR415, LYS418
T86	-9.63	83.34	04	GLY57, ARG58, SER59, GLY117, CYS129
T87	-10.44	19.64	04	LYS134, SER228, TYR314, CYS387, VAL365
T88	-9.88	61.46	03	ARG58, SER59, GLY117, THR118, CYS129
PZA	-5.3	21.74μM	04	GLY57, ARG58, SER59, GLY125, CYS129
INN	-8.2	17.93μM	04	ALA53, ARG54, THR122, GLY125, ILE184
STM	-9.1	201.09	06	GLY117, HIS132, SER228, GLN336, TYR415
RIF	-9.5	110.43	04	GLY117, ARG325, GLN336, ASN385, CYS387

Comp.: Compound, PZA: Pyrazinamide, INN: Ciprofloxacin, STM: Streptomycin

4.4 Conclusions

The drug-likeness of all synthesized compounds (**T1-T88**) was assessed by calculating their pharmacokinetic and pharmacodynamic parameters. They all strictly adhered to Lipinski's Rule of Five, a fundamental criterion for oral bioavailability. Moreover, all compounds demonstrated higher human oral absorption. Furthermore,

DFT calculations were conducted on all synthesized compounds. The results revealed that most compounds exhibited smaller energy differences, indicating higher chemical reactivity and potential for intermolecular interactions, making the molecules soft. Additionally, the chemical reactivity parameters of all compounds fell within the specified range. To gain insight into the mechanism of action of active molecules, *in silico* molecular docking was performed. The results showed that most active molecules inhibited the flavoenzyme DprE1 by forming a noncovalent adduct with the amino acid Cys387. Interactions with Cys387 were observed in most synthesized compounds, and they exhibited higher binding energy values compared to standard drugs.

****

CHAPTER 5

SUMMARY AND CONCLUSIONS

Abstract

This chapter provides a summary of the research findings and draws conclusions based on them. Additionally, it outlines potential avenues for future research.

5.1 Summary

Antimicrobial drugs have significantly altered the landscape of infectious disease treatment and have had profound implications for humanity. Initially, there was great optimism that infectious diseases could be effectively eradicated due to advancements in antimicrobial chemotherapy. However, antimicrobial resistance has emerged as a pressing global health issue, influenced by both human and non-human use of antimicrobials. The consequences of antimicrobial resistance become particularly severe when pathogens develop resistance to crucial antimicrobials used in human medicine. Despite initial hopes, the reality is that emerging and re-emerging infectious diseases continue to pose significant challenges, leading to ongoing battles against infections caused by drug-resistant organisms in clinical settings. Considering these factors, the current study aimed to combine the biologically active pyrazine moiety with various active heterocyclic moieties using an active functional system. This process aimed to create a novel molecular framework and assess their biological activities. Consequently, five new series of target molecules were synthesized through a multistep organic synthetic protocol.

1) Two sets of 1,3,4-oxadiazole/[1,2,4]triazolo[3,4-*b*][1,3,4]thiadiazine incorporated pyrazine derivatives (**T1-T18**): Out of the 18 derivatives, compounds **T7, T8,** and **T17** exhibited the highest potency, each with a MIC

value of 1.56 µg/mL, while exhibiting non-toxicity towards non-cancerous cells.

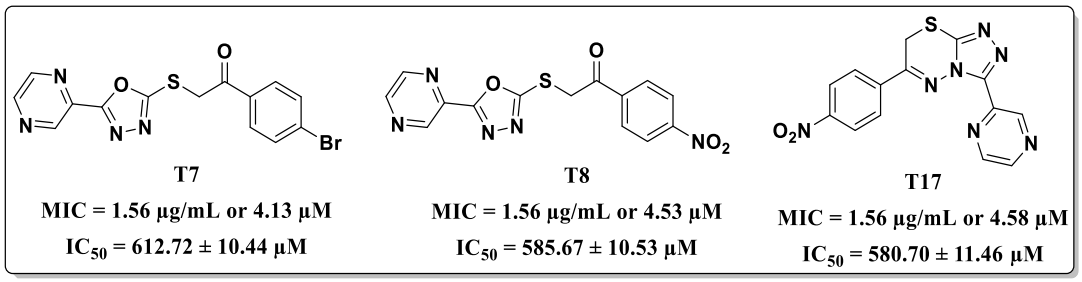

T7
MIC = 1.56 µg/mL or 4.13 µM
IC_{50} = 612.72 ± 10.44 µM

T8
MIC = 1.56 µg/mL or 4.53 µM
IC_{50} = 585.67 ± 10.53 µM

T17
MIC = 1.56 µg/mL or 4.58 µM
IC_{50} = 580.70 ± 11.46 µM

2) Two sets of 1,2,4-triazole incorporated pyrazine derivatives (**T19-T36**): Among the 18 synthesized molecules in this series, compound **T29** demonstrated the highest potency, with a MIC value of 3.12 µg/mL, while also exhibiting non-toxicity towards normal cells.

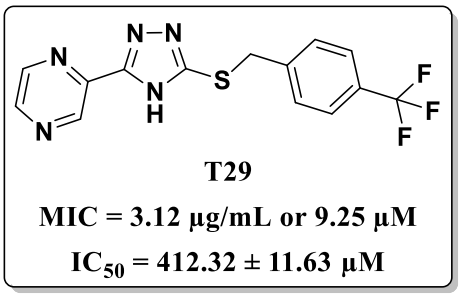

T29
MIC = 3.12 µg/mL or 9.25 µM
IC_{50} = 412.32 ± 11.63 µM

3) Two sets of pyrazine hydrazinylidene derivatives containing benzenesulfonate scaffold (**T37-T52**): In this series, a total of 16 molecules were synthesized. Out of these, three compounds (**T40, T43**, and **T48**) demonstrated significant antitubercular activity, each having a MIC value of 1.56 µg/mL. Additionally, MTT assay results indicate that these active compounds are non-toxic to non-cancerous cells.

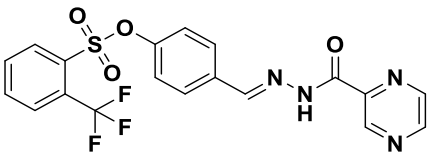

T40

MIC = 1.56 µg/mL or 3.45 µM

IC_{50} = 501.36 ± 10.64 µM

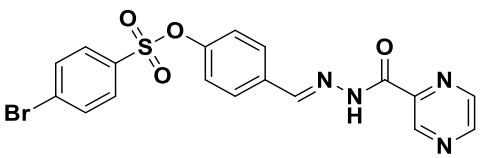

T43

MIC = 1.56 µg/mL or 3.46 µM

IC_{50} = 457.03 ± 11.48 µM

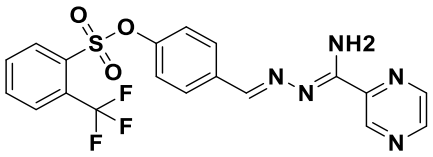

T48

MIC = 1.56 µg/mL or 3.38 µM

IC_{50} = 463.88 ± 10.84 µM

4) One set of 4-quinazolinone incorporated pyrazine derivatives (**T53-T68**): In this series, 16 derivatives were synthesized, and among them, compounds **T60** and **T65** exhibited the highest potency with a MIC value of 3.12 µg/mL.

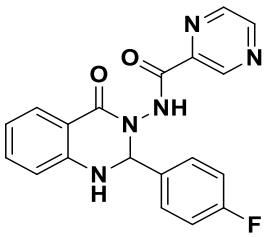

T60

MIC = 3.12 µg/mL or 7.99 µM

IC_{50} = 419.57 ± 10.28 µM

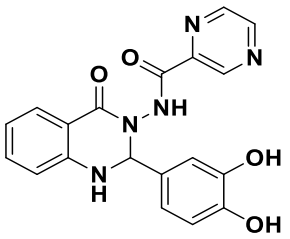

T65

MIC = 3.12 µg/mL or 8.27 µM

IC_{50} = 418.32 ± 10.56 µM

5) Four sets of 2-aminophenyl and 2-oxoacetyl incorporated pyrazine-2-carbohydrazide derivatives (**T69-T88**): In this series, 20 derivatives were synthesized and screened for their antitubercular activity. The findings indicate that compounds **T84** and **T87** showed promising activity, each with a MIC value of 1.56 µg/mL. Furthermore, the MTT assay confirmed that these active compounds are non-toxic to normal cells.

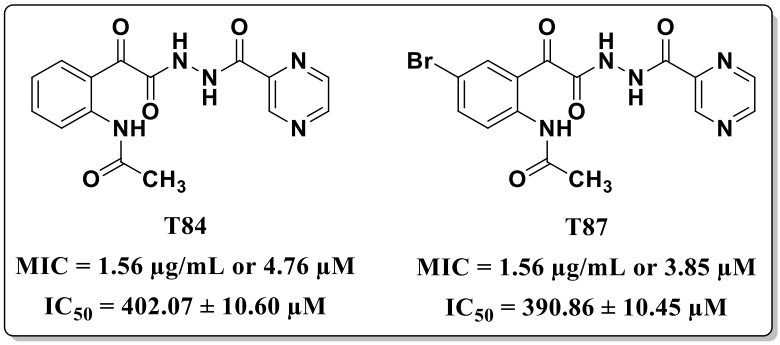

T84

MIC = 1.56 µg/mL or 4.76 µM

IC_{50} = 402.07 ± 10.60 µM

T87

MIC = 1.56 µg/mL or 3.85 µM

IC_{50} = 390.86 ± 10.45 µM

The newly synthesized compounds underwent purification through either recrystallization or column chromatography techniques. The structures of all intermediates and final compounds were confirmed using ^{1}H-NMR, ^{13}C-NMR, and HRMS/ESI-MS. Subsequently, all final compounds were evaluated for their *in vitro* antitubercular, antibacterial, and antifungal activities. The results indicated promising activity against the tested strains for most synthesized compounds. Compounds exhibiting potent activity against the *M. tuberculosis* H37Rv strain were selected for cytotoxicity studies using MTT assay against non-cancerous cells. Additionally, *in silico* ADME studies were conducted to assess their drug-likeness, while DFT calculations were performed to evaluate their molecular properties. Furthermore, *in silico* molecular docking was employed to elucidate the mechanism of action of the synthesized molecules against the DprE1 of *M. tuberculosis*.

5.2 Conclusions

- Designed and synthesized five new series of pyrazine-based molecules (**88 molecules**) using a multistep organic synthetic protocol.
- All the synthesized compounds were characterized by ^{1}H-NMR, ^{13}C-NMR, and HRMS/ESI-MS.
- Out of a total of **88** molecules, **08** demonstrated the highest potency against the *M. tuberculosis* H37Rv strain, with a Minimum Inhibitory Concentration of **1.56 µg/mL**. Additionally, **20** molecules exhibited promising activity against the same strain, with an MIC of **3.12 µg/mL**. The rest of the compounds displayed moderate activity with MIC varying from **6.25** to **12.5 µg/mL**.

- **12** compounds showed promising antibacterial activity and **06** compounds showed promising antifungal activity against the tested strains.
- All the active compounds showed minimal toxicity against non-cancerous cells with IC_{50} values > **350 µM**.
- Analysis from *in silico* molecular docking revealed that most of the active compounds exerted inhibitory effects on the flavoenzyme DprE1 through the formation of noncovalent adducts with the amino acid **Cys387**.
- All the synthesized compounds displayed adequate physicochemical, pharmacokinetic, and electronic properties.
- This study emphasizes the crucial need for a thorough examination of the pharmacological properties of these compounds, including *in vivo* studies, to fully grasp their potential in treating infectious diseases.

5.3 Scope for Future Work

- Twenty-eight molecules demonstrated significant inhibition activity against *M. tuberculosis* without toxicity to normal cell lines, suggesting their potential as lead compounds for further *in vivo* and enzymatic studies in drug development.
- While these compounds were only tested against normal bacteria, evaluating them against multidrug-resistant tuberculosis, extensively drug-resistant tuberculosis, methicillin-resistant *Staphylococcus aureus* (MRSA), etc., could provide valuable insights.
- Future research could focus on structurally modifying the active backbone to enhance potency and understand the antitubercular behavior of resulting structures in biological settings.
- The Structure-Activity Relationship information from this study could be utilized in computer-aided drug design (CADD) or Quantitative Structure-Activity Relationship (QSAR) studies to develop new pyrazine-based lead molecules.

****

References

Beard, H., Cholleti, A., Pearlman, D., Sherman, W., and Loving, K. A. (2013). "Applying physics-based scoring to calculate free energies of binding for single amino acid mutations in protein-protein complexes." *PLoS One*, 8(12), e82849.

Bradford, F. E., Connor, L. P., Kilner, C. A., and Halcrow, M. A. (2004). "Iron complexes of 3-(pyrazinyl)-1,2,4-triazole ligands." *Polyhedron*, 23(13), 2141-2151.

Castelo-Branco, F. S., Lima, E. C. de, Domingos, J. L. de O., Pinto, A. C., Lourenço, M. C. S., Gomes, K. M., Costa-Lima, M. M., Araujo-Lima, C. F., Aiub, C. A. F., Felzenszwalb, I., Costa, T. E. M. M., Penido, C., Henriques, M. G., and Boechat, N. (2018). "New hydrazides derivatives of isoniazid against Mycobacterium tuberculosis: Higher potency and lower hepatocytotoxicity." *Eur. J. Med. Chem.*, 146, 529-540.

Cousins, K. R. (2005). "ChemDraw Ultra 9.0. Cambridge Soft, 100 Cambridge Park Drive, Cambridge, MA 02140. www. cambridgesoft.com. See Web site for pricing options." *J. Am. Chem. Soc.*, 127(11), 4115-4116.

Eberhardt, J., Santos-Martins, D., Tillack, A. F., and Forli, S. (2021). "AutoDock Vina 1.2.0: New Docking Methods, Expanded Force Field, and Python Bindings." *J. Chem. Inf. Model.*, 61(8), 3891-3898.

Espíndola, M. R., Varotti, F. de P., Aguiar, A. C. C., Andrade, S. N., and Rocha, E. M. M. da. (2022). "In vitro assessment for cytotoxicity screening of new antimalarial candidates." *Brazilian J. Pharm. Sci.*, 58, e18308.

Fiser, A., Kinh, R., Do, G., and Ali, A. S. (2000). "Modeling of loops in protein structures." *Protein Sci.*, 9(9), 1753-73.

Franzblau, S. G., Witzig, R. S., Mclaughlin, J. C., Torres, P., Madico, G., Hernandez, A., Degnan, M. T., Cook, M. B., Quenzer, V. K., Ferguson, R. M., and Gilman, R. H. (1998). "Rapid, Low-Technology MIC Determination with Clinical Mycobacterium tuberculosis Isolates by Using the Microplate Alamar Blue Assay." *J. Clin. Microbiol,* 36(2), 362-366.

Heatley, N. G. (1943). “A Method for the Assay of Penicillin.” *Biochem J.*, 38(1), 61-65.

Koçak Aslan, E., Han, M. İ., Krishna, V. S., Tamhaev, R., Dengiz, C., Doğan, Ş. D., Lherbet, C., Mourey, L., Tønjum, T., and Gündüz, M. G. (2022). “Isoniazid Linked to Sulfonate Esters via Hydrazone Functionality: Design, Synthesis, and Evaluation of Antitubercular Activity.” *Pharmaceuticals*, 15(10), 1301.

Ong, K. T., Liu, Z. Q., Meng, and Tay, G. (2017). “Review on the Synthesis of Pyrazine and Its Derivatives.” *Borneo J. Resour. Sci. Technol,* 7(2), 60-75.

Patil, S. R., Asrondkar, A., Patil, V., Sangshetti, J. N., Kalam Khan, F. A., Damale, M. G., Patil, R. H., Bobade, A. S., and Shinde, D. B. (2017). “Antileishmanial potential of fused 5-(pyrazin-2-yl)-4H-1,2,4-triazole-3-thiols: Synthesis, biological evaluations and computational studies.” *Bioorganic Med. Chem. Lett.*, 27(16), 3845-3850.

Tadashi Sasaki, Eikoh Ito, and Ikuo Shimizu (1982). Ring transformation of 1,3,4-oxadiazole to s-triazole-fused heterocycles. New synthetic route for thiazolo[2,3-c]-s-triazole and 7H-s-triazolo[3,4-b][1,3,4]thiadiazine.” *J. Org. Chem*, 47, 2757-2760.

Reddyrajula, R., and Dalimba, U. (2020). “The bioisosteric modification of pyrazinamide derivatives led to potent antitubercular agents: Synthesis via click approach and molecular docking of pyrazine-1,2,3-triazoles.” *Bioorganic Med. Chem. Lett.*, 30(2), 126846.

Servusova-Vanaskova, B., Jandourek, O., Paterova, P., Kordulakova, J., Plevakova, M., Kubicek, V., Kucera, R., Garaj, V., Naesens, L., Kunes, J., Dolezal, M., and Zitko, J. (2015). “Alkylamino derivatives of N-benzylpyrazine-2-carboxamide: synthesis and antimycobacterial evaluation.” *Medchemcomm*, 6(7), 1311-1317.

Servusová, B., Vobicková, J., Paterová, P., Kubíček, V., Kuneš, J., Doležal, M., and Zitko, J. (2013). “Synthesis and antimycobacterial evaluation of N-substituted 5-chloropyrazine-2-carboxamides.” *Bioorganic Med. Chem. Lett.*, 23(12), 3589-3591.

Shmidt, M. S., Reverdito, A. M., Kremenchuzky, L., Perillo, I. A., and Blanco, M. M. (2008). “Simple and Efficient Microwave Assisted N-Alkylation of Isatin.” *Molecules*,

13, 831-840.

Soltan, M. K., Ibrahim, S. M., Abo-Kul, M., Soltan, M. K., and Helal, A. S. (2014). "synthesis and anti-inflammatory activity of new 2-arylidenehydrazinyl-quinazolinone and 3-amino-triazoloquinazolinone derivatives synthesis and anti-inflammatory activity of new 2-arylidenehydrazinyl-quinazolinone and 3-amino-triazolo-quinazolinone derivatives." *Asian J. Pharm. Anal. Med. Chem.*, 2(2), 82-93.

Srinivasarao, S., Nandikolla, A., Suresh, A., Calster, K. Van, Voogt, L. De, Cappoen, D., Ghosh, B., Aggarwal, H., Murugesan, S., and Chandra Sekhar, K. V. G. (2020). "Seeking potent anti-tubercular agents: Design and synthesis of substituted-: N -(6-(4-(pyrazine-2-carbonyl)piperazine/homopiperazine-1-yl)pyridin-3-yl)benzamide derivatives as anti-tubercular agents." *RSC Adv.*, 10(21), 12272-12288.

Tian, X., Jaber, J. J., and Rychnovsky, S. D. (2006). "Synthesis and structure revision of calyxin natural products." *J. Org. Chem.*, 71(8), 3176-3183.

Tirado-Rives, J., and Jorgensen, W. L. (2008). "Performance of B3LYP density functional methods for a large set of organic molecules." *J. Chem. Theory Comput.*, 4(2), 297-306.

Trott, O., and Olson, A. J. (2009). "AutoDock Vina: Improving the speed and accuracy of docking with a new scoring function, efficient optimization, and multithreading." *J. Comput. Chem.*, 31(2), 455-461.

Vrbanac, J., and Slauter, R. (2016). "ADME in Drug Discovery." *A Compr. Guid. to Toxicol. Nonclinical Drug Dev.*, Elsevier, 39-67.

Yang, J., Roy, A., and Zhang, Y. (2013). "Protein-ligand binding site recognition using complementary binding-specific substructure comparison and sequence profile alignment." *Bioinformatics*, 29(20), 2588-2595.

Zhang, L. R., Liu, Z. J., Zhang, H., Sun, J., Luo, Y., Zhao, T. T., Gong, H. Bin, and Zhu, H. L. (2012). "Synthesis, biological evaluation and molecular docking studies of novel 2-(1,3,4-oxadiazol-2-ylthio)-1-phenylethanone derivatives." *Bioorganic Med. Chem.*, 20(11), 3615-3621.

Zhang, Y., Wade, M. M., Scorpio, A., Zhang, H., and Sun, Z. (2003). “Mode of action of pyrazinamide: Disruption of Mycobacterium tuberculosis membrane transport and energetics by pyrazinoic acid.” *J. Antimicrob. Chemother.*, 52(5), 790-795.

Zhou, S., Yang, S., and Huang, G. (2017). “Design, synthesis and biological activity of pyrazinamide derivatives for anti-mycobacterium tuberculosis.” *J. Enzyme Inhib. Med. Chem.*, 32(1), 1183-1186.

Abdel-Aziz, M., and Abdel-Rahman, H. M. (2010). “Synthesis and anti-mycobacterial evaluation of some pyrazine-2-carboxylic acid hydrazide derivatives.” *Eur J Med Chem*, 45(8), 3384-3388.

Ahmad, M., Hameed, S., Tahir, M. N., Israr, M., Anwar, M., Shah, M. A., Khan, S. A., and Din, G. (2016). “Synthesis, characterization and biological evaluation of some 5-methylpyrazine carbohydrazide based hydrazones.” *Pak J Pharm Sci*, 29(3), 811-817.

Al-Tamimi, A. M. S., Mary, Y. S., Miniyar, P. B., Al-Wahaibi, L. H., El-Emam, A. A., Armaković, S., and Armaković, S. J. (2018). “Synthesis, spectroscopic analyses, chemical reactivity and molecular docking study and antitubercular activity of pyrazine and condensed oxadiazole derivatives.” *J Mol Struct*, 1164, 459-469.

Åqvist, J., Medina, C., and Samuelsson, J. E. (1994). “A new method for predicting binding affinity in computer-aided drug design.” *Protein Engineering, Design and Selection*, 7(3), 385-391.

Begland, R. W., Hartter, D. R., Donald, D. S., Cairncross, A., and Sheppard, W. A. (1974). “Hydrogen cyanide chemistry. VII. Diiminosuccinonitrile condensation with diaminomaleonitrile.” *J Org Chem*, 39(9), 1235-1239.

Bouz, G., Juhás, M., Pausas Otero, L., Paredes de la Red, C., Janďourek, O., Konečná, K., Paterová, P., Kubíček, V., Janoušek, J., Doležal, M., and Zitko, J. (2019a). “Substituted N-(Pyrazin-2-yl)benzenesulfonamides; Synthesis, Anti-Infective Evaluation, Cytotoxicity, and In Silico Studies.” *Molecules*, 25(1), 138.

Bouz, G., Semelková, L., Janďourek, O., Konečná, K., Paterová, P., Navrátilová, L., Kubíček, V., Kuneš, J., Doležal, M., and Zitko, J. (2019b). “Derivatives of 3-

Aminopyrazine-2-carboxamides: Synthesis, Antimicrobial Evaluation, and in Vitro Cytotoxicity." *Molecules*, 24(7), 1212.

Bouz, G., Šlechta, P., Jand'ourek, O., Konečná, K., Paterová, P., Bárta, P., Novák, M., Kučera, R., Dal, N. J. K., Fenaroli, F., Zemanová, J., Forbak, M., Korduláková, J., Pavliš, O., Kubíčková, P., Doležal, M., and Zitko, J. (2023). "Hybridization Approach Toward Novel Antituberculars: Design, Synthesis, and Biological Evaluation of Compounds Combining Pyrazinamide and 4-Aminosalicylic Acid." *ACS Infect Dis*, 9(1), 79-96.

Cappoen, D., Claes, P., Jacobs, J., Anthonissen, R., Mathys, V., Verschaeve, L., Huygen, K., and Kimpe, N. De. (2014). "1,2,3,4,8,9,10,11-Octahydrobenzo[j]phenanthridine-7,12-diones as New Leads against Mycobacterium tuberculosis." *J Med Chem*, 57(7), 2895-2907.

Das, R., Shilakari Asthana, G., Suri, K. A., Mehta, D. K., and Asthana, A. (2015). "Synthesis and assessment of antitubercular and antimicrobial activity of some novel triazolo and tetrazolo-fused 1, 3, 4-oxadiazole molecules containing pyrazine moiety." *Journal of Pharmaceutical Sciences and Research*, 7(10), 806-811.

Deore, A. B., Dhumane, J. R., Wagh, R., and Sonawane, R. (2019). "The Stages of Drug Discovery and Development Process." *Asian Journal of Pharmaceutical Research and Development*, 7(6), 62-67.

Dolezal, M., and Zitko, J. (2015). "Pyrazine derivatives: A patent review (June 2012-present)." *Expert Opin Ther Pat*, 25(1), 33-47.

El-Azab, A. S., Mary, Y. S., Abdel-Aziz, A. A. M., Miniyar, P. B., Armaković, S., and Armaković, S. J. (2018). "Synthesis, spectroscopic analyses (FT-IR and NMR), vibrational study, chemical reactivity and molecular docking study and anti-tubercular activity of condensed oxadiazole and pyrazine derivatives." *J Mol Struct*, 1156, 657-674.

Ghosh, P., and Mandal, A. (2012). "Greener approach toward one-pot route to pyrazine synthesis." *Green Chem Lett Rev*, 5(2), 127-134.

Global Tuberculosis Report 2023, *World Health Organization*, ISBN 978-92-4-008385-1.

H. S. Lima, C., G. M. O. Henriques, M., L. P. Candea, A., C. S. Lourenco, M., A. F. M. Bezerra, F., L. Ferreira, M., R. Kaiser, C., and N. de Souza, M. V. (2011). "Synthesis and Antimycobacterial Evaluation of N-(E)-heteroaromaticpyrazine-2-carbohydrazide Derivatives." *Med Chem*, 7(3), 245-249.

Hassan, N. W., Saudi, M. N., Abdel-Ghany, Y. S., Ismail, A., Elzahhar, P. A., Sriram, D., Nassra, R., Abdel-Aziz, M. M., and El-Hawash, S. A. (2020). "Novel pyrazine based anti-tubercular agents: Design, synthesis, biological evaluation and in silico studies." *Bioorg Chem*, 96, 103610.

Itoh, T., Maeda, K., Wada, T., Tomimoto, K., and Mase, T. (2002). "Efficient synthesis of substituted 2-aminopyrazines: FeCl 3-promoted condensation of hydroxyiminoketones with aminoacetonitriles." *Tetrahedron Lett*, 43(51), 9287-9290.

Jing, F., Zhang, Y., Luo, S., Chu, W., Zhang, H., and Shi, X. (2010). "Catalytic synthesis of 2-methylpyrazine over Cr-promoted copper-based catalyst via a cyclo-dehydrogenation reaction route." *J. Chem. Sci.*, 122, 621-630.

Jones, R. G. (1949). "Pyrazines and Related Compounds. I. A New Synthesis of Hydroxypyrazines." *J Am Chem Soc*, 71(1), 78-81.

Juhás, M., Kučerová, L., Horáček, O., Janďourek, O., Kubíček, V., Konečná, K., Kučera, R., Bárta, P., Janoušek, J., Paterová, P., Kuneš, J., Doležal, M., and Zitko, J. (2020). "N-Pyrazinoyl Substituted Amino Acids as Potential Antimycobacterial Agents-the Synthesis and Biological Evaluation of Enantiomers." *Molecules*, 25(7), 1518.

Lazar, C., Kluczyk, A., Kiyota, T., and Konishi, Y. (2004). "Drug evolution concept in drug design: 1. Hybridization method." *J Med Chem*, 47(27), 6973-82.

Lima, L., and Barreiro, E. (2005). "Bioisosterism: A Useful Strategy for Molecular Modification and Drug Design." *Curr Med Chem*, 12(1), 23-49.

Maga, J. A. (1992). “Pyrazine Update.” *Food Reviews International*, 8(4), 479-558.

Miniyar, P. B., Mokale, S. N., and Makhija, S. J. (2017). “Design and synthesis of 5-methylpyrazine-2-carbohydrazide derivatives: A new anti-tubercular scaffold.” *Arabian Journal of Chemistry*, 10(1), 41-46.

Miniyar, P., and Makhija, S. (2009). “Synthesis and characterization of pyrazine-2-carbohydrazide derivatives as antimicrobial agents.” *Journal of Young Pharmacists*, 1(2), 165.

Miniyar, P., Murumkar, P., Patil, P., Barmade, M., and Bothara, K. (2015). “Unequivocal Role of Pyrazine Ring in Medicinally Important Compounds: A Review.” *Mini-Reviews in Medicinal Chemistry*, 13(11), 1607-1625.

Müller, R., and Rappert, S. (2010). “Pyrazines: Occurrence, formation and biodegradation.” *Appl Microbiol Biotechnol*, 85(5), 1315-20.

Occhineri, S., Matucci, T., Rindi, L., Tiseo, G., Falcone, M., Riccardi, N., and Besozzi, G. (2022). “Pretomanid for tuberculosis treatment: an update for clinical purposes.” *Current Research in Pharmacology and Drug Discovery*, 3(1), 100-128.

Ohta, A., Akita, Y., and Hara, M. (1979). “Syntheses and reactions of some 2,5-disubstituted pyrazine monoxides.” *Chem Pharm Bull (Tokyo)*, 27(9), 2027-2041.

Raw, S. A., Wilfred, C. D., and Taylor, R. J. K. (2003). “Preparation of quinoxalines, dihydropyrazines, pyrazines, and piperazines using tandem oxidation processes.” *Chemical Communications*, 3(18), 2286-2287.

Reddyrajula, R., and Dalimba, U. (2020). “The bioisosteric modification of pyrazinamide derivatives led to potent antitubercular agents: Synthesis via click approach and molecular docking of pyrazine-1,2,3-triazoles.” *Bioorg Med Chem Lett*, 30(2), 126846.

Rennane, S., Baker, L., and Mulcahy, A. (2021). “Estimating the Cost of Industry Investment in Drug Research and Development: A Review of Methods and Results.” *Sage Journals*, 58, 19457243.

Shamsel-Din, H. A., and Gizawy, M. A. (2021). “A novel dipeptide coupled with pyrazine-oxadiazole derivative as a potential antitubercular agent: Synthesis, radioiodination and bioevaluation.” *Applied Radiation and Isotopes*, 173, 109719.

Srinivasarao, S., Nandikolla, A., Suresh, A., Calster, K. Van, Voogt, L. De, Cappoen, D., Ghosh, B., Aggarwal, H., Murugesan, S., and Chandra Sekhar, K. V. G. (2020). “Seeking potent anti-tubercular agents: design and synthesis of substituted- N -(6-(4-(pyrazine-2-carbonyl)piperazine/homopiperazine-1-yl)pyridin-3-yl)benzamide derivatives as anti-tubercular agents.” *RSC Adv*, 10(21), 12272-12288.

Vogl, O., and Taylor, E. C. (1959). “A Direct Synthesis of 2-Aminopyrazine-3-carboxamides.” *J Am Chem Soc*, 81(10), 2472-2474.

Worley, M. V., and Estrada, S. J. (2014). “Bedaquiline: A novel antitubercular agent for the treatment of multidrug-resistant tuberculosis.” *Pharmacotherapy*, 34(11), 1187-1197.

Xavier, A. S., and Lakshmanan, M. (2014). “Delamanid: A new armor in combating drug-resistant tuberculosis.” *J Pharmacol Pharmacother*, 5(3), 222-224.

Yee, D., Valiquette, C., Pelletier, M., Parisien, I., Rocher, I., and Menzies, D. (2003). “Incidence of Serious Side Effects from First-Line Antituberculosis Drugs among Patients Treated for Active Tuberculosis.” *Am J Respir Crit Care Med*, 167(11), 1472-1477.

Young K. Lee, Sang-Eon Park, and Young S. Kwon. (1990). “Process for manufacturing pyrazines.” US4966970A.

Zheng, X., and Av-Gay, Y. (2016). “New Era of TB Drug Discovery and Its Impact on Disease Management.” *Curr Treat Options Infect Dis*, 8(4), 299-310.

Zitko, J., Servusová-Vaňásková, B., Paterová, P., Navrátilová, L., Trejtnar, F., Kuneš, J., and Doležal, M. (2015). “Design, synthesis and anti-mycobacterial evaluation of some new N-phenylpyrazine-2-carboxamides.” *Chemical Papers*, 70, 649-657.

Zulqurnain, M., Aijijiyah, N. P., Wati, F. A., Fadlan, A., Azminah, A., and Santoso, M. (2023). "Synthesis, Mycobacterium tuberculosis H37Rv inhibitory activity, and molecular docking study of pyrazinamide analogs." *J Appl Pharm Sci*, 13(11), 170-177.

Zumla, A., Nahid, P., and Cole, S. T. (2013). "Advances in the development of new tuberculosis drugs and treatment regimens." *Nat Rev Drug Discov*, 12(5), 388-404.

****

LIST OF PUBLICATIONS

Papers published/communicated in international journals

1. **Shivakumar**, P. Dinesha, U. Kumar D., Varsha P. S., V. K. Deekshit, Design, Synthesis, Characterization, and biological evaluation of novel pyrazine-1,3,4-oxadiazole/[1,2,4]triazolo[3,4-b][1,3,4]thiadiazine derivatives as potent antimycobacterial agents, **Journal of Molecular Structure**. (2024). https://doi.org/10.1016/j.molstruc.2024.137657
2. **Shivakumar**, Vanishree A. L., U. Kumar D., Varsha P. S., Chaithra Prabhu, V. K. Deekshit, Design, Synthesis, and Biological Evaluation of Novel Hybrid Compounds Bearing Pyrazine and 1,2,4-triazole Analogues as Potent Antitubercular Agents, **RSC Pharmaceutics**. (2024). https://doi.org/10.1039/D3PM00054K
3. **Shivakumar**, Dinesha P, U. Kumar D., Structure-Based Drug Design and Characterization of Novel Pyrazine Hydrazinylidene Derivatives with a Benzenesulfonate Scaffold as Noncovalent Inhibitors of DprE1 for Tuberculosis Treatment, **Molecular diversity**. (2024). https://doi.org/10.1007/s11030-024-10812-0
4. **Shivakumar**, Dinesha P, U. Kumar D., Noncovalent Inhibitors of DprE1 for Tuberculosis Treatment: Design, Synthesis, Characterization, *In vitro*, and *In-silico* Studies of 4-oxo-1,4-dihydroquinazolinylpyrazine-2-carboxamides, **J Biomol Struct Dyn.**, Accepted.
5. **Shivakumar**, Dinesha P, U. Kumar D., Varsha P. S., Chaithra Prabhu, V. K. Deekshit, Synthesis and *In vitro* Screening of Pyrazine-2-Carbohydrazide Derivatives as Potential Antitubercular Agents, **Journal of Computational Biophysics and Chemistry**. (2024). https://doi.org/10.1142/S2737416524500042

Other publications

1. Anupriya James, **Shivakumar**, John D. Rodney, Sindhur Joshi, U. Kumar D., N.K Udayashankar, Mechanistic Insights and DFT Analysis of Bimetal Doped Styrofoam-like LaFeO3 Perovskites with In-built Dual Redox Couples for

Enhanced Photo-Fenton Degradation of Tetracycline, **Journal of Chemical Engineering**. (2024). https://doi.org/10.1016/j.cej.2023.148466

2. S. Deshpande N, **Shivakumar**, U. Kumar D., S.D. Ghate, S.R. Dixit, A. Awasthi, B.C. Revanasiddappa, Benzothiazole derivatives as p53-MDM2 inhibitors: *in-silico* design, ADMET predictions, molecular docking, MM-GBSA Assay, MD simulations studies, **J Biomol Struct Dyn.** (2023). https://doi.org/10.1080/07391102.2023.2294836
3. M.G. Srinivasa, **Shivakumar**, U. Kumar, C.H. Mehta, U.Y. Nayak, B.C. Revanasiddappa, In silico studies of (Z)-3-(2-chloro-4-nitrophenyl)-5-(4-nitrobenzylidene)-2-thioxothiazolidin-4-one derivatives as PPAR-α agonist: Design, Molecular Docking, MM-GBSA Assay, Toxicity Predictions, DFT Calculations and MD Simulation Studies, **Journal of Computational Biophysics and Chemistry**. (2023). https://doi.org/10.1142/S2737416523500540
4. Shridhar D. N., **Shivakumar**, Udayakumar D., Ashwini Prabhu, Vinitha Rani, Mahendra G. S., S. R. Dixit, Deepshikha S., Revanasiddappa B. C., Synthesis, Characterization, *in silico* studies, and anticancer activity of Novel 1, 3, 4-Oxadiazole derivatives against Ehrlich ascites carcinoma (EAC) cell lines, **Journal of Computational Biophysics and Chemistry**. (2024). https://doi.org/10.1142/S2737416524500030
5. Lavanya Rao, John D. Rodney, **Shivakumar**, U. Kumar D., N.K. Udayashankar, B. Ramachandra Bhat, Elucidating Mechanisms and DFT Analysis of Monometallic Vanadium Incorporated Nano porous TiO_2 as Advanced Material for Enzyme-Free Electrochemical Blood Glucose Biosensors with Exceptional Performance Tailored for Point-Of-Care Applications, **Microchemical Journal**. (2024). https://doi.org/10.1016/j.microc.2024.111172
6. Banylla F. D., **Shivakumar**, U. Kumar D., Madan Kumar, Natasha N. A., S. Ghetia, Ashwini Somayaji, Chaithra Raviraj, Shridhar N. D., Mahendra G. S, B.C. Revanasiddappa, Development and evaluation of novel 4-thiazolidinone derivatives as potential antidiabetic agents: design, synthesis, characterization,

in silico studies, and *in vivo* assessment, **Journal of Computational Biophysics and Chemistry** - Under review.

7. Shreeganesh Subraya Hegde, **Shivakumar**, Badekai Ramachandra Bhat, Praveen Mishra, Udayakumar Dalimba, Minhaz Uddin Ahmed, Gil Nonato Santos, A novel and ultrasensitive high-surface porous carbon-based electrochemical biosensor for early detection of dengue virus, **Biosensors and Bioelectronics: X**. (2024). https://doi.org/10.1016/j.biosx.2024.100525
8. Vinay K. K., Bodke Y. D., **Shivakumar**, U. Kumar D., Nagaraja O., Chethan Krishnamurthy, Synthesis, Computational and UV-Vis Absorption Studies of Novel Sulfathiazole Azo Sulfonamides acting as Potent Antitubercular Agents, **Journal of Molecular Structure**. (2024). https://doi.org/10.1016/j.molstruc.2024.139358
9. Kavitha G. M., **Shivakumar**, U. Kumar D., A. Dharnappa S., Mahendra G.S., Revanasiddappa B. C., Shrikrishna Isloor, Nemat Ali, Sushma Pradeep, Devananda D., Chandan S., Shiva Prasad K., Contriving Multiepitope Vaccine Against Glycoprotein of Rabies Virus Using Computational Informatics Approach, **Current Bioinformatics** - Under Review.

Research papers presented in national/international conference

1. **Shivakumar** and Udayakumar Dalimba (2024). "Design, Synthesis, Characterization, and biological evaluation of novel pyrazine-1,3,4-oxadiazole/[1,2,4]triazolo[3,4-b][1,3,4]thiadiazine derivatives as potent antimycobacterial agents." National Conference on Current Progress in Biochemistry-2024. Karnatak University, Karnataka, India. January 24-25, 2024.
2. **Shivakumar** and Udayakumar Dalimba (2024). "Design, Synthesis, and Biological Evaluation of Novel Hybrid Compounds Bearing Pyrazine and 1,2,4-triazole Analogues as Potent Antitubercular Agents." National Conference on Advanced Materials for Chemical and Biological Applications, SDM College (Autonomous), Ujire, Karnataka, India. March 06-07, 2024.
3. **Shivakumar** and Udayakumar Dalimba (2024). "Structure-Based Drug

Design and Characterization of Novel Pyrazine Hydrazinylidene Derivatives with a Benzenesulfonate Scaffold as Noncovalent Inhibitors of DprE1 for Tuberculosis Treatment." National Conference on Advanced Materials for Chemical and Biological Applications, SDM College (Autonomous), Ujire, Karnataka, India. March 06-07, 2024.

4. **Shivakumar** and Udayakumar Dalimba (2024). "Synthesis and *In vitro* Screening of Pyrazine-2-Carbohydrazide Derivatives as Potential Antitubercular Agents." Internation conference on Transformative chemistry for a sustainable future, St. Aloysius (Deemed to be University), Mangalore, Karnataka, India. March 15, 2024.

BIODATA

SHIVAKUMAR

Senior Research Fellow, Department of Chemistry

National Institute of Technology Karnataka (NITK), Surathkal, Mangalore

575025, Karnataka, India. Mob. +91-7090462847;

Email:shiva244668@gmail.com

Personal Information:

Date of Birth: June 01, 1996

Sex: Male

Nationality: Indian

Languages: 1. English: Proficient, 2. Kannada: Proficient, 3. Telugu: Proficient

Hobbies: Gardening, Cooking, Traveling.

Academic Qualifications:

- **Doctor of Philosophy (Sep 2020 - Apr 2024)** at the Department of Chemistry, National Institute of Technology Karnataka (NITK), Surathkal, India. Secured First Class in coursework (8.31/10).
  Thesis Title: "Design and Development of new pyrazine-based molecules as potent antitubercular agents."
- **Master of Science (June 2017 - May 2019)** in Chemistry from Tumkur University,Karnataka, India. Secured First Class (7.01/10).
- **Bachelor of Science (June 2014 - May 2017)** in Physics, Chemistry, and Mathematics from Tumkur University, Karnataka, India. Secured First Class (76.54 %).

Experience:

Guest Faculty (Aug 2019 - Feb 2020):

Guest Faculty at the Department of Chemistry, University College of Science, Tumkur University, Tumkur, Karnataka, India. Responsibilities include teaching and administrative duties.

Areas of Interest:

Synthetic Organic Chemistry, Medicinal Chemistry, Drug Discovery, Computational and Theoretical Chemistry, and Material Science.

Awards & Honors:

1. **Junior Research Fellowship** (Sep 2020 - June 2023) awarded by the National Institute of Technology Karnataka (NITK).
2. **Senior Research Fellowship** (July 2023 - March 2024) awarded by the National Institute of Technology Karnataka (NITK).
3. Qualified **GATE** (2020) conducted by the Indian Institute of Technology Delhi (IITD), India.
4. Received the **Best Oral and Poster Presentation Award** at the National and International Conferences.

Professional Training/ Workshop:

1. Organized a two-week comprehensive training session that provided practical instruction in Molecular Docking, Molecular Dynamic Simulations, and Density Functional Theory.
2. Week-long Synergistic Training Program Utilizing the Scientific and Technological Infrastructure (STUTI) by Pondicherry University, India under the supervision of the Department of Science and Technology (Oct 2022).
3. Week-long Synergistic Training Program Utilizing the Scientific and Technological Infrastructure (STUTI) by Mangalore University, India under the supervision of the Department of Science and Technology (Nov 2022).
4. Participated in a total of 24 workshops and conferences, both at the national and international levels.

Instrumentation Skills:

Hands-on experience in both handling and interpreting data generated by a diverse array of analytical instruments. These instruments include **FT-NMR, GC-MS, LC-MS, HRMS, single crystal XRD, Powder XRD, HPLC, FTIR, UV spectrophotometer, and fluorimeter.**

Computational Skills:

I have strong computational skills, particularly in the realm of scientific software applications like **Gaussian, Schrödinger, Materials Studio, GROMACS, Desmond, AutoDock Vina, Avogadro, ChemDraw, Origin, PyMOL, COMSOL Multiphysics, Ansys, MestReNova, TopSpin, Mendeley, Reaxys, and SciFinder**. I excel in conducting various *in silico* studies, including molecular docking, molecular dynamics simulations, homology modeling, virtual screening, 2D and 3D QSAR studies, MM-GBSA assay, ADMET assessments, Catalysis, Adsorption and sensing studies, Materials design using ML/AI, and density functional theory (DFT) calculations.

Experimental Skills:

- Proficient in the synthesis of organic compounds, utilizing a variety of methods such as conventional, microwave, ultrasonication, solvent-free synthesis, and high-pressure reactions.
- Proficient in performing Recrystallization, Solvent extraction, TLC, and Column chromatography.
- Proficient in handling a wide array of laboratory instruments, including electronic and analytical balances, multiscale reactors, autoclaves, parallel synthesizers, digital melting point apparatus, rotor evaporators, Glove box, and flash chromatography systems.
- I am well-versed in laboratory safety protocols including proper handling of chemicals, disposal of hazardous waste, and use of personal protective equipment.

- Highly skilled in conducting thorough literature surveys to find appropriate synthetic methods, characterization techniques, and background information for research projects.

Declaration:

I hereby confirm that the information provided is accurate to the best of my understanding.

Yours Sincerely,

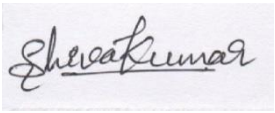

(SHIVAKUMAR)

Place: NITK, Surathkal

Date: 20 - 08 - 2024